

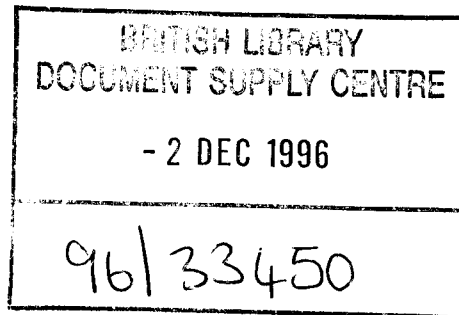
# Magnetization Oscillations *and* Waves

A.G. Gurevich, Ph.D., D.Sci.

Chief Researcher and Professor  
Magnetic Laboratory  
Ioffe Physico-Technical Institute  
St. Petersburg, Russia

G.A. Melkov, Ph.D., D.Sci.

Professor  
Dean of Department, Radiophysical  
Shevchenko Kiev National University  
Kiev, Ukraina



CRC Press

Boca Raton New York London Tokyo

**Library of Congress Cataloging-in-Publication Data**

Catalog record is available from the Library of Congress.

This book contains information obtained from authentic and highly regarded sources. Reprinted material is quoted with permission, and sources are indicated. A wide variety of references are listed. Reasonable efforts have been made to publish reliable data and information, but the author and the publisher cannot assume responsibility for the validity of all materials or for the consequences of their use.

Neither this book nor any part may be reproduced or transmitted in any form or by any means, electronic or mechanical, including photocopying, microfilming, and recording, or by any information storage or retrieval system, without prior permission in writing from the publisher.

CRC Press, Inc.'s consent does not extend to copying for general distribution, for promotion, for creating new works, or for resale. Specific permission must be obtained in writing from CRC Press for such copying.

Direct all inquiries to CRC Press, Inc., 2000 Corporate Blvd., N.W., Boca Raton, Florida 33431.

© 1996 by CRC Press, Inc.

No claim to original U.S. Government works  
International Standard Book Number 0-8493-9460-0  
Printed in the United States of America 1 2 3 4 5 6 7 8 9 0  
Printed on acid-free paper

---

# *Contents*

---

<b>Preface</b>	<b>ix</b>
<b>1 Isotropic ferromagnet magnetized to saturation</b>	<b>1</b>
1.1 Ferromagnetism . . . . .	1
1.1.1 Elementary magnetic moments . . . . .	2
1.1.2 Paramagnetism . . . . .	4
1.1.3 Weiss theory . . . . .	6
1.1.4 Exchange interaction . . . . .	7
1.2 Equation of motion of magnetization . . . . .	8
1.3 High-frequency magnetic susceptibility . . . . .	10
1.3.1 Solution of the linearized equation of motion . . . . .	11
1.3.2 Peculiarities of the susceptibility tensor . . . . .	12
1.3.3 High-frequency permeability . . . . .	14
1.4 Allowance for magnetic losses . . . . .	17
1.4.1 Dissipative terms and dissipation parameters . . . . .	17
1.4.2 Susceptibility tensor components . . . . .	19
1.5 Uniform oscillations in a small ellipsoid . . . . .	22
1.5.1 Internal and external magnetic fields . . . . .	23
1.5.2 Eigenoscillations . . . . .	24
1.5.3 Forced oscillations . . . . .	27
<b>2 Anisotropic ferromagnet</b>	<b>31</b>
2.1 Landau–Lifshitz equation . . . . .	31
2.1.1 Generalization of equation of motion . . . . .	32
2.1.2 Methods of analysis of ferromagnetic resonance in anisotropic ferromagnet . . . . .	35
2.2 Magnetocrystalline anisotropy . . . . .	37
2.2.1 Origins of magnetocrystalline anisotropy . . . . .	37
2.2.2 Phenomenological description . . . . .	39
2.2.3 Equilibrium orientations of magnetization . . . . .	41
2.3 Ferromagnetic resonance in a single crystal . . . . .	43
2.3.1 Sphere of a uniaxial ferromagnet . . . . .	44

2.3.2	Sphere of a cubic ferromagnet . . . . .	47
2.3.3	Simultaneous allowance for different kinds of anisotropy . . . . .	50
2.4	Ferromagnetic resonance in a polycrystal . . . . .	53
2.4.1	Independent-grain and strongly-coupled-grain approximations . . . . .	54
2.4.2	Influence of porosity . . . . .	56
<b>3</b>	<b>Antiferromagnets and ferrites</b> . . . . .	<b>59</b>
3.1	Antiferromagnetism and ferrimagnetism . . . . .	59
3.1.1	Crystal and magnetic structures . . . . .	60
3.1.2	Equations of motion and energy terms . . . . .	64
3.1.3	Ground states and small oscillations . . . . .	65
3.2	Antiferromagnetic resonance . . . . .	68
3.2.1	Antiferromagnet with an easy axis of anisotropy: steady states . . . . .	68
3.2.2	Oscillations in antiparallel state . . . . .	71
3.2.3	Oscillations in noncollinear state . . . . .	73
3.2.4	Oscillations in transverse and arbitrarily oriented fields . . . . .	74
3.2.5	Antiferromagnet with easy plane of anisotropy . . . . .	76
3.3	Magnetic oscillations in ferrimagnets . . . . .	81
3.3.1	Ground states of two-sublattice ferrimagnet . . . . .	81
3.3.2	Oscillations in antiparallel ground state . . . . .	83
3.3.3	Oscillations in noncollinear ground state . . . . .	86
3.3.4	Damped and forced oscillations . . . . .	87
<b>4</b>	<b>Fundamentals of electrodynamics of gyrotropic media</b> . . . . .	<b>91</b>
4.1	Equations . . . . .	91
4.1.1	General equations and boundary conditions . . . . .	91
4.1.2	Equations for bigyrotropic media . . . . .	94
4.2	Uniform plane waves . . . . .	96
4.2.1	General relations . . . . .	96
4.2.2	Longitudinal magnetization . . . . .	98
4.2.3	Transverse magnetization . . . . .	102
4.3	Nonreciprocity . . . . .	104
4.4	Energy relations . . . . .	106
4.4.1	Equation of energy balance . . . . .	107
4.4.2	Energy losses . . . . .	108
4.5	Perturbation method . . . . .	109
4.5.1	Gyrotropic perturbation of a waveguide . . . . .	110
4.5.2	Gyrotropic perturbation of a resonator . . . . .	111
4.5.3	Quasistatic approximation . . . . .	111
4.5.4	Resonator with walls of real metal . . . . .	114

<b>5</b>	<b>Waveguides and resonators with gyrotropic media. Microwave ferrite devices</b>	<b>117</b>
5.1	Waveguide with longitudinally magnetized medium . . . . .	117
5.1.1	Circular waveguide . . . . .	118
5.1.2	Circular waveguide with ferrite rod . . . . .	119
5.1.3	Faraday ferrite devices . . . . .	121
5.2	Waveguide with transversely magnetized ferrite . . . . .	123
5.2.1	Rectangular waveguide filled with ferrite . . . . .	123
5.2.2	Rectangular waveguide with ferrite plates . . . . .	125
5.2.3	Microwave ferrite devices . . . . .	128
5.3	Resonators with gyrotropic media . . . . .	130
5.3.1	Eigenoscillations and forced oscillations . . . . .	131
5.3.2	Waveguide resonators . . . . .	133
5.3.3	Ferrite resonators . . . . .	134
5.3.4	Use of perturbation method . . . . .	137
5.4	Waveguides and waveguide junctions with ferrite samples . . . . .	138
5.4.1	Ferrite ellipsoid in a waveguide . . . . .	139
5.4.2	Coupling of orthogonal waveguides. Ferrite band-pass filters . . . . .	141
5.4.3	General properties of nonreciprocal junctions . . . . .	143
<b>6</b>	<b>Magnetostatic waves and oscillations</b>	<b>147</b>
6.1	Magnetostatic approximation . . . . .	147
6.2	Nonexchange magnetostatic waves in plates and rods . . . . .	153
6.2.1	Volume waves in plates . . . . .	153
6.2.2	Surface waves . . . . .	157
6.2.3	Magnetostatic waves in waveguides with finite cross section . . . . .	162
6.2.4	Energy flow and losses . . . . .	166
6.2.5	Magnetostatic waves in ferrite films: excitation, applications . . . . .	168
6.3	Magnetostatic oscillations (Walker's modes) . . . . .	170
6.3.1	Metallized cylinder . . . . .	171
6.3.2	Sphere and ellipsoid of revolution . . . . .	171
6.3.3	Damping, excitation, and coupling . . . . .	176
<b>7</b>	<b>Spin waves</b>	<b>179</b>
7.1	Spin waves in unbounded ferromagnet . . . . .	179
7.1.1	Energy and effective field of exchange interaction . . . . .	179
7.1.2	Dispersion law . . . . .	180
7.1.3	Magnetization, field components, and damping . . . . .	184
7.2	Spin waves in bounded bodies . . . . .	186
7.2.1	Exchange boundary conditions . . . . .	186
7.2.2	Standing spin waves in films . . . . .	189

7.2.3	Propagating spin waves in films . . . . .	194
7.2.4	Spin waves in nonuniform magnetic fields . . . . .	198
7.3	Magnons . . . . .	199
7.3.1	Quantization of magnetic oscillations and waves . . . . .	199
7.3.2	Thermal magnons . . . . .	202
7.4	Elements of microscopic spin-wave theory . . . . .	205
7.4.1	Diagonalization of the Hamiltonian . . . . .	206
7.4.2	Discussion of the dispersion law . . . . .	209
7.4.3	Allowance for dipole–dipole interaction and anisotropy . . . . .	212
7.4.4	Interaction of magnons . . . . .	214
<b>8</b>	<b>Magnetic oscillations and waves in unsaturated ferromagnet</b>	<b>215</b>
8.1	Oscillations of domain walls . . . . .	215
8.1.1	Domain walls and domain structures . . . . .	215
8.1.2	Equation of motion of a domain wall . . . . .	219
8.1.3	Dynamic susceptibility . . . . .	220
8.2	Ferromagnetic resonance in samples with domain structure . . . . .	222
8.2.1	Ellipsoid of uniaxial ferromagnet . . . . .	224
8.2.2	Sphere of cubic ferromagnet . . . . .	226
8.2.3	Nonuniform modes in unsaturated samples . . . . .	229
<b>9</b>	<b>Nonlinear oscillations of magnetization</b>	<b>231</b>
9.1	Ferromagnetic resonance in strong alternating fields . . . . .	231
9.1.1	Rigorous solution of equation of motion . . . . .	231
9.1.2	Approximate methods . . . . .	234
9.2	Harmonic generation and frequency conversion . . . . .	237
9.2.1	Frequency doubling . . . . .	238
9.2.2	Frequency mixing . . . . .	242
<b>10</b>	<b>Parametric excitation of magnetic oscillations and waves</b>	<b>245</b>
10.1	Nonlinear coupling of magnetic modes . . . . .	245
10.2	Thresholds of parametric excitation under transverse pumping . . . . .	249
10.2.1	First-order and second-order instabilities . . . . .	249
10.2.2	Threshold fields . . . . .	252
10.2.3	Effect of pumping-field polarization . . . . .	254
10.3	Longitudinal and oblique pumping . . . . .	255
10.3.1	Longitudinal pumping . . . . .	255
10.3.2	Effect of nonuniformities . . . . .	259
10.3.3	Oblique pumping . . . . .	261
10.4	Instability of nonuniform modes and nonuniform pumping . . . . .	263
10.4.1	Parametric excitation of magnetostatic oscillations and waves . . . . .	263
10.4.2	Ferrite parametric amplifier . . . . .	267

10.4.3	Nonuniform pumping . . . . .	268
10.5	Above-threshold state . . . . .	271
10.5.1	Reaction of parametric spin waves on pumping . . . . .	271
10.5.2	Phase mechanism . . . . .	274
10.5.3	Nonlinear damping . . . . .	276
10.5.4	Stability of the above-threshold state . . . . .	279
10.5.5	Nonlinear microwave ferrite devices . . . . .	279
<b>11</b>	<b>Spin-spin relaxation</b>	<b>283</b>
11.1	Relaxation processes in magnetically ordered substances . . . . .	283
11.1.1	Kinds of relaxation processes . . . . .	283
11.1.2	Methods of theoretical study . . . . .	285
11.2	Inherent spin-spin processes . . . . .	288
11.2.1	Three-magnon splitting . . . . .	289
11.2.2	Three-magnon confluence . . . . .	292
11.2.3	Four-magnon scattering . . . . .	294
11.2.4	Inherent processes for uniform precession . . . . .	296
11.2.5	Experimental data . . . . .	296
11.3	Two-magnon processes . . . . .	299
11.3.1	Theory of two-magnon processes . . . . .	300
11.3.2	Disorder in distribution of ions over lattice sites . . . . .	305
11.3.3	Anisotropy-field variations and pores in polycrystals . . . . .	306
11.3.4	Surface roughness . . . . .	308
<b>12</b>	<b>Magnetoelastic coupling</b>	<b>311</b>
12.1	Elastic properties and magnetoelastic interaction . . . . .	311
12.1.1	Elastic waves and oscillations . . . . .	311
12.1.2	Magnetoelastic energy and equations of motion . . . . .	314
12.2	Effect of elastic stresses on ferromagnetic resonance . . . . .	318
12.3	Magnetoelastic waves . . . . .	319
12.3.1	Normal waves . . . . .	320
12.3.2	Damping and excitation . . . . .	323
12.3.3	Magnetoelastic waves in nonuniform steady magnetic field . . . . .	324
12.4	Parametric excitation of magnetoelastic waves . . . . .	326
12.4.1	Longitudinal pumping of magnetoelastic waves . . . . .	326
12.4.2	Parametric excitation caused by magnetoelastic coupling . . . . .	329
12.4.3	Elastic pumping . . . . .	330
12.5	Spin-lattice relaxation . . . . .	331

<b>13 Ionic anisotropy and relaxation</b>	<b>337</b>
13.1 Anisotropy caused by impurity ions . . . . .	337
13.1.1 Energy levels of ions . . . . .	337
13.1.2 One-ion theory of ferromagnetic resonance anisotropy . . . . .	342
13.1.3 Near-crossing energy levels . . . . .	343
13.1.4 Experimental data . . . . .	344
13.2 Ionic relaxation processes . . . . .	347
13.2.1 Transverse relaxation . . . . .	347
13.2.2 Longitudinal (slow) relaxation . . . . .	349
13.2.3 Relaxation of ionic-level populations . . . . .	356
13.2.4 Experimental data . . . . .	357
<b>14 Interaction of magnetic oscillations and waves with charge carriers</b>	<b>363</b>
14.1 Effect of charge carriers in semiconductors . . . . .	363
14.1.1 Damping of magnetic oscillations caused by conductivity . . . . .	363
14.1.2 Influence of interionic electron transitions . . . . .	365
14.1.3 Interaction of spin waves with charge carriers . . . . .	367
14.2 Ferromagnetic resonance and spin waves in metals . . . . .	372
14.2.1 Thin-film model . . . . .	373
14.2.2 Theory without allowance for exchange interaction . . . . .	375
14.2.3 Influence of exchange interaction . . . . .	378
14.2.4 Antiresonance . . . . .	384
14.2.5 Processes of magnetic relaxation . . . . .	386
<b>Appendices</b>	<b>391</b>
A Units and constants . . . . .	391
B Demagnetization factors . . . . .	397
C Dirac delta function and Kronecker delta symbol . . . . .	401
<b>Bibliography</b>	<b>403</b>
<b>Subject Index to the Bibliography</b>	<b>431</b>
<b>Index</b>	<b>435</b>



---

## *Preface*

---

In this book the high-frequency processes, i.e., oscillations and waves in magnetically ordered substances: ferromagnets, antiferromagnets, and ferrimagnets (ferrites) are treated. This subject is of interest, at least, from three points of view: (i) as a part of the fundamental problem of interaction of electromagnetic field with matter, (ii) as a basis for designing nonreciprocal and controllable devices that are used now (and will be used more widely in the future) in microwave and optical systems in radar, space communication, radioastronomy, etc., (iii) as a technique for measuring the parameters of magnetic materials.

The problems studied in the book include ferromagnetic and antiferromagnetic resonances, spin waves, nonlinear processes, and high-frequency manifestations of interactions between the magnetic system and other systems of magnetically ordered substances (crystal lattice, charge carriers). Fundamentals of electrodynamics of such substances and principles of their applications in microwave and optical engineering are considered, as well. These problems are treated mainly in terms of classical theory using the Maxwell equations and the Landau–Lifshitz equation of motion of magnetization. It is well known that the magnetic ordering is a result of the quantum-mechanical exchange interaction, which cannot be understood in the framework of the classical theory. Nevertheless, the existence of this interaction does not prevent but, on the contrary, makes possible and reasonable the classical treatment of dynamic processes in magnetically ordered substances. The quantum-mechanical approach should be used (and is used in this book) only in the study of relaxation processes, which determine the energy losses of magnetic oscillations and waves.

The present book differs from other monographs on this subject in that it treats successively, in a single style, and on the up-to-date level all the main topics of the problem, in a form comprehensible for readers not skilled in mathematics and theoretical physics. The book is intended to be a manual for everybody entering the field of magnetic dynamics: scientists as well as engineers, designers of magnetic materials and devices, and students. The authors hope, however, that it will be used as a reference book by scientists and engineers that already work in the field.

The readers are supposed to have studied mathematics and experimental physics to an extent of usual college courses but may have, perhaps, forgotten some parts of them. Therefore, the background information needed to understand the topics treated in the book is briefly reviewed. Sections 1.1, 2.2, 3.1, and partly, 8.1 and

12.1 are devoted to this. So, no other manuals are needed to understand completely the material presented in the book. (This does not mean, of course, that the study of other books and articles is not recommended.)

The authors tried not only to present some useful theoretical results but to teach the reader to obtain, at least, some of them. Therefore, most of the formulae are derived in detail, so that the reader would be able to reproduce the derivation. The book contains no formulated problems. (The authors' experience tells that not all readers solve them.) Nevertheless, an active study of the book is strongly recommended. It can consist in deriving the formulae given in the book, carrying out the estimates, and in comparing different results. All the data needed for this the reader can obtain from the text and appendices.

The experimental techniques are not described in the book, they should be mastered in laboratories. But the experimental results are cited, especially when they supplement considerably the existing theories or contradict them. The experiment is present 'invisibly' in the book written by experimentalists.

In the selection of topics to be considered we tried to use the following criteria: generality, timeliness, and pedagogical value. When these criteria came into conflict, the decision could not be but subjective. Moreover, some topics satisfying all mentioned criteria have not been included into the book. Among them there are spin waves in antiferromagnets, interaction of spin waves with light, and such nonlinear effects as magnetic envelope solitons and chaos.

The CGS (Gaussian) units are used throughout the book because they are most suitable for describing the physical, in any case the magnetic, processes. Often (when this cannot lead to uncertainty) the units of some cited values are omitted, as is common in lectures and discussions. The relations between CGS and SI units are listed in Appendix A.

The list of references contains, in addition to all sources cited in the text, a few good books and papers not referred to but worth becoming acquainted with in studying the problems treated in the book, as well as some of the above-mentioned problems, which were not included in the book. Neither the completeness of the list of references nor the elucidation of priorities was aimed.

The entire book is written in collaboration by both authors, and they are both responsible for all mistakes. We will be grateful to the readers who will kindly attract our attention to them.

We are very grateful to all our colleagues and friends who, in the course of our long work on this book, improved the content by their critical comments and advices. We regret that it is impossible to mention all of them here. We are especially thankful to the late Professor G. V. Skrotskii, whose advices were very valuable. The authors have the pleasure to thank N. K. Selyanina and V. G. Grigor'yants, whose comments resulted in an essential improvement of the book. We are grateful to the staff of the Editorial Office at the Ioffe Physico-Technical Institute for the skillful preparation of the camera-ready copy of the book.

# 1

---

## *Isotropic ferromagnet magnetized to saturation*

---

### 1.1 Ferromagnetism

The aim of this book is to study the dynamical magnetic properties of magnetically ordered substances. But before treating the dynamical properties, we review in this section the basic concepts of ferromagnetism. We assume the reader to be somewhat familiar with them and only review the most important aspects.<sup>1</sup>

All substances can be classified as diamagnetic and paramagnetic. The latter contain elementary magnetic moments, which can be oriented by magnetic field, what leads to magnetization in the direction of the field. However, in some paramagnetic substances the orientation of magnetic moments occurs *spontaneously*, in the absence of an external magnetic field. Such substances are called magnetically ordered. The simplest type of them is a ferromagnet. All elementary magnetic moments tend to align, in this case, parallel to each other, resulting in large spontaneous magnetization.

Two points should be emphasized. First, the thermal motion hinders the orientation of magnetic moments. Therefore, the spontaneous parallel order is nearly ideal only at low temperatures. At a temperature  $T_C$  called the Curie temperature the thermal motion destroys completely the magnetic order.

Second, the directions of spontaneous magnetization, in the absence of external magnetic field or in a weak field, (in not very small samples) are not parallel to each other throughout the whole sample. The sample is divided into domains, inside of which these directions are approximately the same, but change rather quickly in going from one domain to another.

---

<sup>1</sup>For an overview of the basic concepts of ferromagnetism the textbooks [227, 70] are recommended, and for a more thorough study of the theory of ferromagnetism the monographs [246, 226, 201] can be used.

### 1.1.1 Elementary magnetic moments

Elementary magnetic moments, mentioned above, are the spin and the orbital magnetic moments of electrons. The net moments of all inner (filled) electron shells of atoms are equal to zero. Contributions to paramagnetism appear only from the partly filled 3d, 4d, 5d, or 4f shells and also from outer s electrons. In ionic crystals the total, spin plus orbital, magnetic moments of ions can, generally speaking, be regarded as elementary magnetic moments. However, the orbital moments of some 3d ions are equal to zero (the ions in S state), and the moments of some other ions are quenched (i.e., the lowest energy level of the ion is an orbital singlet, see Section 13.1). In these cases, the spin moments of ions are the elementary magnetic moments.

Magnetic moments in dielectrics and semiconductors can be regarded as localized on crystal-lattice sites. In metals, the magnetic moments of 3d and 4f shells are only partly localized (to a greater degree, in 4f metals), and the delocalized magnetic-moment density of conduction electrons is to be taken into account [445].

Let us, first, consider the localized magnetic moments as *classical* magnetic dipoles. Such a dipole with the moment  $\mathfrak{M}_f$ , situated at a point  $f$ , produces at a point  $f'$  the magnetic field [399]

$$\mathbf{H}_{f'} = \frac{3(\mathfrak{M}_f \mathbf{r}_{ff'}) \mathbf{r}_{ff'}}{r_{ff'}^5} - \frac{\mathfrak{M}_f}{r_{ff'}^3} \quad (1.1)$$

where  $\mathbf{r}_{ff'}$  is a radius-vector connecting points  $f$  and  $f'$ . A force moment acting on another dipole, with a moment  $\mathfrak{M}_{f'}$ , situated at a point  $f'$ , is

$$\mathbf{T}_{f'} = \mathfrak{M}_{f'} \times \mathbf{H}_{f'}. \quad (1.2)$$

The energy of interaction of the two dipoles is [70]

$$\varepsilon_{ff'} = -\mathfrak{M}_{f'} \mathbf{H}_{f'} = -\frac{3(\mathfrak{M}_f \mathbf{r}_{ff'}) (\mathfrak{M}_{f'} \mathbf{r}_{ff'})}{r_{ff'}^5} + \frac{\mathfrak{M}_f \mathfrak{M}_{f'}}{r_{ff'}^3}. \quad (1.3)$$

The energy of magnetic (dipole–dipole) interaction of all magnetic moments of a sample is the double sum of (1.3) over all  $f$  and  $f'$  except  $f = f'$ . This energy, as we shall soon see, is in most cases far too small to be the reason of magnetic ordering.

To begin the elucidation of this reason, we point out, first of all, that the elementary magnetic moments, being microscopic objects, obey the laws of quantum mechanics. The quantum mechanics (e.g., [243, 336]) treats all dynamical variables, including magnetic moments, as operators acting on appropriate wave functions. The quantities that can be observed are the eigenvalues of these operators.

The eigenvalues of the projection of a moment of momentum (or an *angular momentum*) onto a certain axis, chosen as an axis of quantization, are discrete quantities, the nearest of which differ by  $\hbar$ . They are usually expressed in units

of  $\hbar$ . Then, e.g., for spin angular momenta

$$\{\hat{S}_z\} = S, S - 1, \dots, (-S) \quad (1.4)$$

where braces denote the eigenvalues of an operator inside them, and  $S$  is the spin quantum number, which can be an integer or half-integer. For an electron,  $S = 1/2$ , and  $\{\hat{S}_z\} = \pm 1/2$ . For the  $\text{Fe}^{3+}$  ion (which is the main magnetic ion in most magnetic materials),  $S = 5/2$ , and  $\{\hat{S}_z\} = 5/2, 3/2, \dots, (-5/2)$ . The projections  $\hat{L}_z$  of the orbital angular momentum are quantized in an analogous manner, but the orbital quantum numbers are only integers.

The projections of the angular-momentum operator onto  $x$ - and  $y$ -axes have no definite eigenvalues in the representation in which the  $z$ -axis is the axis of quantization. The eigenvalues of the squared vector-length operator are (e.g., for a spin angular momentum)

$$\{\hat{S}^2\} = S(S + 1). \quad (1.5)$$

The total angular momentum  $\hat{J}$  is the geometric sum of spin and orbital angular momenta. The eigenvalues of its projection  $\hat{J}_z$  are quantized analogously to (1.4), and the quantum number  $J$ , for given values of  $S$  and  $L$ , can take the values

$$J = (S + L), (S + L - 1), \dots, |S - L|. \quad (1.6)$$

The *magnetic-moment* operators, the spin  $\hat{\mathfrak{M}}_s$ , the orbital  $\hat{\mathfrak{M}}_L$ , and the total  $\hat{\mathfrak{M}}$ , are proportional to the corresponding angular momenta. Magnetic moments, as distinct from angular momenta, are expressed in *absolute* units. Therefore,

$$\hat{\mathfrak{M}}_s = -\gamma_S \hbar \hat{S} \quad (1.7)$$

where  $\hbar \equiv h/2\pi$  is the Plank's constant, and the gyromagnetic ratio

$$\gamma_S = \frac{g_S |e_0|}{2m_e c}. \quad (1.8)$$

Here  $e_0$  is the charge of an electron,  $m_e$  is its mass at rest,  $c$  is the velocity of light, and  $g_S$  is the spectroscopic splitting factor (Lande factor or  $g$ -factor) for an electron spin. Its value, given by the quantum electrodynamics, is

$$g_S = 2 \left( 1 + \frac{\alpha}{2\pi} - 0.328 \frac{\alpha^2}{\pi^2} \right) \quad (1.9)$$

where  $\alpha = e_0^2/(\hbar c) \approx 1/137$  is the fine-structure constant. The minus sign in (1.7) shows that the magnetic moment and the angular momentum of an electron are antiparallel to each other, the value of  $\gamma_S$  being positive.

An expression analogous to (1.7) can be written for orbital magnetic moment as well, but in this case  $g_L = 1$ . The total magnetic moment

$$\hat{\mathfrak{M}} = -\gamma \hbar \hat{J} = -\frac{g |e_0| \hbar}{2m_e c} \hat{J}. \quad (1.10)$$

The  $g$ -factor in (1.10) depends on the *quantum numbers*  $S$ ,  $L$ , and  $J$ . Assuming  $g_S = 2$ , we get [1]

$$g_J = \frac{3}{2} + \frac{S(S+1) - L(L+1)}{2J(J+1)}. \quad (1.11)$$

It follows from (1.7) and (1.10) that the magnetic moments are quantized in the same way as the angular momenta. In particular,

$$\{\hat{\mathfrak{M}}_z\} = \gamma\hbar J, \gamma\hbar(J-1), \dots, (-\gamma\hbar J). \quad (1.12)$$

The difference between two successive eigenvalues of  $\hat{\mathfrak{M}}_z$  are

$$\delta\mathfrak{M}_z = \gamma\hbar \equiv g\mu_B \quad (1.13)$$

where

$$\mu_B = \frac{|e_0|\hbar}{2m_e c} \quad (1.14)$$

is the Bohr magneton.

### 1.1.2 Paramagnetism

The states with different  $\{\hat{\mathfrak{M}}_z\}$  values are degenerate in the absence of an external magnetic field. When the magnetic field  $\mathbf{H}$  is applied, there appears the potential energy of a magnetic moment in this field (the Zeeman energy)

$$\varepsilon_Z = -\mathfrak{M}H \quad (1.15)$$

and the degeneracy is removed. There are then  $(2J+1)$  equidistant energy levels separated by intervals

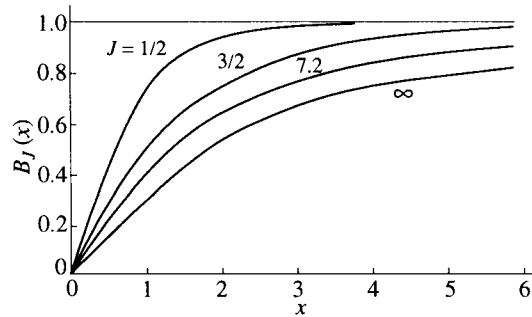
$$\delta\varepsilon = \gamma\hbar H. \quad (1.16)$$

Transitions between these levels, with absorption of electromagnetic energy quanta  $\hbar\omega$ , are called electron paramagnetic, or electron spin, resonance (e.g., [1, 15]). As the transitions only between the neighboring levels are allowed by the selection rules [15], the resonance condition is

$$\omega = \gamma H \equiv \frac{g|e_0|\hbar}{2m_e c} H \quad (1.17)$$

The difference in populations of the levels with different  $\{\hat{\mathfrak{M}}_z\}$  results in the appearance of the net moment in the direction of the field  $\mathbf{H}$ . The calculation, with the use of general formulae of quantum statistics [244], leads to the expression for the magnetization (the net moment per unit volume) [370, 24]

$$M = M^0 B_J \left( \frac{M^0 H}{N\kappa T} \right) \quad (1.18)$$



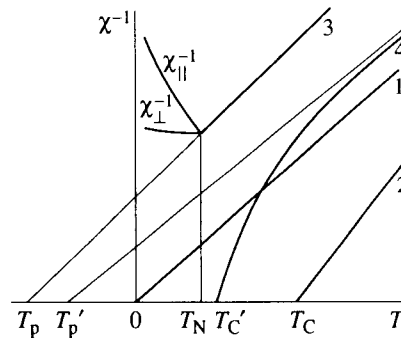
**FIGURE 1.1**  
Brillouin functions. Numbers by the curves indicate  $J$  values.

where  $B_J(x)$  is the Brillouin function

$$B_J(x) = \frac{2J+1}{2J} \coth\left(\frac{2J+1}{2J}x\right) - \frac{1}{2J} \coth\left(\frac{1}{2J}x\right) \quad (1.19)$$

$M^0 = \gamma\hbar JN$  is the saturation magnetization,  $N$  is the number of magnetic moments in a unit volume, and  $\kappa$  is the Boltzmann constant.

The plots of the Brillouin function (1.19) are shown in Figure 1.1. When  $x \rightarrow \infty$ , i.e., in very high magnetic fields or at very low temperatures,  $B_J(x) \rightarrow 1$ , and all magnetic moments are oriented in the direction of the field. For small  $x$ , expanding  $B_J(x)$  in a power series, we obtain from (1.18) that  $M = \chi_p H$ . The paramagnetic susceptibility  $\chi_p$ , which does not depend on  $H$  in this limiting case,



**FIGURE 1.2**  
Reciprocal of susceptibility versus temperature: curve 1 relates to paramagnet (Curie law), curve 2 to ferromagnet (Curie-Weiss law), curve 3 to antiferromagnet, curve 4 to ferrimagnet.

can be written as

$$\chi_p = \frac{C}{T} \quad (1.20)$$

where

$$C = \frac{1}{3} J(J+1) \frac{(\gamma \hbar)^2}{\kappa} N \quad (1.21)$$

is the Curie constant, and (1.20) is the *Curie law* (Figure 1.2).

### 1.1.3 Weiss theory

In ferromagnets large values of the magnetization, nearly equal to the saturation magnetization  $M^0$ , are observed at not very low temperatures and in not very high fields. The formal explanation of this fact was presented by Weiss as early as in 1907. He supposed that, in addition to the external field  $H$ , a high internal (he named it 'molecular') field

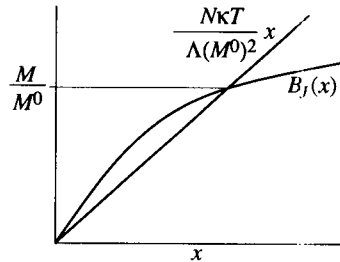
$$H_E = \Lambda M \quad (1.22)$$

acts on the magnetic moments of a ferromagnet. Here  $\Lambda$  is a large constant, the physical nature of which Weiss was not able to explain.

Substituting  $H + H_E$  for  $H$  in (1.17), we obtain

$$M = M^0 B_J \left[ \frac{M^0}{N \kappa T} (H + \Lambda M) \right]. \quad (1.23)$$

It should be noted that Weiss used the classical Langevin (see, e.g., [70]) theory of paramagnetism. We, following [70, 370], have replaced it by the above-mentioned Brillouin approach.



**FIGURE 1.3**

Graphical solution of equation (1.23) for spontaneous magnetization of a ferromagnet.

Solving the transcendental equation (1.23) for  $M$  in the most interesting case of  $H = 0$ , we see (Figure 1.3) that there is a nontrivial solution  $M \neq 0$  if  $T < T_C$  where

$$T_C = \Lambda C \quad (1.24)$$



and  $C$  is the Curie constant (1.21). The temperature  $T_C$  is the Curie point, and  $M$  is the spontaneous magnetization of a ferromagnet.

At  $T > T_C$  the spontaneous magnetization is equal to zero, and the argument of the Brillouin function becomes small. Then, using the expansion of  $B_J(x)$  in a power series, we obtain the susceptibility

$$\chi_f = \frac{C}{T - T_C}. \quad (1.25)$$

This is the *Curie–Weiss law* (Figure 1.2).

#### 1.1.4 Exchange interaction

The magnetic interaction of elementary magnetic moments cannot be the cause of magnetic ordering and hence of the spontaneous magnetization of a ferromagnet, at least not for common ferromagnets with not extremely low Curie temperatures. This follows from the comparison of the thermal energy  $\kappa T_C$ , which destroys the ferromagnetic order, with the energy of magnetic interaction of two magnetic dipoles. The former is of the order of  $10^{-15} - 10^{-13}$  (if  $T_C = 10 - 1000$  K), whereas the latter, according to (1.3) and (1.11), is of the order of  $\mu_B^2/a^3 \sim 10^{-18}$  (here  $a \sim 3 \times 10^{-8}$  is the mean distance between magnetic moments).

The energy  $e_0^2/a$  of the electrostatic (Coulomb) interaction of two electrons at the same distance  $a$  is of the order of  $10^{-11}$ . Thus, even a small fraction of this energy would be enough to give the observed values of  $T_C$ . It is known from quantum mechanics (e.g., [243, 336]) that the form of a wave function and, consequently, the mean energy of the Coulomb interaction of two electrons depend on the mutual orientation of their spins. The part of the Coulomb energy that depends on this orientation is called exchange energy. This energy is the cause of magnetic ordering. In ferromagnets it is minimized at parallel orientation of all electronic spin moments of 3d or 4f shells. Such was the explanation of the nature of ferromagnetism proposed in 1928 independently and almost simultaneously by Frenkel [130] and Heisenberg [178].

Dirac [101] showed that the energy operator (Hamiltonian) of the exchange interaction between two particles with spin angular momenta  $\hat{S}_1$  and  $\hat{S}_2$  can be written in the form

$$\hat{\mathcal{H}}_{\text{ex}} = -2I_{1,2}(r_{12})\hat{S}_1\hat{S}_2 \quad (1.26)$$

where  $I_{1,2}(r_{12})$  is the *exchange integral*. It decreases quickly with increasing distance  $r_{12}$  between the particles.

In many ferromagnets, as well as in antiferromagnetic and ferrimagnetic substances (Chapter 3), the interacting particles are situated at such large distances from each other that the above-considered exchange interaction (referred to as direct exchange interaction) cannot be responsible for magnetic ordering. Different mechanisms of indirect exchange interaction, in which some other particles take part, must be operating in such cases. In ionic crystals, the exchange interaction of

cation spins via the anions situated between them [18] is the dominant mechanism (Section 3.1). In metals (Section 14.2), the interaction via conduction electrons is of the greatest importance. In both these cases, the Hamiltonian can be approximated by the Dirac formula (1.26). The real mechanism of interaction determines the value of the exchange integral and its dependence on  $r_{12}$ .

A system of spin magnetic moments, localized on crystal-lattice sites and interacting with each other according to the Hamiltonian (1.26), is the Heisenberg–Dirac–Van Vleck model (often referred to, briefly, as *Heisenberg model*) of a magnetically ordered substance, in particular, of a ferromagnet if the exchange integral in (1.26)  $I_{1,2} > 0$ . To generalize this model we have to take into consideration the weaker interactions: the magnetic (dipole–dipole) interaction of spin magnetic moments and the Zeeman interaction with the external magnetic field (Section 7.4).

Two important assumptions are made in the Heisenberg model: (i) the spin magnetic moments are assumed to be completely localized, and (ii) orbital magnetic moments are ignored. The first assumption is satisfied for magnetically ordered dielectrics and semiconductors. It is poorly satisfied for metals; the zone model (e.g., [445]) should be used in this case.

The second assumption is satisfied perfectly for ferromagnets with ions in S state, and the stronger the quenching of orbital momenta (if they are present) the better. When the quenching is sufficiently strong, the weak (but still important) influence of orbital moments can be taken into account in the framework of the generalized Heisenberg model. It is assumed, first, that the value of  $\gamma$  in the Zeeman term of the Hamiltonian (Section 7.4) differs from the spin value  $\gamma_S$  given by (1.9). Second, a term describing the magnetocrystalline anisotropy (the main cause of which is the spin–orbital interaction, Section 2.2) is added into the Hamiltonian.

In magnetically ordered substances with 4f (rare-earth) ions, the quenching of orbital angular momenta does not take place, and the spin–orbital interaction, which combines spin and orbital angular momenta in total angular momenta  $\hat{J}$ , is strong. Nevertheless, the Heisenberg model may be used for such substances, but the total angular momenta  $\hat{J}$  must be substituted for spin angular momenta  $\hat{S}$ .

Some other topics of the theory of magnetism will be considered below when the need for them arises.

## 1.2 Equation of motion of magnetization

To describe some phenomena in ferromagnets, in particular, the dynamical processes we are interested in, the *continuum* approach can be used. Applying it, we

digress from the microscopic picture of the ferromagnet and use the magnetization

$$\mathbf{M} = \frac{\sum_{\Delta V} \mathfrak{M}}{\Delta V} \quad (1.27)$$

as a quantity characteristic of its state ( $\sum_{\Delta V} \mathfrak{M}$  is the magnetic moment of a small but macroscopic volume  $\Delta V$ ). Vector  $\mathbf{M}$  is just the quantity that enters the equations of macroscopic electrodynamics (Chapter 4).

The continuum approach allows one to use the *classical* theory. Exchange interaction, which is a quantum-mechanical effect, must be postulated now. If the magnetization  $\mathbf{M}$  is uniform or changes in space slowly, the Weiss ‘molecular’ field (1.22) is sufficient to allow for this interaction. In the case of strong coordinate dependence of  $\mathbf{M}$ , an additional field is to be used, which describes the increase of the exchange energy when the neighboring spin moments are not parallel to each other (Section 7.1).

In the classical treatment of dynamic processes in a ferromagnet, the equations of macroscopic electrodynamics should be supplemented by the material relations (Section 4.1), which express the dependence, in our case, of the magnetization  $\mathbf{M}$  on the magnetic field  $\mathbf{H}$  for the particular substance. The equation of motion of the magnetization can be used as such a relation. In the framework of a classical theory this equation is to be postulated.

The equation of motion of magnetization was proposed by Landau and Lifshitz [241] in 1935. We shall consider this equation, in a general form, in Section 2.1. Now we present a classical ‘derivation’ of it (which cannot be strict, of course) for a special case of uniform oscillations of magnetization in an isotropic ferromagnet.

Suppose the ferromagnet to be a sum of classical tops (the nonstrictness consists just of this assumption) with angular momenta  $\mathbf{J}$  and magnetic moments  $\mathfrak{M}$ . The equation of motion of the top, according to (1.2), can be written as [399]

$$\hbar \frac{\partial \mathbf{J}}{\partial t} = \mathfrak{M} \times \mathbf{H}. \quad (1.28)$$

It has been taken into account that  $\mathbf{J}$  is expressed in units of  $\hbar$  and  $\mathfrak{M}$ , in absolute units. Multiplying (1.28) by the number  $N$  of tops in a unit volume and using the general quantum-mechanical relation (1.10), we obtain the equation of motion of the magnetization

$$\frac{\partial \mathbf{M}}{\partial t} = -\gamma \mathbf{M} \times \mathbf{H}. \quad (1.29)$$

This equation does not allow for ‘losses’, i.e., for the dissipation of magnetic energy. The ways of phenomenological allowance for it are considered in Section 1.4, and the physical processes that result in it will be discussed in Chapters 11 and 13.

In deducing (1.29) we have ignored the exchange interaction. But it is easy to see that the ‘molecular’ field (1.22) does not enter (1.29). The above-mentioned additional exchange field (that arises when  $\mathbf{M}$  is nonuniform) will enter the equation

of motion (Section 7.1). Thus, (1.29) is valid strictly for uniform magnetization and approximately, if  $\mathbf{M}$  varies in space sufficiently slowly.

The quantity  $\gamma$  in (1.29), being a characteristic of the collective motion of magnetic moments, should not be and is not equal to the value of  $\gamma$  for the same ions either in the free state or in a paramagnetic crystal. In the framework of classical theory,  $\gamma$  is to be regarded as a parameter the value of which must be found from experiment. It is clear, however, that the difference between an actual value of  $\gamma$  and its spin value (1.8) is due to the influence of the orbital magnetic moments. Indeed, the  $g$ -factor (related to  $\gamma$  by (1.10)) is very near to its spin value of 2 in materials in which all the magnetic ions are in S state, for example, in yttrium iron garnet (YIG)  $\text{Y}_3\text{Fe}_5\text{O}_{12}$  [138] and in lithium ferrite  $\text{Li}_{0.5}\text{Fe}_{2.5}\text{O}_4$  [297].

It is worth noting that the influence of orbital moments results in  $g$  values, found from gyromagnetic (Barnett or Einstein–De Haas) experiments (e.g., [70]) which are less than 2. At the same time, this influence leads to the values of  $g$ -factor in (1.29) that are greater than 2. The difference was explained by Kittel [227] and Van Vleck [418]. They took into consideration that  $\gamma$  in (1.29) is the ratio of the total magnetic moment to the spin angular momentum, whereas  $\gamma$  in the mentioned gyromagnetic experiments is the ratio of the same total magnetic moment but to the total angular momentum.

An important feature of the equation of motion (1.29) is that it ensures the conservation of the vector  $\mathbf{M}$  length. Indeed, multiplying both sides of (1.29) by  $\mathbf{M}$  scalarly, we get

$$\frac{\partial}{\partial t} M^2 = 0 \quad (1.30)$$

If we regard  $\mathbf{M}$  as a vector with one end fastened, the other end, according to (1.30), will move on the surface of a sphere. Such movement is called *precession* of the magnetization. In the case of cylindrical symmetry, the end of the vector  $\mathbf{M}$  moves along a circle (circular precession). In other cases, its trajectory is more complicated.

---

### 1.3 High-frequency magnetic susceptibility

Let us consider the oscillations of magnetization at some point of a ferromagnet under the influence of a given internal ac magnetic field at the same point. Having solved this problem, we shall find the high-frequency magnetic susceptibility of a ferromagnet.

We take the magnetic field and magnetization in (1.29) to be the sums of steady and alternating parts:

$$\mathbf{H} = \mathbf{H}_0 + \mathbf{h}_{\sim} \quad \mathbf{M} = \mathbf{M}_0 + \mathbf{m}_{\sim} \quad (1.31)$$

and assume that

$$h_{\sim} \ll H_0 \quad m \ll M_0. \quad (1.32)$$

This assumption will be retained in all first eight chapters.

Substitute the sums (1.31) into (1.29) and, allowing for conditions (1.32), use the method of successive approximations. In the zero approximation, retaining in (1.29) only steady components, we obtain

$$\mathbf{M}_0 \times \mathbf{H}_0 = 0. \quad (1.33)$$

This expression determines the *equilibrium direction* of the magnetization. In the considered case of an isotropic ferromagnet this direction coincides with the direction of the internal magnetic field  $\mathbf{H}_0$ . The length of the vector  $\mathbf{M}_0$  is, of course, not determined by (1.33), and, in the framework of considered theory, should be regarded as known quantity.

In the first approximation, neglecting the products of ac quantities and taking into account (1.33), we obtain

$$\frac{\partial \mathbf{m}_{\sim}}{\partial t} + \gamma \mathbf{m}_{\sim} \times \mathbf{H}_0 = -\gamma \mathbf{M}_0 \times \mathbf{h}_{\sim}. \quad (1.34)$$

The derivation of this equation is called *linearization* of the equation of motion.

### 1.3.1 Solution of the linearized equation of motion

We shall solve (1.34) assuming the *harmonic* (sinusoidal) time dependence of  $\mathbf{h}_{\sim}$ . As the equation is linear, the time dependence of  $\mathbf{m}_{\sim}$  will be also harmonic. Using the method of complex amplitudes (e.g., [321]), we introduce complex variables

$$\dot{\mathbf{m}} = \mathbf{m} \exp(i\omega t) \quad \dot{\mathbf{h}} = \mathbf{h} \exp(i\omega t) \quad (1.35)$$

the real parts of which are  $\mathbf{m}_{\sim}$  and  $\mathbf{h}_{\sim}$ . The complex vector quantities  $\mathbf{m}$  and  $\mathbf{h}$  in (1.35) are the *complex amplitudes* of the vectors  $\mathbf{m}_{\sim}$  and  $\mathbf{h}_{\sim}$ . They satisfy the equation

$$i\omega \mathbf{m} + \gamma \mathbf{m} \times \mathbf{H}_0 = -\gamma \mathbf{M}_0 \times \mathbf{h}. \quad (1.36)$$

Projecting (1.36) onto the axes of a Cartesian coordinate system, with the  $z$ -axis coinciding with the direction of  $\mathbf{H}_0$  and  $\mathbf{M}_0$ , we get

$$\begin{aligned} i\omega m_x + \gamma H_0 m_y &= \gamma M_0 h_y \\ -\gamma H_0 m_x + i\omega m_y &= -\gamma M_0 h_x \\ i\omega m_z &= 0. \end{aligned} \quad (1.37)$$

The solution of the system (1.37) is

$$m_x = \chi h_x + i\chi_a h_y \quad m_y = -i\chi_a h_x + \chi h_y \quad m_z = 0 \quad (1.38)$$

$$\chi = \frac{\gamma M_0 \omega_H}{\omega_H^2 - \omega^2} \quad \chi_a = \frac{\gamma M_0 \omega}{\omega_H^2 - \omega^2} \quad (1.39)$$

where the following notation is used:

$$\omega_H = \gamma H_0. \quad (1.40)$$

Expressions (1.38) and (1.39) were obtained first by Polder [319]. They can be written in a tensor form

$$\mathbf{m} = \vec{\chi} \mathbf{h} \quad (1.41)$$

where the high-frequency magnetic susceptibility  $\vec{\chi}$  is a nonsymmetric second-rank tensor (e.g., [273]):

$$\vec{\chi} = \begin{vmatrix} \chi & i\chi_a & 0 \\ -i\chi_a & \chi & 0 \\ 0 & 0 & 0 \end{vmatrix}. \quad (1.42)$$

The solution (1.38) can be written, as well, in a vector form

$$\mathbf{m} = \chi \mathbf{h}_\perp + i \mathbf{h}_\perp \times \mathbf{G}_m \quad (1.43)$$

where  $\mathbf{h}_\perp = x_0 h_x + y_0 h_y \equiv \mathbf{h} - z_0 h_z$  and

$$\mathbf{G}_m = z_0 \chi_a \quad (1.44)$$

is the magnetic gyration vector ( $x_0$ ,  $y_0$ , and  $z_0$  are the unit vectors directed along the corresponding axes).

### 1.3.2 Peculiarities of the susceptibility tensor

In the considered case of an isotropic and lossless ferromagnet, magnetized to saturation, the longitudinal component of the ac field does not produce the ac magnetization. The transverse ac field  $\mathbf{h}_\perp$  excites not only the magnetization component parallel to the field, but also a component that is perpendicular to it. The latter, according to the factors  $i$  in (1.38) or (1.42), has a phase shift of  $\pi/2$  with respect to  $\mathbf{h}_\perp$ . Such property of a medium, caused by nonsymmetry of the susceptibility tensor, is called *gyrotropy*. It should be noted that there exist media in which the electric susceptibility in the presence of a steady magnetic field becomes a nonsymmetric tensor. All substances containing magnetic ions (i.e., ions with partly filled 3d or 4f shells), in particular, ferromagnets, belong to such media. Their electric gyrotropy results in Faraday and Kerr effects at optical frequencies [246]. In our case the *magnetic* susceptibility tensor contains antisymmetric components and hence the gyrotropy may be called magnetic. In ferromagnets it dominates at microwave and far infrared frequencies.

Thus, the *nonsymmetry* of the magnetic susceptibility tensor is the first peculiarity of the obtained solution of the equation of motion. The second one is the

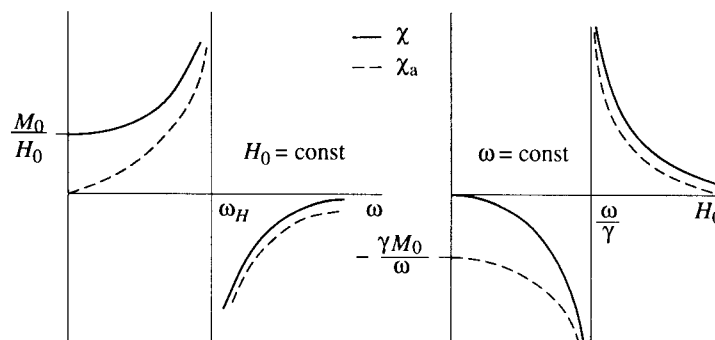


FIGURE 1.4

Dependence of the susceptibility-tensor components on frequency  $\omega$  ( $H_0 = \text{const}$ ) and steady magnetic field  $H_0$  ( $\omega = \text{const}$ ).

*resonant dependence* of the components of this tensor on frequency  $\omega$  and magnetic field  $H_0$ . In the idealized case of a lossless ferromagnet, considered in this section, these components grow unlimitedly when  $\omega$  or  $H_0$  approaches the pole

$$\omega = \omega_H \equiv \gamma H_0. \quad (1.45)$$

The dependence of  $\chi$  and  $\chi_a$  on  $\omega$  and  $H_0$  is shown in Figure 1.4.

The resonant dependence of the tensor  $\vec{\chi}$  components results in the phenomenon of *ferromagnetic resonance*, i.e., of the resonant absorption of electromagnetic energy in a ferromagnetic sample. This phenomenon was predicted as early as in 1912 by Arkadyev [22] on a classical model. In 1923 Dorfman [102] pointed out the possibility of it on a quantum model, but without allowance for spin (or exchange) nature of ferromagnetism because the electron spin was discovered only in 1925 and the nature of ferromagnetism was explained in 1928. The first theory of ferromagnetic resonance based on the correct understanding of ferromagnetism was proposed by Landau and Lifshitz in 1935 [241]. Experimentally, ferromagnetic resonance was discovered in 1946 by Griffiths [149] and, independently but somewhat later, by Zavoiskii [461].

An important contribution to the theory of ferromagnetic resonance was made by Kittel [220]. He showed that the ferromagnetic-resonance frequency (i.e., the frequency at which the maximal absorption of electromagnetic energy by a ferromagnetic sample occurs) is not at all the frequency (1.45), and it depends essentially on the sample shape. This dependence will be treated in Section 1.5.

The third peculiarity of the solution of the equation of motion (1.36), i.e., of the ac magnetization in a ferromagnet, is that the resonant behavior of the oscillation amplitudes occurs only under the influence of an ac magnetic field *circular* component with *right-hand rotation* (relative to the direction of  $M_0$ ).

The circular components of ac field and ac magnetization are defined as

$$h_{\pm} = h_x \pm ih_y \quad m_{\pm} = m_x \pm im_y. \quad (1.46)$$

If the complex amplitude of a vector, e.g.,  $\mathbf{m}_{\sim}$  has only a component  $m_+$ , then it is a transverse vector (relative to the  $z$ -axis) circularly polarized with right-hand rotation. Indeed, from  $m_- = 0$  it follows that  $m_y = -im_x$ . Let the  $x$  component of the real vector  $\mathbf{m}_{\sim}$  (the complex amplitude of which is  $m$ ) have the form  $m_{\sim x} = m_0 \cos \omega t$ . Then  $m_{\sim y} = \text{Re}[-im_0 \exp(i\omega t)] = m_0 \sin \omega t$ . These expressions for  $m_{\sim x}$  and  $m_{\sim y}$  mean that the transverse vector  $\mathbf{m}_{\sim}$  rotates in the  $xy$  plane, taking the shortest way from the positive semiaxis  $x$  to the positive semiaxis  $y$ . This is just the definition of the vector  $\mathbf{m}_{\sim}$  circular polarization with the right-hand direction of rotation relative to the  $z$ -axis. (This definition is equivalent to the following: the tip of the vector is moving as the head of a right-hand screw that shifts in a given direction.) It can be shown in the same manner that, if there is only the component  $m_-$ , i.e.,  $m_y = im_x$ , then the vector  $\mathbf{m}_{\sim}$  is circularly polarized with the left-hand rotation.

Thus, the relations between the complex amplitudes

$$m_y = \mp im_x \quad (1.47)$$

correspond to circular polarization of the real vector with the right-hand (upper sign) or left-hand (lower sign) rotation.

From (1.46), (1.38), and (1.39) it follows that

$$m_{\pm} = \chi_{\pm} h_{\pm} \quad (1.48)$$

where

$$\chi_{\pm} = \chi \pm \chi_a = \frac{\gamma M_0}{\omega_H \mp \omega}. \quad (1.49)$$

So, the component  $h_+$  produces only  $m_+$ , and  $h_-$  produces only  $m_-$ . In other words, in the variables  $h_+$ ,  $h_-$ ,  $h_z$  and  $m_+$ ,  $m_-$ ,  $m_z$  the susceptibility tensor becomes *diagonal*, with components  $\chi_+$ ,  $\chi_-$ , and  $\chi_z = 0$ . It is seen from (1.48) and (1.49) that only the magnetization component  $m_+$ , which is excited by the field component  $h_+$ , depends in a resonant manner on  $\omega$  or  $H_0$ .

### 1.3.3 High-frequency permeability

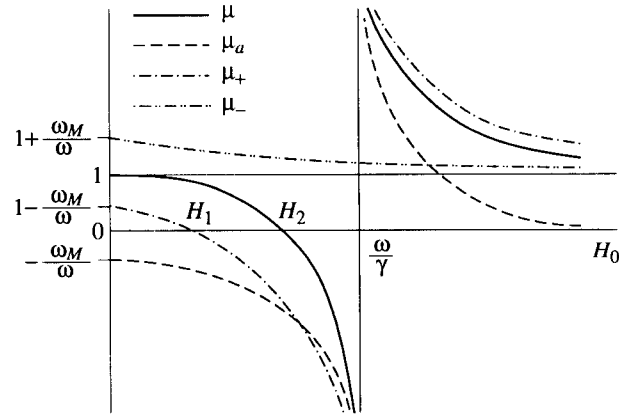
The complex amplitude of ac magnetic induction is

$$\mathbf{b} = \mathbf{h} + 4\pi\mathbf{m}. \quad (1.50)$$

Substituting (1.41) into (1.50), we get

$$\mathbf{b} = \vec{\mu} \mathbf{h} \quad (1.51)$$





**FIGURE 1.5**  
Permeability-tensor components versus magnetic field.

where the high-frequency permeability tensor

$$\vec{\mu} = \vec{I} + 4\pi\vec{\chi}. \quad (1.52)$$

Here  $\vec{I}$  is a unit tensor, i.e., a diagonal tensor with all nonzero components equal to unity.<sup>2</sup>

Taking into account (1.42) and (1.39), we find

$$\vec{\mu} = \begin{vmatrix} \mu & i\mu_a & 0 \\ -i\mu_a & \mu & 0 \\ 0 & 0 & 1 \end{vmatrix} \quad (1.53)$$

where

$$\mu = 1 + 4\pi\chi = \frac{\omega_H(\omega_H + \omega_M) - \omega^2}{\omega_H^2 - \omega^2} \quad \mu_a = 4\pi\chi_a = \frac{\omega\omega_M}{\omega_H^2 - \omega^2}. \quad (1.54)$$

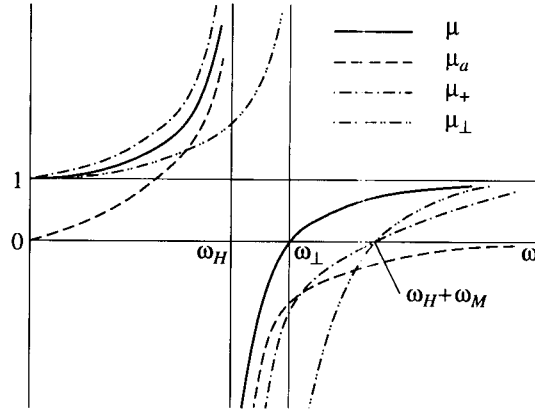
Here we have used the notation

$$\omega_M = \gamma 4\pi M_0. \quad (1.55)$$

The dependence of  $\mu$  and  $\mu_a$  on  $H_0$  is shown in Figure 1.5. One can see that the diagonal component  $\mu$  is negative in the magnetic-field interval from  $H_2$  to the resonance field  $\omega/\gamma$ . The *antiresonance* field, at which  $\mu = 0$ , is

$$H_2 = \sqrt{\left(\frac{\omega}{\gamma}\right)^2 + (2\pi M_0)^2} - 2\pi M_0. \quad (1.56)$$

<sup>2</sup>In what follows we shall write 1 instead of  $\vec{I}$ .



**FIGURE 1.6**  
Permeability-tensor components and effective permeabilities versus frequency.

The condition of antiresonance ( $H_0 = H_2$ ) can be written also as  $\omega = \omega_{\perp}$  where

$$\omega_{\perp} = \sqrt{\omega_H(\omega_H + \omega_M)}. \quad (1.57)$$

The circular components of the tensor  $\vec{\mu}$ , relating the circular components of  $\mathbf{m}$  to such components of  $\mathbf{h}$ , as it is easy to make sure, are

$$\mu_{\pm} = 1 + 4\pi\chi_{\pm} = \mu + \mu_a = \frac{\omega_H + \omega_M \mp \omega}{\omega_H \mp \omega}. \quad (1.58)$$

Only  $\mu_+$  has a pole at  $\omega = \omega_H$ . This component becomes equal to zero at  $H_0 = H_1$  where

$$H_1 = \frac{\omega}{\gamma} - 4\pi M_0. \quad (1.59)$$

The frequency dependence of different tensor  $\vec{\mu}$  components is shown in Figure 1.6. The frequency dependence of

$$\mu_{\perp} \equiv \mu - \frac{\mu_a^2}{\mu} = \frac{(\omega_H + \omega_M)^2 - \omega^2}{\omega_{\perp}^2 - \omega^2} \quad (1.60)$$

is also plotted. This quantity is an effective permeability for one of the electromagnetic waves propagating in a ferromagnetic medium in the direction perpendicular to  $\mathbf{M}_0$  (Section 4.2). It should be noted that the circular components  $\mu_+$  and  $\mu_-$  are the effective permeabilities for two waves propagating in the direction of  $\mathbf{M}_0$ .

## 1.4 Allowance for magnetic losses

The oscillations of magnetization are inevitably accompanied by *dissipation* of their energy, which is transformed into other kinds of energy, mainly, into the thermal energy. Various physical processes that lead to the dissipation will be treated in Chapter 11 and subsequent chapters. The purpose of this section is to discuss the ways of formal, phenomenological allowance for the dissipation of energy of magnetization oscillations.

### 1.4.1 Dissipative terms and dissipation parameters

The simplest way to take dissipation into account is to correct the final expressions of the tensor  $\overleftrightarrow{\chi}$  components. It is sufficient, e.g., to replace the real frequency  $\omega$  in (1.39) by the complex quantity  $\omega' + i\omega''$ . This will result in the appearance of the imaginary parts of  $\chi$  and  $\chi_a$  leading to the absorption of electromagnetic energy (Section 4.4).

However, it is better to change in a proper way the *equation of motion* of the magnetization (1.29). A comparatively small term, leading to dissipation, should be added into the right-hand side of this equation. This is the method used by *Landau and Lifshitz* [241]; the proposed equation can be written as

$$\frac{\partial \mathbf{M}}{\partial t} = -\gamma \mathbf{M} \times \mathbf{H} - \frac{\gamma \lambda}{M^2} \mathbf{M} \times (\mathbf{M} \times \mathbf{H}) \quad (1.61)$$

where  $\lambda$  is a dissipation parameter with the dimensionality of magnetic field.<sup>3</sup>

If we replace  $\mathbf{M} \times \mathbf{H}$  in the dissipative term of (1.61) by  $(-\gamma^{-1} \partial \mathbf{M} / \partial t)$  (using the equation of motion without dissipation) and introduce a dimensionless parameter  $\alpha = \lambda / M$ , we obtain the equation of motion proposed by *Gilbert*:

$$\frac{\partial \mathbf{M}}{\partial t} = -\gamma \mathbf{M} \times \mathbf{H} + \frac{\alpha}{M} \mathbf{M} \times \frac{\partial \mathbf{M}}{\partial t}. \quad (1.62)$$

The dissipative term in this equation can be written supposing, simply, that an effective field of ‘friction’, proportional to the rate of the change of  $\mathbf{M}$ , is acting on  $\mathbf{M}$ . It is easy to show that the substitution

$$\gamma \rightarrow \frac{\gamma}{1 + \alpha^2} \quad \lambda \rightarrow \frac{\alpha M}{1 + \alpha^2} \quad (1.63)$$

transforms (1.61) into (1.62) *exactly*.

Both equations (1.61) and (1.62) ensure the condition (1.30) for the conservation of the vector  $\mathbf{M}$  length. We shall see in Chapter 11 that the length of  $\mathbf{M}$  is conserved in some dissipation processes and is not conserved in others. Equations

<sup>3</sup>In some later papers the quantity  $\lambda_1 = \gamma \lambda$  (with the dimensionality of frequency) was named ‘the Landau–Lifshitz dissipation parameter’.

tions (1.61) and (1.62) do not hold, strictly speaking (but, nevertheless, are often used), in the presence of the processes of the second type.

An example of equations of motion that allow the change of the vector  $\mathbf{M}$  length is the *modified Bloch* equation, or Bloch–Bloembergen equation (e.g., [366]):

$$\frac{\partial \mathbf{M}}{\partial t} = -\gamma \mathbf{M} \times \mathbf{H} - \omega_r \left( \mathbf{M} - \frac{M_0}{H_0} \mathbf{H} \right) \quad (1.64)$$

where  $\omega_r$  is the relaxation frequency. The dissipative term in (1.64) is proportional to the difference between the instantaneous magnetization  $\mathbf{M}$  and the magnetization that would be if the instantaneous field  $\mathbf{H}$  were ‘frozen’.

Equations (1.61), (1.62), and (1.64) differ, first, in the form of the dissipative term and, second, in the dimensionality of the dissipation parameter. The latter difference is due to tradition only; in each of these equations it is possible to use a dissipation parameter with any dimensionality.

Equations of motion with more than one dissipation parameter have also been proposed. In particular, the Bloch equation [53] with two relaxation times, which is commonly used for paramagnetic resonance (e.g., [15]), has been applied to ferromagnetic resonance, too. However, the processes of energy dissipation in ferromagnets, being numerous and complicated, cannot be described strictly by an equation of motion either with one or with two dissipation parameters. For an approximate treatment, especially in the case of small losses, each of the above-discussed equations can be used.

Consider now the linearization of equation of motion in the presence of losses. Using, as in Section 1.3, the method of successive approximations, we make sure, first of all, that the condition for equilibrium (1.33) has not changed. Then we obtain from (1.61) the linearized equation for the complex amplitudes of the ac quantities

$$i\omega \mathbf{m} + \gamma \mathbf{m} \times \mathbf{H}_0 + \gamma \lambda \frac{H_0}{M_0} \mathbf{m} = -\gamma \mathbf{M}_0 \times \mathbf{h} + \gamma \lambda \mathbf{h}. \quad (1.65)$$

Linearization of (1.62) yields

$$i\omega \mathbf{m} + \gamma \mathbf{m} \times \mathbf{H}_0 + \frac{i\alpha\omega}{M_0} \mathbf{m} \times \mathbf{M}_0 = -\gamma \mathbf{M}_0 \times \mathbf{h}. \quad (1.66)$$

The linearized equation, obtained from (1.64), coincides with (1.65) when  $\omega_r = \gamma \lambda H_0 / M_0$ .

If the losses are small, the second term in the right-hand side of (1.65) can be neglected, and the second expression in (1.63) transforms into  $\lambda \rightarrow \alpha M$ . Thus, in the case of *small amplitudes* (linear approximation) and, simultaneously, *small losses*, all three considered equations of motion are equivalent, and the following relations hold for the dissipation parameters in these equations:

$$\alpha = \frac{\lambda}{M_0} = \frac{\omega_r}{\omega_H}. \quad (1.67)$$

### 1.4.2 Susceptibility tensor components

To find the tensor  $\vec{\chi}$  components in the presence of losses, we have to project the linearized equation (1.65) or (1.66) onto coordinate axes and solve the obtained set of linear equations. But this is not necessary for equation (1.66) because (1.36), with allowance for (1.33), transforms into (1.66) after the replacement

$$\omega_H \rightarrow \omega_H + i\alpha\omega. \quad (1.68)$$

Thus, we can make this replacement in the final expressions (1.39). Then, taking  $\chi = \chi' - i\chi''$  and  $\chi_a = \chi'_a - i\chi''_a$ , we get

$$\begin{aligned} \chi' &= \frac{1}{D} \gamma M_0 \omega_H [\omega_H^2 - (1 - \alpha^2)\omega^2] \\ \chi'' &= \frac{1}{D} \alpha \gamma M_0 \omega [\omega_H^2 + (1 + \alpha^2)\omega^2] \\ \chi'_a &= \frac{1}{D} \gamma M_0 \omega [\omega_H^2 - (1 + \alpha^2)\omega^2] \\ \chi''_a &= 2\alpha \gamma M_0 \omega^2 \omega_H \\ D &= [\omega_H^2 - (1 + \alpha^2)\omega^2]^2 + 4\alpha^2 \omega^2 \omega_H^2. \end{aligned} \quad (1.69)$$

The dependence of real and imaginary parts of the tensor  $\vec{\chi}$  components on  $H_0$  is shown in Figure 1.7. The real parts, as should be expected, change their sign, and the imaginary parts pass through maxima at resonance. The resonance condition is given now by

$$\omega = \frac{\omega_H}{1 + \alpha^2}. \quad (1.70)$$

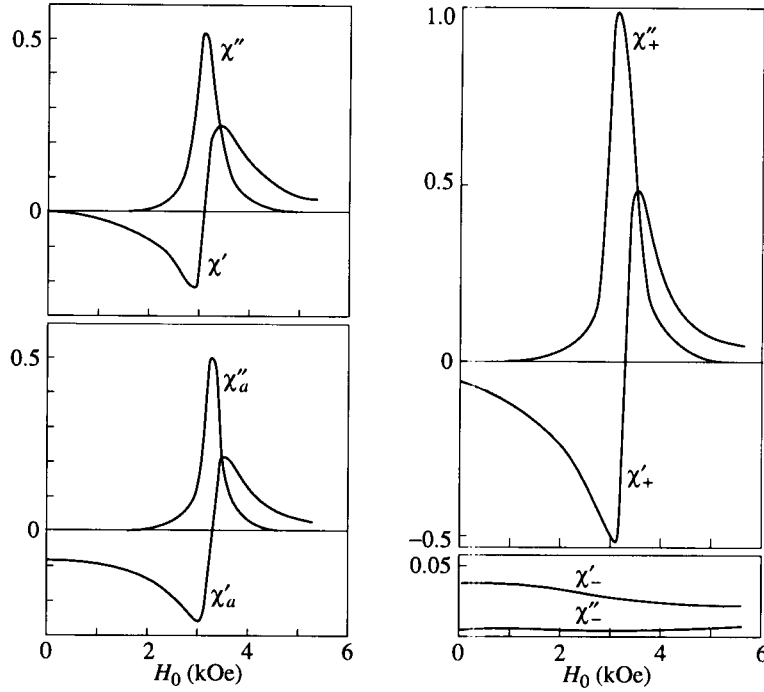
At resonance

$$\begin{aligned} \chi'_{\text{res}} &= \frac{\gamma M_0}{2\omega_H} & \chi''_{\text{res}} &= \frac{\gamma M_0}{2\alpha\omega} \\ \chi'_{a \text{ res}} &= 0 & \chi''_{a \text{ res}} &= \frac{\gamma M_0}{2\alpha\omega_H} \approx \chi''_{\text{res}}. \end{aligned} \quad (1.71)$$

It follows from (1.71) that the *smaller* the dissipation parameter, the greater the absorption of electromagnetic energy by a ferromagnet (Section 4.4) *at resonance*. On the contrary, the absorption of energy *far from resonance* is greater the *greater* the dissipation parameter, as can easily be shown using (1.69).

Solution of equation (1.65) gives the tensor

$$\vec{\chi} = \begin{vmatrix} \chi & i\chi_a & 0 \\ -i\chi_a & \chi & 0 \\ 0 & 0 & \chi_{\parallel} \end{vmatrix} \quad (1.72)$$



**FIGURE 1.7**

Real and imaginary parts of tensor  $\vec{\chi}$  components vs  $H_0$  calculated using (1.69) with  $M_0 = 160$  G,  $f = 9.4$  GHz, and  $\alpha = 0.025$ .

with a nonzero, but small (in the case of small losses) longitudinal component

$$\chi_{\parallel} = \frac{i\gamma\lambda}{\omega - i\lambda\omega_H/M_0}. \quad (1.73)$$

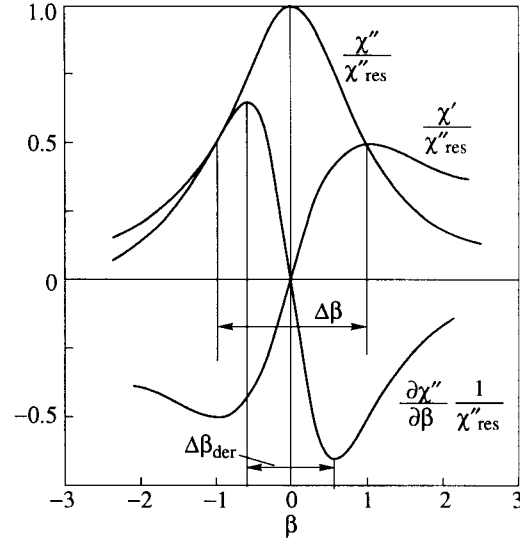
The transverse components of the tensor (1.72) coincide approximately in this case with (1.69) after the substitution of  $\alpha M_0$  for  $\lambda$ .

At frequencies or fields near resonance, expressions (1.69) can be approximated by

$$\frac{\chi'}{\chi'_{\text{res}}} \approx \frac{\chi'_a}{\chi'_{\text{res}}} \approx \frac{\beta}{1 + \beta^2} \quad \frac{\chi''}{\chi''_{\text{res}}} \approx \frac{\chi''_a}{\chi''_{\text{res}}} \approx \frac{1}{1 + \beta^2} \quad (1.74)$$

where  $\beta = (\omega - \omega_H)/(\alpha\omega_H)$  if  $H_0 = \text{const}$ , or  $\beta = (H_0 - \omega/\gamma)/(\alpha\omega)$  if  $\omega = \text{const}$ . Expressions (1.74) represent the *Lorentz resonance curves* (Figure 1.8). The widths of them, defined as the intervals between  $\omega$  or  $H_0$  values at points where  $\chi'' = \chi''_{\text{res}}/2$ , are

$$\Delta\omega = 2\alpha\omega \quad \Delta H = \frac{2\alpha\omega}{\gamma}. \quad (1.75)$$



**FIGURE 1.8**  
Lorentz resonance curves.

In experiments, the derivative  $\partial\chi''/\partial\beta$  is often measured (usually, varying  $H_0$  at  $\omega = \text{const}$ ), and the linewidth  $\Delta H_{\text{der}}$  is defined as the interval between the extrema of this derivative (Figure 1.8). It is easy to make sure that

$$\Delta H_{\text{der}} = \frac{1}{\sqrt{3}} \Delta H. \quad (1.76)$$

It follows from (1.71) and (1.75) that for a Lorentz resonance curve

$$\Delta H \chi''_{\text{res}} = M_0. \quad (1.77)$$

It can be shown that this important relation is valid approximately for the actual resonance curves determined by the expressions (1.69).

Assuming  $\alpha$  to be constant, and integrating  $\chi''$  and  $\chi''_a$  given by (1.69), we get

$$\int_0^\infty \chi'' dH_0 \approx \int_0^\infty \chi''_a dH_0 \approx \frac{1}{\gamma} \int_0^\infty \chi'' d\omega \approx \frac{1}{\gamma} \int_0^\infty \chi''_a d\omega = CM_0 \quad (1.78)$$

where  $C$  is a dimensionless constant factor of the order of 1. For the Lorentz curve  $C = \pi/2$ . Note that (1.78) remains valid in the limit of  $\alpha \rightarrow 0$ . Hence, it follows that

$$\lim_{\alpha \rightarrow 0} \chi''_{\text{res}} = \lim_{\alpha \rightarrow 0} \chi''_{a \text{ res}} = CM_0 \delta \left( H_0 - \frac{\omega}{\gamma} \right) \quad (1.79)$$

where  $\delta(x)$  is the Dirac delta function (Appendix C).

The circular components of the susceptibility tensor in the presence of losses are

$$\chi_{\pm} = \chi \pm \chi_a = \frac{\gamma M_0}{\omega_H \mp \omega + i\alpha\omega}. \quad (1.80)$$

The quantities  $\chi'_+$  and  $\chi''_+$  behave near resonance (Figure 1.7) similar to the real and imaginary parts of  $\chi$  and  $\chi_a$ , but the values of  $\chi'_+$  and  $\chi''_+$  are twice as large. The values of  $\chi'_-$  and  $\chi''_-$  remain small at any  $\omega$  and  $H_0$ .

The tensor  $\vec{\mu}$  components in the presence of losses are easily obtained using (1.69) or applying (1.68) directly to (1.54), and we shall not cite them. We note only that the antiresonance point can be defined now as a point at which  $\mu' = 0$ , the value of  $\mu''$  being small. In the case of small losses the condition for antiresonance differs only slightly from (1.56), and

$$\mu''_{\text{antires}} \approx \frac{2\alpha\omega}{\omega_M} \left( 1 + \frac{\omega_M}{2\omega_H} \right) \quad (1.81)$$

where  $\omega_M$  is determined by (1.55).

In ferromagnetic and ferrimagnetic (Section 3.3) substances the  $\vec{\mu}$  components reach very high values at resonance. For example, in YIG perfect single crystals at frequency of 9 GHz, the dissipation parameter  $\alpha \sim 5 \times 10^{-5}$  and  $\mu''_{\text{res}} \sim 6000$ .

It is worth noting that different dissipation parameters depend differently on  $\omega$ ,  $H_0$ , and  $M_0$ , as well as on temperature. In choosing a parameter to use, preference should be given to one the variation of which, in certain ranges of  $\omega$ ,  $H_0$ , etc., is the least.

## 1.5 Uniform oscillations in a small ellipsoid

In the preceding sections the ac magnetization at a certain point of a ferromagnet was calculated, regarding the magnetic field *at the same point* as given. However, this field cannot be, usually, regarded as given but depends on magnetization distribution in the entire system. Only such quantities as the power flux of the incident electromagnetic wave at the input of the system can be regarded as given. The field and magnetization distribution over the system can be found by solving the boundary problem, with the use of Maxwell's equations and appropriate boundary conditions. The expressions for magnetic susceptibility  $\vec{\chi}$ , obtained in the preceding section, are to be used as material relations (Section 4.1) in such computations. Some of these boundary problems will be considered in Chapters 5 and 6. But the simplest of them, the problem of uniform oscillations of magnetization in a small ferromagnetic ellipsoid, is to be considered now. Having solved it, we shall be able to interpret the results of numerous experiments on ferromagnetic resonance in ferrites, which are usually carried out on small samples, mostly, on spheres.



### 1.5.1 Internal and external magnetic fields

Small dimensions of an ellipsoid, in comparison with other dimensions of the system, permit us to regard the external magnetic fields, both dc and ac, as given. (External field can be defined as a field at the place of the sample, in the absence of it.) Then, without solving the boundary problem, we may use the relation known from magnetostatics (e.g., [131, 44]):

$$\mathbf{H} = \mathbf{H}_e - \vec{N}\mathbf{M} \equiv \mathbf{H}_e + \mathbf{H}_{\text{dem}} \quad (1.82)$$

where  $\mathbf{H}_e$  is the external magnetic field,  $\mathbf{H}$  is the internal field, and  $\mathbf{M}$  is the magnetization; both  $\mathbf{H}$  and  $\mathbf{M}$  are uniform if  $\mathbf{H}_e$  is uniform in and near the ellipsoid. The tensor  $\vec{N}$  in (1.82) is the *demagnetization tensor*. It is symmetric and becomes diagonal in the axes coinciding with the axes of the ellipsoid. The components of  $\vec{N}$  in these axes,  $N_x$ ,  $N_y$ , and  $N_z$ , are called *demagnetization factors*. They depend only on the shape of the ellipsoid (Appendix B), and their sum is

$$N_x + N_y + N_z = 4\pi. \quad (1.83)$$

[Sometimes this sum is normalized to 1, then the factor  $4\pi$  appears in (1.82).] The quantity  $\mathbf{H}_{\text{dem}} = -\vec{N}\mathbf{M}$  in (1.82) is the demagnetizing field.

Substituting the sums of dc and ac components of  $\mathbf{H}_e$ ,  $\mathbf{H}$ , and  $\mathbf{M}$  into (1.82), we get

$$\mathbf{H}_0 = \mathbf{H}_{e0} - \vec{N}\mathbf{M}_0 \quad (1.84)$$

$$\mathbf{h} = \mathbf{h}_e - \vec{N}\mathbf{m} \quad (1.85)$$

Let us discuss now the conditions of applicability of (1.85).

1. The sample must be an *ellipsoid* [this is the condition of applicability of (1.84), too].
2. The sample dimensions must be *small* in comparison with the length of electromagnetic wave in the substance of the sample. This condition is satisfied, usually, for materials with small conductivity, e.g., for ferrites, small samples are used in experiments on ferromagnetic resonance in such materials. But in metals (Section 14.2) the depth of penetration of electromagnetic field into the substance (the skin depth) is very small ( $\sim 10^{-4}$  cm at microwaves), and (1.85) becomes meaningless for samples with all dimensions larger than the skin depth.
3. The alternating magnetization must be *uniform*. For nonuniform oscillations of magnetization (Section 6.3) expression (1.85) does not hold.

Taking (1.84) into account, we get the equilibrium condition

$$\mathbf{M}_0 \times \left( \mathbf{H}_{e0} - \vec{N}\mathbf{M}_0 \right) = 0. \quad (1.86)$$

The linearized equation of motion (1.66), with allowance for (1.84) and (1.85), can be written as

$$i\omega m + \gamma m \left( \mathbf{H}_{e0} - \vec{N} \mathbf{M}_0 \right) + \gamma \left( \vec{N} m \right) \times \mathbf{M}_0 - \frac{i\alpha\omega}{M_0} m \times \mathbf{M}_0 = -\gamma \mathbf{M}_0 \times \mathbf{h}_e. \quad (1.87)$$

Equations (1.86) and (1.87) contain the *external* fields  $\mathbf{H}_{e0}$  and  $\mathbf{h}_e$ , which can be regarded as given quantities, as distinct from the internal fields  $\mathbf{H}_0$  and  $\mathbf{h}$ .

### 1.5.2 Eigenoscillations

In the study of any oscillations we have to begin with the eigenoscillations, i.e., *free* (in the absence of external fields) and *nondamped*. So, assume in (1.87)  $\mathbf{h}_e = 0$  and  $\alpha = 0$  and project it onto the axes of a Cartesian coordinate system in which the  $z$ -axis coincides with the direction of  $\mathbf{M}_0$ . Let the demagnetization tensor have, in these axes, the form

$$\vec{N} = \begin{vmatrix} N_{11} & N_{12} & N_{13} \\ N_{12} & N_{22} & N_{23} \\ N_{13} & N_{23} & N_{33} \end{vmatrix}. \quad (1.88)$$

Then we get two linear equations

$$\begin{aligned} (i\omega + \gamma N_{12} M_0) m_x + \gamma (H_{e0z} - N_{33} M_0 + N_{22} M_0) m_y &= 0 \\ -\gamma (H_{e0z} - N_{33} M_0 + N_{11} M_0) m_x + (i\omega + \gamma N_{12} M_0) m_y &= 0. \end{aligned} \quad (1.89)$$

The condition of compatibility of these equations gives the expression for the *eigenfrequency* (i.e., the frequency of eigenoscillations):

$$\omega_0 = [(\omega_H + \gamma N_{11} M_0)(\omega_H + \gamma N_{22} M_0) - \gamma^2 N_{12}^2 M_0^2]^{1/2} \quad (1.90)$$

where

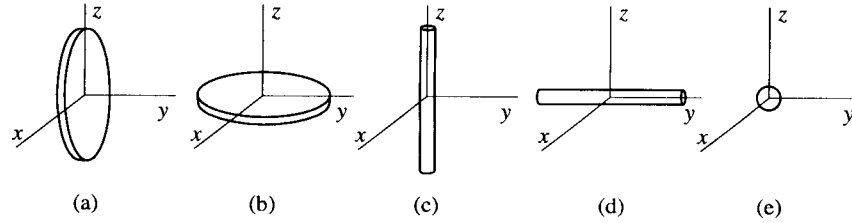
$$\omega_H = \gamma (H_{e0z} - N_{33} M_0). \quad (1.91)$$

The maximal absorption of electromagnetic energy by a small ferromagnetic ellipsoid takes place, as it will be shown below, at a frequency very near to the eigenfrequency (1.90). So, this frequency, which depends on the shape of the sample, is the *frequency of ferromagnetic resonance*. It should be emphasized that, before using (1.90) to calculate the ferromagnetic-resonance frequency, the direction of  $\mathbf{M}_0$  (and, so, of the  $z$  axis) must be found.

If the external field  $\mathbf{H}_{e0}$  is directed along one of the axes of an ellipsoid, then  $\mathbf{M}_0$  and, consequently, the  $z$ -axis are also oriented along this ellipsoid axis. The tensor  $\vec{N}$  becomes diagonal, and (1.90) acquires the form

$$\omega_0 = \gamma \left\{ [H_{e0} + (N_x - N_z) M_0] [H_{e0} + (N_y - N_z) M_0] \right\}^{1/2}. \quad (1.92)$$

It is the famous formula obtained by Kittel [220].



**FIGURE 1.9**  
Limiting cases of an ellipsoid.

The ferromagnetic-resonance frequencies for limiting cases of an ellipsoid (Figure 1.9) are listed in Table 1.1.

**TABLE 1.1**  
Frequencies of ferromagnetic resonance in small samples

Sample	Magnetization direction	See Fig. 1.9	Demagnetization factors			Eigenfrequency
			$N_x$	$N_y$	$N_z$	
Infinitely thin plate	Tangential	(a)	0	$4\pi$	0	$(\frac{\omega_0}{\gamma})^2 = H_{e0}(H_{e0} + 4\pi M_0)$ (1.93)
	Normal	(b)	0	0	$4\pi$	$\frac{\omega_0}{\gamma} = H_{e0} - 4\pi M_0$ (1.94)
Infinitely thin cylinder	Longitudinal	(c)	$2\pi$	$2\pi$	0	$\frac{\omega_0}{\gamma} = H_{e0} + 2\pi M_0$ (1.95)
Infinitely thin cylinder	Transverse	(d)	$2\pi$	0	$2\pi$	$(\frac{\omega_0}{\gamma})^2 = H_{e0}(H_{e0} - 2\pi M_0)$ (1.96)
Sphere		(e)	$\frac{4\pi}{3}$	$\frac{4\pi}{3}$	$\frac{4\pi}{3}$	$\frac{\omega_0}{\gamma} = H_{e0}$ (1.97)

For a sphere, expression (1.97) is extremely simple and does not include  $M_0$ . This is the main reason why spherical samples are widely used in ferromagnetic-resonance experiments. Another reason is that small spheres (with diameters from several millimeters down to  $\sim 0.2$  mm) with very smooth surfaces, necessary for such experiments, are made by very simple techniques (e.g., [146]).

It follows from (1.87) that for a *sphere*

$$i\omega \mathbf{m} + \gamma \mathbf{m} \times \mathbf{H}_{e0} + \frac{i\alpha\omega}{M_0} \mathbf{m} \times \mathbf{M}_0 = -\gamma \mathbf{M}_0 \times \mathbf{h}_e. \quad (1.98)$$

Comparing this equation with (1.66), we see that the motion of the ac magnetization in a sphere occurs as if in the external fields. Formula (1.97) follows from (1.98).

It should be noted that  $N_{11}$ ,  $N_{22}$ , and  $N_{12}$  in (1.90) or  $N_x$  and  $N_y$  in (1.92) are the demagnetization factors for ac fields, while  $N_{33}$  or  $N_z$  are the demagnetization factors for dc fields. They differ from each other in two cases: (i) when (1.90) or (1.92) is used to find the ferromagnetic-resonance condition in metals (Section 14.2), and (ii) when an ac magnetic field exists only in a fraction of a nonmetallic sample, which is excited, e.g., through a hole in a resonator wall. In both cases formulae (1.90) or (1.92) can be used only approximately, because the ac field is nonuniform.

Consider now the *polarization* of eigenoscillations in a small ferromagnetic ellipsoid. From (1.89), taking (1.90) into account, we get

$$\frac{m_y}{m_x} = -i\sqrt{\frac{H_0 + N_{11}M_0}{H_0 + N_{22}M_0}} - \xi^2 - \xi \quad (1.99)$$

where  $\xi = N_{12}(N_{22} + H_0/M_0)$  and  $H_0$  is the internal dc field (1.84). One can see from (1.99) that the ac magnetization is elliptically polarized. The axes of the polarization ellipse do not coincide with  $x$ - and  $y$ -axes, as the phase difference between  $m_y$  and  $m_x$  is not equal to  $\pi/2$ .

If  $H_{e0}$  is directed along one of the ellipsoid axes (the 'Kittel case'), so that  $N_{12} = 0$ , then

$$\frac{m_y}{m_x} = -i\sqrt{\frac{H_{e0} + (N_x - N_z)}{H_{e0} + (N_y - N_z)}} \quad (1.100)$$

Now the axes of the polarization ellipse do coincide with  $x$ - and  $y$ -axes, the transverse axes of the sample. The large axis of the polarization ellipse coincides with the larger of these transverse axes. If the sample is a spheroid, the polarization is circular. It approaches circular in a general ellipsoid with increasing  $H_{e0}$ .

Polarization can be characterized by a parameter named *ellipticity* and defined as

$$\mathcal{E} = 1 - \frac{|m_{\min}|^2}{|m_{\max}|^2} \quad (1.101)$$

where  $|m_{\max}|$  and  $|m_{\min}|$  are, respectively, the large and the small axes of the polarization ellipse. In the Kittel case they coincide with  $|m_x|$  and  $|m_y|$ , and, if, e.g.,  $N_y > N_x$ , then

$$\mathcal{E} = \frac{N_y - N_x}{N_y - N_x + H_{e0}/M_0} \quad (1.102)$$

Assume now in (1.87)  $h_e = 0$ , as before, but  $\alpha \neq 0$ . It is easy to see that the obtained equation differs from the equation with  $\alpha = 0$  only by the substitution (1.68) where  $\omega_H$  is determined now by (1.91). After this substitution we get the complex equation

$$\omega_0^2 - \omega^2(1 + \alpha^2) + 2i\alpha\omega\omega_1 = 0 \quad (1.103)$$

where  $\omega_0$  is the eigenfrequency (1.90) and

$$\omega_1 = \omega_H + \frac{1}{2}(N_{11} + N_{22})\gamma M_0. \quad (1.104)$$

Substituting  $\omega = \omega' + i\omega''$  into (1.103), we obtain

$$(\omega')^2 = \frac{1}{(1 + \alpha^2)^2} \left\{ \omega_0^2 - \alpha^2 \left[ \frac{1}{4}(N_{11} + N_{22})^2 + N_{12}^2 \right] \gamma^2 M_0^2 \right\} \quad (1.105)$$

$$\omega'' = \frac{\alpha\omega_1}{1 + \alpha^2}. \quad (1.106)$$

Here,  $\omega'$  is the frequency and  $\omega''$  is the damping coefficient of free oscillations. One can see from (1.105) that losses lead to the shift of the oscillation frequency which is of the second order in  $\alpha$ .

The damping of oscillations is usually characterized by the *quality factor*  $Q$  defined as

$$Q = \frac{\omega'}{2\omega''} = \frac{\omega'W}{P} \quad (1.107)$$

where  $W$  is the energy stored in the system and  $P$  is the losses of energy per unit time. In our case, to a first approximation ( $\alpha \ll 1$ ),

$$Q_0 \approx \frac{\omega_0}{2\alpha\omega_1}. \quad (1.108)$$

This quantity can be called internal quality factor, as the losses only inside the sample are taken into account.

Expressions (1.105), (1.106), and (1.108) become especially simple for a spheroid magnetized in the direction of the axis of revolution. Then  $N_{12} = 0$ ,  $N_{11} = N_{22}$ ,  $\omega_1 = \omega_0$ , and

$$Q_0 = \frac{1}{2\alpha}. \quad (1.109)$$

This formula, as distinct from (1.108), holds for *any value* of  $\alpha$ .

### 1.5.3 Forced oscillations

Assume now that  $h_e \neq 0$  and  $\alpha \neq 0$  in (1.87). The solution of this linear equation can be written in the form

$$\mathbf{m} = \vec{\chi}^e \mathbf{h}_e \quad (1.110)$$

where  $\vec{\chi}^e$  is the *external susceptibility* tensor. It differs essentially from the tensor  $\vec{\chi}$  defined by (1.41). The tensor  $\vec{\chi}^e$  is introduced in the framework of magnetostatic approximation and only for a certain, uniform mode of oscillation in a sample of a certain, ellipsoidal shape. It characterizes the response of such a sample to an external ac magnetic field. The tensor  $\vec{\chi}$ , on the contrary, is the susceptibility of a substance, it 'does not know' whether the magnetostatic

approximation can be used or not and what the oscillation mode and the sample shape are. However, the latter is true only to the first approximation; some dependence of the tensor  $\vec{\chi}$  components on the oscillation mode and sample shape does exist because the values of the dissipation parameters depend on these factors (Sections 11.2 and 11.3).

If the tensor  $\vec{\chi}$  and the shape of the sample (an ellipsoid) are known, the external tensor  $\vec{\chi}^e$  can be found by eliminating  $\vec{h}$  from two tensor equations (1.41) and (1.85). It leads to

$$\left(\vec{\chi}^e\right)^{-1} = \left(\vec{\chi}\right)^{-1} + \vec{N} \quad (1.111)$$

where  $\left(\vec{\chi}^e\right)^{-1}$  and  $\left(\vec{\chi}\right)^{-1}$  are the reciprocal tensors (the components of which form an inverse matrix [273], relative to the matrix formed by the components of tensor  $\vec{\chi}$  or  $\vec{\chi}^e$ ). The quantity  $\left(\vec{N}\right)^{-1}$ , the reciprocal value of which appears in (1.111), can be called 'susceptibility of the shape'.

However, the calculation of tensor  $\vec{\chi}^e$  components by the use of (1.111) is *cumbersome*, and it is easier to solve equation (1.87) directly. In the lossless case ( $\alpha = 0$ ) it results in

$$\vec{\chi}^e = \begin{vmatrix} \chi_x^e & \chi_s^e + i\chi_a^e & 0 \\ \chi_s^e - i\chi_a^e & \chi_y^e & 0 \\ 0 & 0 & 0 \end{vmatrix} \quad (1.112)$$

$$\chi_{x,y,s}^e = D^{-1}\gamma M_0 \omega_{x,y,s} \quad \chi_a^e = D^{-1}\gamma M_0 \omega \quad (1.113)$$

$$\omega_x = \omega_H + \gamma N_{22} M_0 \quad \omega_y = \omega_H + \gamma N_{11} M_0 \quad \omega_s = -\gamma N_{12} M_0 \quad (1.114)$$

$$D = \omega_0^2 - \omega^2 \quad \omega_0^2 = \omega_x \omega_y - \omega_s^2 \quad (1.115)$$

where  $\omega_0$  is the eigenfrequency (1.90) and  $\omega_H$  is defined by (1.91).

To take *losses* into account the replacement (1.68) should be made in (1.114). We cite here only the formulae for  $\vec{\chi}^e$  components at resonance when  $\omega_0^2 = \omega^2(1 + \alpha^2)$ :

$$\begin{aligned} (\chi_{x,y}^e)'_{\text{res}} &= \frac{\gamma M_0}{2\omega_1} & (\chi_{x,y}^e)''_{\text{res}} &= \frac{\gamma M_0(\omega_H + N_{22,11}\gamma M_0)}{2\alpha\omega\omega_1} \\ (\chi_s^e)'_{\text{res}} &= (\chi_a^e)'_{\text{res}} = 0 & (\chi_s^e)''_{\text{res}} &= \frac{N_{12}\gamma^2 M_0^2}{2\alpha\omega\omega_1} & (\chi_a^e)''_{\text{res}} &= \frac{\gamma M_0}{2\alpha\omega_1} \end{aligned} \quad (1.116)$$

where  $\omega_1$  is determined by (1.104).

For an ellipsoid of revolution (around the  $z$ -axis)

$$(\chi_s^e)''_{\text{res}} = 0 \quad (\chi_x^e)''_{\text{res}} = (\chi_y^e)''_{\text{res}} = (\chi_a^e)''_{\text{res}} = \frac{\gamma M_0}{2\alpha\omega_0} \equiv \chi_{\text{res}}^{e''}. \quad (1.117)$$

The *linewidth*  $\Delta H$  is defined (analogous to Section 1.4) as an interval between  $H_{e0}$  values at which  $(\chi_x^e)''$ ,  $(\chi_y^e)''$ , or  $(\chi_a^e)''$  are equal to one half their values at

resonance. In the case of small losses, taking into account (1.68) and (1.107), it can be shown that

$$\Delta H = \frac{2\alpha\omega_0}{\gamma} = \frac{2\omega_r\omega_0}{\gamma\omega_H} = \frac{2\lambda\omega_0}{\gamma M_0} = \frac{\omega_0^2}{\gamma\omega_1 Q_0}. \quad (1.118)$$

The linewidth  $\Delta\omega$  (when  $\omega$  is varied at constant  $H_{e0}$ ) is

$$\Delta\omega = 2\alpha\omega_1 = \frac{\omega_0}{Q_0}. \quad (1.119)$$

For an ellipsoid of revolution, in particular, for a sphere,  $\omega_1 = \omega_0$  and  $\Delta\omega = \gamma\Delta H$ .

If a certain dissipation parameter,  $\alpha$ ,  $\omega_r$ , or  $\lambda$ , is assumed to be constant, the expressions (1.118) or (1.119) give, formally, the dependence of  $\Delta H$  or  $\Delta\omega$  on  $\omega$ ,  $H_{e0}$ , and  $M_0$ , as well as on the shape of the sample, because the tensor  $\vec{N}$  components enter the expressions for  $\omega_H$ ,  $\omega_0$ , and  $\omega_1$ . However, the dissipation parameters depend on all mentioned quantities (Chapter 11). This dependence, found experimentally or theoretically, must be taken into account to obtain the actual dependence of  $\Delta H$  on  $\omega$ ,  $H_{e0}$ , and other quantities.

For high-quality YIG single crystals the dissipation parameter  $\alpha$  depends weakly on frequency in the microwave range and is of the order of  $5 \times 10^{-5}$ . Then the linewidth  $\Delta H$ , according to (1.118), increases with growing frequency. At frequency of 9 GHz,  $\Delta H \sim 0.3$  Oe.

From (1.117) and (1.118) it follows, for an ellipsoid of revolution, that

$$\Delta H \chi_{\text{res}}^e{}'' = M_0. \quad (1.120)$$

For an arbitrary ellipsoid, a factor of the order of unity will appear in (1.120).

The components of the ac magnetization for forced oscillations can be easily calculated, using the expressions obtained from (1.113)–(1.115) by the substitution (1.68). The polarization of oscillations can be also found. We mention here only that, as it is clear from symmetry considerations, the polarization is circular when the external field is circularly polarized and the sample is an ellipsoid of revolution around the direction of  $\vec{M}_0$ . However, if the sample is an ellipsoid of revolution and the dissipation is small ( $\alpha \ll 1$ ), then the polarization of the ac magnetization at ferromagnetic resonance is very near to circular (i.e., the ellipticity is small) even in the case of linear polarization of the external ac magnetic field.

It will be shown in Sections 5.3 and 5.4 that the interaction of a small ferromagnetic ellipsoid with the electromagnetic field in a resonator or a waveguide is determined by the external susceptibility  $\vec{\chi}^e$ . Thus, the  $\vec{\chi}^e$  components considered in this section and, consequently, the values of the dissipation parameters can be found from the measured characteristics of resonators or waveguides containing ferromagnetic (or ferrimagnetic, see Section 3.3) ellipsoids.





# 2

---

## *Anisotropic ferromagnet*

---

---

### 2.1 Landau–Lifshitz equation

In this chapter uniform oscillations of magnetization in an anisotropic ferromagnet magnetized to saturation will be studied.

Anisotropy is a dependence of the properties of a substance or a body on the angles between the directions of applied fields and some preferred directions. These directions can be determined by the substance structure, by the shape of the body, or (if we consider the properties in ac fields) by the directions of some external steady fields. Two kinds of anisotropy were already treated in Chapter 1. First, the *gyrotropy* when the direction of the steady magnetization  $M_0$  was the preferred one, and the high-frequency magnetic susceptibility acquired the tensor form (1.42). Second, we have seen in Section 1.5 that the ferromagnetic-resonance conditions depend on the orientation of  $M_0$  relative to the ellipsoid axes. Such anisotropy can be referred to as the *shape anisotropy*. However, it was assumed throughout Chapter 1 that the substance itself (a ferromagnet), in the absence of steady magnetization, is isotropic.

Actually, most of ferromagnets are crystals characterized by the *magnetocrystalline anisotropy*. Then the preferred directions are the crystal axes, and all the quantities depend on the angles of  $M_0$  relative to these axes. The *magnetoelastic anisotropy* is also present in ferromagnets, in this case the preferred directions are the directions of the external mechanical stresses. Other kinds of anisotropy, e.g., the anisotropy caused by electric fields or temperature gradients, exist, as well, but usually play a smaller role. The aim of this chapter is, first, to study general methods of allowance for the influence of anisotropy on ferromagnetic resonance and, second, to investigate, using these methods, the most important case of magnetocrystalline anisotropy.

In the classical theory of ferromagnetic resonance, different interactions leading to anisotropy are taken into account by corresponding terms of internal (at temperature  $T = 0$ ) or free (at  $T > 0$ ) energy. We are not concerned about the processes at the boundaries between different media, which are important only

for very small ferromagnetic bodies. Therefore, we shall deal only with *volume densities* of internal  $U_i$  or free  $U_f$  energy. It is known from thermodynamics (e.g., [244]) that

$$U_f = U_i - ST \quad (2.1)$$

where  $S$  is the volume density of entropy.<sup>1</sup> The term  $ST$  in (2.1) in many cases is not written explicitly but ‘spread’ over the whole expression for  $U_f$ . All constants in this expression, as well as the magnetization  $M$ , become then functions of temperature.

### 2.1.1 Generalization of equation of motion

The equation of motion for the magnetization of a ferromagnet was proposed by Landau and Lifshitz [241]. It can not be derived strictly in the framework of a classical theory. We show this equation to be a reasonable generalization of the equation of motion (1.29) for an isotropic ferromagnet (which cannot be derived strictly in the framework of classical theory either).

Consider first the *equilibrium state* of an anisotropic ferromagnet. The necessary condition of it is that the energy should be stationary, i.e., the variation of it

$$\delta \int_V U dV = 0. \quad (2.2)$$

The condition of the vector  $M$  length conservation is also to be taken into account. As we have seen in Chapter 1, this condition (1.30) holds for an isotropic ferromagnet. The conservation of the vector  $M$  length is a result of the strong exchange interaction; the interactions leading to anisotropy are much weaker. Therefore, we may assume (1.30) to be valid for an anisotropic ferromagnet, too.

The condition of stationarity of energy under the supplementary condition (1.30) is (e.g., [273])

$$\frac{\delta}{\delta M} (U + \lambda M^2) = \frac{\delta U}{\delta M} + 2\lambda M = 0 \quad (2.3)$$

where  $\lambda$  is the Lagrange arbitrary factor. It follows from (2.3) that

$$M \times \frac{\delta U}{\delta M} = 0. \quad (2.4)$$

The variational derivative  $\delta U/\delta M$  has the form [273]

$$\frac{\delta U}{\delta M} = \frac{\partial U}{\partial M} - \sum_{p=1}^3 \frac{\partial}{\partial x_p} \left[ \frac{\partial U}{\partial(\partial M/\partial x_p)} \right]. \quad (2.5)$$

---

<sup>1</sup>In what follows we shall omit the words ‘volume density’. The indices ‘i’ and ‘f’ will be also omitted when it does not lead to ambiguity.

Comparing (2.4) with (1.33), we see that the magnetic field in the condition of *equilibrium* is replaced by the quantity  $\delta U/\delta \mathbf{M}$ . It is reasonable to suppose that an analogous replacement is to be made in the *equation of motion* (1.29), as well as in equations (1.61), (1.62), or (1.64) allowing for dissipation. Only the sign must be reversed because in these equations  $\mathbf{H} = -\partial U/\partial \mathbf{M}$ . We obtain then the *Landau–Lifshitz equation*

$$\frac{\partial \mathbf{M}}{\partial t} = -\gamma \mathbf{M} \times \mathbf{H}_{\text{ef}} + \mathbf{R} \quad (2.6)$$

where the effective field

$$\mathbf{H}_{\text{ef}} = -\frac{\delta U}{\delta \mathbf{M}} \equiv -\frac{\partial U}{\partial \mathbf{M}} + \sum_{p=1}^3 \frac{\partial}{\partial x_p} \left[ \frac{\partial U}{\partial (\partial \mathbf{M} / \partial x_p)} \right] \quad (2.7)$$

and  $\mathbf{R}$  is the dissipative term. The condition of equilibrium can be written now as

$$\mathbf{M}_0 \times \mathbf{H}_{\text{ef}0} = 0. \quad (2.8)$$

The dissipative term in (1.62) can be supposed to be unchanged, and the equation of motion takes the form

$$\frac{\partial \mathbf{M}}{\partial t} = -\gamma \mathbf{M} \times \mathbf{H}_{\text{ef}} + \frac{\alpha}{M} \mathbf{M} \times \frac{\partial \mathbf{M}}{\partial t}. \quad (2.9)$$

In the dissipative terms of (1.61) and (1.64) the field  $\mathbf{H}$  can be replaced by  $\mathbf{H}_{\text{ef}}$ .

The quantity  $\gamma$  should be, in general, a *tensor*. In the case of paramagnetic resonance (e.g., [1]) the entire anisotropy is taken into account by means of a tensor  $g$ -factor. There are experimental data [166] showing that, when the anisotropy is large, the allowance for the tensor  $g$ -factor becomes necessary in the case of a ferromagnet, too. However, it is not quite clear what equation of motion should be used in this case. The influence of the tensor character of the  $g$ -factor is usually small for ferromagnets, and so, we shall regard the quantities  $\gamma$  and  $g$  as *scalars*.

For an anisotropic ferromagnet,

$$U = U_{\text{ex}} + U_{\text{mag}} + U_{\text{an}} \quad (2.10)$$

where  $U_{\text{ex}}$  is the exchange energy,  $U_{\text{mag}}$  is the magnetic energy, and  $U_{\text{an}}$  is the energy of anisotropy.

The *exchange energy* can be regarded as a sum of two terms:

$$U_{\text{ex}} = U_{\text{ex}0} + U_{\text{ex}\sim}. \quad (2.11)$$

Here,  $U_{\text{ex}0}$  is the value of exchange energy when the magnetization is uniform, and  $U_{\text{ex}\sim}$  corresponds to the increase of this energy due to the nonuniformity of magnetization. The term  $U_{\text{ex}0}$  can be written in the form

$$U_{\text{ex}0} = \frac{1}{2} \mathbf{M} \overleftrightarrow{\Lambda} \mathbf{M} \quad (2.12)$$

where  $\vec{\Lambda}$  is the exchange tensor. In many cases it can be regarded as a scalar. Then,

$$U_{\text{ex}0} = \frac{1}{2} \Lambda M^2. \quad (2.13)$$

The effective field that, according to (2.7), corresponds to the energy term (2.13) is the ‘molecular’ field (1.22). This field does not enter the equation of motion, in any case, the main term  $\mathbf{M} \times \mathbf{H}_{\text{ef}}$  and the dissipative terms in the Landau–Lifshitz and Gilbert forms. As we now deal only with uniform magnetization oscillations, we do not touch on the term  $U_{\text{ex}0}$ . It will be considered in Section 7.1.

The *magnetic* energy can be written as

$$U_{\text{mag}} = U_Z + U_M \quad (2.14)$$

where

$$U_Z = -\mathbf{M} \mathbf{H}_e \quad (2.15)$$

is the Zeeman energy, i.e., the energy of the magnetization in an external magnetic field  $\mathbf{H}_e$ , and  $U_M$  is the internal magnetic energy resulting from the magnetic (dipole–dipole) interaction between magnetic moments of the sample. For a small ferromagnetic ellipsoid (Section 1.5) the effective field of this interaction is  $-\vec{N}\mathbf{M}$ , hence,

$$U_M = \frac{1}{2} \mathbf{M} \left( \vec{N} \mathbf{M} \right). \quad (2.16)$$

The term  $U_{\text{an}}$  represents all kinds of anisotropy. The expressions for this term in the case of magnetocrystalline anisotropy will be cited in Section 2.2.

To linearize the Landau–Lifshitz equation let us substitute  $\mathbf{M} = \mathbf{M}_0 + \mathbf{m} \exp(i\omega t)$  and

$$\mathbf{H}_{\text{ef}} = \mathbf{H}_{\text{ef}0} + \mathbf{h}_{\text{ef}} \exp(i\omega t) + \mathbf{h} \exp(i\omega t) \quad (2.17)$$

into (2.9). In (2.17) we have excluded the given ac field  $\mathbf{h}$  from the effective ac field, whereas the given *steady* field has been left in  $\mathbf{H}_{\text{ef}0}$ . The field  $\mathbf{h}$  can be either an internal or an external field, according to what quantity we have to find, the susceptibility of the substance  $\vec{\chi}$  or the external susceptibility  $\vec{\chi}^e$  (Section 1.5). Taking into account the equilibrium condition (2.8) and assuming all alternating quantities to be small, we obtain a *linear* equation for the complex amplitudes:

$$i\omega \mathbf{m} + \gamma \mathbf{m} \times \mathbf{H}_{\text{ef}0} + \gamma \mathbf{M}_0 \times \mathbf{h}_{\text{ef}} + \frac{i\alpha\omega}{M_0} \mathbf{m} \times \mathbf{M}_0 = -\gamma \mathbf{M}_0 \times \mathbf{h}. \quad (2.18)$$

It is easy to make sure that the results of Section 1.5 can be obtained by the formalism of the present section, as well. Actually, if the external fields  $\mathbf{H}_{e0}$  and  $\mathbf{h}_e$  are given, and the ferromagnet is isotropic, the energy  $U$  will be the sum of Zeeman energy (2.15) and the demagnetization energy (2.16). Applying (2.7), we find  $\mathbf{H}_{\text{ef}0} = \mathbf{H}_{e0} - \vec{N}\mathbf{M}_0$  and  $\mathbf{h}_{\text{ef}} = -\vec{N}\mathbf{m}$ . Substituting these quantities

into (2.18), we obtain equation (1.87), from which all the results of Section 1.5 follow.

### 2.1.2 Methods of analysis of ferromagnetic resonance in anisotropic ferromagnet

One of these methods, the method of *effective demagnetization factors*, was suggested by Kittel [220] and elaborated by MacDonald [266]. Following this method, we try to represent the effective field in the form analogous to the demagnetizing field:

$$\vec{H}_{ef} = -\vec{N}^{ef} \vec{M} \quad (2.19)$$

introducing the tensor of effective demagnetization factors  $\vec{N}^{ef}$ . It will be demonstrated in Section 2.3 that such representation is possible in the case of small oscillations ( $m \ll M_0$ ) if the  $z$ -axis is directed along the steady magnetization  $\vec{M}_0$ . The effective field having been written in the form (2.19), the problem of allowance for the anisotropy is solved, in principle, because all the formulae of Section 1.5 can be used. One must only replace the tensor  $\vec{N}$  components in these formulae by the corresponding components of tensor  $\vec{N}^{ef}$  or the sum  $\vec{N} + \vec{N}^{ef}$ , according to Table 2.1.

**TABLE 2.1**

Replacement of the demagnetization tensor components when the formulae of Section 1.5 are used to take the anisotropy into account.

Components of tensor $\vec{N}^a$	Components of tensor $\vec{N}$ have to be replaced by	
	in calculating $\vec{\chi}$ components	in calculating $\vec{\chi}^c$ components and resonance conditions for an ellipsoid
$N_{ij}$ ( $i, j = 1, 2$ )	$N_{ij}^{ef}$	$N_{ij} + N_{ij}^{ef}$
$N_{33}$	$N_{33} + N_{33}^{ef}$	$N_{33} + N_{33}^{ef}$

<sup>a</sup> Axis 3 coincides with the direction of  $\vec{M}_0$ .

Another method used to analyze the ferromagnetic resonance in anisotropic media is the method of *spherical coordinates* proposed by Smit and Beljers [371] and by Suhl [390]. Skrotskii and Kurbatov [366] generalized it taking dissipation into account. This method is based on the transition from the variables  $M_x$ ,  $M_y$ , and  $M_z$  to the variables  $\theta$ ,  $\varphi$ , and  $M$  where  $\theta$  and  $\varphi$  are the angles of  $\vec{M}$  in a spherical coordinate system, and  $M$  is the vector  $\vec{M}$  length. If the latter is conserved, two variables,  $\theta$  and  $\varphi$ , are enough.

Let us obtain the equations of motion in new variables using equation (2.9) (which assures the conservation of  $M$ ) and assuming the magnetization to be

uniform. Then, it is easy to show that all three equations, projections of (2.9) onto the axes  $x$ ,  $y$ , and  $z$ , are satisfied if the following *two* equations are valid (we write them in the case of small dissipation, i.e.,  $\alpha \ll 1$ ):

$$\begin{aligned}\frac{\partial \theta}{\partial t} &= -\frac{\gamma}{M \sin \theta} \frac{\partial U}{\partial \varphi} - \frac{\alpha \gamma}{M} \frac{\partial U}{\partial \theta} \\ \frac{\partial \varphi}{\partial t} &= \frac{\gamma}{M \sin \theta} \frac{\partial U}{\partial \theta} - \frac{\alpha \gamma}{M \sin^2 \theta} \frac{\partial U}{\partial \varphi}.\end{aligned}\quad (2.20)$$

If we use equation (1.64) with the dissipative term that does not assure the conservation of  $M$ , two equations would be identical to (2.20) after the substitution  $\omega_r \rightarrow \alpha \omega_H$ , and the third would be

$$\frac{\partial M}{\partial t} = -\omega_r \left( \frac{M_0}{H_0} \frac{\partial U}{\partial M} - M \right). \quad (2.21)$$

Consider now the case of *small* deviations of  $M$  from  $M_0$ . The angles  $\theta_0$  and  $\varphi_0$  of  $M_0$  can be found from the equilibrium conditions

$$\left( \frac{\partial U}{\partial \theta} \right)_{\theta=\theta_0, \varphi=\varphi_0} = 0 \quad \left( \frac{\partial U}{\partial \varphi} \right)_{\theta=\theta_0, \varphi=\varphi_0} = 0 \quad (2.22)$$

which are equivalent to the condition (2.8). (One is to make certain, of course, that the obtained  $\theta_0$  and  $\varphi_0$  values correspond to a *minimum* of energy.)

The derivatives  $\partial U / \partial \theta$  and  $\partial U / \partial \varphi$  in (2.20) are expressed as power series in small quantities  $\delta \theta \sim \theta - \theta_0 = \delta \theta \exp(i\omega t)$  and  $\delta \varphi \sim \varphi - \varphi_0 = \delta \varphi \exp(i\omega t)$ . Taking into account the conditions (2.22) and discarding the terms with powers of  $\delta \theta$  and  $\delta \varphi$  higher than unity, we obtain *linear* equations

$$\begin{aligned}& \left( i\omega + \frac{\gamma}{M_0 \sin \theta_0} U_{\theta\varphi} + \frac{\alpha \gamma}{M_0} U_{\theta\theta} \right) \delta \theta \\ & + \left( \frac{\gamma}{M_0 \sin \theta_0} U_{\varphi\varphi} + \frac{\alpha \gamma}{M_0} U_{\theta\varphi} \right) \delta \varphi = 0 \\ & \left( i\omega - \frac{\gamma}{M_0 \sin \theta_0} U_{\theta\varphi} + \frac{\alpha \gamma}{M_0 \sin^2 \theta_0} U_{\varphi\varphi} \right) \delta \varphi \\ & - \left( \frac{\gamma}{M_0 \sin \theta_0} U_{\theta\theta} - \frac{\alpha \gamma}{M_0 \sin^2 \theta_0} U_{\theta\varphi} \right) \delta \theta = 0\end{aligned}\quad (2.23)$$

where  $U_{\theta\theta} = \partial^2 U / \partial \theta^2$ ,  $U_{\varphi\varphi} = \partial^2 U / \partial \varphi^2$ , and  $U_{\theta\varphi} = \partial^2 U / \partial \theta \partial \varphi$  at *equilibrium* ( $\theta = \theta_0$  and  $\varphi = \varphi_0$ ).

Consider first the *eigenoscillations*. Then, the condition of compatibility of equations (2.23) with  $\alpha = 0$  yields the expression for the eigenfrequency

$$\omega_0 = \frac{\gamma}{M_0 \sin \theta_0} (U_{\theta\theta} U_{\varphi\varphi} - U_{\theta\varphi}^2)^{1/2} \quad (2.24)$$

known as the Smit–Suhl formula.

If the *dissipation* is taken into account, the frequency of free oscillations becomes complex. The real part of it is given, to a first approximation, by (2.24), and the imaginary part is

$$\omega'' = \frac{1}{2} \frac{\alpha\gamma}{M_0} \left( U_{\theta\theta} + \frac{1}{\sin^2 \theta_0} U_{\varphi\varphi} \right). \quad (2.25)$$

The Zeeman energy (2.15) (which is one of the parts of  $U$ ) is written in spherical coordinates as

$$U_Z = -MH_e [\cos \theta \cos \theta_H + \sin \theta \sin \theta_H \cos(\varphi - \varphi_H)] \quad (2.26)$$

where  $\theta_H$  and  $\varphi_H$  are the angles of the vector  $H_e$ . The total magnetic energy can be written analogously.

When the *forced oscillations* are considered, a term  $U_h$ , depending on a given ac field  $h$ , should be included in the energy. This field can be internal or external, depending on what problem is solved. The term  $U_h$  can be written by analogy with (2.26). We shall preserve the symbol  $U$  for the energy without this term, the total energy will be  $U_1 = U + U_h$ . Then, the same operations as in deriving (2.23), but with substitution of  $U_1$  for  $U$ , lead to equations the left-hand sides of which are the same as in (2.23). In the right-hand sides of the first and of the second equations (2.23), respectively, the following terms appear:

$$\gamma h \sin \theta_h \sin(\varphi_0 - \varphi_h) \quad \gamma h [\cot \theta_0 \sin \theta_h \cos(\varphi_0 - \varphi_h) - \cos \theta_h] \quad (2.27)$$

where  $\theta_h$  and  $\varphi_h$  are the angles of the vector  $h$ , and  $h$  is its length.

Using the method of spherical coordinates, we must carefully take into account the equilibrium conditions. For instance, we ought not to take  $\theta_0 = \theta_H$  even when the difference between these angles is small. We also must not direct the  $z$  axis along  $M_0$  to avoid indeterminacies arising from  $\sin \theta_0 = 0$ . On the contrary, when the method of effective demagnetization factors is used, the  $z$  axis should coincide with the direction of  $M_0$ .

## 2.2 Magnetocrystalline anisotropy

In this section we review briefly some general aspects of the most important kind of anisotropy in ferromagnets, the magnetocrystalline anisotropy.

### 2.2.1 Origins of magnetocrystalline anisotropy

The exchange interaction of spins, in the absence of orbital moments, is isotropic. Therefore, the magnetocrystalline anisotropy can be caused either by other interactions of spins or by the spin-orbital interaction.

One of the origins of the magnetocrystalline anisotropy in magnetically ordered crystals is the *magnetic* (dipole–dipole) interaction of elementary magnetic moments (Section 1.1). The energy of magnetic interaction of two magnetic moments with the same values and orientations, according to (1.3), is

$$\varepsilon_{ff'} = -\frac{3\mathfrak{M}^2}{r_{ff'}^3} \left( \cos^2 \theta_{ff'} - \frac{1}{3} \right) \equiv -C \left( \cos^2 \theta_{ff'} - \frac{1}{3} \right) \quad (2.28)$$

where  $\theta_{ff'}$  is the angle between  $\mathfrak{M}$  and  $r_{ff'}$ . If the magnetic moments form a lattice, the internal magnetic energy  $U_M$ , which is the sum of the energies (2.28), should depend, in general, on the orientation of the moments relative to the lattice axes. However, for all cubic crystals,  $U_M$  turns out to be isotropic [208]. For non-cubic *ferromagnets*, the contribution of  $U_M$  to the energy of anisotropy is very small.

Another origin of the magnetocrystalline anisotropy is the *anisotropy of the exchange interaction*, which arises due to the spin–orbital interaction. It can be explained in the following manner [208]. The turns of spins, due to the spin–orbital interaction, result in the change of the shapes of atomic electron shells. This leads to the alteration of the exchange energy (which is a fraction of Coulomb energy of these shells).

The energy of anisotropic exchange interaction can be written (assuming the magnetization to be uniform) as (2.12). However, it is customary to regard the exchange constant  $\Lambda$  as a scalar and include the angle-dependent part of the energy (2.12) into the energy of anisotropy.

Both the above-considered origins of magnetocrystalline anisotropy, in spite of their different physical nature, are alike in the sense that they are both based on *pair interactions* of elementary magnetic moments. The angular dependence (2.28) is the first term of the expansion of an arbitrary angular dependence in the natural functions for this problem, the Legendre polynomials of  $\cos \theta$  [273]. That is why Van Vleck proposed (e.g., [208]) the *pseudodipole* interaction [with such angular dependence as in (2.28) but with another coefficient  $C$ ] as a formal origin of magnetocrystalline anisotropy. If we try to use such interaction to allow for the values of anisotropy in real ferromagnets, we find  $C$  to be 2–3 orders higher than in (2.28). A substantial contribution to the  $C$  values, found in such way, arises from the above-mentioned anisotropic exchange interaction.

The *one-ion origin* of magnetocrystalline anisotropy is quite different, at first sight, from the above-considered origins. Now the angle-dependent free energy is not the sum of pair-interaction energies, but is a sum of energies of *individual* ions (depending, of course, on their interaction). The ions are characterized by their energy spectrum, i.e., by the set of allowed energy levels. The Boltzmann distribution holds for them, and the free-energy density (in the case of one sort of



ions) can be calculated with the formula [244]

$$U_{\text{ion}} = -\kappa T \ln \left[ N \sum_{j=1}^n \exp \left( -\frac{\varepsilon_j}{\kappa T} \right) \right] \quad (2.29)$$

where  $\varepsilon_j$  are the ion energy levels, and  $N$  is the concentration of ions. The angular dependence of the energies  $\varepsilon_j$  is now the origin of the anisotropy. Numerous calculations of the one-ion contributions to magnetocrystalline anisotropy of ionic crystals, both ferromagnetic and antiferromagnetic, are in good agreement with experiment.

It is worth pointing out that in both cases, of anisotropic exchange and of one-ion anisotropy, the real cause of anisotropy is the spin-orbital interaction. The exchange interaction, which is anisotropic in the presence of spin-orbital coupling, influences the ionic energy levels and determines, together with the crystal field, their angular dependence. Therefore, the anisotropic exchange and the one-ion anisotropy should be considered, strictly speaking, not as independent mechanisms but models or theories corresponding more or less to the real experimental situation.

### 2.2.2 Phenomenological description

Irrespective of the nature of magnetocrystalline anisotropy, it is possible, as Akulov proposed (e.g., [208, 70]), to write down expressions for the energy of anisotropy in the form of power series in  $M$  projections on crystal axes. Such expressions must be compatible with the symmetry of the crystal lattice, i.e., remain invariant under all operations which form its symmetry group. The coefficients in these series are called *anisotropy constants*. Only the terms with odd powers of the magnetization projections can be present in these expressions, because magnetization, being an axial vector, changes its sign under the reversal of time, whereas energy must be invariant [410, 208].

For *rhombic* crystals the energy of anisotropy can be written as

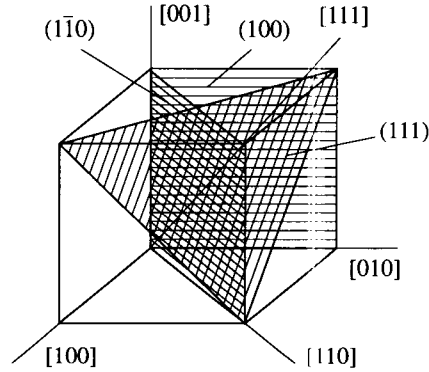
$$U_{\text{an}} = K_1^{(1)} \alpha_1^2 + K_1^{(2)} \alpha_2^2 + U'_{\text{an}} \quad (2.30)$$

where  $\alpha_j = M_j/M$  ( $j = 1, 2, 3$ ) are the direction cosines of  $M$  with respect to the symmetry axes, and  $U'_{\text{an}}$  is the sum of terms of higher order. We have taken into account that  $\alpha_1^2 + \alpha_2^2 + \alpha_3^2 = 1$  and, therefore, omitted one of the terms  $K_1^{(j)} \alpha_j^2$ .

For so-called *uniaxial* ferromagnets: trigonal, tetragonal, and hexagonal (with one main axis, respectively, of the third, fourth, and sixth order), we can neglect, to a first approximation, the anisotropy in the basal plane (perpendicular to the main axis). Then, we get

$$U_{\text{an}} = K_1 \sin^2 \theta + K_2 \sin^4 \theta + K_3 \sin^6 \theta + \dots \quad (2.31)$$

where  $\theta$  is the angle between  $M$  and the main axis. If the anisotropy in the



**FIGURE 2.1**  
Symmetry axes and planes in a cubic crystal.

basal plane is taken into account, additional terms appear in  $U_{\text{an}}$ : the term  $K'_2 \sin^4 \theta \cos 4\varphi$  for a tetragonal crystal and  $K'_3 \sin^6 \theta \cos 6\varphi$  for trigonal and hexagonal crystals,  $\varphi$  being the angle in the basal plane.

In the case of *cubic* crystals, the magnetocrystalline-anisotropy energy is written usually in the form proposed by Akulov

$$U_{\text{an}} = K_1 (\alpha_1^2 \alpha_2^2 + \alpha_2^2 \alpha_3^2 + \alpha_3^2 \alpha_1^2) + K_2 \alpha_1^2 \alpha_2^2 \alpha_3^2 + \dots \quad (2.32)$$

where  $\alpha_{1,2,3}$  are the direction cosines of  $\mathbf{M}$  with respect to the directions [100], [010], and [001] (Figure 2.1). The first term in (2.32) can be replaced by  $K'_1 (\alpha_1^4 + \alpha_2^4 + \alpha_3^4)$ , where  $K'_1 = -K_1/2$ . Passing in (2.32) from the direction cosines to the angles  $\theta$  and  $\varphi$ , we obtain

$$U_{\text{an}} = \frac{1}{4} K_1 (\sin^2 2\theta + \sin^4 \theta \sin^2 2\varphi) + \frac{1}{16} K_2 \sin^2 \theta \sin^2 2\theta \sin^2 2\varphi. \quad (2.33)$$

The angle-dependent parts of elastic and magnetoelastic energies of a ferromagnet (Section 12.1) are usually included in the energy of magnetocrystalline anisotropy. As the expressions (2.30)–(2.32) are determined only by the crystal symmetry, they also hold for the total anisotropy energy. But the values of anisotropy constants are changed, ‘renormalized’. The measurement of anisotropy constants by ‘static’ methods, i.e., at small rates of the change of magnetization direction, yields these renormalized constants. But if the rate of magnetization change is high enough, e.g., at ferromagnetic resonance, the measurement of anisotropy constants gives another values of anisotropy constants. Fortunately, for many substances the difference is small. This topic will be discussed in Section 12.2.

### 2.2.3 Equilibrium orientations of magnetization

To study small oscillations of magnetization, in particular, at ferromagnetic resonance, we must first find the *steady state*, i.e., the equilibrium orientations of magnetization. If only the energy of magnetocrystalline anisotropy is taken into account, the equilibrium directions of magnetization are determined by the condition of minimum of this energy. These directions are referred to as the axes of easy magnetization or, simply, easy axes. (The directions of  $U_{\text{an}}$  maxima are called hard axes.)

Consider a *uniaxial* ferromagnet and limit ourselves in (2.31) to the first constant  $K_1$ . Then, if  $K_1 > 0$ , the axis of anisotropy ( $\theta = 0$ ) is the easy axis. If  $K_1 < 0$ , this axis is the hard one, and the plane  $\theta = \pi/2$  is the easy plane. The allowance for the anisotropy in this plane results in the appearance of some easy directions lying in it.

In the case of *cubic* crystals, we also limit ourselves, at first, to the constant  $K_1$ . Then, if  $K_1 > 0$ , the directions  $\langle 100 \rangle$  are the easy axes,<sup>2</sup> and the directions  $\langle 111 \rangle$  ( $\varphi = 45^\circ$ ,  $\theta = \arccos \sqrt{1/3} = 54^\circ 44'$ ) are the hard axes (Figure 2.1). If  $K_1 < 0$ , directions  $\langle 111 \rangle$  are the easy axes, and directions  $\langle 100 \rangle$  are the hard axes. When  $K_2 \neq 0$  but  $|K_2| < (9/4)|K_1|$ , the easy and hard directions are the same as in the case of  $K_2 = 0$ .

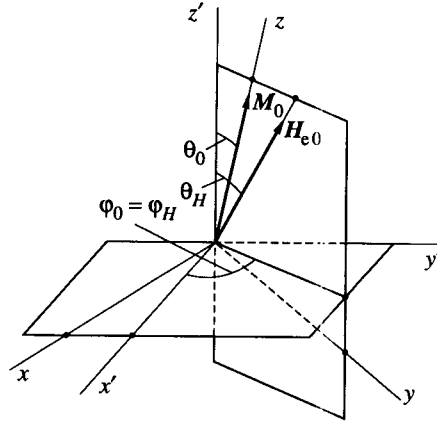
In reality, to find the equilibrium orientation of magnetization it is necessary, along with the energy of magnetocrystalline anisotropy, to take into account the Zeeman energy (2.15), the internal magnetic energy (2.16), and also elastic and magnetoelastic energies (Section 12.1) if the external elastic stresses are present. In doing so one can choose between two quite equivalent methods: to minimize the total energy or to use the condition (2.8).

It should be noted that the uniform magnetization of the whole sample is not always the equilibrium state. In the absence of an external magnetic field or in a weak field, a ferromagnetic sample (with not too small dimensions) is divided into domains (Section 8.1). In the present chapter we assume the external field to be high enough to magnetize the sample to saturation. And, if we consider ellipsoidal samples in a uniform external field, the equilibrium magnetization is also uniform.

Let us first examine a *sphere of uniaxial ferromagnet* (Figure 2.2). For spherical samples there is no shape anisotropy, and the equilibrium orientation of magnetization can be found by minimizing the sum  $U = U_{\text{an}} + U_Z$  where  $U_{\text{an}}$  is the magnetocrystalline energy (2.31), and  $U_Z$  is the Zeeman energy (2.26). The conditions for equilibrium are (2.22). From  $\partial U / \partial \varphi = 0$  it follows that  $\varphi_0 = \varphi_H$ . Limiting ourselves to the first term in (2.31) we obtain from  $\partial U / \partial \theta = 0$  an equation

$$H_{A1} \sin 2\theta_0 = H_{e0} \sin 2(\theta_H - \theta_0) \quad (2.34)$$

<sup>2</sup>The symbol  $\langle \rangle$  denotes one of the equivalent directions, e.g.,  $\langle 100 \rangle$  denotes one of the directions  $[100]$ ,  $[010]$ , and  $[001]$ . The symbol  $\{ \}$  denotes one of the equivalent planes, e.g., the plane  $\{100\}$  is one of the planes  $(100)$ ,  $(010)$ , and  $(001)$ .

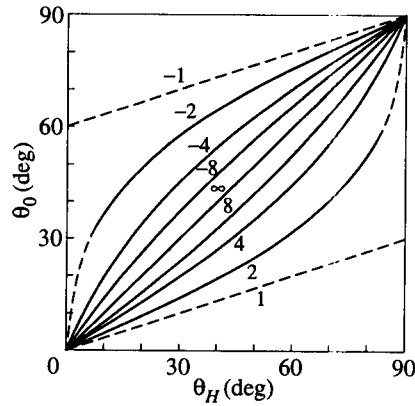


**FIGURE 2.2**  
Coordinate axes for a sphere of a uniaxial ferromagnet ( $K_1 < 0$ ).

where the following notation is introduced:

$$H_{A1} = \frac{K_1}{M_0}. \quad (2.35)$$

The analysis of (2.34) shows (Figure 2.3) that the orientations of  $M_0$  and  $H_{e0}$  coincide when  $H_{e0}$  is directed along the easy axis (if  $K_1 > 0$ ) or lies in the



**FIGURE 2.3**  
Equilibrium orientations of magnetization in a sphere of a uniaxial ferromagnet. Numbers at the curves indicate the  $H_{e0}/H_{A1}$  values. It has been taken  $H_{A1} = 4\pi M_0$ . Dashed lines show that the solution is not realized, because the assumed steady state (uniform magnetization) is not realized, and domains appear.

easy plane (if  $K_1 < 0$ ). When  $\mathbf{H}_{e0}$  is directed along the hard axis or lies in the hard plane, the orientations of  $\mathbf{M}_0$  and  $\mathbf{H}_{e0}$  coincide if  $H_{e0} > 2|H_{A1}|$ . But the condition of the uniformity of magnetization (Section 8.3) is in our case:  $H_{e0} > 2H_{A1} + (4\pi/3)M_0$ . Thus, in a *uniformly* magnetized sphere the  $\mathbf{M}_0$  direction coincides with the direction of  $\mathbf{H}_{e0}$  if the latter is oriented along an easy or a hard axis, or lies in an easy or a hard plane. For all other  $\mathbf{H}_{e0}$  orientations the direction of  $\mathbf{M}_0$  approaches the  $\mathbf{H}_{e0}$  direction asymptotically as  $H_{e0}$  increases (Figure 2.3).

The behavior of the steady magnetization  $\mathbf{M}_0$  in *cubic* crystals is analogous to the behavior of it in uniaxial crystals. Namely, when  $\mathbf{M}_0$  is uniform, its direction coincides with the direction of  $\mathbf{H}_{e0}$  if the latter is oriented along one of the axes  $\langle 100 \rangle$ ,  $\langle 110 \rangle$ , or  $\langle 111 \rangle$  and approaches the direction of  $\mathbf{H}_{e0}$  asymptotically with growing  $H_{e0}$  for all other orientations.

Let us discuss briefly the problem of *measurement* of the magnetocrystalline-anisotropy constants. Single-crystal samples in the form of ellipsoids should be used because in this case, the  $M_0$  value being known, the shape anisotropy can be taken into account. It is very convenient to use spherical samples, for which the shape anisotropy does not exist and, so, the knowledge of  $M_0$  is not obligatory. The samples must be turned around some axes, so that the  $\mathbf{M}_0$  vector will change its orientation with respect to the crystal axes. The values that are measured directly are either the torsion torques (e.g., [208, 70]) or the frequencies (or the steady magnetic fields at constant frequency) of ferromagnetic resonance. The latter case will be discussed in the next section.

---

### 2.3 Ferromagnetic resonance in a single crystal

Studying the influence of magnetocrystalline anisotropy on the magnetization oscillations in single crystals, we shall use, mainly, the method of effective demagnetization factors mentioned in Section 2.1. According to this method we represent the effective field of magnetocrystalline anisotropy (in the case of uniform magnetization):

$$\mathbf{H}_{\text{an}} = -\frac{\partial U_{\text{an}}}{\partial \mathbf{M}} \quad (2.36)$$

in the form

$$\mathbf{H}_{\text{an}} = -\vec{N}^{\text{an}} \mathbf{M}. \quad (2.37)$$

Two problems are to be solved: (i) calculation of permeability tensor  $\vec{\mu}$  components of a single-crystal ferromagnet, and (ii) derivation of ferromagnetic-resonance conditions for a small single-crystal ellipsoid.

Solving the *first problem*, we have to replace, according to Table 2.1, the transverse  $\vec{N}$  components in the formulae of Section 1.5 by the transverse components

of the tensor  $\vec{N}^{\text{an}}$ , and replace  $N_{33}$  by the sum  $N_{33} + N_{33}^{\text{an}}$ . The components of both tensors must be written in the same coordinate system, in which the third axis is directed along  $\mathbf{M}_0$ . Only in such system is it possible to express  $\mathbf{H}_{\text{an}}$  in the form (2.37). The direction of  $\mathbf{M}_0$  should be, of course, found beforehand.

The general expressions for the permeability-tensor components follow from (1.112) and (1.113):

$$\vec{\mu} = \begin{vmatrix} \mu_x & \mu_s + i\mu_a & 0 \\ \mu_s - i\mu_a & \mu_y & 0 \\ 0 & 0 & 1 \end{vmatrix} \quad (2.38)$$

$$\mu_{x,y} = 1 + \frac{\omega_M \omega_{x,y}}{\omega_0^2 - \omega^2} \quad \mu_s = \frac{\omega_M \omega_s}{\omega_0^2 - \omega^2} \quad \mu_a = \frac{\omega_M \omega}{\omega_0^2 - \omega^2} \quad (2.39)$$

where the frequency  $\omega_0$  has the form (1.115). The quantities  $\omega_{x,y,s}$  are determined (if dissipation is not taken into account) by the formulae (1.114), in which the above-mentioned replacements must be made. To take dissipation into account it is sufficient to replace  $\omega_H$  (in  $\omega_x$ ,  $\omega_y$ , and  $\omega_0$ ) by  $\omega_H + i\alpha\omega$ .

### 2.3.1 Sphere of a uniaxial ferromagnet

Turning to the *second problem*, consider first the ferromagnetic resonance in a *uniaxial ferromagnet*. We ignore the anisotropy in the basal plane and take into account only the first anisotropy constant  $K_1$ . Then

$$U_{\text{an}} = K_1 \sin^2 \theta_0 \equiv K_1 \left( 1 - \frac{M_{z'}^2}{M_0^2} \right) \quad (2.40)$$

where the  $z'$ -axis is the axis of anisotropy. We write down the  $x'$ ,  $y'$ , and  $z'$  components of the effective field (2.36) and pass then to the coordinate system  $x, y, z$ , in which the  $z$ -axis is directed along  $\mathbf{M}_0$  and the  $x$ -axis coincides with the axis  $x'$  (Figure 2.2). Then, we obtain, as it is easy to make sure,

$$\begin{aligned} H_{\text{an}x} &= 0 & H_{\text{an}y} &= \frac{2H_{A1}}{M_0} (M_z \cos \theta_0 - M_y \sin \theta_0) \sin \theta_0 \\ H_{\text{an}z} &= \frac{2H_{A1}}{M_0} (M_z \cos \theta_0 - M_y \sin \theta_0) \cos \theta_0 \end{aligned} \quad (2.41)$$

where  $\theta_0$  is the angle between the axes  $z$  and  $z'$ , and  $H_{A1}$  is determined by (2.35). Expressions (2.41) have the form (2.37). It should be noted that for small oscillations ( $M_{x,y} \ll M_z \cong M_0$ ) the field  $\mathbf{H}_{\text{an}}$  can be written in the form (2.37) even when we take into account the higher terms in (2.31). Taking into account two first terms, we obtain [266]

$$N_{11}^{\text{an}} = N_{12}^{\text{an}} = 0 \quad N_{22}^{\text{an}} = -\frac{2H_{A1}}{M_0} \sin^2 \theta_0 + \frac{4H_{A2}}{M_0} (2 \sin^2 \theta_0 - 3 \sin^4 \theta_0)$$

$$N_{33}^{\text{an}} = -\frac{2H_{A1}}{M_0} \cos^2 \theta_0 - \frac{4H_{A2}}{M_0} (\cos^2 \theta_0 - \cos^4 \theta_0) \quad (2.42)$$

where

$$H_{A2} = \frac{K_2}{M_0}. \quad (2.43)$$

(Other  $\vec{N}^{\text{an}}$  components do not enter the ferromagnetic-resonance formulae.)

Let us now derive the expression for the ferromagnetic-resonance frequency in a *sphere* of uniaxial single crystal. According to Table 2.1 we have to substitute the sums of the tensor  $\vec{N}$  components and the components (2.42) of the effective demagnetization tensor into (1.90) and (1.91). But for a sphere all  $\vec{N}$  components are the same, and they cancel out. Then,

$$\begin{aligned} \frac{\omega_0^2}{\gamma^2} &= [H_{e0z} + 2H_{A1} \cos 2\theta_0 + 4H_{A2} \sin^2 \theta_0 (1 + 2 \cos 2\theta_0)] \\ &\times [H_{e0z} + 2H_{A1} \cos^2 \theta_0 - 2H_{A2} \sin^2 2\theta_0] \end{aligned} \quad (2.44)$$

where  $H_{e0z} = H_{e0} \cos(\theta_0 - \theta_H)$ ; here  $\theta_H$  and  $\theta_0$  are the angles between the vectors  $\mathbf{H}_{e0}$  and  $\mathbf{M}_0$ , respectively, and the axis of anisotropy. The angle  $\theta_H$  is given, and  $\theta_0$  must be found by solving the problem of the equilibrium state discussed in Section 2.2.

We now show (taking into consideration, for simplicity, only the first anisotropy constant  $K_1$ ) that the expression (2.44) can be obtained by the method of spherical coordinates (Section 2.1) as well. The energy  $U$  in the Smit–Suhl formula (2.24) is now the sum of Zeeman energy and the energy of magnetocrystalline anisotropy. Using the equilibrium condition  $\varphi_0 = \varphi_H$ , we find from (2.24)

$$\frac{\omega_0^2}{\gamma^2} = [H_{e0} \cos(\theta_0 - \theta_H) + 2H_{A1} \cos 2\theta_0] H_{e0} \frac{\sin \theta_H}{\sin \theta_0}. \quad (2.45)$$

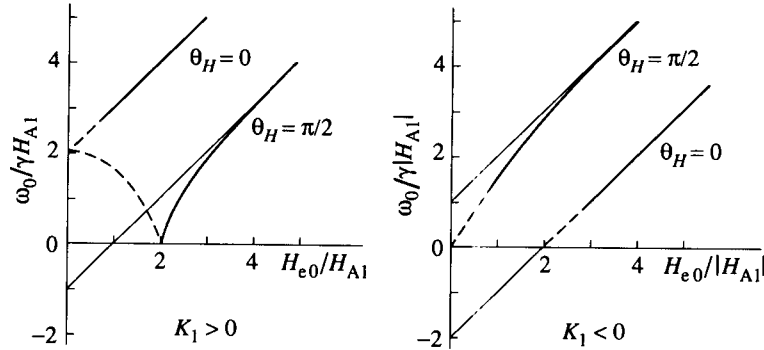
Using the second equilibrium condition (2.34), it is easy to show that (2.45) coincides with (2.44) if  $K_2 = 0$ . Thus, it is inadmissible to ignore the difference between  $\theta_0$  and  $\theta_H$  in (2.45) even if this difference is small.

However, in (2.44) we may assume  $\theta_0 = \theta_H$  in the case of small anisotropy. And if we disregard the terms of second order in the ratios  $H_{A1}/H_{e0}$  and  $H_{A2}/H_{e0}$ , the expression (2.44) takes the form

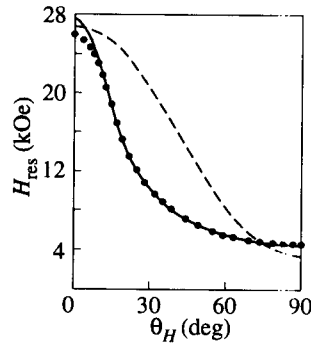
$$\frac{\omega_0}{\gamma} = H_{e0} + H_{A1} \left( \frac{1}{2} + \frac{3}{2} \cos 2\theta_H \right) + H_{A2} \left( -\frac{1}{4} + \cos 2\theta_H - \frac{3}{4} \cos 4\theta_H \right). \quad (2.46)$$

The results of calculation of the ferromagnetic-resonance conditions for a sphere of a uniaxial crystal with the use of (2.46), i.e., with the assumption  $\theta_0 = \theta_H$ , are shown in Figure (2.4).

The angular dependence of the resonance field (at  $\omega = \text{const}$ ), calculated *without* the assumption that the directions of  $\mathbf{M}_0$  and  $\mathbf{H}_{e0}$  coincide, is shown in

**FIGURE 2.4**

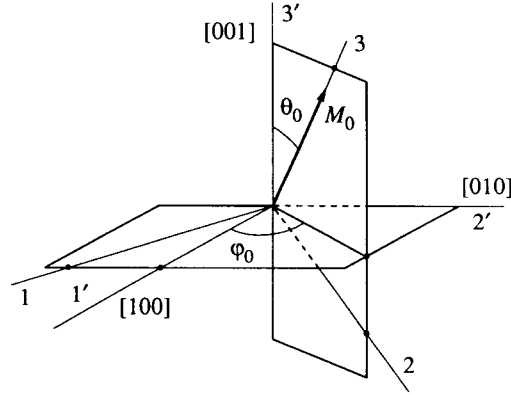
Ferromagnetic-resonance frequencies for a sphere of a uniaxial crystal, calculated by (2.48) with  $H_{A1} = 4\pi M_0$  and  $H_{A2} = 0$ . Dashed lines show that the calculation is not correct, because the assumed uniform magnetization is not realized.

**FIGURE 2.5**

Angular dependence of  $H_{res}$  for a sphere of a crystal with easy plane of anisotropy. Solid curve is calculated using (2.34) and (2.44) with  $g = 2.24$ ,  $H_{A1} = -8.3$  kOe, and  $H_{A2} = 0$ . Dashed curve is calculated by (2.46) with the same values of parameters. Points represent the experimental data for the ferrimagnet  $RbNiF_3$  at frequency of 31.4 GHz and temperature 78 K [143].

Figure 2.5; the result of calculation *with* this assumption and the experimental data are also plotted. One can see from this figure that for this crystal, with rather large anisotropy, the allowance for the difference between  $M_0$  and  $H_{e0}$  directions is necessary.





**FIGURE 2.6**  
Coordinate axes for a sphere of a cubic ferromagnet.

### 2.3.2 Sphere of a cubic ferromagnet

The derivation of the conditions for ferromagnetic resonance in cubic crystals leads to rather cumbersome calculations (e.g., [266]). Without dwelling on them, we shall cite the most important results.

If only the first constant  $K_1$  in (2.32) is taken into account, the components of the tensor of effective demagnetization factors  $\vec{N}^{\text{an}}$  have the form [266]

$$\begin{aligned}
 N_{11}^{\text{an}} &= -3 \frac{H_{A1}}{M_0} \sin^2 \theta_0 \sin^2 2\varphi_0 \\
 N_{22}^{\text{an}} &= -3 \frac{H_{A1}}{M_0} \sin^2 \theta_0 \left( 1 - \frac{1}{4} \sin^2 2\varphi_0 \right) \\
 N_{12}^{\text{an}} &= -3 \frac{H_{A1}}{M_0} \sin^2 \theta_0 \cos \theta_0 \sin 4\varphi_0 \\
 N_{33}^{\text{an}} &= \frac{H_{A1}}{M_0} (1 + \cos^2 2\theta_0 - \sin^4 \theta_0 \sin^2 2\varphi_0)
 \end{aligned} \tag{2.47}$$

(the coordinate axes are directed as in Figure 2.6). Substituting them for the tensor  $\vec{N}$  components in (1.90) and (1.91), we obtain the expression for the resonance frequency in a sphere of a cubic ferromagnet

$$\begin{aligned}
 \frac{\omega_0^2}{\gamma^2} &= \left\{ H_{e0z} + H_{A1} \right. \\
 &\quad \left. \times \left[ \frac{3}{2} + \frac{1}{2} \cos 4\theta_0 + \left( -\frac{15}{8} + 2 \cos 2\theta_0 - \frac{1}{8} \cos 4\theta_0 \right) \sin^2 2\varphi_0 \right] \right\}
 \end{aligned}$$

$$\times \left\{ H_{e0z} + H_{A1} \left[ 2 \cos 4\theta_0 + \left( \frac{1}{2} \cos 2\theta_0 - \frac{1}{2} \cos 4\theta_0 \right) \sin^2 2\varphi_0 \right] \right\} \\ - \frac{9}{4} H_{A1}^2 \sin^2 \theta_0 \sin^2 2\theta_0 \sin^2 4\varphi_0. \quad (2.48)$$

(According to Table 2.1, the components of the sum  $\vec{N}^{an} + \vec{N}$  should be substituted, but, for a sphere, the components of  $\vec{N}$  cancel out.)

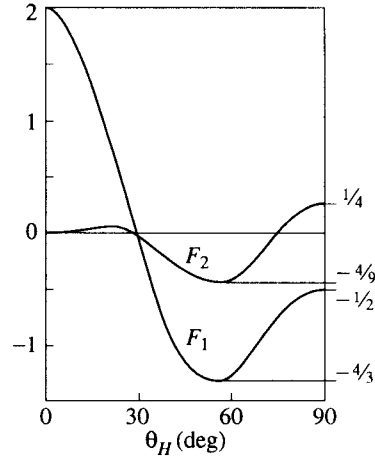
The most interesting is the case when the steady magnetization  $\mathbf{M}_0$  is in the  $\{110\}$  plane, in which all symmetry axes of a cubic crystal lie. We cite the resonance condition for this case ( $\varphi_0 = \pi/4$ ) taking into account two anisotropy constants [176]:

$$\frac{(\omega_0^2)_{\{110\}}}{\gamma^2} = \left[ H_{e0z} + H_{A1} \left( -\frac{3}{8} + 2 \cos 2\theta_0 + \frac{3}{8} \cos 4\theta_0 \right) \right. \\ \left. + H_{A2} \left( \frac{5}{8} + \frac{5}{4} \cos 2\theta_0 + \frac{9}{8} \cos 4\theta_0 \right) \sin^2 \theta_0 \right] \\ \times \left[ H_{e0z} + H_{A1} \left( \frac{1}{2} \cos 2\theta_0 + \frac{3}{2} \cos 4\theta_0 \right) \right. \\ \left. + H_{A2} \left( -\frac{7}{16} + \frac{3}{16} \cos 2\theta_0 \right) \sin^2 2\theta_0 \right]. \quad (2.49)$$

The formulae following from (2.49), in the particular cases when  $\mathbf{M}_0$  direction coincides with the symmetry axes, are given in Table 2.2. In this table  $H_{e0z}$  is replaced by  $H_{e0}$ , because the directions of  $\mathbf{M}_0$  and  $\mathbf{H}_{e0}$  coincide for the symmetry axes (if  $H_{e0}$  is large enough to assure the absence of domains). Attention should be paid to the difference in the structure between formula (2.52) and the first two formulae in Table 2.2. This is due to the fact that the directions  $\langle 100 \rangle$  and  $\langle 111 \rangle$  are the directions of extrema, whereas the  $\langle 110 \rangle$  direction is the saddle 'point' of the  $U_{an}(\theta, \varphi)$  surface.

**TABLE 2.2**  
Ferromagnetic-resonance frequencies for a sphere of a cubic crystal.

Direction of $\mathbf{M}_0$	$\theta_H$	$\frac{\omega}{\gamma}$	
$\langle 100 \rangle$	0	$H_{e0} + 2H_{A1}$	(2.50)
$\langle 111 \rangle$	$54^\circ 44'$	$H_{e0} - \frac{4}{3}H_{A1} - \frac{4}{9}H_{A2}$	(2.51)
$\langle 110 \rangle$	$90^\circ$	$[(H_{e0} - 2H_{A1})(H_{e0} + H_{A1} + \frac{1}{2}H_{A2})]^{1/2}$	(2.52)



**FIGURE 2.7**  
Functions defining the anisotropy of a cubic ferromagnet.

If the anisotropy is *small* ( $H_{A1}, H_{A2} \ll H_{e0}$ ), (2.49) can be written as

$$\frac{\omega_0}{\gamma} = H_{e0} + H_{A1}F_1(\theta_H) + H_{A2}F_2(\theta_H) \quad (2.53)$$

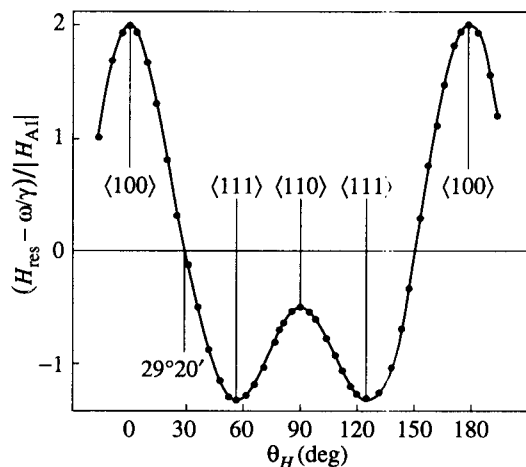
where (Figure 2.7)

$$F_1(\theta) = -\frac{3}{16} + \frac{5}{4} \cos 2\theta + \frac{15}{16} \cos 4\theta \quad (2.54)$$

$$F_2(\theta) = -\frac{7}{64} + \frac{5}{128} \cos 2\theta + \frac{15}{64} \cos 4\theta - \frac{21}{128} \cos 6\theta. \quad (2.55)$$

The angular dependence of the resonance field calculated with formulae (2.53) and (2.54) is plotted in Figure (2.8). The experimental results for YIG are also shown. One can see that in the present case of small anisotropy, sufficiently high frequency, and room temperature, neither  $K_2$  nor the difference between  $\theta_0$  and  $\theta_H$  must be taken into account.

An expression for the resonance frequency in the case, when  $M_0$  lies in the  $\langle 100 \rangle$  plane, can also be easily obtained from (2.48). The angular dependence of  $H_{res}$ , which was calculated disregarding  $K_2$  and the difference between  $\theta_0$  and  $\theta_H$ , is shown, for this case, in Figure 2.9. One can see from Figures 2.8 and 2.9 that in both planes there are directions in which  $H_{e0} = \omega/\gamma$ . When single-crystal spheres are used in microwave ferrite devices, it is reasonable to orient them so that  $M_0$  will coincide with one of these directions; then the resonance field is independent of  $K_1$  and, hence, of the temperature.



**FIGURE 2.8**

Angular dependence of  $H_{\text{res}}$  for a sphere of a cubic ferromagnet with  $K_1 < 0$ .  $\theta_H$  is the angle between  $\mathbf{H}_{e0}$  and the axis  $\langle 100 \rangle$  in the  $\{110\}$  plane. The curve is calculated by (2.53) at  $H_{A2} = 0$ . Points represent experimental data for a YIG sphere at a frequency of 9.3 GHz and at room temperature [159].

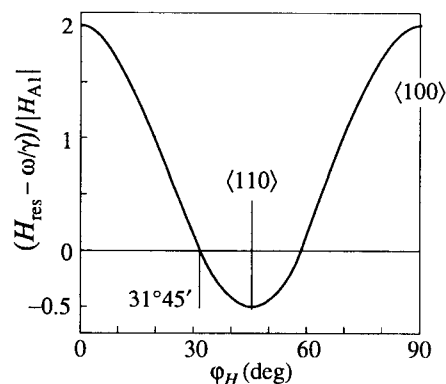
Consider now the case when  $\mathbf{M}_0$  lies in the  $\{111\}$  plane. It is easy to show that, if  $H_{A1} \ll H_{e0}$  and  $H_{A2} = 0$ , the  $\{111\}$  plane is approximately isotropic. The anisotropy in this plane arises, first, due to the influence of the effective demagnetization factor  $N_{12}^{\text{an}}$ , i.e., of the last term in (2.48), and, second, due to the influence of  $K_2$ . The  $\langle 111 \rangle$  axis is the sixth order axis of this anisotropy, and the expression for the resonance frequency of a sphere, when  $H_{A2} \ll H_{A1} \ll H_{e0}$ , takes the form [72]

$$\frac{\omega_0}{\gamma} = H_{e0} - \frac{1}{2}H_{A1} + \frac{1}{18}H_{A2} - \frac{1}{2}\frac{H_{A1}^2}{H_{e0}} + \left( -\frac{1}{2}\frac{H_{A1}^2}{H_{e0}} + \frac{7}{36}H_{A2} \right) \cos 6\psi_0 \quad (2.56)$$

where  $\psi_0$  is the angle between  $\mathbf{M}_0$  and the  $\langle 110 \rangle$  axis in the  $\{111\}$  plane. The general case of  $\mathbf{M}_0$  lying in an arbitrary plane of a cubic crystal was treated by Yakovlev and Burdin [453].

### 2.3.3 Simultaneous allowance for different kinds of anisotropy

In the problems discussed above the sample was a sphere, and only one kind of magnetocrystalline anisotropy, uniaxial or cubic, was taken into account. But often we have to consider simultaneously the shape anisotropy and one or more kinds of magnetocrystalline anisotropy. A typical example is the single-crystal YIG *film* grown epitaxially on a paramagnetic substrate. In such films there appears a growth anisotropy, usually the uniaxial, with the axis directed along the



**FIGURE 2.9**

Angular dependence of  $H_{\text{res}}$  for a sphere of a cubic ferromagnet with  $K_1 < 0$ .  $\varphi_H$  is the angle between  $\mathbf{H}_{e0}$  and the axis  $[100]$  in the  $(100)$  plane. The curve is calculated by (2.48) with  $\theta_0 = \pi/2$ , and  $H_{A1} \ll H_{e0}$  (so that  $H_{e0z} \simeq H_{e0}$  and  $\varphi_0 \simeq \varphi_H$ ).

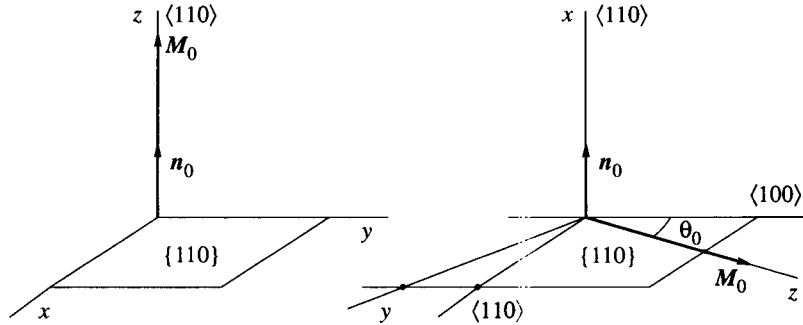
normal to the film surface.

Both methods, of effective demagnetization factors and of spherical coordinates (Section 2.1), can be used to study the simultaneous influence of several kinds of anisotropy. Using the first method, we have to assume the effective demagnetization factors to be the sums of such factors for all kinds of anisotropy. When the second method is used, the energy  $U$  in (2.24) and (2.25) must be the sum of the Zeeman energy and the energies of all considered kinds of anisotropy (except the shape anisotropy if we want to find the tensor  $\vec{\chi}$ ). It should be noted that from the additivity of energies, or effective demagnetization factors for different kinds of anisotropy, the additivity of their contributions to resonance frequency or resonance field does not follow, in general. One can see this, e.g., from formulae (1.90) or (2.24). But the additivity takes place *approximately* in the case of small contributions.

The calculations of the tensor  $\vec{\chi}$  or  $\vec{\chi}^e$  components and of the resonance fields or frequencies, in the presence of different kinds of anisotropy, by the method of effective demagnetization factors are usually cumbersome because one has to write down the components of all effective demagnetization tensors in the same coordinate system. We will limit ourselves to one simple example.

Let us find the ferromagnetic-resonance condition for a *thin film of a cubic ferromagnet* magnetized normally or tangentially to the surface of the film, which coincides with the  $\{110\}$  plane. We take into account only the first cubic anisotropy constant  $K_1^c$  and the constant  $K_1^u$  of the uniaxial growth anisotropy with the axis normal to the film surface.

If the film is *normally* magnetized and assumed to be infinitely thin, the shape

**FIGURE 2.10**

Coordinate axes for a film of a cubic single crystal magnetized normally and tangentially to its surface.  $\mathbf{n}_0$  is a unit vector of the normal to the film surface.

demagnetization factors, in the axes shown in Figure 2.10, are:  $N_{11} = N_{22} = N_{12} = 0$ ,  $N_{33} = 4\pi$ . To find the effective demagnetization factors of the cubic anisotropy we have to take in (2.47)  $\varphi_0 = \pi/4$  and  $\theta_0 = \pi/2$ . Then we get:  $N_{11}^c = -3H_{A1}/M_0$ ,  $N_{22}^c = N_{12}^c = 0$ ,  $N_{33}^c = -H_{A1}/M_0$ . To get the effective demagnetization factors of the uniaxial growth anisotropy, we must take  $\theta_0 = 0$  in (2.42):  $N_{11}^u = N_{22}^u = N_{12}^u = 0$ ,  $N_{33}^u = -2H_{Au}$ , where  $H_{Au} = K_1^u/M_0$ . Substituting the sums of these factors for the corresponding  $\bar{N}$  components in (1.90), we obtain the ferromagnetic-resonance frequency in a normally magnetized film. We write the approximate expression for it in the case of small cubic anisotropy ( $H_{A1} \ll H_{e0}$ ):

$$\frac{\omega}{\gamma} = H_{e0} - 4\pi M_0 + 2H_{Au} - \frac{1}{2}H_{A1}. \quad (2.57)$$

For a film magnetized *tangentially*, at an angle  $\theta$  with the  $\langle 100 \rangle$  axis, the shape demagnetization factors are:  $N_{11} = 4\pi$ ,  $N_{22} = N_{12} = N_{33} = 0$ . To find the effective demagnetization factors of cubic anisotropy it is sufficient to take  $\varphi_0 = \pi/4$  in (2.47). The effective demagnetization factors of uniaxial anisotropy are:  $N_{11}^u = -2H_{Au}/M_0$ ,  $N_{22}^u = N_{12}^u = N_{33}^u = 0$ . The expression for the resonance frequency is obtained by substituting the sums of these demagnetization factors into (1.90). We write it again in the case of small cubic anisotropy:

$$\frac{\omega}{\gamma} = \sqrt{H_{e0}(H_{e0} - 4\pi M_0 + 2H_{Au})} + H_{A1}F_1(\theta) \quad (2.58)$$

where  $F_1(\theta)$  is given by (2.54). If  $H_{e0}$  and  $M_0$  are directed along  $\langle 110 \rangle$  axis,  $F_1 = 1/2$ .

The measurement of the angular dependence of ferromagnetic-resonance field is the most precise and widely used technique for studying the magnetocrystalline anisotropy. From this dependence the values of  $g$ -factor and anisotropy constants

can be found, as well as the magnetization  $M_0$  if a non-spherical sample is used. For weakly conducting substances, spherical samples are usually applied; if only the cubic anisotropy is present and two constants are enough to describe it, then these constants and the  $g$ -factor can be found from the measurement of resonance field in three  $H_{e0}$  directions, as in Table 2.2.

For a film grown so that its surface is the  $\{110\}$  plane, two cubic anisotropy constants can be found at tangential magnetization of the film. If the resonance field at normal magnetization is measured, too, and there is no uniaxial anisotropy, the value of  $M_0$  can be found. In the presence of this anisotropy, only the quantity  $M_0 - K_1^u/(2\pi M_0)$  can be found, as one can see from (2.57) and (2.58).

The values of the anisotropy constants, found in ferromagnetic-resonance experiment, do not coincide, in general, with the values found from static measurement. One reason, already mentioned in Section 2.1, is the difference between the contributions of magnetostriction stresses in these two cases. The second reason is the difference in contributions of the so-called fast-relaxing ions (Section 13.2). However, for ferrites with small anisotropy used in microwave devices, e.g., for YIG, both mentioned contributions are small, and the difference between the values of anisotropy constants, found by resonance and by static methods, is negligible.

## 2.4 Ferromagnetic resonance in a polycrystal

A polycrystal is an assembly of small single crystals (grains) irregular in shape, with dimensions of  $10^{-4}$  to  $10^{-2}$  cm. There are cavities (pores) between them, which occupy often an essential part of the entire volume. Crystal axes of the grains are usually oriented randomly. Only when special measures are taken in preparation of polycrystalline samples, e.g., pressing or thermal treatment in a magnetic field, the uniformity of the angular distribution of grains is broken. The properties of such *textured* polycrystals approach more or less the properties of single crystals.

We will consider only polycrystals without texture, which are, on the average, isotropic. For such media any tensor parameter, in particular, the magnetic susceptibility, has the form

$$\vec{\chi} = \begin{vmatrix} \chi & i\chi_a & 0 \\ -i\chi_a & \chi & 0 \\ 0 & 0 & \chi_{\parallel} \end{vmatrix} \quad (2.59)$$

where the third axis coincides with the preferred direction, in our case, with the direction of the steady magnetization  $M_0$ . Thus, all high-frequency properties of a polycrystalline ferromagnet are determined by three quantities:  $\chi$ ,  $\chi_a$ , and  $\chi_{\parallel}$ . In sufficiently high magnetic fields, when the material is magnetized to saturation,  $\chi_{\parallel}$  is either equal to zero or has a small, non-resonant value (Section 1.4). So, to

describe the high-frequency properties of a polycrystal only two quantities,  $\chi$  and  $\chi_a$ , are usually needed. But since the polycrystal is a very complicated system, the dependence of its parameters  $\chi$  and  $\chi_a$  on frequency and steady magnetic field differs materially from such dependence for a truly isotropic medium treated in Chapter 1.

#### 2.4.1 Independent-grain and strongly-coupled-grain approximations

At the very beginning of the ferromagnetic-resonance investigations, Van Vleck [418] proposed to regard a polycrystal as an ensemble of independent (non-interacting) grains, the resonance condition in each grain depending on the orientation of the crystal axes of the grain with respect to the external magnetic field. The applicability of such a model is based on two assumptions: disregard of the interactions between the magnetization oscillations in different grains and neglect of the influence of the shapes of grains and pores. A system in which these assumptions are strictly satisfied is an assembly of single-crystal spheres situated in a non-magnetic medium far from one another.

But suppose that the following condition holds:

$$H_A \gg 4\pi M_0 \quad (2.60)$$

where  $H_A$  is some anisotropy field, e.g.,  $H_{A1}$  if the higher-order anisotropy constants are not larger than  $K_1$ . Then both mentioned assumptions are satisfied approximately, and the model of independent grains can be applied.

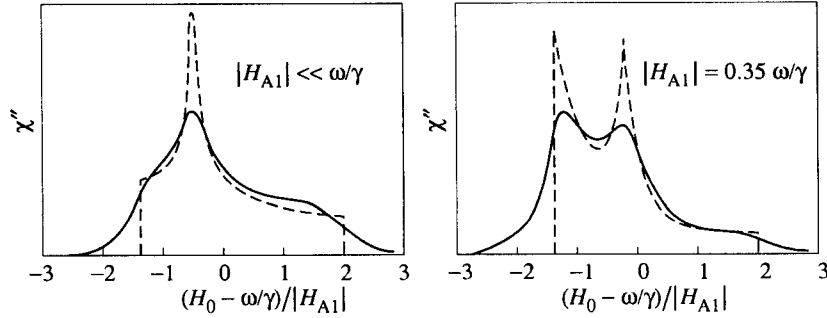
To calculate  $\chi$  and  $\chi_a$  for a polycrystal on the independent-grain model, we should write the expressions for  $\chi^e$  components in a grain with arbitrary shape and orientation and average them. Such calculations are very difficult, if realizable, especially if the finite linewidths  $(\Delta H)_0$  of the grains are taken into account. Therefore, Schlömann [339] supposed that  $(\Delta H)_0 = 0$  and limited himself to the calculation of  $\chi''$ . Assuming a uniform distribution of grains over the orientations (a non-textured polycrystal), he obtained

$$\chi''(\omega, H_0) = \frac{\pi M_0}{4} \int_{\theta=-\pi/2}^{\pi/2} \int_{\varphi=0}^{2\pi} \delta [H_0 - H_{\text{res}}(\omega, \theta, \varphi)] \sin \theta d\theta d\varphi \quad (2.61)$$

where  $H_{\text{res}}(\omega, \theta, \varphi)$  is the resonance field of a grain, and  $\delta(x)$  is the Dirac delta function (Appendix C).

The integral in (2.61) is the distribution function  $w(H_0)$  of the grains over the values of  $H_0$ . The following properties of such functions turned out to be useful in calculating  $\chi''$ : the discontinuities of  $w(H_0)$  take place at the extrema of  $H_{\text{res}}(\theta, \varphi)$ , and the logarithmic singularities appear at the saddle points of  $H_{\text{res}}(\theta, \varphi)$ . If, for a cubic crystal,  $K_1 < 0$  and other anisotropy constants can be neglected,  $w(H_0) \neq 0$  in the range from  $H_{\text{min}} = \omega/\gamma - (4/3)|H_{A1}|$  to  $H_{\text{max}} = \omega/\gamma + 2|H_{A1}|$  (Figure 2.8), and the peak of  $w(H_0)$  appears at  $H_0 = \omega/\gamma - (1/2)|H_{A1}|$ .



**FIGURE 2.11**

Ferromagnetic-resonance curves for a sphere of a cubic polycrystal with  $K_1 < 0$  calculated in the independent-grain approximation. Dashed curves correspond to  $(\Delta H)_0 = 0$  [339], and solid curves, to a finite  $(\Delta H)_0$  value, where  $(\Delta H)_0$  is the intrinsic linewidth of grains.

The calculated curves  $\chi''(H_0)$  are plotted in Figure 2.11. The allowance for a finite  $(\Delta H)_0$  results in smoothing out the singularities of these curves (Figure 2.11). But even then the resonance curve of a polycrystal, calculated on the model of independent grains, differs essentially from the resonance curve of an isotropic ferromagnet or a single crystal: it has ledges on the slopes and, if the anisotropy is large enough, has two maxima. These peculiarities were observed in ferrites with very large anisotropy, for which the condition (2.60) was satisfied [341]. They were also observed in ferrites with compensation points (Section 3.3) near these points [337] where the condition (2.60) holds as well.

When  $(\Delta H)_0$  is sufficiently small, the linewidth of a polycrystal, in the independent-grain approximation, as one can see from Figure 2.11, is

$$(\Delta H)_{\text{an}} \sim \frac{2K_1}{M_0} \quad (2.62)$$

and the shift of the resonance-curve maximum is

$$(\delta H)_{\text{an}} \sim \frac{1}{2} \frac{K_1}{M_0}. \quad (2.63)$$

For most polycrystalline ferromagnetic and ferrimagnetic materials the condition (2.60) does not hold, the experimental resonance curves do not have the specific shapes as in Figure 2.11, and their widths are much less than it follows from (2.62). The main reason for this is that the magnetization oscillations in different grains are *coupled* with each other by the alternating demagnetization fields. It leads to the 'dipole narrowing' of the resonance curves, i.e., to the appearance of the factor

$$\xi_d = \frac{|H_{A1}|}{4\pi M_0} \quad (2.64)$$

in expression (2.62). This factor is usually much less than unity for ferrites applied in microwave devices. The model of strongly coupled grains is more suitable for such materials. The polycrystal is regarded then as a *uniform* medium, subjected to a *nonuniform* effective field, which simulates different orientations of the grain axes. This field leads to the coupling of the initial uniform mode, excited by the external field, with other (non-uniform) modes. The coupling results in the transfer of energy from the initial mode to other modes and, hence, in the broadening of the resonance line of the initially excited mode. The theory of such process will be studied in detail in Section 11.3. It yields, for polycrystals, the  $\Delta H$  values that agree on the order of magnitude with the result of multiplying (2.62) by the factor (2.64).

#### 2.4.2 Influence of porosity

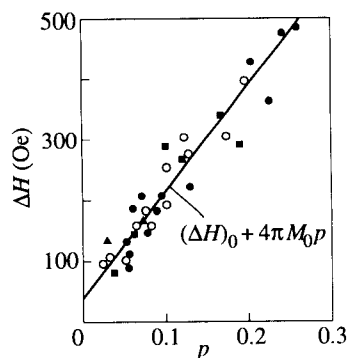
Pores and, in some cases, inclusions of other phases are an important cause of broadening of resonance curves in polycrystals. Porosity is the main reason why  $\Delta H$  values of polycrystalline YIG samples (usually, as large as  $\sim 50$  Oe) exceed considerably the contribution of anisotropy. Both models discussed above may be used to explain the influence of pores: the model of independent, in the present case, not grains but *regions*, and the model of non-uniform perturbation field, which leads to the coupling of *different modes*. We may assume (as a rough estimation based on the independent-region model) that, on the order of magnitude, the linewidth is equal to the demagnetization field of pores, averaged over the sample. This assumption leads to an approximate expression

$$(\Delta H)_p \simeq 4\pi M_0 p \quad (2.65)$$

where  $p = V_p/V_0$  is the porosity,  $V_p$  is the entire volume of all pores, and  $V_0$  is the volume of the sample. The calculation carried out by Schlömann (cited in [377]) on the model of a spherical pore in the center of a spherical sample results in an expression that differs from (2.65) by a factor of  $\sim 1.5$ . This calculation yields also the shift of the resonance-curve maximum

$$(\delta H)_p \simeq \frac{4\pi}{3} M_0 p. \quad (2.66)$$

In Figure 2.12 the values of  $(\Delta H)_p$  are plotted vs porosity for a great number of YIG spheres. The spread of points in the figure, which is due to the difference in dimensions and shapes of pores, is rather large. Nevertheless, the experimental data in Figure 2.12, as well as the data of numerous other experiments, are in agreement with the result (2.65) of the estimate based on the model of independent regions. In reality, the magnetization oscillations in different regions of a porous sample are, of course, not independent, and the model of strongly coupled regions should be used. But in the case of porosity, the results of calculations based on this model (Section 11.3) coincide on the order of magnitude with the above-mentioned estimate on the basis of the independent-region model. The reason is

**FIGURE 2.12**

Dependence of  $\Delta H$  on porosity for YIG polycrystalline spheres [160]. Different marks represent experimental points for spheres prepared by different methods. Measurements were made at frequency of 9 GHz and room temperature.

that, in the case of porosity, both the numerator and the denominator of the factor that represents the dipole narrowing contain, as distinct from (2.64), the values of the same order of  $\pi M_0$ .

It follows from (2.65) and from Figure 2.12 that the contribution of porosity to the linewidth of polycrystalline samples can be very large even in the materials with not very high magnetization. Only in very dense samples ( $p \ll 1\%$ ), can this contribution be made small. And if measures are taken simultaneously to diminish the contribution of anisotropy and the internal linewidth of grains, then very small values of  $\Delta H$  can be obtained in polycrystalline samples, e.g.,  $\Delta H \sim 1$  Oe in YIG [311].



# 3

---

## *Antiferromagnets and ferrites*

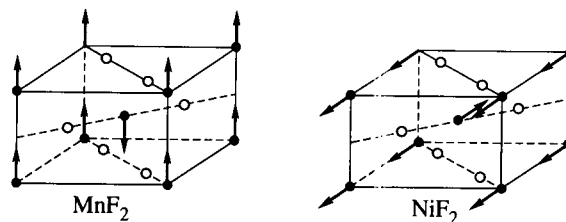
---

### 3.1 Antiferromagnetism and ferrimagnetism

*Antiferromagnets* are defined as substances in which the elementary magnetic moments are ordered, but the spontaneous (in the absence of an external magnetic field) magnetic moment of an elementary magnetic cell (and, hence, the moment of any macroscopic region) is either equal to zero or has a small value, as compared to the sum of elementary magnetic moments. The possibility of the existence of a small moment is included into this definition because the substances with an antiferromagnetic type of magnetic ordering but with a small average moment—the so-called *weak ferromagnets*—are usually related to antiferromagnets. In many antiferromagnets the elementary magnetic cell contains equal numbers of the same magnetic moments aligned in opposite directions. The static and dynamic magnetic susceptibilities of an antiferromagnet are small and (in single crystals) highly anisotropic.

In *ferrimagnets* the magnetic ordering is of the same type as in antiferromagnets. But the magnetic moment of an elementary magnetic cell has a great value, smaller than but comparable to the sum of elementary moments. The elementary magnetic cell of a ferrimagnet contains, in the simplest case, two groups of elementary magnetic moments directed in opposite sides. The numbers of the moments, or their values, or both are not equal to each other. The static and the dynamic susceptibilities of a ferrimagnet, in contrast to antiferromagnets, are of the same order as for ferromagnets.

The cause of ordering of magnetic moments in antiferromagnets and ferrimagnets is the *exchange* interaction of spins (Section 1.1). The exchange integrals in (1.26), corresponding to interactions between different moments, may have different signs. But the sign of the integral which corresponds to the strongest of these interactions should be *negative*, to stimulate the antiparallel orientation of the moments. The exchange interaction in antiferromagnets and ferrimagnets, as well as in most ferromagnets, is mainly *indirect*. In nonmetallic crystals the indirect exchange interaction via anions plays the main role [18].



**FIGURE 3.1**

Magnetic structures of tetragonal antiferromagnets [29]. Full circles are  $\text{Mn}^{2+}$  and  $\text{Ni}^{2+}$  ions, open circles are  $\text{F}^-$  ions. The  $\text{Ni}^{2+}$  magnetic moments are slightly noncollinear.

At temperatures higher than the Neel temperature<sup>1</sup>  $T_N$ , magnetic order in antiferromagnets and ferrimagnets is destroyed by thermal motion, and these substances become paramagnets.

### 3.1.1 Crystal and magnetic structures

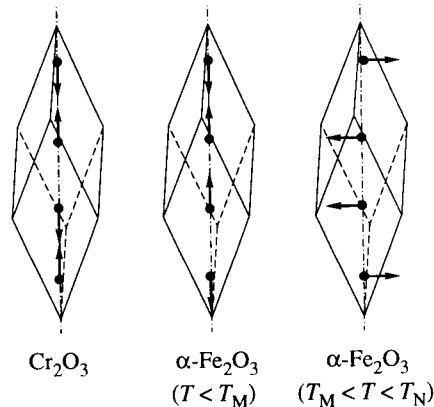
The idea of *antiferromagnetic ordering* was proposed independently by Landau and Neel as a hypothesis used to explain the unusual properties of some 'paramagnetic' crystals. Landau [240] suggested the model of *layers* of magnetic moments directed in opposite sides. Neel proposed the '*staggered*' order, in which the nearest neighbors of each moment are oriented opposite to it. The magnetic neutronography (e.g., [29]) proved the reality of antiferromagnetic ordering and allowed the determination of magnetic structures of many substances. It became clear that both types of antiferromagnetic order, the layered and the staggered, as well as many more complicated types of magnetic order, do exist.

For example, in an antiferromagnetic crystal  $\text{MnF}_2$ , which has the body-centered tetragonal lattice (Figure 3.1), the moments at the apices and in the center of an elementary cell, directed along the fourth-order axis, are antiparallel to each other. So, the Neel order is realized. The same order takes place in another tetragonal antiferromagnet,  $\text{NiF}_2$  (Figure 3.1), but the moments lie now in the basal (perpendicular to the fourth-order axis) plane. Furthermore, the angle between the moments at the apices and in the center of the cell, in  $\text{NiF}_2$ , differs slightly from  $\pi$ . So, a small spontaneous magnetization arises, and this antiferromagnet belongs to the above-mentioned weak ferromagnets.

Magnetic structures of some trigonal antiferromagnets are shown in Figure 3.2. For one of them, the hematite  $\alpha\text{-Fe}_2\text{O}_3$ ,<sup>2</sup> a phase transition (the change of the magnetic-moment direction) occurs at the temperature  $T_M = 250$  K (the Morin point). In the temperature range  $T_M < T < T_N$ ,  $\alpha\text{-Fe}_2\text{O}_3$  is a weak ferromagnet.

<sup>1</sup>The ordering temperature for *ferrimagnets* is referred sometimes to as Curie temperature.

<sup>2</sup>The cubic modification of the ferric oxide,  $\gamma\text{-Fe}_2\text{O}_3$ , is a ferrimagnet.

**FIGURE 3.2**

Magnetic structures of trigonal antiferromagnets [29]. Full circles are  $\text{Cr}^{3+}$  and  $\text{Fe}^{3+}$  ions, anions are not shown. The  $\text{Fe}^{3+}$  magnetic moments at  $T_M < T < T_N$  are slightly noncollinear.

Another trigonal antiferromagnet  $\text{MnCO}_3$  is a weak ferromagnet in the whole range of magnetic ordering,  $T < T_N$  [60].

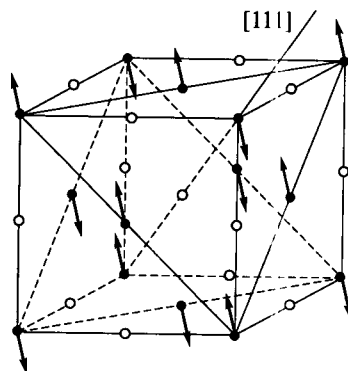
An example of antiferromagnets with the Landau ordering is the cubic crystal (with small trigonal distortions below the Neel temperature)  $\text{MnO}$  (Figure 3.3). In this antiferromagnet, unlike those shown in Figures 3.1 and 3.2, magnetic ordering results in the *doubling* of the dimensions of the magnetic elementary cell, as compared with the crystallographic (or crystallochemical) cell.

Most ferrimagnets, as well as most antiferromagnets, are ionic crystals. The base of their crystal structure is the lattice of anions. Cations are located in the voids between them. Voids occupied by cations are called cation positions (or *sites*). They differ in the number  $N$  of the nearest-neighbor anions. If  $N = 4$ , these anions form a more or less regular tetrahedron, and the site is called tetrahedral. If  $N = 6$ , the site is called octahedral, and if  $N = 8$ , dodecahedral. The same ions can be in different sites, and different ions can be distributed, randomly or in regular manner, over the same sites.

Ferrimagnets, or ferrites,<sup>3</sup> with two cubic crystal structures, spinels and garnets, and some hexagonal structures are most widely used in engineering and science.

Ferrites  $\text{M}^{2+}\text{Fe}_2^{3+}\text{O}_4$  have the *spinel* structure (e.g., [236]). The cation  $\text{M}^{2+}$  can be Ni, Co, Fe, Mg, Mn or a combination of ions, as  $\text{Li}_{0.5}^+\text{Fe}_{0.5}^{3+}$ . Other trivalent ions, as  $\text{Cr}^{3+}$  and  $\text{Al}^{3+}$ , can be substituted for  $\text{Fe}^{3+}$ . Anions in spinel structure form a close-packed cubic lattice with tetrahedral and octahedral voids. The

<sup>3</sup>Ferrites, in a narrow sense, are the combinations  $\text{MFe}_2\text{O}_4$ , where M is a divalent ion. But this term is often used, in a broader sense, for any nonmetal ferrimagnets (and sometimes, nonmetal ferromagnets, as well).



**FIGURE 3.3**

Magnetic structure of antiferromagnet MnO [29]. Full circles are  $\text{Mn}^{2+}$  ions, open circles are  $\text{O}^{2-}$  ions. Magnetic moments lie in  $\{111\}$  planes. Small contraction in the  $\langle 111 \rangle$  direction (in magnetically ordered state) is not shown.

number of occupied tetrahedral voids (so-called A-sites) is half the number of occupied octahedral voids (B-sites). As a result, a rather complicated cubic lattice is formed with a cubic elementary cell containing eight formula units  $\text{MFe}_2\text{O}_4$ . For oxygenous spinels, the size of elementary cell (the lattice constant)  $a \cong 8.5 \text{ \AA}$ . The local symmetry is cubic in tetrahedral sites and is trigonal in octahedral sites. In the latter case there are four nonequivalent sites, which differ from each other in the direction of the third-order local axis.

The distribution of cations over the sites in spinels is usually written in the form  $(\text{M}_x\text{Fe}_{1-x})[\text{M}_{1-x}\text{Fe}_{1+x}\text{O}_4]$  where parentheses include the ions on tetrahedral sites and brackets, the ions on octahedral sites. If  $x = 1$ , the spinel is called *normal*, and if  $x = 0$ , it is called (completely) *inversed*. All ferrimagnetic oxide spinels are completely or partly inversed. Chalcogenide ferromagnets  $\text{M}'\text{Cr}_2\text{X}_4$  ( $\text{X} = \text{S}, \text{Se}$ ;  $\text{M}' = \text{Cd}, \text{Hg}$ ) have normal spinel structure [417]. Normal oxide spinels ( $\text{M} = \text{Zn}, \text{Cd}$ ) and normal chalcogenide spinel  $\text{ZnCr}_2\text{Se}_4$  are antiferromagnets.

The cubic *garnet* structure (e.g., [138]) is even more complicated than the spinel structure. A cubic elementary cell, with the edge larger than  $12 \text{ \AA}$  ( $12.376 \text{ \AA}$  for yttrium iron garnet or YIG), contains eight formula units  $\text{R}_3\text{Fe}_5\text{O}_{12}$  where R is a trivalent rare-earth or yttrium ion. There are three types of cation sites in the garnet lattice: tetrahedral sites with tetragonal local symmetry, four nonequivalent octahedral sites with trigonal local symmetry, and six nonequivalent dodecahedral sites with orthorhombic symmetry. The distribution of ions over the sites in YIG is  $\{\text{Y}_3\}(\text{Fe}_3)[\text{Fe}_2]\text{O}_4$  where braces include ions on dodecahedral sites.

The ferrites  $\text{M}''\text{Fe}_{12}\text{O}_{19}$ ,  $\text{M}''_2\text{M}_2\text{Fe}_{12}\text{O}_{22}$ , and some others [229, 389] (where  $\text{M}''$  is a big divalent ion, as Ba, Sr, Pb, and M is one of the divalent ions listed above) are highly anisotropic *hexagonal* ferrimagnets. The dimensions of their



elementary cells along the main axis are  $\sim 50 \text{ \AA}$ , while the transverse dimensions are on the order of  $5 \text{ \AA}$ .

The strongest exchange interaction in the considered ferrimagnets is the indirect interaction between cations on tetrahedral and on octahedral sites. The effective exchange integral of this interaction is negative, which leads to antiparallel orientation of the magnetic moments of these ions. Other exchange interactions may be either ferromagnetic or antiferromagnetic.

The phenomenological, quasiclassical treatment of antiferromagnets and ferrimagnets is based on the *sublattice model* proposed by Neel [296]. According to this model, we combine into sublattices all elementary magnetic moments which are situated on identical lattice sites and are parallel to each other. The magnetizations of the sublattices are defined as

$$M_j = \frac{1}{\delta V} \sum_f \langle \hat{\mathfrak{M}}_{j f} \rangle \quad (3.1)$$

where  $\langle \hat{\mathfrak{M}} \rangle$  is the quantum-mechanical average of the elementary magnetic moment in the  $j$ th sublattice, and the summation is performed over all such moments in a small volume  $\delta V$ . The total magnetization is

$$M = \sum_{j=1}^N M_j \quad (3.2)$$

where  $N$  is the number of sublattices.

The fitness of this model is not obvious. It is proved, in addition to some quantum-mechanical considerations, by the agreement of numerous results, obtained on the base of this model, with experimental data.

The *number of sublattices*  $N$  should be equal to the number of magnetic ions in the *primitive* magnetic cell (i.e., in the elementary magnetic cell of the smallest volume). For example,  $N = 2$  for the antiferromagnets  $\text{MnF}_2$  and  $\text{NiF}_2$  (Figure 3.1), and  $N = 4$  for the trigonal antiferromagnets shown in Figure 3.2. For crystals with more complicated magnetic structures, the number of sublattices can be rather large. For example, in YIG the primitive magnetic cell (the volume of which is half the volume of the above-mentioned cubic elementary cell) contains  $20 \text{ Fe}^{3+}$  ions, and such must be the number of sublattices.

However, to describe approximately certain properties of antiferromagnet or ferrimagnet, some sublattices can be combined with each other. In particular, we can combine in one sublattice all moments with the same orientation or the moments on the same sites, in spite of their different orientations. Eventually, we obtain two sublattices. The *two-sublattice* model is strict only for antiferromagnets with two magnetic ions in a primitive magnetic cell, as  $\text{MnF}_2$  and  $\text{NiF}_2$ . But this model is often used in approximate treatment of more complicated substances. For YIG,  $12 \text{ Fe}^{3+}$  ions on tetrahedral sites and 8 such ions on octahedral sites can be combined, in considering some problems, into two sublattices with antiparallel orientations.

### 3.1.2 Equations of motion and energy terms

The theory of antiferromagnets and ferrimagnets, based on the sublattice model, can be constructed in a way analogous to the continual theory of ferromagnets (Section 2.1). The expression for the energy density  $U$ , depending on all the vectors  $M_j$ , is the initial point. It is reasonable to suggest that the *Landau-Lifshitz equations* hold for the sublattice magnetizations, too:

$$\frac{\partial M_j}{\partial t} = -\gamma_j M_j \times H_{\text{eff}j} + R_j \quad (3.3)$$

where  $\gamma_j$  are the magneto-mechanical ratios, different, in general, for different sublattices, and  $H_{\text{eff}j}$  are the effective fields acting on the sublattices, which are defined by the expressions analogous to (2.7) but with substitution of  $M_j$  for  $M$ . The dissipative terms  $R_j$  can be written in one of the forms considered in Section 1.4. The Gilbert form, as in (1.62), is the most convenient because it does not contain the effective fields.

The uniform part of the *exchange energy* can be written now as

$$U_{\text{ex}0} = -\frac{1}{2} \sum_{j=1}^N \sum_{j'=1}^N \Lambda_{jj'} M_j M_{j'} \quad (3.4)$$

where the constants  $\Lambda_{jj'}$  represent the exchange interactions between sublattices ( $j \neq j'$ ) and inside them ( $j = j'$ ). We regard these constants as scalars, attributing the anisotropic (usually, small) part of the exchange energy to the energy of anisotropy. The effective field of the exchange interaction that acts on the  $j$ th sublattice is

$$H_{\text{ex}0j} = \sum_{j'=1}^N \Lambda_{jj'} M_{j'}. \quad (3.5)$$

If  $\Lambda_{jj'} > 0$ , the exchange interaction between  $j$ th and  $j'$ th sublattices stimulates ferromagnetic ordering, and if  $\Lambda_{jj'} < 0$ , it stimulates the antiferromagnetic order. It is very important that the effective fields that represent the exchange interaction *between* the sublattices enter the equations of motion (3.3).

The energy of *magnetocrystalline anisotropy* for an antiferromagnet or a ferrimagnet must be written as a series in powers of the components  $M_{jx,y,z}$  allowed by the symmetry of the lattice. The effective fields acting on each sublattice are found by differentiating the entire anisotropy energy with respect to the corresponding  $M_j$ .

Two points are worth noting. First, an assumption of the additivity of sublattice anisotropy energies is often made, i.e., the 'cross-terms', which contain the products of different-sublattice magnetization components, are excluded from the mentioned series. This is strictly valid only for one-ion source of anisotropy (Section 2.2). Second, in the case of antiferromagnets, the role of magnetocrystalline anisotropy, as we shall see, turns out to be much more important than for ferromagnets.

The *Zeeman* energy for antiferromagnets and ferrimagnets should be written in the form (2.15), where  $\mathbf{M}$  is the total magnetization (3.2). The magnetic sublattices in these substances are intermixed ('put into each other') on the microscopic level. Therefore, the *internal magnetic* energy  $U_M$ , which is the result of the long-range dipole–dipole interaction, also depends only on the total magnetization  $\mathbf{M}$ . The demagnetizing fields, acting on all sublattices, are equal to each other. For an ellipsoid, the expressions (2.16) and (1.82) hold.

### 3.1.3 Ground states and small oscillations

Before studying magnetic oscillations in antiferromagnets and ferrimagnets, the *ground states*, i.e., the lengths and directions of all vectors  $\mathbf{M}_{j0}$ , must be found. At  $T = 0$ , the lengths of  $\mathbf{M}_{j0}$  are to be regarded as known, and the problem is to find the angles  $\theta_{j0}$  and  $\varphi_{j0}$  of these vectors. This problem can be solved by the same two equivalent ways as for ferromagnets (Section 2.1): by the minimization of the total energy  $U$  and by the use of the conditions

$$\mathbf{M}_{j0} \times \mathbf{H}_{\text{eff}j0} = 0 \quad (3.6)$$

which follow from the equations of motion (3.3).

Some problems of this kind will be considered in Sections 3.2 and 3.3. Here we briefly discuss only the phenomenon of *weak ferromagnetism* (e.g., [392]). Dzyaloshinskii has shown [106] that the cause of this phenomenon is the presence of energy terms which are of the same nature as the 'ordinary' anisotropy-energy terms, but are minimized at angles between the vectors  $\mathbf{M}_{j0}$ , different from those (e.g., zero or  $\pi$ ) at which the exchange energy is minimal. Such terms are allowed by the symmetry only in some crystals. This problem was studied in detail by Turov [410]. We note only that in two-sublattice antiferromagnets, two types of such terms, of the second order in  $\mathbf{M}_j$  components, can be present:

$$U_D = -Dz_0 (\mathbf{M}_1 \times \mathbf{M}_2) \quad (3.7)$$

$$U_F = -F (M_{1x}M_{2y} - M_{2x}M_{1y}) \quad (3.8)$$

where the  $z$ -axis is the main axis of anisotropy, tetragonal or trigonal.

The anisotropic exchange interaction (Section 2.2) can lead to the term (3.7), and the one-ion anisotropy, as Moria has shown [372], to the term (3.8). The term (3.7), the only one allowed in trigonal antiferromagnets, is responsible for weak ferromagnetism of  $\alpha\text{-Fe}_2\text{O}_3$  and  $\text{MnCO}_3$ . The term (3.8) is allowed in some tetragonal crystals and leads to weak ferromagnetism of  $\text{NiF}_2$ .

Both terms  $U_D$  and  $U_F$  have minima at the angle of  $\pi/2$  between  $\mathbf{M}_1$  and  $\mathbf{M}_2$ . The term (3.8) 'demands', in addition, these vectors to be directed at angles  $\pi/4$  and  $-\pi/4$  with respect to the  $x$ -axis. The minimization of the total energy, consisting of  $U_D$  or  $U_F$  and the exchange energy  $U_{\text{ex}}$ , results in small (because  $U_{\text{ex}} \gg U_D, U_F$ ) spontaneous noncollinearity of the vectors  $\mathbf{M}_{10}$  and  $\mathbf{M}_{20}$ .

At  $T > 0$  the *lengths* of the vectors  $M_{j0}$  depend on magnetic field and temperature. To find the ground state we must use now, in addition to the equilibrium conditions, some supplementary equations. The expressions analogous to (1.18)

$$M_{j0} = M_j^0 B_{J_j} \left( \frac{M_{j0}}{N_j \kappa T} H_{\text{ef}j0} \right) \quad (3.9)$$

may be used as such equations. Here  $M_j^0 = \gamma_j \hbar J_j N_j$  is the sublattice magnetization at  $T = 0$ , and  $B_{J_j}(x)$  is the Brillouin function (1.19). Solving equations (3.9) together with the expressions, relating  $H_{\text{ef}j0}$  to  $M_{j0}$ , and the equilibrium conditions, we can obtain, in principle, the lengths and orientations of  $M_{j0}$  at given  $H_{e0}$  and  $T$ .

This problem can be solved easily only for temperatures very *near* to or *higher* than the *Neel temperature*  $T_N$ . Then all  $M_{j0}$  values, as well as the anisotropy constants, are small, and it is possible, first, to neglect the demagnetizing and anisotropy fields, and, second, to limit oneself to the first terms in the series expansions of the Brillouin functions. Let us consider a *two-sublattice* antiferromagnet or ferrimagnet. Then the effective fields, according to (3.5), are

$$H_{\text{ef}10} = H_{e0} + \Lambda_{11} M_{10} + \Lambda_{12} M_{20} \quad H_{\text{ef}20} = H_{e0} + \Lambda_{12} M_{10} + \Lambda_{22} M_{20}. \quad (3.10)$$

The collinearity of  $H_{e0}$ ,  $M_{10}$ , and  $M_{20}$  follows from (3.6), and, taking into account the first terms in the expansions of  $B_{J_j}$ , we get from (3.9) a system of linear equations for  $M_{10}$  and  $M_{20}$ . To find the *Neel temperature* we must set equal to zero the determinant of this system. Then, for an antiferromagnet with two identical sublattices, we get (designating  $\Lambda_{11} = \Lambda_{22} = -\Lambda_i$  and  $\Lambda_{12} = -\Lambda$ )

$$T_N = C(\Lambda - \Lambda_i) \quad (3.11)$$

where  $C$  has the same form as the Curie constant (1.21), but all quantities,  $J$ ,  $\gamma$ , and  $N$  relate now to a sublattice. Solving the mentioned system for  $H_0 \neq 0$ , we find the *paramagnetic susceptibility* of an antiferromagnet

$$\chi_p = \frac{2C}{T - T_p} \quad (3.12)$$

where  $T_p = -C(\Lambda - \Lambda_i)$  is the negative paramagnetic Curie temperature (Figure 1.3).

For a *ferrimagnet*, taking  $|\Lambda_{11}|, |\Lambda_{22}| \ll |\Lambda_{12}|$ , we obtain

$$T_N \cong \sqrt{C_1 C_2} \Lambda \quad (3.13)$$

where  $\Lambda = -\Lambda_{12}$ , and  $C_1$  and  $C_2$  are the Curie constants of the corresponding sublattices. The temperature dependence of  $\chi_p^{-1}$  is nonlinear in this case (Figure 1.3).

In ferrimagnets, the steady sublattice magnetizations not only differ from each other in magnitude but can differently depend on composition and temperature.

At certain compositions or certain temperatures, the total magnetization  $\sum \mathbf{M}_j 0$  can become equal to zero. Such compositions or temperatures are called *magnetic compensation points*. As the sublattice magneto-mechanical ratios can also differ from each other, the *mechanical compensation points* (where  $\sum \mathbf{M}_j 0 / \gamma_j = 0$ ) do not coincide with the magnetic compensation points.

To *linearize* the equations of motion (3.3) we write the magnetizations and effective fields as sums of steady and ac components and substitute these sums into (3.3). Assuming the ac components to be small as compared with the steady components, we obtain, in a zero approximation, conditions (3.6) and, in the first approximation, the system of  $N$  linear equations for the complex amplitudes

$$i\omega \mathbf{m}_j + \gamma_j \mathbf{m}_j \times \mathbf{H}_{\text{ef}j0} + \gamma_j \mathbf{M}_j 0 \times \mathbf{h}_{\text{ef}j} + \frac{i\alpha_j \omega}{M_j 0} \mathbf{m}_j \times \mathbf{M}_j 0 = -\gamma_j \mathbf{M}_j 0 \times \mathbf{h}. \quad (3.14)$$

Here  $\mathbf{h}_{\text{ef}j}$  are the complex amplitudes of the ac effective fields (without the field which we regard as given) and  $\mathbf{h}$  is the complex amplitude of the given ac field. Equations (3.14) are coupled to each other, because every  $\mathbf{h}_{\text{ef}j}$  depends, in general, on all the sublattice ac magnetizations.

Solving the coupled equations (3.14) is the basis of the theory of magnetic oscillations in antiferromagnets and ferrimagnets. Sections 3.2 and 3.3 will be devoted to this theory. Here we limit ourselves to some general remarks.

Setting equal to zero the determinant of  $3N$  scalar equations that follow from (3.14), we obtain the characteristic equation for the frequencies of free oscillations. If we take  $\alpha_j = 0$ , the solutions of this equation will be the *eigenfrequencies*. We will see below that there are always  $N$  positive roots of this equation, corresponding to eigenoscillations of the considered system with  $N$  degrees of freedom.

If  $\mathbf{h} \neq 0$ , the system of  $3N$  nonuniform linear equations, obtained by projecting (3.14), has  $3N$  solutions, which are complex amplitudes<sup>4</sup> of  $\mathbf{m}_j$  components for *forced oscillations*. All these components are linear functions of the  $\mathbf{h}$  components, and the total ac magnetization is

$$\mathbf{m} \equiv \sum_{j=1}^N \mathbf{m}_j = \vec{\chi} \mathbf{h} \quad (3.15)$$

where  $\vec{\chi}$  is the ac susceptibility tensor of an antiferromagnet or a ferrimagnet. If the ac demagnetizing field is *included* in  $\mathbf{h}_{\text{ef}j}$ , the field  $\mathbf{h}$  is the *external* field, and the tensor  $\vec{\chi}$  in (3.15) is the *external* susceptibility tensor analogous to the tensor  $\vec{\chi}^e$  of a ferromagnetic sample (Section 1.5). If the demagnetizing field is *not included* in  $\mathbf{h}_{\text{ef}j}$ , then  $\mathbf{h}$  is the *internal* ac field, and  $\vec{\chi}$  in (3.15) is the susceptibility of the *substance*. The difference between these tensors is small for antiferromagnets in comparatively low steady magnetic fields. But for ferrimagnets this difference is as essential as for ferromagnets.

<sup>4</sup>The words 'complex amplitude' will be omitted from here on.

### 3.2 Antiferromagnetic resonance

Antiferromagnetic resonance was first investigated theoretically by Kittel [221] and Nagamiya [294] and was discovered experimentally in 1952 by Ubbink *et al.* [413]. Since then a lot of works has been devoted to the investigation of antiferromagnetic resonance in substances with different crystal and magnetic structures (e.g., [122]). The aim of the present section is, first, to show how the theory, discussed in the previous section, is applied to magnetic oscillations in antiferromagnets and, second, to expose the principal features of these oscillations. Therefore, we limit ourselves to the simplest case of antiferromagnet with uniaxial anisotropy and two identical sublattices.

The following *assumptions* are made:

1. The energy of anisotropy  $U_{\text{an}}$  is the sum of the anisotropy energies of the sublattices; writing them in the form (2.31), we allow for only the first constant of anisotropy. The anisotropy in the basal plane is also neglected.
2. The difference in the length of the  $M_{j0}$  vectors is neglected, i.e., strictly speaking, the case of  $T = 0$  is considered (Section 3.1.).
3. The demagnetizing fields are not taken into account.

As the effective fields of *intra-sublattice* exchange interaction do not enter the equations of motion, we may write the total energy as

$$U = \Lambda M_1 M_2 - H(M_1 + M_2) + K(\sin^2 \theta_1 + \sin^2 \theta_2) \quad (3.16)$$

where  $\Lambda \equiv -\Lambda_{12}$ ,  $K \equiv K_1$ , and  $\theta_1$  and  $\theta_2$  are the angles of  $M_1$  and  $M_2$  with respect to the axis of anisotropy (the  $z$ -axis). The magnetizations  $M_1$  and  $M_2$  are uniform; so, according to (2.6),

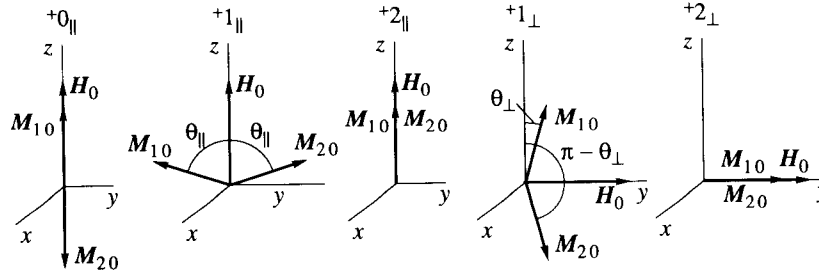
$$H_{\text{ef},1,2} = -\frac{\partial U}{\partial M_{1,2}} = -\Lambda M_{2,1} + H + \frac{K}{(M^0)^2} z_0 (M_{1,2} z_0) \quad (3.17)$$

where  $M^0$  is the length of the vectors  $M_1$  and  $M_2$ .

#### 3.2.1 Antiferromagnet with an easy axis of anisotropy: steady states

Consider, first, the case of  $K > 0$ . It is clear from symmetry considerations that the steady magnetizations  $M_{10}$  and  $M_{20}$ , the field  $H_0$ , and the axis of anisotropy (the  $z$ -axis) lie in one plane. The angles between the  $z$ -axis and the vectors  $M_{10}$ ,  $M_{20}$ , and  $H_0$  are, respectively,  $\theta_{10}$ ,  $\theta_{20}$ , and  $\theta_H$ . To find the angles<sup>5</sup>  $\theta_{10}$  and  $\theta_{20}$  we have to set equal to zero the derivatives of  $U$  with respect to  $\theta_1$  and  $\theta_2$ , or use the conditions (3.6). Both ways lead to the following *necessary* conditions for

<sup>5</sup>In what follows we omit the subscripts 0 at the angles  $\theta_{10}$  and  $\theta_{20}$ .

**FIGURE 3.4**

Ground states of a two-sublattice antiferromagnet with easy axis of anisotropy.

equilibrium:

$$\Lambda (M^0)^2 \sin(\theta_{1,2} - \theta_{2,1}) - H_0 M^0 \sin(\theta_H - \theta_{1,2}) + K \sin \theta_{1,2} \cos \theta_{1,2} = 0. \quad (3.18)$$

When the angles satisfying these conditions are obtained, we have to find out which of them corresponds to the minimum of energy.

Let us consider two particular cases: when the field  $\mathbf{H}_0$  is directed along the anisotropy axis ( $\mathbf{H}_0 \parallel z_0$ ) and when  $\mathbf{H}_0$  is perpendicular to this axis ( $\mathbf{H}_0 \perp z_0$ ). The symmetry allows, in these cases, the ground states shown in Figure 3.4.

It follows from (3.18) that

$$\cos \theta_{\parallel} = \frac{H_0}{2H_E - H_A} \quad (3.19)$$

$$\sin \theta_{\perp} = \frac{H_0}{2H_E + H_A} \quad (3.20)$$

where the angles  $\theta_{\parallel}$  and  $\theta_{\perp}$  are shown in Figure 3.4 and the following notations are used:

$$H_E = \Lambda M^0 \quad H_A = K/M^0. \quad (3.21)$$

It is easy to make sure that the energy (3.16) is minimal, for different states, in the  $H_0$  intervals given in Table 3.1.

One can see from the table that, in the case of  $\mathbf{H}_0 \parallel z_0$ , an antiparallel state  $+0_{\parallel}$  takes place in weak fields. With growing field the transition into state  $+1_{\parallel}$  (*spin-flop*) occurs, which is the first-order phase transition. In a very narrow field interval  $H_{C1} < H_0 < H_{C2}$  (Table 3.1) both states are stable. Domain structures and hysteresis appear in this interval. With the further increase of  $H_0$  the angle between the vectors  $\mathbf{M}_{10}$  and  $\mathbf{M}_{20}$  decreases, and at  $H_0 = H_{E\parallel}$  a transition to the state  $+2_{\parallel}$  (*spin-flip*) occurs, which is usually a second-order phase transition.

In the case of  $\mathbf{H}_0 \perp z_0$ , the angle between  $\mathbf{M}_{10}$  and  $\mathbf{M}_{20}$  decreases gradually with growing  $H_0$ , and at  $H_0 = H_{E\perp}$  a transition from  $+1_{\perp}$  state to  $+2_{\perp}$  state takes place.

For both considered orientations of  $\mathbf{H}_0$ , the total magnetization  $\mathbf{M}_0 = \mathbf{M}_{10} + \mathbf{M}_{20}$  is parallel to  $\mathbf{H}_0$  in all states, and a scalar static susceptibility  $\chi_0 = M_0/H_0$  can be defined. The dependence of  $M_0$  and  $\chi_0$  on  $H_0$  is shown in Figure 3.5. One can see that at low fields a strong anisotropy of the susceptibility is present.

TABLE 3.1

Ground states and eigenfrequencies for a two-sublattice antiferromagnet with easy axis of anisotropy ( $H_A > 0$ ) at  $T = 0$ .

Field direction <sup>a</sup>	Ground state (Fig. 3.4)	Field range <sup>b</sup>	Eigenfrequencies <sup>c</sup> ( $\gamma_1 = \gamma_2 \equiv \gamma$ )
	<sup>+0</sup> <sub>  </sub> Antiparallel	$0 < H_0 < H_{C2}$	$\frac{\omega_{\pm}}{\gamma} = H_{C2} \pm H_0$ (3.22)
$\mathbf{H}_0 \parallel \mathbf{z}_0$	<sup>+1</sup> <sub>  </sub> Noncollinear	$H_{C1} < H_0 < H_{E  }$	$\frac{\omega_{  1}}{\gamma} = \left( \frac{2H_E H_{E\perp}}{H_{E  }^2} H_0^2 - 2H_E H_A \right)^{1/2}$ { $\omega_{  2} = 0$ }
	<sup>+2</sup> <sub>  </sub> Parallel	$H_{E  } < H_0$	$\frac{\omega_{  1}}{\gamma} = H_0 + H_A$ { $\frac{\omega_{  2}}{\gamma} = H_0 - H_{E  }$ }
	<sup>+1</sup> <sub>⊥</sub> Noncollinear	$0 < H_0 < H_{E\perp}$	$\frac{\omega_{\perp 1}}{\gamma} = \left( H_{C2}^2 + \frac{H_{E  }}{H_{E\perp}} H_0^2 \right)^{1/2}$ (3.25)
$\mathbf{H}_0 \perp \mathbf{z}_0$			$\frac{\omega_{\perp 2}}{\gamma} = \left( H_{C2}^2 - \frac{H_A}{H_{E\perp}} H_0^2 \right)^{1/2}$ (3.26)
	<sup>+2</sup> <sub>⊥</sub> Parallel	$H_{E\perp} < H_0$	$\frac{\omega_{\perp 1}}{\gamma} = \sqrt{H_0(H_0 - H_A)}$ { $\frac{\omega_{\perp 2}}{\gamma} = \sqrt{(H_0 - 2H_E)(H_0 - H_E)}$ }

<sup>a</sup>  $\mathbf{z}_0$  is a unit vector parallel to the anisotropy axis.

<sup>b</sup>  $H_{C1} = \sqrt{H_A(2H_E - H_A)}$ ,  $H_{E||} = 2H_E - H_A$ ,  $H_A = K/M^0$ ,  
 $H_{C2} = \sqrt{H_A(2H_E + H_A)}$ ,  $H_{E\perp} = 2H_E + H_A$ ,  $H_E = \Lambda/M^0$ .

<sup>c</sup> Braces indicate the frequencies of modes that are not excited by a uniform ac magnetic field.

For most antiferromagnets,  $H_A \ll H_E$ . Then, the difference between  $H_{C1}$  and  $H_{C2}$ , as well as the difference between  $H_{E||}$  and  $H_{E\perp}$  (Table 3.1) can be ignored, and these approximate expressions can be used:

$$H_{C1} \cong H_{C2} \equiv H_C = \sqrt{2H_E H_A} \quad H_{E||} \cong H_{E\perp} \cong 2H_E. \quad (3.28)$$

Taking (3.11) and (3.21) into account, we get the following estimates for antiferromagnets with Neel temperatures  $T_N \sim 100$  K and  $H_A \sim 10$ – $100$  Oe:  $H_E \sim 10^6$  Oe and  $H_C \sim 10^4$ – $10^5$  Oe.



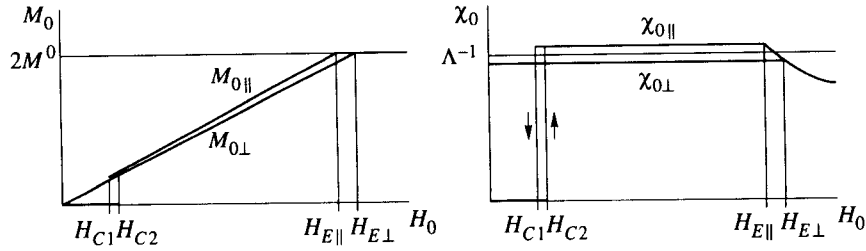


FIGURE 3.5

Steady magnetizations and susceptibilities of an antiferromagnet with easy axis of anisotropy in the field  $\mathbf{H}_0$  parallel (subscripts  $\parallel$ ) and perpendicular (subscripts  $\perp$ ) to the axis.  $H_0$  is plotted not to scale to make the small intervals  $H_{C2} - H_{C1}$  and  $H_{E\perp} - H_{E\parallel}$  visible.

### 3.2.2 Oscillations in antiparallel state

We project now the linearized equations of motion (3.14) onto the coordinate axes and take into account (3.17). In the case of the *antiparallel* state  $^+0_{\parallel}$  (Figure 3.4), we get  $m_{1z} = m_{2z} = 0$  and obtain a system of four equations for  $m_{1x}$ ,  $m_{2x}$ ,  $m_{1y}$ , and  $m_{2y}$ . After transition to circular variables  $m_{j\pm} = m_{jx} \pm m_{jy}$  ( $j = 1, 2$ ), we get two independent systems for the pairs of variables  $m_{1+}$ ,  $m_{2+}$  and  $m_{1-}$ ,  $m_{2-}$ :

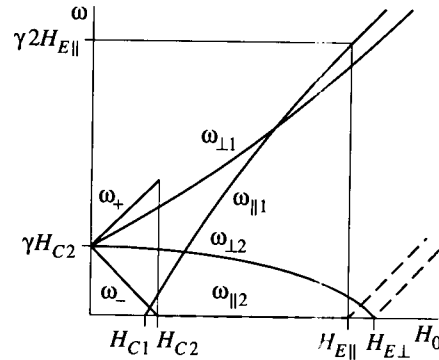
$$\begin{aligned} [\pm\omega - i\alpha\omega - \gamma(H_0 + H_E + H_A)]m_{1\pm} - \gamma H_E m_{2\pm} &= -\gamma M^0 h_{\pm} \\ \gamma H_E m_{1\pm} + [\pm\omega - i\alpha\omega - \gamma(H_0 - H_E - H_A)]m_{2\pm} &= \gamma M^0 h_{\pm}. \end{aligned} \quad (3.29)$$

To find the *eigenfrequencies* we set equal to zero the determinants of systems (3.29) with  $\alpha_j = 0$ . We get two frequencies  $\omega_+$  and  $\omega_-$  given in Table 3.1. Their dependence on  $H_0$  is shown in Figure 3.6. If  $H_0 = 0$ , then  $\omega_+ = \omega_- = \omega_0$ . The values of  $\omega_0$  are usually rather high, e.g.,  $f_0 = \omega_0/2\pi = 165$  GHz for  $\text{Cr}_2\text{O}_3$ .

To analyze the *character of eigenoscillations* we can reason in the following way (as in Section 1.3). For the mode with frequency  $\omega_+$ , the determinant of system (3.29) with lower signs is not equal to zero. Therefore, this system has only the trivial solution  $m_{1-} = m_{2-} = 0$  at  $\omega = \omega_+$ . It means that  $m_{1y} = -m_{1x}$  and  $m_{2y} = -m_{2x}$ , i.e., a circular precession of the vectors  $\mathbf{M}_1$  and  $\mathbf{M}_2$  with right-hand rotation takes place. It is possible to make sure in the same way that the mode with frequency  $\omega_-$  is a left-hand circular precession.

The ratios of the sublattice ac magnetizations can be found from any of equations (3.29) (with  $\alpha = 0$  and  $h_{\pm} = 0$ ) using the values (3.24) of  $\omega_+$  or  $\omega_-$ . If  $H_A \ll H_E$ , these ratios are

$$m_{2\pm}/m_{1\pm} = -(1 \mp H_C/H_E). \quad (3.30)$$



**FIGURE 3.6**

Eigenfrequencies of an antiferromagnet with easy axis of anisotropy. Subscripts  $\parallel$  and  $\perp$  correspond, respectively, to  $\mathbf{H}_0$  parallel and perpendicular to the axis.  $H_0$  is plotted not to scale, as in Figure 3.5. Dashed lines relate to modes with  $m = 0$ .

It follows from (3.30) that the total ac magnetization is small. The precession of the vectors  $\mathbf{M}_1$  and  $\mathbf{M}_2$  in the  $^+0_{\parallel}$  state is illustrated for both modes by Figure 3.7.

To find the *damping* of free oscillations we must set equal to zero the determinant of (3.29) with  $h_{\pm} = 0$  but  $\alpha \neq 0$ . To the first approximation ( $\alpha \ll 1$ ), we obtain the same expressions (3.24) for  $\omega'_{\pm}$  and (if  $H_A \ll H_E$ )

$$\omega''_{\pm} \cong \alpha \omega'_{\pm} H_E / H_A. \quad (3.31)$$

Comparing (3.31) with the relation  $\omega'' = \alpha \omega'$  for the ferromagnet, we see that, if the values of  $\alpha$  are the same, the damping in antiferromagnet is much stronger. However, the  $\alpha$  values in antiferromagnets and ferromagnets can differ essentially from each other.

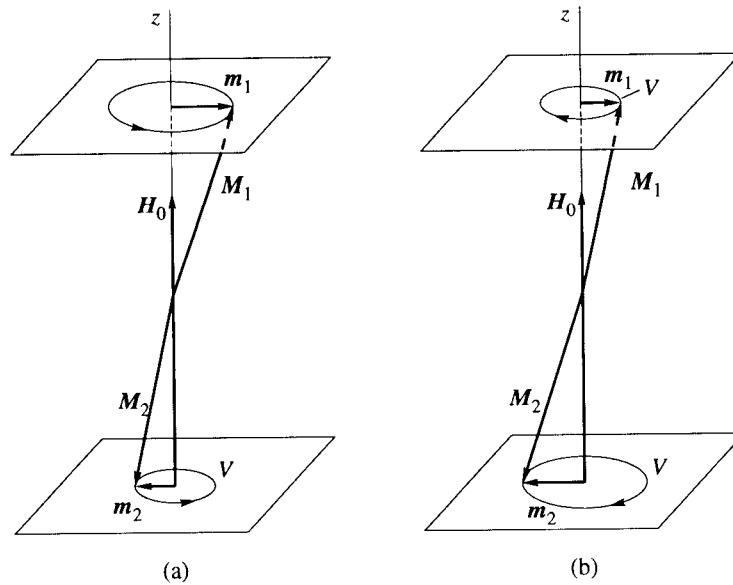
Consider now the *forced* oscillations. The total ac magnetization  $m = m_1 + m_2$ , which determines all the observed effects in antiferromagnetic resonance, is of the most interest. Solving the system (3.29), we obtain, for small dissipation ( $\alpha \ll 1$ ) and  $H_A \ll H_E$ ,

$$m_{\pm} = m_{1\pm} + m_{2\pm} \cong \frac{2\gamma^2 M^0 H_A}{(\omega_+ - \omega)(\omega_- - \omega) + 2i\alpha\omega\gamma H_E} h_{\pm} \equiv \chi_{\pm} h_{\pm}. \quad (3.32)$$

Here  $\chi_+$  and  $\chi_-$  are the tensor  $\vec{\chi}$  circular components (Section 1.3). At resonance ( $\omega = \omega_+$  or  $\omega = \omega_-$ ) we get

$$(\chi_{\pm})_{\text{res}} = \frac{\gamma M^0 H_A}{\alpha \omega_{\pm} H_E}. \quad (3.33)$$

This quantity differs by a factor  $H_A / H_E$  from the resonance circular susceptibility

**FIGURE 3.7**

Precession of the sublattice-magnetization vectors in an antiferromagnet with easy axis of anisotropy in the antiparallel ground state  $^+0_{\parallel}$ : (a) mode with frequency  $\omega_+$  and (b) mode with frequency  $\omega_-$ . The difference between  $|m_1|$  and  $|m_2|$  is exaggerated.

of a ferromagnet (Section 1.4) with the same values of  $\omega$  and  $\alpha$ .

The *linewidths*  $\Delta H_{\pm}$  (or  $\Delta\omega_{\pm}$ ) can be defined, analogously to a ferromagnet, as the differences of the  $H_0$  (or  $\omega$ ) values at which  $\chi''_{\pm} = 1/2(\chi''_{\pm})_{\text{res}}$ . If we take again  $\alpha \ll 1$  and  $H_A \ll H_E$ , we find

$$\Delta H_{\pm} = \frac{\Delta\omega_{\pm}}{\gamma} = \frac{2\alpha\omega_{\pm}}{\gamma} \frac{H_E}{H_A}. \quad (3.34)$$

### 3.2.3 Oscillations in noncollinear state

The steady magnetizations in  $^+1_{\parallel}$  state (Figure 3.4) are

$$\mathbf{M}_{10} = (z_0 \cos \theta_{\parallel} - y_0 \sin \theta_{\parallel}) M^0 \quad \mathbf{M}_{20} = (z_0 \cos \theta_{\parallel} + y_0 \sin \theta_{\parallel}) M^0. \quad (3.35)$$

Projecting now two equations (3.14) with  $\alpha = 0$  and  $h_{\pm} = 0$  onto the coordinate axis, we obtain, with account for (3.17) and (3.35), a system of six equations for the components of vectors  $\mathbf{m}_1$  and  $\mathbf{m}_2$ . To get two *independent* systems (which should correspond to the eigenmodes) we must pass to the components of vectors  $\mathbf{m} = \mathbf{m}_1 + \mathbf{m}_2$  and  $\mathbf{l} = \mathbf{m}_1 - \mathbf{m}_2$ . It should be noted that  $\mathbf{l}$  is the complex amplitude of the ac component of the vector  $\mathbf{L} = \mathbf{M}_1 - \mathbf{M}_2$ , which is referred to

as the *vector of antiferromagnetism*.

One of the independent systems will contain the components  $m_x$ ,  $m_y$ , and  $l_z$  and the other will contain  $m_z$ ,  $l_x$ , and  $l_y$ . If we set equal to zero the determinant of the first system, we find expression (3.25) (in Table 3.1) for the *eigenfrequency*  $\omega_{\parallel 1}$ . The dependence of  $\omega_{\parallel 1}$  on  $H_0$  is shown in Figure 3.6. If we set equal to zero the determinant of the second system, we get  $\omega_{\parallel 2} = 0$ .

The *character of the eigenmodes* in  $+1_{\parallel}$  state can be analyzed in the manner used above. For the first mode, the second of the above-mentioned independent system has only zero solutions. Thus, for this mode (Figure 3.8)

$$m_{1x} = m_{2x} \quad m_{1y} = m_{2y} \quad m_{1z} = -m_{2z}. \quad (3.36)$$

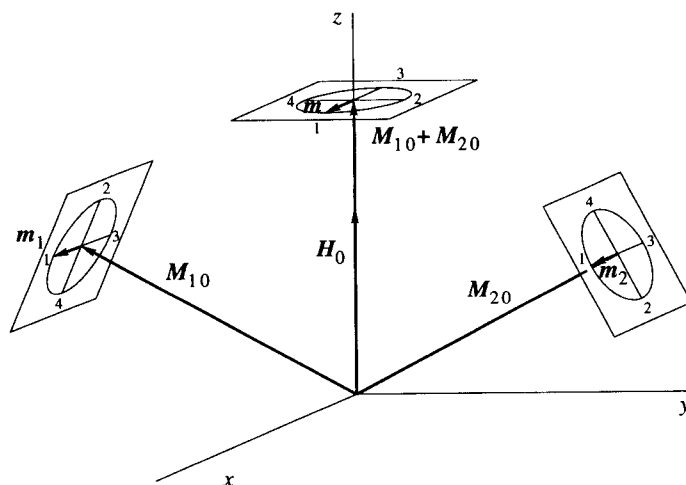
For the second mode,  $m_x = m_y = 0$ ; the component  $m_z$  is also equal to zero, as it follows directly from the second system. This mode is an infinitely slow rotation of vectors  $\mathbf{M}_1$  and  $\mathbf{M}_2$  around the  $z$ -axis. Such motion occurs without changing the energy of the system, and that is why the eigenfrequency is equal to zero. In reality, some factors not taken into account, e.g., the anisotropy in a basal plane, lead to the distinction of  $\omega_{\parallel 2}$  from zero. But, nevertheless, the frequency of this mode will be small as compared with other eigenfrequencies of the system. Such modes are called *soft modes*. The appearance of a soft mode in the present case is due to the fact that the ground state  $+1_{\parallel}$  breaks the cylindrical symmetry of the energy. A general statement that a soft mode should appear, when the ground state breaks the symmetry of the energy of the system, is known as the Goldstone theorem (e.g., [218]).

It is clear from the character of the vector  $\mathbf{M}$  precession (Figure 3.8) that the mode with eigenfrequency  $\omega_1$  is excited by the *transverse* (with respect to  $\mathbf{H}_0$ ) component of the ac magnetic field. The second mode cannot be excited by a uniform ac magnetic field at all. Thus, the tensor  $\vec{\chi}$  for state  $+1_{\parallel}$  (as well as for state  $+0_{\parallel}$ ) has the form (1.47). The non-zero components of this tensor can be found by solving the system of equations for  $m_x$ ,  $m_y$ , and  $l_z$  with  $h \neq 0$  and  $\alpha \neq 0$ . It is clear that these components will pass through resonance, approximately, at  $\omega = \omega_{\parallel 1}$ .

Solving system (3.14) for the *parallel* state  $+2_{\parallel}$ , we get two modes with frequencies given in Table 3.1. However, for the second mode  $\mathbf{m} = 0$ , i.e., this mode cannot be excited by a uniform ac magnetic field. The first mode coincides with the magnetization oscillations in a uniaxial ferromagnet (Section 2.3) with the steady magnetization  $2M^0$  and the anisotropy constant  $K$ .

### 3.2.4 Oscillations in transverse and arbitrarily oriented fields

For the ground state  $+1_{\perp}$  (Figure 3.4) we obtain, in the same way as for the state  $+1_{\parallel}$ , two independent systems of equations: in variables  $m_x$ ,  $m_z$ ,  $l_y$  and in variables  $m_y$ ,  $l_x$ ,  $l_z$  ( $\mathbf{H}_0$  is directed along the  $y$ -axis). Setting the determinants of these systems equal to zero, we obtain the *eigenfrequencies* of the two modes

**FIGURE 3.8**

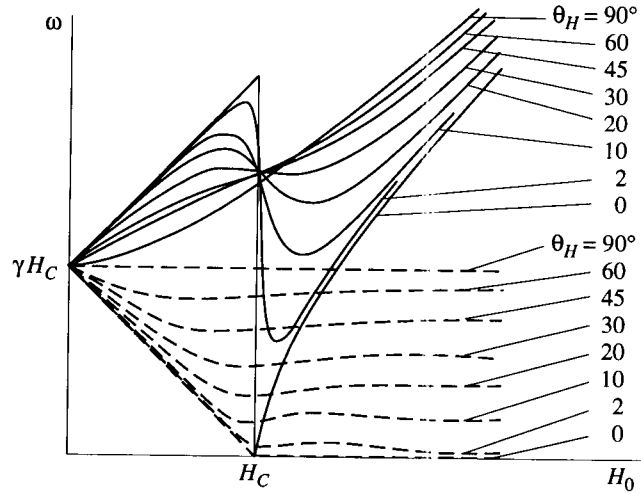
Precession of the sublattice-magnetization and total-magnetization vectors in an antiferromagnet with easy axis of anisotropy in the noncollinear ground state  $^+1_{\parallel}$ . Numbers denote the positions of the tips of the vectors at successive instants.

(Table 3.1). Their dependence on  $H_0$  is shown in Figure 3.6. As  $m_y = 0$  for the first mode, this mode is excited by the *transverse* (with respect to  $\mathbf{H}_0$ ) ac magnetic field component. For the second mode  $m_x = m_z = 0$ , and this mode is excited by the *longitudinal* (parallel to  $\mathbf{H}_0$ ) ac field component. Thus, the susceptibility tensor has the form

$$\vec{\chi} = \begin{vmatrix} \chi_{11} & 0 & i\chi_a \\ 0 & \chi_{22} & 0 \\ -i\chi_a & 0 & \chi_{33} \end{vmatrix}. \quad (3.37)$$

The frequency  $\omega_1$  is the resonance frequency for the components  $\chi_{11}$ ,  $\chi_{33}$ , and  $\chi_a$  of this tensor, and  $\omega_2$  is the resonance frequency for  $\chi_{22}$ . At  $H_0 = H_{E\perp}$  the first mode transforms into the 'ferromagnetic' mode in the parallel ground state  $^+2_{\perp}$ . Its frequency coincides with the eigenfrequency for a uniaxial ferromagnet (Section 2.3) with the corresponding orientation of  $\mathbf{H}_0$ .

The eigenfrequencies for *arbitrarily*  $\mathbf{H}_0$  orientations are shown in Figure 3.9. Using these data, the antiferromagnetic-resonance spectra in a polycrystal can be found in the approximation of independent grains (Section 2.4). This approximation is well suited for antiferromagnets if  $H_0 \ll H_E$ , because the total magnetizations, both steady and ac, are small in this case. One can see from Figure 3.9 that very broad absorption 'lines' should be observed in polycrystalline antiferromagnets in both cases: of variable  $H_0$  at  $\omega = \text{const}$  and of variable  $\omega$  at  $H_0 = \text{const}$ .



**FIGURE 3.9**

Eigenfrequencies of an antiferromagnet with easy axis of anisotropy for different angles between  $\mathbf{H}_0$  and the axis. Solid and dashed lines correspond to two modes. It is assumed  $H_A \ll H_E$ , and the small interval  $H_{C2} - H_{C1}$  is not shown.

### 3.2.5 Antiferromagnet with easy plane of anisotropy

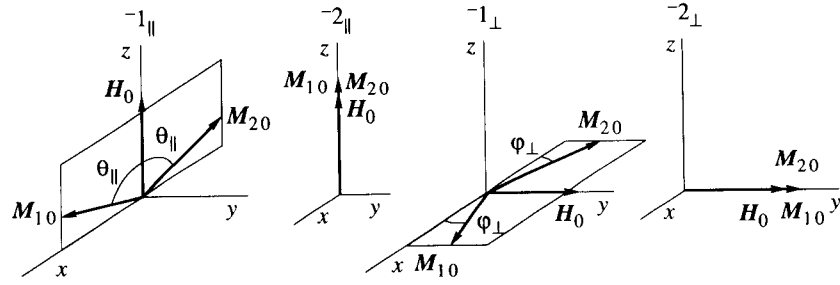
Consider now the case of  $K < 0$ , when  $\mathbf{M}_1$  and  $\mathbf{M}_2$  easy directions lie in the *basal plane*. Only the main results will be cited in this case; the method of obtaining them is the same as that used above.

Two ground states exist now for both  $\mathbf{H}_0$  orientations: a noncollinear state and a parallel state (Figure 3.10 and Table 3.2). The equilibrium angles in *noncollinear* states  $-1_{\parallel}$  and  $-1_{\perp}$  are determined by

$$\cos \theta_{\parallel} = \frac{H_0}{2H_E - H_A} \quad (3.38)$$

$$\sin \varphi_{\perp} = \frac{H_0}{2H_E} \quad (3.39)$$

where  $H_E$  and  $H_A$  are defined by (3.21), as before, but  $H_A < 0$ . Comparing Figure 3.10 with Figure 3.4, we see that the states  $-1_{\parallel}$ ,  $-2_{\parallel}$ , and  $-2_{\perp}$  do not differ from the states  $+1_{\parallel}$ ,  $+2_{\parallel}$ , and  $+2_{\perp}$ , respectively. Therefore, the *expressions* for the eigenfrequencies in all the mentioned states with  $K < 0$  are the same as in the corresponding states with  $K > 0$  (Table 3.1). The difference is, however, in the sign of  $H_A$ . As a result, the *actual dependence* of  $\omega_{\parallel 1}$  on  $H_0$  in the state  $-1_{\parallel}$  (Figure 3.11) differs from such dependence in  $+1_{\parallel}$  state. It coincides approximately (if  $|H_A| \ll H_E$ ) with  $\omega_{\perp 1}$  vs  $H_0$  dependence in the state  $+1_{\perp}$  (Figure 3.6).



**FIGURE 3.10**  
Ground states of a two-sublattice antiferromagnet with easy plane of anisotropy.

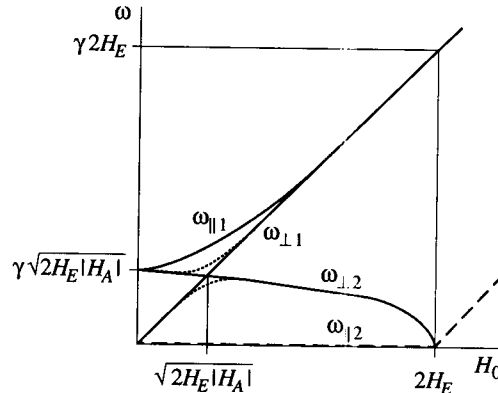
The state  $^{-1}_{\perp}$ , for  $K < 0$  and  $\mathbf{H}_0$  lying in the easy plane, is an *essentially new* one. The eigenfrequencies in this state are given in Table 3.2, and their dependence on  $H_0$  is shown in Figure 3.11. The character of oscillations of the vectors  $\mathbf{M}_1$  and  $\mathbf{M}_2$  in this state is illustrated by Figure 3.12. For the mode with frequency  $\omega_{\perp 1}$ , the components  $m_x$ ,  $m_z$ , and  $l_y$  exist, and this mode is excited by the transverse component of ac magnetic field (with respect to  $\mathbf{H}_0$ , which is directed along the  $y$ -axis). The second mode, with  $m_y$ ,  $l_x$ , and  $l_z$  not equal to zero, is excited by a longitudinal (parallel to  $\mathbf{H}_0$ ) ac field.

**TABLE 3.2**  
Ground states and eigenfrequencies for a two-sublattice antiferromagnet with easy plane of anisotropy ( $H_A < 0$ ) at  $T = 0$ .

Field direction <sup>a</sup>	Ground state (Fig. 3.10)	Field range <sup>b</sup>	Eigenfrequencies ( $\gamma_1 = \gamma_2 \equiv \gamma$ )
$\mathbf{H}_0 \parallel \mathbf{z}_0$	$^{-1}_{\parallel}$ Noncollinear	$0 < H_0 < 2H_E +  H_A $	Expression for $\omega_{\parallel 1}$ coincides with (3.23)
	$^{-2}_{\parallel}$ Parallel	$2H_E +  H_A  < H_0$	Expression for $\omega_{\parallel 1}$ coincides with (3.24)
$\mathbf{H}_0 \perp \mathbf{z}_0$	$^{-1}_{\perp}$ Noncollinear	$0 < H_0 < 2H_E$	$\frac{\omega_{\perp 1}}{\gamma} = H_0 \sqrt{1 + \frac{ H_A }{2H_E}}$ (3.40) $\frac{\omega_{\perp 2}}{\gamma} = \left(2H_E  H_A  - \frac{ H_A }{2H_E} H_0^2\right)^{1/2}$ (3.41)
	$^{-2}_{\perp}$ Parallel	$2H_E < H_0$	Expression for $\omega_{\perp 1}$ coincides with (3.27)

<sup>a</sup>  $\mathbf{z}_0$  is a unit vector perpendicular to the anisotropy plane.

<sup>b</sup>  $H_A = K/M^0$ ,  $H_E = \Lambda M^0$ ; it is assumed that  $|H_A| \ll H_E$ .



**FIGURE 3.11**

Eigenfrequencies of an antiferromagnet with easy plane of anisotropy at  $\mathbf{H}_0 \parallel \mathbf{z}_0$  (subscripts  $\parallel$ ) and  $\mathbf{H}_0 \perp \mathbf{z}_0$  (subscripts  $\perp$ ) where  $\mathbf{z}_0$  is a unit vector of the normal to the easy plane. Dashed lines relate to the modes with  $m = 0$ . Dotted lines correspond to a small distinction of the angle between  $\mathbf{H}_0$  and  $\mathbf{z}_0$  from  $\pi/2$ .

Thus, the frequencies  $\omega_{\perp 2}$  in different ground states  $+1_{\perp}$  and  $-1_{\perp}$  do not differ strongly from one another. On the contrary, the behavior of the frequency  $\omega_{\perp 1}$  in  $-1_{\perp}$  state has no analog in the case of  $K > 0$ . This frequency *approaches zero* at  $H_0 \rightarrow 0$ . Such an important feature of the considered mode is due to the fact that the angle between  $\mathbf{M}_1$  and  $\mathbf{M}_2$  (Figure 3.12) does not change in the precession of these vectors. The antiferromagnetic resonance, in this case, can be and really was observed at rather low frequencies in weak steady magnetic fields (e.g. [300]).

Another peculiarity of the antiferromagnetic-resonance spectrum for  $K < 0$  and  $\mathbf{H}_0$ , lying in the easy plane, is a *crossover* of the branches, i.e., the degeneration of the modes at  $H \cong H_C$  (Figure 3.11). The degeneracy is removed with the deflection of  $\mathbf{H}_0$  from the easy plane.

The anisotropy in the basal plane influences materially only the first mode for  $K < 0$  and  $H_0$  lying in the easy plane. It results in the appearance of a *gap* in the spectrum, i.e., leads to a finite  $\omega_{\perp 1}$  value at zero field. This value depends on the angle between  $\mathbf{H}_0$  and a certain direction in the basal plane. It should be noted that the gap can appear due to other factors, as well, e.g., due to the magnetoelastic interaction (Section 12.2).

Consider now the influence of a *weak moment* (i.e., of the noncollinearity of the sublattice steady magnetizations, Section 3.1) on the magnetic oscillations in the antiferromagnet with an easy plane of anisotropy and  $\mathbf{H}_0$  lying in this plane. The energy term (3.7) does not lead to a qualitative change of the ground state  $-1_{\perp}$



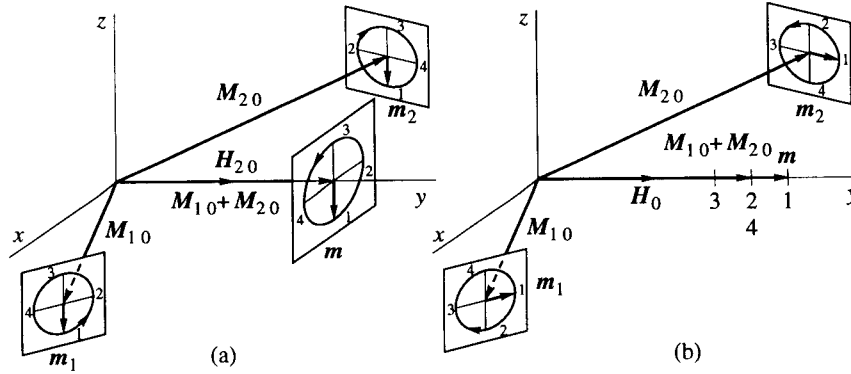


FIGURE 3.12

Precession of the sublattice-magnetization and total-magnetization vectors of an antiferromagnet with easy plane of anisotropy in the ground state  $^{-1}1_{\perp}$  (Figure 3.10) for modes with frequencies (a)  $\omega_{\perp 1}$  and (b)  $\omega_{\perp 2}$ . Numbers are as in Figure 3.8.

(Figure 3.10), but now

$$\sin \varphi_{\perp} = \frac{H_0 + H_D}{2H_E} \quad (3.42)$$

where  $H_D = DM^0$ . The term (3.8), in contrary to the term (3.7), is not invariant under rotations around the  $z$ -axis. Therefore, this term, aside from the fact that it stimulates a certain angle between  $M_{10}$  and  $M_{20}$ , is a source of the anisotropy in the basal plane. If, for simplicity, we suppose  $H_0$  to be directed along the  $y$ -axis, the ground state will remain qualitatively the same as in Figure 3.10. Then, the effective field  $H_F = FM^0$  will appear in (3.42) instead of  $H_D$ .

In the case of the term (3.7), the eigenfrequency of the first mode (for small  $\varphi_{\perp}$ ) is

$$\left(\frac{\omega_1}{\gamma}\right)^2 = H_0(H_0 + H_D) \quad (3.43)$$

and in the case of the term (3.8),

$$\left(\frac{\omega_1}{\gamma}\right)^2 = (H_0 + H_F)(H_0 + 4H_F). \quad (3.44)$$

Comparing these expressions with (3.30), one can see that the allowance for weak ferromagnetism results in an essential change of the spectrum of the mode, for which there was no gap. In the case of the term (3.7), the spectrum changes but remains without a gap. In the case of the term (3.8), a gap appears, as one can see from (3.44).

We have considered the antiferromagnetic resonance in the simple case of a uniaxial two-sublattice antiferromagnet at  $T = 0$ , without taking into account

the shape anisotropy of the sample (i.e., assuming it to be a sphere), and without regard for the sample dimensions. The study of more complicated cases is beyond the scope of this book. We limit ourselves to some brief remarks.

The *shape* of the sample, assuming it to be a small ellipsoid, can be taken into account, in magnetostatic approximation, in the same way as for a ferromagnet (Section 1.5). However, the magnetizations of an antiferromagnet, both steady and ac, are small if  $H_0 \ll H_E$ . Therefore, in such fields the influence of the sample shape on the antiferromagnetic resonance may be neglected.

The requirement for the sample *dimensions* to be small, as compared with the electromagnetic-wave length, is the condition for the applicability of the magnetostatic approximation. As the antiferromagnetic-resonance frequencies are usually very high (lie in the millimeter or submillimeter wavelength ranges), this requirement is difficult to fulfill in experiment.

The next remark concerns the influence of *temperature*. At  $T > 0$  the sublattice magnetizations  $M_{10}$  and  $M_{20}$  differ from  $M^0$  and, in general, from each other. If their values are found, the above-considered theory of antiferromagnetic resonance can be applied almost without changes. It is necessary only to use the values of the parameters  $\gamma$ ,  $H_A$ , and  $H_E$  at a given temperature and to take into account the difference between  $M_{10}$  and  $M_{20}$ . We cite here only the expression for eigenfrequencies in the *antiparallel* state  $^+0_{\parallel}$  found (at  $H_A \ll H_E$ ) with allowance for this difference [122]:

$$\frac{\omega_{\pm}}{\gamma} = \sqrt{2H_A H_E + H_0^2 \frac{\beta}{4}} \pm H_0 \left(1 - \frac{\beta}{2}\right). \quad (3.45)$$

Here  $H_A$  and  $H_E$  are defined according to (3.21) but with substitution of  $\sqrt{M_{10}M_{20}}$  for  $M^0$ , and  $\beta = \Lambda(M_{10} - M_{20})/H_0 \equiv \chi_{0\parallel}/\chi_{0\perp}$  where  $\chi_{0\parallel}$  and  $\chi_{0\perp}$  are the steady susceptibilities for  $\mathbf{H}_0$  directed, respectively, along and perpendicular to the axis of anisotropy. The quantities  $\gamma$  and  $H_E$  are almost independent of temperature. Therefore, the actual temperature dependence of antiferromagnetic-resonance frequencies is determined by the temperature dependence of  $\chi_{0\parallel}$  and  $H_A$ .

The last remark is related to antiferromagnets with more *complicated magnetic structures*. The number  $N$  of the sublattices, which is equal to the number of magnetic ions in a primitive magnetic cell (Section 3.1), can be rather large in such substances. The number of eigenmodes in each ground state is always equal to the number of sublattices. However, as it has been already mentioned in Section 3.1, some sublattices can be combined with each other to form ultimately two sublattices with antiparallel magnetizations. Then the above-discussed two-sublattice theory can be used. It yields, sometimes to a high accuracy, the spectra of two modes with the lowest frequencies. But the remaining  $(N - 2)$  modes are lost.

In conclusion, we point out the peculiarities of antiferromagnetic resonance, as compared with the ferromagnetic resonance.

1. In antiferromagnets, there are several different ground states in different ranges of  $H_0$ ; in every state there are as many modes as there are magnetic ions in a primitive magnetic cell.
2. The character and the value of the magnetocrystalline anisotropy influence materially the antiferromagnetic-resonance spectra; the contribution of the anisotropy is determined, as a rule, by the geometrical mean of the anisotropy field and large exchange field.
3. Antiferromagnetic-resonance spectra have, as a rule, gaps (finite frequencies at zero steady fields); only one of the branches for  $H_0$ , lying in an easy plane of anisotropy, has no gap; the frequency increases for some branches, and decreases for others with growing  $H_0$ .
4. The ac susceptibility-tensor components in antiferromagnets have small values in not very high steady magnetic fields.

The last peculiarity does not exclude, however, the possibility of antiferromagnets to be used in magnetic devices for the high-frequency part of the microwave range.

---

### 3.3 Magnetic oscillations in ferrimagnets

The theory of ferromagnetic resonance considered in Chapters 1 and 2 is applicable with some restrictions, as we will see, to one of the oscillation modes in ferrimagnets, just to the mode used in practice. The aim of the present section is to prove this statement and to discuss the restrictions.

#### 3.3.1 Ground states of two-sublattice ferrimagnet

In contrast to antiferromagnets, the study of ferrimagnets (excluding the regions near the compensation points) can be performed, in the first approximation, without allowance for the magnetocrystalline anisotropy.

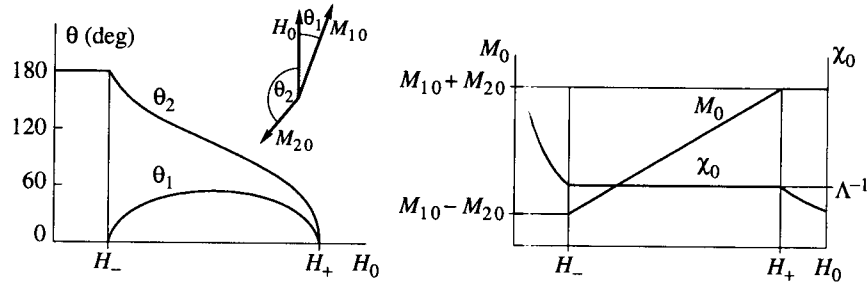
Consider, according to Schlömann [342], the ground states of a *two-sublattice* isotropic ferrimagnet.<sup>6</sup> The energy density can be written as

$$U = -\frac{1}{2}\Lambda_{11}M_1^2 - \frac{1}{2}\Lambda_{22}M_2^2 - \Lambda_{12}\mathbf{M}_1\mathbf{M}_2 - H_0(\mathbf{M}_1 + \mathbf{M}_2) \quad (3.46)$$

where  $\Lambda_{11}$ ,  $\Lambda_{22}$ , and  $\Lambda_{12}$  are the constants of the exchange interaction inside sublattices and between them. Limiting our consideration to the zero temperature, we will regard the lengths of the vectors  $\mathbf{M}_1$  and  $\mathbf{M}_2$  as given. To find the equilibrium orientations of these vectors we set equal to zero the derivatives

---

<sup>6</sup>This problem was first solved by Tyablikov [412] on a microscopic model.

**FIGURE 3.13**

Equilibrium angles of the sublattice magnetizations, the total steady magnetization, and the static susceptibility of an isotropic two-sublattice ferrimagnet vs steady magnetic field.  $M_{10} = 1.5M_{20}$ .

of (3.46) with respect to  $\theta_1$  and  $\theta_2$ . We get that either  $\sin \theta_1 = \sin \theta_2 = 0$  or

$$\cos \theta_1 = \frac{H_0^2 + H_+ H_-}{2H_0 \Lambda M_{10}} \quad \cos \theta_2 = \frac{H_0^2 - H_+ H_-}{2H_0 \Lambda M_{20}} \quad (3.47)$$

where  $\Lambda \equiv -\Lambda_{12}$ , and  $H_{\pm} = \Lambda(M_{10} \pm M_{20})$  are the so-called exchange fields. It is easy to see that

$$M_{10} \sin \theta_1 = -M_{20} \sin \theta_2. \quad (3.48)$$

One can make sure that the energy (3.46) is minimal at  $\theta_1$  and  $\theta_2$  values given in Table 3.3. These equilibrium values are plotted vs  $H_0$  in Figure 3.13. In ferrites, usually,  $\Lambda \gtrsim 10^3$ , and the first exchange field  $H_- \sim 10^5$  Oe, the second exchange field  $H_+$  is several times larger.

**TABLE 3.3**

Ground states of isotropic two-sublattice ferrimagnet at  $T = 0$ .

Ground state	Field range <sup>a</sup>	Equilibrium values of $\theta_1$ and $\theta_2$ (Figure 3.13)
Antiparallel	$0 < H_0 < H_-$	$\theta_{10} = 0 \quad \theta_{20} = \pi$
Noncollinear	$H_- < H_0 < H_+$	Formulae (3.47)
Parallel	$H_+ < H_0$	$\theta_{10} = \theta_{20} = 0$

<sup>a</sup> $H_{\pm} = \Lambda(M_{10} \pm M_{20})$ .

It follows from (3.48) that the total steady magnetization  $M_0 = M_{10} + M_{20}$  is always parallel to  $H_0$ . The dependence of  $M_0$  and  $\chi_0 = M_0/H_0$  on  $H_0$  is also shown in Figure 3.13.

To find the ground states at  $T > 0$  it is necessary to take into account the temperature dependence of  $M_{10}$  and  $M_{20}$ . If the larger (at  $T = 0$ ) magnetization decreases faster with growing temperature than the smaller one, then a temperature

compensation point (Section 3.1) appears. A typical example is the rare-earth garnets (e.g., [447, 138]), in which the magnetization of the dodecahedral (rare-earth) sublattice decreases faster with growing temperature than the magnetization of the combined (tetrahedral plus octahedral) iron sublattice.

### 3.3.2 Oscillations in antiparallel ground state

As we do not take into account for the present the demagnetizing fields and magnetocrystalline anisotropy, the effective fields that enter the equations of motion are, according to (3.46),

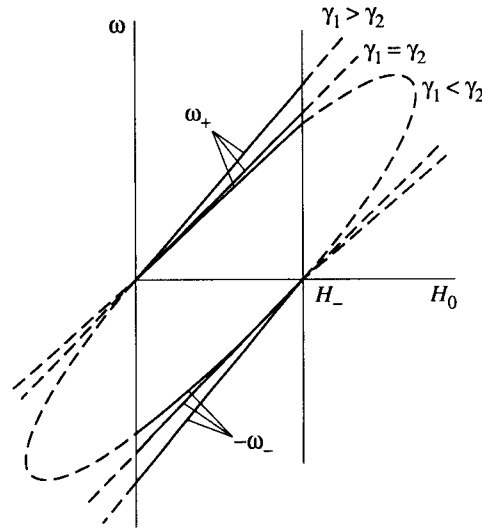
$$\mathbf{H}_{\text{ef},1,2} = \mathbf{H}_0 - \Lambda \mathbf{M}_{2,1}. \quad (3.49)$$

Projecting the equations of motion (3.14) onto the coordinate axes and passing to the circular variables, we get

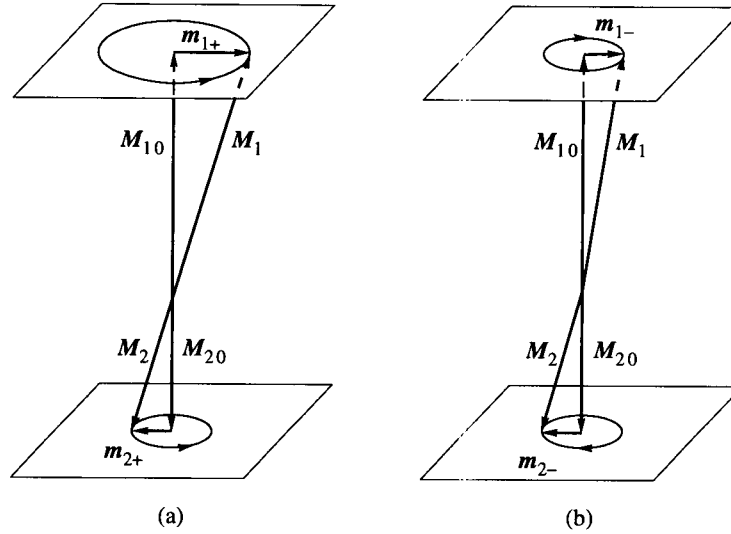
$$\begin{aligned} [\pm\omega - \gamma_1 (H_0 + \Lambda M_{20}) - i\alpha_1\omega] m_{1\pm} - \gamma_1 \Lambda M_{10} m_{2\pm} &= -\gamma_1 M_{10} h_{\pm} \\ \gamma_2 \Lambda M_{20} m_{1\pm} + [\pm\omega - \gamma_2 (H_0 - \Lambda M_{10}) + i\alpha_2\omega] m_{2\pm} &= \gamma_2 M_{20} h_{\pm}. \end{aligned} \quad (3.50)$$

Setting the determinant of this system with  $\alpha_{1,2} = 0$  and  $h_{\pm} = 0$  equal to zero, we obtain the equation for the *eigenfrequencies*:

$$\begin{aligned} \omega^2 \pm \omega [\Lambda (\gamma_2 M_{10} - \gamma_1 M_{20}) - (\gamma_1 + \gamma_2) H_0] \\ - \gamma_1 \gamma_2 H_0 [\Lambda (M_{10} - M_{20}) H_0]. \end{aligned} \quad (3.51)$$



**FIGURE 3.14**  
Eigenfrequencies of a two-sublattice ferrimagnet in the antiparallel ground state.

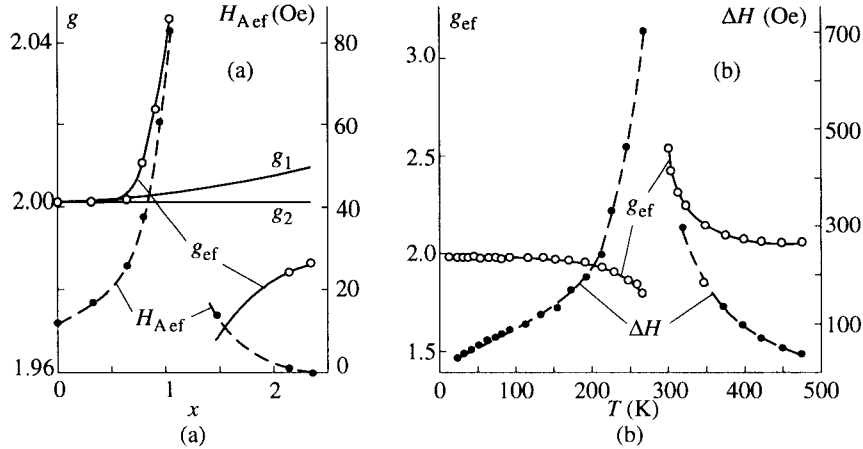
**FIGURE 3.15**

Precession of the sublattice magnetizations of a ferrimagnet in the antiparallel ground state for (a) the 'ferromagnetic' and (b) exchange modes. A small difference between the values of  $m_{1-}$  and  $m_{2-}$  is not shown.

The signs  $\pm$  in (3.51) correspond to the two modes of eigenoscillations. It is appropriate to replace these signs by the single sign  $+$ . Then we obtain an equation the roots of which represent the frequency  $\omega_+$  of the first mode and the frequency of the second mode with reversed sign ( $-\omega_-$ ). It is easy to make sure that it will be the equation of hyperbolas in  $(\omega, H_0)$  plane (Figure 3.14). The form of the hyperbolas depends on the value of  $(\gamma_1 - \gamma_2)$ ; if  $\gamma_1 = \gamma_2$ , the hyperbolas transform into a pair of parallel straight lines. Of course, only the segments of the hyperbolas in the limits  $0 < H_0 < H_-$  have physical sense because only in these limits the ground state is the assumed antiparallel state. As the eigenfrequencies must be positive, the segments with  $\omega > 0$  give the frequencies  $\omega_+$ , and those with  $\omega < 0$  give  $(-\omega_-)$ . One can see from Figure 3.14 that the dependence of  $\omega_+$ , as well as of  $\omega_-$ , on  $H_0$  is, in general ( $\gamma_1 \neq \gamma_2$ ), nonlinear. The frequency  $\omega_-$  is high at  $H_0 = 0$  and decreases with growing  $H_0$ . At  $H_0 \cong H_-/2$  the degeneration of the two modes occurs.

Approximate expressions for  $\omega_+$  and  $\omega_-$  (when  $H_0 \ll H_-$ ), obtained by Wangness [434], have the form

$$\omega_+ \cong \frac{M_{10} - M_{20}}{M_{10}/\gamma_1 - M_{20}/\gamma_2} H_0 \equiv \gamma_{\text{ef}} H_0 \quad (3.52)$$

**FIGURE 3.16**

Effective parameters of ferrimagnets with (a) compositional and (b) temperature compensation points. (a) Garnet  $\text{Y}_3\text{Fe}_{5-x}\text{Ga}_x\text{O}_{12}$ ,  $T = 77$  K;  $g$ -factor of the tetrahedral sublattice  $g_1$  was calculated assuming  $g$ -factor of the octahedral sublattice  $g_2$  to be independent of  $x$  [331]. (b) Garnet  $\text{Gd}_3\text{Fe}_5\text{O}_{12}$ ;  $\Delta H$  values are for  $\mathbf{H} \parallel \langle 111 \rangle$  [329].

$$\omega_- \cong \Lambda (\gamma_2 M_{10} - \gamma_1 M_{20}) - \frac{M_{10}\gamma_2/\gamma_1 - M_{20}\gamma_1/\gamma_2}{M_{10}/\gamma_1 - M_{20}/\gamma_2} H_0 \equiv \omega_E - \gamma'_{\text{ef}} H_0. \quad (3.53)$$

The quantity  $\gamma'_{\text{ef}}$  in (3.52) is the ratio of the total steady magnetic moment to the total steady moment of momentum.

It is easy to make sure, in the same way as for antiferromagnets (Section 3.2), that the mode with frequency  $\omega_+$  is a *right-hand* circular precession, and the mode with frequency  $\omega_-$  is a *left-hand* precession around the direction of  $\mathbf{H}_0$  and  $\mathbf{M}_0$  (Figure 3.15). The ratios of the amplitudes of the sublattice ac magnetizations for these modes (if  $H_0 \ll H_-$ ) are

$$\frac{m_{1+}}{m_{2+}} \cong -\frac{M_{10}}{M_{20}} \quad \frac{m_{1-}}{m_{2-}} \cong \frac{\gamma_1}{\gamma_2}. \quad (3.54)$$

The first relation (3.54) means that the vectors  $\mathbf{M}_1$  and  $\mathbf{M}_2$  are always antiparallel to each other. No work is done against the exchange forces in such a movement, which is why the exchange constant  $\Lambda$  does not appear in expression (3.52). For the second mode, the vectors  $\mathbf{M}_1$  and  $\mathbf{M}_2$  do not remain antiparallel, and the frequency  $\omega_-$  essentially depends on  $\Lambda$ . This mode is called the *exchange mode*, and the first one (with frequency  $\omega_+$ ) is called the *ferromagnetic mode*.

It follows from (3.52) that the frequency  $\omega_+$  tends to zero when approaching the magnetic compensation point and tends to infinity when approaching the mechanical compensation point. The frequency  $\omega_-$ , which, at low  $H_0$  values, lies usually in the infrared region, decreases when approaching the compensation

points, so that it can appear in the microwave region. Although formulae (3.52) and (3.53) hold (approximately) only under condition  $H_0 \ll H_- \equiv \Lambda(M_{10} - M_{20})$ , i.e., far from the compensation points, the mentioned tendencies agree with the experiment (Figure 3.16). However, the theory of magnetic oscillations in ferrimagnets *near the compensation points*, as the antiferromagnetic-resonance theory, can be developed only with allowance for the anisotropy (see, e.g., the paper by Geschwind and Walker [136]).

### 3.3.3 Oscillations in noncollinear ground state

The steady sublattice magnetizations for the noncollinear ground state (Table 3.3) can be written in the form

$$\mathbf{M}_{1,20} = (z_0 \cos \theta_{1,2} + y_0 \sin \theta_{1,2}) M_{1,20} \quad (3.55)$$

where the angles  $\theta_1$  and  $\theta_2$  are determined by (3.47). Projecting the equations of motion (3.14) with  $\alpha_{1,2} = 0$  and  $\mathbf{h} = 0$  onto the coordinate axes and taking into account (3.49) and (3.55), we obtain a set of six uniform linear equations for the components of  $\mathbf{m}_1$  and  $\mathbf{m}_2$ . Limiting ourselves, for simplicity, to the case  $\gamma_1 = \gamma_2$ , we get from the mentioned system the following equations for the vector  $\mathbf{m} = \mathbf{m}_1 + \mathbf{m}_2$  components:

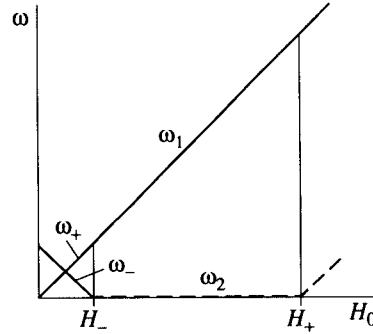
$$\frac{i\omega}{\gamma} m_x + H_0 m_y = 0 \quad -H_0 m_x + \frac{i\omega}{\gamma} m_y = 0 \quad \frac{i\omega}{\gamma} m_z = 0. \quad (3.56)$$

It follows from these equations that two modes are possible. For the first mode,  $\omega_1 = \gamma H_0$  (Figure 3.17),  $m_y = -im_x$ , and  $m_z = 0$ . For the second mode,  $\omega_2 = 0$  and  $m_x = m_y = 0$ . The appearance of the mode with zero frequency (a *soft* mode) could be expected because the ground state breaks the cylindrical symmetry of the energy.

Equations (3.56) and the frequency  $\omega_1 = \gamma H_0$  coincide with the corresponding expressions for a *ferromagnet* (Section 1.3). Thus, in the noncollinear state, as in the antiparallel state, there exists a 'ferromagnetic' mode. The *character of precession* of the sublattice-magnetization vectors  $\mathbf{M}_1$  and  $\mathbf{M}_2$  can be found with the use of the initial equations for the components of  $\mathbf{m}_1$  and  $\mathbf{m}_2$ . For the second (soft) mode, an infinitely slow precession of both vectors  $\mathbf{M}_1$  and  $\mathbf{M}_2$  around the  $z$ -axis takes place. For the first mode, the tips of these vectors move along the ellipses, but the projections of the ellipses on the  $xy$  plane are circles, as well as the trajectory of the tip of the total magnetization vector  $\mathbf{M}$ . One can assure that, for the first mode, the angle between the vectors  $\mathbf{M}_1$  and  $\mathbf{M}_2$  *does not change* in the precession; and that is why the frequency of this mode is independent of the exchange constant.

One of the modes in the third (parallel) ground state (Table 3.3) coincides with the oscillation mode for a ferromagnet with the steady magnetization  $\mathbf{M}_{10} + \mathbf{M}_{20}$ .



**FIGURE 3.17**

Eigenfrequencies of a two-sublattice ferrimagnet with  $\gamma_1 = \gamma_2$ . Dashed lines correspond to modes with  $m = 0$ .

### 3.3.4 Damped and forced oscillations

Let us limit ourselves to the oscillations in the *antiparallel* state. Then, to consider the influence of losses, we have to set equal to zero the determinant of system (3.50) with  $\alpha_{1,2} \neq 0$ . Assume  $\alpha_1$  and  $\alpha_2$  to be less than or of the order of unity. Assume also that the steady magnetic field is sufficiently low and we are far from the compensation points, so that the conditions  $H_0 \ll H_-$  and (for the first mode)  $\omega \ll \gamma_{1,2}H_-$  are satisfied. Then, for the first mode, we find

$$\omega' = \frac{\gamma_{\text{ef}}H_0}{1 + \alpha_{\text{ef}}^2} \quad (3.57)$$

$$\omega'' = \alpha_{\text{ef}}\omega' \quad (3.58)$$

where  $\gamma_{\text{ef}}$  is determined by (3.52) and

$$\alpha_{\text{ef}} = \frac{\alpha_1 M_{10}/\gamma_1 + \alpha_2 M_{20}/\gamma_2}{M_{10}/\gamma_1 - M_{20}/\gamma_2}. \quad (3.59)$$

According to (3.61),  $\alpha_{\text{ef}}$  tends to infinity at approaching the *mechanical* compensation point.

The damping of the mode with frequency  $\omega_-$  can be treated in the same manner. Assuming  $\alpha_{1,2} \ll 1$  and, as before,  $H_0 \ll H_-$ , we get an expression analogous to (3.58) but with a somewhat different effective dissipation parameter.

Consider now the *forced* oscillations, again in the antiparallel ground state. Solving system (3.50) with the *upper* signs in the presence of an ac field  $h_+$ , we find  $m_+ = m_{1+} + m_{2+} = \chi_+ h_+$ , where, with the same assumptions as before ( $H_0 \ll H_-$  and  $\alpha_{1,2} \lesssim 1$ ), we get

$$\chi_+ = \frac{\gamma_{\text{ef}}(M_{10} - M_{20})}{\omega_+ - \omega + i\alpha_{\text{ef}}\omega}. \quad (3.60)$$

This result is of great importance: (3.60) coincides with the expression for the

circular susceptibility of a ferromagnet [which is obtained from (1.49) with the substitution (1.68)] if we replace  $M_0$  by  $(M_{10} - M_{20})$  and substitute  $\gamma_{ef}$  and  $\alpha_{ef}$  for  $\gamma$  and  $\alpha$ .

It follows from (3.60), with regard for (3.52) and (3.59), that

$$\Delta H = 2\omega \frac{\alpha_1 M_{10}/\gamma_1 + \alpha_2 M_{20}/\gamma_2}{M_{10} - M_{20}}. \quad (3.61)$$

The linewidth (3.61) increases with the approach to the *magnetic* compensation point. It should be noted that this increase, as well as the increase of  $\Delta\omega = 2\alpha_{ef}\omega$  at approach to the mechanical compensation point, is a phenomenological effect not related to any new relaxation mechanism.

If  $\gamma_1$  and  $\gamma_2$  differ only slightly from each other, so that the magnetic and the mechanical compensation points are very near to each other, then both  $\Delta H$  and  $\Delta\omega$  increase in the field or frequency range in which the compensation points lie (Figure 3.16). But if there is a great difference between  $\gamma_1$  and  $\gamma_2$ , then large  $\gamma_{ef}$  values can be observed at a mechanical compensation point where the  $\Delta H$  value is small. This effect was observed [250] in the garnet  $\text{Eu}_3\text{Fe}_{5-x}\text{Ga}_x\text{O}_{12}$ .

Solving system (3.50) with *lower* signs at  $H_0 \ll H_-$  and  $\alpha_{1,2} \ll 1$ , we can find the susceptibility  $\chi_-$  to be proportional to  $(\gamma_1 - \gamma_2)^2$ . The difference between  $\gamma_1$  and  $\gamma_2$  is usually small. Therefore, the ferrimagnetic resonance for the exchange mode, with frequency  $\omega_-$  (which lies in the infrared range), is a weak effect. However, it was observed in rare-earth garnets [360].

An arbitrary transverse ac field is the sum of fields with right-hand and left-hand circular polarizations. Each of them excites ac magnetization with circular polarization and the corresponding direction of rotation. As the eigenfrequencies  $\omega_+$  and  $\omega_-$  differ strongly from each other (except in the small regions near the compensation points or near  $H_0 = H_-/2$ ), the magnetizations  $m_+$  and  $m_-$ , as a rule, are not excited simultaneously.

We have not yet taken into account the *demagnetizing fields*. So, the considered quantities  $\chi_+$  and  $\chi_-$  are components of the susceptibility  $\vec{\chi}$  of a *substance* (a ferrimagnet). The transition from  $\vec{\chi}$  to the susceptibility  $\vec{\chi}^e$  of a small ellipsoidal sample is a magnetostatic problem, independent of the properties of the substance. Therefore, all expressions for the eigenfrequencies and  $\vec{\chi}^e$  components, obtained in Section 1.5, will be valid for a ferrimagnet with the *effective* parameters.

The above-considered theory of magnetic oscillations in ferrimagnets is valid, furthermore, only at  $T = 0$ , if we regard the parameters  $M_{j0}$ ,  $\gamma_j$ , and  $\alpha_j$  as given quantities, which are independent of temperature. But if we take into account the *temperature dependence* of all parameters, the theory will be valid at  $T > 0$ , too. The lengths of the sublattice steady magnetization vectors  $M_{j0}$ , and, hence, the length of the total magnetization vector  $M_0$ , depend now on temperature and must be found, together with the directions of these vectors, as mentioned in Section 3.1. For the 'ferromagnetic' mode in low fields and far from compensation points, the only parameters for which the temperature dependence is, practically, to be taken into account are: the total magnetization  $M_0$ , the effective dissipation parameter

$\alpha_{\text{ef}}$ , and also the effective anisotropy constant (see below).

To take into account the magnetocrystalline anisotropy in ferrimagnets we have to add the energy terms that describe the anisotropy to the energy (3.46). It is often assumed, as in the case of antiferromagnets, that the energy of anisotropy is the sum of anisotropy energies of sublattices.

In the most important case of the 'ferromagnetic' mode, at  $H_0 \ll H_-$  and far from compensation points, we obtain for the eigenfrequencies and  $\vec{\chi}$  components the same expressions as for ferromagnets, but the anisotropy constants in these expressions are the effective constants. If the additivity of sublattice anisotropy energies takes place, the effective anisotropy constants are, simply, the sums of the corresponding sublattice constants. The effective anisotropy fields are obtained by dividing the effective anisotropy constants by the total magnetization  $M_{10} - M_{20}$ . These fields increase with the approach to the *magnetic* compensation points (Figure 3.16).

Far enough from compensation points (or if there are no such points in the considered ferrimagnet), the influence of the magnetocrystalline anisotropy is, in common with ferromagnets, a first-order effect, the oscillations in an isotropic medium being the zero approximation. The angular dependence of the resonance frequencies or fields are then the same as for ferromagnets. That is why the experimental data obtained in ferrimagnets  $\text{RbNiF}_3$  and  $\text{Y}_3\text{Fe}_5\text{O}_{12}$  have been used in Section 2.3 (Figures 2.5 and 2.8) to illustrate the angular dependence of the ferromagnetic resonance fields. But near the compensation points the magnetocrystalline anisotropy, as it has been already mentioned, should be taken into account in the zero approximation, no matter how small the anisotropy is.

The equivalence of a ferrimagnet—under certain conditions—to a ferromagnet holds for an *arbitrary* number of sublattices. The sublattice steady magnetizations may even be noncollinear, but the total magnetization  $M_0 = |\sum \mathbf{M}_{j0}|$  should be large. Turov has shown [410] that in this case there always exists a 'ferromagnetic' mode, for which, in a sufficiently weak steady magnetic field, the 'bunch' of the sublattice-magnetization vectors precesses, as a whole, around the  $\mathbf{M}_0$  direction.

Ferrimagnets are the only magnetic materials widely used presently at *microwave* frequencies. Therefore, it is very important that, under the above-mentioned conditions (which are usually satisfied in practice), ferrimagnets are equivalent to ferromagnets. We can 'forget' that they are ferrimagnets and apply all the results of the comparatively simple ferromagnetic-resonance theory.

However, the following peculiarities of magnetic oscillations in ferrimagnets are to be kept in mind:

1. In addition to the 'ferromagnetic' mode, there exist  $(N - 1)$  *exchange modes* ( $N$  is the number of sublattices), the frequencies of which, in weak steady magnetic fields, lie usually in the infrared range.
2. In *strong steady magnetic fields*, on the order of  $\Lambda M_0$ , the frequencies of the 'ferromagnetic' and the exchange modes become comparable and both *depend on the exchange constants*.

3. In the vicinity of *compensation points*, the frequencies of the ferromagnetic and the exchange modes draw near and *depend on the exchange constants* even in weak steady fields; magnetocrystalline anisotropy influences here essentially the frequencies and the character of oscillations.
4. In the range of steady magnetic fields from  $H_- = \Lambda(M_{10} - M_{20})$  to  $H_+ = \Lambda(M_{10} + M_{20})$  (in the case of two sublattices) the ground state is *noncollinear*; a *soft mode* appears in this range in addition to a ferromagnetic mode.

# 4

---

## *Fundamentals of electrodynamics of gyrotropic media*

---

---

### 4.1 Equations

In the preceding chapters we considered the behavior of ferromagnets, antiferromagnets, and ferrimagnets in *given* ac magnetic fields and obtained the tensor magnetic susceptibilities of these substances. However, the ac magnetic field cannot be, usually, regarded as given; it is to be found, together with the ac magnetization, by solving the corresponding electrodynamic problem. The simplest of such problems was already treated in Section 1.5. The magnetostatic approximation was applicable in that case, and a well-known solution of magnetostatic equations was used. We now pass to the general case when full Maxwell's equations, together with boundary conditions, are to be used.

The aim of the present chapter is to discuss the peculiarities of Maxwell's equations, as well as some methods of solving them and some general consequences of them, for the case of gyrotropic media. We define a gyrotropic medium as having nonsymmetric tensor parameters  $\vec{\epsilon}$  and  $\vec{\mu}$ . In this and two following chapters the components of these tensors will be assumed to depend on  $\omega$ ,  $\mathbf{H}_0$ , and  $\mathbf{M}_0$  but not on the wave vector  $\mathbf{k}$ . The dependence on  $\mathbf{k}$ , i.e., the spatial dispersion, will be taken into account in Chapter 7.

#### 4.1.1 General equations and boundary conditions

The fundamental equations of macroscopic electrodynamics, the *Maxwell equations* (e.g., [246, 191]) are

$$\begin{aligned} \operatorname{rot} \mathbf{E} + \frac{1}{c} \frac{\partial \mathbf{B}}{\partial t} &= 0 & \operatorname{div} \mathbf{B} &= 0 \\ \operatorname{rot} \mathbf{H} - \frac{1}{c} \frac{\partial \mathbf{D}}{\partial t} &= \frac{4\pi}{c} \mathbf{J} & \operatorname{div} \mathbf{D} &= 4\pi R. \end{aligned} \quad (4.1)$$

Here  $\mathbf{E}$  and  $\mathbf{D}$  are the macroscopic electric-field and electric-displacement vectors,  $\mathbf{H}$  and  $\mathbf{B}$  are the macroscopic magnetic-field and magnetic-induction vectors, and  $\mathbf{J}$  and  $R$  are the free electric-current and electric-charge densities. The quantities  $\mathbf{E}$  and  $\mathbf{B}$  are the space and time averages of the microscopic fields, respectively, electric and magnetic. The vectors  $\mathbf{D}$  and  $\mathbf{H}$  in (4.1) are defined as

$$\mathbf{D} = \mathbf{E} + 4\pi\mathbf{P} \quad \mathbf{H} = \mathbf{B} - 4\pi\mathbf{M} \quad (4.2)$$

where  $\mathbf{P}$  is the polarization, i.e., the electric-dipole-moment density, and  $\mathbf{M}$  is the magnetization, which we dealt with in the previous chapters. The equation of charge conservation follows from (4.1):

$$\operatorname{div}\mathbf{J} + \frac{\partial R}{\partial t} = 0. \quad (4.3)$$

The *boundary conditions*, which hold for the field vectors in two adjacent media at their interface, follow also from the Maxwell equations (4.1) and can be written in the form

$$\begin{aligned} \mathbf{E}_1 \times \mathbf{n}_0 - \mathbf{E}_2 \times \mathbf{n}_0 &= 0 & \mathbf{H}_1 \times \mathbf{n}_0 - \mathbf{H}_2 \times \mathbf{n}_0 &= \frac{4\pi}{c}\mathbf{I} \\ \mathbf{D}_1 \mathbf{n}_0 - \mathbf{D}_2 \mathbf{n}_0 &= 4\pi\eta & \mathbf{B}_1 \mathbf{n}_0 - \mathbf{B}_2 \mathbf{n}_0 &= 0 \end{aligned} \quad (4.4)$$

where  $\mathbf{n}_0$  is a unit normal to the interface directed from the first medium into the second;  $\eta$  and  $\mathbf{I}$  are the surface densities, respectively, of the electric charge and of the current. For real media,  $\eta$  and  $\mathbf{I}$  are equal to zero, but they are introduced for an interface of dielectric and metal. Now, the following conditions are satisfied, to a first approximation, by the fields in dielectric

$$\mathbf{E}_1 \times \mathbf{n}_0 = 0 \quad \mathbf{D}_1 \mathbf{n}_0 = 4\pi\eta \quad \mathbf{H}_1 \times \mathbf{n}_0 = \frac{4\pi}{c}\mathbf{I} \quad \mathbf{B}_1 \mathbf{n}_0 = 0. \quad (4.5)$$

To obtain a complete systems of equations the *material equations* are to be added to Maxwell's equations (4.1). The material equations reflect the properties of the considered substances and can be found from theories that describe these substances or from experiment. As the charge density is related to the current density by equation (4.3), it is sufficient to take into account the material equations that express the dependence of  $\mathbf{D}$ ,  $\mathbf{B}$ , and  $\mathbf{J}$  on  $\mathbf{E}$  and  $\mathbf{H}$ . It should be noted that in some cases, e.g., for metals (Section 14.2), it is impossible to consider separately the problems of obtaining the material equations and of integrating the Maxwell equations. But for weakly conducting ferro- or ferrimagnets magnetized to saturation, these problems can be separated. The Landau–Lifshitz equation of motion, as well as the expressions for the tensor  $\vec{\chi}$  components, which are obtained by solving this equation, can be regarded as material equations for such substances.

The magnetic field in our case is a sum of the steady and ac fields. Suppose all the quantities in (4.1), including electric field, to be such sums. Assume that the ac components  $h_{\sim}$ ,  $e_{\sim}$ ,  $b_{\sim}$ ,  $d_{\sim}$ ,  $\rho_{\sim}$ , and  $j_{\sim}$  are small as compared with the

steady components, respectively,  $\mathbf{H}_0$ ,  $\mathbf{E}_0$ ,  $\mathbf{B}_0$ ,  $\mathbf{D}_0$ ,  $R_0$ , and  $\mathbf{J}_0$ . Then, if the given fields and currents vary harmonically with time, all ac quantities have such time dependence, and we can use the method of complex amplitudes (Section 1.3).

Substituting the sums of steady and ac components of all quantities into (4.1), we obtain two independent systems of equations: for steady components and, according to the method of complex amplitudes, for the complex amplitudes of ac components. The first system, in its turn, divides into two independent systems: the electrostatic and the *magnetostatic*, which has the form

$$\operatorname{rot}\mathbf{H}_0 = \frac{4\pi}{c}\mathbf{J}_0 \quad \operatorname{div}\mathbf{B}_0 = 0. \quad (4.6)$$

The system for the *complex amplitudes* of the ac quantities<sup>1</sup> is

$$\operatorname{rote} + ik_0\mathbf{b} = 0 \quad (4.7)$$

$$\operatorname{roth} - ik_0\mathbf{d} = \frac{4\pi}{c}\mathbf{j} \quad (4.8)$$

$$\operatorname{div}\mathbf{b} = 0 \quad (4.9)$$

$$\operatorname{div}\mathbf{d} = 4\pi\rho \quad (4.10)$$

where  $k_0 = \omega/c$ . The boundary conditions for the ac components are of the same form as (4.4) or (4.5).

Consider now the material equations for ac components. Neglecting the small 'mixed' terms, assume that  $\mathbf{d}$  depends only on  $\mathbf{e}$ , and  $\mathbf{b}$  depends only on  $\mathbf{h}$ . Then, for small amplitudes (in linear approximation)

$$\mathbf{d} = \vec{\epsilon}_d \mathbf{e} \quad (4.11)$$

$$\mathbf{b} = \vec{\mu} \mathbf{h} \quad (4.12)$$

where  $\vec{\epsilon}_d$  is the *dielectric constant* (which can depend, nevertheless, on frequency, temperature, etc.) and  $\vec{\mu}$  is the *permeability*, which was considered in detail in the preceding chapters. The current density can be written as

$$\mathbf{j} = \vec{\sigma} \mathbf{e} + \mathbf{j}_{\text{ext}} \quad (4.13)$$

where  $\vec{\sigma}$  is the high-frequency conductivity ( $\mathbf{j} = \vec{\sigma} \mathbf{e}$  is the Ohm law). The quantity  $\mathbf{j}_{\text{ext}}$  is the density of an *external* current, which is excited by the fields not taken into account explicitly in the considered problem.

Using (4.11)–(4.13), we can exclude  $\mathbf{d}$ ,  $\mathbf{b}$ , and  $\mathbf{j}$  from Maxwell's equations (4.7)–(4.10) and obtain

$$\operatorname{rote} + ik_0 \vec{\mu} \mathbf{h} = 0 \quad (4.14)$$

$$\operatorname{roth} - ik_0 \vec{\epsilon} \mathbf{e} = \frac{4\pi}{c} \mathbf{j}_{\text{ext}} \quad (4.15)$$

<sup>1</sup>Later on we will omit, as in the preceding chapters, the words 'complex amplitudes'.

$$\operatorname{div}(\vec{\mu} \mathbf{h}) = 0 \quad (4.16)$$

$$\operatorname{div}(\vec{\varepsilon} \mathbf{e}) = 4\pi \rho_{\text{ext}} \quad (4.17)$$

where  $\rho_{\text{ext}} = (i/\omega)\operatorname{div}\mathbf{j}_{\text{ext}}$  and

$$\vec{\varepsilon} = \vec{\varepsilon}_d - i\frac{4\pi}{\omega}\vec{\sigma}. \quad (4.18)$$

The tensor  $\vec{\varepsilon}$ , as distinct from  $\vec{\varepsilon}_d$ , will be called *permittivity*. We can exclude  $\mathbf{e}$  or  $\mathbf{h}$  from (4.14) and (4.16) to obtain a second-order differential equation for each of these vectors.

Let us introduce designations for the tensor  $\vec{\mu}$  components. (Analogous designations can be introduced for the components of the tensor  $\vec{\varepsilon}$ .) Represent  $\vec{\mu}$  as a sum of a symmetric  $\vec{\mu}_s$  and an antisymmetric  $\vec{\mu}_{\text{as}}$  tensors. The components of the former are

$$(\mu_s)_{pq} = (\mu_s)_{qp} \equiv \mu_{pq} = \mu'_{pq} - i\mu''_{pq} \quad p, q = 1, 2, 3 \equiv x, y, z \quad (4.19)$$

and the components of the latter are

$$(\mu_{\text{as}})_{pq} = -(\mu_{\text{as}})_{qp} \equiv i\mu_{\alpha pq} = i(\mu'_{\alpha pq} - i\mu''_{\alpha pq}) \quad p \neq q \quad (4.20)$$

where all the quantities  $\mu'_{pq}$ ,  $\mu''_{pq}$ ,  $\mu'_{\alpha pq}$ , and  $\mu''_{\alpha pq}$  are real. Three tensor  $\vec{\mu}_{\text{as}}$  components  $\mu_{\alpha 12}$ ,  $\mu_{\alpha 23}$ , and  $\mu_{\alpha 31}$  can be regarded as components of the vector  $4\pi\mathbf{G}_m$ , where  $\mathbf{G}_m$  is the magnetic gyration vector (1.44). Then,

$$\mathbf{b} = \vec{\mu}_s \mathbf{h} + i4\pi \mathbf{h} \times \mathbf{G}_m. \quad (4.21)$$

The tensor  $\vec{\mu}$  can be also represented as a sum of a Hermitian ( $\vec{\mu}_H$ ) and an anti-Hermitian ( $\vec{\mu}_{\text{aH}}$ ) tensor with components

$$(\mu_H)_{pq} = \mu'_{pq} + i\mu'_{\alpha pq} \quad (\mu_{\text{aH}})_{pq} = \mu''_{\alpha pq} - i\mu''_{pq}. \quad (4.22)$$

#### 4.1.2 Equations for bigyrotropic media

Consider a medium which is isotropic in the absence of steady magnetization. The only preferred direction is then the direction of  $\mathbf{M}_0$ , and the parameters of such a medium have the form

$$\vec{\mu} = \begin{vmatrix} \mu & i\mu_\alpha & 0 \\ -i\mu_\alpha & \mu & 0 \\ 0 & 0 & \mu_{\parallel} \end{vmatrix} \quad \vec{\varepsilon} = \begin{vmatrix} \varepsilon & i\varepsilon_\alpha & 0 \\ -i\varepsilon_\alpha & \varepsilon & 0 \\ 0 & 0 & \varepsilon_{\parallel} \end{vmatrix} \quad (4.23)$$

(the third axis is directed along  $\mathbf{M}_0$ ). For polycrystalline ferrites in microwave range,  $\varepsilon$  can be regarded as a scalar. In visible light and at higher frequencies,  $\mu$  differs only slightly from unity. Nevertheless, we will deal with the medium the tensor parameters of which have *simultaneously* the form (4.23). The main reason



for considering such a medium (we call it bigyrotropic) is that the antisymmetric components of  $\vec{\varepsilon}$  and of  $\vec{\mu}$  can be of the same order for ferrites in the infrared range and for some ferromagnetic semiconductors, even at microwave frequencies.

Let us consider the peculiarities of the electrodynamic equations for the medium with parameters (4.23) in the case of  $\mathbf{j}_{\text{ext}} = 0$ . Excluding the transverse (with respect to  $\mathbf{M}_0$ )  $\mathbf{h}$  and  $\mathbf{e}$  components from the projections of Maxwell's equations, we get the following equations for the longitudinal components:

$$\begin{aligned} \left( \nabla_{\perp}^2 + \frac{\varepsilon_{\parallel}}{\varepsilon} \frac{\partial^2}{\partial z^2} + k_0^2 \varepsilon_{\parallel} \mu_{\perp} \right) e_z + k_0 \mu_{\parallel} \left( \frac{\varepsilon_a}{\varepsilon} + \frac{\mu_a}{\mu} \right) \frac{\partial}{\partial z} h_z &= 0 \\ \left( \nabla_{\perp}^2 + \frac{\mu_{\parallel}}{\mu} \frac{\partial^2}{\partial z^2} + k_0^2 \varepsilon_{\perp} \mu_{\parallel} \right) h_z - k_0 \varepsilon_{\parallel} \left( \frac{\varepsilon_a}{\varepsilon} + \frac{\mu_a}{\mu} \right) \frac{\partial}{\partial z} e_z &= 0 \end{aligned} \quad (4.24)$$

where

$$\varepsilon_{\perp} = \varepsilon - \frac{\varepsilon_a^2}{\varepsilon} \quad \mu_{\perp} = \mu - \frac{\mu_a^2}{\mu}. \quad (4.25)$$

Here  $\nabla_{\perp}$  is the Hamilton nabla operator in the  $xy$  plane:

$$\nabla_{\perp} = x_0 \frac{\partial}{\partial x} + y_0 \frac{\partial}{\partial y} \quad \nabla_{\perp}^2 = \frac{\partial^2}{\partial x^2} + \frac{\partial^2}{\partial y^2}.$$

It follows from (4.24) that the TE field (with  $e_z = 0$  and  $h_z \neq 0$ ) and the TM field (with  $h_z = 0$  and  $e_z \neq 0$ ) *cannot exist* in a gyrotropic medium except if  $\partial/\partial z = 0$ . As to the TEM field, its existence is not forbidden by equations (4.24).

It is possible to exclude  $e_z$  or  $h_z$  from equations (4.24) and get the differential equation  $\mathcal{L}(h_z) = 0$  or  $\mathcal{L}(e_z) = 0$ , where  $\mathcal{L}$  is a certain fourth-order linear operator [109] (see also [153]). The same equations hold for transverse components of  $\mathbf{e}$  and  $\mathbf{h}$ . The scalar potential function  $\psi$  can be introduced [109], which also satisfies the equation  $\mathcal{L}(\psi) = 0$ ; all  $\mathbf{e}$  and  $\mathbf{h}$  components can be obtained from this function by differential operations. However, the fourth-order differential equation for the function  $\psi$  can be integrated analytically only in a limited number of problems.<sup>2</sup>

The situation becomes simpler in the particular, but important, case when the dependence of the  $\psi$  function on the coordinate  $z$  (in the direction of steady magnetization) is harmonic. It means that  $\psi = Z(z)\psi_{\perp}(x, y)$ , where  $Z(z)$  has the form of  $\exp(\pm ik_z z)$ ,  $\cos(k_z z)$ ,  $\sin(k_z z)$  or is a linear combination of these functions. This case includes also the absence of the dependence on  $z$ , i.e.,  $k_z = 0$ . If the  $z$  dependence is harmonic, so that  $\partial^2/\partial z^2 = -k_z^2$ , then  $\mathcal{L}$  is a product of two second-order operators:

$$\mathcal{L} = (\nabla_{\perp}^2 + \kappa_1^2)(\nabla_{\perp}^2 + \kappa_2^2). \quad (4.26)$$

<sup>2</sup>For a detailed discussion of this subject see [153].

The quantities  $\kappa_{1,2}^2$  are the roots of the quadratic equation

$$\kappa^4 - p\kappa^2 + q = 0 \quad (4.27)$$

where

$$p = (\varepsilon_{\parallel}\mu_{\perp} + \varepsilon_{\perp}\mu_{\parallel})k_0^2 - \left(\frac{\varepsilon_{\parallel}}{\varepsilon} + \frac{\mu_{\parallel}}{\mu}\right)k_z^2$$

$$q = \varepsilon_{\parallel}\mu_{\parallel}\varepsilon_{\perp}\mu_{\perp}k_0^4 + \frac{\varepsilon_{\parallel}\mu_{\parallel}}{\varepsilon\mu}k_z^4 - 2\varepsilon_{\parallel}\mu_{\parallel}\left(1 + \frac{\varepsilon_a\mu_a}{\varepsilon\mu}\right)k_0^2k_z^2. \quad (4.28)$$

Thus, in the case of harmonic  $z$  dependence there are two modes; the  $\psi_{\perp}$  function for them satisfies the Helmholtz equation

$$\nabla_{\perp}^2\psi_{\perp} + \kappa_{1,2}^2\psi_{\perp} = 0. \quad (4.29)$$

The eigenvalues  $\kappa_1$  and  $\kappa_2$  determine the dependence of the fields on the transverse coordinates. After these values and the functions  $\psi_1$  and  $\psi_2$  are found—by solving (4.29) with corresponding boundary conditions—the  $\mathbf{e}$  and  $\mathbf{h}$  components can be rather easily calculated. Such a technique of solving the boundary electrodynamic problems for media with parameters (4.23) in the case of harmonic  $z$  dependence (or for fields independent on  $z$ ) is considered in [153]; some examples will be given in Chapter 5.

## 4.2 Uniform plane waves

We consider first of all the propagation of a uniform plane wave in an unbounded medium with parameters (4.23). The wave is called *uniform* when the fields depend only on one coordinate, in the direction of propagation. For a uniform *plane* wave this coordinate is Cartesian, i.e., the wave front is a plane.

### 4.2.1 General relations

The complex amplitudes of the field vectors for a uniform plane wave can be written in the form

$$\mathbf{e} = \mathbf{e}_0 \exp(-i\mathbf{k}\mathbf{r}) \quad \mathbf{h} = \mathbf{h}_0 \exp(-i\mathbf{k}\mathbf{r}) \quad (4.30)$$

where  $\mathbf{e}_0$  and  $\mathbf{h}_0$  are constant complex vectors and  $\mathbf{k}$  is the wave vector. Substituting (4.30) into (4.14) and (4.16) with  $\mathbf{j}_{\text{ext}} = 0$ , we get

$$\mathbf{k} \times \mathbf{e} - k_0 \vec{\mu} \mathbf{h} = 0 \quad \mathbf{k} \times \mathbf{h} + k_0 \vec{\varepsilon} \mathbf{e} = 0 \quad (4.31)$$

where  $k_0 = \omega/c$ .

Projecting (4.31) onto the coordinate axes and setting equal to zero the determinant of the obtained system, we could find the dispersion relation, i.e., the dependence of  $\omega$  on the length and direction of the wave vector  $\mathbf{k}$ . This relation can be found, however, in a simpler manner if we use the technique considered in the preceding section. The quantities that appeared there now have the following sense:  $\kappa = k \sin \theta_k$  and  $k_z = k \cos \theta_k$ , where  $\theta_k$  is the angle between  $\mathbf{k}$  and the direction of the steady magnetization  $\mathbf{M}_0$ . Substituting these quantities into (4.27) and (4.28), we obtain directly the *dispersion relation*

$$\begin{aligned} & \frac{k^4}{k_0^4} \left( \frac{\sin^2 \theta_k}{\varepsilon_{\parallel}} + \frac{\cos^2 \theta_k}{\varepsilon} \right) \left( \frac{\sin^2 \theta_k}{\mu_{\parallel}} + \frac{\cos^2 \theta_k}{\mu} \right) - \frac{k^2}{k_0^2} \left[ \left( \frac{\varepsilon_{\perp}}{\varepsilon_{\parallel}} + \frac{\mu_{\perp}}{\mu_{\parallel}} \right) \sin^2 \theta_k \right. \\ & \left. + 2 \left( 1 + \frac{\varepsilon_a \mu_a}{\varepsilon \mu} \right) \cos^2 \theta_k \right] + \varepsilon_{\perp} \mu_{\perp} = 0 \end{aligned} \quad (4.32)$$

where  $\varepsilon_{\perp}$  and  $\mu_{\perp}$  are determined by (4.25). Two roots of this equation correspond to the two normal waves that propagate at the angle  $\theta_k$  to  $\mathbf{M}_0$ .

It should be noted that the roots of (4.32), in general, *cannot* be written in the form

$$k^2 = k_0^2 \varepsilon_{\text{ef}} \mu_{\text{ef}} \quad (4.33)$$

where  $\varepsilon_{\text{ef}}$  would depend only on components of  $\vec{\varepsilon}$  and  $\mu_{\text{ef}}$  would depend only on components of  $\vec{\mu}$ . But (4.33) holds if either  $\varepsilon$  or  $\mu$  is a scalar. In particular, for scalar  $\varepsilon$ , it follows from (4.32) that

$$\begin{aligned} k^2 &= k_0^2 \varepsilon \mu_{\text{ef}}(\theta_k) \\ &= k_0^2 \varepsilon \frac{2 + \left( \frac{\mu_{\perp}}{\mu_{\parallel}} - 1 \right) \sin^2 \theta_k \pm \sqrt{\left( \frac{\mu_{\perp}}{\mu_{\parallel}} - 1 \right)^2 \sin^4 \theta_k + 4 \frac{\mu_{\perp}^2}{\mu_{\parallel}^2} \cos^2 \theta_k}}{2 \left( \frac{\sin^2 \theta_k}{\mu_{\parallel}} + \frac{\cos^2 \theta_k}{\mu} \right)}. \end{aligned} \quad (4.34)$$

If (4.33) is valid, it is easy to make sure that

$$\begin{aligned} k' &= \frac{1}{\sqrt{2}} k_0 (|\varepsilon_{\text{ef}}| |\mu_{\text{ef}}| + \varepsilon'_{\text{ef}} \mu'_{\text{ef}} - \varepsilon''_{\text{ef}} \mu''_{\text{ef}})^{1/2} \\ k'' &= \frac{1}{\sqrt{2}} k_0 (|\varepsilon_{\text{ef}}| |\mu_{\text{ef}}| - \varepsilon'_{\text{ef}} \mu'_{\text{ef}} + \varepsilon''_{\text{ef}} \mu''_{\text{ef}})^{1/2} \end{aligned} \quad (4.35)$$

where it has been assumed that  $\varepsilon_{\text{ef}} = \varepsilon'_{\text{ef}} - i\varepsilon''_{\text{ef}}$ ,  $\mu_{\text{ef}} = \mu'_{\text{ef}} - i\mu''_{\text{ef}}$ , and  $k = k' - ik''$ .

Consider two limiting cases of a medium with scalar  $\varepsilon$ . In the first case, of an ideal *dielectric*,  $\varepsilon'' = 0$ ,  $\varepsilon' = \varepsilon$ , and from (4.35), it follows that

$$k' = \frac{1}{\sqrt{2}} k_0 \sqrt{\varepsilon} (|\mu_{\text{ef}}| + \mu'_{\text{ef}})^{1/2} \quad (4.36)$$

$$k'' = \frac{1}{\sqrt{2}} k_0 \sqrt{\varepsilon} (|\mu_{\text{ef}}| - \mu'_{\text{ef}})^{1/2}. \quad (4.37)$$

In the second case, of a well-conducting *metal*, we may assume, to the first approximation, that  $\varepsilon' = 0$  and, according to (4.18),  $\varepsilon'' = 4\pi\sigma/\omega$ . Then, it follows from (4.35) that

$$k' = k_0 \sqrt{\frac{2\pi\sigma}{\omega}} (|\mu_{\text{ef}}| - \mu_{\text{ef}}'')^{1/2} \equiv \frac{1}{\delta_1} \sqrt{\mu_{\text{ef}} L} \quad (4.38)$$

$$k'' = k_0 \sqrt{\frac{2\pi\sigma}{\omega}} (|\mu_{\text{ef}}| + \mu_{\text{ef}}'')^{1/2} \equiv \frac{1}{\delta_1} \sqrt{\mu_{\text{ef}} R}. \quad (4.39)$$

Here

$$\delta_1 = \frac{1}{k_0} \sqrt{\frac{\omega}{2\pi\sigma}} = \frac{c}{\sqrt{2\pi\sigma\omega}} \quad (4.40)$$

is the skin depth, i.e., the penetration length of an electromagnetic field into metal. Note that if the magnetic losses are taken into account ( $\mu_{\text{ef}}'' \neq 0$ ), then  $k' \neq k''$ .

If the value of  $\varepsilon''$  is finite but small ( $\varepsilon'' \ll \varepsilon'$ ), we get, taking for simplicity  $\mu_{\text{ef}}'' = 0$ , that  $k' \cong k_0 \sqrt{\varepsilon' \mu_{\text{ef}}'}$  and

$$k'' = \frac{1}{2} k_0 \varepsilon'' \sqrt{\frac{\mu_{\text{ef}}'}{\varepsilon'}} \equiv \frac{2\pi\sigma}{c} \sqrt{\frac{\mu_{\text{ef}}'}{\varepsilon'}}. \quad (4.41)$$

#### 4.2.2 Longitudinal magnetization

In the case of so-called longitudinal magnetization, i.e., of wave propagation in the direction of steady magnetization ( $\theta_k = 0$ ) the roots of (4.32) are

$$k_{\pm} = k_0 \sqrt{(\varepsilon \pm \varepsilon_a)(\mu \pm \mu_a)}. \quad (4.42)$$

Upper and lower signs in (4.42) correspond to two waves. To find the field structure for these waves we project equations (4.31) for  $\theta_k = 0$  onto the coordinate axes and, according to the symmetry of the problem, pass to the circular components (Section 1.3) of  $e$  and  $h$ . Then, we get

$$\begin{aligned} k e_{\pm} \pm i k_0 (\mu \pm \mu_a) h_{\pm} &= 0 \\ -k h_{\pm} \pm i k_0 (\varepsilon \pm \varepsilon_a) e_{\pm} &= 0 \end{aligned} \quad (4.43)$$

and  $e_z = h_z = 0$ . It is easy to make sure that upper and lower signs in (4.43) correspond to the same signs in (4.42). It can be shown, in the same manner as in Sections 1.3 and 3.2, that the transverse fields  $e$  and  $h$  have the right-hand circular polarization for the plus signs in (4.42) and (4.43), and have the left-hand circular polarization for the minus signs.

Substituting (4.42) into (4.43), we find

$$\frac{e_{\pm}}{h_{\pm}} = \mp i \sqrt{\frac{\mu \pm \mu_a}{\varepsilon \pm \varepsilon_a}} \equiv \mp i \zeta_{\pm}. \quad (4.44)$$

The quantity  $\zeta_{\pm}$  can be called *wave impedance* of the medium for waves with the right-hand and left-hand circular polarizations propagating in the direction of steady magnetization. It is easy to make sure that for both waves

$$\zeta = \frac{e_x}{h_y} = -\frac{e_y}{h_x}. \quad (4.45)$$

It is clear that all relations, obtained above for  $\theta_k = 0$ , are valid for  $\theta_k = \pi$ , too, if the sense of polarization rotation (right-hand or left-hand) is determined in both cases with respect to  $\mathbf{M}_0$ . It follows from (4.42) and (4.44) that for  $\theta_k = 0, \pi$ , i.e., in the case of longitudinal magnetization, it is possible to introduce the effective parameters  $\varepsilon_{ef\pm} = \varepsilon \pm \varepsilon_a$  and  $\mu_{ef\pm} = \mu \pm \mu_a$ .

The constancy of the field structure in the course of propagation is the definition of a *normal wave*. The waves with right-hand and left-hand circular polarization are the normal waves in the considered case of the longitudinal magnetization. Any other wave can be represented as a sum of normal waves. The difference between their propagation constants  $k_z$  leads to the variation of the field structure (polarization) of the total wave in the course of propagation.

Suppose, e.g., that at  $z = 0$  there is a linearly polarized wave with the electric field  $e(0) = e_0 x_0$ . It can be represented as a sum of the right-hand and the left-hand circularly polarized waves:

$$e(0) = \frac{e_0}{2}(x_0 - iy_0) + \frac{e_0}{2}(x_0 + iy_0). \quad (4.46)$$

At  $z = l$  the wave transforms into

$$e(l) = \frac{e_0}{2}(x_0 - iy_0) \exp[-i(k'_+ - ik''_+)l] + \frac{e_0}{2}(x_0 + iy_0) \exp[-i(k'_- - ik''_-)l]. \quad (4.47)$$

It can be shown that (4.47) corresponds to an elliptically polarized wave and that the major axis of the polarization ellipse makes the angle

$$\vartheta = \frac{1}{2}(k'_+ - k'_-)l \quad (4.48)$$

with the direction of the linear polarization at  $z = 0$ . The ellipticity of the wave can be defined analogously to (1.101). At  $z = 0$  the ellipticity  $\mathcal{E} = 1$ , and at  $z = l$

$$\mathcal{E} = \cosh^{-2} \left( \frac{1}{2} |k''_+ - k''_-| l \right). \quad (4.49)$$

If there are no losses ( $k''_+ = k''_- = 0$ ), the polarization at  $z = l$  remains linear ( $\mathcal{E} = 1$ ).

Formula (4.48) is valid for an arbitrary elliptical polarization of the wave at  $z = 0$ , as well. In this case,  $\vartheta$  is the angle of the turn of the major axis of polarization ellipse on the way from  $z = 0$  to  $z = l$ .

The turn of polarization in a longitudinally magnetized medium is the *Fara-*

day effect.<sup>3</sup> It follows from (4.48) and (4.42) that this effect is caused by the antisymmetric components of  $\vec{\varepsilon}$  and  $\vec{\mu}$ . As the signs of these components are determined by the direction of the steady magnetization  $M_0$  and are independent of the direction of the wave propagation, the sign of the angle  $\vartheta$  remains the same when the wave propagates in opposite direction. This is an important feature of the Faraday effect. For instance, the angle  $\vartheta$  is doubled when a wave traverses the distance  $l$  in the forward and reverse directions.

Let us consider now in more detail the propagation of electromagnetic waves in longitudinally magnetized weakly conducting *ferromagnet*, or ferrimagnet (ferrite). Two cases are of the most interest: one is realized at microwave frequencies, another, in optics. In the first case,  $\varepsilon$  can be regarded as a scalar independent of frequency, and the expressions obtained in the previous chapters can be used for  $\vec{\mu}$  components. Suppose that the ferromagnet (or ferrimagnet) is isotropic and is magnetized to saturation and, at first, do not take losses into account. Then expression (1.58) for  $\mu \pm \mu_a$  can be used. Substituting it into (4.42), we get the *dispersion relation*

$$(\omega_H \mp \omega) \left( \frac{k^2}{k_0^2 \varepsilon} - 1 \right) - \omega_M = 0 \quad (4.50)$$

where  $\omega_H$  and  $\omega_M$  are determined by (1.40) and (1.55), and the upper and lower signs correspond to the waves with right-hand and left-hand rotation of the polarization, respectively. The  $\omega$  vs  $k$  curves for these waves are plotted in Figure 4.1. For the wave with left-hand rotation (it can be called ordinary), the  $\omega(k)$  dependence differs but slightly from such that would take place if  $\mu$  was a scalar independent of frequency. For the wave with right-hand rotation (extraordinary wave) the  $\omega(k)$  dependence contains two branches. At one of them  $\omega$  infinitely increases with growing  $k$ , approaching the straight line  $\omega = c\sqrt{\varepsilon}k$ . At the second branch,  $\omega$  tends to the constant value  $\omega_H$  with growing  $k$ . The phase velocity  $v_{ph} = \omega/k$  and the group velocity  $v_{gr} = \partial\omega/\partial k$  become very small at this branch at large  $k$  values.

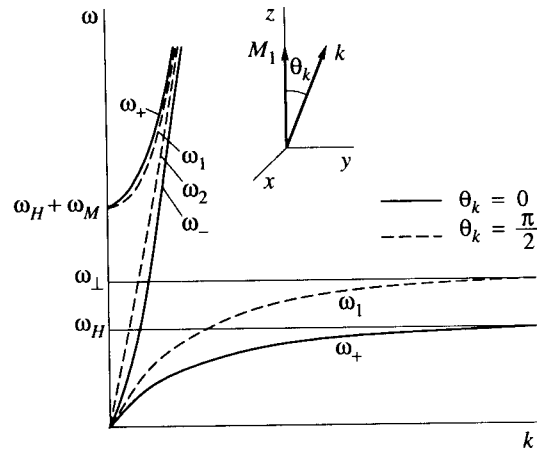
One can see from Figure 4.1 that (without allowing for losses) the wave with right-hand rotation does not exist in the frequency range  $\omega_H < \omega < \omega_H + \omega_M$ , in which the effective permeability  $\mu + \mu_a$  is negative (Figure 1.6). If losses are taken into account, the extraordinary wave does exist in this range, but the damping of it is very strong ( $k'' > k'$ ).

In the other case, which is realized at *optical* frequencies,  $\omega \gg \omega_H, \omega_M$ . From (1.69) we get then to the first approximation, assuming  $\alpha \ll 1$ ,

$$\mu' \cong 1 \quad \mu'_a \cong -\frac{\omega_M}{\omega} \quad \mu'' \cong \alpha \frac{\omega_M}{\omega} \quad \mu''_a \cong 0. \quad (4.51)$$

Now we may not regard  $\varepsilon$  as a scalar,  $\varepsilon'_a$  can be even larger than  $\mu'_a$ . But we can take  $\varepsilon'_a \ll \varepsilon'$  and  $\varepsilon'' \ll \varepsilon'$ . Then, from (4.48) and (4.42) with regard for (4.51) it

<sup>3</sup>We use the term 'turn of polarization' instead of the traditional term 'rotation of the plane of polarization'.

**FIGURE 4.1**

Dispersion relations for electromagnetic waves in an unbounded nonconducting ferromagnet magnetized to saturation (without allowing for losses).

follows that

$$\vartheta = \frac{1}{2c} \left( -\omega_M \sqrt{\epsilon'} + \epsilon'_a \frac{\omega}{\sqrt{\epsilon'}} \right) l. \quad (4.52)$$

The first term in (4.52) is the 'magnetic' (i.e., determined by  $\mu'_a$ ) Faraday turn of polarization; in the considered approximation it is *independent* of frequency. Its value for usual ferrites ( $\epsilon' \sim 15$ ,  $M_0 \sim 200$  G) is  $\sim 40$  deg  $\text{cm}^{-1}$ . The second term is the 'electric' Faraday turn; it usually depends strongly on frequency because  $\epsilon'_a$  changes rapidly with frequency near the absorption lines of the substance. It should be noted that, in some papers on the propagation of optical waves in ferromagnets, a statement can be found that all the observed effects can be described using only  $\vec{\epsilon}$  components, i.e., taking  $\mu = 1$ . It follows from the content of this chapter that such a statement is absolutely groundless.

The problems of reflection from and passing through interfaces, normal to the direction of propagation, are easily solved in the case of longitudinal magnetization, as well as the problem of passage through a gyrotropic layer. Waves with circular polarization pass through and reflect from the interfaces of different media without change of the polarization, and the complex amplitudes of the reflected and transmitted waves are easily found from the boundary conditions. The incident wave with an arbitrary elliptical (e.g., a linear) polarization is resolved into two waves with circular polarization. Their transmission and reflection are considered, and then the complex amplitudes of transmitted and reflected waves with circular polarization are summed to get the total transmitted and reflected waves. Two results of such calculations are to be mentioned. First, the magneto-optical

Kerr effect, i.e., the turn of the major axis of the polarization ellipse of the wave reflected from an interface of an isotropic and lossy gyrotropic media. The second interesting result is the oscillating dependence of the angle of the polarization turn on the thickness of the gyrotropic layer [140].

### 4.2.3 Transverse magnetization

In the case of  $\theta_k = \pi/2$ , the solutions of the dispersion equation (4.32) are

$$k_1 = k_0 \sqrt{\varepsilon_{\parallel} \mu_{\perp}} \quad (4.53)$$

$$k_2 = k_0 \sqrt{\varepsilon_{\perp} \mu_{\parallel}} \quad (4.54)$$

where  $\varepsilon_{\perp}$  and  $\mu_{\perp}$  are determined by (4.25). The system of six equations, the projections of (4.31), splits now into two independent systems. One of them is ( $z$ -axis is the direction of steady magnetization and  $y$ -axis is the direction of propagation)

$$\begin{aligned} k e_z - k_0 \mu h_x - i k_0 \mu_a h_y &= 0 \\ -i \mu_a h_x + \mu h_y &= 0 \\ k_0 \varepsilon_{\parallel} e_z - k h_x &= 0. \end{aligned} \quad (4.55)$$

The second system is obtained from (4.55) by the substitutions  $e \rightleftharpoons h$  and  $\vec{\varepsilon} \rightleftharpoons -\vec{\mu}$ . It is easy to show that (4.53) is the compatibility condition of the system (4.55), and (4.54) is the compatibility condition of the second system.

So, for the first normal wave, the nonzero field components are  $e_z$ ,  $h_x$ , and  $h_y$ . According to the second equation of (4.55),  $b_y = 0$  for this wave. Thus, the vectors  $e$  and  $b$  are transverse (with respect to the direction of propagation), linearly polarized, and perpendicular to each other. The vector  $h$  is elliptically polarized in the plane perpendicular to  $M_0$ . For the second wave, with the dispersion relation (4.54), the nonzero components are  $h_z$ ,  $e_x$ , and  $e_y$ ; the vectors  $h$  and  $d$  are now transverse and linearly polarized.

The wave impedance can be defined, in the case of transverse magnetization, as the ratio of transverse (with respect to the propagation direction) components of  $e$  and  $h$ . It follows from (4.55) and (4.53) that the wave impedance of the first normal wave is

$$\zeta_1 = \frac{e_z}{h_x} = \sqrt{\frac{\mu_{\perp}}{\varepsilon_{\parallel}}}. \quad (4.56)$$

For the second normal wave,

$$\zeta_2 = \frac{e_x}{h_z} = \sqrt{\frac{\mu_{\parallel}}{\varepsilon_{\perp}}}. \quad (4.57)$$

It is clear from the expressions for  $k_{1,2}$  and  $\zeta_{1,2}$  that the effective parameters for the first wave are  $\mu_{\perp}$  and  $\varepsilon_{\parallel}$ , and for the second wave,  $\mu_{\parallel}$  and  $\varepsilon_{\perp}$ .



If a wave with field structure (polarization), different from the field structure of a normal wave, propagates in a transversely magnetized medium, the polarization of this wave changes in the course of propagation. It should be emphasized that the transformation of polarization in this case has the same cause as the Cotton–Mouton effect [246]. In contrast to the Faraday effect, it *does not depend* on the direction of  $\mathbf{M}_0$  because  $\mu_a$  and  $\varepsilon_a$  appear in (4.53) and (4.54) only in second powers. This transformation, also in contrast to Faraday effect, occurs in the opposite direction when the propagation direction is reversed.

Consider now the particular case of a transversely magnetized *ferrite* in the microwave range. In this case,  $\varepsilon$  can be regarded as a scalar independent of frequency. If the ferrite is magnetized to saturation, then  $\mu_{\parallel} = 1$  and  $k_{\parallel} = k_0\sqrt{\varepsilon\mu_{\parallel}}$  while  $k_{\perp} = k_0\sqrt{\varepsilon}$ . The second (ordinary) wave propagates now as in a nonmagnetic dielectric. To obtain the *dispersion law* of the first (extraordinary) wave we substitute (1.60) (without allowance for losses) into the expression for  $k_{\perp}$ . Then, we get

$$(\omega_{\perp}^2 - \omega^2) \left( \frac{k^2}{k_0^2 \varepsilon} - 1 \right) - \omega_{\perp}^2 = 0. \quad (4.58)$$

The  $\omega(k)$  dependence that follows from (4.58) contains two branches (Figure 4.1). One of them asymptotically approaches, with growing  $k$ , the dispersion curve of the ordinary wave. The frequency in the second branch tends to the constant value  $\omega_{\perp}$ .

One can see from Figure 4.1 that the extraordinary wave *does not exist* (if losses are not taken into account) in the frequency range  $\omega_{\perp} < \omega < \omega_H + \omega_M$ , in which (Figure 1.6) the effective permeability  $\mu_{\perp}$  is negative. With allowance for losses, the extraordinary wave exists but is strongly damped in this range.

At the lower limit of the forbidden frequency range  $\mu_{\perp} \rightarrow \infty$ , and at the upper limit,  $\mu_{\perp} = 0$ . So, these limits are, respectively, the *resonance* and *antiresonance* points of the effective permeability. We have come across an analogous situation in the case of the longitudinal magnetization. The resonance points of the effective permeabilities are different in the two cases, whereas the antiresonance points coincide (Figure 1.6). It is easy to show, using (4.34), that the antiresonance frequency  $\omega_{\text{antires}}$  (defined by the condition  $\mu_{\text{ef}} = 0$ ) is

$$\omega_{\text{antires}} = \omega_H + \omega_M \quad (4.59)$$

irrespective of the propagation direction.

If the losses are taken into account, the resonance point is defined as a point where  $\mu_{\text{ef}}''$  is maximal, and the antiresonance point is defined as a point where  $\mu_{\text{ef}}' = 0$  and  $\mu_{\text{ef}}''$  is small. It is easy to make sure that  $k' = k''$  at the antiresonance point, as well as near the resonance point (where  $\mu_{\text{ef}}' = 0$ ). Near resonance the value of  $k' = k''$  is large, approximately proportional to  $\alpha^{-1/2}$ , whereas at antiresonance it is small, proportional to  $\alpha$ .

Expressions (4.50) and (4.58) can be regarded as dispersion equations for pairs of *coupled waves*. The first waves in these pairs are magnetic or spin waves. To

obtain their ‘uncoupled’ dispersion relations we must set to zero the expressions in the first parentheses in (4.50) and (4.58). Dispersion relations for the second waves, which are the electromagnetic waves in a medium with  $\mu = 1$ , are found by setting equal to zero the expressions in the second parentheses in (4.50) and (4.58). The last terms in these equations represent the coupling of the waves. It results in the repulsion of the dispersion curves of spin waves and electromagnetic waves (Figure 4.1). Such treatment, ‘in terms of coupled modes’, brings nothing new in the considered problem of waves in an unbounded uniform medium. But for more complicated problems it can be very useful.

---

### 4.3 Nonreciprocity

The presence of  $\vec{\epsilon}$  or  $\vec{\mu}$  antisymmetric components, caused by steady magnetization, results in some phenomena in systems containing such media, which are referred to as *nonreciprocal effects*. This term is used because in such effects the well-known reciprocal theorem (e.g., [191]) is violated. One of the nonreciprocal effects is the turn of polarization of a linearly polarized wave (the Faraday effect) in a longitudinally magnetized gyrotropic medium. This effect was considered in the preceding section for an unbounded medium. Analogous effects are observed, as we will see in Chapter 5, in waveguides containing gyrotropic media, as well. Other nonreciprocal effects, which are possible only in systems, containing *boundaries* between different media, will be studied in Chapters 5 and 6.

The aim of the present section is to consider some general relationships that can be used in the analysis of nonreciprocal effects. The most important of these relationships is the generalized Lorentz lemma.

The Lorentz lemma was proposed for media with symmetric tensor parameters and was used in deriving the reciprocal theorem. We will generalize this lemma to a system containing media with arbitrary tensors  $\vec{\epsilon}$  and  $\vec{\mu}$ . The system can contain any boundaries, including metallic surfaces. Two ac electromagnetic fields with the same frequency and complex amplitudes  $e_1, h_1$  and  $e_2, h_2$  are excited by the external currents, respectively,  $j_{\text{ext}1}$  and  $j_{\text{ext}2}$ .

We write the Maxwell equation (4.14) for the fields with subscripts 1 and 2, and equation (4.16) for the same fields, and scalarly multiply these equations, respectively, by  $h_2, (-h_1), e_2$ , and  $(-e_1)$ . Then, we sum all the obtained expressions and represent the tensors  $\vec{\mu}$  and  $\vec{\epsilon}$  as sums of symmetric and antisymmetric tensors (Section 4.1). It is easy to make sure that

$$h_1 \vec{\mu}_s h_2 = h_2 \vec{\mu}_s h_1 \quad h_1 \vec{\mu}_{\text{as}} h_2 = -h_2 \vec{\mu}_{\text{as}} h_1. \quad (4.60)$$

Taking into account (4.60) and analogous relationships for the electric fields and

tensors  $\vec{\epsilon}_s$  and  $\vec{\epsilon}_{as}$ , we get

$$\frac{c}{4\pi} \operatorname{div} (\mathbf{e}_1 \times \mathbf{h}_2 - \mathbf{e}_2 \times \mathbf{h}_1) + \frac{i\omega}{2\pi} (\mathbf{h}_2 \vec{\mu}_{as} \mathbf{h}_1 - \mathbf{e}_2 \vec{\epsilon}_{as} \mathbf{e}_1) = \mathbf{j}_{\text{ext}1} \mathbf{e}_2 - \mathbf{j}_{\text{ext}2} \mathbf{e}_1. \quad (4.61)$$

This expression represents the Lorentz lemma generalized to media with nonsymmetric tensor parameters.

Integrating (4.61) over a volume  $V$ , we obtain, with the use of the Gauss theorem (e.g., [273]),

$$\begin{aligned} \frac{c}{4\pi} \int_S (\mathbf{e}_1 \times \mathbf{h}_2 - \mathbf{e}_2 \times \mathbf{h}_1) \mathbf{n}_0 dS + \frac{i\omega}{2\pi} \int_{V_a} (\mathbf{h}_2 \vec{\mu}_{as} \mathbf{h}_1 - \mathbf{e}_2 \vec{\epsilon}_{as} \mathbf{e}_1) dV \\ = \int_{V_1} \mathbf{j}_{\text{ext}1} \mathbf{e}_2 dV - \int_{V_2} \mathbf{j}_{\text{ext}2} \mathbf{e}_1 dV. \end{aligned} \quad (4.62)$$

Here  $S$  is the surface that encloses the volume  $V$ ,  $\mathbf{n}_0$  is a unit outward normal to  $S$ ,  $V_a$  is the part of the volume  $V$  that contains gyrotropic media, and  $V_{1,2}$  are the parts of  $V$  in which the currents  $\mathbf{j}_{\text{ext}1}$  and  $\mathbf{j}_{\text{ext}2}$  exist. The expression (4.62) is the generalized Lorentz lemma in the *integral* form.

The volume  $V$  must be chosen according to the character of the problem. In the antenna theory (e.g., [191]) the infinitely large volume  $V$  includes both the transmitting and the receiving antennae. Then, the surface integral in (4.62) tends to zero; and, if  $\vec{\mu}$  and  $\vec{\epsilon}$  of all media are symmetric tensors (in particular, scalars), the reciprocity theorem follows from (4.62).

When *waveguide devices* are investigated, the volume  $V$  is restricted (Section 5.4) by the walls of waveguides (or of a waveguide junction) and the waveguide cross sections. The currents  $\mathbf{j}_{\text{ext}1,2}$  are in this case, usually, outside the volume  $V$ , so that the right-hand side of (4.62) is equal to zero. And, if we assume the metallic waveguide walls to be ideally conducting, the surface integral over the walls is equal to zero, too. Then, it follows from (4.62) that

$$\begin{aligned} \frac{c}{4\pi} \sum_{p=1}^n \int_{S_p} (\mathbf{e}_{p1} \times \mathbf{h}_{p2} - \mathbf{e}_{p2} \times \mathbf{h}_{p1}) \mathbf{n}_{0p} dS \\ = -\frac{i\omega}{2\pi} \int_{V_a} (\mathbf{h}_1 \vec{\mu}_{as} \mathbf{h}_2 - \mathbf{e}_1 \vec{\epsilon}_{as} \mathbf{e}_2) dV \equiv J_a. \end{aligned} \quad (4.63)$$

Here  $p$  is the number of an input or an output waveguide,  $S_p$  is its cross section,  $\mathbf{n}_{0p}$  is a unit normal to this cross section,  $\mathbf{e}_p$  and  $\mathbf{h}_p$  are the fields at it. The nonreciprocal microwave ferrite devices, for which  $J_a \neq 0$ , will be treated in Chapter 5. Here we limit ourselves to some general remarks. For a *magnetically* gyrotropic medium, it follows from (4.21) that  $\vec{\mu}_{as} \mathbf{h}_2 = i4\pi \mathbf{h}_2 \times \mathbf{G}_m$ . Taking this into account, we get

$$J_a = 2\omega \int_{V_a} \mathbf{G}_m (\mathbf{h}_1 \times \mathbf{h}_2) dV. \quad (4.64)$$

The antisymmetric components of  $\vec{\chi}$  and  $\vec{\mu}$  and, hence, the vector  $G_m$  are proportional to  $M_0$ . Therefore, the quantity  $J_a$  changes its sign when the direction of the steady magnetization is reversed.

The quantity  $J_a$  can be equal to zero, besides the trivial case  $\mu_a = 0$ , for two reasons. The first reason is related to the structure of the fields  $h_1$  and  $h_2$ . One can see from (4.64) that  $J_a = 0$  if the complex amplitudes  $h_1$  and  $h_2$  are parallel to each other in the entire volume  $V_a$ . This takes place when a small ferrite sample is situated in the waveguide at a point of *linear* polarization of the magnetic field. The second reason relates to the *symmetry of the device*: the integrals in (4.64) over different parts of the volume  $V_a$  can compensate each other. A representative example is a ferrite slab located symmetrically in a rectangular waveguide (Section 5.2). It should be emphasized that the entire system can be reciprocal in the above-discussed sense ( $J_a = 0$ ), while the field structures are nonreciprocal, i.e., different for opposite directions of propagation.

Thus, the existence of steady magnetization is not sufficient but necessary for observing nonreciprocal effects (and designing nonreciprocal devices). This is in agreement with the principle of symmetry of the kinetic coefficients (the *Onsager principle*) [246], which, for  $\vec{\mu}$  components, can be written as

$$\mu_{pq}(\omega, \mathbf{k}, \mathbf{B}_0) = \mu_{qp}(\omega, -\mathbf{k}, -\mathbf{B}_0) \quad (4.65)$$

where  $\mathbf{B}_0 = \mathbf{H}_0 + 4\pi\mathbf{M}_0$ .

It should be noted that antisymmetric components of  $\vec{\epsilon}$  (may be of  $\vec{\mu}$ , too) can arise in some substances without any action of steady magnetization. These components depend linearly on  $k$  and, so, are equal to zero if  $k = 0$ . The sense of the turn of polarization in such substances changes, as distinct from the Faraday effect, to the opposite when the direction of propagation is reversed. This phenomenon is called natural optical activity [246], as distinguished from gyrotropy, which is discussed in detail in this book.

#### 4.4 Energy relations

The energy relations are quadratic (in field amplitudes) expressions that follow from Maxwell's equations and represent the relationship between energy flows and energy losses in an electromagnetic field. As we are interested in *stationary* processes, when all the linear quantities are harmonic functions of time, we consider in the present section, as in Section 4.3, the quadratic relations for the *complex amplitudes*.

Suppose that there are two real quantities  $a_{\sim} = a_0 \cos(\omega t + \varphi_a)$  and  $b_{\sim} = b_0 \cos(\omega t + \varphi_b)$ , and the complex quantities  $\hat{a} = a_0 \exp(i\omega t + i\varphi_a)$  and  $\hat{b} = b_0 \exp(i\omega t + i\varphi_b)$  are introduced, so that  $a_{\sim}$  and  $b_{\sim}$  are the real parts of  $\hat{a}$  and  $\hat{b}$ . Then, it is easy to show that the average of the product  $a_{\sim}b_{\sim}$  over the period of

oscillations is

$$\overline{a_{\sim} b_{\sim}} \equiv \int_0^T a_{\sim} b_{\sim} dt = \frac{1}{2} \operatorname{Re}(ab^*) = \frac{1}{2} \operatorname{Re}(a^* b) \quad (4.66)$$

(the quantities  $a = a_0 \exp(i\varphi_a)$  and  $b = b_0 \exp(i\varphi_b)$  are the complex amplitudes of  $a_{\sim}$  and  $b_{\sim}$ ). Expressions analogous to (4.66) hold for both scalar and vector products of vector quantities.

#### 4.4.1 Equation of energy balance

We multiply the Maxwell equation (4.14) scalarly by  $\mathbf{h}^*$  and the complex conjugate of (4.16), by  $-e$ . Summing the obtained expressions, we get

$$\frac{c}{4\pi} \operatorname{div}(\mathbf{e} \times \mathbf{h}^*) + \frac{i\omega}{4\pi} (\mathbf{h}^* \vec{\mu} \mathbf{h} - \mathbf{e}^* \vec{\varepsilon}^* \mathbf{e}) + e \mathbf{j}_{\text{ext}}^* = 0. \quad (4.67)$$

The real part of (4.67) can be written in the form

$$\operatorname{div} \mathbf{II} + P + P_{\text{ext}} = 0 \quad (4.68)$$

where

$$\mathbf{II} = \frac{c}{8\pi} \operatorname{Re}(\mathbf{e} \times \mathbf{h}^*) \quad (4.69)$$

$$P = -\frac{\omega}{8\pi} \operatorname{Im}(\mathbf{h}^* \vec{\mu} \mathbf{h} - \mathbf{e}^* \vec{\varepsilon}^* \mathbf{e}) \quad (4.70)$$

$$P_{\text{ext}} = \frac{1}{2} \operatorname{Re}(e \mathbf{j}_{\text{ext}}^*). \quad (4.71)$$

Taking into account the relationships, analogous to (4.66), for the vector and scalar products, we make sure that  $\mathbf{II}$  is the time-averaged Poynting vector, i.e., the mean value of the density of the electromagnetic-energy flow,  $P$  is the mean value of the density of the energy losses, and  $P_{\text{ext}}$  is the mean value of the density of the power of losses due to external currents. Thus, (4.68) is the equation of *energy balance* for the ac electromagnetic field (in differential form).

Using (4.18) and (4.13), it is possible to rewrite (4.68) as

$$\operatorname{div} \mathbf{II} + P_{\text{m}} + P_{\text{e}} = 0 \quad (4.72)$$

where  $P_{\text{m}} = -\omega/(8\pi) \operatorname{Im}(\mathbf{h}^* \vec{\mu} \mathbf{h})$  is the density of magnetic losses, and

$$P_{\text{e}} = \frac{1}{2} \operatorname{Re}(e \mathbf{j}^*) \quad (4.73)$$

is the density of *total* electric losses due to both ohmic and external currents.

Integrating (4.68) over a volume  $V$ , we find

$$\int_S \mathbf{II} \mathbf{n}_0 dS + \int_V P dV + \int_V P_{\text{ext}} dV = 0 \quad (4.74)$$

where  $S$  is the surface that encloses the volume  $V$  and  $\mathbf{n}_0$  is a unit outward normal to  $S$ . Expression (4.74) is the energy balance equation in integral form, i.e., the complex Poynting theorem for an ac electromagnetic field.

#### 4.4.2 Energy losses

Let us consider in more detail the quantity (4.70). It is easy to show that Hermitian tensors  $\vec{\mu}_H$  (Section 4.1) and  $\vec{\varepsilon}_H$  do not contribute to  $P$ , and the contribution of anti-Hermitian tensors can be written in the form

$$P = \frac{\omega}{8\pi} \text{Im} \left( \mathbf{h} \vec{\mu}_{\text{aH}}^* \mathbf{h}^* + \mathbf{e} \vec{\varepsilon}_{\text{aH}}^* \mathbf{e}^* \right). \quad (4.75)$$

So, the energy losses are determined by *anti-Hermitian* parts of the tensors  $\vec{\mu}$  and  $\vec{\varepsilon}$ , i.e., by the imaginary parts of their symmetric components and the real parts of the antisymmetric components. [That is why the factor  $i$  has been introduced before the antisymmetric components in (4.20).]

Consider, e.g., a medium with permeability as in (4.23) but with scalar permittivity. Such a medium represents, for microwave range, a ferromagnet or a ferrimagnet (ferrite) which, in the absence of steady magnetization, is assumed to be isotropic. For this medium

$$\vec{\mu}_{\text{aH}}^* = \begin{vmatrix} i\mu'' & \mu''_a & 0 \\ -\mu''_a & i\mu'' & 0 \\ 0 & 0 & i\mu''_{\parallel} \end{vmatrix} \quad \vec{\varepsilon}_{\text{aH}}^* = \begin{vmatrix} i\varepsilon'' & 0 & 0 \\ 0 & i\varepsilon'' & 0 \\ 0 & 0 & i\varepsilon'' \end{vmatrix}. \quad (4.76)$$

The complex amplitudes of the components of  $\mathbf{h}$  and  $\mathbf{e}$  vectors with arbitrary polarization can be written as  $h_p = h'_p + ih''_p$  and  $e_p = e'_p + ie''_p$ , where  $p = 1, 2, 3 \equiv x, y, z$ . Then, as it is easy to make sure,

$$P = \frac{\omega}{8\pi} \left[ \mu'' (|h_x|^2 + |h_y|^2) + \mu''_{\parallel} |h_z|^2 + 2\mu''_a (h'_y h''_x - h'_x h''_y) + \varepsilon'' |e|^2 \right]. \quad (4.77)$$

For media with tensor  $\vec{\varepsilon}$  (e.g., for plasmas, both gaseous and solid-state, and for ferromagnets or ferrimagnets in optical range) the power of electrical losses should be written analogous to magnetic losses in (4.77).

One can see from (4.77) that the dissipation (positive losses) of electromagnetic energy is determined by *positive* values of  $\mu''$ ,  $\mu''_{\parallel}$ , and  $\varepsilon''$ , if the signs are chosen as in (4.19). Such a conclusion cannot be made concerning  $\mu''_a$  (as well as  $\varepsilon''_a$ ), because the quantity  $h'_y h''_x - h'_x h''_y$  in (4.77) and analogous quantity for electric field components can have different signs depending on the polarization of the fields. These quantities are positive for circularly or elliptically polarized fields with right-hand rotation (with respect to the direction of steady magnetization), and are negative in the case of left-hand rotation. For linearly polarized fields these quantities are equal to zero. Thus, the same values of  $\mu''_a$  and  $\varepsilon''_a$  make positive, negative, or zero contribution to dissipation of electromagnetic energy, depending on the polarization of the field.

For a passive medium (without any intrinsic energy sources), it should be  $P > 0$  for any polarization. This leads to the following *limitations* on the values of anti-Hermitian parts of  $\vec{\mu}$  components:

$$\mu'' > 0 \quad \mu''_{\parallel} > 0 \quad |\mu''_{\alpha}| < \mu'' \quad (4.78)$$

and to analogous limitations on the values of the components of  $\vec{\varepsilon}$ . The signs of  $\mu''_{\alpha}$  and  $\varepsilon''_{\alpha}$  can be arbitrary, and just as the signs of  $\mu'_{\alpha}$  and  $\varepsilon'_{\alpha}$ , they depended on the direction of the steady magnetization.

## 4.5 Perturbation method

The difficulties we meet with in solving boundary electro-dynamical problems are especially great in the case of gyrotropic media. Therefore, in this case the approximate methods are of particular importance. The simplest and most general of them is the perturbation method. The unperturbed system is, usually, a system containing no gyrotropic media, and the perturbation is either a small change of parameters in an arbitrary large volume or a substantial change of parameters but in a small volume. The second case is more interesting from the practical point of view.

The perturbation method is effective in calculating the quantities that are functionals of the electromagnetic field, such as eigenfrequencies of resonators or propagation constants of waveguides. The perturbation formulae for these quantities can be deduced from general quadratic relations, which can be called *perturbation lemmas*.

To derive these lemmas consider two systems: an unperturbed (initial), with scalar parameters  $\mu_0$  and  $\varepsilon_0$ , and a perturbed, with tensor parameters  $\vec{\mu}$  and  $\vec{\varepsilon}$ . An electromagnetic field with frequency  $\omega_0$  and complex amplitudes of the field vectors  $\mathbf{h}_0$  and  $\mathbf{e}_0$  exists in the initial system, and a field with frequency  $\omega$  and complex amplitudes  $\mathbf{h}$  and  $\mathbf{e}$  exists in the perturbed system. There are no external currents in both systems. We write equations (4.14) and (4.16) for the perturbed system and the complex conjugates of these equations, for the initial system. Then we multiply these equations by the appropriate vectors, as in the derivation of (4.61) or (4.67). Summing all the obtained expressions, we find (assuming  $\mu_0$  and  $\varepsilon_0$  to be real) the perturbation lemma

$$\operatorname{div} (\mathbf{e} \times \mathbf{h}_0^* + \mathbf{e}_0^* \times \mathbf{h}) + \frac{i}{c} \left( \omega \mathbf{h}_0^* \vec{\mu} \mathbf{h} - \omega_0 \mathbf{h} \mu_0 \mathbf{h}_0^* + \omega \mathbf{e}_0^* \vec{\varepsilon} \mathbf{e} - \omega_0 \mathbf{e} \varepsilon_0 \mathbf{e}^* \right) = 0. \quad (4.79)$$

In the same manner, but starting from equations (4.14) and (4.16) for both systems (not from the complex conjugate of (4.16) for the initial one), we can obtain a lemma that differs from (4.79) by the replacement  $\mathbf{h}_0^* \rightarrow \mathbf{h}_0$  and  $\mathbf{e}_0^* \rightarrow -\mathbf{e}_0$ .

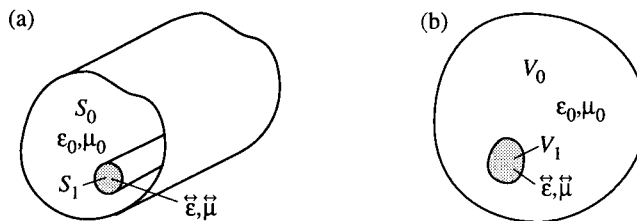


FIGURE 4.2

Gyrotropic perturbations (a) of a waveguide and (b) of a resonator.

#### 4.5.1 Gyrotropic perturbation of a waveguide

Consider an infinite waveguide with cross section  $S_0$  filled, in the unperturbed state, with a medium the parameters of which are  $\mu_0$  and  $\epsilon_0$ . A wave with complex amplitudes  $e_0 = e_0^0 \exp(-ik_{\eta_0}\eta)$  and  $h_0 = h_0^0 \exp(-ik_{\eta_0}\eta)$  propagates in this waveguide ( $\eta$ -axis is directed along the axis of the waveguide). The eigenfunctions of the unperturbed waveguide  $e_0^0$  and  $h_0^0$  and the propagation constant  $k_{\eta_0}$  are assumed to be known. The perturbation is an infinite cylinder with cross section  $S_1$  and parameters  $\vec{\mu}$  and  $\vec{\epsilon}$  inserted in the waveguide (Figure 4.2). The complex amplitudes of the field in the perturbed waveguide are  $e = e^0 \exp(-ik_{\eta}\eta)$  and  $h = h^0 \exp(-ik_{\eta}\eta)$ . The propagation constant  $k_{\eta}$  is to be found.

Substituting the quantities  $e_0$ ,  $h_0$ ,  $e$ , and  $h$  into the lemma (4.79) (where, in the present case,  $\omega = \omega_0$ ), integrating it over the waveguide cross section  $S_0$ , and taking into account the boundary conditions at the waveguide walls, we obtain, according to Nikolskii [299],

$$k_{\eta} - k_{\eta_0} = \frac{\omega}{c} \frac{\int_{S_1} \left( h_0^{0*} \delta \vec{\mu} h^0 + e_0^{0*} \delta \vec{\epsilon} e^0 \right) dS}{\int_{S_0} \left( e_{\perp}^0 \times h_{0\perp}^{0*} + e_{0\perp}^{0*} \times h_{\perp}^0 \right) \eta_0 dS}. \quad (4.80)$$

Here the subscript  $\perp$  denotes the transverse (with respect to the waveguide axis) components of the eigenfunctions of the waveguide,  $\delta \vec{\mu} = \vec{\mu} - \mu_0$ ,  $\delta \vec{\epsilon} = \vec{\epsilon} - \epsilon_0$ , and  $\eta_0$  is a unit vector directed along the waveguide axis.

Formula (4.80), as well as the lemma (4.79), is rigorous, but the eigenfunctions  $e^0$  and  $h^0$  are unknown. If the surface  $S_1$  is small as compared with  $S_0$ , then, in the denominator of (4.80), we can approximately replace the unknown functions  $e^0$  and  $h^0$  by the known functions  $e_0^0$  and  $h_0^0$ . Taking into consideration the formula of the waveguide theory (e.g., [151])  $h_{0\perp}^0 = (\eta_0 \times e_{0\perp}^0) / \zeta_0$  (where  $\zeta_0$  is the characteristic impedance of the unperturbed waveguide), we get

$$k_{\eta} - k_{\eta_0} \cong \frac{\omega \zeta_0}{2cN_0} \int_{S_1} \left( h_0^{0*} \delta \vec{\mu} h^0 + e_0^{0*} \delta \vec{\epsilon} e^0 \right) dS \quad (4.81)$$

where  $N_0 = \int_{S_0} |e_{0\perp}^0|^2 dS$  is the normalization constant of the unperturbed-waveguide eigenfunctions.



### 4.5.2 Gyrotropic perturbation of a resonator

Let us derive a formula for the eigenfrequency of a hollow electromagnetic resonator with a small gyrotropic sample (Figure 4.2). The field  $(e_0, h_0)$  in (4.79) represents now the field of one of the modes of the unperturbed resonator, and  $(e, h)$  is the field of 'the same' mode of the resonator with the sample. ('The same' means that this mode transforms into the mode of an unperturbed resonator when the sample volume  $V_1 \rightarrow 0$ .) Integrating (4.79) over the resonator volume  $V_0$  and taking into account the boundary conditions at the resonator walls (regarded as ideally conducting), we find [298]

$$\frac{\omega - \omega_0}{\omega} = - \frac{\int_{V_1} (h_0^* \delta \vec{\mu} h + e_0^* \delta \vec{\epsilon} e) dV}{\int_{V_0} (h_0^* \mu_0 h + e_0^* \epsilon_0 e) dV}. \quad (4.82)$$

If  $V_1 \ll V_0$ , we may, as in the previous case, replace the perturbed fields in the denominator by the unperturbed fields. Then we get

$$\frac{\omega - \omega_0}{\omega} \cong - \frac{1}{2W_0} \int_{V_1} (h_0^* \delta \vec{\mu} h + e_0^* \delta \vec{\epsilon} e) dV \quad (4.83)$$

where

$$W_0 = \int_{V_0} \epsilon_0 |e_0|^2 dV = \int_{V_0} \mu_0 |h_0|^2 dV \quad (4.84)$$

is the energy of the electromagnetic field in the unperturbed resonator multiplied by  $8\pi$ .

In (4.81) and (4.83), the quantities of the type  $h_0^* \delta \vec{\mu} h$  take place. We write them down in the particular case of a medium with parameters (4.23). For instance,

$$h_0^* \delta \vec{\mu} h = \delta \mu h_{0\perp}^* h_{\perp} + i\mu_a z_0 (h_{0\perp}^* \times h_{\perp}) + \delta \mu_{\parallel} h_{0z}^* h_z \quad (4.85)$$

where  $\delta \mu = \mu - \mu_0$ ,  $\delta \mu_{\parallel} = \mu_{\parallel} - \mu_0$ , the  $z$ -axis is directed along the steady magnetization  $M_0$ , and the subscripts  $\perp$  denote now the components perpendicular to this axis.

If we allow for dissipation, i.e., take into account the anti-Hermitian parts of  $\vec{\epsilon}$  and  $\vec{\mu}$ , the right-hand sides of (4.81) and (4.83) become complex. These formulae then give the changes of both the real parts and the imaginary parts of  $k_{\eta}$  or  $\omega$ . Therefore, they can be used to calculate the decrement of a wave in a ferrite-loaded waveguide and the quality factor of a resonator with a ferrite sample, which is related to the imaginary part of the eigenfrequency by the expression (1.107).

### 4.5.3 Quasistatic approximation

The perturbed fields in (4.81) and (4.83) differ essentially from the unperturbed fields, no matter how small the sample may be, and are to be approximated in some way or other. The simplest is the quasistatic approximation, which consists in the following: the relation between the perturbed (internal) ac field in the sample

and the unperturbed ac field is assumed to be the same as the relation between the *static* internal and external fields. (The external field is the field at the point of a waveguide or a resonator where the sample is, but without the sample.)

This is just the approximation used in Section 1.5. The magnetostatic problem of the relation between the internal and the external fields has a simple solution (1.85) if the sample is a small ellipsoid in a nonmagnetic medium ( $\mu_0 = 1$ ). Having excluded the internal field  $\mathbf{h}$  from (1.85) and the expression

$$\mathbf{h} + 4\pi\mathbf{m} = \vec{\mu}\mathbf{h} \quad (4.86)$$

we obtained, in Section 1.5, the relation between the magnetization  $\mathbf{m}$  and the external field  $\mathbf{h}_e$  (now designated as  $\mathbf{h}_0$ ). To find the relation between  $\mathbf{h}$  and  $\mathbf{h}_0$ , which we are interested in at the present, we exclude  $\mathbf{m}$  from (1.85) and (4.86) and obtain (for  $\mu_0 = 1$ )

$$\mathbf{h} = \left(1 + \frac{1}{4\pi}\vec{N}\delta\vec{\mu}\right)^{-1}\mathbf{h}_0 \equiv \vec{T}\mathbf{h}_0 \quad (4.87)$$

where the superscript  $-1$  denotes the inverse tensor. If  $\mu_0 \neq 1$ , the quantity  $\delta\vec{\mu}$  is replaced by  $\delta\vec{\mu}/\mu_0$ .

Assume that  $\vec{\mu}$  has the form (4.23),  $\mu_0 = 1$ , and  $\mathbf{M}_0$  is directed along one of the ellipsoid axes. The tensor  $\vec{T}$  components, i.e., the relations between the components of  $\mathbf{h}$  and  $\mathbf{h}_0$ , found on these assumptions, are listed in Table 4.1 for the limiting cases of an ellipsoid. Analogous relations hold between the components of  $\mathbf{e}$  and  $\mathbf{e}_0$ .

A *necessary condition* for the applicability of the quasistatic approximation is that at least one of the sample dimensions ( $d$ ) must be small as compared with the length of electromagnetic wave in the sample. If we take into account that the transverse diagonal components  $\mu$  and  $\varepsilon$  are of the same order of magnitude as other components, respectively, of  $\vec{\mu}$  and  $\vec{\varepsilon}$ , then we may write this condition as

$$\frac{\omega}{c}\sqrt{|\mu||\varepsilon|}d \lesssim \frac{\pi}{6}. \quad (4.93)$$

Here  $d$  is the diameter of a sphere, the diameter of a cylinder, or the thickness of a slab. It must be emphasized that other dimensions of a cylinder or a slab should not be small. Then, the internal field will vary in the plane of the slab or along the length of the cylinder, but in the same way as the external field.

If all dimensions of the sample are small, the integration in (4.83) can be replaced by multiplication by  $V_1$ . The integration in (4.81) can be replaced by multiplication by  $S_1$  if all dimensions of the cylinder cross section are small.

The second necessary condition for the applicability of the quasistatistical approximation (in the considered form), already mentioned in Section 1.5, is that the oscillation mode must be uniform.

The above-obtained perturbation formulae contain the tensor parameters of the substance  $\vec{\mu} = 1 + 4\pi\vec{\chi}$  and  $\vec{\varepsilon} = 1 + 4\pi\vec{\chi}_{\text{el}}$  (where  $\vec{\chi}_{\text{el}}$  is the ac electric

**TABLE 4.1**  
Relations between components of perturbed and unperturbed fields in the quasistatic approximation.

Sample	Direction of magnetization	Notation in Figure (1.9)	$h_x$	$h_y$	$h_z$	
Slab	Tangential	(a)	$h_{0x}$	$\frac{i\mu_a}{\mu} h_{0x} + \frac{1}{\mu} h_{0y}$	$h_{0z}$	(4.88)
	Normal	(b)	$h_{0z}$	$h_{0y}$	$\frac{1}{\mu_{\parallel}} h_{0z}$	(4.89)
Cylinder	Longitudinal	(c)	$\frac{2(\mu+1)}{(\mu+1)^2 - \mu_a^2} h_{0x} - \frac{2i\mu_a}{(\mu+1)^2 - \mu_a^2} h_{0y}$	$\frac{2i\mu_a}{(\mu+1)^2 - \mu_a^2} h_{0x} + \frac{2(\mu+1)}{(\mu+1)^2 - \mu_a^2} h_{0y}$	$h_{0z}$	(4.90)
	Transverse	(d)	$\frac{2}{\mu+1} h_{0z} - \frac{i\mu_a}{\mu+1} h_{0y}$	$h_{0y}$	$\frac{2}{\mu_{\parallel}+1} h_{0z}$	(4.91)
Sphere		(e)	$\frac{3(\mu+2)}{(\mu+2)^2 - \mu_a^2} h_{0x} - \frac{3i\mu_a}{(\mu+2)^2 - \mu_a^2} h_{0y}$	$\frac{3i\mu_a}{(\mu+2)^2 - \mu_a^2} h_{0x} + \frac{3(\mu+2)}{(\mu+2)^2 - \mu_a^2} h_{0y}$	$\frac{3}{\mu_{\parallel}+2} h_{0z}$	(4.92)

susceptibility). But, if the sample is a small ellipsoid or, in limiting cases, a thin slab or a thin cylinder, the *external* susceptibility tensors  $\vec{\chi}^e$  and  $\vec{\chi}_{el}^e$  (Section 1.5), which relate the ac magnetization  $m$  and ac polarization to the *external* ac fields, can be inserted into the perturbation formulae. Consider, e.g., formula (4.83) and assume  $\mu_0 = 1$  and  $\varepsilon_0 = 1$ . The expression  $h_0^* \delta \vec{\mu} h$  in (4.83) can be rewritten as follows:

$$h_0^* \delta \vec{\mu} h = h_0^* 4\pi \vec{\chi} h = 4\pi h_0^* \vec{\chi}^e h_0. \quad (4.94)$$

The expression  $e_0^* \delta \vec{\varepsilon} e$ , as well as the analogous expressions in (4.81) can be transformed in the same way. Thus, the introduction of external susceptibilities allows one to exclude the internal (perturbed) fields from the perturbation formulae, and there is no need in approximating them.

If the substance (ferromagnet or ferrite) is isotropic, in the absence of steady magnetization, and the sample (an ellipsoid) is magnetized along one of its axes, the tensor  $\vec{\chi}^e$  is given by (1.112) with  $\chi_s = 0$ . Then, the expression  $h_0^* \vec{\chi}^e h_0$ , which appears in (4.83), takes the form

$$h_0^* \vec{\chi}^e h_0 = \chi_x^e |h_{0x}^2|^2 + \chi_y^e |h_{0y}|^2 + i\chi_a^e z_0 (h_0^* \times h_0). \quad (4.95)$$

It is easy to make sure that the last term in (4.95) is equal to zero for a linear polarization of  $h_0$ , and is real and has different signs, for circular polarization of  $h_0$  with different senses of rotation.

#### 4.5.4 Resonator with walls of real metal

The perturbation method can be used, as well, to calculate approximately the parameters of electromagnetic resonators or waveguides with walls made of non-ideal, in particular, ferromagnetic metal. Consider, e.g., a resonator, a part  $S_1$  of the surface of which is a boundary with metal having high but *finite* conductivity. The rest of the resonator surface is a boundary with ideally conducting metal. There are no gyrotropic samples inside the resonator.

We integrate (4.79) over the volume of this resonator and take into account that the tangential component of the electric field is not equal to zero on  $S_1$ . Then, neglecting the distinction between the perturbed ( $\omega$ ) and unperturbed ( $\omega_0$ ) values of frequency, except in the difference  $(\omega - \omega_0)$ , we get the perturbation formula obtained by Slater [367]:

$$\frac{\omega - \omega_0}{\omega_0} \equiv \frac{\omega' - \omega_0}{\omega_0} + i \frac{1}{2Q} = \frac{ic}{2\omega_0 W_0} \int_{S_1} (e \times h^*) n_0 dS. \quad (4.96)$$

Here  $W_0$  is determined by (4.84),  $n_0$  is a unit outward normal to  $S_1$ , and  $e$  and  $h$  are the perturbed field vectors. It should be noted that the real part of the integral in (4.96) is the energy flow through  $S_1$  multiplied by  $8\pi/c$ ; this is in agreement with the definition (1.108) of the quality factor  $Q$ .

According to the perturbation method, it is possible to substitute  $h_0$  for  $h$  in (4.96). The unperturbed field  $h_0$  is now the field in the resonator with ideally

conducting walls, which is tangential to  $S_1$ . The relation of the tangential electric-field component  $e_\tau$  to  $h_0$  can be found from the analysis of the wave propagation within the wall in the direction from the surface of the resonator. Note that such calculation in the case of nonferromagnetic well-conducting metal leads to the Leontovich boundary condition (e.g., [191])

$$\frac{e_\tau}{h_0} = \frac{1+i}{2} k_0 \delta_1 \quad (4.97)$$

where  $\delta_1$  is the skin depth (4.40) in metal with  $\mu = 1$ . The case of ferromagnetic metal will be considered in Section 14.2.



# 5

---

## *Waveguides and resonators with gyrotropic media. Microwave ferrite devices*

---

---

### 5.1 Waveguide with longitudinally magnetized medium

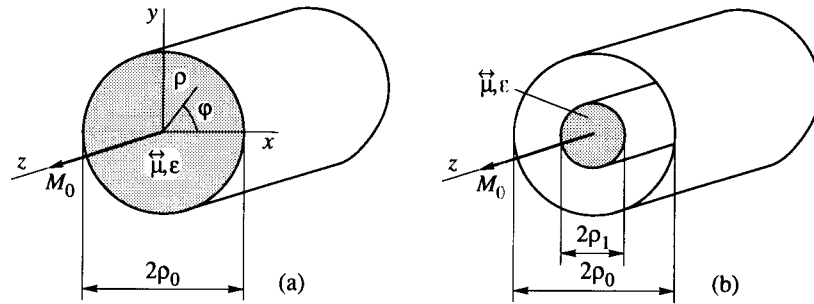
In this chapter we will study electromagnetic waves in waveguides and oscillations in resonators containing gyrotropic media, in particular, the magnetized ferrites. We will limit ourselves to the media with parameters (4.23) and often will regard  $\varepsilon$  as a scalar. The first two sections of this chapter will be devoted to the so-called *regular* waveguides (infinitely long and with constant cross section) completely or partly filled with a gyrotropic medium.

The case of a medium magnetized in the direction of the waveguide axis (a longitudinally magnetized medium) will be treated first. In this case, the longitudinal field components satisfy the equations that are obtained from (4.24) by the replacement  $\partial/\partial z \rightarrow -ik_z$ . It follows from these equations (as mentioned in Section 4.1) that, if  $h_z = 0$ , then  $e_z = 0$ , too, and vice versa. Thus, the modes of the waveguide filled with a longitudinally magnetized gyrotropic medium *are not* TE or TM waves. However, they turn into TE or TM waves when  $\mu_a \rightarrow 0$  and  $\varepsilon_a \rightarrow 0$ . Therefore, they can be referred to as quasi-TE and quasi-TM waves. Furthermore, they turn into TE or TM modes when  $k_z \rightarrow 0$ . Equations (4.24) coincide then with the equations for an isotropic medium with parameters  $\varepsilon_{\parallel}$  and  $\mu_{\perp}$  (for TM waves) or with parameters  $\varepsilon_{\perp}$  and  $\mu_{\parallel}$  (for TE waves). It can be shown (e.g., [153]) that for magnetically-gyrotropic media ( $\varepsilon_a = 0$ ), in particular, for ferrites at microwaves, the boundary conditions at  $k_z = 0$  coincide, as well, with the boundary conditions for an isotropic medium. Therefore, the following expressions for the critical wavelengths, analogous with such expressions for an isotropic medium, are valid:

$$\lambda_{\text{crTM}} = (\lambda_{\text{crTM}})_0 \sqrt{\varepsilon\mu_{\perp}} \quad \lambda_{\text{crTE}} = (\lambda_{\text{crTE}})_0 \sqrt{\varepsilon\mu_{\parallel}} \quad (5.1)$$

where  $(\lambda_{\text{crTM}})_0$  and  $(\lambda_{\text{crTE}})_0$  are the critical wavelengths in an empty waveguide.

To find the propagation constant  $k_z$  and the field structure in a waveguide with



**FIGURE 5.1**  
Circular waveguides with longitudinally magnetized ferrite.

a longitudinally magnetized gyrotropic medium the method of scalar potential functions mentioned in Section 4.1 can be used. This method is described in considerable detail in [153]. Here we will limit ourselves to some remarks. As the  $z$  dependence is harmonic for a wave propagating—as in our case—in  $z$  direction, the functions  $\psi_{\perp 1,2}$  satisfy equation (4.29), and the quantities  $\kappa_{1,2}$  are the roots of (4.27). The boundary conditions at the waveguide walls can be satisfied only by some linear combinations of two fields that correspond to the functions  $\psi_{\perp 1}$  and  $\psi_{\perp 2}$ . These combinations are the normal modes of the waveguide. However, this problem can be solved analytically only in a limited number of cases. A circular waveguide filled with a longitudinally magnetized medium belongs to them.

### 5.1.1 Circular waveguide

Consider first a circular waveguide [Figure 5.1(a)] with perfectly conducting walls completely filled with the medium for which  $\vec{\mu}$  has the form (4.23) and  $\varepsilon$  is a scalar. A particular solution of (4.29) in cylindrical coordinates (Figure 5.1) that remains finite at  $\rho = 0$  has the form [293]

$$\psi = J_m(\kappa\rho)\exp(im\varphi) \quad (5.2)$$

where  $J_m$  is the Bessel function and  $m = 0, \pm 1, \pm 2, \dots$ . The scalar function  $\psi$  that corresponds to a *normal wave* can be written as

$$\psi = [A_1 J_m(\kappa_1\rho) + A_2 J_m(\kappa_2\rho)] \exp(im\varphi - ik_z z). \quad (5.3)$$

Substituting (5.3) into the boundary conditions for the function  $\psi$  [151] at  $\rho = \rho_0$ , we obtain a system of two uniform linear equations for  $A_1$  and  $A_2$ . Setting equal to zero the determinant of this system, we get the transcendental



equation

$$F_1 - F_2 = 0$$

$$F_{1,2} = \left( \frac{k_0^2 \varepsilon \mu_{\perp} - k_z^2}{\kappa_{1,2}} - \kappa_{1,2} \right) \frac{J'_m(\kappa_{1,2} \rho_0)}{J_m(\kappa_{1,2} \rho_0)} + \frac{\mu_a m}{\mu \rho_0} \frac{k_z^2}{\kappa_{1,2}^2} \quad (5.4)$$

where  $J'(\kappa \rho_0)$  is the derivative of  $J(\kappa \rho_0)$  with respect to the argument. This equation was derived independently by Kales [203], Gintsburg [139], and Suhl and Walker [397]. Solving it together with the expressions for the roots  $\kappa_{1,2}$  of (4.27), we can find  $\kappa_1$ ,  $\kappa_2$ , and the propagation constant  $k_z$ .

It is very important that  $k_z$  occurs in (5.4), as well as in (4.27), only to the *second power*. Therefore, the value of  $|k_z|$  is independent of the direction of propagation. At the same time,  $\mu_a$  and  $m$  occur in (5.4) to the *first powers*, as a product  $\mu_a m$ . The sign of  $\mu_a$  is determined by the direction of  $\mathbf{M}_0$ , and the sign of  $m$  represents the direction of the polarization rotation (right-hand for  $m < 0$  and left-hand for  $m > 0$ ) with respect to the direction of propagation. Therefore, the sign of  $\mu_a m$  shows the direction of the polarization rotation with respect to the direction of the steady magnetization. The waves with right-hand and left-hand rotation with respect to this direction have different propagation constants  $|k_{z+}|$  and  $|k_{z-}|$ . This distinction, in analogy with the unbounded medium (Section 4.2), leads to the turn of polarization, i.e., to the Faraday effect.

The analysis of equation (5.4) was carried out in detail in [397]. It was shown, in particular, that formula (4.48) is to be replaced now by

$$\vartheta = \frac{1}{2|m|} (k'_{z+} - k'_{z-}) l. \quad (5.5)$$

We can define a vector which lies in the cross section of the waveguide and is rigidly bound to the field structure. This vector can be referred to as a vector of *polarization of the wave*. It plays, in the case of a waveguide, the role of the field-polarization vector (Section 4.2), the turn of which is the Faraday effect.

### 5.1.2 Circular waveguide with ferrite rod

The circular (as well as any other) waveguide completely filled with gyrotropic medium (ferrite) is disadvantageous from the practical point of view. First, it has a low 'quality factor' (i.e., the ratio of the angle  $\vartheta$  to the losses). Second, strong reflections at the boundary of this waveguide and the empty waveguide make matching difficult. These shortcomings can be diminished if the waveguide is *partly* filled with ferrite, e.g., if the circular waveguide contains a circular ferrite rod [Figure 5.1(a)].

This problem can also be solved strictly. The field in the ferrite rod ( $\rho < \rho_1$ ) must be represented by a sum of two fields corresponding to  $\kappa_1$  and  $\kappa_2$ . The field in the isotropic medium ( $\rho_1 < \rho < \rho_0$ ) with parameters  $\mu_0 = 1$  and  $\varepsilon_0$  is a sum of TE and TM fields. Each of them should contain Bessel functions  $J_m(\kappa_0 \rho)$  as

well as Bessel functions of the second kind (or Neumann functions)  $N_m(\kappa_0\rho)$  [293] because the point  $\rho = 0$  (at which  $N_m \rightarrow \infty$ ) does not belong now to the considered region. Thus, six arbitrary constants appear in the expressions for field components. The boundary conditions at  $\rho = \rho_0$  and  $\rho = \rho_1$  yield a system of six equations. Setting equal to zero the determinant of this system, we get a transcendental equation for the quantities  $k_z$ ,  $\kappa_1$ ,  $\kappa_2$ , and  $\kappa_0$ , which is to be solved together with the expressions for the roots  $\kappa_1$  and  $\kappa_2$  of (4.27) and the expression  $\kappa_0^2 = k_0^2\varepsilon_0 - k_z^2$ . Omitting cumbersome calculations [285], we note that only  $k_z^2$  and the product  $\mu_a m$  occur in the mentioned equation as well as in (5.4). Therefore, the properties of the circular waveguide with a longitudinally magnetized ferrite rod are, qualitatively, the same as those of the circular waveguide filled with ferrite. In particular, formula (5.5) is valid now, too.

If  $\rho_1/\rho_0 \ll 1$ , formula (4.81) with the quasistatic approximation of the perturbed field (Table 4.1) can be used to calculate  $k_{z\pm}$  and the angle  $\vartheta$  for the circular waveguide with ferrite rod. Such calculation [153], in the most interesting case of the quasi-TE<sub>11</sub> wave, yields

$$\vartheta = 4.2k_{z0} \left( \frac{\rho_1}{\rho_0} \right)^2 \frac{\mu_a}{(\mu + 1)^2 - \mu_a^2} l \quad (5.6)$$

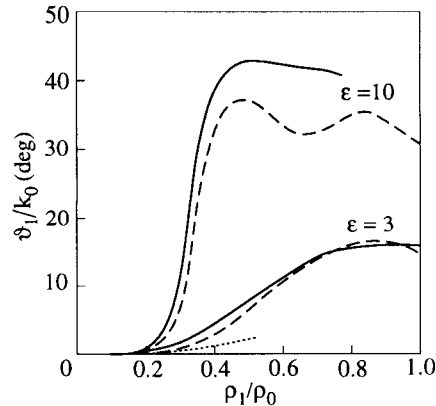
where  $k_{z0}$  is the propagation constant in an empty waveguide. To estimate the limit of validity of this expression we use formula (4.93) and get, for  $\varepsilon_0 = 10$ ,  $\rho_1/\rho_0 \lesssim 0.05$ .

Another variant of the perturbation method (Section 4.5), the weakly-gyrotropic approximation, can also be used [285]. Now the waveguide with the same  $\varepsilon$  and  $\mu$  but with  $\mu_a = 0$  is regarded as the unperturbed system, and the appearance of the antisymmetric component  $\mu_a$  is the perturbation; the ratio  $\mu_a/\mu$  is a small parameter. The results of calculations of the angle  $\vartheta$  by all mentioned methods are shown in Figure 5.2.

The turn of polarization (the Faraday effect) in a circular waveguide can be regarded alternatively as a result of energy transfer from a linearly polarized, e.g., quasi-TE<sub>11</sub>, wave to another wave, also linearly polarized quasi-TE<sub>11</sub> but with the polarization vector (or the field pattern) turned through the angle of  $\pi/2$  with respect to the polarization of the first wave. These waves are the normal waves of an empty waveguide, but they become *coupled* in a waveguide with longitudinally magnetized gyrotropic medium. Such treatment can be applied, as well, in the case of waveguide with a square cross section. The longitudinally magnetized gyrotropic medium leads to the coupling of the waves quasi-TE<sub>10</sub> and quasi-TE<sub>01</sub> in this waveguide.

The treatment in terms of *coupled waves* is especially useful if the distinction between the waves in the waveguide with a gyrotropic medium and the corresponding waves in the waveguide with an isotropic medium is small. This takes place when the radius of the ferrite rod is small, or the values of  $\varepsilon_a$  and  $\mu_a$  are small.

The latter case is realized in *optics*. Consider, for instance, a plane optical

**FIGURE 5.2**

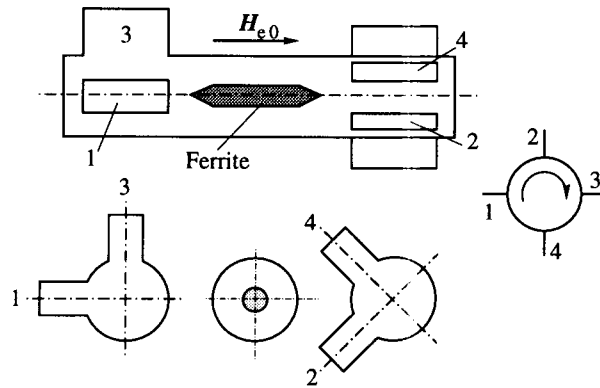
Turn of polarization in a circular waveguide with ferrite rod [285].  $\vartheta_1$  is the angle of the turn on a distance  $l$ , and  $k_0$  is the wave number in free space. Solid curves correspond to the rigorous calculation, dashed curves, to the calculation in the weakly-gyrotropic approximation, and the dotted curve, to the calculation using (5.6).  $\mu = 1$ ,  $\mu_a = 0.5$ ,  $k_0 = 0.6\pi/\rho_0$ .

waveguide (e.g., [7]), which consists of three dielectric layers with permittivities  $\epsilon_1$ ,  $\epsilon_2$ , and  $\epsilon_3$ , the permittivity of the middle layer  $\epsilon_2$  being the greatest. (In fact, this waveguide is a thin film with  $\epsilon_2$  on a substrate with  $\epsilon_1 < \epsilon_2$ , a third ‘layer’ is air.) In the absence of gyrotropic media the normal waves in such waveguide are TE and TM waves. But if one of the layers is gyrotropic, these waves are coupled. If one of them is excited at the input, its energy is transferred into another wave during the propagation. Of course, this process can be considered, as well, in terms of *normal waves* of gyrotropic waveguide, which are neither TE nor TM. They are not transformed into one another but have different  $k_z$  values, and this results in the transformation of the structure of the propagating wave, which is the sum of these normal waves.

### 5.1.3 Faraday ferrite devices

The direction of the turn of the wave polarization in a waveguide with a longitudinally magnetized gyrotropic medium does not depend, as previously mentioned, on the direction of propagation, and it is reversed when the direction of the steady magnetization is changed. This effect, which is a manifestation of the nonreciprocity of such systems (Section 4.3), is used in designing nonreciprocal microwave and optical ferrite devices. The devices of such type (referred to as polarization or Faraday devices) were investigated by Hogan [183] (see also [247]).

Let us consider the device shown schematically in Figure 5.3. It is a section of a circular waveguide with a longitudinally magnetized ferrite cylinder on its



**FIGURE 5.3**  
Faraday circulator.

axis and with two pairs of input and output rectangular waveguides. The linear polarization of the wave  $TE_{11}$  is turned by the ferrite sample through the angle  $\vartheta = \pi/4$ . The angle between the pairs of rectangular waveguides has the same value. It is easy to see that the wave coming, e.g., from port 1 (Figure 5.3) passes into port 2, and the wave from port 3 passes into port 4. As the sign of the angle  $\vartheta$  is independent of the direction of propagation, the wave from port 2 will pass into port 3, and the wave from port 4 will pass into port 1. A device with such properties is called a *circulator* (in the considered case, a four-port circulator). If the external steady field  $H_{e0}$  is turned to the opposite direction, the direction of energy circulation is reversed.

When matched loads are connected to ports 3 and 4, the circulator becomes an *isolator*, i.e., a device that isolates a generator (connected to port 1) from a load, e.g., from an antenna (connected to port 2). If a transmitter and an antenna are connected, as before, to ports 1 and 2, respectively, and a receiver is connected to port 3, the device works as a *duplexer* [247]. A Faraday circulator and, hence, an isolator or a duplexer have usually, in a frequency band of  $\sim 10\%$ , the following parameters: forward losses less than 0.5 dB and backward losses 25–30 dB. Changing, continuously or discretely, the magnetic field  $H_{e0}$ , we obtain an amplitude *modulator* or a *switch*. The frequencies of modulation as high as  $\sim 10$  MHz can be reached with comparatively low magnetic-field amplitudes. All the above-mentioned Faraday devices can be constructed using the waveguide with square cross section, as well.

A circular or a square waveguide with a longitudinally magnetized ferrite sample can also be applied in a controllable phase shifter or phase modulator. In this case, the circularly polarized wave is to be used with  $k_z$ , depending on magnetic field. It is worth noting, however, that a linearly polarized wave in a waveguide in which only this wave propagates can be used, as well, to design a controllable phase

shifter. As an example, the reciprocal Reggia–Spencer phase shifter [326] (see also [247]) may be mentioned.

---

## 5.2 Waveguide with transversely magnetized ferrite

In this section we will study the propagation of waves in waveguides that contain gyrotropic media magnetized at right angle to the waveguide axis. First of all, the rectangular waveguide completely filled with such a medium will be treated.

### 5.2.1 Rectangular waveguide filled with ferrite

Consider a rectangular waveguide (Figure 5.4) filled with the medium with parameters (4.23). The direction of magnetization, which coincides, as usual, with the  $z$ -axis, is normal to the wide waveguide walls. The simplest modes in this waveguide are such for which the fields *do not depend on*  $z$ . Let us first ignore the boundary conditions. Then, as it follows from (4.24), TE waves (with  $h_z = 0$ ) and TM waves (with  $e_z = 0$ ) can exist if  $\partial/\partial z = 0$ . Substituting  $e = e_0 \exp(-ik_y y)$  and  $h = h_0 \exp(-ik_y y)$  into equations (4.14) and (4.16) and projecting these equations onto the coordinate axes, we obtain two independent systems: the following one<sup>1</sup>

$$\begin{aligned} k_y e_z - k_0 \mu h_x - ik_0 \mu_a h_y &= 0 \\ i \frac{\partial e_z}{\partial x} - ik_0 \mu_a h_x + k_0 \mu h_y &= 0 \\ k_0 \varepsilon_{||} e_z - k_y h_x + i \frac{\partial h_y}{\partial x} &= 0 \end{aligned} \quad (5.7)$$

and a system for the components  $e_x$ ,  $e_y$ , and  $h_z$ . The system (5.7) represents the waves  $TE_{n0}$ , and the second one represents the waves  $TM_{n0}$  (the subscripts  $n$  and  $0$  indicate the numbers of variations of the field-component amplitudes along the axes, respectively,  $x$  and  $z$ ).

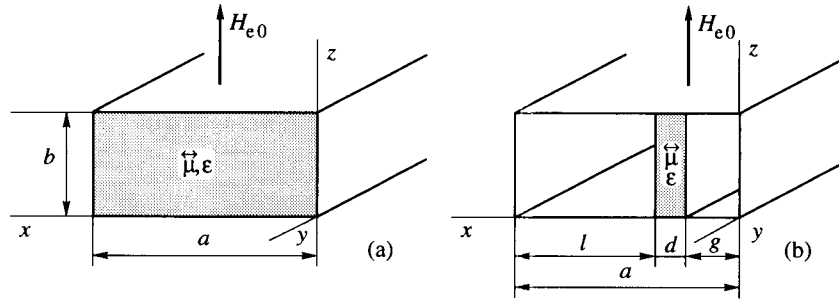
However, the waves  $TM_{n0}$  *do not exist* in this waveguide because they do not satisfy the boundary conditions. Indeed, the components  $e_x$  and  $e_y$  should be equal to zero at the walls  $z = 0$  and  $z = b$  and, hence, everywhere because  $\partial/\partial z = 0$ .

For  $TE_{n0}$  waves, excluding  $h_x$  and  $h_y$  from (5.7), we find

$$\frac{d^2 e_z}{dx^2} + \kappa_x^2 e_z = 0 \quad (5.8)$$

---

<sup>1</sup>In (5.7) and later on we omit the subscripts  $0$  at the components of  $e_0$  and  $h_0$ .



**FIGURE 5.4**  
Rectangular waveguides with transversely magnetized ferrite.

where

$$\kappa_x^2 = k_0^2 \varepsilon_{\parallel} \mu_{\perp} - k_y^2. \quad (5.9)$$

The solution of (5.8), which satisfies the boundary conditions at  $x = 0$  and  $x = a$ , has the form

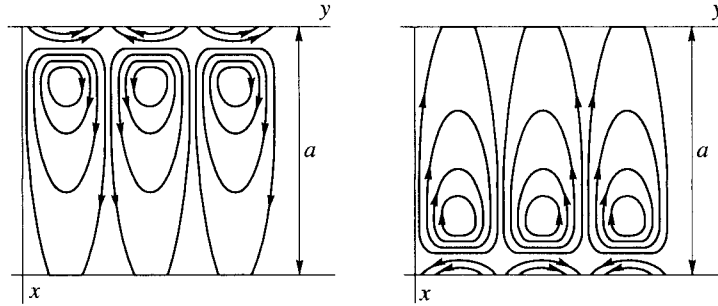
$$e_z = A \sin \kappa_x x \quad \kappa_x = \frac{n\pi}{a} \quad n = 1, 2, 3, \dots \quad (5.10)$$

From (5.9) and (5.10) we obtain the propagation constant

$$k_y = \sqrt{k_0^2 \varepsilon_{\parallel} \mu_{\perp} - \left(\frac{n\pi}{a}\right)^2}. \quad (5.11)$$

Thus, the structure of the electric field of the waves  $TE_{n0}$  in a rectangular waveguide filled with transversely magnetized ferrite is the same as in the waveguide filled with an isotropic medium. It is easy to make sure that the structure of the ac magnetic induction is also the same as in the case of an isotropic medium. However, the structure of the ac magnetic field is quite different (Figure 5.5) and nonreciprocal. It changes with the reversal of the direction of propagation or the direction of magnetization and remains the same if both these directions are reversed.

The field structure in a rectangular waveguide filled with transversely magnetized medium is much more complicated if we allow for the field dependence on both transverse coordinates  $x$  and  $z$ . Normal waves are, then, the superpositions of partial waves with two values of  $\kappa_x$ . They are no more waves TE or TM but have six field components [356, 285]. It follows from (5.11) that, if  $\mu_{\perp} < 0$ , only such modes can propagate. The  $x$  dependences of the fields are represented, then, either by hyperbolic (with imaginary  $\kappa_x$ ) or by trigonometric functions. In the first case, the fields 'press themselves' to one of the narrow (perpendicular to the  $x$ -axis) walls of the waveguide, depending on the direction of propagation. Such modes are referred to as ferrite-metal modes.

**FIGURE 5.5**

Magnetic force lines of a  $TE_{10}$  wave in a rectangular waveguide filled with ferrite for two directions of propagation.  $\varepsilon = 9$ ,  $\mu = 0.9$ ,  $\mu_a = 0.6$ ,  $k_0 = 1.41\pi/a$ .

### 5.2.2 Rectangular waveguide with ferrite plates

Let us turn now to waveguides *partly filled* with transversely magnetized gyrotropic medium. The simplest case is a rectangular waveguide with a ferrite plate parallel to the narrow waveguide walls (Figure 5.4). We limit ourselves again to the modes with  $\partial/\partial z = 0$ . Equation (5.8) is valid inside the plate; outside the plate

$$\frac{de_z^2}{dx^2} + \kappa_{x0}^2 e_z = 0 \quad (5.12)$$

$$\kappa_{x0}^2 = k_0^2 - k_y^2. \quad (5.13)$$

The solutions of (5.8) and (5.12) that satisfy the boundary conditions at  $x = 0$  and  $x = a$  are

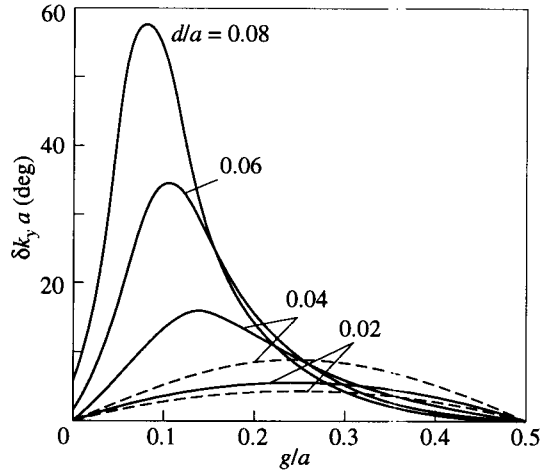
$$\begin{aligned} e_z &= A \sin \kappa_{x0} x & 0 < x < g \\ e_z &= B \sin \kappa_x (x - g) + C \cos \kappa_x (x - g) & g < x < g + d \\ e_z &= D \sin \kappa_{x0} (a - x) & g + d < x < a. \end{aligned} \quad (5.14)$$

Four conditions of continuity of  $e_z$  and  $h_y$  at  $x = g$  and  $x = g + d$  yield a system of equations for the coefficients  $A$ ,  $B$ ,  $C$ , and  $D$ . Setting equal to zero the determinant of this system, we obtain the equation derived first by Kales, Chait and Sakiotis [204]:

$$\begin{aligned} p \kappa_{x0} \cot \kappa_x d (\tan \kappa_{x0} g + \tan \kappa_{x0} l) - (p^2 + q^2) \tan \kappa_{x0} g \tan \kappa_{x0} l \\ + \kappa_{x0}^2 + \kappa_{x0} q (\tan \kappa_{x0} g - \tan \kappa_{x0} l) = 0 \end{aligned} \quad (5.15)$$

where  $p = \kappa_x / \mu_{\perp}$ ,  $q = \mu_a k_y / (\mu \mu_{\perp})$  and  $l = a - g - d$ .

Equation (5.15) contains the product  $\mu_a k_y$ . Therefore, the roots of this equation,  $|k_y^+|$  and  $|k_y^-|$ , as well as the field patterns, are different for opposite directions



**FIGURE 5.6**

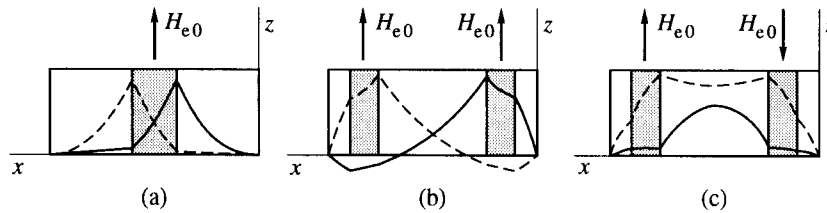
Dependence of nonreciprocal difference of propagation constants in a rectangular waveguide with ferrite plate on the location and thickness of the plate [Figure 5.4(b)]. Solid curves represent the results of rigorous calculation [158], dashed curves correspond to the calculation by the perturbation method (Section 4.5).  $\epsilon = 9$ ,  $\mu = 0.9$ ,  $\mu_a = 0.5$ ,  $k_0 = 1.44\pi/a$ .

of propagation or opposite directions of magnetization; they remain the same if both of these directions are reversed. The replacement  $g \rightleftharpoons l$  results in the same change of  $|k_y|$ . If  $g = l$ , then  $|k_y^+| = |k_y^-|$ . An equation for critical frequency (or for critical waveguide dimensions at constant frequency) is obtained by taking  $k_y = 0$  in (5.15). Then,  $\mu_a$  will appear in this equation only to the second power. So, the critical values of frequency or of waveguide dimensions are independent of the directions of magnetization and propagation.

The dependence of the nonreciprocal difference  $\delta k_y = |k_y^+| - |k_y^-|$  on the thickness and location of the ferrite plate obtained by numerical solution of equation (5.15) [158] is shown in Figure (5.6). The results of calculation by the perturbation method with quasistatic approximation of the internal field (Section 4.5) are also plotted. One can see that the perturbation method may be used only for  $d \lesssim 0.02a$ .

The field structures in a waveguide with a transversely magnetized plate are quite different, as it follows from (5.13), for  $|k_y| < k_0$  and  $|k_y| > k_0$ . In the first case the  $x$  dependence outside the plate is represented by trigonometric functions, while in the second case it is represented by hyperbolic functions. The field structure inside the plate, according to (5.9), depends on the value of  $\mu_\perp$ . If  $\mu_\perp < 0$ , i.e., the frequency lies in the range  $\omega_\perp < \omega < \omega_H + \omega_M$  (Figure 1.6), the  $x$  dependence of the fields in the ferrite plate is represented by hyperbolic functions. In unbounded transversely magnetized ferrite, the wave propagation





**FIGURE 5.7**

Electric-field patterns in waveguides with magnetized ferrite plates ( $\partial/\partial z = 0$ ). Solid and dashed lines correspond to opposite directions of propagation. (a)  $\mu_{\perp} < 0$  and (b,c)  $\mu_{\perp} > 0$ .

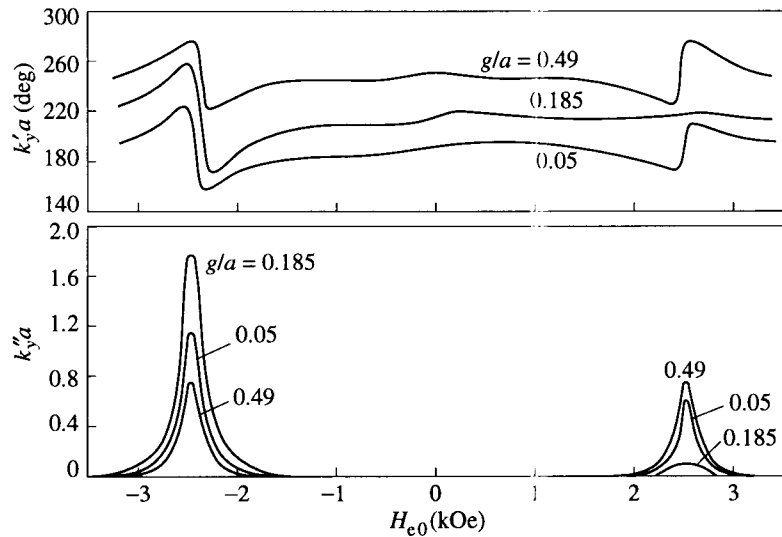
in this case would be impossible. In a waveguide containing a ferrite plate with  $\mu_{\perp} < 0$  the wave does propagate, but its field is 'pushed out' of the regions where the polarization of magnetic field is near right-hand circular. For opposite directions of propagation—as well as for opposite directions of magnetization—the fields 'press themselves' to the opposite surfaces of the plate (Figure 5.7). This is a manifestation of the *nonreciprocal field-displacement* effect.

The transcendental equations analogous to (5.15) can be obtained, in the case of  $\partial/\partial z = 0$ , for rectangular waveguides with an arbitrary number of transversely magnetized ferrite plates parallel to the narrow waveguide walls. The most interesting is the case of two plates located symmetrically in the waveguide and magnetized either in the same or in opposite directions (Figure 5.7). In the first case the propagation constants  $|k_y|$  do not differ from each other for opposite directions of propagation, but the field structures are different. In the second case both the  $|k_y|$  values and the field structures depend on the direction of propagation.

When the *energy losses* in ferrite are taken into account, the  $\vec{\mu}$  components and  $\varepsilon$  gain imaginary parts and the dispersion equations, e.g., (5.15), become complex. Solutions of these equations yield complex propagation constants  $k_y = k'_y - ik''_y$ ; the quantities  $k''_y$  are the damping coefficients (decrements) of the waves. If the imaginary parts of  $\mu$ ,  $\mu_a$ , and  $\varepsilon$  are small as compared with the real parts, the following approximate formula can be used:

$$k''_y = \frac{\partial k'_y}{\partial \varepsilon'} \varepsilon'' + \frac{\partial k'_y}{\partial \mu'} \mu'' + \frac{\partial k'_y}{\partial \mu'_a} \mu''_a. \quad (5.16)$$

Near ferromagnetic resonance, where  $\mu''$  and  $\mu''_a$  are of the same order of magnitude as  $\mu'$  and  $\mu'_a$ , this formula cannot be applied and it is necessary to find the complex roots of the dispersion equations. The results of this calculation [158] are shown in Figure 5.8. One can see from this figure that, in a position of the ferrite plate near the point of circular polarization of the magnetic field, the losses depend strongly on the direction of propagation. This phenomenon, which can be named *nonreciprocal damping*, is widely used in microwave ferrite devices. Note that the

**FIGURE 5.8**

Real and imaginary parts of the propagation constant versus the external steady magnetic field for different locations of the magnetized ferrite plate in a rectangular waveguide [Figure 5.4(b)] calculated by computer solving of (5.15) [158]. Thickness of the plate  $d = 0.02a$ . Frequency is 9.4 GHz,  $M_0 = 170$  G,  $\omega_r = 2 \times 10^9$  s<sup>-1</sup>,  $\epsilon = 9$ , the values of  $\mu$  and  $\mu_a$  were obtained using (1.69).

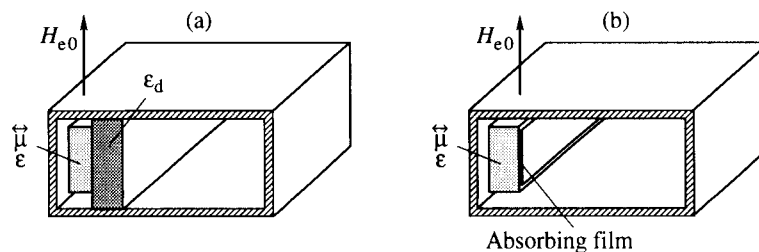
maximal damping occurs at the external magnetic-field value that coincides with the ferromagnetic-resonance field calculated with formula (1.92) for an ellipsoid with the same ratio of dimensions as for the ferrite plate in the waveguide.

### 5.2.3 Microwave ferrite devices

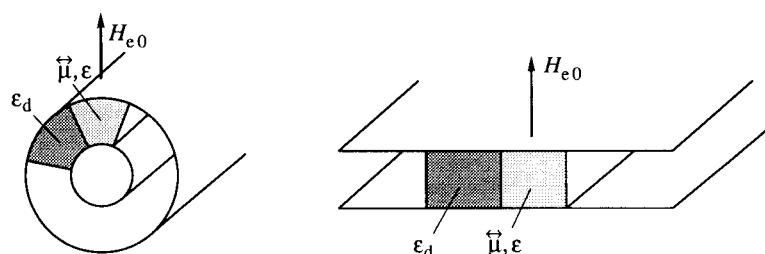
Devices in which the waveguides with transversely magnetized ferrite are used can perform almost all functions that perform the Faraday devices discussed in the previous section. Their parameters, in most cases, are not worse than the parameters of Faraday devices, whereas the constructions are simpler.

Consider first the isolators. One of them, a *resonance isolator*, in which the above-mentioned effect of nonreciprocal damping is used, is shown schematically in Figure 5.9(a). The dielectric plate serves to enhance the concentration of the field in the ferrite plate. Resonance isolators of this type have, in centimeter-wavelength range, forward losses of 0.2–0.3 dB and isolation (the ratio of backward to the forward losses) of more than 100 in a frequency band of approximately 20%.

Every waveguide that contains points with circular (or nearly circular) polarization of the magnetic field can be used to design the resonance isolator. In the case of a microstrip or a coaxial waveguide, a dielectric sample should be inserted to

**FIGURE 5.9**

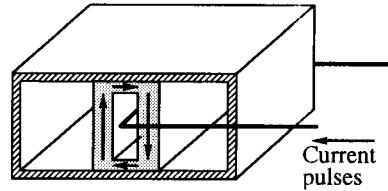
Microwave ferrite isolators using (a) resonance absorptions and (b) field-displacement effect.

**FIGURE 5.10**

Coaxial resonance isolator and its parallel-plane analog.

obtain such points. Microstrip and coaxial waveguides with dielectric and ferrite samples cannot be analyzed rigorously, and a parallel-plane waveguide is often used as an approximate model. In Figure 5.10, a coaxial isolator and its parallel-plane analog are shown. It is clear from symmetry considerations that, without the dielectric sample, it is impossible to attain different losses at different directions of propagation. The microstrip and coaxial waveguides are wide-band. To get a wide-band isolator it is necessary only to ensure the ferromagnetic-resonance condition in the whole frequency band. This can be achieved, for instance, by the use of a nonuniform steady magnetic field. The frequency band of such isolators can be as large as an octave, the forward losses being 0.2–0.4 dB, and isolation, not less than 50.

The design of an isolator that uses the above-mentioned *field-displacement* effect is shown schematically in Figure 5.9(b). The dimensions and the position of the ferrite plate are chosen to make the electric field of the forward wave equal to zero at the place of the absorber. It has been pointed out above that one of the waves is effectively ‘pushed out’ of the ferrite plate if  $\mu_{\perp} < 0$ . This requirement must be fulfilled for good performance of a field-displacement isolator. The characteristic parameters of this device are: forward losses 0.1–0.3 dB and isolation  $\sim 100$ . The field-displacement effect has been applied, as well, in constructing nonreciprocal



**FIGURE 5.11**  
Latching ferrite phase shifter. The arrows show one of the two magnetization directions.

devices, isolators and circulators using wide microstrip waveguides [330]. These devices have been called *edge guided* devices.

Let us briefly consider the ferrite microwave phase shifters. The rectangular waveguide with a magnetized ferrite plate, which has been discussed above, is the simplest nonreciprocal phase shifter. The steady magnetic field is, in this case, much less (or, sometimes, greater) than its resonance value  $H_{\text{res}}$ . Then the decrement  $k''_y$  can be sufficiently small at required values of the nonreciprocal difference  $\delta k'_y$ , as seen in Figure 5.8. The fields exceeding  $H_{\text{res}}$  are used at low frequencies to avoid the so-called *initial losses* caused by intrinsic ferromagnetic resonance (Section 8.3).

To design a *reciprocal* phase shifter we must put the ferrite plate into the central plane of the waveguide ( $g = l$  in Figure 5.4) or use two plates symmetrically placed and magnetized in the same directions (Figure 5.7).

A 'toroidal' *nonreciprocal* phase shifter is shown schematically in Figure 5.11. If the ferrite has a sufficiently great value of remanent induction  $B_r$  and low coercive field  $H_c$ , then the phase shift can be controlled by short (e.g., microsecond) current pulses, and the phase shifter is a '*latching*' device (with 'magnetic memory'). It should be noted that the phase shifts in this device can be calculated approximately on a model of a waveguide with two ferrite plates magnetized in opposite directions (Figure 5.7). The typical parameters of such devices are: losses 0.5–1 dB for the phase shift of  $360^\circ$  (i.e., the figure of merit is more than  $300 \text{ deg dB}^{-1}$ ) in a 10% frequency band.

---

### 5.3 Resonators with gyrotropic media

We turn now to another fundamental problem of the electrodynamics of systems with gyrotropic media, to the problem of oscillations of an electromagnetic resonator containing such medium.

### 5.3.1 Eigenoscillations and forced oscillations

Consider a hollow resonator containing a medium the parameters of which,  $\vec{\varepsilon}$  and  $\vec{\mu}$  are arbitrary functions of coordinates. Let us neglect, first, all kinds of losses, i.e., assume  $\vec{\varepsilon}$  and  $\vec{\mu}$  to be Hermitian tensors (Section 4.1) and suppose the conductivity of the walls to be infinite. We introduce the complex amplitudes  $C e_\nu$  and  $iCh_\nu$  of the fields of *eigenoscillations* ( $C$  is an arbitrary real quantity, and  $e_\nu$  and  $h_\nu$  are the eigenvectors). These complex amplitudes must satisfy the Maxwell equations (4.14) and (4.16) with  $j_{\text{ext}} = 0$  and the boundary conditions (4.5). Hence,

$$\text{roth}_\nu = \frac{\omega_\nu}{c} \vec{\varepsilon} e_\nu \quad \text{rote}_\nu = \frac{\omega_\nu}{c} \vec{\mu} h_\nu \quad (5.17)$$

and, at the resonator surface  $S$ ,

$$e_\nu \times \mathbf{n}_0 = 0 \quad \mathbf{n}_0 \vec{\mu} h_\nu = 0 \quad (5.18)$$

where  $\mathbf{n}_0$  is a unit normal to  $S$ ,  $\omega_\nu$  is the eigenfrequency corresponding to eigenvectors  $e_\nu$  and  $h_\nu$ , and  $\nu$  indicates the number of an oscillation mode.

If  $\vec{\varepsilon}$  and  $\vec{\mu}$  are symmetric tensors (in particular, scalars), their components are real in the absence of losses. Then, the eigenvectors  $e_\nu$  and  $h_\nu$  satisfy equations (5.17) with real coefficients and can be taken as real. The corresponding eigenoscillations are standing waves. However, if  $\vec{\mu}$  or  $\vec{\varepsilon}$  have *antisymmetric* components (which are imaginary in the absence of losses), the solutions of (5.17) are complex. It means that the fields of eigenoscillations of a resonator with gyrotropic medium *are not* standing waves. The eigenfrequencies, nevertheless, remain real [153], as it should be for a system without losses.

Consider now the *forced oscillations* of the resonator, i.e., the excitation of harmonic oscillations, with frequency  $\omega$ , under the action of external current density  $j_{\text{ext}}$ , external charge density  $\rho_{\text{ext}}$ , external magnetization  $m_{\text{ext}}$ , and external fields at the apertures  $S_1$  in the resonator walls. The quantities  $j_{\text{ext}}$ ,  $\rho_{\text{ext}}$ , and  $m_{\text{ext}}$ , as well as the external electric field  $e_{\text{ext}}$  and the external magnetic induction  $b_{\text{ext}}$  at  $S_1$ , are assumed to be known. The Maxwell equations for the fields of forced oscillation and the boundary conditions are written as follows:

$$\text{rote} + ik_0 \vec{\mu} \mathbf{h} = -i4\pi k_0 m_{\text{ext}} \quad (5.19)$$

$$\text{div} \left( \vec{\mu} \mathbf{h} \right) = -4\pi \text{div} m_{\text{ext}} \quad (5.20)$$

$$\text{roth} - ik_0 \vec{\varepsilon} \mathbf{e} = \frac{4\pi}{c} j_{\text{ext}} \quad (5.21)$$

$$\text{div} \left( \vec{\varepsilon} \mathbf{e} \right) = 4\pi \rho_{\text{ext}} \quad (5.22)$$

$$\begin{aligned} \mathbf{n}_0 \times (\mathbf{e} \times \mathbf{n}_0) &= \mathbf{e}_{\text{ext}} & \mathbf{n}_0 \vec{\mu} \mathbf{h} &= \mathbf{n}_0 b_{\text{ext}} & \text{on } S_1 \\ \mathbf{n}_0 \times (\mathbf{e} \times \mathbf{n}_0) &= 0 & \mathbf{n}_0 \vec{\mu} \mathbf{h} &= 0 & \text{on } S - S_1. \end{aligned} \quad (5.23)$$

The complex amplitudes of the forced-oscillation fields can be represented in the form

$$\mathbf{e} = \sum_{\nu=1}^{\infty} \mathcal{E}_{\nu} \mathbf{e}_{\nu} - \nabla \varphi \quad \mathbf{h} = \sum_{\nu=1}^{\infty} \mathcal{H}_{\nu} \mathbf{h}_{\nu} + \nabla \psi \quad (5.24)$$

where  $\mathbf{e}_{\nu}$  and  $\mathbf{h}_{\nu}$  are the above-considered eigenvectors, and the coefficients  $\mathcal{E}_{\nu}$  and  $\mathcal{H}_{\nu}$ , as well as the gradient functions  $\varphi$  and  $\psi$ , are to be found. (The distinction of the signs before  $\nabla \varphi$  and  $\nabla \psi$  in (5.24) is due to tradition.)

Note that the eigenvectors  $\mathbf{e}_{\nu}$  and  $\mathbf{h}_{\nu}$  satisfy the *orthogonality* relations [153]

$$\int_{V_0} \mathbf{e}_{\nu}^* \vec{\varepsilon} \nabla \varphi dV = \int_{V_0} \mathbf{h}_{\nu}^* \vec{\mu} \nabla \psi dV = 0 \quad (5.25)$$

$$\int_{V_0} \mathbf{e}_{\nu}^* \vec{\varepsilon} \mathbf{e}_{\nu'} dV = \int_{V_0} \mathbf{h}_{\nu}^* \vec{\mu} \mathbf{h}_{\nu'} dV = \Delta_{\nu\nu'} \quad (5.26)$$

where  $V_0$  is the resonator volume and  $\Delta_{\nu\nu'}$  is the Kronecker delta symbol (Appendix C).

To find the coefficients  $\mathcal{E}_{\nu}$  and  $\mathcal{H}_{\nu}$  we multiply the first expression in (5.24) by  $\vec{\varepsilon}$  and then multiply it scalarly by  $\mathbf{e}_{\nu}$ . The second expression in (5.24) is multiplied, similarly, by  $\vec{\mu}$  and by  $\mathbf{h}_{\nu}$ . Integrating the obtained expressions over  $V_0$  and taking into account the orthogonality relations (5.25) and (5.26), we get the formulae

$$\mathcal{E}_{\nu} = \int_{V_0} \mathbf{e}_{\nu}^* \vec{\varepsilon} \mathbf{e} dV \quad \mathcal{H}_{\nu} = \int_{V_0} \mathbf{h}_{\nu}^* \vec{\mu} \mathbf{h} dV. \quad (5.27)$$

Then we multiply (5.19) by  $\mathbf{h}_{\nu}^*$  and (5.21) by  $\mathbf{e}_{\nu}^*$  and integrate over  $V_0$ . After some transformations, using (5.27) and the boundary conditions and taking into account that  $\vec{\varepsilon}$  and  $\vec{\mu}$  are Hermitian tensors, we obtain ultimately

$$\mathcal{E}_{\nu} = \frac{-i\omega I_{\nu} + \omega_{\nu} F_{\nu} - i\omega\omega_{\nu} G_{\nu}}{\omega_{\nu}^2 - \omega^2} \quad (5.28)$$

$$\mathcal{H}_{\nu} = \frac{\omega_{\nu} I_{\nu} + i\omega F_{\nu} + \omega^2 G_{\nu}}{\omega_{\nu}^2 - \omega^2} \quad (5.29)$$

where

$$I_{\nu} = 4\pi \int_{V_0} \mathbf{e}_{\nu}^* \mathbf{j}_{\text{ext}} dV \quad (5.30)$$

$$G_{\nu} = c \int_{V_0} \mathbf{h}_{\nu}^* \mathbf{m}_{\text{ext}} dV \quad (5.31)$$

$$F_{\nu} = c \int_{S_1} (\mathbf{h}_{\nu}^* \times \mathbf{e}_{\text{ext}}) n_0 dS. \quad (5.32)$$

If the losses are small ( $\mu'' \ll \mu'$ ,  $\mu_a'' \ll \mu_a'$ , etc.), they can be taken into account approximately by the following substitution in (5.28) and (5.30):

$$\omega_\nu \rightarrow \omega'_\nu + i\omega''_\nu \equiv \omega'_\nu + i\frac{\omega'_\nu}{2Q_\nu} \quad (5.33)$$

where  $\omega'_\nu$  can be assumed to be equal to  $\omega_\nu$  calculated without allowance for losses, and  $Q_\nu$  is the quality factor of the resonator for the  $\nu$ th mode.

We do not consider the calculation of the gradient functions as they do not play an important role in most cases. We note only that  $\varphi$  is determined by  $\rho_{\text{ext}}$  and  $\psi$  is determined by  $m_{\text{ext}}$  and  $b_{\text{ext}}$ .

### 5.3.2 Waveguide resonators

A waveguide resonator is a section of a waveguide bounded by two metal planes perpendicular to the waveguide axis. The transverse components of the electric field (which is a superposition of fields of the incident and reflected waves) should be equal to zero at these planes. This boundary condition can be satisfied by the waves of a single mode only if the electric field structure for this mode is *reciprocal*. If the propagation constant  $k(\omega)$  is also reciprocal, the equation for the resonator eigenfrequencies  $\omega_\nu$  has the form

$$k(\omega_\nu) = \frac{p\pi}{l} \quad p = 1, 2, 3, \dots \quad (5.34)$$

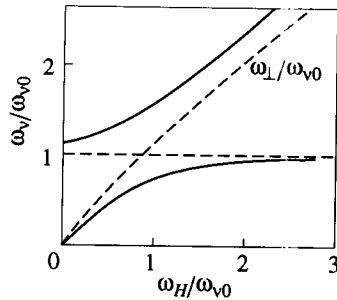
where  $l$  is the resonator length. If the propagation constant is *nonreciprocal*, then  $k(\omega)$  in the left-hand side of (5.34) is replaced by  $[k_+(\omega) + k_-(\omega)]/2$ .

It was shown in the previous section that both electric-field structure and propagation constant are reciprocal for waves  $\text{TE}_{n0}$  in a *rectangular waveguide filled* with transversely magnetized ferrite. Therefore, an equation for the eigenfrequencies  $\omega_\nu$  of a resonator that is a section of such a waveguide can easily be found using (5.11) and (5.34) [247]

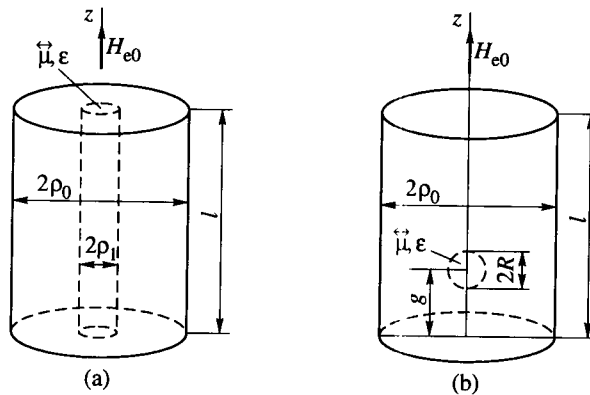
$$\left(\frac{\omega_\nu}{\omega_{\nu 0}}\right)^2 = \frac{\omega_H(\omega_H + \omega_M) - \omega_\nu^2}{(\omega_H + \omega_M)^2 - \omega_\nu^2} \quad (5.35)$$

where  $\omega_{\nu 0} = (c/\sqrt{\varepsilon})\sqrt{(n\pi/a)^2 + (p\pi/l)^2}$  is the eigenfrequency of the rectangular resonator filled with isotropic medium with the same permittivity  $\varepsilon$  and  $\mu = 1$ . The dependence of  $\omega_\nu$  on  $\omega_H$  calculated by equations (5.35) is shown in Figure 5.12. It resembles the Wien graph for the eigenfrequencies of coupled oscillatory circuits (e.g., [256]). Thus, the resonator with ferrite can be regarded as a system consisting of two coupled subsystems: the resonator and ferrite.

The electric field structure and the propagation constant of a circular waveguide with a longitudinally magnetized *ferrite cylinder* (Section 5.1) are also both reciprocal. Therefore, the eigenfrequencies of the waveguide resonator that is a section of such a waveguide (Figure 5.13) can be, as well, calculated using equation (5.34). These frequencies will be different for the right-hand and the left-hand

**FIGURE 5.12**

Magnetic-field dependence of the eigenfrequencies of a rectangular resonator filled with magnetized ferrite calculated using (5.35) (solid curves). Dashed lines show the uncoupled frequencies of the resonator ( $\omega_{v0}$ ) and of ferrite ( $\omega_{\perp}$ ).  $\omega_M = 0.5\omega_{v0}$ .

**FIGURE 5.13**

Cylindrical resonators with ferrite samples.

circular polarizations (relative to the direction of the steady magnetization), i.e., for  $\exp(-i\varphi)$  and  $\exp(i\varphi)$  dependences of the resonator fields on the azimuth angle. It should be noted that the repulsion of the  $\omega_v$  vs  $\omega_H$  curves (analogous to that shown in Figure 5.12) will be much stronger for the right-hand polarized mode because in this case the resonator—in terms of coupled oscillations—interacts stronger with ferrite.

### 5.3.3 Ferrite resonators

The concept of coupled oscillations can be applied, as well, to open resonators consisting of dielectric (with  $\epsilon \gg 1$ ) and ferrite samples. However, of greater in-



terest are the so-called ferrite resonators, i.e., open resonators that contain nothing but a ferrite sample. The oscillations of such resonators, which can be regarded as coupled oscillations of an open dielectric resonator and ferrite, are called *magnetodynamic* oscillations. It should be pointed out that these oscillations take place in all experiments on ferromagnetic resonance in samples (e.g., ellipsoids) of a weakly conducting substance. The treatment of ferromagnetic resonance in Section 1.5, in which this fact was ignored, is approximately correct only if the dimensions of the sample are small in comparison with the wavelength  $2\pi c/(\omega\sqrt{\epsilon})$ .

The eigenfrequencies of magnetodynamic oscillations can be calculated using the *method of coupled oscillations* in the form proposed by Auld [25]. Let us consider briefly this method. We rewrite, first, equations (5.17) for *eigenoscillations* (assuming  $\epsilon$  to be a scalar and omitting the subscripts  $\nu$ ) in the form resembling (5.19) and (5.21):

$$\text{rote} + ik_0\mathbf{h} = -ik_04\pi\mathbf{m} \quad \text{roth} - ik_0\epsilon\mathbf{e} = 0. \quad (5.36)$$

These equations can be regarded as equations for *forced* oscillations of a resonator with an isotropic medium excited by the magnetization  $\mathbf{m}$ . Together with the equation of motion of the magnetization (1.36) they form a system of equations for coupled oscillations of a resonator and ferrite.

Taking into account (5.24), we can write (1.36) as

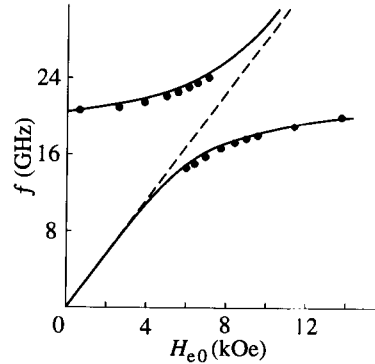
$$i\omega\mathbf{m} + \gamma\mathbf{m} \times \mathbf{H}_0 + \gamma\mathbf{M}_0 \times \nabla\psi = -\gamma\mathbf{M}_0 \times \sum_{\nu} \mathcal{H}_{\nu}\mathbf{h}_{\nu}. \quad (5.37)$$

As  $I_{\nu} = F_{\nu} = 0$  and  $G_{\nu}$  is determined by (5.31), expression (5.29) now has the form

$$\mathcal{H}_{\nu} = \frac{c\omega^2}{\omega_{\nu}^2 - \omega^2} \int_{V_1} \mathbf{h}_{\nu}^* \mathbf{m} dV \quad (5.38)$$

where the integration is over the volume of the sample. So, we have obtained a system of equations (5.37) and (5.38), in which  $\omega_{\nu}$  are the eigenfrequencies of the resonator with isotropic medium,  $\mathbf{h}_{\nu}$  and  $\nabla\psi$  are the eigenfunctions of this resonator, and  $\omega$  is the unknown frequency of the coupled oscillations. The magnetization  $\mathbf{m}$  in (5.38) can be represented by an infinite sum of eigenfunctions. If the sample dimensions are small, the magnetizations of magnetostatic modes (Section 6.3) may be taken as such eigenfunctions. The infinite system of equations (5.37) and (5.38) is rigorous, but it is difficult to find its strict solutions. Approximate solutions can be found if we limit ourselves to a finite number of eigenmodes of the resonator and the sample, which most strongly interact with each other.

This method was used [276] to analyze the *magnetodynamic* oscillations of a *ferrite sphere*. Only the uniform mode of the magnetization oscillations and the two lowest degenerate modes of a dielectric sphere were taken into account. The frequency  $\omega_1$  of these modes is equal approximately (if  $\epsilon \gg 1$ ) to  $\pi c/(R\sqrt{\epsilon})$  where  $R$  is the radius of the sphere. The calculation yields the following expression for



**FIGURE 5.14**

Eigenfrequencies of magnetodynamic oscillations of a YIG sphere with  $2R = 3.72$  mm. Solid curves represent the theoretical dependence (5.39), circles represent the experimental data [328], the dashed line corresponds to the Kittel frequency of uniform ferromagnetic resonance at  $R \rightarrow 0$ .

the ferromagnetic-resonance field in a ferrite sphere:

$$H_{\text{res}} = \frac{\omega}{\gamma} + \frac{4}{\pi^2} 4\pi M_0 \frac{\omega^2}{\omega_1^2 - \omega^2}. \quad (5.39)$$

The field dependence of the resonance frequency calculated by (5.39) is plotted in Figure 5.14 together with experimental data. One can see from this figure, as well as from (5.39), that the 'usual' condition for ferromagnetic resonance in a sphere ( $H_{\text{res}} = \omega/\gamma$ ) is *approximately* valid only if  $\omega \ll \omega_1$ , i.e., at low frequencies or for small spheres. In this case, it follows from (5.39) that

$$H_{\text{res}} = \frac{\omega}{\gamma} + \frac{4}{\pi^4} 4\pi M_0 \varepsilon (k_0 R)^2. \quad (5.40)$$

It should be noted that the influence of the sample dimensions on the frequency of ferromagnetic resonance (or, more correctly, of magnetodynamic oscillations) was calculated by Hurd [187] in another way, solving Maxwell's equations by the method of successive approximations. He obtained

$$H_{\text{res}} = \frac{\omega}{\gamma} + \frac{2}{45} 4\pi M_0 (\varepsilon + 5) (k_0 R)^2. \quad (5.41)$$

If  $\varepsilon \gg 1$ , this expression differs from (5.40) only by a factor very near to 1. Formula (5.41), in contrast to (5.40), is valid at *arbitrary* values of  $\varepsilon$ , but, as well as (5.40), it holds only for *small spheres*. Formula (5.39) is not limited by this condition but is valid only at  $\varepsilon \gg 1$ .

### 5.3.4 Use of perturbation method

Let us return to the case of a ferrite sample in a hollow resonator. If the volume of the sample is small, as compared with the resonator volume, the perturbation method with quasistatic approximation of the internal field (Section 4.5) can be used to calculate the eigenfrequencies and the quality factors of the resonator. As an example of the application of this method, consider a *cylindrical resonator* with the mode  $TE_{mnp}$  containing a *small ferrite sphere* on its axis [Figure 5.13(b)]. (Some other examples can be found in [153].) If the sphere is magnetized along the resonator axis, the mode with circular polarization should be taken as an unperturbed mode because this mode will remain an eigenmode after perturbation.

The unperturbed-field components can be written in the form [151] (see also [153]):

$$\begin{aligned} h_z &= \kappa^2 Z \psi_{\perp} & \mathbf{h}_{\perp} &= \frac{dZ}{dz} \nabla \psi_{\perp} & \mathbf{e} &= k_0 Z \mathbf{z}_0 \times \nabla \psi_{\perp} \\ Z &= \sin k_z z & \psi_{\perp} &= J_{|m|}(\kappa \rho) \exp(im\varphi) & k_z &= \frac{\pi p}{e} \end{aligned} \quad (5.42)$$

where  $\kappa \rho_0$  is the  $n$ th root of the equation  $J'_{|m|}(\kappa \rho_0) = 0$  ( $J'_{|m|}$  is the derivative of the Bessel function with respect to the argument) and  $\rho_0$  is the radius of the resonator. Using formula (4.83) and Table 4.1, we obtain for the mode  $TE_{111}$

$$\frac{\omega - \omega_0}{\omega} = -8.4 \frac{R^3}{l \rho_0^2} \left[ \left( \frac{\pi}{k_0 l} \right)^2 \frac{\mu \pm \mu_a - 1}{\mu \pm \mu_a + 2} \cos^2 \frac{\pi g}{l} + \frac{\varepsilon - 1}{\varepsilon + 2} \sin^2 \frac{\pi g}{l} \right] \quad (5.43)$$

where  $R$  is the radius of the ferrite sphere, and the signs  $\pm$  correspond, respectively, to the right-hand and left-hand polarizations of the mode.

If the sphere is magnetized in the direction perpendicular to the resonator axis and parallel to the ac magnetic field, both the unperturbed and perturbed eigenmodes are the modes with linear polarization. In this case,  $\mu \pm \mu_a$  in (5.43) will be replaced by  $\mu_{\parallel}$ .

Resonators with small ferrite samples can be used, as Nikol'skii proposed [298], (see also [153]) to *measure*  $\vec{\mu}$  *components* and  $\varepsilon$  of ferrites. For polycrystalline ferrites, there are four complex parameters:  $\mu$ ,  $\mu_a$ ,  $\mu_{\parallel}$ , and  $\varepsilon$ . To find their real and imaginary parts it is necessary to measure the changes of the resonance frequency and of the quality factor of a resonator in four independent experiments. Suppose that a sphere in the cylindrical resonator with  $TE_{111}$  mode (Figure 5.13) is used. Then the real and imaginary parts of  $\mu$  and  $\mu_a$  can be found, according to (5.43), from the measurements with a sphere magnetized along the resonator axis and put at  $g = 0$ . The component  $\mu_{\parallel}$  is found using the sphere in the same position but magnetized in the direction perpendicular to the resonator axis. To find  $\varepsilon$  the sphere must be put at  $g = l/2$ .

Resonators with small ferromagnetic, ferrimagnetic, or antiferromagnetic samples, mostly spheres, are widely used in measurements of the *magnetic-resonance parameters*: the resonance field and the resonance linewidth. In this case, the

second term in the integrand of (4.83) can be neglected, either because it is small as compared with the first term, or because the frequency difference is measured with respect to the frequency of the resonator with the same sample but far from the magnetic resonance. The first term in the integrand of (4.83) can be transformed according to (4.94), and (4.83) takes the form

$$\frac{\omega - \omega_0}{\omega} = -\frac{2\pi}{W_0} \int_{V_1} \mathbf{h}_0^* \vec{\chi}^e \mathbf{h}_0 dV \quad (5.44)$$

where  $\mathbf{h}_0$  is the external magnetic field and  $\vec{\chi}^e$  is the external susceptibility tensor.

Consider the most important case in which the sample is in the region of a linearly polarized ac magnetic field and the dimensions of the sample are *small* enough to regard this field as independent of coordinates in the volume of the sample. Then, taking (4.84) into account, we find from (5.44) that

$$\delta\omega = -2\pi\omega_0\alpha \frac{V_1}{V_0} \chi^{e'} \quad (5.45)$$

$$\delta\left(\frac{1}{Q}\right) = 4\pi\alpha \frac{V_1}{V_0} \chi^{e''}. \quad (5.46)$$

Here  $\chi^e$  is the transverse diagonal component of  $\vec{\chi}^e$ ,  $V_1$  is the volume of the sample,  $V_0$  is the volume of the resonator, and

$$\alpha = \frac{V_0 |\mathbf{h}_0^0|^2}{\int_{V_0} |\mathbf{h}_0|^2 dV} \quad (5.47)$$

( $\mathbf{h}_0^0$  is the field at the point where the sample is located). The factor  $\alpha$  can be easily calculated for resonators of simple shapes. For instance,  $\alpha = 2$  in the case of a sample in the magnetic-field maximum of a rectangular resonator with  $TE_{n,0}$  mode. For other convex resonators,  $\alpha$  differs but not very strongly from this value. It should be pointed out that  $\delta\omega$  [or  $\delta(1/Q)$ ] is the difference between  $\omega$  (or  $1/Q$ ) values measured either with and without the sample or, in both cases, with the sample but at and far from ferromagnetic resonance. The latter case is more often used (if the resonance curve is not too wide).

---

#### 5.4 Waveguides and waveguide junctions with ferrite samples

In this section the properties of waveguides with ferrite samples will be studied. We begin with the simplest problem of this type, the problem of a small ferrite sample in a *regular* (i.e., unbounded and with constant cross section) waveguide.

### 5.4.1 Ferrite ellipsoid in a waveguide

Consider, according to [154], an ellipsoid with parameters  $\vec{\mu}$  and  $\varepsilon$  in a regular waveguide. The amplitude of the incident wave is given, and the electromagnetic field in the waveguide far from the ellipsoid is to be found. The perturbation method in such a variant, when the given field of the incident wave is assumed to be the unperturbed field acting on the sample, can lead to an approximately correct solution only if the ferrite sample is very small. For realistic dimensions and parameters of the sample, we must suppose that the sample magnetization is determined by the *self-consistent* field, which is the sum of field  $\mathbf{h}_0$  of the incident wave and the field  $\mathbf{h}_r$  radiated by the sample. If condition (4.93) is satisfied, the magnetization can be written as

$$\mathbf{m} = \vec{\chi}^e (\mathbf{h}_0 + \mathbf{h}_r). \quad (5.48)$$

The radiation field excited by the magnetization  $\mathbf{m}$ , in general, is the sum of all normal waves propagating in the waveguide and the near (nonpropagating) modes. However, it is of no sense to substitute the highly nonuniform near fields into equation (5.48), which is valid only for the uniform fields. And if there exists only one propagating wave, then only the field of this wave must be taken into account.

Assume, e.g., that the ellipsoid is located (Figure 5.15) *at the axis* of a rectangular waveguide in which only the wave  $\text{TE}_{10}$  propagates. The transverse component of the given magnetic field of this wave is

$$h_{0x} = \sin \frac{\pi x}{a} \exp(-ik_y y). \quad (5.49)$$

The radiation field should be calculated by solving the problem of excitation of the field in a waveguide by a given magnetization, which is analogous, in some sense, to the problem of excitation of the field in a resonator considered in the preceding section. We write down the result of such calculation for the field  $\text{TE}_{10}$  [154]:

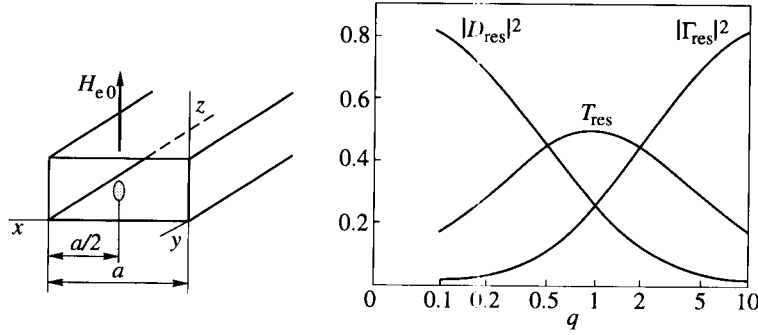
$$h_{rx} = -i\omega m_x \sin \frac{\pi x}{a} \exp(\mp ik_y y) \quad w = 4\pi \frac{V_1 k_y}{S} \quad (5.50)$$

where  $V_1$  is the volume of the ellipsoid and  $S$  is the area of the waveguide cross section. Substituting (5.49) and (5.50) into the projection of (5.48), we find  $m_x$  and the transverse component of the radiation field

$$h_{rx} = -\frac{i\omega\chi^e}{1 + i\omega\chi^e} \sin \frac{\pi x}{a} \exp(\mp ik_y y). \quad (5.51)$$

The *reflection* coefficient related to the cross section in which the center of the sample lies is

$$\Gamma \equiv \frac{h_{rx}(y=0)}{h_{0x}(y=0)} = \frac{-i\omega\chi^e}{1 + i\omega\chi^e}. \quad (5.52)$$



**FIGURE 5.15**

Dependence of the transmission  $|D|$  and reflection  $|\Gamma|$  coefficients and of the relative absorbed power  $T$  at resonance on the coefficient of coupling for a magnetized ferrite ellipsoid in a rectangular waveguide [154].

The *transmission* coefficient related to the same cross section

$$D \equiv \frac{h_{0x}(y=0) + h_{rx}(y=0)}{h_{0x}(y=0)} = \frac{1}{1 + iw\chi^e}. \quad (5.53)$$

The ratio of the power absorbed by the sample to the power of the incident wave

$$T = 1 - |\Gamma|^2 - |D|^2. \quad (5.54)$$

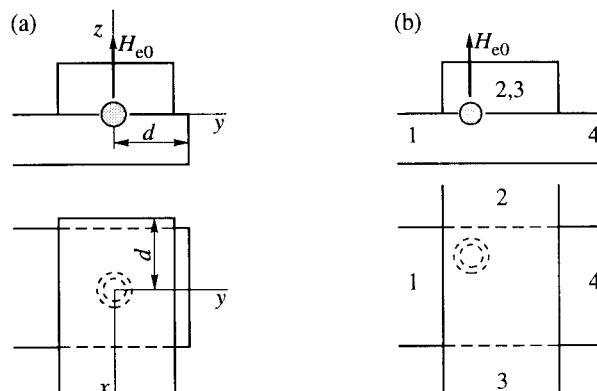
At ferromagnetic resonance ( $\chi^{e'} \cong 0$ ,  $\chi^{e''} = \chi_{\text{res}}^{e''}$ )

$$\Gamma_{\text{res}} = \frac{-q}{1+q} \quad D_{\text{res}} = \frac{1}{1+q} \quad T_{\text{res}} = \frac{2q}{(1+q)^2} \quad (5.55)$$

$$q = w\chi_{\text{res}}^{e''} = 4\pi \frac{V_1}{S} k_y \lambda_{\text{res}}^{e''}. \quad (5.56)$$

The quantity  $q$  can be called the *coefficient of coupling* of the sample with the waveguide. The dependences of  $\Gamma_{\text{res}}$ ,  $D_{\text{res}}$ , and  $T_{\text{res}}$  on  $q$  are plotted in Figure 5.15. With increasing  $q$ , i.e., with growing sample volume and narrowing resonance line,  $|\Gamma| \rightarrow 1$ ,  $D \rightarrow 0$ , and  $T \rightarrow 0$ .

Analogous calculation for the sample at a point of *circular polarization* of the magnetic field with right-hand rotation (with respect to the direction of the steady magnetization) shows that, in this case,  $\Gamma_{\text{res}} = 0$  at any value of  $q$ , while  $D \rightarrow 1$  and  $T \rightarrow 0$  at  $q = 0$  and  $q \rightarrow \infty$ ; the total absorption ( $T = 1$ ) occurs at  $q = 1$ . The sample located at a point of the left-hand circular polarization does not influence, as could be expected, the wave propagation in the waveguide. So, a section of a rectangular waveguide with a ferrite sample located at a point of circular polarization and magnetized along a normal to the wide waveguide wall is a nonreciprocal *band-rejection filter*.

**FIGURE 5.16**

Rectangular waveguides coupled by a magnetized ferrite sphere located (a) at points with linear polarization of the ac magnetic field (a band-pass filter) and (b) at points with circular polarization (a four-port circulator).

The problem of an ellipsoid in a *short-circuited* waveguide can be solved, as well [154]. Both the external ( $\mathbf{h}_0$ ) and the radiation ( $\mathbf{h}_r$ ) fields are, in this case, the sums of the fields of incident waves and waves reflected from the shorting plane. If this plane is located at a distance  $d = n\pi/k_y$  ( $n = 0, 1, 2, \dots$ ) from the sample, then

$$\Gamma_{\text{res}} = \frac{1 - 2q}{1 + 2q}. \quad (5.57)$$

#### 5.4.2 Coupling of orthogonal waveguides. Ferrite band-pass filters

Let us discuss now the problem of a ferrite ellipsoid that couples two waveguides. Consider, e.g., two rectangular waveguides perpendicular to each other, with a hole in their common wall and a small ferrite ellipsoid in the hole [154]. Assume that the ac magnetic field is uniform in the volume of the sample and is the sum of  $\text{TE}_{10}$  fields of both waveguides. Of course, these assumptions are not valid strictly, but they allow one to solve the problem rather easily and obtain qualitatively correct results.

If the hole is in the *middle* of both the waveguide wide walls, as in Figure 5.16(a), then, with the mentioned assumptions, it follows from (5.48) that

$$\begin{aligned} m_x &= \chi^e (h_{0x1} + h_{rx1}) + i\chi_a^e (h_{0y2} + h_{ry2}) \\ m_y &= -i\chi_a^e (h_{0x1} + h_{rx1}) + \chi^e (h_{0y2} + h_{ry2}) \end{aligned} \quad (5.58)$$

where the subscripts 1 and 2 correspond, respectively, to the lower and upper waveguides in Figure 5.16, and the axes are directed as in this figure. The

characteristics of the considered waveguide junction can be obtained [154] in the same manner as in the above-treated problem. We cite, as an example, the expression for the transmission coefficient in the case of Figure 5.16(a) when both waveguides are short-circuited at the distance  $d$  from the sample:

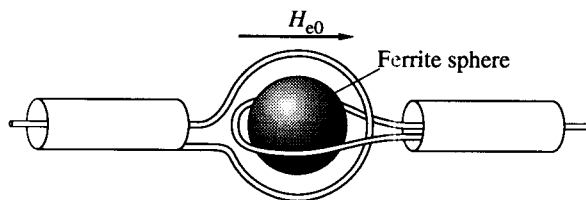
$$D_{\text{res}} = \frac{4iq \cos^2 k_y d \exp(-2ik_y d)}{1 + 4q \cos k_y d \exp(-ik_y d)}. \quad (5.59)$$

One can see that  $|D_{\text{res}}| \rightarrow 1$  (if  $k_y d = 0, \pi$ ) when  $q \rightarrow \infty$ . This means that the ferrite sample of sufficiently large dimensions or with sufficiently narrow resonance line reradiates almost all power into the second waveguide.

Ferrite samples in waveguides and waveguide junctions are widely used in microwave engineering to design ferrite filters (e.g., [179]), which can be tuned over very broad frequency ranges by changing the steady magnetic field. It has been already mentioned above that a nonreciprocal absorption band-rejection filter is realized with the use of a ferrite sample at a point of the magnetic-field circular polarization. Using a sample at a point of linear polarization (at the waveguide axis), a reflection-type band-rejection filter can be made.

The above-considered junction of two short-circuited waveguides with a ferrite sample in a hole between them [Figure 5.16(a)] is a *band-pass* filter. Small losses in the center of the transmission band (at ferromagnetic resonance) take place in such filter if  $q \gg 1$ . But if the sample is put at a point of the circular polarization, the minimal losses would occur when  $q = 1$ .

The nonreciprocity, which appears when the ferrite sample is located at a point of the circular polarization of the magnetic field, provides a possibility to realize a *filter-circulator* [Figure 5.16(b)]. If the device is feeded from port 1, the ac magnetic field of the incident wave has, at the point where the sample is located, the right-hand circular polarization (relative to the direction of the steady magnetization shown in the figure). Only such a wave, i.e., the wave that propagates towards port 2, will be excited by the sample in the upper waveguide. There will be no reflected wave in the input port 1, and no power will be transmitted to port 4. It is easy to make sure that the power from port 2 is transmitted into port 3, and so on. Thus, the device is a circulator (Section 5.1). At the same time, it is a filter, which can be tuned by changing the steady magnetic field.



**FIGURE 5.17**  
Coaxial ferrite filter.



Other waveguides can also be applied in designing microwave ferrite filters [179]. The *coaxial* filters (Figure 5.17) are the most widely used. As the parameters of the coaxial waveguide and of the coils weakly depend on frequency, such filters can be tuned (by changing the steady magnetic field) in frequency bands up to several octaves, which lie in a very broad range, approximately, of 0.1–20 GHz.

The losses (at the central frequency) of the band-pass ferrite filters, in which, as in the above-considered examples, one ferrite sample is used, are 0.5–1 dB. The bands (at constant magnetic field) are some tens of megacycles. To improve the shape of the amplitude-frequency characteristic, filters with two, three, and even more ferrite samples can be used.

### 5.4.3 General properties of nonreciprocal junctions

Ferrite band-pass and band-rejection filters discussed above are examples of nonreciprocal waveguide junctions. To study the general characteristics of such junctions the scattering matrix is used to great advantage (e.g., [247]). Let us review briefly some properties of this matrix.

Consider a junction with  $n$  waveguide ports (Figure 5.18). In every port there are, in general, an incident wave and a wave reflected from the junction. Their fields can be written as

$$\begin{aligned} e_p^+ &= A_p \mathcal{E}_p \exp(-ik_{zp}z) & e_p^- &= B_p \mathcal{E}_p \exp(ik_{zp}z) \\ h_p^+ &= A_p \mathcal{H}_p \exp(-ik_{zp}z) & h_p^- &= B_p \mathcal{H}_p \exp(ik_{zp}z) \end{aligned} \quad (5.60)$$

where  $\mathcal{E}_p$  and  $\mathcal{H}_p$  are the eigenfunctions of the waveguides that form the ports and  $p$  is the number of a port ( $p = 1, 2, \dots, n$ ).

Assuming the junction to be linear, we can write

$$B_p = \sum_{q=1}^n S_{pq} A_q \quad (5.61)$$

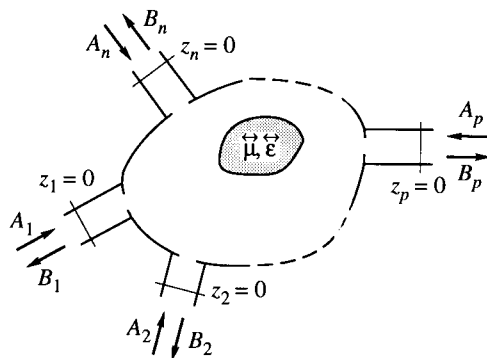
or, in the matrix form,

$$\|B\| = \|S\| \|A\| \quad (5.62)$$

where  $\|A\|$  and  $\|B\|$  are column matrices of the amplitudes  $A_p$  and  $B_p$  and  $\|S\|$  is a square *scattering matrix*:

$$\|S\| = \begin{vmatrix} S_{11} & S_{12} & \dots & S_{1n} \\ S_{21} & S_{22} & \dots & S_{2n} \\ \dots & \dots & \dots & \dots \\ S_{n1} & S_{n2} & \dots & S_{nn} \end{vmatrix}. \quad (5.63)$$

The element  $S_{pp}$  is the reflection coefficient in the port  $p$  in the absence of incident waves (i.e., in the absence of sources and unmatched loads) in all other ports. The



**FIGURE 5.18**  
Nonreciprocal waveguide junction.

element  $S_{pq}$  is the transmission coefficient *from* port  $q$  *into* port  $p$  in the absence of incident waves in all ports but the  $q$  port.

For a junction *without losses* the scattering matrix  $\|S\|$  is *unitary*<sup>2</sup> (e.g., [247]). The scattering matrix for a reciprocal junction is *symmetric* ( $S_{pq} = S_{qp}$ ). For a *nonreciprocal* junction,

$$S_{qp} - S_{pq} \equiv \delta S_{pq} \neq 0. \quad (5.64)$$

To find the nonreciprocal difference  $\delta S_{pq}$  formula (4.63) can be used. The fields with subscripts 1 and 2 in this formula are the sums of the fields of incident and reflected waves. Suppose that, for a process 1, the incident wave exists only in port  $p$ , and for a process 2, only in port  $q$ . Then, taking (5.60) into account, we can obtain from (4.63)

$$\delta S_{pq} = \frac{1}{2} \frac{J_a}{A_p A_q}. \quad (5.65)$$

Thus,  $J_a \neq 0$  is the condition for nonsymmetry of the scattering matrix, i.e., for the nonreciprocity of the junction.

Consider, first, a *two-port* junction. In the absence of losses, the unitary matrix of this junction can be written in the form [247]

$$\|S\| = \left\| \begin{array}{cc} a \exp(i\alpha) & \sqrt{1-a^2} \exp(i\alpha + i\varphi) \\ -\sqrt{1-a^2} \exp(i\beta - i\varphi) & a \exp(i\beta) \end{array} \right\| \quad (5.66)$$

where  $a$ ,  $\alpha$ ,  $\beta$ , and  $\varphi$  are arbitrary (but  $a \leq 1$ ) real quantities. One can see from (5.66) that the two-port junction *without losses* can be a nonreciprocal

<sup>2</sup>A matrix  $\|S\|$  is called unitary (e.g., [293]) if  $\|\tilde{S}\| \cdot \|S\|^* = \|I\|$ , where  $\|\tilde{S}\|$  is a transpose matrix with elements  $(\tilde{S})_{pq} = S_{qp}$ ,  $\|S\|^*$  is a complex conjugate matrix with elements  $(S^*)_{pq} = S_{pq}^*$ , and  $\|I\|$  is a diagonal matrix with elements  $I_{pp} = 1$  (a unit matrix).

phase shifter but cannot be an isolator. The scattering matrix of an ideal isolator ( $S_{11} = S_{22} = S_{21} = 0, |S_{12}| = 1$ ) is not unitary. A junction with such matrix can be realized only in the presence of *losses*. One more interesting conclusion follows from (5.66): as  $|S_{11}| = |S_{22}|$ , if we match an arbitrary two-port junction (without losses) from one side, it will be matched from another side, too.

Let us pass now to *three-port* junctions. It is easy to show, using the unitarity of the scattering matrix, that a reciprocal three-port junction without losses cannot be matched simultaneously from all three ports. A *nonreciprocal* three-port junction *without losses* can be matched from all three ports and then becomes an ideal circulator. Let us prove this important theorem.

If the junction is matched, i.e.,  $S_{11} = S_{22} = S_{33} = 0$ , then it follows from the unitarity of the scattering matrix that

$$\begin{aligned} S_{12}^* S_{13} &= 0 & S_{21}^* S_{23} &= 0 & S_{31}^* S_{32} &= 0 \\ |S_{12}|^2 + |S_{32}|^2 &= 1 & |S_{21}|^2 + |S_{31}|^2 &= 1 & |S_{13}|^2 + |S_{23}|^2 &= 1. \end{aligned} \quad (5.67)$$

The condition  $S_{12}^* S_{13} = 0$  can be satisfied if either  $S_{12} = 0$  or  $S_{13} = 0$ . In the first case, it follows from other conditions (5.67) that

$$S_{12} = S_{23} = S_{31} = 0 \quad |S_{21}| = |S_{13}| = |S_{32}| = 1 \quad (5.68)$$

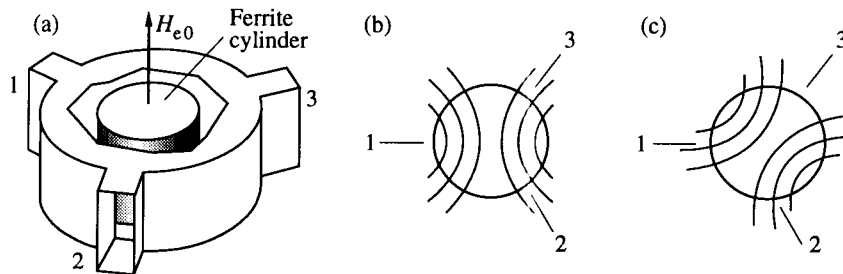
and in the second case

$$S_{21} = S_{13} = S_{32} = 0 \quad |S_{12}| = |S_{23}| = |S_{31}| = 1. \quad (5.69)$$

The matrices with elements (5.68) and (5.69) represent ideal circulators with the directions of energy transmission, respectively,  $1 \rightarrow 2 \rightarrow 3 \rightarrow 1$  and  $1 \rightarrow 3 \rightarrow 2 \rightarrow 1$ . The direction realized, depends, of course, on the direction of the *magnetization* of the ferrite sample in the junction.

Circulators with four and even more ports can be made, as well. But then, the reciprocity and perfect matching are not sufficient for the junction to be a circulator. The phase shifts between transmission coefficients into different ports must have definite values.

*Symmetric three-port* circulators, called *Y* circulators, have been designed using different waveguides: rectangular, coaxial, microstrip. These circulators are, perhaps, the most used microwave ferrite devices. The rectangular-waveguide *Y* circulator is shown in Figure 5.19. Its operation can be explained in the following way. The ferrite cylinder in the circulator can be regarded as a ferrite rod in a cylindrical resonator with the quasi-TM<sub>110</sub> mode (independent of coordinate  $z$  in the direction of the rod axis). The magnetic force lines for this mode are shown in Figure 5.19 in the cases of isotropic ( $\mu_a = 0$ ) and gyrotropic ( $\mu_a \neq 0$ ) rods. As pointed out in Section 5.3, the field in the resonator is the sum of the fields of the right-hand and left-hand circular polarized oscillations, i.e., waves propagating in opposite directions 'along the azimuth'. In the case of an isotropic (not magnetized) ferrite rod [Figure 5.19(b)] the wavelengths of these waves are

**FIGURE 5.19**

Y circulator: (a) an example of design, (b) ac magnetic force lines in and near the ferrite cylinder when  $\mu_a = 0$ , and (c) magnetic force lines when  $\mu_a \neq 0$ .

equal, and the maximum of the total field is located opposite the center of the input port (e.g., port 1) cross section. The power coming from this port is divided into equal parts between ports 2 and 3. However, if the ferrite cylinder is magnetized, the wavelengths of the waves propagating along the azimuth in opposite directions are different, and the field maximum shifts to one of ports 2 or 3. By choosing the proper parameters of the device (dimensions and the value of the steady magnetic field) one can make the field minimum to coincide [Figure 5.19(c)] with the center of port 2 or 3 (depending on the direction of magnetization of the ferrite cylinder). Then, all the power from port 1 will be transmitted into one of these ports.

The above-stated reasoning can be applied, as well, to other designs of a Y circulator because the main part of energy is concentrated in the ferrite sample, and the configuration of the surroundings does not play an important role.

The Y circulator is a resonance device, and its frequency band cannot be very large. To broaden it a ferrite sample with a highly nonuniform internal steady magnetic field can be used. Frequency bands wider than 30% can be achieved in such way. The forward losses of a Y circulator are usually less than 0.5 dB, and isolation is more than 20 dB [179, 330, 352].

# 6

---

## *Magnetostatic waves and oscillations*

---

### 6.1 Magnetostatic approximation

It was shown in Section 4.2 that ‘slow branches’ (with small phase and group velocities) appear in the spectrum of electromagnetic waves in an unbounded magnetized ferromagnet. Similar branches exist, as well, in the spectra of waves in waveguides containing ferromagnetic (or ferrimagnetic) media [356]. Solving boundary problems for systems with gyrotropic media, we meet with great difficulties. They increase especially in the regions of strong dispersion, in which the slow branches appear. At the same time, for slow waves

$$k \gg k_0 \equiv \frac{\omega}{c}. \quad (6.1)$$

This allows us to use the method of successive approximations. In the *zero approximation*, taking (6.1) into account, we neglect the term  $ik_0 \vec{\epsilon} \mathbf{e}$  in the Maxwell equation (4.16). Then, this equation and (4.15) take the same form as the magnetostatic equations (4.6). In the problems we deal with,  $\mathbf{j}_{\text{ext}} = 0$ . Hence, the equations can be written as

$$\text{rot} \mathbf{h} = 0 \quad \text{div} \left( \vec{\mu} \mathbf{h} \right) = 0. \quad (6.2)$$

Having solved these equations with regard for boundary conditions, we find  $\mathbf{h}$  and  $\mathbf{m} = \vec{\chi} \mathbf{h}$ , the dispersion relations for normal waves, the eigenfrequencies of resonators, etc.

In the *first* approximation with respect to  $k_0/k$ , the electric field  $\mathbf{e}$  can be found from (4.14) and (4.17). In the case of  $\rho_{\text{ext}} = 0$  and constant scalar  $\epsilon$ , these equations take the form

$$\text{rote} = -k_0 \vec{\mu} \mathbf{h} \quad \text{dive} = 0. \quad (6.3)$$

In the *second* approximation, using equation (4.16), we can calculate corrections to the dispersion relations and eigenfrequencies. The waves and oscillations for which this method can be applied are called magnetostatic waves and oscillations.

The above-mentioned zero approximation was already used in Sections 1.5 and 4.5. However, only *ellipsoidal* samples were considered, and an additional assumption of the *uniformity* of the ac magnetization was made. Therefore, it was possible to use the solution (1.82) of the magnetostatic problem for an ellipsoid. Now we have to solve the magnetostatic equations for other boundary conditions and without assumption of uniformity of the magnetization.

With increasing wave number  $k$  the exchange interaction (Section 1.1) becomes important. But in a certain interval of  $k$  values (which will be defined below) it is possible to neglect this interaction. Magnetostatic waves with such wave numbers must be called nonexchange magnetostatic waves. Often they are called, simply, magnetostatic waves, and magnetostatic waves with allowance for exchange interaction are called spin waves, although both of them are spin waves, and both are magnetostatic waves. Moreover, the greater  $k$  is, the more applicable is the magnetostatic approximation.

We consider first the nonexchange magnetostatic waves as a limiting case of the waves studied in Section 4.2. If (6.1) holds, it is possible to retain only the first term in (4.32). Then, for scalar  $\varepsilon$ , we get

$$\frac{\mu}{\mu_{\parallel}} = -\cot^2 \theta_k \equiv \frac{k_z^2}{k_x^2 + k_y^2} \quad (6.4)$$

where  $\theta_k$  is the angle between  $\mathbf{M}_0$  and  $\mathbf{k}$ . For a ferromagnet magnetized to saturation,  $\mu_{\parallel} = 1$ , and, neglecting losses, we find from (6.4) and (1.54) that

$$\omega^2 = \omega_H (\omega_H + \omega_M \sin^2 \theta_k). \quad (6.5)$$

One can see from (6.5) that  $\omega$  depends on the *direction of propagation* and lies in the range

$$\omega_H \leq \omega \leq \omega_{\perp} \equiv \sqrt{\omega_H(\omega_H + \omega_M)} \quad (6.6)$$

in which  $\mu < 0$ . The frequency  $\omega$  is *independent* of the wave number  $k$ , i.e., the group velocity  $v_{\text{gr}} \equiv \partial\omega/\partial k = 0$ .

The *field structure* of the considered waves can be easily found using the general results of Section 4.2. In particular, for  $\theta_k = 0$  vectors  $\mathbf{e}$  and  $\mathbf{h}$  are transverse and right-hand circularly polarized. For  $\theta_k = \pi/2$  the vector  $\mathbf{e}$  is parallel to  $\mathbf{M}_0$ , and  $\mathbf{h}$  is parallel to the propagation direction. It is easy to make sure that in both cases and for arbitrary  $\theta_k$  values, as well, the power flow (Section 4.4) is equal to zero. It correlates with the fact that  $v_{\text{gr}} = 0$  because the velocity of the energy transport coincides (rigorously in the absence of losses) with the group velocity.

The decrement  $k''$  of the nonexchange magnetostatic waves in an unbounded medium is *infinite* for an arbitrary value of the dissipation parameter of the medium. This follows from the general relation

$$\omega'' = v_{\text{gr}} k'' \quad (6.7)$$

which is valid for an arbitrary dispersion law in the case of small amplitudes and

small losses. In this relation,  $k''$  is the imaginary part of the wave number for a stationary wave ( $\omega'' = 0$ ), and  $\omega''$  is the imaginary part of the eigenfrequency ( $k'' = 0$ ), which differs from the dissipation parameter  $\omega_r$  (Section 1.4) only by a factor of the order of unity.

In reality, there are three reasons that lead to *finite group velocity* and, therefore, to finite values of energy flow and damping of magnetostatic waves: the influence of the term in Maxwell's equation neglected in the zero magnetostatic approximation, the influence of the exchange interaction, and the influence of boundary conditions (Section 6.2). However, in a certain range of  $k'$  values the influence of all three factors on the dispersion law appears to be small, and expression (6.5) can be used in the analysis of some important problems.

One of them is the *degeneration* of uniform magnetization oscillations and nonexchange magnetostatic waves. Comparing (6.5) with formula (1.92) for the eigenfrequency  $\omega_0$  of uniform oscillations of an ellipsoid (when the directions of  $\mathbf{H}_{e0}$  and  $\mathbf{M}_0$  coincide), we see that  $\omega_0$  lies either in the interval (6.6) or above it. It is easy to make sure that the condition for degeneration (i.e., for  $\omega_0$  to lie in the mentioned interval) is

$$H_{e0} > \left( N_z + \frac{N_x N_y}{N_z} \right) M_0 \quad (6.8)$$

where  $H_{e0}$  is the external field and  $N_{x,y,z}$  are the demagnetization factors of the sample. This condition cannot be satisfied for a thin cylinder magnetized along its axis, and it is always satisfied for normally magnetized thin film. For a sphere (6.8) can be written as

$$\omega_0 > \frac{2}{3} \omega_M. \quad (6.9)$$

We now have to derive the equations that can be used to solve more complicated boundary problems in the magnetostatic approximation. According to the first equation (6.2), the *magnetostatic potential*  $\psi$  can be introduced:

$$\mathbf{h} = \nabla \psi. \quad (6.10)$$

Substituting (6.10) into the second equation (6.2), we obtain an equation

$$\operatorname{div} \left( \vec{\mu} \nabla \psi \right) = 0 \quad (6.11)$$

which can be called *generalized Walker's equation*. To obtain the *boundary conditions* we introduce local coordinates  $\xi, \eta, \zeta$  with the  $\zeta$  axis coinciding with the normal to the boundary surface  $S$ . It follows then from the general conditions (4.4) that on  $S$

$$\frac{\partial \psi_1}{\partial \xi} = \frac{\partial \psi_2}{\partial \xi} \quad \frac{\partial \psi_1}{\partial \eta} = \frac{\partial \psi_2}{\partial \eta} \quad \left( \vec{\mu}_1 \nabla \psi_1 \right)_\zeta = \left( \vec{\mu}_2 \nabla \psi_2 \right)_\zeta \quad (6.12)$$

where the subscripts 1 and 2 correspond to the two media.

Let us show that expressions (6.4) and (6.5) can be found from equation (6.11). Substituting the complex amplitude  $\psi = \psi_0 \exp(-ik_x x - ik_y y - ik_z z)$  (where  $\psi_0$  is a constant quantity) into (6.11), we get

$$\mathbf{k} \left( \vec{\mu} \mathbf{k} \right) = 0. \quad (6.13)$$

For  $\vec{\mu}$  in the form (4.23), equation (6.4) directly follows from (6.13), and (6.5) follows from (6.4) if  $\mu_{\parallel} = 1$ . In the latter case (6.11) takes the form in which this equation was first written by Walker [432]:

$$\mu \left( \frac{\partial^2 \psi}{\partial x^2} + \frac{\partial^2 \psi}{\partial y^2} \right) + \frac{\partial^2 \psi}{\partial z^2} = 0 \quad (6.14)$$

( $z$  axis is directed along  $\mathbf{M}_0$ ).

For a *single crystal* magnetized to saturation in the  $\mathbf{M}_0$  direction,  $\vec{\mu}$  has the form (2.38), and (6.11) is written as

$$\mu_x \frac{\partial^2 \psi}{\partial x^2} + \mu_y \frac{\partial^2 \psi}{\partial y^2} + 2\mu_s \frac{\partial^2 \psi}{\partial x \partial y} + \frac{\partial^2 \psi}{\partial z^2} = 0 \quad (6.15)$$

where  $\mu_x$ ,  $\mu_y$ , and  $\mu_s$  have the form (2.39). It should be noted that the antisymmetric component  $\mu_a$  does not enter (6.14) and (6.15), but it appears in the boundary conditions (6.12). To obtain the expressions for  $\omega_x$ ,  $\omega_y$ , and  $\omega_s$  [in (2.39)] we have to substitute in (1.114) the components  $N_{11}^{\text{an}}$ ,  $N_{22}^{\text{an}}$ , and  $N_{12}^{\text{an}}$  of the anisotropy tensor  $\vec{N}^{\text{an}}$  for the corresponding components of the demagnetization tensor  $\vec{N}$  and substitute the sum  $N_{33} + N_{33}^{\text{an}}$  for  $N_{33}$  (Table 2.1).

For a uniform plane wave,  $\psi = \psi_0 \exp(-i\mathbf{k}\mathbf{r})$ . Then, it follows from (6.15) that

$$\mu_x \cos^2 \varphi_k + \mu_y \sin^2 \varphi_k + \mu_s \sin 2\varphi_k + \cot \theta_k = 0. \quad (6.16)$$

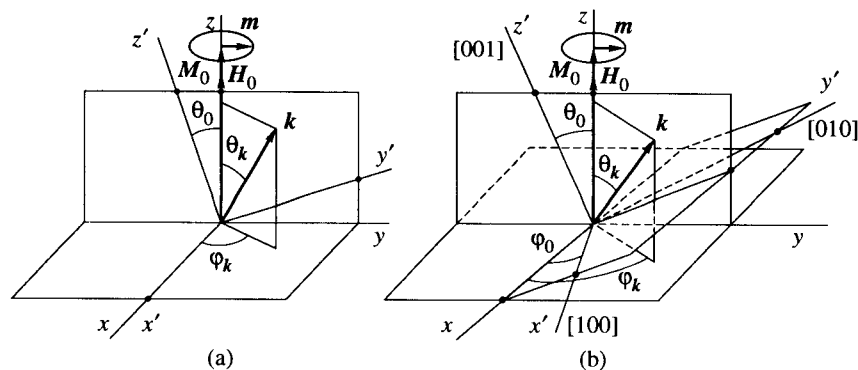
Here  $\theta_k$  and  $\varphi_k$  are the vector  $\mathbf{k}$  angles in the coordinate system in which the polar axis coincides with the  $\mathbf{M}_0$  direction. The tensor  $\vec{N}^{\text{an}}$  components must be written, of course, in the same system. Substituting (2.39) into (6.16), we get

$$\omega^2 = \omega_x \omega_y - \omega_s^2 + \omega_M \left( \frac{1}{2}(\omega_x + \omega_y) + \frac{1}{2}(\omega_x - \omega_y) \cos 2\varphi_k + \omega_s \sin 2\varphi_k \right) \sin^2 \theta_k. \quad (6.17)$$

Consider first a *uniaxial crystal*. Suppose that  $\mathbf{M}_0$  and  $\mathbf{H}_0$  directions coincide, neglect the anisotropy in the basal plane, and take into account only the first anisotropy constant in (2.31). Then, using expressions (2.42) (with  $H_{A2} = 0$ ), we obtain from (6.17)

$$\left( \frac{\omega}{\gamma} \right)^2 = (H_0 + 2H_{A1} \cos 2\theta_0) (H_0 + 2H_{A1} \cos^2 \theta_0) + 4\pi M_0 [H_0 + H_{A1} (3 \cos^2 \theta_0 - 1 - \sin^2 \theta_0 \cos 2\varphi_k)] \sin^2 \theta_k. \quad (6.18)$$



**FIGURE 6.1**

Coordinate axes for magnetostatic waves in (a) uniaxial and (b) cubic crystals. Axes  $x'$ ,  $y'$ , and  $z'$  are the crystallographic axes.

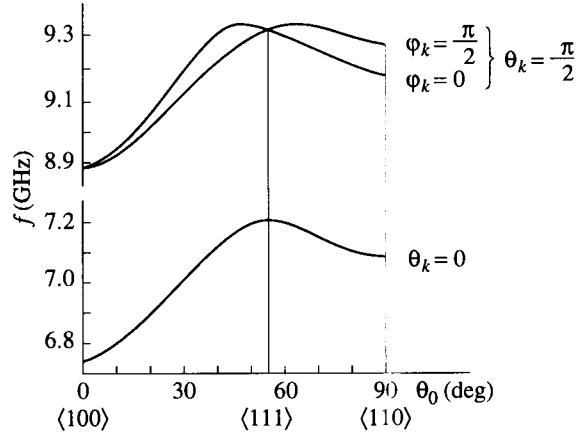
Here  $H_{A1} = K_1/M_0$ ,  $\theta_0$  is the angle between  $\mathbf{M}_0$  and the anisotropy axis  $z'$ , and  $\theta_k$  and  $\varphi_k$  are the angles of the vector  $\mathbf{k}$  (Figure 6.1).

For a *cubic crystal*, we suppose again that the directions of  $\mathbf{M}_0$  and  $\mathbf{H}_0$  coincide, limit ourselves to the case of  $H_{A2} = 0$ , and consider the particularly interesting case when  $\mathbf{M}_0$  lies in the  $\{110\}$  plane. Then, analogously to the previous case but substituting expressions (2.47) into (1.114) with  $\varphi_0 = \pi/4$ , we find

$$\begin{aligned} \left(\frac{\omega}{\gamma}\right)^2 &= \left[ H_0 + H_{A1} \left( -\frac{3}{8} + 2 \cos 2\theta_0 + \frac{3}{8} \cos 4\theta_0 \right) \right] \\ &\times \left[ H_0 + H_{A1} \left( \frac{1}{2} \cos 2\theta_0 + \frac{3}{2} \cos 4\theta_0 \right) \right] \\ &+ 4\pi M_0 \left\{ H_0 + H_{A1} \left[ -\frac{3}{16} + \frac{5}{4} \cos 2\theta_0 + \frac{15}{16} \cos 4\theta_0 \right] \right. \\ &\left. + \left( \frac{3}{16} - \frac{3}{4} \cos 2\theta_0 + \frac{9}{16} \cos 4\theta_0 \right) \cos 2\varphi_k \right\} \sin^2 \theta_k \quad (6.19) \end{aligned}$$

where  $\theta_0$  is the angle between  $\mathbf{M}_0$  and the direction  $\langle 100 \rangle$  (Figure 6.1). The dependence of the frequency on  $\theta_0$  for different directions of propagation is shown in Figure 6.2. One can see from the figure that  $\omega$  does not depend on  $\varphi_k$  when  $\mathbf{M}_0$  is directed along the  $\langle 100 \rangle$  or  $\langle 111 \rangle$  axis, and this dependence is the strongest when  $\mathbf{M}_0$  is directed along the axis  $\langle 110 \rangle$ .

Comparing formulae (6.18) or (6.19) with formula (6.5) for an isotropic medium, we see that, if  $\mathbf{M}_0$  is directed along the anisotropy axis in a uniaxial crystal, as well as along the axes  $\langle 100 \rangle$  or  $\langle 111 \rangle$  in a cubic crystal, these formulae coincide



**FIGURE 6.2**

Dependence of the frequency of a magnetostatic wave in a cubic crystal on the direction of  $\mathbf{M}_0$  for different propagation directions.  $\theta_0$  is the angle between the  $\mathbf{M}_0$  and  $\langle 100 \rangle$  axis in a  $\{110\}$  plane.  $M_0 = 139$  G,  $K_1 = 6 \times 10^3$ ,  $H_0 = 2.5$  kOe.

after the following substitution in (6.5):

$$H_0 \rightarrow H_0 + H^A. \quad (6.20)$$

Here,  $H^A = 2H_{A1}$  for a uniaxial crystal or for the axis  $\langle 100 \rangle$  in a cubic crystal, and  $H^A = -(4/3)H_{A1}$  for the axis  $\langle 111 \rangle$  in a cubic crystal (in the last case, if only the first anisotropy constant is taken into account). These coincidences are the manifestations of a general theorem, which states that, for the mentioned directions of magnetization (the directions of extrema of the energy of anisotropy) and only for them, the solutions of all electrodynamic problems in an anisotropic medium are obtained from the solutions in an isotropic medium by the substitution (6.20).

The validity of the nonexchange magnetostatic approximation is limited, from low  $k$  values, by the need to use full Maxwell's equations, and from high  $k$  values, by the need to take into account the exchange interaction. To estimate the *lower limit* the following condition can be used: the difference between the frequency (6.5) and the correct value of the frequency, found, e.g., from (4.42) or (4.48), must not exceed a certain quantity. For media with narrow resonance lines,  $\gamma\Delta H$  can be taken as such quantity. Then, we get

$$k > k_{\min} = k_0 \sqrt{\frac{4\pi M_0}{\Delta H}}. \quad (6.21)$$

For a YIG single crystal ( $4\pi M_0 = 1750$  G,  $\Delta H = 0.3$  Oe),  $k_{\min} = 250$  cm $^{-1}$ . For uniform oscillations in finite samples,  $k_{\min}$  in (6.21) must be replaced by  $2\pi/d_{\max}$  where  $d$  is the smallest of the sample dimensions.

The exchange interaction leads to the increase of the frequencies of magnetic waves (Section 7.1) by a quantity  $\sim \gamma D k^2$  (where  $D$  is the nonuniform-exchange constant). Requiring that the quantity  $\gamma D k^2$  should not exceed (for a single crystal)  $\gamma \Delta H$ , we obtain the estimate of the *upper limit* of the validity of the nonexchange magnetostatic approximation:

$$k < k_{\max} = \sqrt{\frac{\Delta H}{D}}. \quad (6.22)$$

For a YIG,  $D = 5.2 \times 10^{-9}$ , and  $k_{\max} \cong 6 \times 10^3$ . So, there is an interval of  $k$  values (for a YIG, approximately,  $10^2 - 10^4$ ) in which the nonexchange magnetostatic approximation may be used to calculate the frequencies of magnetic waves or oscillations.

---

## 6.2 Nonexchange magnetostatic waves in plates and rods

Magnetostatic waves in single-crystal ferrite films can be used in microwave engineering to design miniature devices such as filters, resonators, and delay lines. Therefore, we will study these waves in some detail: in this section, in the nonexchange approximation and in Section 7.2, making allowance for exchange interaction.

### 6.2.1 Volume waves in plates

Consider first an isotropic ferromagnetic plate magnetized to saturation *along the normal* to its surfaces (Figure 6.3). Suppose that both surfaces of the plate are *metallized* and there is no dependence of the fields on the coordinate  $x$  in the direction perpendicular to the direction of propagation. Then, the solution of (6.14) is<sup>1</sup>

$$\psi = (A \cos k_z z + B \sin k_z z) \exp(-iky). \quad (6.23)$$

The boundary condition at  $z = 0$  and  $z = d$  is

$$\left( \vec{\mu} \nabla \psi \right) \mathbf{n}_0 = 0 \quad (6.24)$$

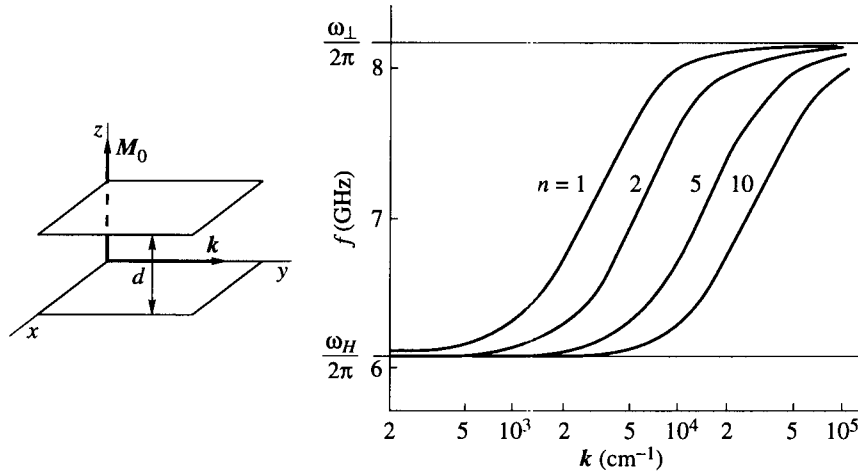
or in our case  $\partial \psi / \partial n = 0$ . Taking this into account, we get  $B = 0$  and

$$k_z = \frac{n\pi}{d} \quad (6.25)$$

where  $d$  is the plate thickness and  $n = 1, 2, 3 \dots$  is the number of half-waves of  $\psi$  (and, hence, of the field components) in  $z$  direction.

---

<sup>1</sup>Here and later on we omit the subscript at the vector  $\mathbf{k}$  component in the direction of propagation.



**FIGURE 6.3**

Dispersion curves of magnetostatic waves in a normally magnetized metallized ferromagnetic plate.  $M_0 = 139$  G,  $H_0 = 3.9$  kOe,  $d = 10$   $\mu\text{m}$ .

Substitution of (6.23) into (6.14) leads to

$$k_z^2 = -\mu k^2. \quad (6.26)$$

As  $k_z^2 > 0$ , the propagating waves ( $k^2 > 0$ ) exist only if  $\mu < 0$ , i.e., in the frequency range (6.6). Expression (6.26), together with (6.25) and the frequency dependence of  $\mu$  (1.54), determine the *dispersion relation*  $\omega(k)$ . It can be written in the form

$$\omega^2 = \omega_H \left( \omega_H + \frac{\omega_M}{1 + Z_n^2/(kd)^2} \right) \quad (6.27)$$

where  $Z_n = n\pi$ . In the limiting case of  $kd \rightarrow \infty$ , (6.27) transforms into the dispersion relation (6.5) for  $\theta_k = \pi/2$ . For finite  $k$  values, unlike the unbounded medium,  $\omega$  depends on  $k$ , and the group velocity  $v_{\text{gr}} \equiv \partial\omega/\partial k \neq 0$ .

In the considered case,  $\omega$  increases with the growth of  $k$  (Figure 6.3) and  $v_{\text{gr}} > 0$ . Such waves are called *forward waves*. The expression for  $v_{\text{gr}}$  is obtained by differentiating (6.27). It follows from this expression, as well as from Figure 6.3, that  $v_{\text{gr}}$  passes through a maximum at a value of  $k$  near  $n\pi/d$ . The maximal  $v_{\text{gr}}$  values are of the order of

$$(v_{\text{gr}})_{\text{max}} \sim \frac{\gamma M_0 d}{n}. \quad (6.28)$$

For a YIG film ( $d = 10$   $\mu\text{m}$ ,  $n = 1$ ),  $(v_{\text{gr}})_{\text{max}} \sim 2.5 \times 10^6$ .

The components of the magnetic field  $\mathbf{h}$  and magnetization  $\mathbf{m} = \vec{\chi} \mathbf{h}$  are found easily from  $\psi = A \cos k_z z \exp(-iky)$ . The electric field  $\mathbf{e}$  can be found, in the first

approximation, from equations (6.3) and the boundary conditions  $e_x = e_y = 0$  at  $z = 0, d$ . It turns out that, if  $k, k_z \ll k_0$  (which is the condition for the magnetostatic approximation to be valid),  $e$  is small as compared to  $h$ .

Consider now, following Bar'yakhtar and Kaganov [39], a ferromagnetic plate magnetized, as before, normally to its surface but *not metallized*. We have now to 'sew together' the fields in three regions:  $z < 0$ ,  $0 < z < d$ , and  $z > d$ , using the boundary conditions at the interfaces between these regions. For the potential inside the plate, the expression (6.23) is valid, and outside the plate

$$\psi_0 = \begin{cases} C \exp(\kappa_{0z}z -iky) & z < 0 \\ D \exp(-\kappa_{0z}z -iky) & z > d \end{cases} \quad (6.29)$$

where  $\kappa_{0z}$  is real and positive. In the plate, (6.26) holds, and the substitution of  $\psi_0$  into the Laplace equation results in

$$\kappa_{0z}^2 = k^2. \quad (6.30)$$

To satisfy the boundary conditions (6.12) it is necessary, in this case, to take  $\psi = \psi_0$  and  $\partial\psi/\partial z = \partial\psi_0/\partial z$  at  $z = 0, d$ . This leads to a system of linear equations for the coefficients  $A, B, C$ , and  $D$ . Equating to zero the determinant of the system and taking into account (6.26) and (6.30), we obtain the transcendental equation

$$\tan Z = \frac{2Zkd}{Z^2 - (kd)^2} \quad (6.31)$$

where  $Z = k_z d = \sqrt{-\mu}kd$ .

Equation (6.31) has an infinite number of roots  $Z_n$  ( $n = 1, 2, 3, \dots$ ) corresponding to different modes. These roots can be found by numerical or graphical (Figure 6.4) methods. Then, taking into account the frequency dependence of  $\mu$ , we obtain the dispersion relation  $\omega(k)$ . It can be written, as before, in the form (6.27), but the quantities  $Z_n$  depend now on  $kd$ . The frequency range remains the same as for the metallized plate, the  $\omega$  vs  $k$  curves are like those shown in Figure 6.3, and the estimate (6.28) is valid.

In the case of a *tangentially magnetized* plate (Figure 6.5), the potential in the plate can be written as

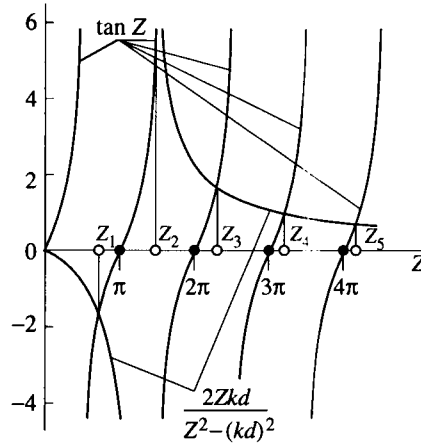
$$\psi = (A \cos k_x x + B \sin k_x x) \exp(-ik_y y - ik_z z). \quad (6.32)$$

Substituting it into equation (6.14), we get

$$-\mu(k_x^2 + k_y^2) = k_z^2. \quad (6.33)$$

Consider, for simplicity, a *metallized* plate. The boundary condition (6.24) leads now to

$$\mu \frac{\partial\psi}{\partial z} + i\mu_a \frac{\partial\psi}{\partial y} = 0 \quad (6.34)$$

**FIGURE 6.4**

Graphical solution of equation (6.31) for a free normally magnetized plate.  $kd = 4$ . Full circles represent  $Z_n$  values for a metallized plate.

at  $x = 0$  and  $x = d$ . Being applied to (6.33), these conditions result in a system of equations for the coefficients  $A$  and  $B$ . Setting the determinant of this system equal to zero, we find

$$(\mu^2 k_x^2 + \mu_a^2 k_y^2) \sin k_x d = 0. \quad (6.35)$$

As we limit ourselves, for the present, to the *volume* waves (with *trigonometric* dependence of the potential in the plate on the coordinate in the direction normal to the plate), we assume  $k_x$  in (6.35) to be real. Then, it follows from (6.35) that

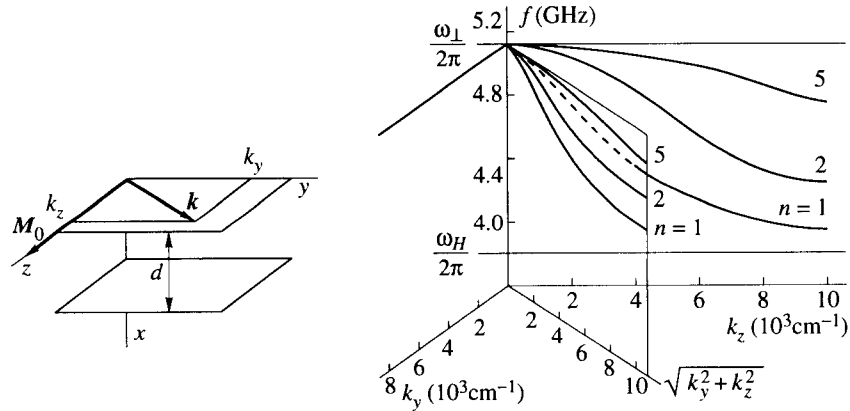
$$k_x d = n\pi \equiv X_n. \quad (6.36)$$

Substituting (6.36) into (6.33) and taking into account the frequency dependence of  $\mu$ , we obtain the dispersion relation

$$\omega^2 = \omega_H \left( \omega_H + \frac{\omega_M}{1 + \frac{k_y^2 d^2}{k_y^2 d^2 + X_n^2}} \right) \equiv \omega_H \left( \omega_H + \frac{\omega_M}{1 + \frac{\cos^2 \theta_k}{\sin^2 \theta_k + X_n^2 / (kd)^2}} \right) \quad (6.37)$$

where  $k^2 = k_y^2 + k_z^2$  and  $\theta_k$  is the angle between the direction of magnetization and the direction of propagation (Figure 6.5).

The dispersion curves, calculated by formula (6.37), are plotted in Figure 6.5. One can see that, for  $\theta_k = \pi/2$ , the frequency does not depend on  $k$ . In the other limiting case of  $\theta_k = 0$ , i.e., when the wave propagates along  $\mathbf{M}_0$ ,  $\omega$  lies in the range (6.6) and decreases with growing  $k$ , i.e.,  $v_{gr}$  is negative. This means

**FIGURE 6.5**

Dispersion curves of volume magnetostatic waves in a tangentially magnetized metallized plate.  $M_0 = 90$  G,  $H_0 = 1.35$  kOe,  $d = 10$   $\mu\text{m}$ .

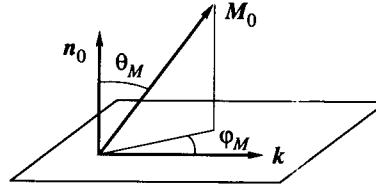
that the group velocity vector  $\mathbf{v}_{\text{gr}} = \partial\omega/\partial\mathbf{k}$  is antiparallel to the vector  $\mathbf{k}$  and to the phase velocity  $\mathbf{v}_{\text{ph}} = \mathbf{k}\omega/k^2$ . Such waves are called *backward waves*. If  $\theta_k \neq 0, \pi/2$ , the dependence of  $\omega$  on  $k = (k_y^2 + k_z^2)^{1/2}$  is also a decreasing one (Figure 6.5), but the angle between group and phase velocities is neither equal to zero nor to  $\pi$ . This is the consequence of the anisotropy in the  $yz$  plane due to magnetization in the  $z$  direction. The direction of  $\mathbf{v}_{\text{ph}}$  is usually determined by the exciting conductor (antenna), and the direction of  $\mathbf{v}_{\text{gr}}$  depends on the direction and value of the steady magnetic field and on  $\omega$ .

We will not consider the problem of magnetostatic volume wave propagation in a *free* (nonmetallized) tangentially magnetized plate, which was treated in detail by Damon and Eshbach [82]. We note only that the frequency range and the character of the dependence of  $\omega$  on  $k_y$  and  $k_z$  remain the same as for the metallized plate. Formula (6.37) also remains valid, but the quantities  $X_n$  depend now on  $k_y$  and  $k_z$ .

### 6.2.2 Surface waves

We have considered as yet only such solutions of equation (6.14) (corresponding to the volume waves) for which the dependence of  $\psi$  inside the ferromagnetic plate on the coordinate  $\zeta$  in the direction of the normal to the plate surface is represented by trigonometric functions. However, there exist solutions with  $k_\zeta^2 < 0$ , for which the dependence of  $\psi$  on  $\zeta$  is represented by *hyperbolic* functions not only outside the ferromagnet but also *inside* it. Waves corresponding to such solutions are called *surface waves*.

For surface waves, the simpler problem of wave propagation along an interface



**FIGURE 6.6**  
Surface wave at the boundary of a ferromagnet with metal or dielectric.

of half-infinite ferromagnet and half-infinite dielectric (or metal) is also meaningful. Gintsburg [141] was the first to study this problem. Consider a *half-infinite* ferromagnet magnetized tangentially to its surface and a wave propagating parallel to the surface and normally to the direction of magnetization ( $\theta_M = \varphi_M = \pi/2$  in Figure 6.6). Consider first the propagation along the interface of the ferromagnet with perfect metal. The potential can be written in the form  $\psi = A \exp(-\kappa x - ik y)$  where  $\kappa$  is real and positive, and

$$k = s_k |k|. \quad (6.38)$$

Here,  $s_k = \pm 1$  where the upper sign corresponds to the propagation in the positive direction, and the lower sign corresponds to the propagation in the negative direction of the  $y$  axis.

Substituting  $\psi$  into equation (6.14), we get

$$\mu (\kappa^2 - k^2) = 0. \quad (6.39)$$

The boundary condition (6.24) leads to

$$\mu \kappa = \mu_a k. \quad (6.40)$$

It follows from (6.39) that either

$$\kappa = |k| \quad (6.41)$$

or  $\mu = 0$ . The latter case is of no interest because then, according to (6.40),  $k = 0$ .

Note that, according to (1.54),  $\mu_a$  changes the sign if the direction of  $M_0$  is changed from positive, with respect to the  $z$  axis [what was assumed in deriving (1.54)], to negative. Hence, we may write

$$\mu_a = \tilde{\mu}_a s_M \quad (6.42)$$

where  $\tilde{\mu}_a$  is defined according to (1.54), and  $s_M = 1$  if  $M_0 = z_0 M_0$ , and  $s_M = -1$  if  $M_0 = -z_0 M_0$ . Substituting (6.38) and (6.42) into (6.40) and taking (6.41) into account, we get

$$\frac{\mu}{\mu_a} = s_M s_k \equiv s. \quad (6.43)$$



It follows from (1.49) or from Figure 1.5 that the ratio  $\mu/\mu_a$  is never equal to +1 and is equal to -1 at

$$\omega = \omega_H + \omega_M. \quad (6.44)$$

Thus, the frequency of a surface nonexchange magnetostatic wave, propagating along the boundary of a ferromagnet with metal, is independent of  $k$  and lies above the range (6.6). The direction of propagation is determined by the condition  $s = -1$ . It is easy to make sure that this condition is equivalent to the condition

$$\frac{\mathbf{k}}{k} = \mathbf{n}_0 \times \frac{\mathbf{M}_0}{M_0} \quad (6.45)$$

where  $\mathbf{n}_0$  is a unit normal to the boundary directed into the ferromagnet.

Consider now the wave propagating along the boundary of a ferromagnet and a dielectric. The potential in the ferromagnet ( $x > 0$ ) is written as before, and expression (6.39) holds. In the dielectric ( $x < 0$ ),  $\psi_0 = C \exp(\kappa_0 x - ik y)$ . Substituting  $\psi_0$  into the Laplace equation, we find  $\kappa_0^2 = k^2$ . So,

$$\kappa_0 = \kappa = |k|. \quad (6.46)$$

From the boundary conditions (6.12) at  $x = 0$ , it follows that  $A = C$  and

$$\kappa_0 + \mu\kappa = \mu_a k. \quad (6.47)$$

Taking into account (6.46), (6.38), and (6.42), we obtain from (6.47)

$$\frac{1 + \mu}{\mu_a} = s_M s_k = s. \quad (6.48)$$

It is easy to make sure that (6.48) is satisfied only for  $s = -1$ , and

$$\omega = \omega_H + \frac{1}{2}\omega_M. \quad (6.49)$$

Thus, the surface wave propagating along the boundary with a dielectric is characterized by the same nonreciprocity as the wave at the boundary with metal. Its frequency also lies above the frequency range of volume waves but nearer to the upper limit of this range.

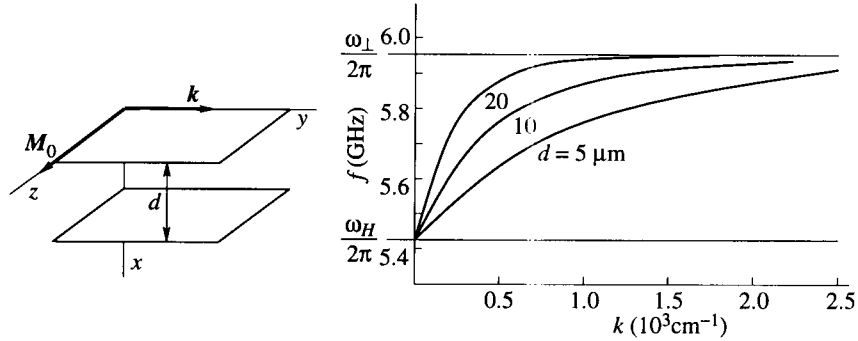
Eshbach and Damon [112] studied surface waves at the boundary ferromagnet-dielectric for *arbitrary directions* of magnetization and propagation (Figure 6.6). It was shown that the waves exist if

$$\sin \theta_M \sin \varphi_M \geq \frac{\omega_H}{\omega_H + \omega_M} \quad (6.50)$$

and their frequencies are determined by a very simple formula:

$$\omega = \frac{\omega_H}{2} \frac{1}{\sin \theta_M \sin \varphi_M} + \frac{\omega_H + \omega_M}{2} \sin \theta_M \sin \varphi_M. \quad (6.51)$$

Expression (6.49) is a particular case of (6.51).

**FIGURE 6.7**

Dispersion curves for surface waves in a free ferromagnetic plate.  $M_0 = 139$  G,  $H = 1.25$  kOe.

Passing to the surface waves in *plates*, we limit ourselves to the simplest but very important case of a wave propagating *normally to the direction of magnetization* in a tangentially magnetized plate. Such a wave in a metallized plate is of no interest because its frequency does not depend on  $k$ , and we consider a *free* plate (Figure 6.7). This problem was studied by Damon and Eshbach [82].

The potential inside the plate can be written in the form

$$\psi = [A \exp(-\kappa x) + B \exp(\kappa x - \kappa d)] \exp(-iky) \quad (6.52)$$

and outside the plate

$$\psi_0 = \begin{cases} C \exp(\kappa_0 x - ik y) & x < 0 \\ D \exp(-\kappa_0 x + \kappa_0 d - ik y) & x > d. \end{cases} \quad (6.53)$$

Expression (6.46) holds as before, and a system of equations for the coefficients  $A$ ,  $B$ ,  $C$ , and  $D$  follows from the boundary conditions. Equating its determinant to zero, we obtain

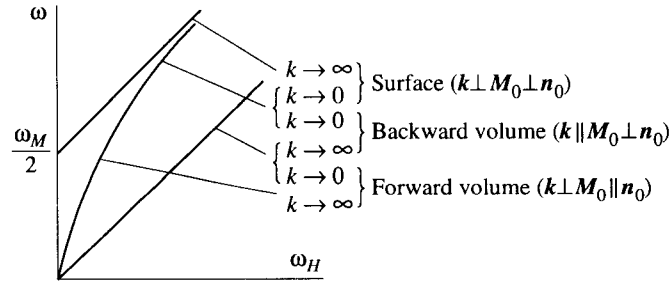
$$\frac{\mu_a^2 k^2 - (\kappa \mu + \kappa_0)^2}{\mu_a^2 k^2 - (\kappa \mu - \kappa_0)^2} = \exp(-2\kappa d). \quad (6.54)$$

Taking into account (6.46) and dependences (1.54) of  $\mu$  and  $\mu_a$  on  $\omega$ ,  $\omega_M$ , and  $\omega_H$ , we find the dispersion relation

$$\omega^2 = \left(\omega_H + \frac{\omega_M}{2}\right)^2 - \left(\frac{\omega_M}{2}\right)^2 \exp(-2\kappa d). \quad (6.55)$$

As it should be expected from the symmetry considerations, the frequency does not depend on the directions of  $M_0$  and  $k$ . It depends on  $k$  (Figure 6.7) and lies in the range

$$\omega_{\perp} \leq \omega \leq \omega_H + \frac{1}{2}\omega_M. \quad (6.56)$$

**FIGURE 6.8**

Regions of existence of nonexchange magnetostatic waves in a free ferromagnetic plate.  $\mathbf{n}_0$  is a unit normal to the plate surface.

This range adjoins the range (6.6), in which the frequencies of the volume waves lie (Figure 6.8). The group velocity of the considered surface wave is positive. This is in accordance with the general rule that magnetostatic waves, propagating normally to the direction of magnetization, are forward waves, and waves, propagating along this direction, are backward waves. The value of the *group velocity* is easily found by differentiating (6.55):

$$v_{\text{gr}} = \frac{d\omega_M^2}{4\omega} \exp(-2kd). \quad (6.57)$$

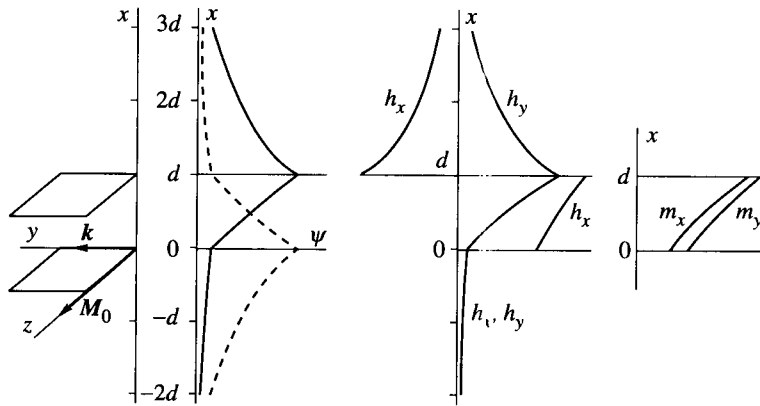
In contrast to volume waves, this quantity decreases *monotonically* with growing  $k$ .

Having solved the system of equations for the coefficients  $A$ ,  $B$ ,  $C$ , and  $D$ , we find the potentials  $\psi$  and  $\psi_0$  and can calculate the magnetic field  $\mathbf{h} = \nabla\psi$ , the magnetization  $\mathbf{m} = \vec{\chi}\mathbf{h}$ , and, in the first approximation, the electric field  $\mathbf{e}$ . We cite here only some qualitative results of these calculations. The potentials and all field components turn out to be nonreciprocal, i.e., their coordinate dependences change with the reversal of  $\mathbf{M}_0$  or  $\mathbf{k}$  (Figure 6.9). The fields and magnetization 'press themselves' to one of the plate surfaces, depending on the direction of the  $\mathbf{M}_0 \times \mathbf{k}$  vector (or on the sign of  $s = s_M s_k$ ). The magnetic field and magnetization inside the plate are elliptically polarized. The magnetic field outside the plate is circularly polarized, the directions of polarization rotation being opposite at opposite sides of the plate. The electric field is linearly polarized in  $z$  direction.

Seshadri [358] studied a more complicated case when a tangentially magnetized ferromagnetic plate *adjoins metal* at one side ( $x = 0$ ) and air at the other side ( $x = d$ ). The dispersion relation for the surface wave, in this case, has the form

$$\left(1 + 2\frac{\omega_H}{\omega_M} + 2s\frac{\omega}{\omega_M}\right) \frac{\omega_H + \omega_M - s\omega}{\omega_H + \omega_M + s\omega} = \exp(-2kd). \quad (6.58)$$

In contrast to (6.55),  $s$  appears in this expression, i.e., the dispersion relation is

**FIGURE 6.9**

Potential, field, and magnetization patterns for a surface magnetostatic wave in a tangentially magnetized plate.  $M_0 = 139$  G,  $H_0 = 1.25$  kOe,  $d = 10$   $\mu$ m. Solid and dashed lines correspond to different directions of propagation.

*nonreciprocal*. If  $s = 1$ , the frequency lies in the range

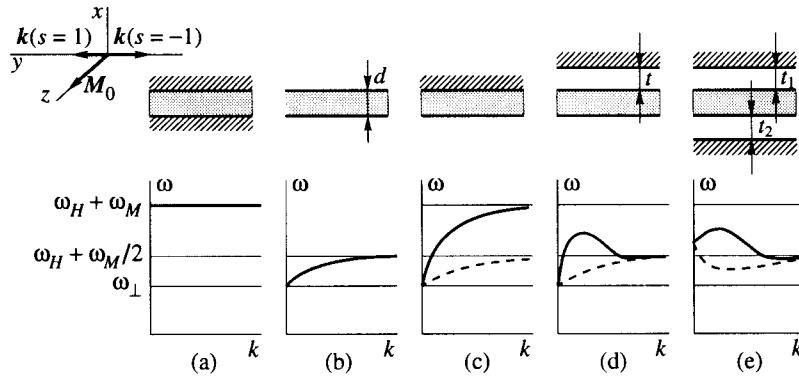
$$\omega_{\perp} \leq \omega \leq \omega_H + \omega_M. \quad (6.59)$$

When  $kd \rightarrow \infty$ , it approaches the frequency (6.44) of the wave propagating along the boundary of ferromagnet with metal. If  $s = -1$ , the frequency lies in the range (6.56) and approaches, when  $kd \rightarrow \infty$ , the frequency (6.49) of the wave propagating along the boundary of a ferromagnet and a dielectric. The curves  $\omega$  vs  $k$  for both values of  $s$  are plotted in Figure 6.10(c).

The dispersion relations of surface waves have been calculated, as well, for the structures shown in Figure 6.10(d),(e) [58, 457]. An interesting feature of these structures is the nonmonotonical dependence  $\omega(k)$  for  $s = 1$ : the wave is forward at small  $k$  values and is backward at large  $k$  values. Volume and surface waves in some other structures were also investigated (e.g., [8]). By varying the thicknesses and the magnetizations of the layers it is possible to approach the required dispersion relations, in particular, with approximately constant  $v_{gr}$  (for broadband delay lines) or with linear dependence  $v_{gr}(\omega)$  (for pulse-compression devices [4]).

### 6.2.3 Magnetostatic waves in waveguides with finite cross section

The existence of slow electromagnetic waves in ferrite-loaded waveguides with small cross section was first demonstrated theoretically by Seidel [356]. His, rather complicated, analysis was based on full Maxwell's equations. But if the waves are regarded from the very beginning as magnetostatic, such problems can

**FIGURE 6.10**

Frequencies of surface magnetostatic waves in different structures containing a tangentially magnetized ferrite plate. Solid lines and dashed lines correspond to  $s = 1$  and  $s = -1$ , respectively. Curves  $\omega(k)$  relate to  $t = t_1 = 2d$ ,  $t_2 = 5d$ .

be solved easily. In the case of a *metallized rectangular ferrite rod*, the solution was carried out by Auld and Mechta [27].

The magnetostatic potential can be written as

$$\psi = (A_x \cos k_x x + B_x \sin k_x x)(A_z \cos k_z z + B_z \sin k_z z) \exp(-iky). \quad (6.60)$$

Substituting this into the Walker equation (6.14), we get

$$-\mu(k_x^2 + k^2) = k_z^2. \quad (6.61)$$

The boundary conditions at  $z = 0$  and  $z = b$  (Figure 5.4) lead to

$$B_z = 0 \quad k_z = \frac{m\pi}{b} \quad (m = 1, 2, 3 \dots). \quad (6.62)$$

There are two possibilities to satisfy the boundary conditions at  $x = 0$  and  $x = a$ :

$$B_x = -\frac{s\tilde{\mu}_a k}{\mu k_x} A_x \quad k_x = \frac{n\pi}{a} \quad (n = 1, 2, 3 \dots) \quad (6.63)$$

$$B_x = iA_x \quad k_x = i\kappa_x \quad \kappa_x = \frac{sk\tilde{\mu}_a}{\mu}. \quad (6.64)$$

The first possibility corresponds to volume waves. Then, from (6.61)–(6.63) and the frequency dependence of  $\mu$ , it follows:

$$\omega^2 = \omega_H \left[ \omega_H + \omega_M \left( 1 + \frac{(m\pi/b)^2}{(n\pi/a)^2 + k^2} \right)^{-1} \right]. \quad (6.65)$$

The second possibility corresponds to waves with hyperbolic  $x$  dependence and trigonometric  $z$  dependence. In this case, (6.61) transforms into  $k_z^2 = -\mu_\perp k^2$ ,

and, taking (1.60) into account, we get

$$\omega^2 = (\omega_H + \omega_M) \left( \omega_H + \frac{\omega_M}{1 + (m\pi)^2 / (kb)^2} \right). \quad (6.66)$$

The dispersion relations (6.65) and (6.66) are reciprocal, but the potentials and, hence, the field structures are nonreciprocal, as one can see from (6.63) and (6.64). Both waves are forward, as would be expected because the direction of propagation is normal to  $\mathbf{M}_0$ .

The problem of magnetostatic-wave propagation in a longitudinally magnetized *round rod* can also be solved rigorously. We must now use cylindrical coordinates (Figure 5.1), in which equation (6.11) takes the form

$$\mu \left( \frac{\partial^2 \psi}{\partial \rho^2} + \frac{1}{\rho} \frac{\partial \psi}{\partial \rho} + \frac{1}{\rho^2} \frac{\partial^2 \psi}{\partial \varphi^2} \right) - \frac{\partial^2 \psi}{\partial z^2} = 0. \quad (6.67)$$

Consider, for simplicity, a *metallized rod*. Note that it is the same problem as in Section 5.1 but solved now in the magnetostatic approximation. The solution of (6.67) can be written in the form

$$\psi = J_m(\kappa\rho) \exp(im\varphi - ikz) \quad (6.68)$$

where  $J_m$  is the Bessel function and  $m = 0, \pm 1, \pm 2, \dots$ . The boundary condition

$$\mu \frac{\partial \psi}{\partial \rho} + i\mu_a \frac{1}{\rho} \frac{\partial \psi}{\partial \varphi} = 0 \quad \text{at } \rho = \rho_0 \quad (6.69)$$

follows from (6.24). Substituting (6.68) into (6.67), we find  $k^2 = -\mu\kappa^2$ , and it follows from (6.69):

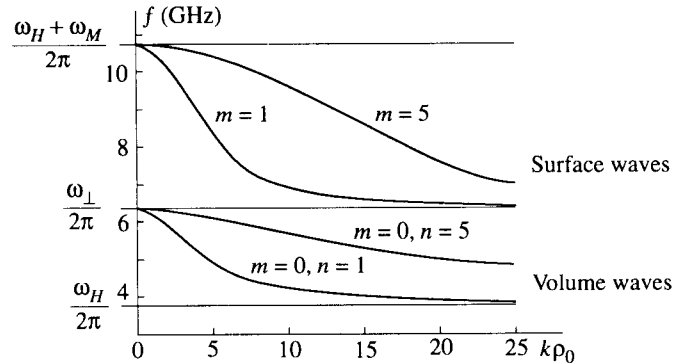
$$\frac{X J'_m(X)}{J_m(X)} = m \frac{\mu_a}{\mu} \quad (6.70)$$

where  $X = \kappa\rho_0$ , and prime denotes the differentiation with respect to  $X$ . This equation is much simpler than equation (5.4), which was obtained without using the magnetostatic approximation. Taking into account the frequency dependence of  $\mu$  and  $\mu_a$ , we find from (6.70) the dispersion relation

$$\omega^2 = \omega_H \left( \omega_H + \frac{\omega_M}{1 + (k\rho_0)^2 / X_{mn}^2(\omega)} \right) \quad (6.71)$$

where  $X_{mn}(\omega)$  is the  $n$ th root of (6.70).

If  $m = 0$ , equation (6.70) becomes  $J_1(X) = 0$  and has only real roots independent of  $\omega$ , which correspond to volume waves. Formula (6.71) gives, in this case, the explicit dependence  $\omega(k)$  (Figure 6.11). If  $m \neq 0$ , equation (6.70) has, at each  $|m|$ , an infinite number of real roots, which depend on frequency and the sign of  $mM_{0z}$ , i.e., on the direction of polarization rotation with respect to the direction of the steady magnetization. For the left-hand rotation, equation (6.70) has imaginary roots, too, one root at each value of  $|m|$ . These roots correspond to

**FIGURE 6.11**

Dispersion characteristics of magnetostatic waves in a round metal waveguide filled with longitudinally magnetized ferrite.  $M_0 = 200$  G,  $H_0 = 1.35$  kOe.

surface waves (Figure 6.11). One can see from the figure that, in accordance with the above-mentioned rule, all waves are backward.

The magnetostatic waves in a *nonmetallized* rod were investigated by Joseph and Schlömann [192]. The volume-wave dispersion characteristics, in this case, do not differ qualitatively from the dispersion characteristics in a metallized rod. However, the surface waves exist in a smaller range (6.56).

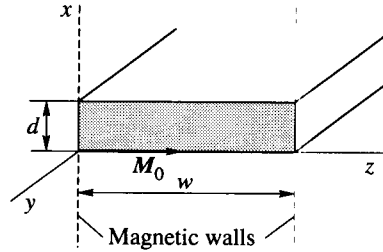
Magnetostatic waves in ferrite *films of finite width* are of certain interest from the practical point of view. Such films can be regarded as rectangular rods. But the problem of wave propagation in a free (nonmetallized) rectangular rod has no strict analytical solution. To solve it approximately the method of 'magnetic walls' can be used. According to this method, we exclude the regions  $z < 0$  and  $z > w$  (Figure 6.12) from consideration and assume fictitious boundary conditions  $(\vec{\mu} \mathbf{h}) \mathbf{n}_0$  at the planes  $z = 0$  and  $z = w$ . At the surfaces  $x = 0$  and  $x = d$ , the real boundary conditions are to be satisfied. Such problem has a simple solution, which is a good approximation if the dimension in the direction normal to the 'magnetic walls' ( $w$  in Figure 6.12) is much larger than another dimension ( $d$ ).

Consider, e.g., a surface wave. The potential can be written as

$$\psi = \psi_{\perp} (F \cos k_z z + G \sin k_z z) \quad (6.72)$$

where  $\psi_{\perp}$  has the form (6.52) inside the plate and the form (6.53) outside it. The boundary conditions at  $x = 0$  and  $x = d$  lead to (6.54), and from the boundary conditions at the magnetic walls  $z = 0$  and  $z = w$  it follows that  $F = 0$  and

$$k_z = \frac{n\pi}{w} \quad (n = 1, 2, 3, \dots). \quad (6.73)$$



**FIGURE 6.12**  
Tangentially magnetized ferromagnetic plate of finite width.

Substituting (6.72) into the Walker equation (6.14), we get, instead of (6.39),

$$\mu(\kappa^2 - k^2) - k_z^2 = 0. \quad (6.74)$$

From the Laplace equation for the potential outside the plate, it follows that

$$\kappa_0^2 - k^2 - k_z^2 = 0. \quad (6.75)$$

Expressions (6.54) and (6.73)–(6.75), together with the dependence of  $\mu$  and  $\mu_a$  on  $\omega$ , determine the dispersion relation. It differs essentially from the dispersion relation in an infinite film only for small values of  $kw$ .

Using the method of magnetic walls, O'Keefe and Patterson [303] considered a more complicated structure, shown in Figure 6.10(d). Some interesting features were found, in particular, the existence of a *volume* wave in a certain frequency range below  $\omega_{\perp}$ .

#### 6.2.4 Energy flow and losses

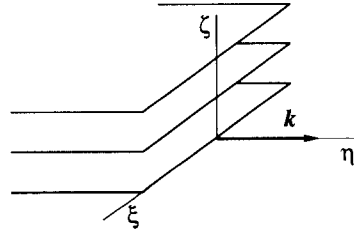
Let us limit ourselves to magnetostatic waves in plane structures, which are of most practical interest. Consider a structure (Figure 6.13) consisting of  $N$  ferrite and dielectric layers and suppose that  $v_{ph}$  and  $v_{gr}$  are both directed along the  $\eta$  axis. Then, the *energy flow* in this direction, related to the unit length of the structure in the  $\xi$  direction, is

$$P_{\parallel}(\xi) = \sum_{j=1}^N \int_{(j)} \Pi_{j\eta}(\xi, \zeta) d\zeta \quad (6.76)$$

where  $\Pi_j$  is the mean value of the Poynting vector (4.67), and integration is over the thickness of each layer of the structure. The electric field, needed to calculate  $\Pi_{j\eta}$ , can be found using equations (6.3). If there is no dependence on  $\xi$ , it follows from (6.3):

$$e_{\xi} = -\frac{k_0}{k} b_{\zeta} \quad (6.77)$$





**FIGURE 6.13**  
A planar structure.

and, as  $h_\xi = 0$ , we obtain

$$\Pi_\eta = -\frac{c}{8\pi} \operatorname{Re} (e_\xi h_\zeta^*) = \frac{\omega}{8\pi k} \operatorname{Re} \left[ h_\zeta^* \left( \vec{\mu} \mathbf{h} \right)_\zeta \right]. \quad (6.78)$$

As a simple example, consider a volume wave in a normally magnetized metallized plate (Figure 6.3). Then,

$$P_1 = \int_0^d \Pi_y dz = \frac{1}{16\pi} \frac{\omega d}{k} h_{z \max}^2. \quad (6.79)$$

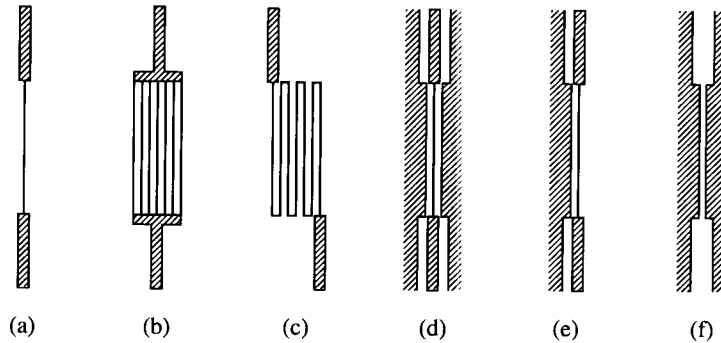
The energy flow for a wave in a free (nonmetallized) plate is to be found by summing in (6.76) the integrals over three regions: the plate and two dielectric half-spaces. The energy flows in different regions may have different signs, but the total flow, of course, is in the direction of group velocity.

The losses of magnetostatic waves have the following sources: magnetic losses determined by anti-Hermitian parts of  $\vec{\mu}$  components (Section 4.4); electric losses determined by imaginary parts of  $\varepsilon$  in ferrite and dielectric layers; losses in metallic layers; electromagnetic radiation (if the structure is not entirely screened); excitation of other types of waves in the structure, first of all, of the elastic waves.

The first source is, usually, the most important. To find its contribution we can use the above-discussed dispersion relation assuming  $\mu$  and  $\mu_a$  in these relations to be complex. If the dispersion relation is written in the form  $F(\omega, \omega_H, k) = 0$  [as, e.g., relations (6.27), (6.37), or (6.55)], then it is sufficient to make the replacement (1.68). Solving the obtained complex equation, we can get  $k = k' - ik''$ . If the losses are *small*, we can expand  $F(\omega, \omega_H + i\alpha\omega, k' - ik'')$  in power series in  $i\alpha\omega$  and  $(-ik'')$ . Equating to zero the sum of linear terms in these series, we obtain

$$k'' = \alpha \frac{\omega}{v_{gr}} \frac{\partial \omega}{\partial \omega_H}. \quad (6.80)$$

The quantity  $\omega_\tau$  can be introduced which characterizes the attenuation of the wave per *unit time* of propagation. If we turn, in the factor  $\exp(i\omega t - ik'y - k''y)$ ,

**FIGURE 6.14**

Transducers used to excite and receive magnetostatic waves in ferrite films. Microstrip transducers: (a) single microstrip, (b) lattice, (c) meander. Coplanar transducers: (d) symmetric, (e) nonsymmetric, (f) slot-line.

to the coordinate system moving in the direction of the wave propagation with the velocity  $v_{gr}$ , we see that in the new system the attenuation is determined by the factor  $\exp(-\omega_{\tau}t)$  where

$$\omega_{\tau} = v_{gr}k'' = \alpha\omega \frac{\partial\omega}{\partial\omega_H}. \quad (6.81)$$

Comparing this expression with (6.7), we make sure that  $\omega_{\tau}$  coincides with the decrement  $\omega''$  of oscillations (when  $k'' = 0$ ). For the surface wave in a free (nonmetallized) film, it follows from (6.81) and (6.55) that

$$\omega_{\tau} = \alpha \left( \omega_H + \frac{1}{2}\omega_M \right). \quad (6.82)$$

### 6.2.5 Magnetostatic waves in ferrite films: excitation, applications

To excite magnetostatic waves in ferrite films (usually, YIG epitaxial films on GGG substrates) thin metal conductors, placed at or near the film surface, are used. The simplest exciting element (transducer or 'antenna') is a straight microstrip or wire conductor (Figure 6.14). Because of relation (6.1), the wave front of the excited wave is approximately parallel to the conductor, i.e.,  $\mathbf{k}$  and  $\mathbf{v}_{gr}$  vectors are perpendicular to it. If the field structure of the wave is reciprocal, waves propagating in both directions have equal amplitudes. But if the field structure is nonreciprocal, the amplitude is larger in the direction for which the fields have greater values at the surface where the transducer is placed.

As the first approximation, the problem of wave excitation by *given currents* can be treated. Such problems were solved by Ganguly and Webb [134], Emtage [108], Kalinikos (see references in [205]), and by others. In reality, the currents in the

transducers are not given and should be found together with the amplitudes of the excited waves. Such *self-consistent* theories were worked out by Vugalter and Makhalin [431] and Gilinskii and Shcheglov [137].

The main result of all theories of magnetostatic-wave excitation is that the amplitude of the wave with a certain  $k$  value is proportional to the  $k$ th space Fourier harmonic of the current.

A comparatively simple problem (which can be used as a starting point in more complicated cases) is the problem of magnetostatic-wave excitation by a *linear current*  $I$  at the surface of the film. The solution of this problem can be written in the form

$$\mathbf{h}(\eta, \zeta) = CI\mathbf{h}^0(\eta, \zeta) \quad (6.83)$$

where  $\mathbf{h}(\eta, \zeta)$  is the complex amplitude of the magnetic field of the excited wave,  $\mathbf{h}^0(\eta, \zeta)$  is the *normalized* magnetic-field eigenfunction, and  $C$  is the complex quantity found by solving the problem; it is assumed that  $\partial/\partial\xi = 0$  where  $\xi$  is the coordinate in the direction of the current.

Consider now a transducer consisting of  $N$  parallel linear conductors with currents  $I_j = |I_j| \exp(i\varphi_j)$ , which are situated at distances  $l_j$  from a certain point. Then,

$$\mathbf{h} = C\mathbf{h}^0 \sum_{j=1}^N |I_j| \exp(i\varphi_j + ikl_j). \quad (6.84)$$

In the particular case of equal ( $|I_j| = \text{const} \equiv I$ ) and cophased ( $\varphi_j = 0$ ) currents at equal distances  $\delta l$  from each other, we get  $\mathbf{h} = CIF_N\mathbf{h}^0$  where 'the structural factor'

$$F_N = \frac{\sin(k\delta l N/2)}{\sin(k\delta l/2)}. \quad (6.85)$$

An analogous expression can be obtained for the antiphased currents ( $\varphi_j - \varphi_{j-1} = \pi$ ). The transducer (b) in Figure 6.13 can be regarded as cophased, and transducers (c), (d), and (e), as antiphased.

Expression (6.85) can be used to find the dependence of the intensity of excitation on the *width*  $b$  of the conductor. Assuming the uniform current distribution over the width of the conductor, we regard the conductor as a system of  $N$  equal cophased currents  $I/N$  at distances  $b/N$ . At  $N \rightarrow \infty$  we get

$$C(b) = C(0)F_b \quad F_b = \frac{\sin(kb/2)}{kb/2}. \quad (6.86)$$

According to (6.86), the decrease of the excitation intensity with increasing  $b$  becomes essential at  $b \gtrsim \pi/(2k)$ . This estimate can be used, notwithstanding that the current distribution over the conductor width is far from uniform.

The power flow of the excited wave, related to a unit length of the transducer,

can be written in the form

$$P_1 = P_1^+ + P_1^- = \frac{1}{2} R_{1\text{rad}}^+ |I|^2 + \frac{1}{2} R_{1\text{rad}}^- |I|^2 = \frac{1}{2} R_{1\text{rad}} |I|^2 \quad (6.87)$$

where  $I$  is the complex amplitude of the transducer current, indices + and – correspond to the waves propagating in opposite directions, and  $R_{1\text{rad}}^+$ ,  $R_{1\text{rad}}^-$ , and  $R_{1\text{rad}}$  are the *radiation resistances*. For the complete calculation of the magnetostatic-wave excitation, we have to find the current distribution along the transducer. The theory of transmission lines with losses (e.g., [191]) can be used for this purpose. The radiation resistance  $R_{1\text{rad}}$  is the main part of the distributed resistance, one of the four distributed parameters of such lines. It was shown [428] that the theory of transmission lines with losses can be applied to the receiving transducer, as well.

In conclusion, we list the main distinctive features of magnetostatic waves in films.

1. Broad frequency range ( $\sim 1\text{--}50$  GHz) limited from above only by the high values of the steady magnetic field, and from below, by the rise of domains.
2. Possibility of tuning by variation of the steady magnetic field.
3. The range of wave numbers ( $\sim 10\text{--}10^4$  cm $^{-1}$ ) independent of frequency and convenient for applications.
4. Low group velocity controllable by the steady magnetic field.
5. Possibility to change the dispersion law by simple means, e.g., by the choice of the wave type and the thickness of layers.
6. Comparatively low propagation losses.
7. Effective excitation by transducers of simple design.

These features result in broad application possibilities of magnetostatic waves in designing miniature controllable and nonreciprocal microwave devices. Among them there are delay lines, filters, resonators (e.g., [3, 189, 5]), as well as nonlinear devices (Section 10.5).

---

### 6.3 Magnetostatic oscillations (Walker's modes)

In ferromagnetic or ferrimagnetic samples of finite dimensions, magnetization oscillations with discrete eigenfrequencies should take place. In this section we will study these oscillations in the magnetostatic approximation. The uniform mode of such oscillations was already considered in this approximation in Section 1.5. *Nonuniform* oscillations were observed, as it became clear afterwards, in early ferromagnetic-resonance experiments as subsidiary maxima superimposed on the main resonance curve. White and Solt [439] and Dillon [93] were the first to resolve these maxima and give a qualitative explanation of them. The rigorous theory was worked out by Walker [432] (see also [433]) for the case of an ellipsoid

of revolution (spheroid). We will cite the main results of this theory below, after considering simpler examples.

### 6.3.1 Metallized cylinder

Consider a 'waveguide' resonator (Section 5.3) obtained from a round metallized ferrite rod magnetized in the direction of its axis (Figure 6.15). As the electric-field structure and the propagation constant  $k$  of this waveguide are both reciprocal (Sections 6.2), the eigenfrequencies of the resonator are determined by expression (5.34). Substituting it into the dispersion relation (6.71), we get the equation for the *eigenfrequencies*

$$\omega^2 = \omega_H \left\{ \omega_H + \omega_M \left[ 1 + \frac{(\pi p)^2}{X_{m,n}^2(\omega)} \left( \frac{\rho_0}{l} \right)^2 \right]^{-1} \right\} \quad (6.88)$$

where  $X_{m,n}(\omega)$  are the roots of (6.70),  $m = 0, \pm 1, \pm 2, \dots$ ,  $n = 1, 2, 3, \dots$ , and  $p = 1, 2, 3, \dots$ . One can see from (6.88) that the eigenfrequencies depend on the *ratio* of the resonator dimensions and on three integral numbers  $m$ ,  $n$ , and  $p$ , which characterize the oscillation mode. The range in which the eigenfrequencies lie is the same as for propagating waves, both volume and surface:

$$\omega_H < \omega < \omega_H + \omega_M. \quad (6.89)$$

If the cylindrical surface is not metallized, the frequency range would be

$$\omega_H < \omega < \omega_H + \frac{1}{2}\omega_M. \quad (6.90)$$

(In this case the plane metal surfaces must be assumed to be infinite in order for the problem to have a rigorous solution).

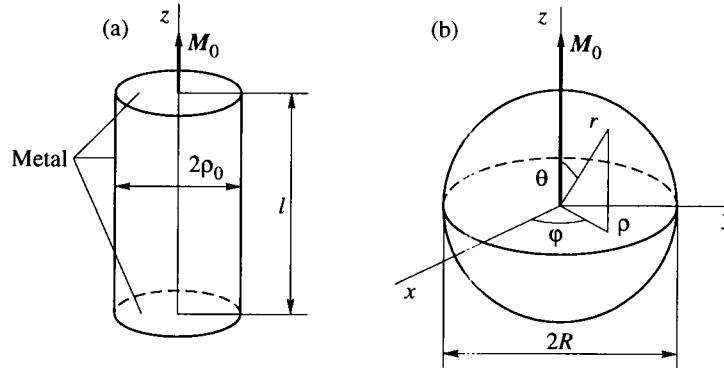
The components of  $\mathbf{h} = \nabla\psi$  and  $\mathbf{m} = \vec{\chi}\mathbf{h}$  can be found from the potential

$$\psi = J_m(\kappa\rho) \exp(-im\varphi) \cos k_z z \quad (6.91)$$

where  $k_z = \pi p/l$ . It should be noted that by taking into account the boundary conditions for the potential (6.91), we can find expression (6.88) without using the dispersion relation for the propagating wave.

### 6.3.2 Sphere and ellipsoid of revolution

The problem of magnetostatic oscillations in a sphere is of great interest because spherical ferrite samples are widely used for ferromagnetic-resonance experiments and in microwave ferrite devices, especially in ferrite filters (Section 5.3). The magnetostatic oscillations in a sphere can be treated as a particular case of such oscillations in an ellipsoid of revolution (spheroid) analyzed by Walker [432]. However, some mathematical difficulties, arising in this way, make an indepen-



**FIGURE 6.15**  
Magnetostatic ferrite resonators: (a) metallized cylinder. (b) sphere.

dent solution of the problem for a sphere more expedient. Such a solution was performed by Fletcher and Bell [119].

Consider a sphere (Figure 6.15) of an isotropic nonconducting ferromagnet magnetized to saturation. We must find the solutions of the Walker equation (6.14) for the potential  $\psi$  inside the sphere and of the Laplace equation for the potential  $\psi_0$  outside it and satisfy the boundary conditions (6.12) at the sphere surface. These conditions lead to

$$\psi = \psi_0 \quad (\vec{\mu} \nabla \psi) \cdot \mathbf{r}_0 = \frac{\partial \psi_0}{\partial r} \quad \text{at } r = R \quad (6.92)$$

where  $\mathbf{r}_0$  is a unit vector directed along the radius. To satisfy the boundary conditions the solutions for  $\psi$  and  $\psi_0$  should be found in a coordinate system in which the surface  $r = R$  is a *coordinate surface*. The spherical coordinate system  $r, \theta, \varphi$  is, of course, such a system, and the solution of Laplace's equation in this system has the form [293]

$$\psi_0 = r^{-(n+1)} P_n^{|m|}(\cos \theta) \exp(-im\varphi) \quad (6.93)$$

where  $P_n^{|m|}$  is the first-kind associated Legendre functions [273],  $n = 1, 2, 3, \dots$ , and  $m = 0, \pm 1, \pm 2, \dots, \pm n$ .

However, the solution of Walker's equation *cannot* be obtained in spherical coordinates. Therefore, more complicated coordinates  $\xi, \eta, \varphi$  were introduced in [119], which are related to the Cartesian coordinates in the following way:

$$\begin{aligned} x &= \sqrt{\mu - 1} R \sqrt{\xi^2 - 1} \sin \eta \cos \varphi \\ y &= \sqrt{\mu - 1} R \sqrt{\xi^2 - 1} \sin \eta \sin \varphi \end{aligned}$$

$$z = \sqrt{\frac{\mu - 1}{\mu}} R \xi \cos \eta. \quad (6.94)$$

The solution of (6.14) in these coordinates, finite at  $r = 0$ , is

$$\psi = P_n^{|m|}(\xi) P_n^{|m|}(\cos \eta) \exp(-im\varphi). \quad (6.95)$$

The sphere surface  $r = R$  is the coordinate surface  $\xi = \xi_R$  where

$$\xi_R = \sqrt{\frac{\mu}{\mu - 1}}. \quad (6.96)$$

Substitution of (6.93) and (6.95) into the boundary conditions (6.92) yields the equation

$$\xi_R \frac{[P_n^{|m|}(\xi_R)]'}{P_n^{|m|}(\xi_R)} + n - 1 + \mu_a m = 0 \quad (6.97)$$

where the prime denotes the differentiation with respect to the argument. This equation and the frequency dependences of  $\mu$  and  $\mu_a$  determine the eigenfrequencies of magnetostatic oscillations in a sphere.

As it should be expected, the eigenfrequencies do not depend on  $R$ . They depend on  $\omega_H$ ,  $\omega_M$ , and on three integers  $n$ ,  $m$ , and  $r$ . The integer  $r$  characterizes the number of the root of equation (6.97); by tradition, the number of the root is  $(r + 1)$  if  $m > 0$  and is  $r$  if  $m \leq 0$ . Therefore the quantity of roots is equal to  $(r_{\max} + 1)$  at  $m > 0$  and is equal to  $r_{\max}$  at  $m \leq 0$ . The analysis of (6.97) shows that  $r_{\max}$  is equal to the integral part of  $(n - |m|)/2$  [119].

The components of  $\mathbf{h} = \nabla\psi$  and  $\mathbf{m} = \vec{\chi}\mathbf{h}$  can be determined, for each mode, from (6.95). Positive and negative  $m$  values correspond, respectively, to the right-hand and to the left-hand rotation of the entire  $\mathbf{h}$  and  $\mathbf{m}$  pattern around the  $\mathbf{M}_0$  direction. The local polarization of  $\mathbf{h}$  and  $\mathbf{m}$  is, in general, elliptic and different at different points of the sphere.

Consider first the case of  $n = |m|$ . Equation (6.97) transforms then into

$$\mu + \frac{m}{|m|} \mu_a = -\frac{|m| + 1}{|m|}. \quad (6.98)$$

It is easy to make sure, taking (1.54) into account, that equation (6.98) can be satisfied only if  $m > 0$ . It has then, for each  $m$  value, only one root

$$\omega_{m,m,0} = \omega_H + \frac{m}{2m + 1} \omega_M \equiv \gamma H_{e0} + \gamma \frac{4\pi}{3} \frac{m - 1}{2m + 1} M_0. \quad (6.99)$$

The potential in this case is

$$\psi = \rho^m \exp(-im\varphi) \equiv (x - iy)^m \quad (6.100)$$

where  $\rho = \sqrt{x^2 + y^2}$ . The magnetization components are

$$m_x = im_y = (x - iy)^{m-1} \equiv \rho^{m-1} \exp[-i(m-1)\varphi]. \quad (6.101)$$

The magnetization has, for these modes, the right-hand circular polarization at all points, and its amplitude increases with growing distance from the  $z$  axis. In the simplest case of  $n = m = 1$  the magnetization does not depend on coordinates, and the frequency is equal to  $\gamma H_{e0}$ . This mode (1,1,0) is the *uniform mode* studied in detail in Section 1.5.

For the family of modes with  $n = m + 1$ , it follows from (6.97):

$$\mu + \frac{m}{|m|} \mu_a = -\frac{|m| + 3}{|m|}. \quad (6.102)$$

This equation is also satisfied only if  $m > 0$  and has, for each  $m$ , one root

$$\omega_{m+1,m,0} = \omega_H + \frac{m}{2m+3} \omega_M \equiv \gamma H_{e0} + \gamma \frac{4\pi}{3} \frac{m-3}{2m+3} M_0. \quad (6.103)$$

The potential and the magnetization components, for this family, gain an additional factor  $z$ , as compared with (6.100) and (6.101), so that the magnetization is equal to zero at the equatorial plane. The polarization is circular with right-hand rotation at every point, as for the family  $(m, m, 0)$ .

One can see from (6.99) and (6.103) that, for both considered families, the differences  $\omega - \gamma H_{e0}$  are proportional to  $M_0$  and *do not depend* on  $H_{e0}$ . This feature, as well as the circular polarization of  $h$  and  $m$ , takes place only for the modes  $(m, m, 0)$  and  $(m+1, m, 0)$ .

The frequencies and magnetization components can also be easily found for the modes with  $m = 0$ . In this case, (6.97) takes the form

$$\xi_R \frac{P'_n(\xi_R)}{P_n(\xi_R)} = -(n+1) \quad (6.104)$$

where  $P_n(\xi)$  are the Legendre polynomials [273]. This equation has no roots for  $n = 1$ . If  $n = 2$ , then  $P_2(\xi) = (3\xi^2 - 1)/2$ , the root of (6.104) is  $\xi_R^2 = 1/5$ , and

$$\omega_{2,0,1}^2 = \omega_H \left( \omega_H + \frac{4}{5} \omega_M \right). \quad (6.105)$$

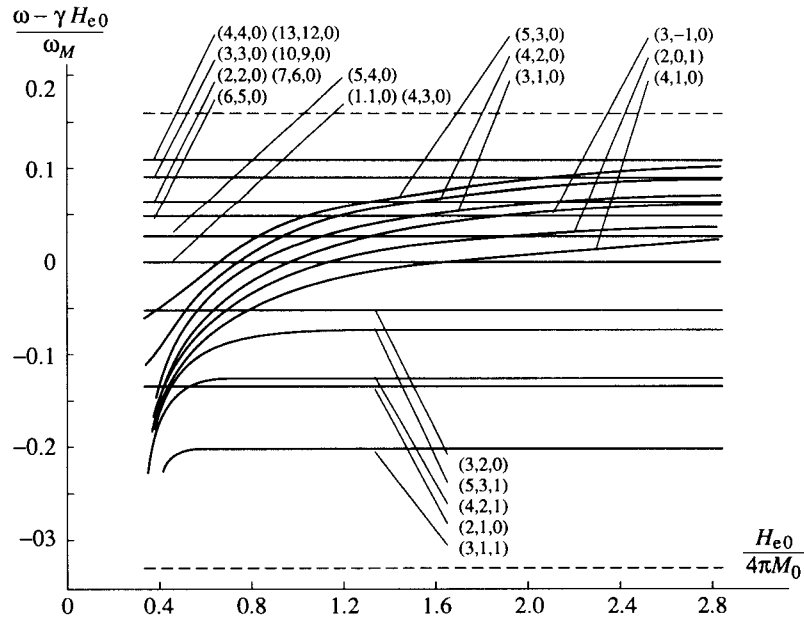
The magnetization components for the mode (2,0,1) are

$$m_x = \chi x + i\chi_a y \quad m_y = -i\chi_a x + \chi y. \quad (6.106)$$

The magnetization is now elliptically polarized, and the difference  $\omega - \gamma H_{e0}$  depends on  $H_{e0}$ , as for all magnetostatic modes of a sphere except the families  $(m, m, 0)$  and  $(m+1, m, 0)$ .

The calculated field and magnetization components and the eigenfrequencies for all magnetostatic modes of a sphere with  $n \leq 5$  are given in [119]. The field dependences of the frequencies for some modes are shown in Figure 6.16. One can see in this figure the numerous degenerations of modes: 'accidental' intersections of  $\omega$  vs  $H_{e0}$  curves, as well as the entire coincidence of the frequencies of modes  $(m, m, 0)$  and  $(3m+1, 3m, 0)$ . The eigenfrequencies of all magnetostatic



**FIGURE 6.16**

Eigenfrequencies of magnetostatic oscillations of a sphere versus external static magnetic field [119]. Dashed lines indicate the limits of the entire magnetostatic-mode spectrum.

modes of a sphere lie in the range (6.90) [119]. Hence, the resonance  $H_{e0}$  values at constant frequency are in the limits

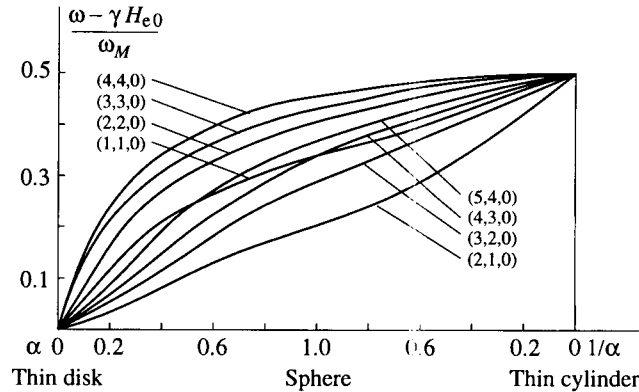
$$\frac{\omega}{\gamma} - \frac{2\pi}{3}M_0 < H_{e0} < \frac{\omega}{\gamma} + \frac{4\pi}{3}M_0. \quad (6.107)$$

It is worth noting that the measurement of differences between the frequencies of two magnetostatic modes from  $(m, m, 0)$  or  $(m + 1, m, 0)$  families is a precise and convenient method to determine the steady magnetization  $M_0$ .

Let us now cite some results concerning magnetostatic modes of an *ellipsoid of revolution* (spheroid) magnetized along the axis of revolution [432]. The setting up of the problem and the assumptions are the same as in the case of a sphere. Many properties of magnetostatic oscillations, mentioned above for a sphere, take place for a spheroid, as well.

In particular, the rule for determining the quantity of modes with given  $m$  and  $n$  remains the same as for a sphere. For the mode families  $(m, m, 0)$  and  $(m + 1, m, 0)$ , the difference  $\omega - \omega_H$  is independent of  $\omega_H$  and the magnetization is circularly polarized.

The frequencies of all magnetostatic modes of a spheroid (with semiaxes  $a$



**FIGURE 6.17**

Dependence of the magnetostatic-mode frequencies of an ellipsoid of revolution on the ratio of ellipsoid axes [432]. Note that  $H_0$  is the internal field.

and  $c$ ) lie in the same range (6.90) where now  $\omega_H = \gamma H_{e0} - \gamma N_z M_0$ . At  $a/c \equiv \alpha \rightarrow 0$  (when the spheroid transforms into an infinitely thin disc), the mode spectrum turns into a point  $\omega = \omega_H = \gamma(H_{e0} - 4\pi M_0)$ . At  $\alpha \rightarrow \infty$  (infinitely thin cylinder) it turns into a point  $\omega = \omega_H + \omega_m/2 = \gamma(H_{e0} + 2\pi M_0)$  (Figure 6.17).

### 6.3.3 Damping, excitation, and coupling

To take the damping of magnetostatic oscillations into account we have to substitute the complex  $\mu$  and  $\mu_a$  values into the characteristic equations, e.g., (6.97). The imaginary parts  $\omega''_{\nu}$  of the roots of these equations represent the damping. It appears that the quality factors of nonuniform magnetostatic oscillations differ little from the quality factor of the uniform mode.

The magnetostatic oscillations in small samples usually are excited by the electromagnetic fields of resonators or waveguides in which the samples are placed. In the theory of such excitation the following *orthogonality relations* [318] are used:

$$\begin{aligned} \int_V \mathbf{m}_{\nu}(\mathbf{r}) \times \mathbf{m}_{\nu'}(\mathbf{r}) dV &= 0 \\ \int_V \mathbf{m}_{\nu}(\mathbf{r}) \mathbf{m}_{\nu'}^*(\mathbf{r}) &= D\Delta_{\nu\nu'} \\ \int_V \mathbf{m}_{\nu}(\mathbf{r}) \times \mathbf{m}_{\nu'}^*(\mathbf{r}) dV &= iz_0 D\Delta_{\nu\nu'}. \end{aligned} \quad (6.108)$$

Here  $\nu$  and  $\nu'$  are the joint mode indices including  $n$ ,  $m$ , and  $r$ ;  $\mathbf{m}_{\nu}(\mathbf{r})$  and  $\mathbf{m}_{\nu'}(\mathbf{r})$

are the normalized magnetizations of different modes,  $D$  is the normalization constant; the integration is over the volume of the sample;  $\Delta_{\nu\nu'}$  is the Kronecker delta-symbol (Appendix C); and  $z_0$  is a unit vector directed along  $\mathbf{M}_0$ .

As the functions  $\mathbf{m}_\nu(\mathbf{r})$  make up a full system, the magnetization of *forced oscillations* can be written in the form

$$\mathbf{m}(\mathbf{r}) = \sum_{\nu} C_{\nu} \mathbf{m}_{\nu}(\mathbf{r}). \quad (6.109)$$

Taking the orthogonality relations (6.108) into account, we can obtain the following expression for the coefficients  $C_{\nu}$ :

$$C_{\nu} = C \omega^2 \frac{\int_V \mathbf{h}(\mathbf{r}) \mathbf{m}_{\nu}^*(\mathbf{r}) dV}{\omega^2 - \omega'_{\nu}{}^2 + 2i\omega'_{\nu}\omega''_{\nu}} \quad (6.110)$$

where  $\mathbf{h}(\mathbf{r})$  is the given field and  $C$  is a constant depending on the normalization of eigenfunctions  $\mathbf{m}_{\nu}(\mathbf{r})$ .

According to (6.110), the coefficients  $C_{\nu}$  change in a resonance manner with varying  $\omega$  or  $H_{e0}$ . And if  $\omega'_{\nu}$  is sufficiently small, the magnetostatic modes are excited one after another as  $\omega$  or  $H_{e0}$  varies.

It is clear from (6.110) that the condition for excitation of a certain mode is that the 'excitation integral' in the numerator of (6.110) should not be equal to zero. If the field  $\mathbf{h}(\mathbf{r})$  is uniform, this integral differs from zero only for the uniform mode (1,1,0). To excite a nonuniform mode, a *nonuniform* field is needed. The amplitude of the excited mode is greater the nearer the field pattern is to the structure of the magnetization of the mode to be excited.

In reality, the nonuniform magnetostatic modes are often observed when the excitation integral in (6.110) seems to be equal to zero. This is due sometimes to the inaccuracy of the sample location or to the disturbance of the field by the sample holder. But there are also more fundamental reasons of such 'illegal' excitation.

One of them is the influence of *magnetocrystalline anisotropy*. If  $\mathbf{M}_0$  is directed along the axis in a uniaxial crystal or along (100) or (111) axes in a cubic crystal, then, according to the above-mentioned general theorem (Section 6.1), the entire spectrum of  $H_{e0}$  resonance values of the magnetostatic modes in a single-crystal sample will be shifted by the quantity  $H^A$  with respect to the spectrum in an isotropic sample. However, the situation becomes much more complicated for an arbitrary  $\mathbf{M}_0$  direction. In this case, the solutions of the magnetostatic equations (the eigenmodes) are no more the Walker modes. But, if the anisotropy is not very large, it is advisable to seek the solutions in the form of series in the Walker modes. Krivchenkov and Pil'shchikov showed [235] that (for a sphere) only such terms in these series are not equal to zero which correspond to the Walker modes with the same parity (even or odd) of the  $n$  values and with the same parity of the  $m$  values, relative to the  $n$  and  $m$  values of the initial mode.

Let us discuss the same problem in terms of coupled oscillations. We now have to say that the anisotropy leads to the *coupling* of oscillations, which were

independent (eigen) modes in an isotropic sample. The coupling results in the frequency shift of the original mode and in the excitation of all modes that are coupled with it. Near the points of degeneration [i.e., of crossing of the unperturbed curves  $\omega(H_{e0})$  of the coupled modes] the repulsion of these curves occurs (e.g., [121]).

Returning to an isotropic medium, we remind the reader that Walker's theory is valid for a system with *cylindrical* symmetry in respect to the  $M_0$  direction. If this symmetry is *broken* (for an arbitrary ellipsoid or for an ellipsoid of revolution but magnetized in an arbitrary direction), the situation is similar to the above-considered situation in the case of an anisotropic medium. Any disturbances of cylindrical symmetry, including macroscopic defects, as pores, clifts, and so on, can be treated (in terms of coupled oscillations) as factors leading to the coupling of Walker's modes. This is the second reason of 'illegal' excitation of the nonuniform magnetostatic oscillations.

The third reason is the *finite* sample *dimensions*. It was pointed out in Section 5.3 that, for a sphere with finite radius, the 'retarding' terms in Maxwell's equations (discarded in the zero magnetostatic approximation) result in the correction (5.41) of the resonance field of the uniform mode. Similar corrections take place for the nonuniform modes [318] but decrease with increasing  $n$  and  $m$ . The influence of the 'retarding' terms is also the source of coupling of magnetostatic modes. Sui Yangshen has shown [398] that the coupling appears, in this case, between modes with the same parity of  $n$  and with the same  $m$  values.

According to Walker's theory, the magnetostatic oscillations arise due to the resonance frequency dependence (1.54) of the  $\vec{\mu}$  components. This dependence takes place for any *magnetized* isotropic substance. Therefore, nonuniform magnetostatic oscillations should be observed even in paramagnets, but the range (6.90) is very narrow in this case at not very low temperatures.

However, neither the specific form (1.54) of the  $\vec{\mu}$  components, nor the existence of the steady magnetization are the necessary conditions for the appearance of nonuniform magnetostatic oscillations. They were observed [45] in a uniaxial *antiferromagnet* in the antiparallel state (Section 3.2), in which the steady magnetization is equal to zero.

# 7

## *Spin waves*

### 7.1 Spin waves in unbounded ferromagnet

In the preceding chapter, the waves of magnetization were considered in such range of wave numbers  $k$  that the influence of exchange interaction on the dispersion law could be ignored. Now we begin to study the waves with larger  $k$  values when this interaction is to be taken into account. Such waves are usually referred to as spin waves, although this term can be related, as well, to the waves studied in Chapter 6.

In Section 7.1 we consider spin waves in an unbounded uniform ferromagnet magnetized to saturation. We will use, as before, the continuum model describing the ferromagnet by the magnetization  $\mathbf{M}(\mathbf{r}, t)$ .

#### 7.1.1 Energy and effective field of exchange interaction

The energy of exchange interaction in a ferromagnet can be represented by the sum (2.11) of the uniform term  $U_{\text{ex}0}$  and the *nonuniform* term  $U_{\text{ex}\sim}$ . The latter is equal to the increase of the exchange energy due to the nonparallelism of neighboring magnetic moments, i.e., to the dependence of  $\mathbf{M}$  on coordinates. This term can be written in the form [14]

$$U_{\text{ex}\sim} = \frac{1}{2} \sum_{p=1}^3 \sum_{s=1}^3 q_{ps} \frac{\partial \mathbf{M}}{\partial x_p} \frac{\partial \mathbf{M}}{\partial x_s} \quad (7.1)$$

where  $q_{ps}$  are the components of a tensor  $\vec{q}$ . Using (2.7), we obtain from (2.12) and (7.1) the effective field of the exchange interaction

$$\mathbf{H}_{\text{ex}} = \mathbf{H}_{\text{ex}0} + \mathbf{H}_{\text{ex}\sim} \equiv \vec{\Lambda} \mathbf{M} + \sum_{p=1}^3 \sum_{s=1}^3 q_{ps} \frac{\partial^2 \mathbf{M}}{\partial x_p \partial x_s}. \quad (7.2)$$

For an *isotropic* ferromagnet,  $\Lambda$  and  $q$  are scalars,  $\mathbf{H}_{\text{ex}0}$  transforms into (1.57),

and  $H_{\text{ex}\sim}$  takes the form

$$H_{\text{ex}\sim} = q\nabla^2 M. \quad (7.3)$$

In this chapter we deal only with a ferromagnet magnetized to saturation, in which  $M_0$  does not change quickly in space. Then, the field  $H_{\text{ex}\sim}$  has only an alternating component. Its complex amplitude in an isotropic ferromagnet is

$$h_{\text{ex}} = q\nabla^2 m. \quad (7.4)$$

The quantities  $D$  and  $\eta$  connected with  $q$  by the relations

$$\eta = \gamma D = \gamma M_0 q \quad (7.5)$$

are also used. All three quantities can be called the *nonuniform exchange constants* or constants of spin stiffness.

### 7.1.2 Dispersion law

The dispersion relation for spin waves was obtained at first by Bloch [52] on the microscopic model. This relation was generalized by Holstein and Primakoff [184] (Section 7.4). On the macroscopic, continuum model, the spin-wave dispersion law can be derived by two, quite equivalent, methods.

The *first* method is based on expression (6.4), which is valid regardless of whether the exchange interaction is taken into account or not; only the form of  $\mu$  depends on that (dealing with a ferromagnet magnetized to saturation, we assume  $\mu_{\parallel} = 1$ ). To obtain the expression for  $\mu$  we must solve the equation of motion, e.g., (2.18) with the effective field (7.4). For a plane wave,  $m = m_0 \exp(-ikr)$ ,  $h = h_0 \exp(-ikr)$ , and it follows from (7.4):

$$h_{\text{ex}} = -qk^2 m. \quad (7.6)$$

It is easy to make sure that equation (2.18) with this field differs from equation (1.66) only by the replacement

$$\omega_H \rightarrow \omega_H + \eta k^2. \quad (7.7)$$

Therefore, we can, without solving anew the equation of motion, make this replacement in the final expressions for  $\mu$  components. In particular, we get from (1.54)

$$\mu = \frac{(\omega_H + \eta k^2)(\omega_H + \eta k^2 + \omega_M) - \omega^2}{(\omega_H + \eta k^2)^2 - \omega^2} \quad \mu_a = \frac{\omega \omega_M}{(\omega_H + \eta k^2)^2 - \omega^2}. \quad (7.8)$$

If the dissipation should be taken into account, it is sufficient to make the replacement (1.68) in (7.8)

The parameters of the medium  $\mu$  and  $\mu_a$  now depend not only on frequency but also on the wave number  $k$ . Such dependence (in general case, the dependence

on the direction of  $\mathbf{k}$ , as well) is called *space dispersion*.<sup>1</sup>

Substituting (7.8) into (6.3) and assuming  $\mu_{\parallel} = 1$ , we get the dispersion relation

$$\begin{aligned}\omega^2 &= \left(\omega_H + \eta k^2\right) \left(\omega_H + \eta k^2 + \omega_M \frac{k_x^2 + k_y^2}{k^2}\right) \\ &\equiv \left(\omega_H + \eta k^2\right) \left(\omega_H + \eta k^2 + \omega_M \sin^2 \theta_k\right).\end{aligned}\quad (7.9)$$

It can be rewritten as

$$\omega^2 = A_k^2 - |B_k|^2 \quad (7.10)$$

where

$$A_k = \omega_H + \eta k^2 + \frac{1}{2}\omega_M \sin^2 \theta_k \quad |B_k| = \frac{1}{2}\omega_M \sin^2 \theta_k. \quad (7.11)$$

The *second* method of deriving the dispersion law (7.9) was used by Herring and Kittel [180]. They found, first of all, the dependence of the internal magnetic field  $\mathbf{h}_M$  on the ac magnetization, which is determined by the magnetostatic equations (6.2). For plane waves, it follows from these equations that

$$\mathbf{h}_M = -\frac{4\pi}{k^2} \mathbf{k}(\mathbf{m}\mathbf{k}). \quad (7.12)$$

This field is substituted, then, into the equation of motion (2.18), which, in this case, takes the form

$$i\omega \mathbf{m} + (\omega_H + i\alpha\omega) \mathbf{m} \times \mathbf{z}_0 + \frac{\omega_M}{4\pi} \mathbf{z}_0 \times (\mathbf{h}_{\text{ex}} + \mathbf{h}_M) = 0 \quad (7.13)$$

( $\mathbf{z}_0$  is a unit vector parallel to  $\mathbf{M}_0$ ). Projecting (7.13) with  $\alpha = 0$  onto the axes  $x$  and  $y$  and equating the determinant of the obtained system to zero, we get (7.9).

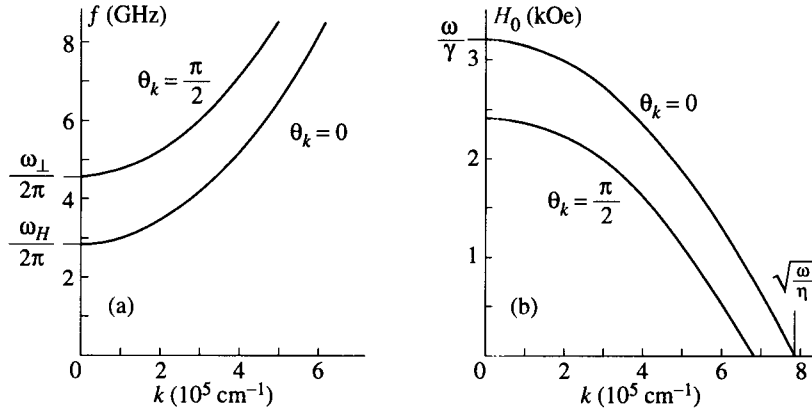
The curves  $\omega$  vs  $k$  at constant  $H_0 = \omega_H/\gamma$  and the curves  $H_0$  vs  $k$  at constant  $\omega$  are plotted in Figure 7.1. At very large  $k$  values, when  $\eta k^2 \gg \omega_H, \omega_M$ , the spin-wave dispersion relation approaches the quadratic law  $\omega = \eta k^2$ , obtained in 1930 by Bloch [52]. If  $\omega_M < \omega_H + \eta k^2$ ,

$$\omega \cong A_k \equiv \omega_H + \eta k^2 + \frac{1}{2}\omega_M \sin^2 \theta_k. \quad (7.14)$$

The spin-wave *phase velocity*  $v_{\text{ph}} = \omega/k$  passes through a minimum at certain values of  $k = k_1$  and  $\omega = \omega_1$  depending on the angle  $\theta_k$ . In particular, at  $\theta_k = 0$

$$k_1 = \sqrt{\frac{\omega_H}{\eta}} \quad \omega_1 = 2\omega_H \quad v_{\text{ph min}} = 2\sqrt{\eta\omega_H}. \quad (7.15)$$

<sup>1</sup>There exists another type of the space dispersion, a linear dependence of the antisymmetric  $\vec{\epsilon}$  components on  $k$  leading to the phenomenon of natural optical activity (e.g., [246]).

**FIGURE 7.1**

Dispersion characteristics of spin waves in an isotropic ferromagnet with  $M_0 = 139$  G and  $\eta = 9.16 \times 10^{-2}$  (YIG at room temperature): (a)  $H_0 = \text{const} = 1$  kOe, (b)  $\omega = \text{const} = 2\pi \cdot 9$  GHz.

The group velocity

$$v_{\text{gr}} \equiv \frac{\partial \omega}{\partial k} = \frac{2\eta k}{\omega} \left( \omega_H + \eta k^2 + \frac{1}{2} \omega_M \sin^2 \theta_k \right) \equiv 2\eta k \xi \quad (7.16)$$

where  $\xi$  is the ratio of the approximate value (7.14) of the frequency to the exact value.

Expression (7.9) can be written in the form

$$\eta k^2 = \omega_{Hc}(\theta_k) - \omega_H \quad (7.17)$$

where

$$\omega_{Hc}(\theta_k) \equiv \gamma H_{0c}(\theta_k) = \sqrt{\omega^2 + \left( \frac{1}{2} \omega_M \sin^2 \theta_k \right)^2} - \frac{1}{2} \omega_M \sin^2 \theta_k. \quad (7.18)$$

One can see from (7.17), as well as from Figure 7.1, that the propagating spin waves (with  $k^2 > 0$ ) exist only if  $H_0 < H_{0c}(\theta_k)$ . The quantity  $H_{0c}(\theta_k)$  is maximal at  $\theta_k = 0$ :

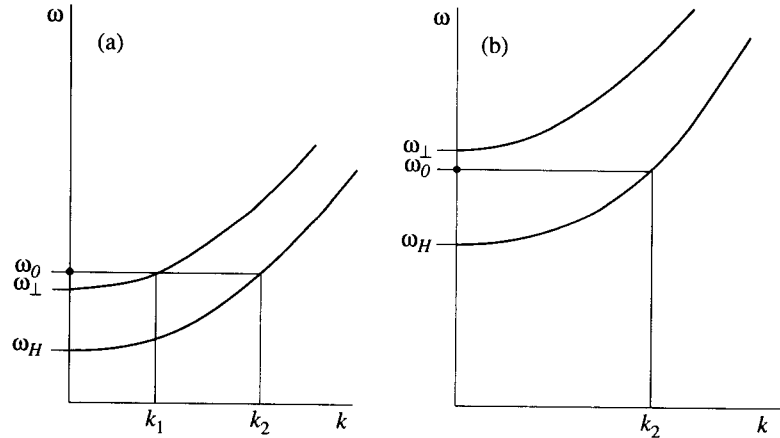
$$H_{0c}(0) = \frac{\omega}{\gamma}. \quad (7.19)$$

The maximal value of  $k$  also takes place at  $\theta_k = 0$ :

$$k_{\text{max}} = \sqrt{\frac{\omega}{\eta}}. \quad (7.20)$$

For YIG at 9 GHz,  $k_{\text{max}} \cong 8 \times 10^5$ .



**FIGURE 7.2**

Degeneration of spin waves with uniform oscillations of magnetization in a ferromagnetic sphere: (a) when condition (6.8) is satisfied, (b) when it is not satisfied.

Let us discuss now the *degeneration* of the uniform precession of magnetization with spin waves. If  $k \gg d^{-1}$  (where  $d$  is the minimal sample dimension), the influence of the boundary conditions for the ac fields on the spin-wave dispersion law is immaterial. Then, expression (7.9) can be used for the spin-wave frequency, together with formula (1.92) for the frequency of uniform precession. It is easy to show that the degeneration always exists if the exchange interaction is taken into account, contrary to nonexchange spin waves (Section 6.1). The degeneration takes place in the range  $k_1 < k < k_2$  (Figure 7.2) if condition (6.8) is satisfied, and in the range  $0 < k < k_2$  if this condition is not satisfied. For an ellipsoid of revolution,

$$k_2 = \sqrt{\frac{\gamma N_{\perp} M_0}{\eta}} \quad (7.21)$$

Consider now spin waves in an *anisotropic* (single-crystal) ferromagnet. We will not take into account the anisotropy of the nonuniform exchange constant (which usually turns out to be small), i.e., we will regard  $q$  as a scalar and use formula (7.4). When we substitute the effective field (7.4) into the linearized equation of motion for an anisotropic ferromagnet (Section 2.3), we notice that this equation differs from the equation without  $\mathbf{h}_{\text{ex}}$  only by the replacement (7.7). Therefore, it is sufficient to make this replacement in the corresponding nonexchange dispersion relations, e.g., in (6.18) or (6.19). Let us cite, as an example, the simple expression

$$\left(\frac{\omega}{\gamma}\right)^2 = (H_0 + H^A + Dk^2) (H_0 + H^A + Dk^2 + 4\pi M_0 \sin^2 \theta_k) \quad (7.22)$$

which is valid in the following cases: when  $M_0$  is directed along the axis—or lies in the easy plane—of a uniaxial crystal, when  $M_0$  is directed along the  $\langle 100 \rangle$  axis of a cubic crystal, and when it is directed along the  $\langle 111 \rangle$  axis of such crystal. In the first two cases, as it was pointed out in Section 6.1,  $H^A = 2K_1/M_0$ , and in the third case  $H^A = -4/3 K_1/M_0$ .

### 7.1.3 Magnetization, field components, and damping

To get the ac magnetization components of a spin wave we must find the solutions of the system obtained by projecting (7.13) (with  $\alpha = 0$ ) onto coordinate axes; expressions (7.6), (7.12), and (7.9) are to be taken into account. Directing the coordinate axes in such way that  $\mathbf{k}$  vector will lie in  $yz$  plane, we get

$$\frac{m_y}{m_x} = -i \left( 1 + \frac{\omega_M \sin^2 \theta_k}{\omega_H + \eta k^2} \right)^{-1/2} \equiv -i \frac{A_k + |B_k|}{A_k - |B_k|}. \quad (7.23)$$

If  $\theta_k = 0$ , then  $m_y = -im_x$ , i.e., the ac magnetization is *right-hand circularly* polarized. If  $\theta_k \neq 0$ , the polarization is *elliptical*; the polarization ellipse, as it follows from (7.23), is compressed in the direction of the  $\mathbf{k}$  projection on  $xy$  plane. The ellipticity (1.101) decreases with increasing  $k$ .

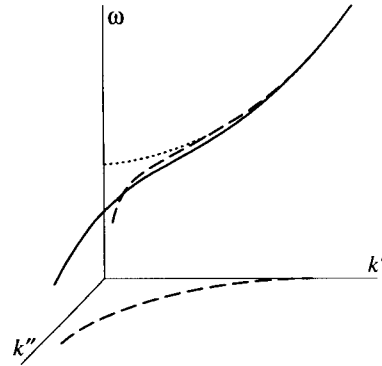
The electromagnetic-field components of a spin wave can be found using the general solutions of Maxwell's equations for propagating waves in an unbounded medium (Section 4.2). But the expressions obtained with allowance for exchange interaction should now be taken for  $\mu$  and  $\mu_a$ . The energy flow can be calculated using the general formula (4.69). In contrast to nonexchange magnetostatic waves in an unbounded medium (Section 6.1), the energy flow is now not equal to zero.

To analyze the *damping* of spin waves we can make the replacement (1.68) in the dispersion relation (7.9). Two statements of the problem are possible. In the first case, the attenuation of a *stationary* propagating wave ( $\omega'' = 0$ ) is considered. In the second case, we are concerned with the damping of a standing wave ( $k'' = 0$ ). Formula (6.7), which relates  $k''$  (for the first case) to the  $\omega''$  (for the second case) holds, if the losses are small, for an arbitrary dispersion law (Section 6.1). Hence, this formula is valid for exchange spin waves, too.

In the first case ( $\omega'' = 0$ ,  $k = k' - ik''$ ) two real equations that are equivalent to the complex dispersion relation give the dependence of  $k'$  and  $k''$  on  $\omega$ . Without dwelling on the solution of these equations, we only cite the *exact* formula

$$k'k'' = \frac{\alpha\omega}{2\eta}. \quad (7.24)$$

The dependence  $\omega(k', k'')$  is shown schematically in Figure 7.3. If  $k'' \ll k'$ , the value of  $k$ , found without regard to losses, can be taken for  $k'$ ; the value of  $k''$  is then obtained from (7.24). But if the condition  $k'' \ll k'$  is not satisfied, one of the quantities,  $k'$  or  $k''$ , should be found from the exact equations following from the complex dispersion relation; the other can be found using (7.24).

**FIGURE 7.3**

Dispersion characteristics of a spin wave ( $\theta_k = 0$ ) with allowance for losses. Dashed lines are projections of the curve  $\omega(k', k'')$  onto the planes  $(\omega, k')$  and  $(k', k'')$ , dotted line represents  $\omega(k')$  dependence when losses are not taken into account.

Expression (7.24) shows that  $k''$  increases with decreasing  $k'$  and becomes equal to it at

$$k' = \sqrt{\frac{\alpha\omega}{2\eta}} \equiv k_{\min}. \quad (7.25)$$

When  $k''$  exceeds  $k'$ , the process cannot be referred to as a propagating wave. An estimate for a YIG single crystal ( $\Delta H = 0.3$  Oe) gives  $k_{\min} = 4 \times 10^3$ . It should be noted that the 'disappearance' of spin waves in an unbounded medium at  $k'' > k'$  is the consequence of the decrease of group velocity, and it is removed by taking boundary conditions into account. So, spin waves with small  $k'$  in plates and rods, considered in Section 6.2, do not disappear.

In the second case ( $k'' = 0$ ,  $\omega = \omega' + i\omega''$ ), the inequality  $\omega'' < \omega'$  is always satisfied if  $\alpha < 1$ . The complex dispersion equation can now be solved in the first approximation assuming  $\omega'$  to be the same as in the absence of losses. Then,

$$\omega'' = \alpha\omega\xi \quad (7.26)$$

where  $\xi$  is the same as in (7.16).

The following quantities are often used in examining the damped spin waves: the *free path*

$$l_k = \frac{1}{2k''} \quad (7.27)$$

and *time of life*

$$\tau_k = \frac{1}{2\omega''}. \quad (7.28)$$

They characterize the damping, respectively, in space and in time of the squared spin-wave amplitude. These quantities have direct meaning for the quasiparticles that correspond to spin waves (Section 7.3).

---

## 7.2 Spin waves in bounded bodies

In this section we will study the influence of the nonuniformity of the medium and, first of all, the influence of the boundaries between different media on spin-wave propagation. As in Section 6.2, the equation of motion and the Maxwell equations should now be solved making allowance for the electrodynamic boundary conditions. The magnetostatic approximation can be used (for nonmetallic ferromagnets)<sup>2</sup> even more rightfully than in Section 6.2. But first, the effective field of exchange interaction should be substituted in the equation of motion. And second, the supplementary (exchange) boundary conditions should be introduced.

### 7.2.1 Exchange boundary conditions

The need of supplementary boundary conditions, when the exchange interaction is taken into account, follows formally from the fact that the *derivatives* of  $\mathbf{m}$ , with respect to coordinates, appear in the equations of motion. Therefore, the order of differential equations which are obtained from the equation of motion and the electrodynamic equations increases. Solutions of these equations contain more arbitrary constants, and 'ordinary' electrodynamic boundary conditions are not enough to find these constants.

The physical reason for introducing the supplementary boundary conditions is that the fields, acting on magnetic moments in a *thin layer* near the boundary, differ essentially from the fields inside the sample

The supplementary (exchange) boundary conditions, as Rado and Weertman have shown [325], can be deduced from the equation of motion of the magnetization, like the electrodynamic boundary conditions are deduced from the Maxwell equations. Let us write the equation of motion (2.9) in the form

$$\frac{1}{\gamma} \frac{\partial \mathbf{M}}{\partial t} + \mathbf{M} \times \mathbf{H}_{\text{ef}} + q \mathbf{M} \times \nabla^2 \mathbf{M} + \mathbf{M} \times \mathbf{H}_s = 0 \quad (7.29)$$

where  $q \nabla^2 \mathbf{M}$  is the nonuniform part (7.3) of the exchange effective field;  $\mathbf{H}_s$  is the effective field of the surface anisotropy, which exists only in the thin boundary layer; and  $\mathbf{H}_{\text{ef}}$  includes the external magnetic field and all effective fields which vary slowly in space: effective fields of anisotropy, effective fields responsible for dissipation, etc.

---

<sup>2</sup>Spin waves in metals will be considered in Section 14.2.

The *surface anisotropy*, which describes the special conditions in the boundary layer, is usually regarded as uniaxial, with easy or hard axis normal to the boundary surface. However, it can be unidirectional, i.e., when the opposite directions of the normal to the boundary are not equivalent. A more general case is also possible when the easy directions lie on a cone with the axis normal to the boundary. We will consider the case of *uniaxial* surface anisotropy. Then, taking into account only the first constant of this anisotropy, we can write, according to (2.7) and (2.40),

$$\mathbf{H}_s = \frac{2K_1}{M_0^2} (\mathbf{M}\mathbf{n}_0)\mathbf{n}_0 \quad (7.30)$$

where  $\mathbf{n}_0$  is a unit external normal to the boundary of the ferromagnet.

Consider a boundary of a ferromagnet with a nonmagnetic medium and integrate (7.29) over a volume  $V$  (Figure 7.4) of a disc 'slit' by the boundary. The thickness of the disc  $2d$  is assumed to be small but larger than the thickness  $d_s$  of the boundary layer. The two first terms of (7.29) make negligible contributions, and the result of integration can be written in the form

$$I_1 + I_2 = 0 \quad I_1 = q \int_V \mathbf{M} \times \nabla^2 \mathbf{M} dV \quad I_2 = 2 \int_V \frac{K_1}{M_0^2} (\mathbf{M}\mathbf{n}_0) \mathbf{M} \times \mathbf{n}_0 dV. \quad (7.31)$$

Transforming  $I_1$  into a surface integral and assuming the area of the disk  $\sigma$  to be small, we get

$$I_1 = -\sigma q \mathbf{M} \times \frac{\partial \mathbf{M}}{\partial n} \quad (7.32)$$

$$I_2 = \sigma \int_0^{-d_s} \frac{2K_1}{M_0^2} (\mathbf{M}\mathbf{n}_0) (\mathbf{M} \times \mathbf{n}_0) d\zeta \quad (7.33)$$

where  $\zeta$  is the coordinate in the direction of  $\mathbf{n}_0$ . Integral (7.33) can be written as

$$I_2 = \sigma \frac{2K_s}{M_0^2} (\mathbf{M}\mathbf{n}_0) \mathbf{M} \times \mathbf{n}_0 \quad (7.34)$$

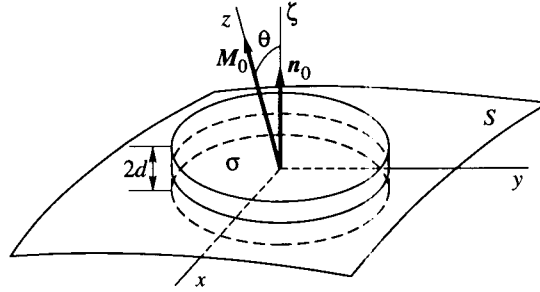
which may be regarded as a definition of the constant of the surface anisotropy  $K_s$ . If  $M_0$  does not depend on  $\zeta$ , then

$$K_s = \int_0^{-d_s} K_1 d\zeta. \quad (7.35)$$

Substituting (7.32) and (7.34) into (7.31), we get the *boundary condition*

$$q \mathbf{M} \times \frac{\partial \mathbf{M}}{\partial n} + \frac{2K_s}{M_0^2} (\mathbf{n}_0 \mathbf{M}) \mathbf{n}_0 \times \mathbf{M} = 0 \quad (7.36)$$

which is applied to the vector  $\mathbf{M}$  in the ferromagnet outside a thin boundary layer. This layer is excluded from consideration, and its properties are taken into account by a single parameter  $K_s$ .



**FIGURE 7.4**  
Boundary of a ferromagnet ( $\zeta < 0$ ) with a nonmagnetic medium.

In the case of *small oscillations* of magnetization, we substitute  $\mathbf{M} = \mathbf{M}_0 + \mathbf{m} \exp(i\omega t)$  into (7.36). Then, assuming  $\mathbf{M}_0 = \text{const}$  (in the absence of domains) and equating the sum of terms linear in  $\mathbf{m}$  to zero, we obtain the exchange boundary condition for the complex amplitude  $\mathbf{m}$ :

$$\mathbf{z}_0 \times \frac{\partial \mathbf{m}}{\partial n} + \xi \left[ (\mathbf{n}_0 \mathbf{m}) \mathbf{n}_0 \times \mathbf{z}_0 + (\mathbf{n}_0 \mathbf{z}_0) \mathbf{n}_0 \times \mathbf{m} \right] = 0. \quad (7.37)$$

Here  $\mathbf{z}_0$  is a unit vector in the direction of  $\mathbf{M}_0$  and

$$\xi = \frac{2K_s}{qM_0^2}. \quad (7.38)$$

This parameter can be either positive or negative, according to the sign of  $K_s$ .

Projecting (7.37) onto the coordinate axes shown in Figure 7.4, we obtain the boundary conditions in the form proposed by Soohoo [374]:

$$\frac{\partial m_x}{\partial n} + \xi m_x \cos 2\theta = 0 \quad \frac{\partial m_y}{\partial n} + \xi m_y \cos^2 \theta = 0 \quad (7.39)$$

where  $\theta$  is the angle between  $\mathbf{M}_0$  and the normal to the boundary surface (Figure 7.4). If  $\theta = 0$  (normal magnetization),

$$\frac{\partial m_{x,y}}{\partial n} + \xi m_{x,y} = 0 \quad (7.40)$$

and for  $\theta = \pi/2$  (tangential magnetization),

$$\frac{\partial m_x}{\partial n} - \xi m_x = 0 \quad \frac{\partial m_y}{\partial n} = 0. \quad (7.41)$$

The parameter  $\xi$  characterizes the degree of fastening ('pinning') of magnetic moments at the boundary and can be called the *pinning parameter*. In the limiting case of  $\xi = 0$  (no pinning or *free magnetic moments*), it follows from (7.39):

$$\frac{\partial \mathbf{m}}{\partial n} = 0. \quad (7.42)$$

In the other limiting case of *perfect pinning* ( $\xi \rightarrow \infty$ ), if  $\theta \neq \pi/2$ ,

$$m = 0. \quad (7.43)$$

The boundary condition (7.42) was first used by Ament and Rado [16], and condition (7.43) was proposed by Kittel [223]. The general case was studied by Rado and Weertman [325] and by Kaganov [195].

It should be noted that the relative values of the first and second terms in (7.39), (7.40), or (7.41) depend not only on  $\xi$  but also on the rate of change of the ac magnetization in the direction of the normal to the boundary surface. For spin waves, these values depend on the projection of  $\mathbf{k}$  onto this direction.

### 7.2.2 Standing spin waves in films

Proceeding to the study of spin waves in ferromagnetic films, consider first the case when the projection of the wave vector onto the film surface  $k_{\parallel} = 0$ . Such standing spin waves can be regarded as magnetization oscillations, uniform over the film surface and nonuniform in the direction normal to the surface. Kittel [223] predicted that such oscillations can be excited by a *uniform* ac magnetic field. Seavey and Tannenwald [355] corroborated this prediction experimentally. This phenomenon was called spin-wave resonance (SWR) and was investigated in a wealth of experimental and theoretical works (see, e.g., books [333, 374] and a review article [125]).

Let us consider first the *eigenmodes* of standing spin waves in films, in the absence of damping and exciting field. We have to find joint solutions of the equation of motion and magnetostatic equations that satisfy the electrodynamic and the above-studied exchange boundary conditions. Solving this problem, we can apply the same two methods as in the case of waves in an unbounded medium (Section 7.1). Using the second of these methods, we must first find the relation between magnetic field and magnetization that follows from magnetostatic equations with electrodynamic boundary conditions. From expression (7.12) we obtain in the present case, when  $\mathbf{k}$  is parallel to  $\mathbf{n}_0$ ,

$$\mathbf{h}_M = -4\pi\mathbf{n}_0(m\mathbf{n}_0). \quad (7.44)$$

For eigenoscillations,  $\mathbf{h}_M$  is the total ac magnetic field. It is equal to zero outside the film and has no tangential component inside. Thus, the electrodynamic boundary condition  $h_{\tau 1} = h_{\tau 2}$  is satisfied. It is easy to make sure that the second boundary condition,  $b_{n 1} = b_{n 2}$ , is also satisfied by the field (7.44). This field must be substituted into (7.13), and the solutions of this equation that satisfy the *exchange* boundary conditions are to be found.

Consider the case of a *normally* magnetized film. In this case,  $\mathbf{h}_M = 0$  not only outside but also inside the film. The cylindrical symmetry of the system requires the use of circular magnetization components  $m_{\pm}$ . The condition of the existence of nonzero solutions of (7.13) (with  $\alpha = 0$ ) results in the expression for

eigenfrequencies

$$\omega_{\pm} = \pm (\omega_H + \eta k_z^2). \quad (7.45)$$

As  $\omega_{\pm} > 0$  by definition, oscillations with left-hand polarization (with frequency  $\omega_-$ ) exist only at imaginary  $k_z$  and sufficiently large  $|k_z|$ . The frequency  $\omega_+$  (for real  $k_z$ ) coincides with the frequency (7.9) of spin waves propagating in the direction of  $M_0$  in an unbounded ferromagnet.

Let us examine the case when the pinning parameter has different values at different sides of the film. The exchange boundary conditions, according to (7.40), should now be written as

$$\begin{aligned} -\frac{\partial m_{\pm}}{\partial z} + \xi_1 m_{\pm} &= 0 & \text{at } z = 0 \\ \frac{\partial m_{\pm}}{\partial z} + \xi_2 m_{\pm} &= 0 & \text{at } z = d. \end{aligned} \quad (7.46)$$

The solutions can be sought in the form

$$m_{\pm} = A_{\pm} \cos k_z z + B_{\pm} \sin k_z z. \quad (7.47)$$

Substituting (7.47) into (7.46), we get an equation for  $k_z$ :

$$\cot k_z d = \frac{k_z^2 - \xi_1 \xi_2}{k_z (\xi_1 + \xi_2)}. \quad (7.48)$$

In the particular case of  $\xi_1 = \xi_2 \equiv \xi$ , (7.48) is equivalent to the equations

$$\cot \frac{k_z d}{2} = \frac{k_z}{\xi} \quad (7.49)$$

$$-\tan \frac{k_z d}{2} = \frac{k_z}{\xi}. \quad (7.50)$$

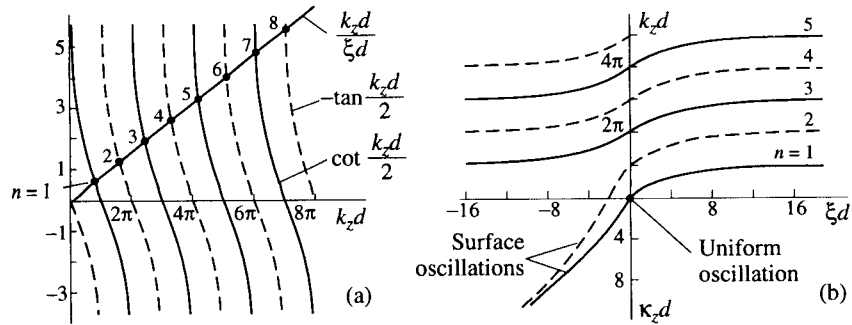
If  $\xi > 0$ , these equations have only *real* roots, and only right-hand polarized oscillations exist. Figure 7.5(a) shows the graphical solution of (7.49) and (7.50) in this case. Denoting the roots by  $k_{zn}$  ( $n = 1, 2, 3, \dots$ ) and taking into account that  $\omega_H = \gamma H_{e0} - \omega_M$ , we obtain from (7.45)

$$\frac{\omega_n}{\gamma} = H_{e0} - 4\pi M_0 + D k_{zn}^2. \quad (7.51)$$

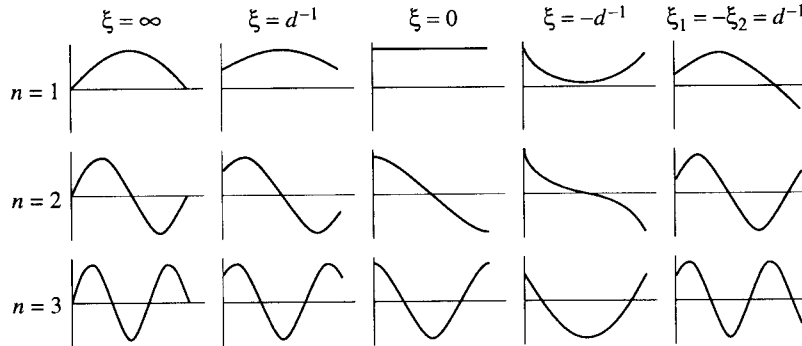
If  $\xi = \infty$  (perfect pinning),  $k_{zn} = n\pi/d$ , and if  $\xi = 0$  (no pinning),  $k_{zn} = (n-1)\pi/d$ .

It is easy to make sure that the roots of (7.49), i.e., the odd  $n$  values, correspond to the dependences  $m_+(z)$  which are symmetric with respect to the middle of the film, and the roots of (7.50), i.e., the even values of  $n$ , correspond to the antisymmetric  $m_+(z)$  dependences. The patterns  $m_+(z)$  are plotted in Figure 7.6. One can see, in particular, that the solution with  $n = 1$  at  $\xi = 0$  represents the



**FIGURE 7.5**

(a) Graphical solution of equations (7.49) and (7.50) for  $\xi d = 4$  and (b) dependence of the roots on the value of  $\xi d$  [333]. Solid lines correspond to (7.49), and dashed lines, to (7.50).

**FIGURE 7.6**

The ac magnetization patterns for standing spin waves in normally magnetized films with symmetric ( $\xi_1 = \xi_2 \equiv \xi$ ) and antisymmetric ( $\xi_1 = -\xi_2$ ) exchange boundary conditions.

uniform oscillation, and its frequency (1.96) follows from (7.51). At  $\xi \neq 0$  the uniform oscillations do not exist.

If  $\xi < 0$ , each equation (7.49) and (7.50) has, in addition to the real roots, one imaginary root  $k_z = i\kappa_z$ . These roots correspond to the *hyperbolic* (or surface) modes (Figure 7.6). The behavior of real and imaginary roots with changing  $\xi$  is shown in Figure 7.5(b). According to this figure and expression (7.51), the frequencies of surface modes decrease with increasing  $|\xi|$  and become equal to zero at  $D\kappa^2 = H_{e0} - 4\pi M_0$ . At still larger  $\kappa$  (or smaller  $H_{e0}$ ) the eigenmode is the left-hand rotating magnetization [215].

Another interesting particular case of  $\xi_1 = -\xi_2 \equiv \xi$  (Figure 7.6) was investigated by Korchagin and Khlebopros [232]. It follows from (7.48) that in this case  $k_z = n\pi/d$ , independently of the value of  $\xi$ . These boundary conditions

can be realized, as Wigen *et al.* have shown [442], by means of depositing thin ( $d_{1,2} \ll d$ ) layers with magnetizations  $M_{01} < M_0$  and  $M_{02} > M_0$  onto the film (with thickness  $d$  and magnetization  $M_0$ ).

Now consider briefly the *excitation* of standing spin waves in a film by a uniform ac magnetic field. The magnetization can be sought in the form

$$m_{\pm} = \sum_{n=1}^{\infty} C_n m_{\pm n} \quad (7.52)$$

where  $m_{\pm n}$  are the magnetizations (7.47) of the eigenmodes. They are orthogonal and can be normalized, e.g., so that  $\sqrt{A_{\pm n}^2 + B_{\pm n}^2} = 1$ . The coefficients  $C_n$  are determined by formula (6.110). If the ac magnetic field is uniform, it can be taken out of the integral, and the quantity

$$\mathfrak{M}_{\pm n} = \int_0^d m_{\pm n} d z \quad (7.53)$$

remains in the numerator of (6.110). This quantity is the normalized magnetic moment of the  $n$ th mode related to unit area of the film.

We will limit ourselves to the case of  $\xi_1 = \xi_2 \equiv \xi > 0$ . Substituting (7.47) (for right-hand polarized modes, which are the only existing modes in this case) into (7.53), we obtain for symmetric modes (with odd  $n$  values)

$$\mathfrak{M}_{+n} = \frac{1}{k_{zn}} \left( 1 + \frac{k_{zn}^2}{\xi^2} \right)^{-1/2} \quad (7.54)$$

For antisymmetric modes,  $\mathfrak{M}_{+n} = 0$ , which is clearly seen from Figure 7.6. Thus, only *symmetric* modes (with  $n = 1, 3, 5, \dots$ ) are excited by a uniform magnetic field. Note that this is also valid in the case of antisymmetric boundary conditions ( $\xi_1 = -\xi_2$ ). It follows from (7.54) that the effectiveness of excitation is the greatest for  $\xi = \infty$  and approaches zero for  $\xi = 0$ .

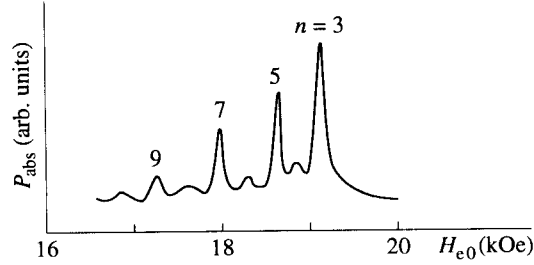
When the frequency or the steady magnetic field is varied, the  $C_n$  values change in a resonance manner and the modes are excited one after another (Figure 7.7). It can be shown that the condition for the absorption maxima of the neighboring modes to be *resolved* is

$$d \lesssim 2\pi \sqrt{\frac{nD}{\Delta H}} \quad (7.55)$$

Therefore, *thin* films should be used to observe the spin-wave resonance. For YIG ( $D = 5.2 \times 10^{-9}$ ,  $\Delta H = 0.5$  Oe) and  $n = 1$ ,  $d_{\max} \simeq 3 \mu\text{m}$ .

The quantity that is measured in experiments on spin-wave resonance is the ac *magnetic moment*  $\mathfrak{M}$ . If condition (7.55) is satisfied, the moment for the  $n$ th mode is

$$\mathfrak{M}^{(n)} = SC\mathfrak{M}_{+n} \quad (7.56)$$

**FIGURE 7.7**

Spectrum of standing spin waves (SWR) in normally magnetized cobalt film with thickness  $d = 0.294 \mu\text{m}$  at frequency of 8.8 GHz [400].

where  $\mathfrak{M}_{+n}$  is the normalized moment (7.53),  $S$  is the film area, and  $C$  is the multiplier in formula (6.110). At resonance ( $\omega = \omega'_n$ ), taking (6.110) and (7.54) into account, we find

$$|\mathfrak{M}^{(n)}| = \frac{CS\omega}{\gamma\Delta H} \left[ k_z^2 n \left( 1 + \frac{k_z^2 n}{\xi^2} \right) \right]^{-1} h_+. \quad (7.57)$$

In the case of perfect pinning ( $\xi = \infty$ ,  $k_z n = n\pi/d$ ), the moment is proportional to  $n^{-2}$ .

Spin-wave resonance in *tangentially* magnetized films was investigated in detail by Salanskii and Erukhimov [333]. Here we will make only some brief remarks. The field (7.44) is not equal to zero in this case. Substituting it into (7.13) and projecting this equation onto axes  $x$  and  $y$  (the axes are directed as in Figure 6.5), we get the expression

$$\omega^2 = (\omega_H + \eta k_x^2) (\omega_H + \eta k_x^2 + \omega_M) \quad (7.58)$$

which coincides with the dispersion relation (7.9) for  $\theta_k = \pi/2$ . Equation (7.58) has, at constant  $\omega$ , two roots,  $k_x^2_{1,2}$ . One of them,  $k_x^2_1$ , is positive if  $\omega > \omega_\perp$ . The second root,  $k_x^2_2$ , is always negative. The *partial* solutions corresponding to the roots  $k_x^2_1$  and  $k_x^2_2$  can satisfy, individually, the exchange boundary conditions at both sides of the film only if  $\xi = 0$ . For all other values of  $\xi$ , the *sum* of these partial solutions satisfies the boundary conditions and, hence, is the eigenmode. The partial solution corresponding to  $k_x^2_2$  decreases quickly with distance from the surfaces of the film. Therefore, it does not materially affect the dispersion law, which can be written in the form similar to (7.49), with certain effective value of the pinning parameter  $\xi_{\text{ef}}$  [333].

Originally metal films were used in the experiments on spin-wave resonance (e.g., [355, 400, 232]). The presence of conductivity was not of great importance because the thickness  $d$  was much smaller than the skin depth  $\delta$  (Section 4.2). Later on nonmetal films were used, as well (e.g., [353, 456]). In many early works

the disagreements with the above-mentioned theoretical dependences took place. The main cause of these disagreements was the nonuniformity of the parameters, e.g., of  $M_0$ , over the thickness of the film [83]. When high-quality uniform films became available, the predictions of the theory were confirmed (e.g., [35, 32]). The spin-wave resonance became one of the techniques for investigation of magnetic films, first of all, for the measurement of the exchange constant  $D$ . It should be noted that the above-mentioned case of antisymmetric boundary conditions ( $\xi_2 = -\xi_1$ ) turned out to be very useful because the value of  $D$  can be found independently of the  $\xi$  value.

### 7.2.3 Propagating spin waves in films

In the analysis of propagating spin waves in films a difficulty arises similar to one discussed above for standing spin waves in tangentially magnetized films: partial solutions, taken separately, cannot satisfy all boundary conditions. However, an exception exists: the normally magnetized *metallized* film with  $\xi = 0$  at both surfaces. Although this case can hardly be realized, it will help us to reveal some features present in more realistic cases.

It was shown in Section 6.2 that the potential  $\psi = \cos k_z z \exp(-ik_y y)$  ensures the satisfaction of the electrodynamic boundary conditions for a normally magnetized metallized plate. It can be easily shown that, if  $\xi = 0$ , the exchange boundary conditions are also satisfied. So, the wave with this potential remains a normal wave. Then, substituting  $k^2 = k_y^2 + k_z^2$  into (7.9), we obtain

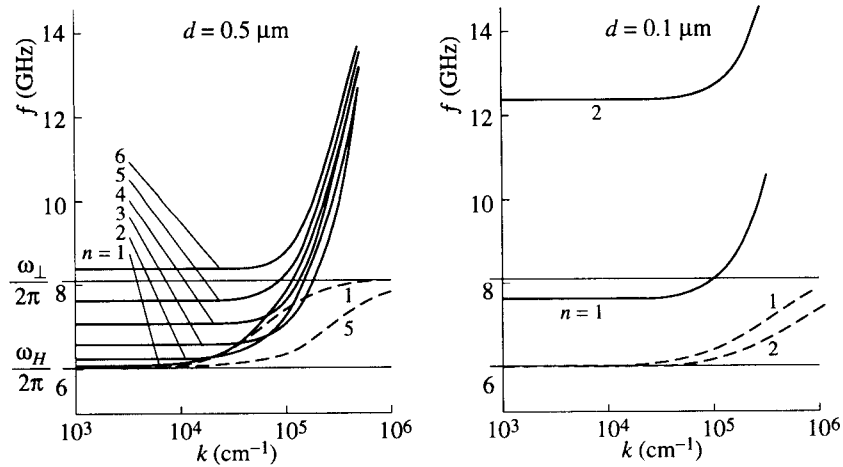
$$\omega^2 = (\omega_H + \eta k_z^2 + \eta k_y^2) \left( \omega_H + \eta k_z^2 + \eta k_y^2 + \frac{\omega_M}{1 + k_z^2/k_y^2} \right) \quad (7.59)$$

where, according to (6.25),  $k_z = n\pi/d$  and  $n = 1, 2, 3, \dots$  denotes the number of the branch. If  $\eta \rightarrow 0$ , (7.59) transforms into (6.27); if  $d \rightarrow \infty$ , (7.59) gives the dispersion relation (7.9) of a spin wave in an unbounded medium for  $\theta_k = \pi/2$ ; and if  $k_y = 0$ , (7.59) transforms into expression (7.51) for the frequencies of standing spin waves. The curves  $\omega$  vs  $k_y$  calculated with (7.59) are plotted in Figure 7.8.

In all other cases the examination of exchange spin waves propagating in magnetic films is much more complicated. Two methods (as in the case of an unbounded medium) can be used. They differ by the order of taking into account the magnetostatic equations and the equation of motion.

The first method was used by Gann [133] (who was the first to solve this problem) and then by Filippov [117], De Wames and Wolfram [90], and by many others. The dependence  $\vec{m}(\vec{h})$ , which follows from the equation of motion and is expressed by the tensor  $\vec{\chi}$ , is found first of all. Then we look for the solution of electrodynamic equations (in magnetostatic approximation) that satisfies both the electrodynamic and the exchange boundary conditions.

The second method was proposed by Vendik, Chartorizhskii, and Kalini-

**FIGURE 7.8**

Dispersion characteristics of spin waves in normally magnetized metallized films with  $\xi = 0$  calculated by formula (7.59) (solid lines). Dashed lines represent the characteristics calculated by (6.27) without allowance for exchange interaction.  $H_{e0} = 3.9$  kOe, YIG at room temperature.

kos [420, 421] and was also widely used (e.g., [205]). Apply this method, we first find the dependence of the demagnetizing field  $h_M$  on magnetization  $m$ , which follows from magnetostatic equations and the *electrodynamic* boundary conditions. Then we look for the solutions of the equation of motion satisfying the *exchange* boundary conditions.

Let us consider in more detail the main steps of both methods for the case of a normally magnetized film assuming that there is no dependence on  $x$  (Figure 6.3). Using the *first* method, we must find the solution of the Walker equation (6.14) satisfying both electrodynamic and exchange boundary conditions. We substitute the potential (6.23) into this equation using formula (7.8) (with  $k^2 = k_y^2 + k_z^2$ ) for  $\mu$ . Then, we obtain an expression of the same form as (7.59), which is, at given  $\omega$  and  $k_y$ , a bicubic equation for  $k_z$ ; the roots of it are  $|k_z| = k_{z p}(\omega)$  ( $p = 1, 2, 3$ ). Substituting these roots into (6.23), we obtain the potentials  $\psi_p$ , which correspond to the *partial waves*. The sum of these potentials contains six arbitrary constants. In the case of a metallized film, there are six boundary conditions: an electrodynamic and two exchange conditions at each side of the film. For a free film, there are two constants more, in the expressions for the potentials outside the film, and two electrodynamic boundary conditions are added. Thus, in both cases the *sum of three partial waves* can satisfy all boundary conditions; so, this sum represents a normal wave. Equating to zero the determinant of six or eight equations obtained from the boundary conditions, we find the dispersion equation  $F(\omega, k_y) = 0$ . The roots  $\omega_n(k_y)$  of this equation correspond to different branches

of the spin-wave spectrum.

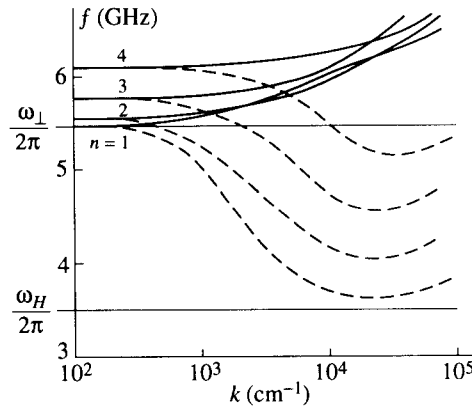
Using the *second* method, we find, first of all, the relationship between the magnetization  $\mathbf{m}$  (regarded at this stage as given) and the field  $\mathbf{h}_M$ , which is the effective field of the internal magnetic energy. This field and the given external magnetic field  $\mathbf{h}_e$  (if the problem of the wave excitation is considered), as well as the effective fields of the exchange interaction and of the anisotropy, are to be substituted into the equation of motion. All these fields, except the field  $\mathbf{h}_e$ , are linear functions of the magnetization  $\mathbf{m}(z, y) = \mathbf{m}(z) \exp(-ik_y y)$ . Solutions of the equation of motion that satisfy the *exchange* boundary conditions are then to be found. It is advisable [205] to represent the functions  $m_x(z)$  and  $m_y(z)$  as series in the solutions  $m_{jx,y}$  of the equation of motion without the field  $\mathbf{h}_M$ . In the considered case of normal magnetization, it is necessary, of course, to use the circular components  $m_{j\pm}$ . These are just the solutions of the above-studied problem of standing spin waves in a normally magnetized film because in that case  $\mathbf{h}_M = 0$ . After substituting the mentioned series into the equation of motion, we get an infinite system of linear equations for the coefficients in the series. The condition of compatibility of these equations yields the dispersion relation  $F(\omega, k_y) = 0$ .

Both methods are, of course, equivalent and both lead to calculations that can be fulfilled with the use of computers. We will cite some qualitative results of such calculations. The frequencies of all branches increase with growing  $k_y$ , as in the simple case considered above (Figure 7.8). But, as distinct from Figure 7.8, now the repulsion of some branches takes place. The character of the exchange boundary conditions has a great influence on the dispersion relations and on the  $m_+(z)$  patterns. At small  $k_y$  values, these patterns are like the patterns in the case of  $k_y = 0$  (Figure 7.6).

The dispersion curves of spin waves in a *tangentially* magnetized film are plotted in Figure 7.9. The values of  $\omega$  at  $k_{\parallel} \rightarrow 0$  ( $k_{\parallel}$  is the wave-vector component in the direction of propagation) are the frequencies of spin-wave resonance. For waves propagating normally to  $\mathbf{M}_0$ , the frequencies of all branches increase with growing  $k_{\parallel}$ , and the repulsion of the branches with the same parity takes place. If losses are taken into account, the  $k_{\parallel}''$  maxima should appear in the regions of repulsion. Waves propagating normally to the  $\mathbf{M}_0$  direction are now no longer pure surface waves, as in the nonexchange case (Section 6.2).

For waves propagating along  $\mathbf{M}_0$ , the dependences of  $\omega$  on  $k_{\parallel}$  are not monotone (Figure 7.9). At small  $k_{\parallel}$  values, the influence of magnetic (dipole-dipole) interaction and of the electrodynamic boundary conditions dominates. This leads, as in the case of nonexchange waves, to the decrease of  $\omega$  with growing  $k_{\parallel}$ . At larger  $k_{\parallel}$ , the exchange interaction dominates and the frequencies increase.

Comparing the dispersion characteristics of the exchange spin waves with the characteristics obtained in the nonexchange approximation (Section 6.2), one can see that the latter are approximately valid at sufficiently small  $k_{\parallel}$  and sufficiently large values of the film thickness  $d$ . It is not obvious, at first sight, that it should be so because the exchange boundary conditions always influence the magnetization.

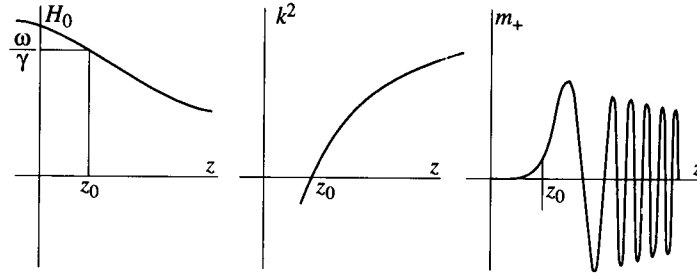
**FIGURE 7.9**

Dispersion characteristics of spin waves in a tangentially magnetized YIG film for different propagation directions (schematically). Solid lines correspond to  $\theta_k = \pi/2$  and dashed lines, to  $\theta_k = 0$ .  $d = 1 \mu\text{m}$ ,  $H_0 = 1.25 \text{ kOe}$ .

Indeed, these conditions materially influence the distribution of magnetization in the regions near the *surfaces* of the film. With decreasing  $k_{\parallel}$  and increasing  $d$ , the relative volume of these regions grows smaller and, hence, the influence of the exchange boundary conditions on the dispersion relations diminishes.

Consider now the exchange spin waves in a film of *finite width* (a spin-wave waveguide) magnetized, e.g., in the direction of a normal to the film surface. The boundary conditions, both electrodynamic and exchange, at surfaces  $x = 0$  and  $x = w$  (for  $0 \leq z \leq d$ ) must now be taken into account, in addition to the boundary conditions at the surfaces  $z = 0$  and  $z = d$ . The problem becomes much more difficult than in the nonexchange case (Section 6.2), in which it also cannot be rigorously solved (except when the waveguide is completely metallized). However, if the film width  $w$  is sufficiently large, we may approximately substitute  $k_x^2 + k_y^2$  for  $k_y^2$  in the dispersion relation and take for  $k_x$  the allowed ('quantized') values  $k_x = n_x \pi/w$ . It will result in splitting of each branch of the spectrum into an infinite number of branches.

If *all dimensions* of the film are *finite*, the spin-wave spectrum, like the spectrum of nonexchange, Walker's oscillations (Section 6.3), should be an infinite discrete set of eigenfrequencies. To find them, taking into account the effective field of exchange interaction and all boundary conditions, is a problem not solved strictly until now. But let us discuss the problem qualitatively. Consider, e.g., a rectangular film of the width  $w$  and the length  $l$ . Suppose that the above-considered problem is solved for a film of the same width and infinite length, so that we know the dispersion law for such a spin-wave waveguide. It is clear that the solution in the form of a standing wave with one value of  $k_y$  cannot satisfy all boundary



**FIGURE 7.10**  
Excitation of a spin wave in a nonuniform steady magnetic field near a turning surface.

conditions at surfaces  $y = 0$  and  $y = l$ . But, if  $l$  is sufficiently large, we can ignore this fact and suppose that a certain 'quantization' condition takes place, e.g.,  $k_y = n_y \pi / l$ . Then, the allowed  $k_y$  values will mark discrete points, i.e., the eigenfrequencies of the spin-wave resonator, at all branches of  $\omega(k_y)$  dependence. The intervals between the neighboring frequencies will be larger the smaller the length  $l$  is.

#### 7.2.4 Spin waves in nonuniform magnetic fields

We will now briefly consider the spin-wave propagation in a ferromagnet with parameters *continuously* changing in space. Of the greatest interest is the case when this change is due to the nonuniformity of the steady magnetic field. If the change of  $H_0$  is slow enough, we may assume that an 'ordinary' spin wave propagates in such a medium with slow-changing parameters, but the wave vector  $\mathbf{k}$  changes continuously in space. The condition of slow change can be written in the form

$$|\nabla H_0| \ll |\mathbf{k}| H_0. \quad (7.60)$$

At certain surfaces the field  $H_0$  can have such value that the wave vector  $\mathbf{k} = 0$ . Near these surfaces condition (7.60) is not satisfied, and we must find a strict solution of the equation of motion with variable parameters. This solution must transform into a wave with slow-changing  $\mathbf{k}$  at one side of the mentioned surface; at another side of this surface it must transform into a spin oscillation with amplitude decreasing exponentially in the direction of  $\nabla H_0$ . By analogy with a quantum-mechanical problem of the motion of a particle near a potential barrier [336], the considered surface can be named the *turning surface*.

The one-dimensional problem of this kind was solved by Schlömann and Joseph [346, 347]. The field was assumed to be directed along the  $z$ -axis and to change monotonically with  $z$  (Figure 7.10). One can suppose that the right-



hand circularly polarized ac magnetization  $m_+$  will depend on  $z$ , as shown in Figure 7.10. Then, a nonzero eigenmoment will arise near the turning plane  $z = z_0$ . And if a uniform ac magnetic field is applied in this region, it will excite a spin wave with changing  $k$  propagating from the turning plane in the direction of decreasing  $H_0$ . A nonuniform internal field can be realized, e.g., in a ferromagnetic or ferrite cylinder put into a uniform external field  $H_{e0}$ .

A similar problem for a normally magnetized *disc* was studied theoretically and experimentally by Eshbach [111]. In this case,  $H_0$  changes in the radial direction, the turning surface is a cylindrical surface, and spin waves propagate to the center of the disc.

Morgenthaler and Stancil later (e.g., [384]) investigated in detail the propagation of spin waves in films in nonuniform magnetic fields. It was found, in particular, that spin waves propagate, as well, *along* the turning surfaces. Of special interest is the case when the closed turning surface bounds a region in which  $k^2 > 0$ . Spin-wave oscillations (standing waves) exist in this region; outside it, the magnetization decreases exponentially. Such a spin-wave resonator ('magnetic pit') can be realized, e.g., by diminishing the external magnetic field in a small region of a normally magnetized film [206]. The losses in such resonators (as well as the losses of waves propagating along the turning surfaces) are small because there are no contributions of the relaxation processes due to the scattering of spin waves by defects present at real boundaries.

### 7.3 Magnons

In this section we will use the general principle of *corpuscule-wave duality* (e.g., [243]) and 'translate into corpuscular language' the results obtained above on the quasiclassical, continuum model.

#### 7.3.1 Quantization of magnetic oscillations and waves

Oscillations and waves of magnetization in magnetically ordered substances can be regarded, respectively, as 'crowds' or flows of quasiparticles with energy

$$\varepsilon = \hbar\omega \quad (7.61)$$

and quasimomentum

$$\mathbf{p} = \hbar\mathbf{k}. \quad (7.62)$$

These quasiparticles are called *magnons*. The dependence  $\omega(\mathbf{k})$ , discussed above in detail, gives at the same time the dispersion law  $\varepsilon(\mathbf{p})$  of magnons.

In the case of uniform oscillations,  $\mathbf{p} = 0$  and  $\varepsilon = \hbar\omega_0$ . In the opposite limiting

case of very large  $k$  values, when  $\omega \simeq \eta k^2$ ,

$$\varepsilon \simeq \frac{\eta}{\hbar} p^2. \quad (7.63)$$

Comparing (7.63) with the relation between the kinetic energy and momentum of a nonrelativistic particle, we see that the magnon with a sufficiently large  $k$  can be regarded approximately as a free particle with the mass  $m_{\text{mag}} = \hbar/(2\eta)$ . For YIG,  $m_{\text{mag}} = 5.7 \times 10^{-27}$ , which is about six times larger than the mass of an electron. The difference between the magnon energy  $\hbar\omega$  and the energy (7.63) can be regarded as the potential energy of a magnon in magnetic fields, external and demagnetizing, and in the effective field of anisotropy.

The energy  $W$  of magnetic oscillations and waves, in the corpuscular language, is the sum of energies of all magnons that exist in the considered body. This sum can be approximately divided into two parts:

$$W = \sum_{\nu} n_{\nu} \varepsilon_{\nu} + \sum_{\mathbf{k}} n_{\mathbf{k}} \varepsilon_{\mathbf{k}}. \quad (7.64)$$

Here  $n_{\nu}$  are the numbers of magnons that correspond to the modes (including the uniform mode) for which the influence of the boundary conditions is important;  $n_{\mathbf{k}}$  are the numbers of magnons with large  $k$  values, which can be treated as corresponding to plane spin waves.

To gain a *discrete* spectrum, which has been assumed in (7.64), without taking into consideration the complicated real boundary conditions, the *periodical* Born-von Karman boundary conditions (e.g., [24]) can be used for the second sum in (7.64). Then, the allowed values of vector  $\mathbf{k}$  projections are

$$k_x = \frac{2\pi p_1}{l_1} \quad k_y = \frac{2\pi p_2}{l_2} \quad k_z = \frac{2\pi p_3}{l_3} \quad (7.65)$$

where  $l_1$ ,  $l_2$ , and  $l_3$  are the periods of the dependence on coordinates  $x$ ,  $y$ , and  $z$ , respectively, and  $p_1$ ,  $p_2$ ,  $p_3$  are integers. As long as the continuum model is used, the values of these integers are not limited.

Writing the energy in the form (7.64), we suppose that different modes do not interact, i.e., the magnon 'gas' is ideal. This supposition is valid if we remain in the limits of a linear theory.

Let us discuss the connection between the *numbers of magnons* and the ac magnetization amplitudes. We have to equate the classical high-frequency magnetic energy to the quantities  $n_{\nu} \hbar \omega_{\nu}$  or  $n_{\mathbf{k}} \hbar \omega_{\mathbf{k}}$ . Consider first the *uniform oscillations* in a small ellipsoid. Their energy consists of the Zeeman energy (2.15), the internal magnetic energy (2.16), and the energy of anisotropy. The last can be included formally into (2.16) if we regard the tensor  $\vec{N}$  in this formula as the sum of the demagnetization tensor and the tensor  $\vec{N}^{\text{an}}$  (Section 2.1). We write down the high-frequency energy terms, which are proportional to the squared ac magnetization

components  $m_{\sim x}$  and  $m_{\sim y}$ , and take into account the expression

$$M_z \simeq M_0 - \frac{m_{\sim x}^2 + m_{\sim y}^2}{2M_0} \quad (7.66)$$

which follows from the condition of conservation of the vector  $M$  length. We then find the energy density

$$U = \frac{H_0}{2M_0} (m_{\sim x}^2 + m_{\sim y}^2) + \frac{1}{2} m_{\sim x}^2 (N_x - N_z) + \frac{1}{2} m_{\sim y}^2 (N_y - N_z). \quad (7.67)$$

Equating it to  $U = n_0 \hbar \omega_0$  (where  $n_0 = n_0/V$  and  $V$  is the sample volume), we can find the connection between  $n_0$  and the amplitudes  $m_{\sim x}$  and  $m_{\sim y}$ . If the sample is an ellipsoid of revolution magnetized along its axis, and the anisotropy axis of a uniaxial crystal or one of the axes  $\langle 100 \rangle$  or  $\langle 111 \rangle$  of a cubic crystal coincides with the axis of the sample, then the ac magnetization is circularly polarized, and

$$n_0 = \frac{m_0^2}{2M_0 \gamma \hbar} \quad (7.68)$$

where  $m_0 = (m_{\sim x}^2 + m_{\sim y}^2)^{1/2}$ .

For *spin waves*, we must include the nonuniform exchange energy and the energy of the volume demagnetizing field  $h_M$  into the energy density  $U$ , but we must exclude the energy of the surface demagnetizing field. The result is again very simple when the magnetization is circularly polarized, i.e., for spin waves with  $\theta_k = 0$ :

$$n_k \equiv \frac{n_k}{V} = \frac{m_k^2}{2M_0 \gamma \hbar} \quad (7.69)$$

where  $m_k = (m_{\sim k x}^2 + m_{\sim k y}^2)^{1/2}$ .

Formulae (7.68) and (7.69) are approximately valid, respectively, for an arbitrary ellipsoid and for spin waves propagating in an arbitrary direction if  $H_0 + Dk^2 \gg 4\pi M_0$ , i.e., when the polarization of the magnetization is nearly circular. If this condition is not satisfied, formulae (7.68) and (7.69) give only the order of magnitude.

Taking into account (7.68), (7.69), and (7.66), we obtain an important formula

$$M_0 - M_z = n \gamma \hbar \quad (7.70)$$

where  $n = n_0 + n_k$ . This means that each magnon of both the uniform precession and spin waves reduces the  $z$  projection of magnetization by a quantity  $\gamma \hbar \equiv g \mu_B$  [ $g$  is the  $g$ -factor and  $\mu_B$  is the Bohr magneton (1.14)].

For *nonuniform* magnetization oscillations (e.g., the Walker modes, Section 6.3), only the numbers of magnons in the *whole sample* have meaning. To find them we must equate the high-frequency magnetic energy of the sample, for a certain mode, to the quantity  $n \nu \hbar \omega_\nu$ . In the case of circularly polarized magnetization

(with the amplitude  $m_\nu$ ), we obtain

$$n_\nu = \frac{1}{2M_0\gamma\hbar} \int_V m_\nu^2(r) dV. \quad (7.71)$$

If uniform oscillations, Walker's modes, and short-wavelength spin waves simultaneously exist in a sample, the total change of the  $z$  component of the sample magnetic moment  $\mathfrak{M}$  is

$$M_0V - \mathfrak{M}_z = \left( Vn_0 + \sum_\nu n_\nu + V \sum_k n_k \right) \gamma\hbar \equiv n\gamma\hbar. \quad (7.72)$$

The transverse  $\mathfrak{M}$  components are equal to zero for all nonuniform modes, both Walker's modes and spin waves. Calculating  $\mathfrak{M}^2 = \mathfrak{M}_x^2 + \mathfrak{M}_y^2 + \mathfrak{M}_z^2$  and taking into account (7.72) and (7.68), we get [376]

$$\mathfrak{M} = M_0V - (n - n_0V) \gamma\hbar. \quad (7.73)$$

Thus, all magnons, except magnons of uniform oscillations, diminish the vector  $\mathfrak{M}$  length.

The numbers of magnons are proportional to the squared ac magnetization amplitudes, just as the numbers of particles in quantum mechanics are proportional to the squared moduli of the wave functions. We can suppose, therefore, that an analogy should exist between the equation of motion of magnetization and the Schrödinger equation. Indeed, it is easy to make sure that, in the case of circular polarization, the equation of motion for the ac magnetization amplitude has the form of Schrödinger's equation. Schlömann was the first to point out this analogy. Tsukernik [407] showed that it takes place in the general case of noncircular magnetization polarization, too.

The magnon energy  $\varepsilon$  and quasimomentum  $p$  are real quantities by definition. The *dissipation* of energy of magnetic oscillations and waves is taken into account, in the corpuscular language, by the finite magnon mean time of life  $\tau_k$  and finite mean path length  $l_k$ . It follows from (7.68) and (7.69) that  $\tau_k$  is equal to the relaxation time (7.28) of the squared oscillation or wave amplitude. The mean path length  $l_k$ , for spin waves, is given by (7.27). For oscillations, both uniform and nonuniform,  $l_k$  is equal to zero.

For damped free oscillations, the numbers of magnons decrease, approaching the equilibrium (thermal) values, due to the collisions with magnons and other quasiparticles (Chapters 11 and 12). For stationary (forced) oscillations and waves, the constancy of magnon numbers is maintained by the processes of their creation, e.g., due to the annihilation of electromagnetic-field photons.

### 7.3.2 Thermal magnons

The magnons we considered above correspond to coherent oscillations and waves and can be called *coherent* magnons. They usually have distinct  $k$  values and

distinct values of energy  $\hbar\omega$  where  $\omega$  is the frequency of the field that excites them. Of course, such a distribution in the  $\mathbf{k}$  space is nonequilibrium one. At the same time, in magnetically ordered substances at any temperature  $T > 0$  there exist noncoherent, *thermal magnons*, which are in thermodynamic equilibrium with other quasiparticles, first of all, with phonons. The distributions of such magnons in the  $\mathbf{k}$  space and over the energies are very broad and depend on temperature and magnetic field. These distributions are determined by the dispersion law of magnons (which was discussed in detail above) and by their statistics.

The magnetic moment of a magnon, as it follows from (7.70), is

$$\mathbf{m} = -z_0\gamma\hbar \equiv -z_0g\mu_B \quad (7.74)$$

where  $z_0$  is a unit vector in the direction of  $\mathbf{M}_0$ . Magnons being the elementary excitations of the electronic magnetic system, we can believe that the magneto-mechanical ratio  $\gamma$  of magnons should be the same as for electrons. It follows, then, from (7.74) that magnons are quasiparticles with the moment of momentum (spin) equal to *unity*. The particles with an integer spin obey the Bose–Einstein statistics (e.g., [244]). If the total number of particles (or quasiparticles) in the system is not fixed, which is the case for magnons, the chemical potential for the system is to be set to zero. Then, the number of particles in a state with energy  $\varepsilon$  (the distribution function) is [244]

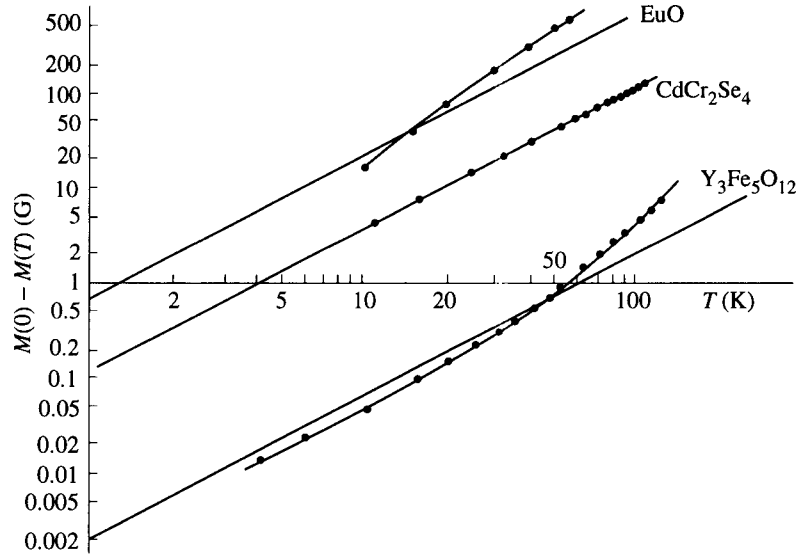
$$\bar{n} = \frac{1}{\exp(\varepsilon/\kappa T) - 1}. \quad (7.75)$$

Thermal magnons materially influence the *thermodynamic* properties of magnetically ordered substances, in particular, *the temperature dependences of magnetization*  $M(T)$ . To find this dependence we use formula (7.70), in which  $M_0$  is now the magnetization  $M(0)$  in the absence of magnons, i.e., at  $T = 0$ ,  $M_z = M(T)$ , and  $n$  is the number of all equilibrium magnons per unit volume. The first sum in (7.64) can be neglected now. Calculating the second sum, we replace the summation over all  $\mathbf{k}$  states by the integration over the  $\mathbf{k}$  space. Then, using the periodic boundary conditions (7.65), we get

$$n = \frac{1}{(2\pi)^3} \int_{\mathbf{k}} \bar{n} d\mathbf{k}. \quad (7.76)$$

Let us consider an isotropic ferromagnet and assume, for simplicity, the dispersion law  $\omega = \eta k^2$ . This will not lead to a great error because we will integrate over the entire  $\mathbf{k}$  space, and the states with large  $k$  values will make the greatest contribution. Substituting (7.75) into (7.76) and integrating over the vector  $\mathbf{k}$  angles  $\theta_k$  and  $\varphi_k$ , we obtain

$$M(0) - M(T) = \frac{\gamma\hbar}{2\pi^2} \int_0^\infty \frac{k^2 dk}{\exp(\hbar\eta k^2/\kappa T) - 1}. \quad (7.77)$$



**FIGURE 7.11**

Temperature dependences of magnetization. Points represent experimental data for EuO [334], CdCr<sub>2</sub>Se<sub>4</sub> [385], and YIG [465]. Straight lines corresponding to the law (7.78) intersect the axis of ordinates at points  $[-4.288 - (3/2) \ln \eta]$ . For EuO and YIG, these lines are drawn according to the  $\eta$  values obtained by other methods [309, 252]; for CdCr<sub>2</sub>Se<sub>4</sub>, they are drawn through the experimental points.

The calculation of the integral in (7.77) results in

$$M(0) - M(T) = 5.863 \times 10^{-2} \gamma \hbar \left( \frac{\kappa T}{\hbar \eta} \right)^{3/2} \equiv 5.157 \times 10^{-5} \eta^{-3/2} T^{3/2}. \quad (7.78)$$

This is the well-known *three-halves power law* obtained first (on the microscopic model) by Bloch [52].

The use of expression (7.78) is one of the ways to measure the exchange constant  $\eta$ . The experimental dependences  $M(0) - M(T)$  for ferromagnets EuO and CdCr<sub>2</sub>Se<sub>4</sub> and ferrimagnet Y<sub>3</sub>Fe<sub>5</sub>O<sub>12</sub> (YIG) are plotted in Figure 7.11. For YIG the three-halves power law is poorly satisfied, especially at high temperatures. The reason is that the spin-wave spectrum for this ferrimagnet contains 20 branches (Section 3.3), and the disregard of all of them but the lowest, 'ferromagnetic', branch is permissible only at low temperatures. The position of the asymptotic straight line at low temperatures agrees with the value of  $\eta = 0.092$ , found for YIG by a more precise method (Section 12.4).

For EuO, the three-halves power law is satisfied badly for another reason: the magnetization of this ferromagnet is very high ( $4\pi M_0 = 24\,000$  G at 4.2 K [284]), and neglecting the term  $\omega_M \sin^2 \theta_k$  in the spin-wave dispersion relation

is not permissible. For  $\text{CdCr}_2\text{Se}_4$  with magnetization five times smaller, this reason is not so important. The law (7.78) is valid for this ferromagnet in a broad temperature range and yields  $\eta = 5.9 \times 10^{-3}$ .

The magnon contribution to *heat capacity* can be found in an analogous manner:

$$(c_v)_{\text{mag}} = \frac{\partial}{\partial T} \int_{\mathbf{k}} \bar{n} \varepsilon d\mathbf{k}. \quad (7.79)$$

The calculation results in [227]

$$(c_v)_{\text{mag}} = 0.113 \kappa^{5/2} (\hbar \eta)^{-3/2} T^{3/2} \equiv 0.71 \eta^{-3/2} T^{3/2}. \quad (7.80)$$

This contribution can be extracted from the measured heat capacity of a nonmetallic ferromagnet by taking into account that the lattice (phonon) contribution is proportional at low temperature to  $T^3$ . Thus, the measurement of  $c_v$  can also be used to find the value of  $\eta$ .

#### 7.4 Elements of microscopic spin-wave theory

Up to now we have regarded the ferromagnet as a medium characterized by the magnetization depending continuously on coordinates. But in reality a ferromagnet, as any solid, is built of discrete microscopic objects: atoms, ions, electrons. To study the influence of the microscopic structure of ferromagnets on their behavior, in particular, on the spin waves, we have to apply microscopic models and, hence, quantum-mechanical methods of analysis.

Spin waves were proposed in 1930 by Bloch [52] on a microscopic model with allowance only for the exchange interaction between the electron spin moments. Ten years later Holstein and Primakoff [184] constructed the microscopic theory of spin waves taking into account, in addition to the exchange interaction, the Zeeman interaction of spins with the external magnetic field and the magnetic (dipole–dipole) interaction. Since then the microscopic spin-wave theory was an object of numerous theoretical investigations; this theory is presented in many excellent books (e.g., [14, 226, 412]). The aim of the present section is to give a brief outline of this theory.

We will use the *Heisenberg model* of a ferromagnet (Section 1.1), which is a system of electron spin moments localized at crystal-lattice points and bound with each other by the exchange interaction. We will see below that the microscopic approach must be used for spin waves with large  $k$  values, comparable with  $1/a$  (where  $a$  is the lattice constant). For such waves, the influence of boundary conditions is negligible, only the spectrum becomes discrete. However, the discrete spectrum can be obtained, in the unbounded medium, by use of the cyclic boundary conditions, as pointed out in the preceding section. Therefore, only an *unbounded* ferromagnet will be treated in the present section. The magne-

to crystalline anisotropy and other effects caused by spin-orbital interaction also will not be taken into account, they are described rather well by the quasiclassical continuum theory.

Then, the Hamiltonian of the model should contain the operators of the exchange energy, of the Zeeman energy, and of the energy of the dipole-dipole interaction. The first is the sum of expressions (1.26). The second can be written by analogy with classical expression (2.15) taking into account that the projection of magnetization onto the  $z$ -axis (directed along the magnetic field) is

$$\hat{M}_z = -\gamma\hbar \sum_f \hat{S}_f^z. \quad (7.81)$$

Here,  $\hat{S}_f^z$  is the  $z$  projection of a spin  $\hat{S}_f$  at the lattice point  $f$ , and the summation is over all spins in a unit volume.

For simplicity, we neglect at present the dipole-dipole interaction. Thus the Hamiltonian takes the form

$$\mathcal{H} = \gamma\hbar \sum_f \hat{S}_f^z - \sum_f \sum_{f' \neq f} I_{ff'} \mathbf{S}_f \mathbf{S}_{f'} \quad (7.82)$$

where  $\hat{S}_f \hat{S}_{f'} = \hat{S}_f^x \hat{S}_{f'}^x + \hat{S}_f^y \hat{S}_{f'}^y + \hat{S}_f^z \hat{S}_{f'}^z$ . The operators  $\hat{S}_{f,f'}^{x,y,z}$  obey the commutation relation [226]

$$[\hat{S}_f^x, \hat{S}_{f'}^y] = i\Delta_{ff'} \hat{S}_f^z \quad (7.83)$$

and the two others obtained from (7.83) by cyclic interchanging of indices;  $\Delta_{ff'}$  is the Kronecker delta-symbol (Appendix C).

#### 7.4.1 Diagonalization of the Hamiltonian

Our objective is to transform the Hamiltonian (7.82) into

$$\hat{\mathcal{H}} = U_0 + \sum_{\mathbf{k}} \hat{n}_{\mathbf{k}} \varepsilon_{\mathbf{k}}(\mathbf{k}) \quad (7.84)$$

where the summation is over all allowed  $\mathbf{k}$  values and  $\hat{n}_{\mathbf{k}}$  is an operator whose eigenvalues are integers. Then  $U_0$  will be the ground-state energy,  $\varepsilon(\mathbf{k})$  will be the energy of an elementary excitation, i.e., of a magnon, and  $\hat{n}_{\mathbf{k}}$  will be the operator of the number of magnons in a certain state.

The conversion of the Hamiltonian (including the energy of the dipole-dipole interaction) into the form (7.84) was carried out in [184] by means of the famous *Holstein-Primakoff transformations*. The first of these transformations is the transition from the spin operators  $\hat{S}_f^{x,y,z}$  to new operators  $\hat{a}_f^+$  and  $\hat{a}_f$ .

Let us pass first to the cyclic combinations

$$\hat{S}_f^{\pm} = \hat{S}_f^x \pm i\hat{S}_f^y \quad (7.85)$$



and then to the operators  $\hat{a}_f^+$  and  $\hat{a}_f$  which satisfy the following commutation relations

$$[\hat{a}_f, \hat{a}_{f'}^+] = \Delta_{ff'}, \quad [a_f, a_{f'}] = 0 \quad [a_f^+, a_{f'}^+] = 0. \quad (7.86)$$

Assuming the expression

$$\hat{S}_f^z = -S + \hat{a}_f^+ \hat{a}_f \quad (7.87)$$

to be valid, it can be shown that

$$\hat{S}_f^+ = \sqrt{2S} \left(1 - \frac{1}{2S} \hat{a}_f^+ \hat{a}_f\right)^{1/2} \hat{a}_f \quad \hat{S}_f^- = \sqrt{2S} \hat{a}_f^+ \left(1 - \frac{1}{2S} \hat{a}_f^+ \hat{a}_f\right)^{1/2} \quad (7.88)$$

where, as well as in (7.87),  $S$  is the spin quantum number, so that the eigenvalues of  $\hat{S}_f^z$  are  $S, (S-1), \dots, (-S)$ .

The operators that satisfy the commutation relations (7.86) are the operators of *creation* and *annihilation* of particles obeying the Bose–Einstein statistics [244]. When they act on the wave functions of the particles in the *secondary-quantization representation* (in which the functions consist of the numbers of particles in different states), the operator  $\hat{a}_f^+$  increases the number of particles in the  $f$  state by unity and does not ‘touch’ the numbers of them in all other states (e.g., [84]). The operator  $\hat{a}_f$  decreases the number of particles in the  $f$  state by unity. The operator  $\hat{a}_f^+ \hat{a}_f \equiv \hat{n}_f$  is the operator of the *number of particles* in the  $f$  state. In our case,  $\hat{a}_f^+$  and  $\hat{a}_f$  are the operators, respectively, of creation and annihilation of spin deviations (i.e., of the change of  $S^z$  by  $\pm 1$ ) at the lattice point  $f$ . The state of the ferromagnetic sample is represented by the numbers of spin deviations at all lattice points.

As the operator expressions (7.88) are very complicated, we expand the radicals in power series and limit ourselves to the first terms of these series:

$$\hat{S}_f^+ \cong \sqrt{2S} \hat{a}_f \quad \hat{S}_f^- \cong \sqrt{2S} \hat{a}_f^+. \quad (7.89)$$

This seems to be a very rough approximation, especially for small  $S$  values. The main assumption of the Holstein–Primakoff theory is that this approximation is, nevertheless, permissible at sufficiently low temperatures when the mean numbers of spin deviations

$$\bar{n}_f \ll 1. \quad (7.90)$$

According to the eigenvalues of  $\hat{S}_f^z$ , the numbers of spin deviations at a lattice point must satisfy the condition

$$n_f \leq 2S. \quad (7.91)$$

This condition restricts the allowed (*‘physical’*) region in the entire spin-deviation space, and so, the spin deviations differ from normal Bose-particles. The exact relations (7.88) ensure the fulfillment of (7.91), but the approximate relations (7.89) do not.

Substituting the new operators  $\hat{a}_f^+$  and  $\hat{a}_f$  into the Hamiltonian (7.82), we get

$$\hat{\mathcal{H}} = U_0 + \hat{\mathcal{H}}_2 + \hat{\mathcal{H}}_4 \quad (7.92)$$

$$U_0 = -\gamma\hbar SNH - S^2 \sum_f \sum_{f'} I_{ff'} \quad (7.93)$$

$$\hat{\mathcal{H}}_2 = \gamma\hbar H \sum_f \hat{a}_f^+ \hat{a}_f + 2S \sum_f \sum_{f'} I_{ff'} (\hat{a}_f^+ \hat{a}_f - \hat{a}_f^+ \hat{a}_{f'}) \quad (7.94)$$

$$\hat{\mathcal{H}}_4 = - \sum_f \sum_{f'} I_{ff'} \hat{a}_f^+ \hat{a}_f \hat{a}_{f'}^+ \hat{a}_{f'}. \quad (7.95)$$

Here the sums are over all lattice points,  $N$  is the number of these points, and  $f \neq f'$  in all double sums.

The Hamiltonian (7.95) can be neglected at sufficiently low temperatures when condition (7.90) is satisfied. But the Hamiltonian (7.94) does not have the required form (7.84). This implies that the spin deviations localized at lattice points are not the elementary excitations of a ferromagnet.

To obtain such excitations (which should be collective excitations of the entire considered system) the *second* Holstein–Primakoff transformation is to be performed. We have to pass from the  $r$  space to the  $k$  space, i.e., to carry out the Fourier transformation of the operators  $\hat{a}_f^+$  and  $\hat{a}_f$ :

$$\hat{a}_f^+ = \frac{1}{\sqrt{N}} \sum_{\mathbf{k}} \exp(-i\mathbf{k}\mathbf{r}_f) \hat{a}_{\mathbf{k}}^+ \quad \hat{a}_f = \frac{1}{\sqrt{N}} \sum_{\mathbf{k}} \exp(i\mathbf{k}\mathbf{r}_f) \hat{a}_{\mathbf{k}}. \quad (7.96)$$

The wave vectors in (7.96) are defined nonuniquely (e.g., [24]), an arbitrary vector of the reciprocal lattice can be added to  $\mathbf{k}$ . Therefore, the  $\mathbf{k}$  space should be restricted to the first Brillouin zone. We will use, as in the preceding section, the periodical Born–von Karman boundary conditions. The allowed  $\mathbf{k}$  values are given, then, by (7.66). But now, in the case of a discrete lattice, these values are *limited* by the first Brillouin zone. The number of the allowed  $\mathbf{k}$  values in this zone is equal to the number of spins  $N$  in the periodicity volume. We will take this volume as  $1 \text{ cm}^3$ , thus,  $N$  will be the number of spins per unit volume.

The operators  $\hat{a}_{\mathbf{k}}^+$  and  $\hat{a}_{\mathbf{k}}$  obey the commutation relations similar to (7.86), with replacement of  $f$  by  $\mathbf{k}$ . Therefore, they can be regarded as creation and annihilation operators of some quasiparticles. These quasiparticles are *not localized* at lattice points but belong to the entire lattice. The operator

$$\hat{n}_{\mathbf{k}} = \hat{a}_{\mathbf{k}}^+ \hat{a}_{\mathbf{k}} \quad (7.97)$$

is the operator of the number of these quasiparticles. The eigenvalues of this operator  $n_{\mathbf{k}} = 0, 1, 2, \dots$  are the numbers of quasiparticles in the  $\mathbf{k}$  states.

Substitution of (7.96) into (7.94) yields

$$\hat{\mathcal{H}}_2 = \gamma\hbar H \sum_{\mathbf{k}} \hat{n}_{\mathbf{k}} + 2S \sum_{\mathbf{k}} \hat{n}_{\mathbf{k}} \sum_g [1 - \exp(i\mathbf{k}\mathbf{r}_g)] I_g \quad (7.98)$$

where  $\mathbf{r}_g = \mathbf{r}_f - \mathbf{r}_{f'}$ ,  $I_g \equiv I_{ff'}$ , and the last sum is over all lattice points except one, the initial. The Hamiltonian (7.98) has the desired form of (7.84), and

$$\varepsilon_k(k) = \gamma\hbar H + 2S \sum_g [1 - \exp(i\mathbf{k}\mathbf{r}_g)] I_g. \quad (7.99)$$

Thus, the transition to the operators  $\hat{a}_k^+$  and  $\hat{a}_k$  has brought approximately the Hamiltonian (7.82) of the Heisenberg model into the diagonal form. Therefore, these operators can be regarded approximately as the creation and annihilation operators of the elementary excitations of this model, i.e., of spin waves or magnons. Such is the case, however, only if the dipole–dipole interaction is not included into the Hamiltonian (7.82).

The spin-operator  $\hat{S}$  projections and, hence, all quantities that depend on them can be represented as functions of  $\hat{a}_k^+$  and  $\hat{a}_k$ . In particular, substituting (7.96) into (7.87) and summing over all lattice points, we get

$$\sum_f \hat{S}_f^z = -SN + \sum_{\mathbf{k}} \hat{n}_k. \quad (7.100)$$

The relation (7.70) follows directly from (7.100); the relation (7.72) can be obtained in a similar manner [376].

#### 7.4.2 Discussion of the dispersion law

The dispersion relation (7.99) is to be compared with the classical expression (7.9) for  $\theta_k = 0$  because, for this direction of spin-wave propagation, there is no influence of the dipole–dipole interaction. In both cases the magnon energy is the sum of the Zeeman term and the exchange term, the difference is in the form of the latter. Now it contains the *microscopic* parameters  $S$  and  $I_g$ , and the  $\mathbf{k}$  dependence is more complicated and governed by magnetic structure.

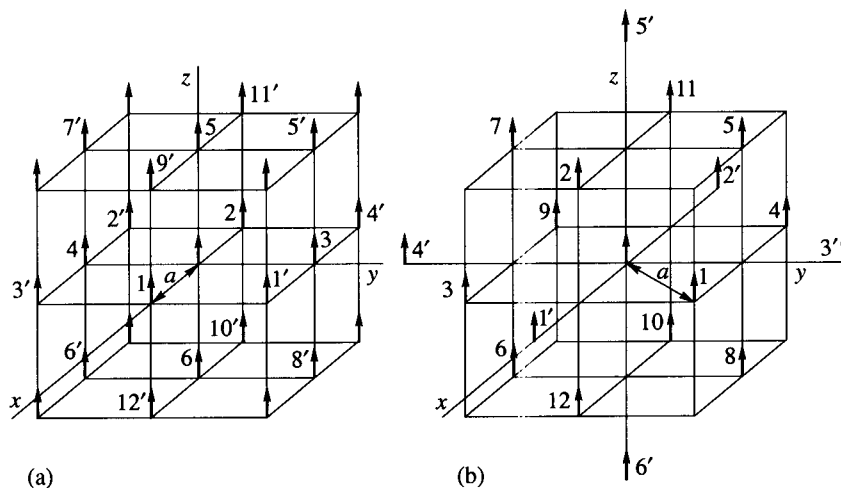
The exchange integrals  $I_g$  decrease quickly with increasing distance  $r_g$  between the spins. Therefore, it is reasonable to take into account only the *nearest neighbors* in (7.99). Consider, first, a *simple cubic* spin lattice (Figure 7.12). Calculating the sum in (7.99) over six nearest neighbors, we get

$$\varepsilon_k = \gamma\hbar H + 4SI_1 (3 - \cos k_x a - \cos k_y a - \cos k_z a) \quad (7.101)$$

where  $I_1$  is the exchange integral, which is assumed to be independent of the  $r_g$  direction. As another example, consider a *face-centered cubic* lattice (Figure 7.12), in which the number of the nearest neighbors  $Z = 12$ . Now it follows from (7.99) that

$$\begin{aligned} \varepsilon_k = \gamma\hbar H + 4SI_1 [6 - \cos(k_x + k_y)a_1 - \cos(k_x - k_y)a_1 - \cos(k_y + k_z)a_1 \\ - \cos(k_y - k_z)a_1 - \cos(k_z + k_x)a_1 - \cos(k_z - k_x)a_1] \end{aligned} \quad (7.102)$$

where  $a_1 = a/\sqrt{2}$ , and  $a$ , as in (7.101), is the distance between the nearest spins.

**FIGURE 7.12**

(a) Simple cubic and (b) face-centered cubic spin lattices. The unprimed numbers correspond to the nearest neighbors of the spin in the center, primed numbers correspond to the next-nearest neighbors.

In the long-wave-length limit ( $ka \ll 1$ ) both expressions (7.101) and (7.102) reduce to

$$\varepsilon_k = \gamma \hbar H + \frac{1}{3} Z S I_1 a^2 k^2. \quad (7.103)$$

This coincides with the classical expression if

$$\eta = \frac{1}{3} \frac{Z S I_1}{\hbar} a^2. \quad (7.104)$$

It is easy to obtain analogous formulae taking into account also the next-nearest neighbors (the second coordination sphere). Then, for a simple cubic lattice,

$$\eta = \frac{2S}{\hbar} \left( I_1 + \frac{1}{4} I_2 \right) a^2 \quad (7.105)$$

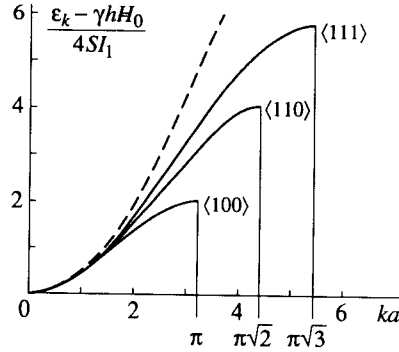
and for a face-centered cubic lattice,

$$\eta = \frac{4S}{\hbar} (I_1 + I_2) a^2 \quad (7.106)$$

where  $I_1$  and  $I_2$  are the exchange integrals, respectively, in the first and second coordination spheres.

If the exchange integrals are unknown, the following expressions can be used to estimate the value of  $\eta$ :

$$\eta = \frac{1}{6} \Lambda M_0 \gamma a^2 \quad (7.107)$$

**FIGURE 7.13**

Dispersion characteristics of spin waves in a ferromagnet with simple cubic spin lattice for different directions of propagation calculated (solid curves) by formula (7.101), i.e., in the nearest-neighbor approximation and without allowance for dipole-dipole interaction. Dashed curve corresponds to the continuum dispersion law.

$$\eta = \frac{1}{2} \frac{\kappa T_C a^2}{\hbar(S+1)}. \quad (7.108)$$

They result from (1.24), (1.21), and the relation

$$\Lambda = \frac{2ZI_1}{\hbar(S+1)} \quad (7.109)$$

which can be found, in the nearest-neighbor approximation, by equating (2.13) to the exchange term in (7.93). Formula (7.107) can be rewritten as

$$D = \frac{1}{6} H_E a^2 \quad (7.110)$$

where  $H_E$  is the 'molecular' field (1.22).

As an example, consider the ferromagnet EuO with NaCl structure, lattice constant  $a_{\text{lat}} = 5.141 \text{ \AA}$ , and  $T_C = 69.5 \text{ K}$  [284]. The  $\text{Eu}^{2+}$  ions ( $S = 7/2$ ) form a face-centered cubic lattice with  $a = a_{\text{lat}}/\sqrt{2}$ . The following values of exchange integrals were found from the neutron-diffraction experiments [309]:  $I_1 = 0.606\kappa$  and  $I_2 = 0.119\kappa$ . From (7.106) we find  $\eta = 1.75 \times 10^{-3}$ , which agrees rather well with the temperature dependence of magnetization (Figure 7.11). Using (7.108), we get  $\eta = 1.34 \times 10^{-3}$ .

For the ferromagnet  $\text{CdCr}_2\text{Se}_4$  (another example), the values of exchange integrals are unknown. To estimate  $\eta$ , using (7.108), we take for  $a$  the mean distance between the  $\text{Cr}^{3+}$  ions in this ferromagnet with rather complicated, spinel structure. This distance can be easily found taking into account that the elementary cell with  $a_{\text{lat}} = 10.75 \text{ \AA}$  [284] contains 16  $\text{Cr}^{3+}$  ions. Using the values of  $T_C = 130 \text{ K}$  [284] and  $S = 3/2$ , we find from (7.108)  $\eta = 6.2 \times 10^{-3}$ , which is

to be compared with the value  $5.9 \times 10^{-3}$  found from the three-halves-power law for the magnetization (Section 7.3). Such excellent coincidence is accidental. But it follows from both examples that expression (7.108) can be used to estimate the exchange constant  $\eta$  for ferromagnets. An attempt to use this expression, as well as other cited formulae, for ferrimagnets meets difficulties connected, first of all, with the uncertainty in determining the value of  $a$ .

Thus, the results of the microscopic and the continuum theories of spin waves coincide if  $ka \ll 1$ , but differ materially when this condition is not valid. According to the continuum theory, the dispersion law is isotropic (i.e.,  $\omega_k$  depends only on  $k$ ) if the dipole-dipole interaction and the magnetocrystalline anisotropy are not taken into consideration. The microscopic theory, even without allowance for these interactions, results in a strong dependence of  $\omega_k$  on the *direction* of  $k$  with respect to the *axes of spin lattice* (Figure 7.13). The values of  $k$  and  $\omega_k$  are unlimited in continuum theory. In microscopic theory the  $k$  vectors are defined only in the first Brillouin zone (i.e.,  $k \lesssim 10^8$ ) and  $\omega_k$  *does not exceed* the value on the order of  $4ZSI_1/\hbar \sim 10^{14} - 10^{15}$ .

Let us discuss briefly the magnon contributions to the thermodynamic characteristics of a ferromagnet, according to the microscopic theory. These contributions depend, in general, on three factors: the statistics of magnons, the region in  $k$  space over which the summation (or integration) is carried out, and the dispersion law. Magnons are approximately Bose-particles in both theories, continuum and microscopic. The fact that the summation in the microscopic theory is performed over the first Brillouin zone has no great effect because, at sufficiently low temperatures, there are few magnons with large  $k$  values. The third factor, i.e., the distinction in the dispersion law, is the most important.

The calculation of the magnetization temperature dependence, analogous to that considered in Section 7.3 but with the use of the dispersion law (7.101) (without the Zeeman term), results in the following expression (e.g., [214]):

$$M(0) - M(T) = C_{3/2}T^{3/2} + C_{5/2}T^{5/2} + C_{7/2}T^{7/2} + \dots \quad (7.111)$$

The coefficient  $C_{3/2}$  is the same as in (7.78), and the consequent coefficients contain the lattice constant  $a$ : the coefficient  $C_{5/2}$  contains it to the second power, the coefficient  $C_{7/2}$ , to the fourth power, and so on. The estimates show that all higher terms can usually be neglected at  $T \lesssim T_c/2$ .

### 7.4.3 Allowance for dipole-dipole interaction and anisotropy

The Hamiltonian of the dipole-dipole interaction can be obtained by replacement  $\mathfrak{M} \rightarrow \gamma\hbar\hat{S}$  in the classical expression, which is the double sum of the energies (1.3). This Hamiltonian should be added to the Hamiltonian (7.82). Then, after the two above-considered Holstein-Primakoff transformations, the entire Hamiltonian will contain, apart from the terms of the second and fourth order in operators  $\hat{a}_k^+$  and  $\hat{a}_k$ , also terms of third order in these operators. The quadratic

term of the Hamiltonian will have the form (e.g., [214])

$$\hat{\mathcal{H}}_2 = \hbar \left[ A_k \hat{a}_k^+ \hat{a}_k + \frac{1}{2} (B_k \hat{a}_k \hat{a}_{-k} + B_k^* \hat{a}_k^+ \hat{a}_{-k}^+) \right] \quad (7.112)$$

$$A_k = \omega_H + 2 \sum_g I_g [1 - \exp(i\mathbf{k}\mathbf{r}_g)] + \frac{1}{2} \omega_M \sin^2 \theta_k \quad (7.113)$$

$$B_k = \frac{1}{2} \omega_M \sin^2 \theta_k \exp(i2\varphi_k). \quad (7.114)$$

Here  $\omega_M = \gamma 4\pi N \gamma \hbar S$ ,  $\theta_k$  and  $\varphi_k$  are the vector  $\mathbf{k}$  angles in the spherical coordinate system with the axis oriented along the direction of magnetization.

The Hamiltonian (7.112) has no diagonal form (7.84). It means that now the operators  $\hat{a}_k^+$  and  $\hat{a}_k$  are not the operators of magnon creation and annihilation. One more transition, to new operators  $\hat{c}_k^+$  and  $\hat{c}_k$ , the *third Holstein–Primakoff transformation* [184], also referred to as the Bogolyubov transformation is needed to bring the Hamiltonian into the diagonal form. This problem is studied in detail in many books (e.g., [14, 412]). We will cite here only the main result: the dispersion relation is now

$$\varepsilon_k = \hbar \sqrt{A_k^2 - |B_k|^2} \quad (7.115)$$

where  $A_k$  and  $B_k$  are determined by (7.113) and (7.114). The difference between this dispersion law and expressions (7.9) and (7.10) obtained in the continuum theory is only in the form of the *exchange* term. The influence of the long-range dipole–dipole interaction is the same in both microscopic and continuum theories.

The dipole–dipole interaction, as mentioned above, does not manifest itself for spin waves with  $\theta_k = 0$ . If  $\theta_k \neq 0$  but  $|B_k| \ll A_k$ , the expression  $\varepsilon_k = \hbar A_k$ , which is the generalization of expression (7.14), is approximately valid. The operators  $\hat{c}_k^+$  and  $\hat{c}_k$  differ, in this case, but slightly from  $\hat{a}_k^+$  and  $\hat{a}_k$ , so that  $\hat{a}_k^+$  and  $\hat{a}_k$  can be regarded approximately as the magnon creation and annihilation operators. For most ferromagnets and ferrimagnets  $|B_k|/\kappa \sim 0.1$  K. Therefore, the considered approximation is valid for thermal magnons, except at very low temperatures. For coherent spin waves with  $k \lesssim 10^6$ , this approximation is valid only at very high frequencies.

The *magnetocrystalline* anisotropy (the main contribution to which makes the spin–orbital interaction) can be taken into account only phenomenologically in the considered microscopic theory based on the Heisenberg model because this model does not allow for the orbital moments. At not very large  $k$  values we may simply replace the term  $Dk^2$  in the continuum spin-wave dispersion relation by its microscopic analog. At large  $k$  values, the magnetocrystalline anisotropy, as well as the dipole–dipole interaction, makes a relatively small contribution to the dispersion relation. In this case, the exchange interaction plays the main role. The contribution of it, as we have seen (Figure 7.13), is strongly anisotropic.

#### 7.4.4 Interaction of magnons

The main assumptions of the Holstein–Primakoff theory are: (i) the possibility to replace the radicals in (7.88) by their series expansions; (ii) the possibility to neglect all terms in the Hamiltonian on the order higher than two in the operators  $\hat{a}_k^+$  and  $\hat{a}_k$  (or  $\hat{c}_k^+$  and  $\hat{c}_k$  if the dipole–dipole interaction has been taken into account); such terms include the terms (7.95), the third-order terms which arise due to the dipole–dipole interaction, and the higher-order terms in the expansions of the radicals.

The second assumption is warrantable at low levels of excitation, i.e., for thermal magnons, at sufficiently low temperatures. The neglected terms represent the collisions of magnons, which have small probabilities at small numbers of magnons.

The first assumption gives rise to strong doubt. The replacement of the radicals by the series removes the ‘automatic’ limitation of the spin-deviation numbers  $n_f$  at each lattice point, and this limitation is to be brought into the theory ‘artificially’. Dyson [104] showed that the allowance for the properties of spin operators  $\tilde{S}_f$ , which leads to the limitation of  $n_f$ , is equivalent to an additional, *kinematic* interaction of the repulsion type. It should be taken into consideration only at  $T \lesssim T_C/2$ .

According to Dyson, the higher terms in the Hamiltonian, which are discarded in the Holstein–Primakoff theory, lead to another, *dynamic*, interaction of the attraction type. It leads to the correction of the spin-wave dispersion law, which is more essential than the correction caused by the kinematic interaction but is also small at low temperatures. The dynamic interaction yields an additional term in the  $M(T)$  dependence, which is proportional to  $T^4$  [105]. This term can be also neglected at  $T < T_C/2$ .

Thus, the ‘Holstein–Primakoff magnons’ [Bose-particles with dispersion law (7.114)] are *not* the elementary excitations of the Heisenberg ferromagnet. But they can be approximately regarded as such at a sufficiently low level of excitation of the spin system.

At higher levels of excitation (for thermal excitations, at higher temperatures) the elementary excitations differ materially, in their dispersion law and properties of their creation and annihilation operators, from the Holstein–Primakoff magnons. However, they can be called magnons or spin waves. The dispersion relations of such excitations and their contributions to thermodynamic quantities have been calculated by the use of more potent modern theoretical techniques (e.g., [412, 370, 414]). The only condition of the validity of the spin-wave (magnon) concept is the relation

$$\varepsilon_k \tau_k > 2\pi\hbar. \quad (7.116)$$

It means that the magnon time of life should be larger than the period of oscillations which correspond to the magnon energy.



# 8

---

## *Magnetic oscillations and waves in unsaturated ferromagnet*

---

### 8.1 Oscillations of domain walls

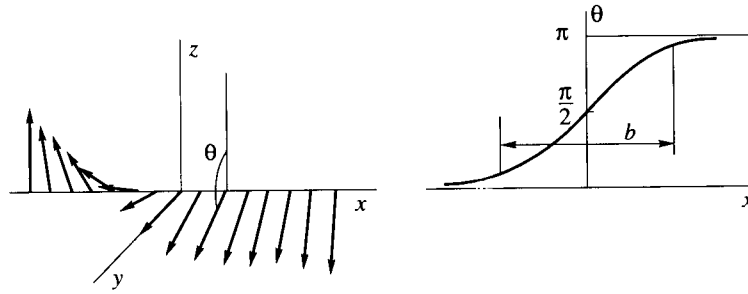
We have supposed until now that the ground state of a ferromagnetic (or a ferromagnetic) body is the uniform magnetization. However, such a state is an equilibrium state only in sufficiently high magnetic fields or for very small samples, less than  $\sim 1 \mu\text{m}$ . In lower fields, in particular, in zero field, samples of larger dimensions split into *magnetic domains*. The magnetizations inside the domains are approximately uniform but vary from one domain to another, so that in zero field the magnetization averaged over a volume containing many domains is usually equal to zero. The cause of the rise of domains is that the magnetic field excited by the sample diminishes materially when the sample is split into domains, and so, the total energy (or free energy, at  $T > 0$ ) is minimized in their presence.

The transition from the magnetization direction in a domain to that in the neighboring domain occurs gradually but, mainly, in a boundary layer, the so-called *domain wall*. The thickness of this layer is usually small as compared with the dimensions of domains.

This chapter is devoted to high-frequency magnetic processes in such 'unsaturated' (i.e., split into domains) ferromagnetic samples. In the present section, the processes caused by oscillations of domain walls are studied, and in the next section, the processes caused by precession of magnetization inside domains will be considered.

#### 8.1.1 Domain walls and domain structures

The behavior of magnetization in a domain wall was first studied by Landau and Lifshitz in their famous paper [241]. Let us consider, following [241], two neighboring domains in a ferromagnetic uniaxial single crystal and a plane domain



**FIGURE 8.1**  
Turn of magnetization vectors in the Bloch domain wall.

wall between them (Figure 8.1). At sufficiently large distances from the boundary ( $x = 0$ ) the magnetizations  $M_1$  and  $M_2$  in the domains are directed along two different easy axes, in the considered case, along the opposite directions of the  $z$ -axis. The energy of magnetocrystalline anisotropy would be minimal if the magnetization turns abruptly from one of these directions to the other. But the exchange energy would be large in that case; this energy is smaller the smoother the turn. Magnetic energy, which is due to the demagnetizing fields in the wall, becomes equal to zero when the vector  $M$  lies in the boundary plane because, then, no magnetization components perpendicular to the boundary arise. Such domain walls, which are called *Bloch walls*, take place in most cases.

The dependence of the magnetization angle  $\theta$  in the Bloch wall on  $x$  (Figure 8.1) can be found by solving the variational problem of minimizing the sum of anisotropy and exchange energies. Having solved this problem, Landau and Lifshitz found [241]

$$\cos \theta = -\tanh \left( \frac{x}{M_0} \sqrt{\frac{K_1}{q}} \right) \equiv -\tanh \frac{\pi}{b} x \quad (8.1)$$

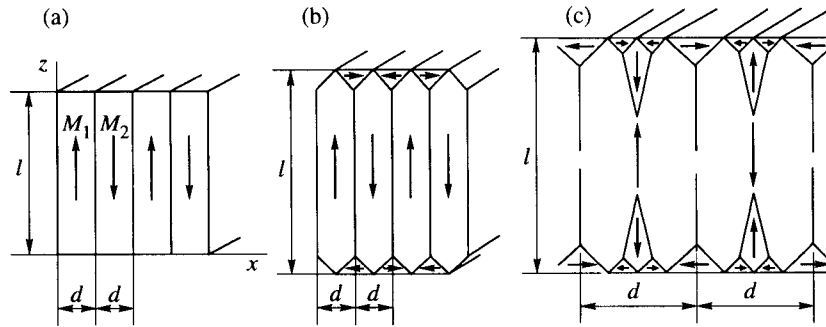
where  $K_1$  is the first constant of uniaxial anisotropy,  $q$  is the nonuniform exchange constant (Section 7.1), and

$$b = \pi M_0 \sqrt{\frac{q}{K_1}} \quad (8.2)$$

can be named the *wall thickness*. It is the distance at which the magnetization turn mainly (by  $\sim 75\%$ ) takes place. The anisotropy and the exchange energies are equal when (8.1) holds, and the total energy of the domain wall per unit of its surface is

$$W_s = 2\pi M_0 \sqrt{qK_1} \equiv 2bK_1. \quad (8.3)$$

Analogous calculations in the case of a cubic crystal (e.g., [61]) lead to the values of  $b$  and  $W_s$  of the same order. For YIG at room temperature ( $|K_1| = 5.5 \times 10^3$ ,



**FIGURE 8.2**  
Domain structures in a plate of uniaxial ferromagnet.

$q = 3.76 \times 10^{-11}$ ,  $b = 3.6 \times 10^{-5}$  cm, and  $W_s = 0.4$  erg cm $^{-2}$ .

In thin films with easy axes of magnetization lying in the plane of the film, Bloch walls do not correspond to the minimum of total energy because of the demagnetizing fields and, hence, of the magnetic energy arising due to magnetization components normal to the film surface. Then, the Neel walls appear, in which the magnetization lies in the plane perpendicular to the domain boundary and parallel to the film surface.

The form and the dimensions of domains depend essentially on the *dimensions of the sample*. Consider, e.g., a plate of uniaxial ferromagnet of the thickness  $l$  with surfaces normal to the easy axis. Suppose that the domains are layers ('stripes') of the width  $d$  parallel to this axis [Figure 8.2(a)]. To find the domain width we have to minimize the sum of the wall energy (8.3) (related to a unit of the plate surface) and the magnetic energy, which in this case (if related also to a unit of the plate surface) is of the order of

$$W_M \sim M_0^2 d. \quad (8.4)$$

The minimization results in

$$d = \frac{\sqrt{W_s l}}{M_0}. \quad (8.5)$$

Near the sample surfaces, more complicated domain structures usually arise. One of them is shown in Figure 8.2(b). In this case, the domain width is determined by a compromise between the wall energy and the anisotropy energy in the surface prisms because the magnetic energy is equal to zero. This results in

$$d = \sqrt{\frac{2W_s l}{K_1}}. \quad (8.6)$$

Such a structure, predicted by Landau and Lifshitz [241], exists in a certain interval of  $l$ . For smaller  $l$  values (in thin films), the simple structure shown in Figure 8.2(a)

is more advantageous, and for larger  $l$  values, more complicated surface structures, as shown in Figure 8.2(c), arise.

The structures similar to that shown in Figure 8.2 can arise in cubic crystals, as well. If  $K_1 > 0$ , the magnetization directions in the prisms [Figure 8.2(b)] are also easy directions, and the domain width  $d$  is determined by the compromise between the wall energy and the magnetoelastic energy (Section 12.1). In the case of  $K_1 < 0$ , the anisotropy energy plays the same role as before, and formula (8.6) is valid on the order of magnitude. For YIG the domain width  $d$  is of the order of  $10^{-2}\sqrt{l}$ . In real crystals, domain structures like those shown in Figures 8.2(b),(c), and even more complicated ones, arise inside the sample near different defects, as pores, grain boundaries in polycrystals, etc. In real crystals, the parallel-plane layered structure usually transforms into a *labyrinth* structure (e.g., [95]).

One can see from (8.5) or (8.6) that the domain dimension  $d$  is proportional to  $\sqrt{l}$ . Therefore, a sufficiently small sample ( $l < l_0$ ) will not split into domains. For small samples expression (8.5) should be used, and

$$l_0 \sim \frac{W_s}{M_0^2}. \quad (8.7)$$

For YIG,  $l_0 \sim 10^{-5}$  cm.

When an external magnetic field  $H_e$  is applied, a new term, the Zeeman energy (2.15), arises in the energy of the sample. Now the equilibrium is reached when a mean magnetization  $\overline{M}$  emerges in the direction coinciding or near the direction of  $H_e$ . This mean magnetization can be formed in two ways [70]: (i) by the shift of domain walls leading to the growth of the domains in which the magnetization makes an acute angle with  $H_e$  (*displacement* processes); (ii) by the turning of the magnetization vectors in domains (*rotation* processes).

The displacement processes dominate at small external fields and are completed with the disappearance of the domain structure. The rotation processes continue after vanishing of the domains and are completed when the magnetization is directed along  $H_e$ .

The magnetization processes become more complicated when the domain structure undergoes transformations at certain  $H_e$  values or at certain temperatures. An important example is the rise of the so-called *bubble domains* in films with large uniaxial anisotropy ( $K_1 > 2\pi M_0^2$ ). In such films, at certain values of the external magnetic field applied normally to the film surface, the above-discussed layered (or stripe) domain structure transforms into isolated cylindrical domains with diameters of the order of  $1 \mu\text{m}$ . The bubble domains exist in a certain magnetic-field range from  $H_{\min}$  to  $H_{\max}$  where  $H_{\min}$  is the so-called field of elliptical instability and  $H_{\max}$  is the collapse field. At  $H < H_{\min}$  the equilibrium structure is the stripe domains, and at  $H > H_{\max}$  the uniform magnetization is the equilibrium state. It should be noted that bubble domains can be generated, annihilated, and moved in the plane of the film by rather simple means (e.g., [301]). Owing to these properties, the bubble domains in epitaxial ferrite (usually, with garnet structure) films are applied in computer memory and signal-processing devices.

### 8.1.2 Equation of motion of a domain wall

If the frequency of the ac magnetic field is much less than all the characteristic frequencies of a ferromagnetic sample, the change of its magnetization is occurring quasistatically. This means that the magnetic state at a certain moment is determined by the value of the ac magnetic field at the same moment (but, of course, with impact of the magnetic prehistory of the sample). With the growth of the frequency of the ac magnetic field, the inertia, first, of the domain-wall displacement and, then, of the magnetization rotation, begins to influence the ac magnetization. Proceeding to study the first of these dynamic processes, we have to derive, first of all, the equation of motion of a domain wall.

Suppose that the steady magnetic field is either absent or small, so that the domain structure is conserved. The ac magnetic field is assumed not to make equal angles with the magnetizations of the neighboring domains, otherwise the displacement processes would not take place.

The displacement of a domain wall is a result of the turns of the magnetization vectors in the wall. Therefore, the equation of motion of the wall must be based on the equation of motion of the *magnetization* (Section 2.1). The effective field in this equation includes the effective fields of anisotropy and of exchange interaction, as well as the demagnetizing field caused by the variation of magnetization in the wall. Such theory was developed by Landau and Lifshitz [241] for the case of a uniaxial ferromagnet and the magnetic field applied in the direction of the easy axis, i.e., along the  $z$ -axis in Figure 8.1. The dissipative term in the equation of motion was taken as in (1.61). It was shown that the equation of motion has a solution depending on coordinate  $x$  (Figure 8.1) and time in the combination  $(x - vt)$  where

$$v = \frac{M_0 H}{\rho} \quad (8.8)$$

$$\rho = \frac{\lambda}{\gamma M_0} \sqrt{\frac{K_1}{q}}. \quad (8.9)$$

This solution corresponds to the displacement of the wall without its deformation. Expression (8.8) written in the form

$$\rho \frac{dx}{dt} = M_0 H \quad (8.10)$$

can be regarded as an equation of motion of the domain wall. The right-hand side of (8.10) is the force acting on the wall.

Becker [43] and Döring [103] later showed that it is necessary to add an *elastic* force and an *inertial* term to the equation of motion (8.10). Then this equation takes the form

$$m_w \frac{d^2 x}{dt^2} + \rho \frac{dx}{dt} + \zeta x = M_0 H \quad (8.11)$$

which is the equation of a harmonic oscillator. The appearance of the inertial term  $m_w d^2x/dt^2$  in (8.11) is associated with kinetic energy of the moving wall. It was shown [43] that the effective mass (per unit surface of the wall) is

$$m_w \sim \frac{1}{\gamma^2 b} \quad (8.12)$$

where  $b$  is the wall thickness (8.2). Expression (8.12) is also valid for cubic crystals. For YIG,  $b = 3.6 \times 10^{-5}$  cm and  $m_w \sim 10^{-10}$  g cm $^{-2}$ .

The presence of the term  $\zeta x$  in (8.11) is caused by the fact that, in a real crystal, the domain wall at equilibrium is located in a 'potential well', and when it moves from this equilibrium position, an elastic force  $-\zeta x$  arises. The coefficient  $\zeta$  can be related to the initial *static* susceptibility  $\chi_i = \overline{M}/H_0$  where  $\overline{M}$  is the mean magnetization in a small steady field  $H_0$  caused by the displacement process. This magnetization is a result of the shifts of the neighboring walls in opposite directions by the distance  $x$ , so that

$$\overline{M} = \frac{2x}{d} M_0 \quad (8.13)$$

where  $d$  is the domain width. Equation (8.11) gives in the static case  $\zeta x = M_0 H$ , and taking (8.13) into account, we get

$$\zeta = \frac{2M_0^2}{\chi_i d}. \quad (8.14)$$

### 8.1.3 Dynamic susceptibility

Solving equation (8.11) with a harmonic ac field  $h \exp(i\omega t)$  and passing then from  $x$  to the mean ac magnetization  $\overline{m} \exp(i\omega t)$ , according to (8.13), we get the *dynamic* (high-frequency) susceptibility caused by the domain-wall displacement

$$\chi_{||} = \frac{\overline{m}}{h} = \chi_i \left( 1 - \frac{\omega^2}{\omega_{0w}^2} + i \frac{1}{Q_w} \frac{\omega}{\omega_{0w}} \right)^{-1}. \quad (8.15)$$

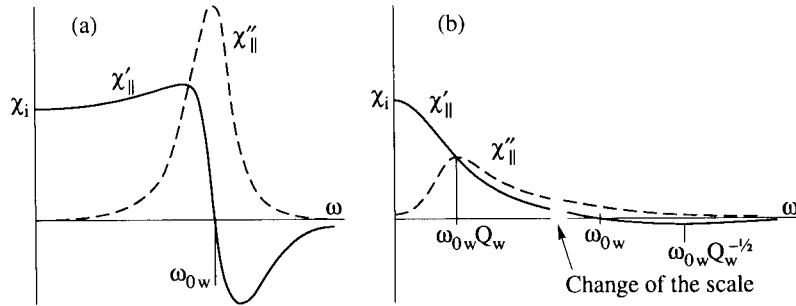
Here,

$$\omega_{0w} = \sqrt{\frac{\zeta}{m_w}} \quad (8.16)$$

is the eigenfrequency and

$$Q_w = \frac{\sqrt{\zeta m_w}}{\rho} \quad (8.17)$$

is the quality factor. The dependence  $\chi_{||}(\omega)$  is of the *resonance* type if  $Q_w \gg 1$  and of the *relaxation* type if  $Q_w < 1$  (Figure 8.3).

**FIGURE 8.3**

Magnetic spectra caused by domain-wall oscillations (schematically): (a) of resonance-type ( $Q_w = 5$ ) and (b) of relaxation-type ( $Q_w = 0.2$ ).

From (8.16), taking into account (8.12), (8.14), (8.2), (8.6), and (8.3), we obtain

$$\omega_{0w} = \gamma M_0^{5/4} \left( \frac{q}{K_1} \right)^{1/8} l^{1/4} \chi_i^{-1/2}. \quad (8.18)$$

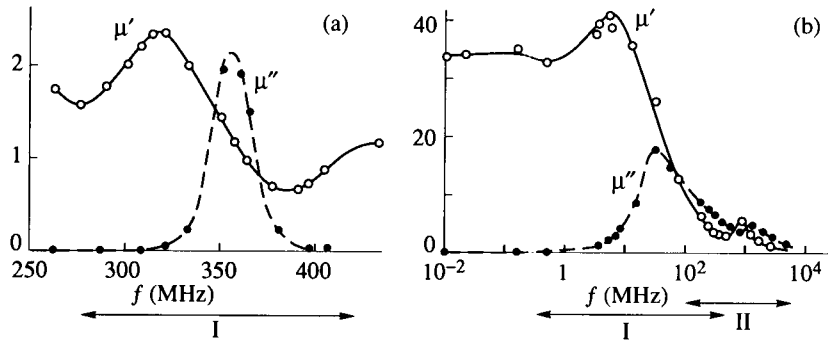
When this expression is used to estimate the value of  $\omega_{0w}$ , the sample dimension must be taken for  $l$  in the case of a single crystal, and the mean grain dimension (usually  $10^{-3}$ – $10^{-4}$  cm), in the case of a polycrystal. Then, for the YIG polycrystal (with  $\chi_i \sim 10$ ), we get  $f_{0w} \equiv \omega_{0w}/2\pi = 25$ – $45$  MHz, and for the cobalt-ferrite polycrystal ( $\chi_i \sim 3$ ),  $f_{0w} = 200$ – $300$  MHz. For single crystals, the  $f_{0w}$  values will be several times greater.

From (8.16) and (8.17), with regard to (8.9), (8.12), and (8.2), a simple formula for the resonance-line width follows:

$$\Delta\omega_w \equiv \frac{\omega_{0w}}{Q_w} = \pi\gamma\lambda. \quad (8.19)$$

However, trying to estimate the value of  $\lambda$  in this formula, we come across some difficulties. The ferromagnetic-resonance experiments, commonly used to get this value, are performed generally at higher frequencies. Taking the  $\lambda$  value obtained by Galt [132] from the direct measurement of domain-wall velocity in a nickel-ferrite single crystal, we get  $\Delta f_w = 35$  MHz. An estimate of  $f_{0w}$  in a polycrystal of this ferrite yields, according to (8.18),  $f_{0w} = 280$  MHz. So, in this case, as well as in many others, the estimates result in  $Q_w > 1$ , i.e., in the resonance-type frequency dependence of  $\chi_{\parallel}$ .

The frequency dependences of the real and imaginary parts of the permeability in the absence of a steady magnetic field are called *magnetic spectra*. The experimental magnetic spectrum for the cobalt-ferrite single crystal is shown in Figure 8.4(a). It is determined, certainly, by the domain-wall oscillations because the eigenfrequencies of the rotation process (Section 8.2) should be much higher in this ferrite with very large anisotropy. The experimental values of

**FIGURE 8.4**

Magnetic spectra (a) of single-crystal cobalt ferrite [312] and (b) of polycrystal nickel ferrite [288] at room temperature. The region of domain-wall oscillations is denoted by I and the region of natural ferromagnetic resonance, by II.

$f_{0w} = 360$  MHz and  $\Delta f_w = 25$  MHz [Figure 8.4(a)] agree with the estimates using the formulae (8.18) and (8.19).

As distinct from single crystals, narrow regions of resonance variation of  $\mu'$  and  $\mu''$  caused by domain-wall oscillations are never observed in polycrystals. The reason for this is the spread in forms, dimensions, and orientations of domains. The magnetic spectra caused by domain-wall oscillations are very broad in polycrystals and often overlap with the regions of resonance  $\mu'$  and  $\mu''$  variation [Figure 8.4(b)] caused by rotation processes, which will be considered in the next section.

## 8.2 Ferromagnetic resonance in samples with domain structure

The ac magnetizations in the neighboring domains are strongly coupled, analogously, in some sense, to the ac sublattice magnetizations in antiferromagnets and ferrimagnets (Section 3.1). An important difference, however, is that in an antiferromagnet or ferrimagnet the sublattices are 'mixed' on the microscopic level and the coupling is performed by the exchange interaction. Domains, on the contrary, are macroscopic regions coupled mainly by the *demagnetizing* fields, which arise at the domain boundaries and, as we will see below, at the sample surfaces. We will study in this section the *coupled* oscillations of the domain magnetizations, i.e., the ferromagnetic resonance in the presence of domains.

The equations of motion for the magnetizations in the domains have the same form (3.3) as for the sublattice magnetizations, but  $j = 1, 2, \dots$  is now the number



of a group of identical domains. The mean magnetization is

$$\overline{\mathbf{M}} = \sum_j \eta_j \mathbf{M}_j \quad (8.20)$$

where  $\eta_j = V_j / \sum_j V_j$  is the relative volume occupied by the domains of the  $j$ th group. The effective field acting on the magnetization  $\mathbf{M}_j$  in the domains of the  $j$ th group can be written, analogously to (2.7), in the form

$$\mathbf{H}_{\text{ef}j} = \frac{1}{\eta_j} \left[ -\frac{\partial U}{\partial \mathbf{M}_j} + \sum_{p=1}^3 \frac{\partial}{\partial x_p} \left( \frac{\partial U}{\partial (\partial \mathbf{M}_j / \partial x_p)} \right) \right]. \quad (8.21)$$

Here,  $U$  is the energy density per unit volume of the *entire* sample (which is the reason for the factor  $1/\eta_j$  arising in this formula). The energy  $U$  must include all kinds of energy associated with domains: the domain-wall energy and the magnetic energy caused by the demagnetizing fields.

Let us consider the energy of the demagnetizing fields at the plane boundary of two domains. The condition of the continuity of the magnetic induction component normal to the domain boundary is

$$\mathbf{H}_1 \mathbf{n}_0 - \mathbf{H}_2 \mathbf{n}_0 = -4\pi (\mathbf{M}_1 \mathbf{n}_0 - \mathbf{M}_2 \mathbf{n}_0) \quad (8.22)$$

where the indices 1 and 2 correspond to the neighboring domains, and  $\mathbf{n}_0$  is a unit normal to the boundary. In the case when the domains are infinite plane layers of equal thickness, the demagnetizing fields satisfying the conditions (8.22) are

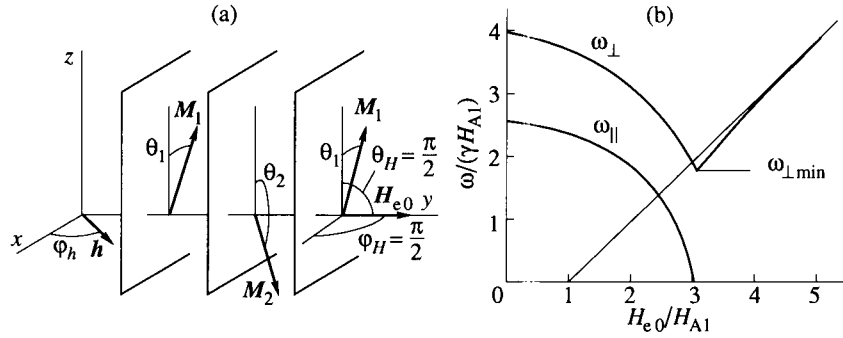
$$\mathbf{H}_{M_{1,2}} = \pm 2\pi (M_{1n} - M_{2n}) \mathbf{n}_0 \quad (8.23)$$

where  $M_{1,2n}$  are the normal components of  $\mathbf{M}_{1,2}$ . The energy of these fields is

$$U_{Mw} = \frac{1}{8\pi} H_{M_{1,2}}^2 = \frac{\pi}{2} (M_{1n} - M_{2n})^2. \quad (8.24)$$

The demagnetizing fields for more complicated domain structures were found by solving the appropriate magnetostatic problems [425, 194].

A rigorous theory of magnetization oscillations in an unsaturated sample can be developed only under some simple assumption as to the domain structure. Nagamiya [295] was the first to work out such a theory for a disk of tetragonal ferromagnet. The case of a spheroid of uniaxial ferromagnet was investigated by Smit and Beljers [371], and the ferromagnetic resonance in a sphere of cubic ferromagnet was studied by Artman [23]. In all these theories a regular and simple domain structure consisting of thin parallel-plane layers of equal thickness, was assumed. Domain walls were regarded as infinitely thin and immovable, and their energy was not taken into account. The domain walls can be assumed to be immovable (i.e., the domain structure does not change when the external steady magnetic field is applied) if the field makes *equal angles* with the magnetizations of both domain groups (as in Figure 8.5). Then, the magnetizing of the sample

**FIGURE 8.5**

Ferromagnetic resonance in an unsaturated sphere of a uniaxial ferromagnet ( $K_1 > 0$ ) [371]: (a) accepted domain structure, (b) eigenfrequencies vs external steady magnetic field. Vectors  $\mathbf{M}_{10}$  and  $\mathbf{M}_{20}$  lie in the  $yz$  plane,  $H_{A1} = (4\pi/3)M_0$ .

is achieved only by the turning of magnetization vectors in the domains, i.e., by rotation process. This condition was satisfied in all mentioned theories.

### 8.2.1 Ellipsoid of uniaxial ferromagnet

Assume, according to [371], that the easy axis of anisotropy coincides with one of the ellipsoid axes and the steady magnetic field is perpendicular to this axis (Figure 8.5). Then, in compliance with the above-mentioned condition, the domain structure shown in this figure will not change with the growth of the steady field  $H_{e0}$ , and the directions of  $\mathbf{M}_1$  and  $\mathbf{M}_2$  will approach the  $\mathbf{H}_{e0}$  direction until the domain structure disappears at  $H_{e0} = H_s$ . The ac magnetic field lies in the plane perpendicular to the anisotropy axis (Figure 8.5).

The following energy terms are taken into account: the Zeeman energy  $U_Z$ , the anisotropy energy  $U_{an}$ , and the magnetic energies associated with the demagnetizing fields both at the ellipsoid surface ( $U_{Mel}$ ) and at the domain boundaries ( $U_{Mw}$ ). As the domain widths are equal ( $\eta_1 = \eta_2 = 1/2$ ), the Zeeman energy is

$$U_Z = \frac{1}{2} (\mathbf{M}_1 + \mathbf{M}_2) [\mathbf{H}_{e0} + h \exp(i\omega t)]. \quad (8.25)$$

The anisotropy energy, according to (2.40), can be written in the form

$$U_{an} = K_1 \left( 1 - \frac{1}{2} \frac{M_{1z}^2}{M_0^2} - \frac{1}{2} \frac{M_{2z}^2}{M_0^2} \right). \quad (8.26)$$

Assuming the domain width to be much less than the sample dimensions, we can neglect the magnetization nonuniformity when calculating  $U_{Mel}$ . Then, according

to (2.16),

$$U_{M \text{ el}} = \frac{1}{2} (N_x \overline{M}_x^2 + N_y \overline{M}_y^2 + N_z \overline{M}_z^2) \quad (8.27)$$

where  $\overline{M}_{x,y,z}$  are the components of  $\overline{\mathbf{M}} = (\mathbf{M}_1 + \mathbf{M}_2)/2$  and  $N_{x,y,z}$  are the demagnetization factors of the sample. The energy  $U_{M \text{ w}}$  is written in the form (8.24) with  $M_{1,2n} = M_{1,2y}$ .

The equations of motion of the domain magnetizations have the form (3.3). Following [371], we will use the method of spherical coordinates (Section 2.1) and write the equations of motion, by analogy with (2.20)—but without dissipation terms—in the form

$$\frac{\partial \theta_{1,2}}{\partial t} = -\frac{2\gamma}{M_0 \sin \theta_{1,2}} \frac{\partial U}{\partial \varphi_{1,2}} \quad \frac{\partial \varphi_{1,2}}{\partial t} = \frac{2\gamma}{M_0 \sin \theta_{1,2}} \frac{\partial U}{\partial \theta_{1,2}} \quad (8.28)$$

where  $\theta_{1,2}$  and  $\varphi_{1,2}$  are the polar and the azimuthal angles of  $\mathbf{M}_{1,2}$ .

First of all, we have to find the *equilibrium* values  $(\theta_{1,2})_0$  and  $(\varphi_{1,2})_0$  of these angles. The equilibrium conditions are the extensions of conditions (2.22). Restrict ourselves, for simplicity, to the case of  $\varphi_H = \pi/2$  (Figure 8.5); as it has been already emphasized, the condition  $\theta_H = \pi/2$  is to be satisfied to exclude the domain-wall displacement. Then, from symmetry considerations,

$$(\varphi_1)_0 = (\varphi_2)_0 = \frac{\pi}{2} \quad (\theta_1)_0 = \pi - (\theta_2)_0 \equiv \theta_0. \quad (8.29)$$

The angle  $\theta_0$  is found from the condition  $\partial U / \partial \theta_1 = 0$  at  $\theta_1 = 0$ , which yields

$$\begin{aligned} \sin \theta_0 &= \frac{H_{e0}}{H_s} & \text{at } H_{e0} \leq H_s \\ \theta_0 &= \frac{\pi}{2} & \text{at } H_{e0} \geq H_s \end{aligned} \quad (8.30)$$

where  $H_s = 2H_{A1} + N_y M_0$  and, as before,  $H_{A1} = K_1/M_0$ .

Now we have to *linearize* equations (8.28). Taking  $\theta_{1,2} = (\theta_{1,2})_0 + \alpha_{1,2} \exp(i\omega t)$  and  $\varphi_{1,2} = (\varphi_{1,2})_0 + \beta_{1,2} \exp(i\omega t)$ , we expand the derivatives in (8.28) into power series in ac components of  $\theta_{1,2}$  and  $\varphi_{1,2}$ . We restrict ourselves to the first two terms of the series and take into account the equilibrium conditions. In the obtained four linear equations, we pass to the new variables  $\alpha^\pm = (\alpha_1 \pm \alpha_2)/2$  and  $\beta^\pm = (\beta_1 \pm \beta_2)/2$ . In these variables, we get two *independent* systems:

$$\begin{aligned} 2(U_{\theta\theta} + U_{\theta_1\theta_2}) \alpha^+ - i\xi\omega\beta^+ &= 0 \\ i\xi\omega\alpha^+ + 2(U_{\varphi\varphi} + U_{\varphi_1\varphi_2}) \beta^+ &= hM_0 \sin \theta_0 \cos \varphi_h \end{aligned} \quad (8.31)$$

$$\begin{aligned} 2(U_{\theta\theta} - U_{\theta_1\theta_2}) \alpha^- - i\xi\omega\beta^- &= hM_0 \cos \theta_0 \sin \varphi_h \\ i\xi\omega\alpha^- + 2(U_{\varphi\varphi} - U_{\varphi_1\varphi_2}) \beta^- &= 0. \end{aligned} \quad (8.32)$$

Here  $U_{\theta\theta} = U_{\theta_1\theta_1} = U_{\theta_2\theta_2}$  and  $U_{\varphi\varphi} = U_{\varphi_1\varphi_1} = U_{\varphi_2\varphi_2}$  ( $U_{\theta_1\theta_1}$ ,  $U_{\theta_1\theta_2}$ , etc., are the second derivatives of the energy  $U$  with respect to the corresponding angles),

$\xi = M_0 \sin \theta_0 / \gamma$ , and  $\varphi_h$  is the angle that the ac field  $h$  makes with the domain boundaries (Figure 8.5).

The first mode [which corresponds to system (8.31)] is excited by the  $h$  component perpendicular to  $H_{e0}$ , and the second mode [corresponding to system (8.32)] is excited by the  $h$  component parallel to  $H_{e0}$ . The eigenfrequencies of these modes,  $\omega_{\perp}$  and  $\omega_{\parallel}$ , are obtained by equalizing to zero the determinants of (8.31) and (8.32). Taking into account expressions (8.24)–(8.27) for the terms of the energy  $U$ , we get [371]

$$\left(\frac{\omega_{\perp}}{\gamma}\right)^2 = (2H_{A1} + 4\pi M_0)(2H_{A1} + N_x M_0) - \frac{(2H_{A1} + N_x M_0)[2H_{A1} + (N_x + N_y)M_0]}{2H_{A1} + N_y M_0} H_{e0}^2 \quad (8.33)$$

$$\left(\frac{\omega_{\parallel}}{\gamma}\right)^2 = 2H_{A1}(2H_{A1} + N_y M_0) - \frac{2H_{A1}}{2H_{A1} + N_y M_0} H_{e0}^2. \quad (8.34)$$

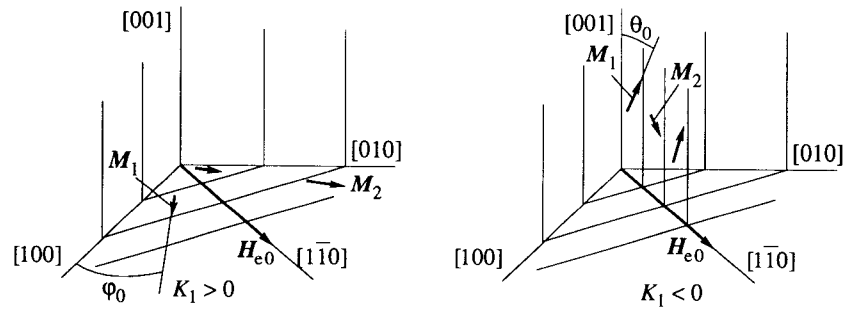
The curves of  $\omega_{\perp}$  and  $\omega_{\parallel}$  vs  $H_{e0}$  computed with (8.33) and (8.34) are plotted, in the case of a sphere, in Figure 8.5. The existence of domains leads, first, to the fact that the frequency  $\omega_{\perp}$  of the mode excited by the transverse (with respect to  $H_{e0}$ ) ac field *does not go to zero* at any value of  $H_{e0}$ . Second, a mode arises that is excited by the ac field *parallel* to  $H_{e0}$ . The frequencies  $\omega_{\perp}$  and  $\omega_{\parallel}$ , in the absence of  $H_{e0}$ , i.e., the frequencies of the so-called ‘natural’ ferromagnetic resonance, are finite and different.

In a more general case of an arbitrary value of the angle  $\varphi_H$ , two modes are excited at *any* orientation of  $h$  [425]. The eigenfrequencies of these modes, at all values of  $H_{e0}$ , lie between the above-considered frequencies  $\omega_{\perp}$  and  $\omega_{\parallel}$  and coincide with them at  $H_{e0} = 0$  and  $H_{e0} = H_s$ .

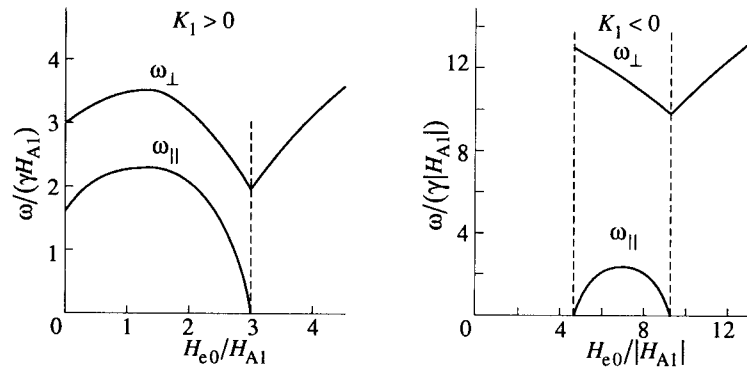
### 8.2.2 Sphere of cubic ferromagnet

Consider, following [23], an unsaturated single-crystal sphere of a cubic ferromagnet, suppose the field  $H_{e0}$  to be directed along the  $\langle 110 \rangle$  axis, and take into account only the first constant  $K_1$  of the cubic anisotropy. In this case, the layered domain structure with domains of equal width are conserved in certain intervals of  $H_{e0}$  values. If  $K_1 > 0$ , the equilibrium magnetizations  $M_{10}$  and  $M_{20}$ , at  $H_{e0} = 0$ , are directed along the easy axes  $[100]$  and  $[010]$  (Figure 8.6). With growing  $H_{e0}$  these magnetizations, lying in the  $(001)$  plane, approach the  $H_{e0}$  direction. If  $K_1 < 0$ , the magnetizations  $M_{10}$  and  $M_{20}$  are directed, at  $H_{e0} = 0$ , along the easy axes  $[111]$  and  $[11\bar{1}]$ . With growing  $H_{e0}$ , the magnetizations  $M_{10}$  and  $M_{20}$ , lying in the  $(1\bar{1}0)$  plane, approach the  $H_{e0}$  direction.

The calculation, similar to the above-considered, shows that, for a cubic crystal, two oscillation modes take place, as well [23]. One mode, with frequency  $\omega_{\perp}$ , is excited by the ac magnetic field perpendicular to  $H_{e0}$ , and the other, with

**FIGURE 8.6**

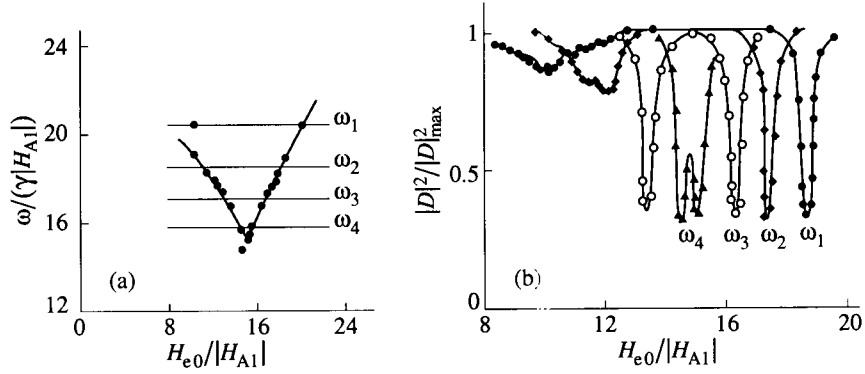
Domain structures accepted in the calculation of the ferromagnetic-resonance conditions in an unsaturated sphere of a cubic ferromagnet [23]. Vectors  $M_{10}$  and  $M_{20}$  lie in the plane (001) for  $K_1 > 0$  and in the plane (110) for  $K_1 < 0$ .

**FIGURE 8.7**

Ferromagnetic-resonance eigenfrequencies in an unsaturated sphere of a cubic ferromagnet [23]. Accepted domain structure is shown in Figure 8.6.  $H_{A1} = (4\pi/3)M_0$  for  $K_1 > 0$ , and  $|H_{A1}| = (1/2)M_0$  for  $K_1 < 0$ . Dashed lines indicate the regions in which the accepted domain structure exists.

frequency  $\omega_{\parallel}$ , is excited by the field parallel to  $H_{e0}$ . The dependences of both frequencies on the steady magnetic field  $H_{e0}$  are shown in Figure 8.7.

In this section we have regarded the domain walls as immovable. However, the magnetization oscillations within domains and the domain-wall oscillations, more rigorously, should be considered *simultaneously* [425]. *Three* eigenmodes then take place. Their frequencies differ most strongly from the frequencies of the magnetization oscillations in domains (considered in this section) and from the frequencies of the domain-wall oscillations (Section 8.1) when these unperturbed frequencies approach each other.

**FIGURE 8.8**

Results of experimental investigation of ferromagnetic resonance in an unsaturated YIG single-crystal sphere [269]. (a) Dependence of resonance frequency on an external steady magnetic field; bold lines represent values calculated according to [23] (Figure 8.7), circles denote the experimental data. (b) Absorption curves at frequencies shown in (a);  $D$  is the transmission coefficient through a resonator containing the YIG sphere.

The susceptibility tensor of a ferromagnetic sample with domain structure is defined by the expression

$$\overline{\mathbf{m}} = \overline{\overline{\chi}}^e \mathbf{h} \quad (8.35)$$

where  $\overline{\mathbf{m}}$  is the ac magnetization averaged over all domains and  $\mathbf{h}$  is the external ac magnetic field. It should be noted that this definition makes sense only under the condition that the domain widths are small as compared with both the sample dimensions and the electromagnetic wavelength. If this condition is satisfied,  $\overline{\mathbf{m}}$  and, hence, the tensor  $\overline{\overline{\chi}}$  can be found by solving the equations of motion, e.g., (8.31) and (8.32) containing the external field  $\mathbf{h}$ . As distinct from the susceptibility tensor of a sample magnetized to saturation, the tensor  $\overline{\overline{\chi}}$  will have, in general, all nine components passing through resonance at the eigenfrequencies of the unsaturated sample.

In both considered examples the domain structure was regular, i.e., it contained a small number of groups of equivalent domains (two groups in these examples). In this case, the  $\overline{\overline{\chi}}^e$  components obtained by solving the coupled equations of motion for these groups and, hence, the amplitudes and widths of ferromagnetic resonance curves corresponding to each coupled mode should be of the same order of magnitude as for a sample magnetized to saturation. This is convincingly illustrated by Figure 8.8.

But if the domain structure is *irregular*, contains many domains of different dimensions and shapes (as is always the case in polycrystals), then a single but 'nonuniformly broadened' and distorted resonance curve is observed. The

irregularity of the domain structure is the main reason for the fact that the region of the 'natural' (in the absence of a steady magnetic field) ferromagnetic resonance in magnetic spectra of polycrystals is usually very broad (as, e.g., in Figure 8.4). This region sometimes overlaps with the region of domain-wall oscillations [288].

The boundaries of the *natural* ferromagnetic-resonance region in *polycrystals* can be estimated in the following way. One can see from (8.33) and (8.34) that  $\omega_{\perp}$  and  $\omega_{\parallel}$  at  $H_{e0} = 0$  depend on the demagnetization factors  $N_x$  and  $N_y$ , in the considered case, of the polycrystal grains. Allowing for arbitrary forms and orientations of the grains, we see that these factors can vary from 0 to  $4\pi$ , and therefore,

$$\omega_{\min} = 2\gamma H_{A1} \quad \omega_{\max} = \gamma(2H_{A1} + 4\pi M_0). \quad (8.36)$$

This estimate was first made by Polder and Smit [320]. The value of  $\omega_{\max}$  is very important because it is the borderline frequency of the so-called *initial losses* in ferrites: at frequencies less than  $\omega_{\max}$ , large losses caused by the natural ferromagnetic resonance prevent the use of the material in devices operating at zero or small steady magnetic fields.

### 8.2.3 Nonuniform modes in unsaturated samples

Rigorous analysis of nonuniform modes (Walker's oscillations and spin waves) in samples with domain structure must be based on the simultaneous solution of the equations of motion for all domain groups and the electrodynamic equations, with regard to all boundary conditions. They include the conditions at the sample surface and at the domain boundaries, assuming the domain-wall thickness to be small as compared with the domain dimensions. Even with this assumption and for simple regular domain structures, like the above-considered, the solution leads to complicated integro-differential equations [38]. A rather simple solution is possible only when the wavelength of the nonuniform mode is much larger than the domain dimensions. Then, the problem can be solved in the same way as for the sample without domains but using the *averaged* susceptibility  $\bar{\chi}^e$ .

The nonexchange oscillation modes found in such way are of two types. The modes of the first type are excited by the transverse (with respect to  $\mathbf{H}_{e0}$ ) ac magnetic field and transform into conventional Walker's modes at  $H_{e0}$  higher than the saturation field. The modes of the second type excited by the longitudinal ac field have no analog in saturated samples.

An approximate analysis of *spin waves* in the presence of domain structure is possible under one of the following conditions:

$$(1) \quad \frac{2\pi}{k} \gg d, b \quad (2) \quad \frac{2\pi}{k} \sim d \gg b \quad (3) \quad \frac{2\pi}{k} \ll d \gg b. \quad (8.37)$$

Here  $k$  is the wave number of the spin wave,  $d$  is the domain width, and  $b$  is the domain-wall thickness.

In the *first* case, an averaged tensor  $\overline{\chi}^e$  can be used. As  $d \sim 1 \mu\text{m}$  and, hence,  $k \ll 10^5$ , the exchange interaction can be neglected for many substances, e.g., for YIG, and the waves are the nonexchange magnetostatic waves (Section 6.2).

In the *second* case, the domain-wall energy can be neglected, as in the case (1), but the averaged susceptibility tensor cannot be used. The solutions of the magnetostatic problem for neighboring domains must be found and bound with each other by the conditions at the domain boundaries.

Consider, for example, *nonexchange* magnetostatic waves in a plate of thickness  $l$  with an easy axis of anisotropy perpendicular to the plate surface. Suppose that a simple layered domain structure [Figure 8.2(a)] takes place. The potential in the  $n$ th domain can be written in the form

$$\psi_n = (A_z \cos k_z z + B_z \sin k_z z)(A_{x_n} \cos k_{x_n} x + B_{x_n} \sin k_{x_n} x) \exp(-ky) \quad (8.38)$$

[compare with (6.60)]. The values of  $A_z$ ,  $B_z$ , and  $k_z$  must be the same in all domains, otherwise it would be impossible to satisfy the boundary conditions at domain boundaries. In the expressions for the potential outside the plate, the factors depending on  $x$  and  $y$  should be the same as in (8.38) in order to satisfy the boundary conditions at the plate surfaces. The factors depending on  $z$  in these expressions must be:  $C \exp(-\kappa_{z0} z)$  at  $z > l$  and  $D \exp(\kappa_{z0} z)$  at  $z < 0$ . The equation for  $k_z$ , which follows from the boundary conditions at the plate surfaces, will differ from (6.31) only by the replacement  $d \rightarrow l$ . Substitution of (8.38) and the potential outside the plate, respectively, into the Walker and the Laplace equations results in the expressions

$$k_z^2 = -\mu(k_{x_n}^2 + k^2) \quad \kappa_{z0}^2 = k_{x_n}^2 + k^2 \quad (8.39)$$

from which one can see that the  $k_{x_n}$  values in all domains are equal.

Consider now the simplest modes with the same potentials in all domains magnetized in the same direction. Then, it is sufficient to take into account the conditions at the boundary of a domain with its neighbor. These conditions are satisfied [69], analogously to the case of a plate magnetized to saturation (Section 6.2), either under the condition (6.36) (but now  $d$  is the *domain* width) or under the condition  $\mu k_x^2 + \mu_a k^2 = 0$ . The first possibility corresponds to volume waves, with trigonometric  $x$  dependence. In the second case, the  $x$  dependence is hyperbolic ( $k_x^2 < 0$ ), i.e., a surface wave propagates along the domain boundary [287, 85]. It should be emphasized that the considered solution is not valid if the condition  $2\pi/k \gg b$  is not satisfied, so that the domain wall cannot be regarded as infinitely thin.

For sufficiently large  $k$  values, i.e., in the *third* case in (8.37), it is possible to assume approximately, paying no attention to domain walls, that in each domain there exist independent spin waves with the dispersion laws as in the unbounded medium with the magnetization of the domain. In Section 10.3 it will be shown that such approximation is adequate in the study of parametric excitation of spin waves in unsaturated samples.



# 9

## *Nonlinear oscillations of magnetization*

### 9.1 Ferromagnetic resonance in strong alternating fields

In all preceding chapters we dealt with linear relations between ac components of magnetization and magnetic field, which were found by solving the linearized equations of motion, e.g., (1.66) or (2.18). But the initial equation of motion for the magnetization, the Landau–Lifshitz equation (2.6), is nonlinear. Hence, at sufficiently high amplitudes of the ac magnetic field and magnetization, the linear relation between them gets broken and nonlinear effects arise. In this chapter some of these effects will be studied.

#### 9.1.1 Rigorous solution of equation of motion

The Landau–Lifshitz equation can be solved rigorously, at arbitrary amplitudes of the ac field, only in a few particular cases. The simplest case is the magnetization precession in the ac field with *circular* polarization. This problem was solved by Skrotskii and Alimov [364]. The solution depends materially (as distinct from the linear case) on the form of a dissipative term in the equation of motion. Consider first equation (1.64) with a dissipative term in the *Bloch–Bloembergen* form.

Assume in (1.64) that

$$\mathbf{H} = \mathbf{H}_0 + \mathbf{h}_{\sim} \quad (9.1)$$

where  $\mathbf{H}_0 = z_0 H_0$  is the internal steady field and  $\mathbf{h}_{\sim}$  is the transverse ac field with right-hand circular polarization. Now, in studying nonlinear processes, we have to do away with the complex-amplitude method (in any case, in its simple form used in previous chapters) and use the *instantaneous* values of all ac quantities. So,

$$\mathbf{h}_{\sim} = h_0 (x_0 \cos \omega t + y_0 \sin \omega t). \quad (9.2)$$

From symmetry considerations, we may seek the solution in the form

$$\mathbf{M} = m_0 [x_0 \cos(\omega t + \varphi) + y_0 \sin(\omega t + \varphi) + z_0 M_z]. \quad (9.3)$$

Substituting (9.1)–(9.3) into (1.64) and projecting the obtained equation onto the coordinate axes, we get three equations for  $m_0$ ,  $\varphi$ , and  $M_z$ . Solving them, we find  $M_z$  and the *nonlinear susceptibility*, which can be defined as

$$\chi_{+n} = \frac{m_0}{h_0} \exp(i\varphi). \quad (9.4)$$

The values of  $M_z$  and of the imaginary part of  $\chi_{+n}$  at resonance ( $\omega = \gamma H_0$ ) are

$$M_{z \text{ res}} = M_0 \left(1 + \frac{\gamma^2 h_0^2}{\omega_r^2}\right)^{-1} \quad \chi''_{+n \text{ res}} = \frac{\gamma}{\omega_r} M_{z \text{ res}}. \quad (9.5)$$

The resonance nonlinear susceptibility is proportional to  $M_{z \text{ res}}$ , and both quantities decrease with the growth of  $h_0$  (Figure 9.1, curves B).

The solution of equation (1.62) with the dissipative term in the *Gilbert* form leads to different results [364] (Figure 9.1, curves G):

$$\begin{aligned} M_{z \text{ res}} &= M_0 \left(1 - \frac{\gamma^2 h_0^2}{\alpha^2 \omega^2}\right)^{1/2} & \chi_{+n \text{ res}} &= \frac{\gamma M_0}{\alpha \omega} & \text{at } h_0 &\leq \frac{\alpha \omega}{\gamma} \\ M_{z \text{ res}} &= 0 & \chi_{+n \text{ res}} &= \frac{M_0}{h_0} & \text{at } h_0 &\geq \frac{\alpha \omega}{\gamma} \end{aligned} \quad (9.6)$$

In (9.5) and (9.6)  $h_0$  is the amplitude of the *internal* ac magnetic field. But expressions (9.6) are valid strictly, and expressions (9.5) are valid approximately for a sphere, too, if  $h_0$  is the amplitude of the *external* field. Actually, the equation of motion for the magnetization of a small ellipsoid (with the Gilbert-type dissipative term) has the form

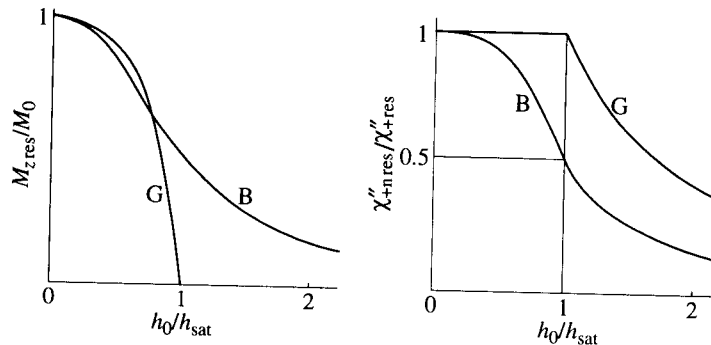
$$\frac{\partial \mathbf{M}}{\partial t} = -\gamma \mathbf{M} \times (\mathbf{H}_{e0} + \mathbf{h}_{e\sim} - \vec{N} \mathbf{M}) + \frac{\alpha}{M} \mathbf{M} \times \frac{\partial \mathbf{M}}{\partial t} \quad (9.7)$$

where  $\mathbf{H}_{e0}$  and  $\mathbf{h}_{e\sim}$  are the steady and the ac external fields. For a sphere,  $\vec{N}$  is a scalar and the demagnetizing field  $\mathbf{N} \mathbf{M}$  drops out of the equation. Then, (9.7) coincides with (1.62) after the replacement of the external fields by the internal ones. This fact was pointed out in Section 1.5 for linearized equations, but it takes place in the case of strong ac fields, too.

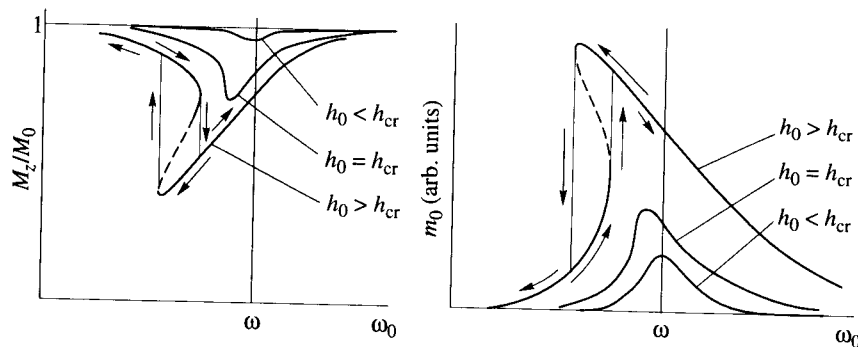
Different behavior of the ac magnetization for different forms of the dissipative term results in, seemingly, the possibility to favor one or the other form using the experiments on ferromagnetic resonance in strong ac fields. But this possibility usually cannot be realized because another nonlinear process, the parametric excitation of spin waves (Chapter 10), arises at field amplitudes much less than  $\alpha \omega / \gamma$  and prevents the manifestation of the above-considered nonlinear process.

A strict solution of the nonlinear equation of motion was found, as well, for an *ellipsoid of revolution* (spheroid) in a steady field parallel to the axis of revolution and a circularly polarized ac field. The solution, in this case, can also be sought in the form of (9.3). But the nonlinear eigenfrequency  $\omega_{0n}$  now has the form

$$\omega_{0n} = \gamma [H_{e0} + (N_{\perp} - N_z) M_z] \quad (9.8)$$

**FIGURE 9.1**

Dependence of  $M_z$  and of the nonlinear susceptibility at resonance on ac field amplitude, found by solving the equations of motion of magnetization with dissipative terms in the Bloch–Bloembergen form (curves B) and in the Gilbert form (curves G). The field  $h_{\text{sat}} = \omega_r/\gamma$  in the case B, and  $h_{\text{sat}} = \alpha\omega/\gamma$  in the case G. In both cases  $h_{\text{sat}} = \Delta H/2$  where  $\Delta H$  is the width of the linear resonance curve.

**FIGURE 9.2**

Solutions of the equation of motion of magnetization for an oblate spheroid ( $N_z - N_\perp > 0$ ) at different ac field amplitudes (schematically). Arrows show the directions of the steady-magnetic-field change.

which differs from the linear eigenfrequency by the substitution of  $M_z$  for the steady magnetization  $M_0$ . According to (9.5) or (9.6),  $M_z$  decreases with growing  $m_0$ . Therefore, the eigenfrequency increases with the growth of  $m_0$  when  $N_z > N_\perp$  (i.e., for an oblate spheroid) and decreases when  $N_z < N_\perp$  (i.e., for a prolate spheroid). The amplitude  $m_0$ , in its turn, depends on the eigenfrequency  $\omega_{0n}$ . Such self-consistent dependences can lead to *instability*.

Assume, e.g., that, in the case of a disk, at the frequency of the ac field  $\omega > \omega_{0n}$ , the amplitude  $m_0$  has accidentally grown. Then,  $M_z$  will decrease and  $\omega_{0n}$  will increase and, so, come nearer to  $\omega$ . This will lead to the further growth of  $m_0$ ,

and so on, until  $\omega_{0n}$  reaches  $\omega$ . The problem was solved strictly by Skrotskii and Alimov [364]. They showed that the instability results in a *nonunique* dependence of  $m_0$  and  $M_z$  on  $\omega$  or  $H_{e0}$  in certain intervals of these parameters (Figure 9.2). The nonuniqueness arises when the amplitude of the ac magnetic field with circular polarization exceeds the critical value  $h_{cr}$  depending on the sample shape. For a sphere,  $h_{cr} = \infty$ . For a thin disk, the critical field is the lowest:

$$h_{cr \min} \cong \frac{1}{2} \frac{(\Delta H)^{3/2}}{\sqrt{4\pi M_0}}. \quad (9.9)$$

For a YIG single crystal ( $\Delta H \simeq 0.5$  Oe),  $h_{cr \min} \simeq 0.004$  Oe, i.e., about 50 times smaller than the field  $\Delta H/2$ , at which, as we have seen, the saturation of ferromagnetic resonance in a sphere takes place.

It is easy to make sure that the instabilities occur at the middle parts of the  $M_z$  and  $m_0$  vs  $\omega_0$  curves (Figure 9.2). As a result, the resonance curves (i.e., the dependences of the absorbed power on  $\omega$  or  $H_{e0}$ ) turn out to be non-Lorentz, and hysteresis takes place. In electrodynamic systems containing nonspherical ferrite samples, low-frequency self-oscillations can arise at sufficiently high microwave-power levels.

Weiss [438] was the first to observe such nonlinear phenomena in ferrite disks. Anderson and Suhl [19] explained them using an approximate solution of the equation of motion, the obtained  $h_{cr}$  value differs from the exact value (9.9) only by a factor of the order of unity. It is worth noting that the work [19] was the first step to Suhl's theory [391, 392] of the parametric excitation of spin waves (Chapter 10).

The instability in the nonlinear motion of the magnetization at high power levels can be caused not only by the shape anisotropy of the sample but also by other kinds of anisotropy (e.g., by the magnetocrystalline anisotropy) that lead to the dependence of the eigenfrequency on the ac magnetization amplitude. Such dependence and, hence, the instability can arise also because of the change of the anisotropy constants due to the heating of the sample by the ac field. This effect was explained by Damon [81].

### 9.1.2 Approximate methods

One of the methods of approximate analysis of nonlinear magnetization oscillations uses the *conservation of the vector  $\mathbf{M}$  length*:

$$M_x^2 + M_y^2 + M_z^2 = M_0^2 \quad (9.10)$$

whence, in the case of  $M_x, M_y \ll M_0$ , it follows that

$$M_z \cong M_0 - \frac{1}{2M_0} (M_x^2 + M_y^2). \quad (9.11)$$

Then, we can use the method of successive approximations and find  $M_x$  and  $M_y$ , in the first approximation, from the linear theory. For an isotropic ferromagnet

$$\begin{aligned} M_x &= \text{Re} [(\chi h_x + i\chi_a h_y) \exp(i\omega t)] \\ M_y &= \text{Re} [(-i\chi_a h_x + \chi h_y) \exp(i\omega t)]. \end{aligned} \quad (9.12)$$

Here  $h_x$  and  $h_y$  are complex amplitudes of the ac magnetic field: of the internal field if  $\chi$  and  $\chi_a$  are components of the linear susceptibility tensor, or of the external ac field if  $\chi$  and  $\chi_a$  are components of the external susceptibility of the sample (Section 1.5). Substituting  $h_x = h_{x0}$  and  $h_y = h_{y0} \exp(i\varphi)$  (where  $h_{x0}$  and  $h_{y0}$  are real quantities) into (9.12) and using (9.11), we find

$$M_z = M_0 - \delta M_z + M_{z2} \quad (9.13)$$

$$\begin{aligned} \delta M_z &= \frac{1}{4M_0} [(|\chi|^2 + |\chi_a|^2) (h_{x0}^2 + h_{y0}^2) \\ &\quad - 4 \sin \varphi (\chi' \chi'_a + \chi'' \chi''_a) h_{x0} h_{y0}] \end{aligned} \quad (9.14)$$

$$\begin{aligned} M_{z2} &= -\frac{1}{4M_0} \{ (\chi'^2 - \chi''^2 - \chi_a'^2 + \chi_a''^2) [h_{x0}^2 \cos 2\omega t + h_{y0}^2 \cos(2\omega t + \varphi)] \\ &\quad + 2 (\chi' \chi'' - \chi'_a \chi''_a) [h_{x0}^2 \sin 2\omega t + h_{y0}^2 \sin(2\omega t + \varphi)] \}. \end{aligned} \quad (9.15)$$

The quantity  $\delta M_z$  represents the effect of *detection* of the magnetization oscillations. One can see from (9.14) that this effect takes place at any polarization of the ac field. For the linear polarization of this field (when, e.g.,  $h_{y0} = 0$ )

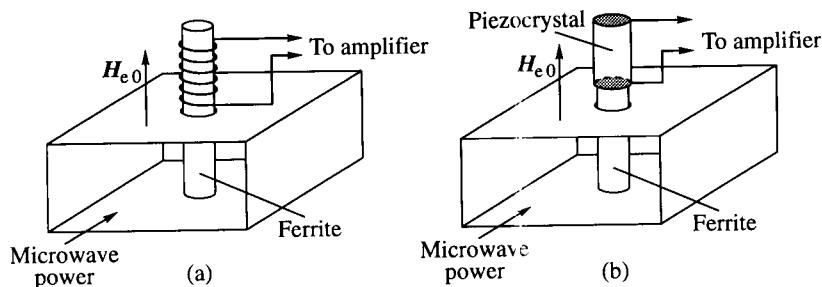
$$\delta M_z = \frac{1}{4M_0} (|\chi|^2 + |\chi_a|^2) h_{x0}^2 \quad (9.16)$$

and for the right-hand circular polarization ( $h_{x0} = h_{y0} = h_0$ ,  $\varphi = -\pi/2$ )

$$\delta M_z = \frac{1}{2M_0} |\chi + \chi_a|^2 h_0^2. \quad (9.17)$$

At resonance [ $\chi' = \chi'_a \cong 0$ ,  $\chi'' = \chi''_a = \gamma M_0 / (2\alpha\omega)$ ], expression (9.17) coincides with the expression that follows from (9.6) in the case of small amplitude  $h_0$ . It should be noted that the  $\delta M_z$  value following from (9.5) is twice as large as (9.17). This results from the fact that equation (1.62), from which (9.5) follows, does not ensure, in contrast to equation (1.64), the conservation of the vector  $\mathbf{M}$  length.

The considered effect of detection can be observed by two methods (Figure 9.3). One of them, used by Bloembergen and Wang [57], is the recording of the emf induced in a coil adjacent to the sample. Another method is the recording of the magnetostrictive deformation of the sample by using the piezoelectric effect in a quartz or ferroelectric sample fastened to the ferromagnetic sample [190]. The



**FIGURE 9.3**  
Ferrite detectors using (a) magnetic induction and (b) magnetostriction [190].

sensitivity of such ferrite detectors is much less than the sensitivity of commonly used semiconductor detectors. But the ferrite detector, which uses the *volume* effect, is more resistant to high power, repeated temperature changes, and radiation damage.

The harmonic functions with frequency  $2\omega$  appear linearly in (9.15); hence, we can use now the method of complex amplitudes. Applying the formulae for  $\chi$  and  $\chi_a$ , which follow from (1.39) after the replacement (1.68), we obtain from (9.15) a very simple expression for the complex amplitude of  $M_{z2}$ :

$$m_{z2} = -\frac{\gamma\chi_a}{4\omega} (h_x^2 + h_y^2). \quad (9.18)$$

Expressions (9.15) and (9.18) represent the effect of *frequency doubling*. It follows from (9.18) that this effect is absent if the field is circularly polarized, provided that the tensor  $\vec{\chi}$  or  $\vec{\chi}^e$  has cylindrical symmetry, which has been assumed in deriving (9.18).

The above-considered approximate method has essential limitations. First, the vector  $\mathbf{M}$  length conservation holds, as was already mentioned, not for every form of the dissipative term in the equation of motion and, as we will see in Chapter 11, not for all relaxation processes. Second, using this method, we can find only the nonlinear terms of the longitudinal magnetization component  $M_z$ . Now we are going to discuss a *more universal* method of successive approximations [153]. We seek the solution of the equation of motion in the form

$$\mathbf{M} = \mathbf{M}_0 + \mathbf{M}^{(1)} + \mathbf{M}^{(2)} + \dots \quad (9.19)$$

and assume that  $M_0 \gg M^{(1)} \gg M^{(2)} \dots$ . Limiting ourselves to the uniform magnetization oscillations, we write the effective field (Section 2.1) as

$$\mathbf{H}_{\text{ef}} = \mathbf{H}_0 + \mathbf{h}_{\sim} - \vec{N}\mathbf{M} \quad (9.20)$$

where  $\mathbf{H}_0$  and  $\mathbf{h}_{\sim}$  are the given magnetic fields ( $H_0 \gg h_{\sim}$ ) and  $\vec{N}$  is the entire tensor of demagnetization factors, including the demagnetization factors of all

kinds of anisotropy.

Substitute now (9.19) and (9.20) into the equation of motion (2.6). To the zero approximation, neglecting  $M^{(1)}$ ,  $M^{(2)}$  . . . , and  $h_{\sim}$ , we obtain the equilibrium condition (1.86) (with the replacement of  $H_{e0}$  by  $H_0$ ). To the *first* approximation, retaining terms of the first order in  $M^{(1)}$  and  $h_{\sim}$  and taking into account the equilibrium condition, we get the linearized equation

$$\begin{aligned} \frac{\partial M^{(1)}}{\partial t} + \gamma M^{(1)} \times \left( H_0 - \vec{N} M_0 \right) - \gamma M_0 \times \vec{N} M^{(1)} \\ + \omega_r \left( 1 + \chi_0 \vec{N} \right) M^{(1)} = -\gamma M_0 \times h_{\sim} + \omega_r \chi_0 h_{\sim} \end{aligned} \quad (9.21)$$

where  $\chi_0 = M_0 / |H_0 - \vec{N} M_0|$ . To the *second* approximation, retaining terms of the second order and taking into account the equilibrium condition and equation (9.21), we obtain the equation for  $M^{(2)}$ . Proceeding with this process, we make sure that the  $n$ th-order magnetization ( $n \geq 2$ ) satisfies the recurrent equation

$$\frac{\partial M^{(n)}}{\partial t} + \gamma \sum_{k=0}^n M^{(k)} \times H_{\text{ef}}^{(n-k)} + \omega_r \left( 1 + \chi_0 \vec{N} \right) M^{(n)} = 0. \quad (9.22)$$

The effective fields  $H_{\text{ef}}^{(n-k)}$  in this equation have the following form:

$$H_{\text{ef}}^{(0)} = H_0 - \vec{N} M_0, \quad H_{\text{ef}}^{(1)} = h_{\sim} - \vec{N} M^{(1)}, \quad H_{\text{ef}}^{(k)} = -\vec{N} M^{(k)} \quad (k \geq 2). \quad (9.23)$$

The considered method can be used either to calculate the magnetization of an ellipsoid in a given external field  $h_{\sim}$  or to find the magnetization in a given internal field  $h_{\sim}$ . And if in the latter case the substance is *isotropic*, we must take  $\vec{N} = 0$  in all expressions (9.23) but the first one. Then equations (9.22) are simplified:

$$\frac{\partial M^{(n)}}{\partial t} + \gamma M^{(n)} \times H_0 + \omega_r M^{(n)} = -\gamma M^{(n-1)} \times h_{\sim} \quad (9.24)$$

where  $H_0 = H_{e0} - \vec{N} M_0$  is the internal steady field. The magnetization  $M^{(n)}$  now depends not on all magnetizations of lower order but on  $M_0$  and  $M^{(n-1)}$  only. It should be noted that equations (9.24) are also valid for a sphere if  $h_{\sim}$  is the external ac field and  $H_0$  is replaced by the external steady field  $H_{e0}$ .

## 9.2 Harmonic generation and frequency conversion

The approximate methods considered above will be applied in this section to the study of nonlinear effects in which magnetization components arise with

frequencies other than the frequency of the external field. The frequency doubling, mentioned in the previous section, is one of such effects.

### 9.2.1 Frequency doubling

Consider first in more detail the component  $M_{z2}$ , for which expressions (9.15) and (9.18) were already found. When the ac magnetic field is circularly polarized and tensor  $\vec{\chi}$  has cylindrical symmetry, the tip of vector  $\mathbf{M}$  moves along the circular trajectory, and no ac component of  $M_z$  appears (as well as no transverse  $\mathbf{M}$  components with frequencies other than the frequency  $\omega$  of the ac field). But if the system has *no cylindrical symmetry* or the ac field is not circularly polarized, the  $M_z$  component with frequency  $2\omega$  arises, as shown in Figure 9.4. One can see from the figure that the amplitude of this component

$$m_{z2} \cong \frac{m_{x0}^2 - m_{y0}^2}{4M_0} \quad (9.25)$$

where  $m_{x0}$  and  $m_{y0}$  are real (not complex) amplitudes of  $M_x$  and  $M_y$ . It is easy to make sure that (9.25) is equivalent to (9.18).

The difference between  $m_{x0}$  and  $m_{y0}$ , which determines the effectiveness of frequency doubling, can be characterized by the *ellipticity* (1.101), and expression (9.25) can be written as

$$m_{z2} = \frac{m_{x0}^2}{4M_0} \mathcal{E}. \quad (9.26)$$

Small ellipticity of ac magnetization arises in a sample with cylindrical symmetry made of isotropic ferrite if the polarization of the ac field is not circular. For the linear polarization of the field, the polarization of magnetization is maximal and, at resonance, is equal to  $2\alpha$  where  $\alpha$  is the Gilbert dissipation parameter. Then, according to (9.24) and (1.117),

$$m_{z2\text{res}} = \frac{\gamma^2 M_0 h_0^2}{8\alpha\omega^2} \quad (9.27)$$

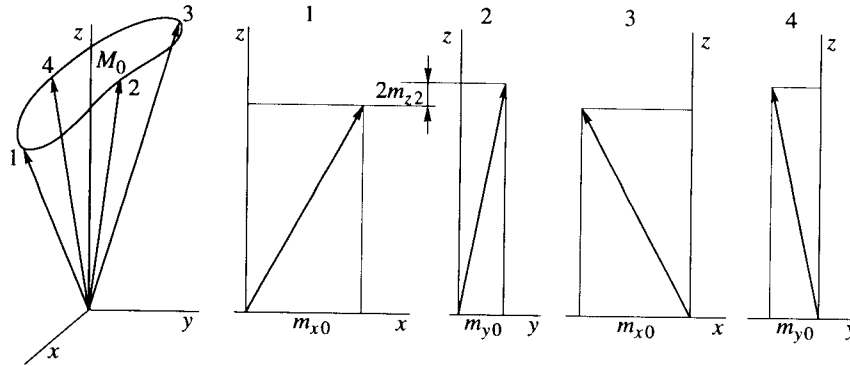
( $h_0$  is here the amplitude of a linearly polarized external field).

The ellipticity of the magnetization is much larger in samples with transverse demagnetization factors *not equal* to each other. Obviously, it is the largest in a thin tangentially magnetized disk. If  $\alpha \ll 1$ , the ellipticity, in this case, weakly depends on the polarization of the ac field. At resonance, it differs but slightly from the ellipticity (1.100) of free oscillations or, in our case, from

$$\mathcal{E} = \frac{4\pi M_0}{H_{e0} + 4\pi M_0}. \quad (9.28)$$

Calculating  $m_{x0}$  at resonance with the use of (1.116), (1.92), and (1.104) and



**FIGURE 9.4**

Positions of the magnetization vector at successive instants in the course of noncircular precession.

substituting it, together with (9.28), into (9.26), we obtain

$$m_{z2\text{res}} = \frac{\pi M_0^2}{4\alpha^2 (H_{e0} + 2\pi M_0)^2 H_{e0}} h_0^2. \quad (9.29)$$

This quantity is three orders of magnitude larger than (9.27) for YIG ( $\Delta H \cong 0.5$  Oe) in 3 cm wavelength range.

To increase the ellipticity of magnetization still more we can use the *magnetocrystalline anisotropy* (Chapter 2). The most advantageous is the case of a tangentially magnetized disk of single-crystal ferrite with the easy plane of anisotropy coinciding with the disk plane [30]. Then,  $4\pi M_0$  in (9.28) is replaced by  $4\pi M_0 + 2|H_{A1}|$  where  $H_{A1} = K_1/M_0$ , and  $K_1$  is the anisotropy constant. The value of  $2|H_{A1}|$  is as high as  $\sim 30$  kOe for some hexagonal ferrites, and  $\mathcal{E}$  becomes very close to unity even at rather high frequencies. High values of ellipticity and, hence, high effectiveness of frequency doubling are also achieved at *magnetodynamic resonance* in comparatively large ferrite samples (Section 5.3).

The frequency doubling is a quadratic effect. Therefore, its efficiency (which can be defined as the ratio of the output power  $P_2$  at frequency  $2\omega$  to the input power  $P_1$  at frequency  $\omega$ ) increases with growing  $P_1$ . The achievable values of the efficiency are limited either by the thermal conditions in the device or by the parametric excitation of spin waves (Chapter 10).

Rather high values of the frequency-doubling efficiency were obtained already in early ferrite devices of this type. Melchor, Ayres, and Vartanian [274] obtained the output pulse power as high as 8 kW at frequency 18 GHz with input power of 32 kW; most likely, the magnetodynamic resonance was used. Later, the efficiency of a frequency doubler with magnetodynamic resonance reached  $-2$  dB, the output power being 2 kW [263]. Output power of 50 W was obtained at

a frequency as high as 140 GHz [28].

Let us consider now the harmonics of the *transverse* magnetization components. The method of successive approximations based on solving the recurrent equations (9.21)–(9.24) must be used in this case. Limit the treatment to an isotropic ferromagnet and examine, to the second approximation, the magnetization in a given internal field. We can use, then, rather simple equation (9.24). Projecting this equation onto coordinate axes, we get for  $n = 2$

$$\begin{aligned} \frac{\partial M_x^{(2)}}{\partial t} + \gamma M_y^{(2)} H_0 + \omega_r M_x^{(2)} &::: -\gamma M_y^{(1)} h_{\sim z} \\ \frac{\partial M_y^{(2)}}{\partial t} - \gamma M_x^{(2)} H_0 + \omega_r M_y^{(2)} &::: \gamma M_x^{(1)} h_{\sim z} \end{aligned} \quad (9.30)$$

$$\frac{\partial M_z^{(2)}}{\partial t} + \omega_r M_z^{(2)} = -\gamma \left( M_x^{(1)} h_{\sim y} - M_y^{(1)} h_{\sim x} \right). \quad (9.31)$$

The first-order magnetization components in the right-hand sides of these equations may be regarded as known.

The quantity  $M_z^{(2)}$  in (9.31) is the longitudinal second-order magnetization component, which was considered above. Equations (9.30) determine the transverse second-order components. They arise, as one can see from (9.30), only if the ac field, besides the transverse components (necessary for the excitation of the first-order magnetization components  $M_x^{(1)}$  and  $M_y^{(1)}$ ), has the *longitudinal* component  $h_{\sim z}$ . Consider the case when this component has the same frequency  $\omega$  as the transverse components, i.e., when there is one ac field making an angle not equal to 0 or  $\pi/2$  with the steady field  $\mathbf{H}_0$ . Then, the solution of (9.30) will contain components with frequency  $2\omega$ , which can be written in a complex form. Assuming  $M_{x,y}^{(2)} = \text{Re}[m_{x,y2} \exp(2i\omega t)]$ , we find

$$m_{x,y2} = -\frac{(2\omega^2 + \gamma^2 H_0^2) h_{x,y} \pm 3i\omega\gamma H_0 h_{y,x}}{2(\gamma^2 H_0^2 - \omega^2 + 2i\omega\omega_r)(\gamma^2 H_0^2 - 4\omega^2 + 4i\omega\omega_r)} \gamma^2 M_0 h_z. \quad (9.32)$$

One can see from (9.32) that the quantities  $m_{x,y2}$  pass through resonance at *two values* of the steady field,

$$H_{01} = \frac{\omega}{\gamma} \quad H_{02} = \frac{2\omega}{\gamma}. \quad (9.33)$$

If we dealt with nonlinear magnetic oscillations in a given *external* ac field with account for the shape and the magnetocrystalline anisotropies, i.e., if we solved equation (9.22), then instead of (9.33) we would get more general resonance conditions

$$\omega_{01} = \omega \quad \omega_{02} = 2\omega \quad (9.34)$$

where  $\omega_0(H_0, M_0, \vec{N})$  is the frequency of linear ferromagnetic resonance in the sample. The maximal values of  $m_{x,y2}$  are equal at both resonances, and in the

case of a linearly polarized ac field (assuming, e.g.,  $h_y = 0$ ) we get

$$-m_{y2} = im_{x2} = \frac{\gamma^2 M_0 h_x h_z}{4\omega\omega_r}. \quad (9.35)$$

Comparing (9.35) with expression (9.27) for the second harmonic of the longitudinal magnetization component in an isotropic sample with cylindrical symmetry, we see that (if  $h_x$  and  $h_z$  are of the same order) the values of the second harmonics of the longitudinal and the transverse magnetizations are approximately the same. But it has been shown above that the values of  $m_{z2}$  increase materially if there is any anisotropy in the  $xy$  plane. No such great increase occurs, as it can be shown, for the transverse second-order components, and it seems that there is no point in using transverse components  $m_{x,y2}$  in devices for frequency doubling. However, these components have maxima at  $\omega_0 = 2\omega$ , e.g., for a small isotropic sphere, at  $H_{e0} = 2\omega/\gamma$ . At such fields the spin-wave spectrum lies above the frequency  $\omega$ , and the low-order processes of the spin-wave parametric excitation (Chapter 10) are forbidden. Therefore, in frequency doublers in which the transverse second harmonics are used, it is possible, under the condition  $\omega_0 = 2\omega$ , to reach high input powers and, hence, obtain the efficiencies of doubling comparable with the efficiencies of the devices that use  $m_{z2}$ . The efficiency as high as  $-5$  dB was obtained in one of the devices using the transverse components [279].

An interesting, though weak, nonlinear effect is observed at  $\omega_0 = 2\omega$  [89]: a maximum of the power absorbed by the sample takes place in the steady field satisfying this condition. By analogy with nonlinear optics (e.g., [55]) this effect can be referred to as *two-quantum absorption*. The qualitative explanation of this effect is obvious—some energy is needed to excite the second harmonic of the transverse magnetization, which passes through a maximum under the condition  $\omega_0 = 2\omega$ . However, such an effect is absent in the framework of the two approximations considered up to now, because the absorption at frequency  $\omega$  is determined by the first-harmonic amplitudes, which, up to the second approximation, have no maximum at  $\omega = 2\omega_0$ . The third approximation is needed to find the nonlinear contributions to these amplitudes. The ratio of the power absorbed at  $\omega = 2\omega_0$  to the power absorbed at ferromagnetic resonance ( $\omega = \omega_0$ ) depends, of course, on the value of the input power  $P_1$ . This ratio was equal to  $-60$  dB for YIG at  $P_1 = 15$  W [89].

Using the chain of equations (9.22) or (9.24), we can find each harmonic of the transverse magnetization components. The  $n$ th harmonic will have maxima in the steady fields determined by the conditions  $\omega_0 = m\omega$  ( $m = 1, 2, 3, \dots, n$ ). The intensities of the harmonics decrease with the growth of their numbers as  $(h_{\sim 0}/H_0)^n$ . The *third* harmonic was observed with the efficiency of  $-24$  dB at an input power of 32 kW [363].

### 9.2.2 Frequency mixing

If several ac magnetic fields with frequencies  $\omega_1, \omega_2, \dots$  are applied, then, along with the above-considered nonlinear effects, the magnetization components with *combination* frequencies  $n_1\omega_1 \pm n_2\omega_2 \pm \dots$  ( $n_{1,2,\dots} = 0, 1, 2, \dots$ ) arise. We limit ourselves to the case of *two* fields  $\mathbf{h}_1$  and  $\mathbf{h}_2$  with frequencies  $\omega_1$  and  $\omega_2$ .

The first-order magnetization  $\mathbf{M}^{(1)}$  is the solution of the linear equation (9.21) and, hence, is the sum of transverse magnetizations  $\mathbf{M}_1^{(1)}$  and  $\mathbf{M}_2^{(1)}$  with frequencies  $\omega_1$  and  $\omega_2$ , excited by the transverse components of the fields  $\mathbf{h}_1$  and  $\mathbf{h}_2$ , respectively. The second-order magnetization  $\mathbf{M}^{(2)}$  satisfies equations (9.22) or (9.24) with  $n = 2$ , which are linear in the unknown  $\mathbf{M}^{(2)}$  but are nonlinear with respect to the magnetizations  $\mathbf{M}_{1,2}^{(1)}$  and the fields  $\mathbf{h}_{1,2}$ . It is clear that  $\mathbf{M}^{(2)}$  will contain the combination harmonics with frequencies  $\omega_1 + \omega_2$  and  $|\omega_1 - \omega_2|$ . The emergence of these harmonics is the *frequency mixing*.

We will use, for simplicity, equation (9.22) or its projections (9.30) and (9.31). The combination harmonics of  $M_z^{(2)}$  can be found, as well, from the condition of  $M$  conservation. Two particular cases are to be considered: (i) both ac fields are transverse with respect to the steady magnetization, i.e., to the  $z$  axis; (ii) one field is transverse ( $\mathbf{h}_1 z_0 = 0$ ) and the second is longitudinal ( $\mathbf{h}_2 \times \mathbf{z}_0 = 0$ ). If both fields are longitudinal,  $\mathbf{M}^{(1)} = 0$  and, hence,  $\mathbf{M}^{(2)} = 0$ .

The case when *both* fields are *transverse* was first studied by Pippin [315]. In this case, it follows from (9.30) that  $M_x^{(2)} = M_y^{(2)} = 0$ ; the value of  $M_z^{(2)}$  can be found from (9.31) or from (9.11). Assume, first, that both fields  $\mathbf{h}_1$  and  $\mathbf{h}_2$  are *circularly* polarized:

$$\begin{aligned} h_{\sim x} &= h_{10} \cos \omega_1 t + h_{20} \cos \omega_2 t \\ h_{\sim y} &= \pm h_{10} \sin \omega_1 t \pm h_{20} \sin \omega_2 t \end{aligned} \quad (9.36)$$

where the signs  $\pm$  before the two terms are independent and correspond to the right-hand or left-hand rotation of the fields  $\mathbf{h}_1$  and  $\mathbf{h}_2$ . Substituting  $M_{x,y}^{(1)} = \text{Re}[m_{1x,y} \exp(i\omega t) + m_{2x,y} \exp(i\omega t)]$  into (9.11), we find

$$\begin{aligned} M_z - M_0 \equiv M_z^{(2)} &= -\frac{1}{2M_0} (|\chi_{1\pm}|^2 h_{10}^2 + |\chi_{2\pm}|^2 h_{20}^2) \\ &\quad - \frac{1}{M_0} [(-\chi'_{1\pm} \chi'_{2\pm} (\pm) \chi''_{1\pm} \chi''_{2\pm}) \cos (\omega_1 (\pm) \omega_2) t \\ &\quad + (\chi''_{1\pm} \chi'_{2\pm} (\pm) \chi'_{1\pm} \chi''_{2\pm}) \sin (\omega_1 (\pm) \omega_2) t] h_{10} h_{20} \end{aligned} \quad (9.37)$$

where  $\chi_{1,2\pm} = \chi_{1,2} \pm \chi_{a1,2}$  (the upper signs correspond to the right-hand and the lower signs, to the left-hand rotation of the polarization); the signs  $(\pm)$  have the following meaning:  $(+)$  corresponds to the opposite and  $(-)$ , to the identical directions of the polarization rotation for the two fields. One can see from (9.37) that the effects of detection are additive, and the effect of frequency doubling does not exist, as should be expected for circular polarization of both fields. The

alternating terms in (9.37) represent the effect of frequency mixing. The frequency  $\omega_1 - \omega_2$  arises when the directions of the polarization rotation of the both fields are the same, and the frequency  $\omega_1 + \omega_2$  arises when these directions are opposite.

An expression for the complex amplitude of the magnetization with frequency  $\omega_1 - \omega_2$  follows from (9.37):

$$m_{z-} = -\frac{1}{M_0} \chi_{1\pm} \chi_{2\pm}^* h_1 h_2. \quad (9.38)$$

The susceptibilities  $\chi_{1+}''$  and  $\chi_{2+}''$  reach high values near ferromagnetic resonance at frequencies  $\omega_1$  and  $\omega_2$ , respectively. And if  $|\omega_1 - \omega_2| < \omega_r$ , the resonance condition can be approximately satisfied at both frequencies simultaneously. Then, as it is easy to make sure,

$$m_{z-\text{res}} \cong \frac{\gamma^2 M_0}{\omega_r^2} h_{10} h_{20} \quad (9.39)$$

(for the right-hand polarization of both fields). If both fields have the same linear polarization, the value of  $m_{z-\text{res}}$  is eight times smaller.

Consider now the second particular case when *one* field is transverse, and the other is *longitudinal*. Without presenting here the solution of the system (9.30) for this case [153], we note only the following. As in the above-considered case of frequency doubling, the magnetizations with frequencies  $\omega_1 \mp \omega_2$  pass through maxima at two values of the steady field. One of them corresponds to the ferromagnetic resonance at the frequency  $\omega_1$  of the transverse ac field ( $H_{e0} = \omega_1/\gamma$  for a sphere). The second value corresponds to the resonance at the frequency  $|\omega_1 - \omega_2|$  or  $\omega_1 + \omega_2$ . The complex amplitudes of the magnetization harmonic with frequency  $|\omega_1 - \omega_2|$  (when the resonance at  $\omega_1$  takes place and  $|\omega_1 - \omega_2| \ll \gamma H_0 \equiv \omega_H$ ) have the form

$$m_{x-} = im_{y-} = \frac{i\gamma^2 M_0}{4\omega_H \omega_r} h_1 h_2. \quad (9.40)$$

Comparing (9.40) with (9.39), we see that the effectiveness of the frequency mixing is much higher in the case of both transverse fields when the resonance condition is approximately satisfied for both fields.

The designs of ferrite frequency mixers for the difference frequency  $|\omega_1 - \omega_2|$  (e.g. [286]) are like the designs of the ferrite detectors (Figure 9.3), but a resonance system, tuned to the frequency  $|\omega_1 - \omega_2|$ , must be added. This system can be realized, e.g., by putting the coil [Figure 9.3(a)] into a resonance circuit or by matching the dimensions of the piezoelectric sample [Figure 9.3(b)]. Despite all 'tricks' the sensitivity of ferrite frequency mixer appears to be much lower than the sensitivity of commonly used semiconductor devices. But the ferrite mixer, as the above-considered ferrite detector, has an unquestionable advantage of greater resistivity against high microwave power, radiation, etc.



# 10

---

## *Parametric excitation of magnetic oscillations and waves*

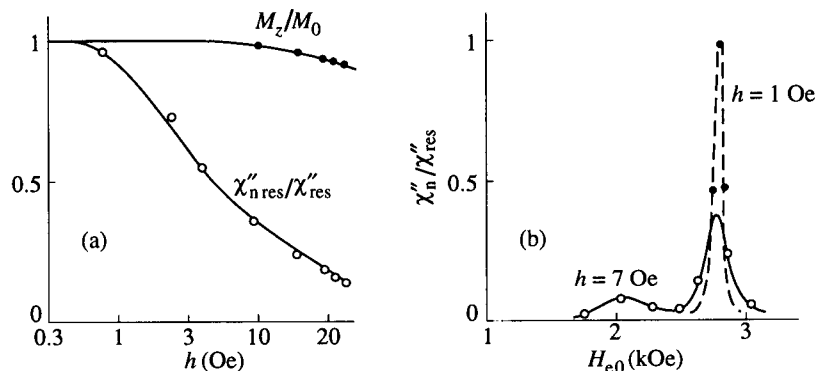
---

### 10.1 Nonlinear coupling of magnetic modes

In Chapter 9 we studied the nonlinear phenomena that occur in ferromagnetic samples in the presence of a *single*, in particular, the uniform mode. However, many different modes can exist in the sample; they were investigated in the previous chapters in linear approximation and, hence, were independent. The nonlinearity of the ferromagnet (and, so, of the equation of motion of magnetization) leads to the *coupling* of the modes, which results in a number of new nonlinear phenomena. The most interesting of them is the parametric excitation of some of these modes under the influence of other modes when the amplitudes of the latter exceed certain threshold values.

The nonlinear phenomena, caused—as it became clear later on—by the parametric excitation of spin waves, were first observed by Bloembergen, Damon, and Wang [56, 57] in the experiments on ferromagnetic resonance in strong ac fields. In these experiments the imaginary part of the tensor  $\bar{\chi}$  and the decrease of the steady magnetization projection  $M_z$  were independently measured. According to (9.5) or (9.6), an essential decrease of both these quantities should occur at ac field amplitude  $h$  of the order of the linear resonance-curve half-width  $\Delta H/2$  (Figure 9.1). Actually, a noticeable decrease of  $M_z$  took place (Figure 10.1) just at such ac field, while  $\chi''$  at resonance started to decrease at much smaller  $h$  value. Besides, an additional maximum of  $\chi''$  arose at steady magnetic field smaller than the resonance field (Figure 10.1). Neither of these effects can be understood within the framework of the one-mode nonlinear theory considered in Chapter 9. They were explained by Anderson and Suhl [19] using the idea of *instability* of certain spin waves under the influence of the uniform-magnetization precession.

Equilibrium (thermal) spin waves with small amplitudes and with frequencies distributed over broad range always exist in magnetically ordered substances (Section 7.3). Due to the nonlinearity of the spin system they are coupled to the

**FIGURE 10.1**

Ferromagnetic resonance in a sphere of single-crystal Ni ferrite in a strong ac field [57]: (a) dependences of  $M_z$  and nonlinear susceptibility  $\chi''_n$  at resonance on the ac field amplitude ( $\chi''$  is the linear susceptibility); (b) resonance curves in weak and strong ac fields. Frequency 9 GHz, room temperature.

uniform magnetization mode excited by the external ac field. When the amplitude of this (pumping) mode exceeds certain threshold value, the energy acquired by spin waves from this mode compensates spin-wave losses, and the instability, i.e., the exponential growth of the spin-wave amplitudes, begins. The theory of such instability was developed by Suhl [391, 392]. As the ac magnetization of the pumping mode is perpendicular to the steady magnetization, this phenomenon can be named spin-wave instability (or parametric excitation of spin waves) under perpendicular or *transverse* pumping.

Later, Schlömann, Green, and Milano [343] discovered spin-wave instability caused not by ac magnetization but directly by ac magnetic field parallel to the steady field. This phenomenon was called parametric excitation of spin waves with *longitudinal* (or parallel) pumping. It should be noted that the fact of nonlinear absorption of the energy of an ac magnetic field parallel to the steady magnetization, at high amplitudes of the ac field, was predicted by Kaganov and Tsukernik [201].

We will restrict ourselves to the study of parametric excitation of spin waves in *ferromagnets*. This will give an explanation of the phenomenon in ferrimagnets (ferrites), too, because at fields and frequencies commonly used, only the lower, 'ferromagnetic' branches of the magnetic spectra in ferrimagnets play a role (Section 3.3). As for antiferromagnets, the excitation of spin waves in these substances occurs, as well, and has a number of interesting features (e.g., [265, 307]).

The theory of spin-wave parametric excitation, which we begin to study, is based on solving the nonlinear equation of motion (2.6). We neglect the dissipation term



in this equation; the losses will be allowed for later. The effective field is

$$\mathbf{H}_{\text{ef}} = \mathbf{H}_0 + \mathbf{h}_{\sim} + \mathbf{h}_M + \mathbf{H}_{\text{ex}} \quad (10.1)$$

where  $\mathbf{H}_0$  is the internal steady field,  $\mathbf{h}_{\sim}$  is the external ac field,  $\mathbf{h}_M$  is the ac effective field of dipole–dipole interaction, i.e., the ac demagnetizing field (the steady demagnetizing field is included in  $\mathbf{H}_0$ ), and  $\mathbf{H}_{\text{ex}}$  is the effective field of exchange interaction.

We seek the solution of the equation of motion in the form

$$\mathbf{M} = z_0 M_0 + \mathbf{m}_{\sim}(\mathbf{r}, t) \quad (10.2)$$

and suppose that  $\mathbf{m}_{\sim} \ll M_0$ . Let us expand the ac magnetization in the Fourier series:

$$\mathbf{m}_{\sim}(\mathbf{r}, t) = \sum_{\mathbf{k}} \mathbf{m}_{\mathbf{k}}(t) \exp(-i\mathbf{k}\mathbf{r}) \quad (10.3)$$

where the summation is over all allowed values of the wave vector  $\mathbf{k}$ . Note that  $\mathbf{m}_{\sim}(\mathbf{r}, t)$  is a real quantity while the coefficients  $\mathbf{m}_{\mathbf{k}}(t)$  are complex; therefore,  $\mathbf{m}_{\mathbf{k}}(t) = \mathbf{m}_{-\mathbf{k}}^*(t)$ . The term with  $\mathbf{k} = 0$  in (10.3) corresponds to the uniform magnetization oscillations, and all other terms correspond to *uniform plane spin waves*. These waves do not satisfy the boundary conditions at the sample surface and, hence, are not the eigenmodes of the problem. Only if  $k > k_{\min}$ , where  $k_{\min}$  is much larger than the inverse dimensions of the sample, can plane waves be regarded approximately as eigenmodes. The main assumption of Suhl's [392], as well as Schlömann's [343, 345], theory is that the expansion (10.3), nevertheless, can be used. It should be noted that magnetostatic waves (Section 6.2) and oscillations (Section 6.3) remain as yet out of consideration; the parametric excitation of these modes will be discussed in Section 10.4.

For the uniform mode, i.e., for the term with  $\mathbf{k} = 0$  in (10.3), the influence of boundary conditions, of course, cannot be neglected. In the case of a small ellipsoid, it can be taken into account by the uniform demagnetizing field  $-\vec{N}\mathbf{m}_{\mathbf{k}=0}$  included in  $\mathbf{h}_M$ . For plane waves with  $\mathbf{k} \neq 0$  (really, with  $k > k_{\min}$ ) the effective fields of the dipole–dipole interaction will have the form (7.12).

Substituting (10.1)–(10.3) into (2.6), projecting the obtained equation onto axes  $x$  and  $y$ , and equating the same harmonics at both sides of the equations, we get two differential equations for each  $\mathbf{k}$ . The components  $m_{\mathbf{k}z}$  can be excluded from these equations using the relation (9.11). Following Suhl [392], we introduce new variables

$$\begin{aligned} a_{\mathbf{k}} &= \frac{1}{M_0} (m_{\mathbf{k}x} + im_{\mathbf{k}y}) \\ a_{-\mathbf{k}}^* &= \frac{1}{M_0} (m_{-\mathbf{k}x}^* - im_{-\mathbf{k}y}^*) = \frac{1}{M_0} (m_{\mathbf{k}x} - im_{\mathbf{k}y}). \end{aligned} \quad (10.4)$$

It can be shown that in these variables

$$m_{\mathbf{k}z} = -\frac{1}{2}M_0 \sum_{\mathbf{k}_1} a_{\mathbf{k}_1} a_{\mathbf{k}_1 - \mathbf{k}}^* \quad (10.5)$$

Consider the case of an ellipsoid of revolution (spheroid) with demagnetization factors  $N_z$  and  $N_x = N_y \equiv N_\perp$ . Then, at  $\mathbf{k} = 0$ , i.e., for the variable  $a_0$  corresponding to the uniform oscillation mode of the spheroid, we obtain a nonlinear equation:

$$-i \frac{da_0}{dt} = \omega_0 a_0 - \gamma (h_{\sim x} + i h_{\sim y}) + \Omega_{n0} \quad (10.6)$$

where  $\omega_0 = \omega_H + \gamma N_\perp M_0$  is the eigenfrequency of the uniform mode,  $h_{\sim}$  is the external ac field, and  $\Omega_{n0}$  is a sum of many nonlinear terms containing the variables  $a_0$ ,  $a_k$ , and  $a_{-k}^*$ . For each  $\mathbf{k} \neq 0$  (or, to be more exact, for  $k > k_{\min}$ ), a pair of equations is obtained:

$$-i \frac{da_k}{dt} = (A_k + \gamma h_z) a_k + B_k a_{-k}^* + \Omega_{nk} \quad (10.7)$$

and the *adjoint* equation obtained from (10.7) by complex conjugation and replacement  $\mathbf{k} \rightarrow -\mathbf{k}$ . Here,  $A_k$  and  $B_k$  are determined by (7.11) and (7.114) and  $\Omega_{nk}$  is a sum of nonlinear terms containing  $a_0$ ,  $a_k$ , and  $a_{-k}^*$ . The nonlinear terms in (10.6) and (10.7) depend on  $M_0$ ,  $N_z$ ,  $N_\perp$ , the components of  $\mathbf{k}$ , and—some terms in (10.7)—on the exchange constant  $\eta$  (Section 7.1).

The solution of *linearized* equation (10.6) (without  $\Omega_{n0}$ ) corresponds to the forced uniform magnetization oscillations in a spheroid, studied in detail in Section 1.5. Equation (10.7) and the adjoint equation describe, in a linear approximation, the coupled oscillations of two harmonic ‘oscillators’  $a_k$  and  $a_{-k}^*$  corresponding to spin waves with wave vectors  $\mathbf{k}$  and  $-\mathbf{k}$ . To find the equations for the *normal* modes a classical analog of the third Holstein–Primakoff transformation (Section 7.4) should be used. This means that we have to pass from  $a_k$  and  $a_{-k}^*$  to new variables  $c_k$  and  $c_{-k}^*$ , in which the linear parts of equation (10.7) and the adjoint equation—neglecting as yet the term  $\gamma h_{\sim z} a_k$ —will have the form

$$\frac{dc_k}{dt} = i\omega_k c_k \quad \frac{dc_{-k}^*}{dt} = -i\omega_k c_{-k}^* \quad (10.8)$$

The new variables are related to the old ones by the expressions (e.g., [14])

$$a_k = u_k c_k + v_k c_{-k}^* \quad a_{-k}^* = v_k^* c_k + u_k c_{-k}^* \quad (10.9)$$

$$u_k = \frac{1}{\sqrt{2}} \sqrt{\frac{A_k}{\omega_k} + 1} \quad v_k = -\frac{1}{\sqrt{2}} \sqrt{\frac{A_k}{\omega_k} - 1} \exp(2i\varphi_k) \quad \varphi_k = \arctan \frac{k_y}{k_x} \quad (10.10)$$

where  $\omega_k$  is the spin-wave frequency (7.9).

The solutions of linear equations (10.8) can be presented in the form

$$c_k = c_k^0 \exp(i\omega_k t) \quad c_{-k}^* = c_{-k}^{0*} \exp(-i\omega_k t) \quad (10.11)$$

and correspond to spin waves with wave vectors  $\mathbf{k}$  and  $-\mathbf{k}$ . Thus, to a linear approximation, the uniform precession excited by an external ac field and the spin waves (with small, equilibrium amplitudes) are independent modes. Nonlinear terms in (10.6) and (10.7) result in the *coupling* of spin waves with each other, with the uniform mode, and [the term  $\gamma h_{\sim z} a_k$  in (10.7)] with the longitudinal external ac magnetic field.

It should be noted that different terms in the classical equation (10.7) are analogous to the corresponding terms in the quantum-mechanical equation of motion for the magnon creation and annihilation operators, which can be obtained from the Hamiltonian expressed in these operators. We will not discuss here this analogy because the parametric excitation of spin waves can be fully described, as Suhl [392] and Schlömann *et al.* [343, 345] have shown, in terms of classical theory.

---

## 10.2 Thresholds of parametric excitation under transverse pumping

Consider the case when  $h_{\sim z} = 0$ , i.e., the ac magnetic field is perpendicular to the steady magnetization. This field (we suppose it to be uniform) excites, to a linear approximation, only the uniform ac magnetization, which plays the role of pumping.

### 10.2.1 First-order and second-order instabilities

As we are interested, at present, only in the *threshold* values of the pumping amplitudes, we regard all spin-wave amplitudes in (10.6) and (10.7) as small in relation to  $a_0$ . Then, supposing the field  $\mathbf{h}_{\sim}$  (with frequency  $\omega_p$ ) to be right-hand circularly polarized, we find from the linearized equation (10.6), after replacement  $\omega_0 \rightarrow \omega_0 + i\omega_{r0}$ ,

$$a_0 = \frac{\gamma h_+}{\omega_0 - \omega_p + i\omega_{r0}} \exp(i\omega_p t) \equiv a_0^0 \exp(i\omega_p t) \quad (10.12)$$

where  $h_+ = h_{\sim x} + ih_{\sim y}$ .

In equation (10.7) and the adjoint equation, we retain only the terms of the first and second order in  $a_0$  and, turning to the variables  $c_k$  and  $c_{-k}^*$ , we get the equation

$$\frac{dc_k}{dt} = i(\omega_k + T_k |a_0|^2) c_k + i(\rho_k a_0 + \xi_k a_0^2) c_{-k}^* \quad (10.13)$$

and the adjoint equation where

$$\rho_k = \rho_{-k} = -\frac{\omega_M}{4\omega_k} (\omega_k + \omega_H + \eta k^2) \sin 2\theta_k \exp(i\varphi_k) \quad (10.14)$$

$$\xi_k = \xi_{-k} = \frac{\omega_k + A_k}{4\omega_k} \left( \omega_M \cos^2 \theta_k - \omega_M \frac{N_{\perp}}{4\pi} + \eta k^2 \right) \quad (10.15)$$

$$T_k = \frac{\omega_M}{4\omega_k} \left[ 2A_k \left( \cos^2 \theta_k - \frac{1}{2} \sin^2 \theta_k + \frac{N_z - N_{\perp}}{4\pi} \right) + \frac{\omega_M}{2} \sin^4 \theta_k \right]. \quad (10.16)$$

Note that spin-wave losses are not yet taken into account. Comparing (10.13)–(10.16) with (10.8), we see that the coupling of spin waves with the uniform mode results, first, in the *nonlinear shift* of the eigenfrequency of spin waves:  $\omega_k \rightarrow \tilde{\omega}_k = \omega_k + T|a_0|^2$ . Second, the coupling *between spin waves* with wave vectors  $\mathbf{k}$  and  $-\mathbf{k}$  arises, and the coupling coefficients contain time-dependent factors  $a_0$  and  $a_0^2$ .

It is known [256] that the time-dependent coupling between two oscillators can lead to the energy transfer from the source that modulates the coupling to the oscillators. This process is most effective if the following condition holds:

$$n\omega_p = \omega_1 + \omega_2 \quad (10.17)$$

where  $n = 1, 2, 3, \dots$ ,  $\omega_1$  and  $\omega_2$  are the eigenfrequencies of the oscillators, and  $\omega_p$  is the coupling-modulation (pumping) frequency. In the corpuscular ‘language’, relation (10.17) is the condition of energy conservation in the elementary process of annihilation of  $n$  particles with energy  $\hbar\omega_p$  and creation of a pair of particles with energies  $\hbar\omega_1$  and  $\hbar\omega_2$ .

At a certain threshold value of the pumping amplitude, the energy transferred to the oscillators exceeds their losses, and their amplitudes begin to increase exponentially, i.e., the *instability* arises. The value of  $n$  in (10.17) is the order of instability. In our case, spin waves with wave vectors  $\mathbf{k}$  and  $-\mathbf{k}$  are the coupled ‘oscillators’, and the degeneracy takes place ( $\omega_1 = \omega_2$ ).

One can see from (10.13) and the adjoint equation that the increase of  $c_k$  and  $c_{-k}^*$ , i.e., the instability, can be caused only by the terms that change with frequency  $\tilde{\omega}_k$ ; other terms may be neglected while examining the threshold of instability. It can be shown that, at amplitudes  $a_0$  up to threshold, the difference between  $\tilde{\omega}_k$  and  $\omega_k$  is small, and we will neglect it. Then, as it follows from (10.11) and (10.12), the term  $i\rho_k a_0 c_{-k}^*$  in (10.13) must be taken into account, and the term  $i\xi_k a_0^2 c_{-k}^*$  can be neglected if  $\omega_p \simeq 2\omega_k$ , [i.e.,  $n = 1$  in (10.17)]. If  $\omega_p \simeq \omega_k$ , i.e.,  $n = 2$ , the latter term is to be taken into account and the former can be neglected.

Thus, for spin waves with  $\omega_k \simeq \omega_p/2$ , i.e., for the *first order* spin-wave instability, equation (10.13) and the adjoint equation become

$$\frac{dc_k}{dt} = i\omega_k c_k + i\rho_k a_0 c_{-k}^* \quad \frac{dc_{-k}^*}{dt} = -i\omega_k c_k - i\rho_k^* a_0^* c_k. \quad (10.18)$$

Solution of these equations can be sought in the form

$$c_k = c_k^0 \exp\left(i\frac{\omega_p}{2}t\right) \quad c_{-k}^* = c_{-k}^{0*} \exp\left(-i\frac{\omega_p}{2}t\right) \quad (10.19)$$

where  $c_k^0$  and  $c_{-k}^{0*}$  are slowly varying functions of time:

$$c_k^0 = c_{k0}^0 \exp(\lambda t) \quad c_{-k}^{0*} = c_{-k0}^{0*} \exp(\lambda t). \quad (10.20)$$

Here,  $c_{k0}^0$  and  $c_{-k0}^{0*}$  are constants, and  $\lambda$  is a real quantity. The condition for instability is  $\lambda > 0$ .

At this point we allow for spin-wave losses replacing  $\omega_k$  by  $\omega_k + i\omega_{rk}$  in (10.18). Inserting (10.19) into (10.18), we obtain a system of two homogeneous linear algebraic equations in  $c_{k0}^0$  and  $c_{-k0}^{0*}$ . Setting the determinant of this system to zero, we get

$$(\lambda + \omega_{rk})^2 + \left(\omega_k - \frac{\omega_p}{2}\right)^2 = a_0^2 |\rho_k|^2. \quad (10.21)$$

The threshold amplitude of the uniform mode  $a_{0\text{thr}1}^0$  is determined by the condition  $\lambda = 0$ :

$$a_{0\text{thr}1}^0 = \frac{1}{|\rho_k|} \sqrt{\omega_{rk}^2 + \left(\frac{\omega_p}{2} - \omega_k\right)^2}. \quad (10.22)$$

To find the actual value of the threshold we must *minimize* expression (10.22). We see, first of all, that the threshold, as it was supposed, is the lowest for spin waves with  $\omega_k = \omega_p/2$ . Then, taking into account (10.14), we get

$$a_{0\text{thr}1}^0 = \min \left\{ \frac{\omega_{rk}}{|\rho_k|} \right\} = \min \left\{ \frac{\omega_{rk}\omega_p}{\omega_M (\omega_k + \omega_H + \eta k^2) \sin 2\theta_k} \right\}. \quad (10.23)$$

Minimization should be performed here with respect to  $k$  or  $\theta_k$ , subject to the condition  $\omega_k(k, \theta_k) = \omega_p/2$ . It follows from (10.23) that, if the dependence of  $\omega_{rk}$  on  $k$  and  $\theta_k$  can be neglected, the threshold pumping amplitude  $a_{0\text{thr}1}^0$  is the smallest for spin waves with  $\theta_k$  somewhat smaller (due to the term  $\eta k^2$ ) than  $45^\circ$  (provided such spin waves do exist at given  $\omega_p$  and  $\omega_H$ ).

For the *second-order* instability ( $\omega_k \simeq \omega_p$ ), equation (10.13) and the adjoint equation reduce to

$$\frac{dc_k}{dt} = i\omega_k c_k + i\xi_k a_0^2 c_{-k}^* \quad \frac{dc_{-k}^*}{dt} = -i\omega_k c_{-k}^* - i\xi_k^* a_0^{*2} c_k \quad (10.24)$$

and the solution must be sought in the form

$$c_k = c_k^0 \exp(i\omega_p t) \quad c_{-k}^* = c_{-k}^{0*} \exp(-i\omega_p t). \quad (10.25)$$

By a method similar to the one used above, we get at  $\omega_k = \omega_p$

$$a_{0\text{thr}2}^0 = \min \left\{ \sqrt{\frac{\omega_{rk}}{2\xi_k}} \right\} \quad (10.26)$$

where  $\xi_k$  is determined by (10.15). Without taking into account the dependence of  $\omega_{rk}$  on  $k$  and  $\theta_k$ , we see that  $a_{0\text{thr}2}^0$  is the lowest for spin waves with  $\theta_k = 0$ . The coupling parameters  $\rho_k$  and  $\xi_k$  are both of the order of  $\omega_M$ , as it follows

from (10.14) and (10.15); for 'good' single-crystal ferrites, applied usually in experiments on parametric excitation of spin waves,  $\omega_{rk} \ll \omega_M$ . Therefore, the threshold amplitudes  $a_{0\text{thr}2}^0$  are much larger than the amplitudes  $a_{0\text{thr}1}^0$ .

For the first-order instability to occur, the frequency  $\omega_p/2$  must lie above the lower boundary  $\omega_H$  of the spin-wave spectrum (7.9). In the case of an ellipsoid, this leads to the condition

$$H_{e0} < \frac{\omega_p}{2\gamma} + N_z M_0. \quad (10.27)$$

For the second-order instability,  $\omega_p/2$  in (10.27) is replaced by  $\omega_p$ .

### 10.2.2 Threshold fields

Consider now the threshold values of the external ac magnetic fields, assuming them to be right-hand circularly polarized. For the *first-order* process, we find from (10.12) and (10.23)

$$h_{\text{thr}1} = \min \left\{ \frac{2\omega_{rk}\omega_p \sqrt{\omega_{r0}^2 + (\omega_p - \omega_0)^2}}{\gamma\omega_M \sin 2\theta_k (\omega_p/2 + \omega_H + \eta k^2)} \right\}. \quad (10.28)$$

This field is the lowest when the pumping frequency  $\omega_p$  is equal to eigenfrequency  $\omega_0$  of the uniform mode. However, this can take place, as it is easy to make sure, only if

$$\omega_p < \omega_M \frac{N_{\perp}}{2\pi} \equiv \omega_{\text{cr}}. \quad (10.29)$$

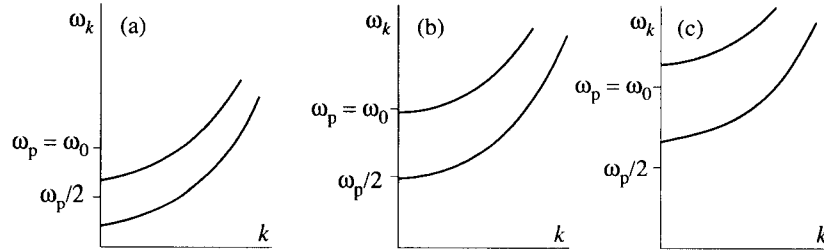
For a sphere,  $\omega_{\text{cr}} = 2\omega_M/3$  coincides with the frequency at which  $\omega_0$  passes the upper boundary of the nonexchange spin-wave spectrum (Section 6.1). For a YIG sphere at room temperature,  $f_{\text{cr}} = 3.27$  GHz.

If the condition (10.29) is only just satisfied [Figure 10.2(b)], the angle  $\theta_k$  is very small, and, as it is seen from (10.28), the threshold field (as well as the threshold amplitude  $a_{0\text{thr}1}^0$ ) is very large. With lowering frequency  $\theta_k$  increases, the threshold field decreases, and at  $\theta_k \sim 45^\circ$  it becomes of the order of<sup>1</sup>

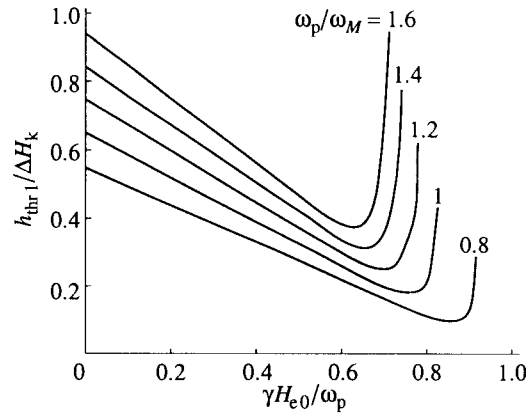
$$h_{\text{thr}1\text{res}} = \frac{\Delta H_0 \Delta H_k}{\pi M_0}. \quad (10.30)$$

Spin waves with small  $k$ , i.e., in the framework of Suhl's theory, with  $k = 0$ , now become unstable. In YIG single crystals ( $\Delta H_0 \sim 0.3$  Oe,  $\Delta H_k \sim 0.15$  Oe) the  $h_{\text{thr}1\text{res}}$  value is as small as  $10^{-4}$  Oe. Further lowering of the frequency  $\omega_p$  (still equal to  $\omega_0$ ) results in excitation of spin waves with increasing  $k$ ,  $\theta_k$  remaining close to  $45^\circ$ .

<sup>1</sup>In this expression and throughout this book,  $\Delta H_0 = 2\omega_{r0}/\gamma$  and  $\Delta H_k = 2\omega_{rk}/\gamma$  are, as distinct from [392], the full widths of resonance curves.

**FIGURE 10.2**

Relative positions of the spin-wave spectrum and the frequency of transverse pumping (equal to the eigenfrequency of uniform oscillations in a sphere) when condition (10.29) (a) is well satisfied, (b) is just satisfied, and (c) is not satisfied.

**FIGURE 10.3**

Threshold field for off-resonance first-order spin-wave instability (subsidiary absorption) in a sphere vs external steady field [392]. © 1957 Elsevier Science Ltd.

At high frequencies ( $\omega > \omega_{cr}$ ), when the condition  $\omega_k = \omega_p/2$  cannot be satisfied at resonance, the minimization of (10.28) [392] shows that the lowest threshold field takes place in the external steady field  $H_{e0 \min}$  less than the resonance field. Spin waves with  $k = 0$  and  $\theta_k = 45^\circ$  then become unstable. The values of  $H_{e0 \min}$ , as well as the values of  $h_{thr1}$ , depend on the sample shape and on the ratio  $\omega_p/\omega_M$ . For spheres, the values of  $H_{e0 \min}$  lie in the range of  $(0.5-0.9) \omega_p/\gamma$  (Figure 10.3). To estimate the value of  $h_{thr1}$  assume, e.g., that  $\omega_p \simeq \omega_M \simeq 1.5\omega_H$  and  $\omega_p - \omega_0 = 0.25\omega_p$ , which corresponds approximately to a YIG sphere at room temperature and frequency of 5 GHz. Then, from (10.28) or Figure 10.3, we obtain  $h_{thr1} = 0.2\Delta H_k$ , or, assuming  $\Delta H_k = 0.15$  Oe, we get  $h_{thr1} = 0.03$  Oe. Thus, the values of threshold field (but not of threshold magnetization) are much

larger in this, off-resonance, case than at resonance ( $\omega_p = \omega_0$ ). However, these values are also easily attainable in experiment, even for polycrystalline ferrites with  $\Delta H_k \sim 10$  Oe.

To the left of the minima in Figure 10.3, spin waves with  $\theta_k$  still close to  $45^\circ$  but with large  $k$  values become unstable. To the right of the minima the unstable spin waves have  $k \simeq 0$  and  $\theta_k < 45^\circ$ . It should be emphasized that all these conclusions were drawn by means of minimizing (10.28) at constant  $\Delta H_k$ ; the  $\Delta H_k$  dependence on  $k$  and  $\theta_k$  can considerably affect them.

The first-order spin-wave instability at  $\omega_p \neq \omega_0$  was named by Suhl [392] the *subsidiary absorption*, and the first order instability at  $\omega_p = \omega_0$  was named the *coincidence* of subsidiary absorption with main resonance.

If condition (10.29) is not satisfied, the *second-order* process comes into action at  $\omega_p \simeq \omega_0$ . The threshold magnetization for this process is determined by (10.26), and the threshold field, with allowance for (10.12), is

$$h_{\text{thr}2} = \min \left\{ \sqrt{\frac{\omega_{rk} [\omega_{r0}^2 + (\omega_p - \omega_0)^2]}{\gamma^2 \xi_k}} \right\}. \quad (10.31)$$

This field is the lowest at resonance ( $\omega_p = \omega_0$ ), and, as it follows from (10.15), a pair of spin waves with  $\theta_k = 0$  and  $\theta_k = \pi$  becomes unstable. For a sphere at resonance,

$$h_{\text{thr}2} = \frac{\Delta H_0}{2} \sqrt{\frac{\Delta H_k}{4\pi M_0}}. \quad (10.32)$$

For YIG at room temperature and a wavelength of 3 cm, an estimate gives  $h_{\text{thr}2} \simeq 2 \times 10^{-3}$  Oe, which is an order of magnitude higher than the threshold field for the first-order process at resonance, and an order of magnitude lower than the threshold field for the off-resonance first-order process. The considered second-order process (the *saturation of main resonance*, according to Suhl) caused the decrease and broadening of the resonance peak in the Bloembergen and Wang experiment (Figure 10.1). The wide maximum at lower steady field in this experiment is a result of the first-order off-resonance process.

### 10.2.3 Effect of pumping-field polarization

All the above-cited expressions for threshold fields relate to the case when the pumping field has the *right-hand circular* polarization and the sample is an ellipsoid of revolution, so that the magnetization is also circularly polarized with right-hand rotation. This is not the case when the field is not circularly (in particular, linearly) polarized, or the sample is an arbitrary ellipsoid. However, if the frequency of the pumping field is equal or very near to resonance frequency, the magnetization component with right-hand circular polarization dominates (Section 1.5). Then, the expressions for threshold fields with *linear* polarization will



differ only by a factor of two from the above-cited expressions for both first-order and second-order processes at resonance.

For the *off-resonance* first-order process (the subsidiary absorption), the left-hand circular magnetization component cannot be neglected a priori. Consider, e.g., the case when a linearly polarized pumping field  $h$  makes an angle  $\varphi_h$  with the  $x$ -axis. Then, the solution of (10.10) is

$$a_0 = a_0^+ \exp(i\omega_p t) + a_0^- \exp(-i\omega_p t) \quad a_0^\pm = \frac{1}{2} \frac{\gamma h \exp(i\varphi_h)}{\omega_0 \mp \omega_p}. \quad (10.33)$$

Here,  $a_0^\pm \exp(i\omega_p t) = m^\pm / M_0$ , where  $m^+$  and  $m^-$  are the amplitudes of magnetization circular components with right-hand and left-hand rotation, respectively. Substituting (10.33) into (10.6) and (10.7), we get, in the same way as in the case of circularly polarized field, the following equation:

$$\frac{dc_k}{dt} = i\omega_k c_k + i(\rho_k a_0^+ + r_k^* a_0^{-*}) \exp(i\omega_p t) c_{-k}^* \quad (10.34)$$

and the adjoint equation where

$$r_k = \frac{1}{2} \frac{\omega_M}{\omega_p} \left( \omega_H + \eta k^2 - \frac{\omega_p}{2} \right) \sin 2\theta_k \exp(-3i\varphi_k). \quad (10.35)$$

The threshold field is now the lowest for spin waves with  $\varphi_k = \varphi_h$  and, of course, with  $\omega_k = \omega_p/2$ . In this case

$$h_{\text{thr 1 lin}} = \min \left\{ \frac{2\omega_r k \omega_p (\omega_p^2 - \omega_0^2)}{\gamma \omega_M \sin 2\theta_k [\omega_p^2/2 + \omega_0 (\omega_H + \eta k^2)]} \right\}. \quad (10.36)$$

Comparing (10.36) with (10.28), we see that the ratio  $h_{\text{thr 1 lin}}/h_{\text{thr 1}}$  differs slightly from 2, i.e., the left-hand circular component of magnetization has small impact on the parametric excitation even in the off-resonance process. However, the case of the pumping-field linear polarization is of interest in that spin waves with distinct values of the azimuthal angle  $\varphi_k$  are excited.

### 10.3 Longitudinal and oblique pumping

We proceed to the study of parametric excitation of spin waves by an ac magnetic field with a longitudinal (parallel to  $M_0$ ) component. The term  $\gamma h_{\sim z} a_k$  in (10.7) should now be taken into account.

#### 10.3.1 Longitudinal pumping

Suppose, first, that the ac magnetic field has *only* a component  $h_{\sim z}$ . Then, the ac magnetization is absent in linear approximation, i.e.,  $a_0 = 0$ . Neglecting,

in (10.7) and in the adjoint equation, the terms that cannot lead to instability and passing, according to (10.9), to the variables  $c_k$  and  $c_{-k}^*$ , we obtain

$$\frac{dc_k}{dt} = i\omega_k c_k + i\gamma h_{\sim z} \frac{B_k}{\omega_k} c_{-k}^* \quad \frac{dc_{-k}^*}{dt} = -i\omega_k c_{-k}^* - i\gamma h_{\sim z} \frac{B_k^*}{\omega_k} c_k. \quad (10.37)$$

It is evident that  $h_{\sim z}$  directly results in the coupling between the 'oscillators'  $c_k$  and  $c_{-k}^*$  if  $B_k \neq 0$ . The quantity  $B_k$  caused by the dipole-dipole interaction is proportional to  $\omega_M \sin^2 \theta_k$  [formula (7.11)] and, in accordance with (7.23) and (1.106), is related to the *ellipticity* of spin waves

$$\mathcal{E} = \frac{2|B_k|}{A_k + |B_k|}. \quad (10.38)$$

The need of ellipticity for parametric excitation of spin waves under longitudinal pumping is easily realized: if  $\mathcal{E} \neq 0$ , the longitudinal component of the spin-wave magnetization with frequency  $2\omega_k$  arises (Section 9.1) and interacts with the longitudinal pumping field, which has the same frequency.

Present the longitudinal ac field in the form

$$h_{\sim z} = \frac{1}{2} h_z [\exp(i\omega_p t) + \exp(-i\omega_p t)] \quad (10.39)$$

and substitute it, as well as expressions (10.11) for  $c_k$  and  $c_{-k}^*$ , into equations (10.37). Assume the frequency  $\omega_p$  to be near  $2\omega_k$  and retain in (10.37) only the terms which vary with frequency close to  $\omega_k$  and, so, can lead to instability. Then, the first equation (10.37) takes the form

$$\frac{dc_k}{dt} = i\omega_k c_k + iV_k h_z \exp(i\omega_p t) c_{-k}^* \quad (10.40)$$

where the *coupling parameter*

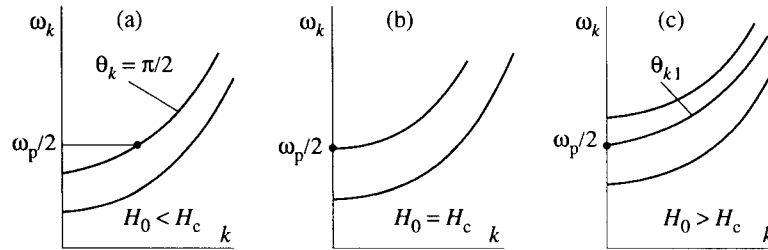
$$V_k = \frac{\gamma B_k}{2\omega_k} = \frac{\gamma \omega_M}{4\omega_k} \sin^2 \theta_k \exp(2i\varphi_k). \quad (10.41)$$

Comparing (10.40) with the first equation (10.18), we see that they differ only by the replacement of  $\rho_k a_0^0$  by  $V_k h_z$ . Thus, we may make this replacement directly in the threshold formula (10.22) or (10.23). For spin waves with  $\omega_k = \omega_p/2$ , when the threshold is the lowest, we get

$$h_{z \text{ thr}} = \min \left\{ \frac{\omega_{rk}}{|V_k|} \right\} = \min \left\{ \frac{\omega_p \Delta H_k}{\omega_M \sin^2 \theta_k} \right\}. \quad (10.42)$$

If  $\Delta H_k$  can be regarded as independent of  $k$  and  $\theta_k$ , then  $h_{z \text{ thr}}$  is lower the closer  $\theta_k$  is to  $\pi/2$ . In small steady magnetic fields, when  $\omega_p/2$  lies above the upper boundary of the nonexchange spin-wave spectrum [Figure 10.4(a)], spin waves with  $\theta_k = \pi/2$  become unstable. Their wave numbers, as it follows, e.g., from (7.17), are determined by the expression

$$Dk^2 = H_c - H_0 \quad (10.43)$$

**FIGURE 10.4**

Relative positions of spin-wave spectra and the frequency of longitudinal pumping. Dots indicate spin waves that become unstable.

where, according to (7.18),

$$H_c \equiv H_{0c}(\pi/2) = \sqrt{\left(\frac{\omega_p}{2\gamma}\right)^2 + (2\pi M_0)^2} - 2\pi M_0. \quad (10.44)$$

The critical field  $H_c$  is the internal steady magnetic field at which spin waves with  $\omega_k = \omega_p/2$  and  $\theta_k = \pi/2$  have  $k = 0$ .

With the decrease of  $H_0$ , the  $k$  value of parametrically excited spin waves<sup>2</sup> increases and at  $H_0 = 0$  reaches the highest value  $k_{\max} = \sqrt{H_c/D}$  possible for given  $\omega_p$ . For YIG at room temperature,  $k_{\max} \simeq 5 \times 10^5$  at  $f_p = 9$  GHz, and  $k_{\max} \simeq 10^6$  at  $f_i = 36$  GHz. The azimuthal angle of parametric spin waves is indeterminable in the case of an isotropic ferromagnet, so that the whole 'fan' of spin waves with wave vectors  $\mathbf{k}$  and  $-\mathbf{k}$  lying in  $\theta_k = \pi/2$  plane is excited.

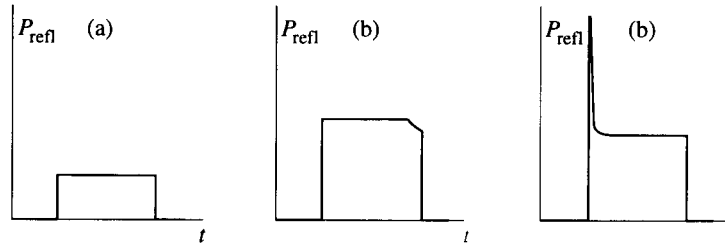
In fields  $H_0$  higher than  $H_c$  [Figure 10.4(c)], the threshold field is the lowest for spin waves with  $k = 0$  and  $\theta_{k1}$  determined by the expression

$$\sin^2 \theta_{k1} = \frac{(\omega_p/2)^2 - \omega_H^2}{\omega_M \omega_H} \quad (10.45)$$

which follows from (10.42) and the condition  $\omega_k = \omega_p/2$ . With increasing  $H_0$ , the angle  $\theta_k$  decreases and the threshold field grows; at  $H_0 = \omega_p/(2\gamma)$  it approaches infinity.

The measurement of spin-wave parametric excitation thresholds under longitudinal pumping is widely used for determining the spin-wave dissipation parameter  $\Delta H_k$ . Samples—usually ferrite spheres or metal films—are placed into resonators. In centimeter or millimeter wavelength ranges, reflection hollow resonators, rectangular or cylindrical, are conventionally used. The threshold values of the incident power  $P_1$  are measured with changing steady field at constant

<sup>2</sup>In what follows, we will for brevity use the term 'parametric spin waves'.

**FIGURE 10.5**

Envelopes of pulses reflected from a resonator with ferrite sphere: (a) in a weak ac field, (b) just above threshold, and (c) far above threshold.

frequency  $\omega_p$ . The threshold ac field is found using the formula

$$h^2 = \frac{8\pi\alpha}{\omega_p V_0} Q_0 \frac{4q}{1+q^2} P_1 \quad (10.46)$$

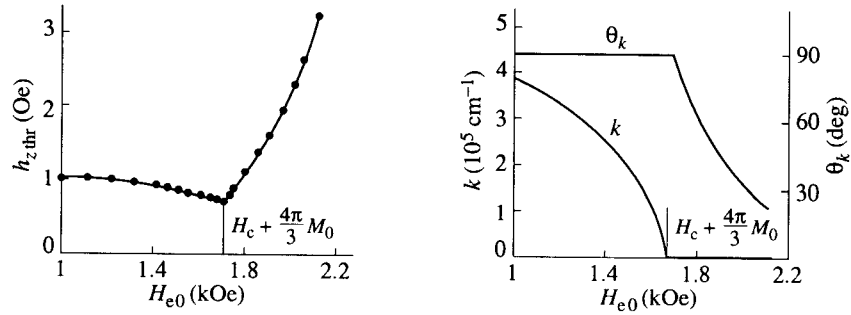
which can be easily derived with the aid of equivalent schemes. In (10.46),  $V_0$  is the resonator volume,  $q = Q_c/Q_0$  ( $Q_0$  and  $Q_c$  are the internal and the external quality factors of the resonator, respectively), and  $\alpha$  is determined by (5.47).

Up to threshold, the sample (in a longitudinal ac field) does not absorb electromagnetic energy. Above threshold, the absorption arises,  $Q_0$  decreases, and the reflection coefficient from the resonator changes (decreases or increases, depending on initial value of  $q$ ). Measurements are usually carried out in pulse regime, and the threshold is indicated by the change of the reflected-pulse envelope (Figure 10.5). The measured value of  $P_{1\text{thr}}$  is smaller the greater the pulse duration  $\tau$ ; the actual value of the threshold can be obtained by extrapolating the dependence  $P_{1\text{thr}}(\tau)$  to  $\tau \rightarrow \infty$  [343].

The  $h_{z\text{thr}}$  values obtained in the described way are plotted vs  $H_{e0}$  in Figure 10.6; the calculated values of  $k$  and  $\theta_k$  of parametric spin values are also shown. The curves  $h_{z\text{thr}}(H_0)$  are called the 'butterfly curves'. Their minima ('bills') are usually located at  $H_0 = H_c$ , where spin waves with  $k \cong 0$  are excited. At left 'wing' the excited spin waves have  $\theta_k = \pi/2$  and  $k > 0$ . The increase in  $h_{z\text{thr}}$  with decreasing  $H_0$  at this wing is due to the dependence of  $\Delta H_k$  on  $k$ . At right wing the excitation of spin waves with small  $k$  (with  $k = 0$  in the framework of the theory considered up to now) and  $\theta_k$  decreasing with the growth of  $H_0$  takes place. The steep increase of  $h_{z\text{thr}}$  at this wing is due to the factor  $\sin^2 \theta_k$  in the denominator of (10.42).

Having measured  $h_{z\text{thr}}$ , we then find  $\Delta H_k$  from (10.42). The corresponding  $k$  values are found from (10.43). The dependences  $\Delta H_k(k)$  obtained in such way will be discussed in Section 11.2.

Let us briefly consider now, using longitudinal pumping as an example, the effect of *magnetocrystalline anisotropy* on the parametric excitation of spin waves. In

**FIGURE 10.6**

Experimental values of threshold field [343] and calculated  $k$  and  $\theta_k$  values of spin waves, parametrically excited under longitudinal pumping, vs external steady field. YIG sphere at frequency 9.4 GHz and room temperature.

the case of longitudinal pumping, the dominating factor is the ellipticity of spin waves, which is significantly influenced by the anisotropy.

To allow for the magnetocrystalline anisotropy we have to insert its effective field in the equation of motion and then, using the same method as above, to obtain the equations for  $c_k$  and  $c_{-k}^*$ . In the particular case of a *cubic* crystal with  $M_0$  lying in the  $\{110\}$  plane, this will result in the replacement of  $V_k$  in (10.40) by  $V_k + \gamma\omega_a/(4\omega_k)$  where

$$\omega_a = \gamma M_0 (N_{11}^a - N_{22}^a). \quad (10.47)$$

Here,  $N_{11}^a$  and  $N_{22}^a$  are the effective demagnetization factors determined by (2.47) with  $\varphi_0 = 45^\circ$ . The threshold field in this case is

$$h_{z \text{ thr}} = \min \left\{ \frac{\omega_p \Delta H_k}{|\omega_M \sin^2 \theta_k \exp(2i\varphi_k) + \omega_a|} \right\}. \quad (10.48)$$

It is minimal for  $M_0$  directed along the  $\langle 110 \rangle$  axis if the contribution of anisotropy to the spin-wave ellipticity is the greatest.

The threshold field depends now on both angles of vector  $k$ . Its minimal value takes place at  $\theta_k = \pi/2$  and  $\varphi_k = \pi/2, 3\pi/2$  for  $K_1 < 0$ , and at  $\theta_k = \pi/2$  and  $\varphi_k = 0, \pi$ , for  $K_1 > 0$ . In both cases [313]

$$h_{z \text{ thr}} = \frac{\omega_p \Delta H_k}{\omega_M + 3\gamma |H_{A1}|}. \quad (10.49)$$

### 10.3.2 Effect of nonuniformities

Nonuniformities (defects), as impurities, pores, surface roughness, and grain boundaries in polycrystals, lead to the so-called *two-magnon* processes, i.e., to the scattering of magnetic oscillations and waves by defects. The contribution of these

processes to the relaxation of linear magnetic modes will be studied in detail in Section 11.3. Here we will consider the influence of such processes on parametric excitation of spin waves under longitudinal pumping, studied theoretically by Zakharov and L'vov [458].

We have to add the terms describing two-magnon processes into equations (10.37). Then, the first of these equations becomes

$$\frac{dc_k}{dt} = i\omega_k c_k + \sum_{k_1} \nu_{k k_1} c_{k_1} + 2ih_{\sim z} V_k c_{-k}^* \quad (10.50)$$

where the summation is over all degenerate spin waves (with  $k_1 = k$ ) and the coefficients  $\nu_{k k_1}$  depend on vectors  $k$  and  $k_1$ , as well as on the nature of nonuniformities. Similar equations can be written for all amplitudes  $c_{k_1}$ .

Two approaches can be applied to this problem (and to many others that will be examined below): an approach of *coupled modes* and an approach of *normal modes*. In using the former, we assume that some external forces excite a certain mode, e.g., spin waves with wave vector  $k$ ; the coupling between this mode and other modes (spin waves with vectors  $k_1$ ) leads to the excitation of these modes. This results in the increase of the dissipation parameter of the primary mode:

$$\omega_{rk} = \omega_{rk}^0 + \omega_{rk}^s \quad (10.51)$$

where  $\omega_{rk}^s$  corresponds to additional dissipation caused by the coupling, in our case, by the two-magnon processes.

In using the second approach, of normal modes, we have to pass, e.g., in equations (10.50) and analogous equations for  $c_{k_1}$ , to new variables in which these equations in linear approximation (i.e., without the terms  $2ih_{\sim z} V_k c_{-k}^*$ ) are uncoupled. These new variables correspond to the *normal modes*. Their dissipation parameters are not equal to  $\omega_{rk}^0 + \omega_{rk}^s$  but are close to  $\omega_{rk}^0$ . However, the eigenfrequencies of the new modes lie in certain bands located near the eigenfrequencies of the 'old' modes (corresponding to the variables  $c_k$  and  $c_{-k}^*$ ), which leads to the broadening of resonance curves.

Without considering any calculations, using either the first or the second approach, we cite some results obtained in [458]. We point out, first of all, that the threshold fields, in the presence of uniformities, are *not* determined by the same expressions as in the absence of them, with the replacement of  $\omega_{rk}^0$  by  $\omega_{rk}^0 + \omega_{rk}^s$ . The reason for this is that the pumping leads to the coupling of a certain pair of normal modes, the dissipation parameters of which are not equal to  $\omega_{rk}^0 + \omega_{rk}^s$ . It might appear (we have met with such a statement in some early works) that nonuniformities have no influence at all on the threshold of spin-wave parametric excitation. This is not true: the nonuniformities lead to chaotization of the phases of excited spin waves, they cease to satisfy the optimal phase relations (Section 10.5), the coupling of spin waves with the pumping field decreases, and the threshold-field value increases.

If the nonuniformities are *randomly* distributed over the sample and their di-

mensions are small as compared with  $k^{-1}$  of the parametric spin waves, then, in the case of  $\omega_{rk}^s \ll \omega_{rk}^0$ ,

$$h_{z \text{ thr}} = \frac{2\omega_p}{\gamma\omega_M} \left[ \omega_{rk}^0 + \frac{1}{2\sqrt{2}} \omega_{rk}^s \ln \left( 0.42 \frac{\omega_{rk}^0}{\omega_{rk}^s} \right) \right] \quad (10.52)$$

and in the case of  $\omega_{rk}^s \gg \omega_{rk}^0$ ,

$$h_{z \text{ thr}} = \frac{2\omega_p}{\gamma\omega_M} \sqrt{\omega_{rk}^0 \omega_{rk}^s}. \quad (10.53)$$

If the scattering of spin waves occurs at the *sample surface* and the sample dimension  $d \gg k^{-1}$ , then

$$h_{z \text{ thr}} = \frac{2\omega_p}{\gamma\omega_M} \sqrt{(\omega_{rk}^0)^2 + (\omega_{rk}^s)^2}. \quad (10.54)$$

In this case, taking (6.7) into account, we have

$$\omega_{rk}^s = \xi \frac{l_k}{d} \omega_{rk}^0 \equiv \xi \frac{v_{gr}}{2d} \quad (10.55)$$

where  $l_k$  is the spin-wave mean free path (7.27) and  $\xi$  is a factor of the order of unity ( $\xi = \pi$  for  $l_k/d \ll 1$  and  $\xi = \pi/2$  for  $l_k/d \gg 1$ ). One can see from (10.54) and (10.55) that the increase of threshold, due to the scattering of parametric spin waves by the sample surface, is larger the larger the group velocity of spin waves. This can be explained by the *removal* of spin waves from the region of interaction: spin waves scatter at the sample boundary before they build up to a sufficient level under the action of pumping. A similar effect takes place for transverse pumping, too.

In polycrystals, the dimension  $d$  is the grain size; threshold fields grow with its reduction. This is widely used to increase the threshold fields and, hence, to raise the maximal operating power of microwave ferrite devices (e.g., [51]). For high-quality ferrite single crystals, the considered effect manifests itself only at low temperatures in very small samples [277].

### 10.3.3 Oblique pumping

If the ac field has both transverse and longitudinal components, then its threshold value is determined by *simultaneous* action of the transverse pumping by the ac magnetization, and of the longitudinal pumping by the  $z$  component of the ac field. Consider the case of an arbitrary oriented linearly polarized ac field:

$$\begin{aligned} h_{\sim x} &= h \sin \theta_h \cos \varphi_h \cos \omega_p t & h_{\sim y} &= h \sin \theta_h \sin \varphi_h \cos \omega_p t \\ h_{\sim z} &= h \cos \theta_h \cos \omega_p t \end{aligned} \quad (10.56)$$

and restrict our treatment to the first-order process in a sample without nonuniformities. The equations for  $c_k$  and  $c_{-k}^*$  will now contain nonlinear terms that are

present both in (10.18) and in (10.37):

$$\frac{dc_k}{dt} = i\omega_k c_k + i(V_k h \cos \theta_h + \rho_k a_0^+ + r_k^* a_0^-) \exp(i\omega_p t) c_{-k}^* \quad (10.57)$$

where

$$a_0^\pm = \frac{1}{2} \frac{\gamma h \sin \theta_h \exp(i\varphi_h)}{\omega_0 \mp \omega_p} \quad (10.58)$$

and  $r_k$  is determined by (10.35). The threshold field can be obtained from equation (10.57) and the adjoint equation in the same way as for pure transverse or pure longitudinal pumping. According to Jakovlev [451],

$$h_{\text{thr}1} = \min \left\{ \frac{\omega_p}{\omega_M} \Delta H_k \left[ \sin^2 \theta_k \cos \theta_h + \frac{\omega_0 (\omega_H + \eta k^2) + \omega_p^2 / 2}{\omega_p^2 - \omega_0^2} \sin 2\theta_k \sin 2\theta_h \right]^{-1} \right\}. \quad (10.59)$$

It is assumed here that  $\varphi_k = \varphi_h$ ; in this case the threshold is the lowest, as for transverse pumping by a linearly polarized field (Section 10.2).

Minimization of (10.59) with respect to  $k$  or  $\theta_k$ , subject to  $\omega_k = \omega_p/2$ , yields the actual value of  $h_{\text{thr}1}$  and the values of  $k$  and  $\theta_k$  of parametric spin waves. At  $H_0 < H_c$ , spin waves with large  $k$  are excited and their polar angles  $\theta_{k1}$  depend on  $\theta_h$  and lie between  $\pi/2$  (for  $\theta_h = 0$ , i.e., for longitudinal pumping) and  $\pi/4$  (for  $\theta_h = \pi/2$ ). At  $H_0 > H_{0c}(\theta_{k1})$ , unstable spin waves have  $k = 0$  and polar angles determined, as in the case of longitudinal pumping, by formula (10.45) [the field  $H_{0c}(\theta_{k1})$  is given by (7.18)]. In the intermediate region  $H_c < H_0 < H_{0c}(\theta_{k1})$ , the values of  $k$ ,  $\theta_{k1}$ , and  $h_{\text{thr}1}$  can be found only with allowance for the dependence of  $\Delta H_k$  on  $k$  and  $\theta_k$ .

The oblique pumping is essential for the understanding of spin-wave parametric excitation in the presence of *domains*. Let us briefly discuss this problem. The spectrum of magnetic oscillations in samples with domain structures can be found only for simple, regular structures (Section 8.2). But even for such structures, additional assumptions must be made to analyze the parametric excitation of spin waves. The main assumption is the neglect of interaction between spin waves in different domains. The processes in domain walls are also to be neglected, and the excited modes, as in all above-considered problems, must be regarded as uniform plane waves.

With all the mentioned assumptions, the method similar to that used many times in this chapter can be applied. It is necessary, however, to allow, first, for the demagnetizing fields in the domains (Section 8.2). Second, we have to take into account that the pumping is oblique, and the angles  $\theta_h$  and  $\varphi_h$  of the ac field with respect to the steady magnetization are different in different domains. With growing ac field, the instability arises first in such domains in which these angles provide the lowest threshold. For the off-resonance first-order process, i.e., when  $\omega_p$  is equal neither to  $\omega_\perp$  nor to  $\omega_\parallel$  (Section 8.2), threshold is the lowest in domains



in which  $\theta_h$  is equal to or near zero, so that the pumping is nearly longitudinal. On the contrary, if  $\omega_p$  is equal to or near  $\omega_\perp$  or  $\omega_\parallel$ , instability occurs first in domains for which the pumping is transverse.

A complete theoretical and experimental investigation of spin-wave parametric excitation in unsaturated samples was carried out by Pil'shchikov *et al.* [314, 248]. The case of a sphere of cubic crystal magnetized along the  $\langle 110 \rangle$  axis was considered, for which the linear ferromagnetic resonance was studied in detail (Section 8.2). The obtained data confirmed the qualitative statements cited above.

## 10.4 Instability of nonuniform modes and nonuniform pumping

It has been assumed so far in this chapter that the parametrically excited modes are uniform plane waves and that the pumping field is uniform. In the present section these assumptions will be discarded.

### 10.4.1 Parametric excitation of magnetostatic oscillations and waves

As already mentioned, the assumption that the parametrically excited modes are uniform plane spin waves ceases to be valid when the minimization of threshold field results in  $k$  values smaller than, or of the order of, the inverse dimensions of the sample. The modes really excited in this case must satisfy the boundary conditions at the sample surface. If the sample is an ellipsoid of revolution, these modes are Walker's modes (Section 6.3). Expansion (10.3) must be replaced, then, by the expansion

$$\mathbf{m}_\sim(\mathbf{r}, t) = \frac{1}{2} \sum_{\nu} [a_\nu \mathbf{m}_\nu(\mathbf{r}) + a_\nu^* \mathbf{m}_\nu^*(\mathbf{r})] \quad (10.60)$$

where  $\mathbf{m}_\nu(\mathbf{r})$  are the normalized magnetizations of the Walker's modes and  $a_\nu$  are time-dependent complex quantities.

Let us consider the case of *longitudinal* pumping. Then, substituting (10.60) and the appropriate effective fields into the equation of motion, taking into account the orthogonality relations (6.108), and neglecting the terms nonlinear in  $a_\nu$ , we get equations [345]

$$\frac{da_\nu}{dt} = i\omega_\nu a_\nu + i\gamma h_z \cos \omega_p t \sum_{\nu'} \lambda_{\nu\nu'} a_{\nu'}^*. \quad (10.61)$$

Here,  $h_z$  is the complex amplitude of the pumping field  $h_{\sim z}$ , and  $\lambda_{\nu\nu'}$  is the *overlapping integral*

$$\lambda_{\nu\nu'} = \frac{1}{D} \int_V \mathbf{m}_\nu^*(\mathbf{r}) \mathbf{m}_{\nu'}(\mathbf{r}) dV \quad (10.62)$$

where integration is carried out over the volume of the sample and  $D$  is the normalization constant in (6.108).

As in Sections 10.2 and 10.3, we leave in equations (10.61) only the terms that vary with frequency  $\omega_p$  and, hence, can lead to instability, i.e., the terms for which  $\omega_{\nu'} = \omega_p - \omega_{\nu}$ . To allow for losses we replace  $\omega_{\nu}$  by  $\omega_{\nu} + i\omega_{r\nu} \equiv \omega_{\nu} + i\Delta H_{\nu}/(2\gamma)$ . The instability will first occur for the pair of modes  $\nu_1$  and  $\nu_2$  for which the threshold field is the lowest. In the same way as in Section 10.3, we obtain for this pair

$$h_{z \text{ thr}} = \min \left\{ \frac{\sqrt{\Delta H_{\nu_1} \Delta H_{\nu_2}}}{|\lambda_{\nu_1 \nu_2}|} \right\}. \quad (10.63)$$

It turns out that, for a *sphere*,  $\lambda_{\nu_1 \nu_2} \neq 0$  if mode indices  $n$  and  $m$  (Section 6.3) satisfy the following selection rules [289]:

$$n_1 = n_2 \quad m_1 = -m_2. \quad (10.64)$$

The *degenerate* instability ( $\omega_{\nu_1} = \omega_{\nu_2}$ ) is possible for modes with  $m = 0$ , e.g., for the mode (2,0,1). For this mode, the magnetization is elliptically polarized (Section 6.3), which is the necessary condition for longitudinal pumping. Using (6.106) to calculate  $\lambda_{(2,0,1)(2,0,1)}$ , we obtain

$$h_{z \text{ thr}} = 1.25 \frac{\omega_p}{\omega_M} \Delta H_{(2,0,1)}. \quad (10.65)$$

The *nondegenerate* instability is possible, e.g., for the pair (3,1,0) and (3, -1, 0); in this case [88]

$$h_{z \text{ thr}} = 1.14 \frac{\omega_p}{\omega_M} \sqrt{\Delta H_{(3,1,0)} \Delta H_{(3,-1,0)}}. \quad (10.66)$$

Expressions (10.65) and (10.66) represent the lowest thresholds for longitudinal pumping of Walker's modes. Comparing them with (10.47), we see that (provided the dissipation parameters are the same) the threshold fields for magnetostatic modes are *slightly higher* than for plane spin waves.

Selection rules for *transverse* pumping of the Walker modes in a sphere, in the case of the first-order process, are [394]

$$n_1 = n_2 \quad m_1 = 1 - m_2. \quad (10.67)$$

The second of these conditions means that the sum of azimuthal indices of the excited modes is equal to the azimuthal index of the pumping mode (1,1,0). The degenerate instability cannot take place under transverse pumping. The threshold, in this case, is the lowest for the pair (2,0,1) and (2,1,0). It is *much higher* than the threshold for plane spin waves.

The parametric excitation of *nonexchange magnetostatic waves* was first investigated theoretically by Schlömann and Joseph [345] in the case of *longitudinal* pumping of waves in a *circular ferrite rod* magnetized along its axis. We will cite

some results of this theory. The selection rules are, in this case,

$$k_{z1} = -k_{z2} \quad m_1 = -m_2 \quad (10.68)$$

where  $k_{z1,2}$  are the wave numbers of waves propagating in opposite directions and  $m_{1,2}$  are the azimuthal indices of these waves with opposite directions of polarization rotation. The degenerate instability is possible for waves with  $m = 0$ , which have the same frequencies for different propagation directions (Section 6.2). The threshold field is minimal in this case, and the expression for it is

$$h_{z \text{ thr}} = \frac{\omega_p \omega_H}{(\omega_p/2)^2 - \omega_H^2} \Delta H_{n0}. \quad (10.69)$$

Note that (10.69) coincides with expression (10.42) for the threshold field of the plane-spin-wave instability at  $H_0 > H_c$ . (To make sure of this, formula (10.45) must be taken into account.)

Consider now the longitudinal pumping of nonexchange magnetostatic waves in *films*. As in the case of a rod, instability occurs for a pair of waves propagating in a film in opposite directions with the same  $k$ . For volume waves, the degenerate instability may take place, and then formula (10.69) holds. For *surface* waves in a tangentially magnetized film, the threshold field has approximately the form

$$h_{z \text{ thr}} \simeq \frac{\omega_p}{2\sqrt{(\omega_H + \omega_M/2)^2 - (\omega_p/2)^2}} \Delta H_k. \quad (10.70)$$

At  $\omega_p/2 = \omega_\perp$ , i.e., for waves with  $k \rightarrow 0$ , the threshold field is equal to  $(\omega_p/\omega_M)\Delta H_k$ , which is the same as follows, in this case, from (10.69). At  $\omega_p/2 = \omega_H + \omega_M/2$ , i.e., for  $k \rightarrow \infty$ , the threshold field approaches infinity. For all intermediate  $k$  values the threshold of surface-wave instability is higher than for volume waves. The reason for this, as well as for the fact that  $h_{z \text{ thr}} \rightarrow \infty$  at  $k \rightarrow \infty$ , is that the magnetization for surface waves is nonreciprocal (Section 6.2), which leads to the decrease of the overlapping integral with growing  $k$ .

Without considering in detail the parametric excitation of magnetostatic waves under *transverse* pumping [259], we note only that thresholds, in this case, are usually higher than under longitudinal pumping and increase infinitely at  $k \rightarrow 0$  and at  $k \rightarrow \infty$ .

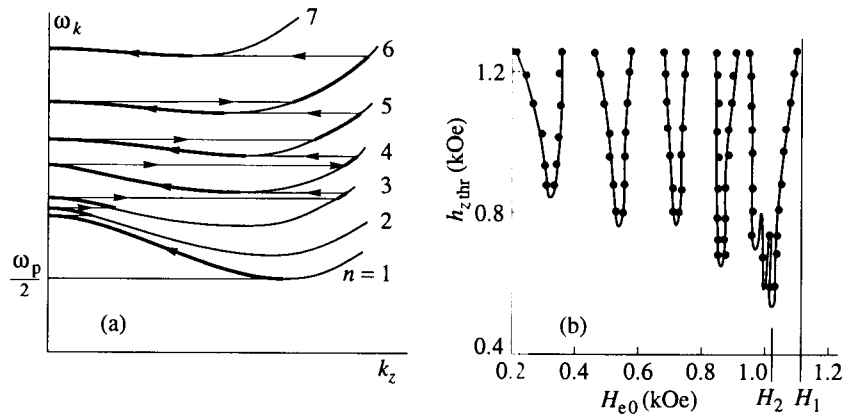
We are now able to discuss the question of what is *actually* excited when, from the theories that deal with uniform plane spin waves, there follows the excitation of such waves with  $k = 0$ . In the case of transverse pumping, magnetostatic modes have higher thresholds than plane spin waves with such  $k$  values that Suhl's theory is already valid, whereas the increase of  $\Delta H_k$  due to the growth of  $k$  is still negligible. Such spin waves with  $k \sim 10^4$  are excited when Suhl's theory gives  $k = 0$ .

As for longitudinal pumping, it has been pointed out above that threshold fields for magnetostatic modes are approximately the same as for plane spin waves. But, actually, the thresholds for magnetostatic modes turn out to be higher due to the

influence of surface inhomogeneities, radiation damping, etc. Thus, spin waves with  $k \sim 10^4$  are excited in the case of longitudinal pumping, as well, at  $H_0 > H_c$  when Schlömann's theory gives  $k = 0$ .

Returning to the parametric excitation of magnetostatic waves in films, consider now the influence of *exchange interaction*, which may not be neglected (Section 7.2) for sufficiently thin films, e.g., for YIG films with thickness smaller than several micrometers. The theory of parametric excitation of spin waves in such films was developed by Lukomskii and Kuz'ko [259] and by Vendik, Kalinikos, and Chertozizhskii [421, 422]. The most interesting effect observed in this case is the *successive* excitation of waves at different branches of the spin-wave spectrum (Section 7.2) when frequency or steady magnetic field is continuously changing.

Consider, e.g., the *longitudinal* pumping of *backward volume* waves in a tangentially magnetized film [207]. The spectrum of these waves is shown schematically in Figure 10.7(a). At each branch of the spectrum, threshold field decreases with decreasing  $k$  due to the growth of ellipticity. At large  $H_{e0}$ , the frequency  $\omega_p/2$  lies below the bottom of the spectrum, and the first-order parametric process is impossible. With decreasing  $H_{e0}$ , the entire spectrum descends; at a certain value of  $H_{e0} = H_1$  the lower branch attains  $\omega_p/2$ , and parametric excitation begins. With further decrease of  $H_{e0}$ , the point  $\omega_p/2$  moves along the lowest branch, and  $h_{z,thr}$  decreases. At a field  $H_2$  [Figure 10.7(b)], the threshold point jumps onto the branch with  $n = 2$ , then it moves to the left along this branch, and so on. As  $n$  values grow, the frequency intervals between branches increase, and one can



**FIGURE 10.7**

Parametric excitation of spin waves in a thin ( $0.5 \mu\text{m}$ ) tangentially magnetized YIG film under longitudinal pumping: (a) spectrum of spin waves propagating along  $\mathbf{M}_0$ , (b) experimental field dependence of the threshold [207]. Spectrum is shown for  $H_{e0} = H_1$ . Arrows indicate the movement of 'threshold point' ( $\omega_k = \omega_p/2$ ) with decreasing  $H_{e0}$ . Bold lines correspond to the portions of the spectrum at which parametric excitation takes place.

observe the regions of  $h_{z \text{ thr}}$  separated by gaps, in which  $h_{z \text{ thr}}$  values exceed the ac field attainable in this experiment. Figure 10.7(b) corresponds to  $d = 0.5 \mu\text{m}$ ; with the increase of film thickness the branches of the spectrum will approach each other, and the curve  $h_{z \text{ thr}}(H_{e0})$  will turn into a monotone left ‘wing’ of the butterfly curve (as in Figure 10.6).

### 10.4.2 Ferrite parametric amplifier

It is clear that pumping can result, as well, in amplification (which can be called parametric amplification) of oscillations or waves excited in a nonlinear medium by an external source. Parametric amplifiers for microwaves have been designed using the nonlinearity of different media: semiconductors, electron streams, etc. [256]. Suhl [393] (see also [394]) suggested the use of the nonlinearity of ferromagnet (ferrite). Three types of ferrite parametric amplifiers can be realized depending on what modes are used: (i) a *magnetostatic* amplifier when both modes are magnetostatic modes; (ii) an *electromagnetic* amplifier when both modes are electromagnetic eigenmodes of a resonator (or normal waves of a waveguide); (iii) a *semistatic* amplifier when one of the modes is magnetostatic and the other is electromagnetic.

The pumping power required for the parametric-amplifier operation is mainly determined by the *filling factor*  $q$  of a resonator with ferrite. For a magnetostatic amplifier, the resonator is the ferrite sample itself and  $q \simeq 1$ . For an electromagnetic amplifier,  $q \ll 1$ . That is why the pumping power of a magnetostatic amplifier is the lowest, and the pumping power of an electromagnetic amplifier is the highest. However, a great shortcoming of a magnetostatic amplifier (characteristic of an electromagnetic amplifier, as well) is the parametric excitation of spin waves, the threshold for which, as we have seen, is lower than the threshold for parametric excitation of magnetostatic modes. It is usually lower than the threshold of parametric *amplification* of these modes, too. The energy of the excited spin waves is partially transformed, as a result of two-magnon processes, into energy of certain long-wavelength modes and is perceived as noise.

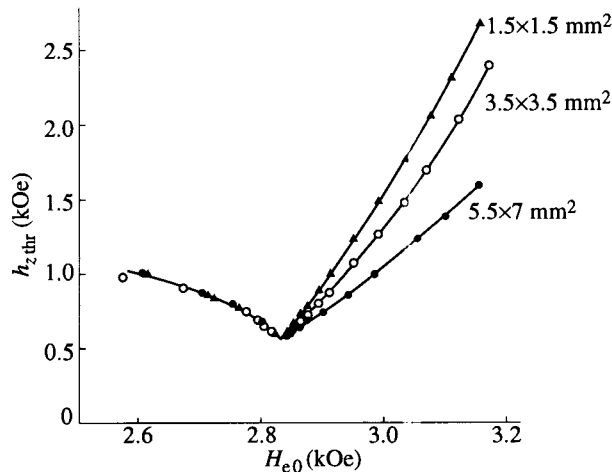
The ferrite parametric amplifier realized first by Weiss [437] was an electromagnetic one. The pumping power being as high as 20 kW, the amplifier was able to operate only in a pulse regime. The magnetostatic amplifier was designed by Denton [88]. Walker’s modes  $(3, 1, 0)$  and  $(3, -1, 1)$  of a YIG sphere with eigenfrequencies, respectively, 4.56 GHz and 4.62 GHz were used. The bandwidth of this amplifier was  $\sim 100$  kHz, and the gain at central frequency was 20 dB, with pumping power, at frequency 9.18 GHz, of 450 mW. The noise factor exceeded 10 dB as a result of the excitation of spin waves.

Numerous investigations with the aim, in particular, to design a travelling-wave amplifier [404] or to use an open dielectric resonator [278], do not result in any material reduction of the noise factor. At present, the ferrite amplifier cannot compete with other types of microwave amplifiers, first of all, with semiconductor amplifiers in which the present-day transistors are used.

### 10.4.3 Nonuniform pumping

Consider, first, the case when the pumping field is present (and has a constant value) only in a small part of the sample. The problem of parametric excitation of spin waves under such (*local*) pumping does not differ, in principle, from the problem of excitation of spin-wave with allowance for their scattering at sample boundaries, which was discussed in the preceding section. In both cases spin waves come out of action when reaching certain surfaces. Therefore, expression (10.54) is also valid in the case of local pumping.

One can see from (10.54) and (10.55) that the threshold is higher the smaller the dimensions of the pumping region and the larger the group velocity of the excited waves. These dependences were verified experimentally in the case of longitudinal pumping using a YIG single-crystal film [281]. Uniform pumping was achieved by putting the film into a hollow resonator, and local pumping, by putting open dielectric resonators with different  $\varepsilon$  (and, hence, with different dimensions) onto the film. The experimental data is shown in Figure 10.8. At  $H_0 < H_c$ , the threshold field does not depend on the dimensions of the pumping region. In such fields, spin waves with  $k \sim 10^4$ – $10^5$  are excited, and their group velocity does not exceed  $\sim 10^5$ . At  $H_0 > H_c$ , the magnetostatic waves with  $k \lesssim 10^3$  are excited, their group velocity (due to the influence of boundary conditions) is of the order of  $10^6$ . According to (10.54) and (10.55), the decrease of pumping-region dimensions leads, then, to a noticeable increase of  $h_{z, \text{thr}}$ , in agreement with experiment.



**FIGURE 10.8**

Threshold fields for longitudinal pumping in a normally magnetized YIG film vs external steady field for different dimensions of the pumping region [281]. Thickness of the film is  $16 \mu\text{m}$ , pumping frequency is 9.37 GHz, room temperature.

Another important case of nonuniform pumping is the excitation of spin waves under the action of a *running wave*. Assume, at first, that the pumping wave is a uniform plane wave with frequency  $\omega_p$  and wave vector  $\mathbf{k}_p$ . The excited modes are also uniform plane waves with frequencies  $\omega_{1,2}$  and wave vectors  $\mathbf{k}_{1,2}$ . We restrict our treatment to the first-order process. Then, besides the condition (10.17) with  $n = 1$ , the condition of *space synchronism*

$$\mathbf{k}_1 + \mathbf{k}_2 = \mathbf{k}_p \quad (10.71)$$

is to be satisfied. In corpuscular 'language', (10.71) is a condition of the impulse conservation, whereas (10.17) is a condition of energy conservation in each elementary process.

In a way similar to the one used in deriving equations (10.13), we obtain the system

$$\frac{dc_1}{dt} = i\omega_1 c_1 + \rho_{12} c_p c_2^* \quad \frac{dc_2^*}{dt} = -i\omega_2 c_2^* - i\rho_{12}^* c_p^* c_1 \quad (10.72)$$

where  $c_p$ ,  $c_1$ , and  $c_2$  are normal variables for the pumping wave and the excited waves, respectively, and  $\rho_{12}$  is the coupling coefficient, which depends on  $\omega_H$  and  $\omega_M$ , as well as on frequencies and wave vectors of all three interacting waves. If  $k_p \ll k_{1,2}$ , so that  $\mathbf{k}_1 \cong -\mathbf{k}_2$ , i.e.,  $\theta_1 \cong \pi - \theta_2 \equiv \theta_k$  and  $\varphi_1 \cong \pi + \varphi_2 \equiv \varphi_k$ , the coupling coefficient can be written in the form

$$\rho_{12} = \rho_{12\perp} + \rho_{12\parallel} \quad (10.73)$$

where  $\rho_{12\perp}$  is given by (10.14) and

$$\rho_{12\parallel} = \frac{\omega_M^2}{4\omega_p} \sin 2\theta_p \exp(-i\varphi_p) \sin^2 \theta_k \exp(2i\varphi_k). \quad (10.74)$$

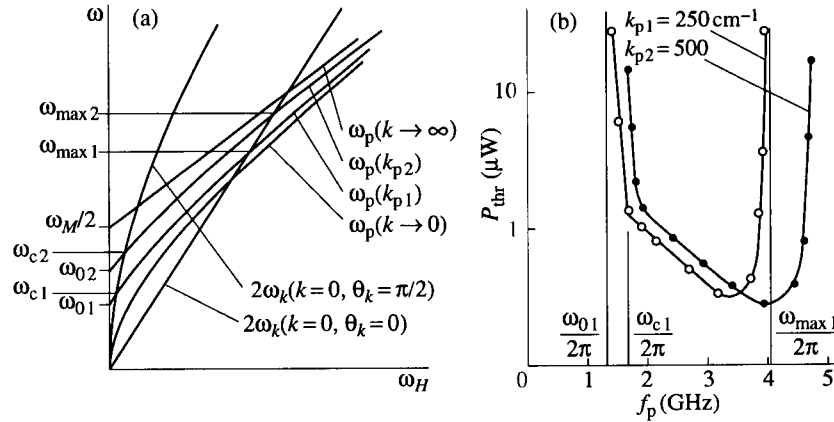
Comparing (10.72) and (10.74) with expressions (10.40) and (10.41), we see that the *combined* action of quasiuniform transverse pumping and quasiuniform longitudinal pumping is present in this case; the effective pumping field for longitudinal pumping is

$$h_z = \frac{\omega_M}{2\gamma} \sin 2\theta_p \exp(-i\varphi_p) c_p. \quad (10.75)$$

It can be shown that  $h_z$  is nothing but the  $z$  component of the magnetic field (7.12) of the pumping wave.

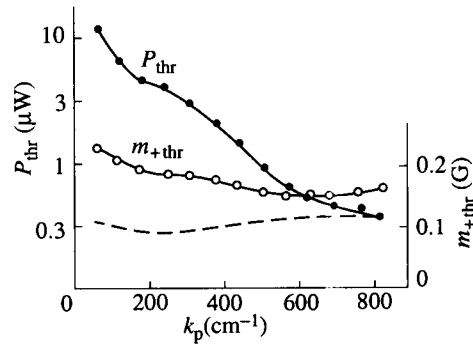
Maximization of the coupling coefficient, e.g., in the case of  $\theta_p = 45^\circ$ , shows that, at  $\omega_p > \omega_M/2$ , the first term in (10.73) dominates. Thus, the waves with  $\theta_k = 45^\circ$  are excited (Section 10.2), and the threshold magnetization is close to that for uniform transverse pumping. At  $\omega_p < \omega_M/2$ , the term  $\rho_{12\parallel}$  dominates, waves with  $\theta_k = \pi/2$  are excited, and the threshold magnetization differs from that for uniform transverse pumping by the factor  $2\omega_p/\omega_M$ .

Consider now a *surface* wave in a tangentially magnetized film (Section 6.2). As the ac magnetic field of this wave has negligibly small  $z$  component, the

**FIGURE 10.9**

First-order parametric spin-wave excitation by a surface magnetostatic wave: (a) frequencies of the pumping waves ( $\omega_p$ ) and twice the spin-wave frequencies ( $2\omega_k$ ), (b) experimental threshold values of input power vs  $\omega_p$  [168].

pumping is *transverse*. We will limit ourselves to the first-order process and suppose the excited modes to be uniform plane spin waves, which can be justified for not-too-thin films ( $d \gtrsim 5 \mu\text{m}$  for YIG). The boundaries of the region in which the first-order instability of such waves takes place under pumping by a surface magnetostatic wave are shown in Figure 10.9(a). The frequency  $\omega_{\max}$  is the upper boundary of this region for the pumping wave with a given wave number  $k_p$ . The

**FIGURE 10.10**

Dependence of threshold values of input power and magnetization on wave number of a pumping surface wave  $k_p$  at  $\omega_p = 3.26 \text{ GHz}$  [71]. YIG film with thickness  $15.2 \mu\text{m}$ , room temperature. Dashed line denotes the theoretical threshold magnetization.



lower boundary of the region is the lower frequency  $\omega_0$  at which the surface wave with given  $k_p$  exists. However, between  $\omega_0$  and the frequency  $\omega_c$ , the threshold fields are high because only exchange spin waves with large  $k$  can be excited. These conclusions agree rather well with experiment [Figure 10.9(b)].

The experimental  $k_p$  dependence of the threshold power  $P_{\text{thr}}$  at the input of a transducer that excites the pumping surface wave is plotted in Figure 10.10. The values of the pumping-wave magnetization, which were found from the threshold power  $P_{\text{thr}}$ , are shown as well. These experimental values are somewhat larger than the values  $(m_{+ \text{thr}})_{\text{theor}}$  calculated by minimization of (10.23). The difference is apparently due to above-discussed effect of local pumping. As for the strong dependence of  $P_{\text{thr}}$  on  $k_p$  (Figure 10.10), it is caused mainly by the change of the pumping-wave group velocity.

For *volume* magnetostatic waves in films, the longitudinal component of an ac magnetic field is comparable with transverse components, and the *oblique* pumping takes place.

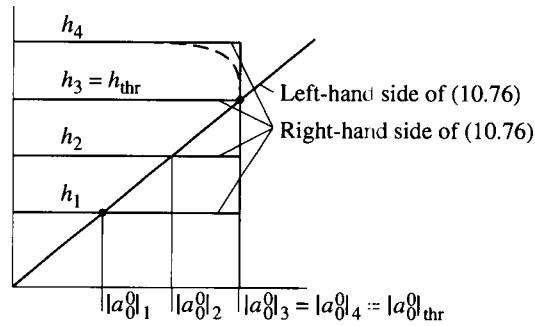
## 10.5 Above-threshold state

In the preceding sections of this chapter, only thresholds of spin-wave parametric excitation were considered, i.e., the values of an ac magnetization or field at which the exponential growth of spin-wave amplitudes (the spin-wave instability) begins. But the growth of these amplitudes cannot be unlimited, and a certain *limiting state* should exist, either a steady state (with constant amplitudes) or an unsteady one (characterized by periodic self-oscillations or chaotic change of these amplitudes). The unlimited exponential growth of spin-wave amplitudes was obtained because we took into account only the lowest nonlinear terms in the equations of motion. Now, studying the above-threshold states, we must take into account the higher-order nonlinear terms, too.

The simplest reason ('mechanism') for the limitation of growth of the parametric spin-wave amplitudes is that the total ac magnetization cannot, in any case, exceed  $M_0$ . However, we will see that the limitation usually occurs much earlier due to other mechanisms. At least three such mechanisms exist: reaction of parametric spin waves on pumping, phase mechanism, and nonlinear damping. In studying these mechanisms, we will limit ourselves to the case when parametric spin waves may be regarded as uniform plane waves and the pumping field is uniform.

### 10.5.1 Reaction of parametric spin waves on pumping

The energy transferred to parametric spin waves is an additional source of losses for the pumping. In the case of longitudinal pumping, the growth of parametric

**FIGURE 10.11**

Graphical solution of equation (10.76) [392]. Solid lines correspond to the approximation (10.77) and dashed line, to the actual dependence of  $\omega_{r0k}$  on  $a_0^0$  (schematically). © 1957 Elsevier Science Ltd.

spin waves leads to the decrease of the quality factor  $Q$  of the resonator in which the sample is placed and, hence, to the slowing down of the increase of  $h_z$  with growing input power. However, the volume of the sample is usually much smaller than the resonator volume, and the decrease of  $Q$  turns out to be small. Therefore, this mechanism does not play any important role in the case of longitudinal pumping.

For *transverse* pumping, this mechanism can be taken into account by introducing an additional dissipation parameter  $\omega_{r0k}$ , so that [compare with (10.12)]

$$a_0^0 = \frac{\gamma h}{\tilde{\omega}_0 - \omega_p + i(\omega_{r0} + \omega_{r0k})}. \quad (10.76)$$

In the case of *first-order* process, the growth of parametric spin waves begins from a very low (thermal) level. The dependence of  $\omega_{r0k}$  on  $a_0^0$  can be approximated, then, as [392]

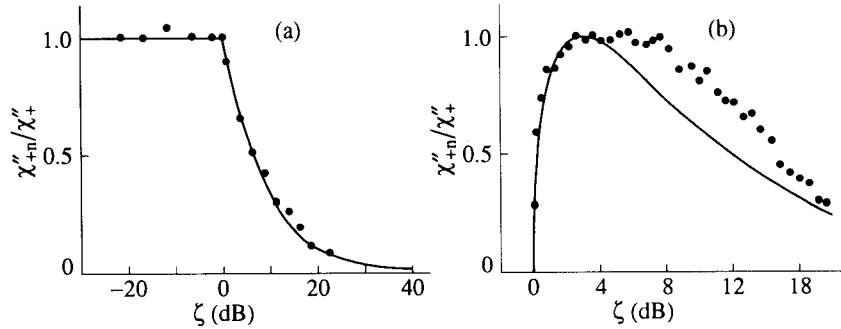
$$\omega_{r0k} = \begin{cases} 0 & \text{at } a_0^0 < a_{0\text{thr}}^0 \\ \infty & \text{at } a_0^0 > a_{0\text{thr}}^0 \end{cases}. \quad (10.77)$$

Equation (10.76), allowing for (10.77), can be solved graphically as shown in Figure 10.11. With the growth of  $h$ , the amplitude  $a_0^0$  increases linearly until  $h$  and  $a_0^0$  reach their threshold values. Then the increase of  $a_0^0$  ceases, and its threshold value 'freezes'. So,

$$a_0^0 = \begin{cases} \gamma h / (\tilde{\omega}_0 - \omega_p + i\omega_{r0}) & \text{at } h < h_{\text{thr}} \\ a_{0\text{thr}}^0 & \text{at } h > h_{\text{thr}} \end{cases} \quad (10.78)$$

where  $a_{0\text{thr}}^0$  is determined by (10.23).

Neglecting the difference between  $\tilde{\omega}_0$  and  $\omega_0$ , we can find from (10.76) and (10.78)

**FIGURE 10.12**

Imaginary parts of the nonlinear susceptibility vs the above-threshold ratio for the first-order parametric spin-wave excitation under transverse pumping: (a) at resonance and (b) off resonance [392]. Dots represent experimental data for a tangentially magnetized disk of Mn ferrite at frequencies (a) 4.04 GHz and (b)  $\sim 9$  GHz. The curves are calculated using (10.80). © 1957 Elsevier Science Ltd.

the expression for the total dissipation parameter

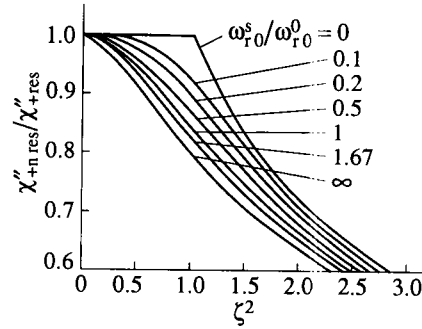
$$\omega_{r0} + \omega_{r0k} = \sqrt{(\zeta^2 - 1)(\omega_0 - \omega_p)^2 + \zeta^2 \omega_{r0}^2} \quad (10.79)$$

where  $\zeta = h/h_{thr}$  is the *above-threshold ratio*. To calculate the components of the nonlinear susceptibility tensor we must substitute the dissipation parameter (10.79) into the expressions for susceptibility components cited in Section 1.5. We obtain, then, e.g.,

$$\frac{\chi''_{+n}}{\chi''_+} = \frac{1}{\zeta^2} \sqrt{(\zeta^2 - 1) \frac{(\omega_0 - \omega_p)^2}{\omega_{r0}^2} + \zeta^2} \quad (10.80)$$

where  $\chi''_+$  and  $\chi''_{+n}$  are imaginary parts of the linear and the nonlinear right-hand circular susceptibilities. The calculated dependences of the ratio (10.80) on  $\zeta$  and the corresponding experimental data are shown in Figure 10.12. The disagreement between experimental data and the calculated curve in Figure 10.12(b) is due to another mechanism of spin-wave amplitude limiting, the phase mechanism, which will be discussed below.

Consider now, following Suhl [395], the steady state above the *second-order instability* threshold. This case differs from the above-considered one in that now the potentially unstable spin waves (with  $\omega_k = \omega_p$ ) are excited, as well, due to the process of *two-magnon scattering* (already discussed in Section 10.3). This process also results in additional excitation of the pumping mode by the parametric spin waves. To allow for these processes we have to add, in equations (10.24) and (10.5), the terms similar to those that have been inserted, with the same purpose, in equation (10.50); the term  $\nu_{k0}a_0$  should be added in (10.24) and the



**FIGURE 10.13**

Influence of two-magnon scattering on the nonlinear susceptibility for the second-order parametric spin-wave excitation [395].

term  $\sum_{k \neq 0} \nu_{0k} c_k$ , in (10.5).

It is necessary, then, to make the replacements  $\omega_0 \rightarrow \omega_0 + i\omega_{r0}^0$  and  $\omega_k \rightarrow \omega_k + i\omega_{rk}^0$  where  $\omega_{r0}^0$  and  $\omega_{rk}^0$  are the dissipation parameters without allowing for two-magnon scattering. Assuming that  $\omega_{rk}^0$ ,  $\nu_{0k}$ , and  $\nu_{k0}$  do not depend on  $k$ , we obtain at resonance ( $\omega_p = \omega_0$ )

$$a_{0res}^0 = \frac{i\gamma h}{\omega_{r0}^0 + \omega_{r0}^s \left[ 1 - (a_{0res}^0/a_{0thr}^0)^4 \right]^{-1/2}}. \quad (10.81)$$

One can see from this expression that the effective dissipation parameter of the pumping mode infinitely increases when  $a_{0res}^0$  approaches  $a_{0thr}^0$ . Hence,  $a_{0res}^0$  reaches  $a_{0thr}^0$  only in the limit of  $h \rightarrow \infty$ . However, a 'threshold' field can be formally defined as  $h_{thref} = a_{0thr}^0 M_0 / \chi''_{+res}$  (where  $\chi''_{+res}$  is the linear susceptibility), and the above-threshold ratio can be also defined as before:  $\zeta = h/h_{thref}$ . Then, the equation

$$\eta = \frac{1+s}{1+s(1-\eta^4/\zeta^4)^{-1/2}} \quad (10.82)$$

where  $\eta = \chi''_{+nres}/\chi''_{+res}$  and  $s = \omega_{r0}^s/\omega_{r0}^0$ , follows from (10.81). The curves  $\eta(\zeta)$  for different values of  $s$ , calculated by solving this equation, are plotted in Figure 10.13. One can see that the threshold of the second-order spin wave instability is 'smeared out' stronger the larger the contribution of two-magnon scattering to the dissipation parameter.

### 10.5.2 Phase mechanism

The phase mechanism of limiting of parametric-spin-wave growth above threshold was suggested by Zakharov, L'vov, and Starobinets [459] (see also [265]).

This mechanism consists in the change of the phase shift between pumping and parametric spin waves, which leads to the decrease of coupling between them with the growth of the pumping field. The phase mechanism plays the most important role for longitudinal pumping, and in discussing it we will restrict ourselves to this case.

To analyze the phase mechanism the following third-order terms must be inserted in equation (10.40) and the adjoint equation:

$$2i \sum_{k_1} T_{k k_1} c_k c_{k_1} c_{k_1}^* + i \sum_{k_1} S_{k k_1} c_{-k}^* c_{k_1} c_{-k_1}. \quad (10.83)$$

Then, these equations turn into the equation

$$\left[ \frac{d}{dt} + \omega_{rk} - i \left( \tilde{\omega} - \frac{\omega_p}{2} \right) \right] c_k^0 - iP_k c_{-k}^0 = 0 \quad (10.84)$$

and the adjoint one where

$$\tilde{\omega}_k = \omega_k + 2 \sum_{k_1} T_{k k_1} |c_{k_1}^0|^2 \quad (10.85)$$

$$P_k = h_z V_k + \sum_{k_1} S_{k k_1} c_{k_1}^0 c_{-k_1}^0. \quad (10.86)$$

Comparing (10.84) with (10.40), we see that the added terms result first in the *change of spin-wave eigenfrequencies* and second, in the 'renormalization' of pumping, i.e., in the replacement of the external pumping  $h_z V_k$  by the effective pumping  $P_k$ . It can be shown that, above the threshold,

$$|P_k| = \sqrt{\omega_{rk}^2 + \left( \tilde{\omega}_k - \frac{\omega_p}{2} \right)^2}. \quad (10.87)$$

According to [459], we introduce new variables  $n_k$  and  $\psi_k$  defined by the following relations (note that  $|c_k| = |c_{-k}|$ ):

$$c_k^0 c_{-k}^0 = |c_k^0|^2 \exp(i\beta_k + i\beta_{-k}) = 2 \frac{\gamma h}{M_0} n_k \exp(i\psi_k). \quad (10.88)$$

The quantity  $n_k$  characterizes the intensity of parametric spin waves with wave vectors  $\mathbf{k}$  and  $-\mathbf{k}$  and is equal to the number of corresponding magnons. The quantity  $\psi_k$  is the sum of phases of spin waves with  $\mathbf{k}$  and with  $-\mathbf{k}$ . It should be emphasized that only the *sum* of these phases is determinable, the difference of them is arbitrary. This means that parametric spin waves are only *partially coherent*.

The new variables satisfy the equations following from (10.84):

$$\frac{dn_k}{dt} = 2n_k \{ -\omega_{rk} + \text{Im} [P_k^* \exp(i\psi_k)] \} \quad (10.89)$$

$$\frac{d\psi_k}{dt} = 2 \left\{ \tilde{\omega}_k - \frac{\omega_p}{2} + \text{Re} [P_k^* \exp(i\psi_k)] \right\}. \quad (10.90)$$

It can be shown, using these equations, that, in a steady state above threshold, only spin waves with a certain pair  $\mathbf{k}$  and  $-\mathbf{k}$  of wave vectors (for which the threshold is the lowest and, hence,  $\tilde{\omega}_k = \omega_p/2$ ) do exist. The solution of (10.89) and (10.90) for these waves has the form [459]

$$n_k = \frac{1}{S} \sqrt{(h_z V)^2 - \omega_{rk}^2} \quad \sin \psi_k = \frac{\omega_{rk}}{h_z V} \quad \cos \psi_k = -\frac{S n_k}{h_z V} \quad (10.91)$$

where

$$S = \frac{1}{4} \left( \frac{\omega_M}{\omega_p} \right)^2 \left( \sqrt{\omega_p^2 + \omega_M^2} - \omega_M + \gamma N_z M_0 \right) \quad (10.92)$$

$$V \equiv \left| V_k \left( \frac{\pi}{2} \right) \right| = \gamma \frac{\omega_M}{2\omega_p}. \quad (10.93)$$

One can see from (10.91) that  $\psi = \pi/2$  at threshold ( $h_z V = \omega_{rk}$ ), which is the optimum condition for energy transfer from pumping to parametric spin waves. With the growth of  $h_z$  this phase relation gets broken, and  $\psi$  approaches  $\pi$  at  $h_z \rightarrow \infty$ .

With the use of (10.91)–(10.93), the  $z$  component of uniform ac magnetization  $m_z$  and the nonlinear susceptibility  $\chi_{zn} = m_z/h_z = \chi'_{zn} - i\chi''_{zn}$  can be calculated:

$$\chi'_{zn} = \frac{M_0 V^2 \zeta^2 - 1}{\gamma S \zeta^2} \quad \chi''_{zn} = \frac{M_0 V^2 \sqrt{\zeta^2 - 1}}{\gamma |S| \zeta^2}. \quad (10.94)$$

These expressions are in rather good agreement with experimental data by Zautkin *et al.* [460] at  $\zeta < \zeta_2 \simeq 7$  (Figure 10.14), which shows the dominant role of the phase mechanism for longitudinal pumping, in any case, if  $\zeta < \zeta_2$ . The phase mechanism operates for transverse pumping as well, especially for the off-resonance first-order process. This mechanism is responsible, e.g., for the deviation of experimental points in Figure 10.12(b) from the calculated curve.

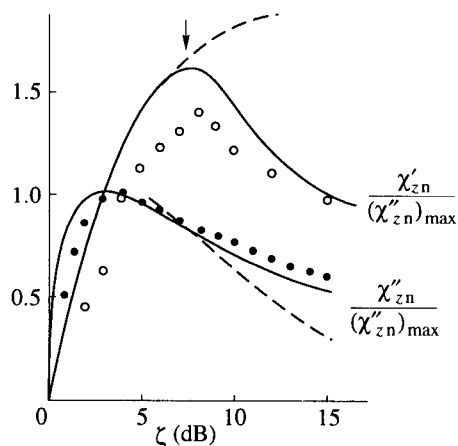
### 10.5.3 Nonlinear damping

The mechanism of nonlinear damping is caused by the dependence of  $\omega_{rk}$  on the parametric-spin-wave amplitudes. The most prominent example is the contribution of the elementary confluence process of *two parametric* magnons. This effect was studied by Gottlieb and Suhl [148]. The contribution of it to  $\omega_{rk}$  is positive and proportional to the number of parametric magnons. This process is allowed by the conditions of energy and impulse conservation if  $H_0 < H_{3cn}$  where

$$H_{3cn} = H_{0c}(\theta_k) - \frac{1}{6\gamma} \left( \sqrt{4\omega_p^2 + \omega_M^2 \sin^4 \theta_k} - \sqrt{\omega_p^2 + \omega_M^2 \sin^4 \theta_k} \right) \quad (10.95)$$

[ $H_{0c}(\theta_k)$  is given by (7.18)].

Three-magnon processes with participation of *only one parametric* magnon can also contribute to nonlinear damping because, at large numbers of parametric

**FIGURE 10.14**

Dependences of real and imaginary parts of nonlinear susceptibility on the above-threshold ratio for longitudinal pumping [460]. Dashed curves are calculated with (10.94), solid curves are calculated allowing for the excitation of the second group of spin waves (see below); the starting point of this excitation is denoted by an arrow. Circles correspond to experimental data for YIG sphere at frequency 9.4 GHz, room temperature, and  $H_0 = H_c - 100$  Oe ( $\mathbf{H}_0 \parallel \langle 111 \rangle$ ).

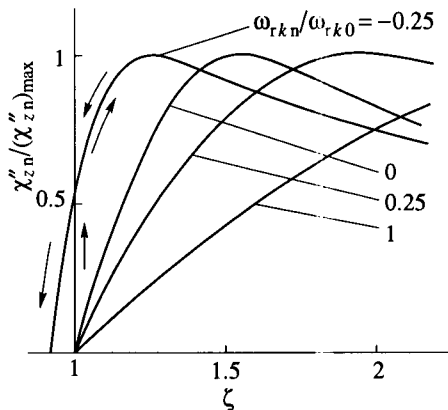
magnons, the numbers of thermal magnons begin to differ from their equilibrium values. It is easy to make sure that the nonlinear contribution of such confluence process is negative, and the contribution of a splitting process is positive, and both are proportional to the number of parametric magnons. In the case of longitudinal pumping in a sphere ( $\theta_k = \pi/2$ ), as L'vov and Fal'kovich have shown [264], the former contribution exists at  $H_0 < H_{3c}$  where

$$H_{3c} = \frac{1}{\gamma} \left( \frac{4}{9} \omega_p^2 - \frac{1}{2} \omega_M^2 \right) \quad (10.96)$$

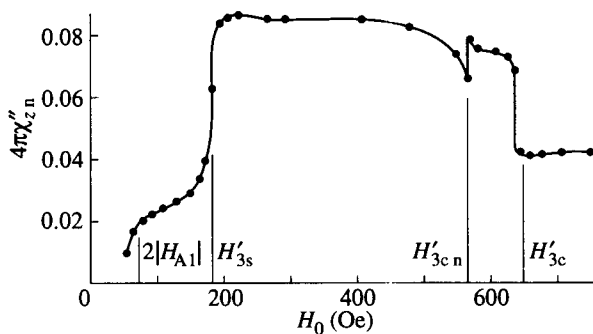
and the latter, at  $H_0 < H_{3s}$  where

$$H_{3s} = H_c - \frac{2}{3\gamma} \left( \sqrt{\omega_p^2 + \omega_M^2} - \sqrt{\frac{1}{4} \omega_p^2 + \omega_M^2} \right). \quad (10.97)$$

The *combined* action of phase mechanism and nonlinear damping can be examined, in the case of longitudinal pumping, if we assume, in equation (10.88), that  $\omega_{rk} = \omega_{rk0} + \omega_{rk n}$  where  $\omega_{rk n}$  is the contribution of nonlinear damping. The nonlinear susceptibilities above threshold calculated in this way are shown in Figure 10.15. One can see that, at small  $\zeta$ , positive nonlinear damping leads to the decrease, and the negative one leads to the increase of  $\chi''_{zn}$ . Such behavior is confirmed by experimental data presented in Figure 10.16. The signs of

**FIGURE 10.15**

Influence of the nonlinear damping on the  $\zeta$  dependences of the nonlinear susceptibility for longitudinal pumping [459].

**FIGURE 10.16**

Field dependence of the nonlinear susceptibility for longitudinal pumping [275]. YIG sphere,  $\mathbf{H}_0 \parallel \langle 100 \rangle$ ,  $f_p = 9.37$  GHz, room temperature,  $\zeta = 1$  dB. The fields  $H'_{3s}$ ,  $H'_{3cn}$ , and  $H'_{3c}$  are calculated with formulae (10.95)–(10.97) with an anisotropy field  $2|H_{A1}|$  added.

$\chi''_{zn}$  quick changes and the experimental steady-field values at which they occur (after a correction for the magnetocrystalline anisotropy) agree with theoretical values (10.95)–(10.97). At sufficiently large  $\zeta$ , the opposite effect takes place (Figure 10.15). Besides, one can see from Figure 10.15 that negative nonlinear damping results in hysteresis or 'hard' excitation of parametric spin waves.



### 10.5.4 Stability of the above-threshold state

It must be pointed out, first of all, that a distinction needs to be drawn between the external stability (relative to the birth of other groups of parametric spin waves) and the internal stability (relative to small changes of the amplitude and phase of the primary group).

For longitudinal pumping, the primary group has  $\theta_{k_1} = \pi/2$  and amplitude and phase determined by (10.89) and (10.90). This state remains stable relative to the creation of another group of spin waves (*external* stability) until the effective pumping (10.86) for the new group reaches the value of  $\omega_{rk}$ . Using this condition, it was found [459] that, in an isotropic ferromagnet, the external stability retains up to  $\zeta = 3.5$ . Then the spin-wave group, with  $\tilde{\omega}_k = \omega_p/2$ , as before, and  $\theta_{k_2} = 50^\circ$ , is excited. Experiment [238] has shown the occurrence of a new group with  $\theta_{k_2} = 45\text{--}50^\circ$  but at larger  $\zeta$  value, of the order 10–20. The distinction is, evidently, due to the dependence of  $\omega_{rk}$  on  $\theta_k$ . With further increase of  $\zeta$ , new groups of spin waves with  $\tilde{\omega}_k = \omega_p/2$  are excited.

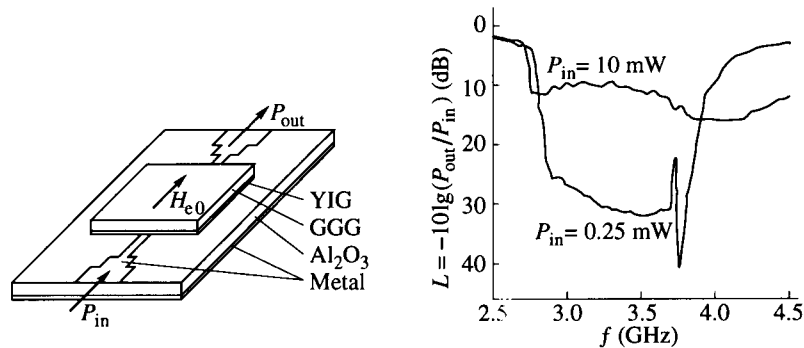
To examine the *internal* stability we must add a small deviation  $\alpha$  to the spin-wave amplitude and, using equation (10.84), see whether  $\alpha$  will grow or damp out with time. If the internal stability does not take place, the collective *self-oscillations*, uniform or nonuniform, of amplitudes and phases of parametric spin waves occur (see review articles [265, 327]). They manifest themselves as oscillations of magnetization, and hence, of the power absorbed by the sample. The frequencies of the oscillations usually lie in the range from tens of kilohertz to tens of megahertz. At small  $\zeta$ , their shape is near sinusoidal, at larger  $\zeta$ , it differs essentially from sinusoidal, and at still larger, it becomes chaotic [327].

Calculation performed for longitudinal pumping in a cubic ferromagnet [459] showed that under assumed conditions (YIG, frequency of 9 GHz, room temperature), the internal stability (relative to uniform deviations) takes place for  $\mathbf{M}_0$  directed along  $\langle 100 \rangle$  axis and does not for  $\mathbf{M}_0 \parallel \langle 111 \rangle$ . This is in agreement with the experimental fact (see, e.g., [256]) that, in YIG under the mentioned conditions, self-oscillations are observed for  $\mathbf{M}_0 \parallel \langle 111 \rangle$  and are not observed if  $\mathbf{M}_0 \parallel \langle 100 \rangle$ .

### 10.5.5 Nonlinear microwave ferrite devices

Let us discuss briefly the practical significance of the nonlinear phenomena considered in the present chapter. First, the parametric excitation of spin waves *restricts the dynamic range* of linear ferrite devices, which are widely used in microwave systems and are starting to be used in optical systems, too. Serious efforts have been made to increase the thresholds of parametric spin-wave excitation in materials intended for use at high microwave power levels. One of the ways, which consists in decreasing the grain dimensions of polycrystalline ferrites, was mentioned in Section 10.4.

Second, as has also been mentioned, the measurement of parametric spin-



**FIGURE 10.17**

Ferrite small-signal suppressor using a surface magnetostatic wave [6]. Thickness of the YIG film is  $26.6 \mu\text{m}$ ,  $H_{e0} = 425 \text{ Oe}$ .

wave excitation thresholds, especially with longitudinal pumping, is a common technique for *determining the dissipation parameters* of ferrite materials.

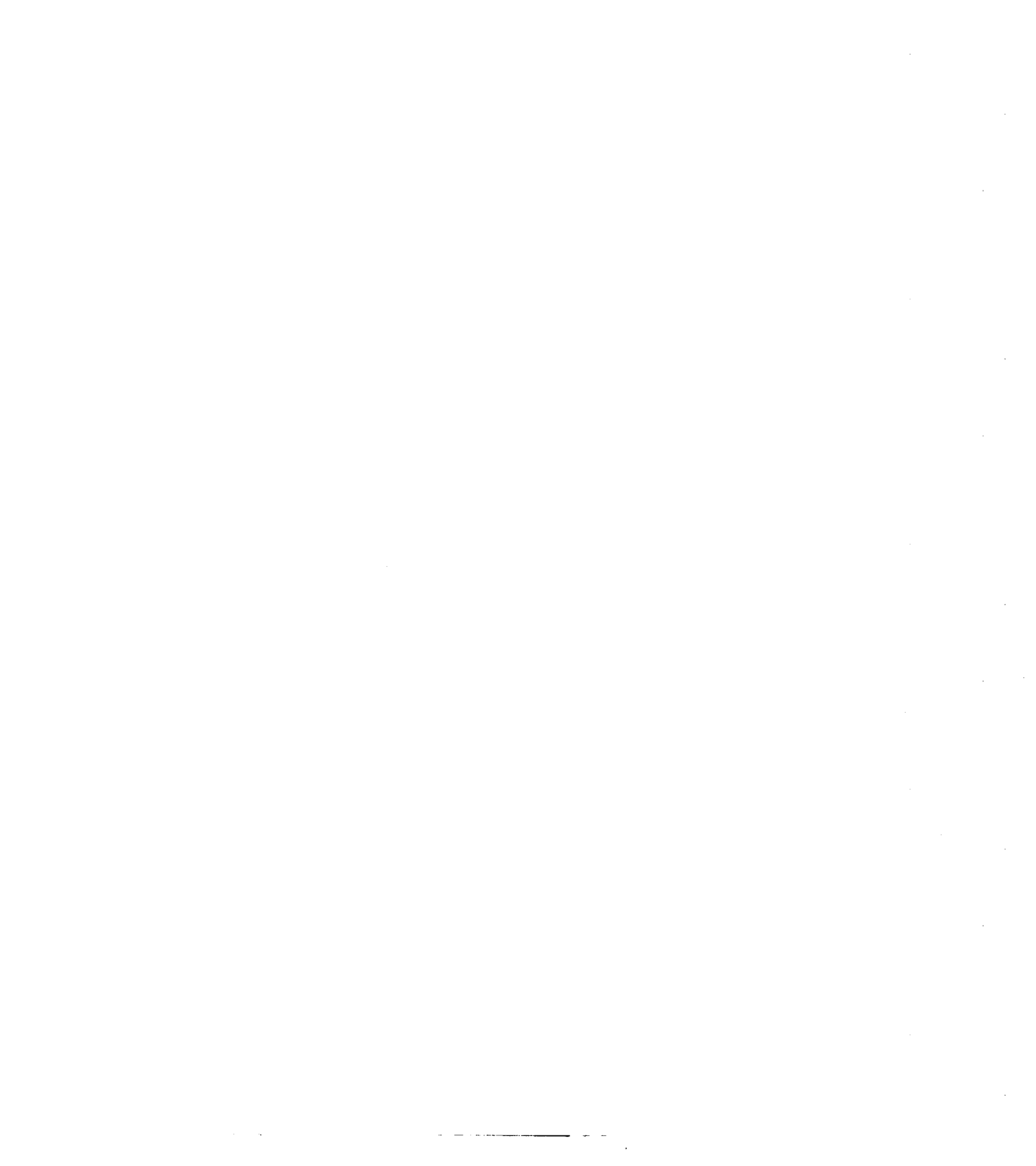
And finally, the above-threshold phenomena, studied in the present section, are applied for *designing nonlinear ferrite devices*. One of such devices is the *power limiter*, e.g., a nonlinear quadripole the output power of which remains approximately constant in a certain range of input power. Such a device is needed, e.g., to protect the input circuit of a microwave receiver against overloads.

To develop a microwave power limiter the *off-resonance* first-order process of spin-wave parametric excitation with transverse or longitudinal pumping can be used. The ferrite sample in a resonator or waveguide, being far from ferromagnetic resonance, practically does not absorb electromagnetic power below the threshold, so that the losses at low signal level are small. Above the threshold, the losses increase due to the parametric excitation of spin waves. Because of the above-discussed ‘freezing’ of pumping amplitude in the first-order process, the output power remains approximately constant in a rather broad dynamic range.

Another type of ferrite power limiter uses the parametric excitation *at ferromagnetic resonance* and therefore has (if the first-order process is applied) much lower threshold power. The ferrite sample in this device reradiates microwave power into an ‘orthogonal’ (i.e., uncoupled in the absence of ferrite) waveguide. It was shown in Section 5.4 that the losses of such a device, a ferrite band-pass filter, are small at low power level. At high power level, above the threshold, the pumping amplitude ‘freezes’, and the losses increase. The threshold input power of such a *filter-limiter*, using the first-order process, is as small as several microwatts, and the dynamic range can be 20–40 dB. However, the first-order process is possible only at low frequencies, e.g., lower than  $\sim 3 \text{ GHz}$  for YIG at room temperature. At higher frequencies the second-order process must be used, and the threshold power substantially increases.

It was pointed out in Section 5.4 that a ferrite band-stop filter can be made, as well. Its simplest design is again a waveguide with a ferrite sample but at ferromagnetic resonance. Such a device operates as a *small-signal suppressor*: at input-power level lower than the threshold of spin-wave parametric excitation, the losses are high, and above the threshold, the losses decrease because the absorbed power is being limited. The threshold is low and the decrease of losses at high power level is essential if the first-order process of parametric excitation is used.

The frequency band of the ferrite small-signal suppressor can be materially enlarged when, instead of ferromagnetic resonance in a sample, a *magnetostatic wave* in a film is excited. It is expedient to use the surface wave in a tangentially magnetized film (Section 6.2) and, of course, the first-order process. Such a device [6] was suggested by Adam and called the 'signal-to-noise ratio enhancer'. Its design and characteristics are shown in Figure 10.17.



# 11

---

## *Spin-spin relaxation*

---

---

### 11.1 Relaxation processes in magnetically ordered substances

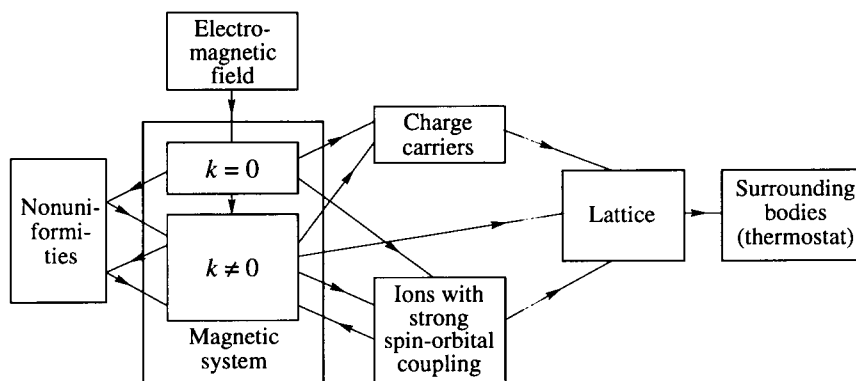
The dissipation of energy of magnetic oscillations and waves was treated in the preceding chapters only phenomenologically. Now we begin to study the physical processes that determine the relaxation. This chapter and, to a large extent, Chapters 12, 13, and 14 will be devoted to this problem.

The relaxation processes move a system to the state of thermodynamical equilibrium. If the forces that had removed it from this state stopped their action, the relaxation processes bring the system to equilibrium. We are interested in the case when in nonequilibrium state there exist one or more modes with amplitudes exceeding their equilibrium values. Then, after the external forces that had excited these modes stop their action, the energy they had passed to these modes is redistributed between all eigenmodes. The relaxation processes determine, in this case, the rate of the decrease of the nonequilibrium mode amplitudes.

However, if the external forces excite some modes continuously, the equilibrium state, of course, will not be reached. The system will remain in a steady nonequilibrium state, in which the amplitudes of the modes excited by the external forces, as well as of some other modes strongly coupled with them, will exceed the equilibrium levels. The relaxation processes now perform the steady energy flow from the modes excited by external forces and determine the dissipative parameters of the system for forced oscillations, i.e., the anti-Hermitian parts of the susceptibility tensor components (Section 4.4).

#### 11.1.1 Kinds of relaxation processes

The system we are interested in is the magnetic system of a magnetically ordered substance. Its eigenmodes are the uniform and nonuniform oscillations and spin waves (or magnons, in terms of corpuscular theory), which were studied in detail above. Some relaxation processes result in the redistribution of energy between the modes of the magnetic system, i.e., in the destruction of magnons excited by the



**FIGURE 11.1**  
Flows of energy in magnetically ordered substances.

external fields and creation of other magnons. Such processes are called spin-spin relaxation processes. They can be subdivided into inherent spin-spin processes, which are characteristic of ideal crystals, and processes caused by defects. The latter can be regarded as scattering of magnons by defects.

The electronic magnetic system<sup>1</sup> is coupled with other systems of the magnetically ordered substance: lattice, free charge carriers, nuclear magnetic system. Therefore, the relaxation processes exist which carry the energy from magnetic system to other systems. In most cases the energy is transferred finally to the lattice that results in heating it (i.e., in the creation of phonons, in terms of corpuscular theory). Therefore, all relaxation processes that result in the flow of energy from the magnetic system are called often spin-lattice processes. They are subdivided into direct and indirect spin-lattice processes. The first are such in which magnons are destructed and, simultaneously, phonons are created. In indirect processes energy is transferred into lattice through some other systems.

The concepts of spin-spin and spin-lattice relaxations were introduced first in the theory of paramagnetic relaxation [68]. In magnetically ordered substances, in which the eigenoscillations are collective modes, these concepts differ essentially from those in paramagnets. In particular, in magnetically ordered substances, as distinct from paramagnets, the relaxation rates of longitudinal and transverse magnetization components are nearly the same and are determined by both the spin-spin and spin-lattice processes [17].

In Figure 11.1 the energy flows are shown which arise in the magnetic system of a ferromagnet and between this system and other systems in a stationary regime when an electromagnetic field excites the uniform mode of magnetic oscillations ( $k = 0$  magnons).

<sup>1</sup>We deal with this system all the time omitting the word 'electronic'.

### 11.1.2 Methods of theoretical study

The relaxation processes in magnetically ordered substances were first studied theoretically by Akhiezer [10]. Since then a lot of works have been devoted to this problem (e.g., monographs and reviews [171, 376, 14]). Two methods were mostly used: the method of coupled equations of motion and the method of transition probabilities (or kinetic equations).

The method of coupled equations of motion<sup>2</sup> is based on the fact that relaxation processes are caused by the interaction of different modes. The allowance for this interaction leads to coupling of the equations of motion of the modes. It results in the energy transfer from one mode to the other, i.e., in the relaxation.

The method of transition probabilities is based on the fact that relaxation processes are the transitions of the system from one state into another, and the quantum-mechanical time-dependent perturbation theory (e.g., [243, 336]) can be used to calculate the probabilities of these transitions. It has been shown [66] that this method gives the same results as the method of coupled equations of motion.

More powerful theoretical techniques were used later to study the relaxation processes in ferro- and ferrimagnets, in particular, the method of Green functions [412]. We will use only the transition probability method, as the most simple, universal, and illuminative.

According to the time-dependent quantum-mechanical perturbation theory [243], the number of transitions per unit time from the state  $l$  into the state  $m$  under the action of time-independent perturbation is

$$w_{lm} = \frac{2\pi}{\hbar} |\langle m | \hat{\mathcal{H}}_p | l \rangle|^2 \delta(\varepsilon_l - \varepsilon_m) \quad (11.1)$$

where  $\langle m | \hat{\mathcal{H}}_p | l \rangle$  is the matrix element of the perturbation energy operator  $\hat{\mathcal{H}}_p$  for transition between states  $l$  and  $m$ ,  $\varepsilon_l$  and  $\varepsilon_m$  are the eigenvalues of energy in these states, and  $\delta(x)$  is the Dirac delta function (Appendix C).

Employing the transition-probability method to study the relaxation processes, we have to pass to the secondary-quantization representation (Section 7.4), in which the transitions from one state to another are the changes of the numbers of quasiparticles: magnons, phonon, etc. The energy operator (Hamiltonian) of the magnetic system can be written in this representation in the form

$$\hat{\mathcal{H}} = U_0 + \hat{\mathcal{H}}_2 + \hat{\mathcal{H}}_p \quad (11.2)$$

where  $\hat{\mathcal{H}}_2$  is the quadratic Hamiltonian that, in the case of the Heisenberg model, was considered in Section 7.4, and  $\hat{\mathcal{H}}_p$  contains terms of higher order in operators  $\hat{a}_k^+$  and  $\hat{a}_k$ .

---

<sup>2</sup>This method was widely used in Chapter 10.

In an ideal (perfectly periodic) crystal the operator  $\hat{\mathcal{H}}_p$  has the form<sup>3</sup> [214, 14]

$$\begin{aligned}\hat{\mathcal{H}}_p = & \sum_1 \sum_2 \sum_3 \Psi_{1,23} \hat{a}_1 \hat{a}_2^+ \hat{a}_3^+ \Delta(\mathbf{k}_1 - \mathbf{k}_2 - \mathbf{k}_3) \\ & + \sum_1 \sum_2 \sum_3 \sum_4 \Psi_{1,234} \hat{a}_1 \hat{a}_2^+ \hat{a}_3^+ \hat{a}_4^+ \Delta(\mathbf{k}_1 - \mathbf{k}_2 - \mathbf{k}_3 - \mathbf{k}_4) \\ & + \sum_1 \sum_2 \sum_3 \sum_4 \Psi_{12,34} \hat{a}_1 \hat{a}_2 \hat{a}_3^+ \hat{a}_4^+ \Delta(\mathbf{k}_1 + \mathbf{k}_2 - \mathbf{k}_3 - \mathbf{k}_4) \\ & + \text{higher terms} + \text{H.c.}\end{aligned}\quad (11.3)$$

Here,  $\Psi_{1,23}$ ,  $\Psi_{1,234}$ , and  $\Psi_{12,34}$  are certain complex quantities,  $\Delta$  is the Kronecker delta symbol (Appendix C), and H.c. denotes Hermitian conjugate terms. It should be noted that  $\hat{a}_k^+$  and  $\hat{a}_k$  are conjugate operators, and the sequence of operators changes to opposite when conjugating.

Each term of the Hamiltonian (11.3) contributes only to the matrix element  $\langle m | \hat{\mathcal{H}}_p | l \rangle$  that corresponds to the transition from state  $l$  to state  $m$ ; in this transition the numbers of quasiparticles whose creation operators appear in the considered term increase by 1, and the numbers of quasiparticles whose annihilation operators appear in this term decrease by 1. For example, the term  $\hat{a}_1 \hat{a}_2^+ \hat{a}_3^+$  gives such a matrix element that  $n_1$  decreases, and  $n_2$  and  $n_3$  increase by 1. This matrix element has the form [84]

$$\begin{aligned}\langle n_1 - 1, n_2 + 1, n_3 + 1 | \hat{\mathcal{H}}_p | n_1, n_2, n_3 \rangle \\ = \sqrt{n_1(n_2 + 1)(n_3 + 1)} \Psi_{1,23} \Delta(\mathbf{k}_1 - \mathbf{k}_2 - \mathbf{k}_3).\end{aligned}\quad (11.4)$$

The Hermitian conjugate term gives the matrix element

$$\langle n_1 + 1, n_2 - 1, n_3 - 1 | \hat{\mathcal{H}}_p | n_1, n_2, n_3 \rangle = \sqrt{(n_1 + 1)n_2 n_3} \Psi_{1,23}^* \Delta(\mathbf{k}_1 - \mathbf{k}_2 - \mathbf{k}_3).\quad (11.5)$$

Thus, each term of the perturbation Hamiltonian  $\hat{\mathcal{H}}_p$  (and hence the associated matrix element) corresponds to a certain elementary process, and the Hermitian conjugate term corresponds to a reverse process. For example, the term  $\hat{a}_1 \hat{a}_2^+ \hat{a}_3^+$  and the matrix element (11.4) correspond to an elementary process of splitting of a magnon into two magnons, and the term  $\hat{a}_3 \hat{a}_2 \hat{a}_1^+$  corresponds to an elementary process of confluence of two magnons. The term  $\hat{a}_1 \hat{a}_2 \hat{a}_3^+ \hat{a}_4^+$  corresponds to an elementary process of scattering, in which two magnons are annihilated and two others are created.<sup>4</sup>

The presence of the delta function in (11.1) results in conservation of energy, and the delta-symbols in (11.3), (11.4), or (11.5) lead to momentum conservation in each elementary process. The momentum conservation, as distinct from energy conservation, is a consequence of the ideality of the crystal and does not take

<sup>3</sup>Here and below the indices 1, 2, 3, ... denote  $\mathbf{k}_1, \mathbf{k}_2, \mathbf{k}_3, \dots$

<sup>4</sup>These elementary processes were already considered in Chapter 10.



place (in each elementary process) for such perturbations that make the crystal non-ideal.

We are usually interested in the rate of change of the numbers of quasiparticles with given  $\varepsilon_1$  and  $k_1$  due to the elementary process of a certain type. We must then sum the probabilities (11.1) over allowed values of all other quasiparticles that take part in this process. The elementary processes both direct and reverse must be taken into account. Then we obtain such expressions as

$$\frac{dn_1}{dt} = \frac{2\pi}{\hbar} \sum_2 \sum_3 \dots \left[ -|\langle m' | \hat{\mathcal{H}}_p | l' \rangle|^2 + |\langle m'' | \hat{\mathcal{H}}_p | l'' \rangle|^2 \right] \delta(\varepsilon_l - \varepsilon_m). \quad (11.6)$$

Here,  $l'$  and  $m'$  denote, respectively, the initial and the final states for direct processes, and  $l''$  and  $m''$  denote such states for reverse processes. The expression (11.6) is a kinetic equation for the number  $n_1$ . Its right side is called the collision sum (or the collision integral if we pass from the summation over  $k$  values to the integration over  $k$  spaces).

The existence of delta functions in (11.6) and delta symbols in the expressions for matrix elements restricts the regions in  $k$  spaces over which (after exclusion of the delta function and delta symbols) integration should really be carried out. For example, in the case of a three-particle process the integration will be carried out over a surface in one of spaces  $k_2$  or  $k_3$ .

Not only  $n_1$  but also numbers  $n_2, n_3, \dots$  of other quasiparticles appear in the right side of (11.6). They, in their turn, depend on the rates of all processes in which these quasiparticles take part, and kinetic equations for them must be also written. Thus, we get a chain of more and more complicated kinetic equations.

The matter is materially simplified if we assume that all numbers  $n_2, n_3, \dots$  except  $n_1$  do not differ from their equilibrium values  $\bar{n}_2, \bar{n}_3, \dots$ . This assumption, as it was mentioned in Section 10.5, is valid only for small numbers  $n_1$ . It is satisfied in the theory of linear relaxation considered in this chapter. Magnons may be regarded as Bose particles (Sections 7.3, 7.4), and their  $\bar{n}_2, \bar{n}_3, \dots$  (as well as  $\bar{n}_1$ ) values can be obtained from (7.78). Then, the kinetic equation (11.6) will contain only one unknown  $\bar{n}_1$ . This equation, as it will be shown by some examples below, can be always represented in the form

$$\frac{dn_1}{dt} = -2\omega_{r1}(n_1 - \bar{n}_1) \quad (11.7)$$

where  $\omega_{r1}$  does not depend on  $n_1$ . The quantity  $\omega_{r1}$  is the frequency of relaxation of the number  $n_1$  to its equilibrium value  $\bar{n}_1$  due to elementary processes of the considered type. The reverse quantity  $\tau_{r1} = 1/(2\omega_{r1})$  is the relaxation time. As the numbers of magnons are proportional to the squared amplitudes of the ac magnetization components,  $\omega_{r1}$  is the relaxation frequency of these amplitudes. It represents a contribution of the considered processes to the phenomenological dissipation parameter  $\omega_r$  (Section 1.4).

Experiment yields directly only the entire parameter  $\omega_r$ . To draw conclusions concerning the contributions of different relaxation processes to this parameter

we have to compare the experimental  $\omega_r$  temperature or other dependences with theoretical predictions, or to perform experiments in such conditions that stimulate one or the other process.

## 11.2 Inherent spin-spin processes

The inherent spin-spin relaxation processes are caused by elementary processes in which three, four, or more magnons take part. The probabilities of such processes are, in general, greater the less the number of magnons taking part in one elementary process. However, the three-magnon processes cannot be caused by the strongest, exchange interaction. The reason for this is that in these processes the number of magnons, and consequently, according to (7.72), the  $M_z$  value are not conserved; whereas the exchange Hamiltonian commutes with  $\hat{M}_z$ , and therefore, the  $M_z$  value must be conserved in processes resulting from exchange interaction. The four-magnon scattering process, in which two magnons are annihilated and two are created, can be caused by the exchange interaction. Therefore, the probability of this process can be comparable with and, in some cases, as we shall see, even higher than the probability of the three-magnon process caused by the weaker, dipole-dipole interaction.

Three-magnon relaxation processes were first studied theoretically by Akhiezer [10] and then by Kaganov and Tsukernik [199], Akhiezer, Baryakhtar, and Peletminskii [15], Sparks, Loudon, and Kittel [378], Schlömann [344], and many others.

The factor  $\Psi_{1,23}$  in (11.3) and (11.4) caused by the dipole-dipole interaction in the long-wavelength approximation and without account for the third Holstein-Primakoff transformation (Section 7.4) has the following form [10]:

$$\Psi_{1,23} = -\pi \sqrt{\frac{M_0}{2V}} (\gamma \hbar)^{3/2} [\sin 2\theta_2 \exp(-i\varphi_2) + \sin 2\theta_3 \exp(-i\varphi_3)]. \quad (11.8)$$

Here,  $V$  is the volume of the sample (that will be canceled afterwards),  $\theta_{2,3}$  and  $\varphi_{2,3}$  are the angles of  $\mathbf{k}_2$  and  $\mathbf{k}_3$  vectors.

Two kinds of three-magnon relaxation processes are to be distinguished: splitting and confluence. They are based on the same elementary processes (Table 11.1). But for the splitting, the *elementary* splitting processes are the direct processes (leading to the decrease of the number of magnons of which the relaxation is examined) and the elementary confluence processes are the reverse processes. For the confluence, on the contrary, the elementary confluence processes are the direct processes and the elementary splitting processes are the reverse ones. This distinction, as we shall see, leads to essentially different ranges of existence of the processes and different contributions to the dissipation parameter.

**TABLE 11.1**  
Elementary processes in three-magnon relaxation processes.

Relaxation processes	Elementary processes <sup>a</sup>	
	direct	reverse
Splitting		
Confluence		

<sup>a</sup> Magnons of which the relaxation is considered are denoted by thick arrows.

### 11.2.1 Three-magnon splitting

According to (11.6) we can write for the splitting process:

$$\begin{aligned} \frac{dn_1}{dt} = & \frac{2\pi}{\hbar} \frac{1}{2} \sum_2 \sum_3 \left[ -|\langle n_1 - 1, n_2 + 1, n_3 + 1 | \mathcal{H}_{3d} | n_1, n_2, n_3 \rangle|^2 \right. \\ & \left. + |\langle n_1 + 1, n_2 - 1, n_3 - 1 | \mathcal{H}_{3d} | n_1, n_2, n_3 \rangle|^2 \right] \delta(\hbar\omega_1 - \hbar\omega_2 - \hbar\omega_3). \end{aligned} \quad (11.9)$$

The factor 1/2 is inserted before the sum because the same states  $|n_1, n_2, n_3\rangle$  and  $|n_1, n_3, n_2\rangle$  enter the sum twice. The matrix elements in (11.9) are obtained from (11.4) and (11.5) by substituting the sum  $\Psi_{1,23} + \Psi_{1,32}$  for  $\Psi_{1,23}$ . The reason for this is that both terms  $\hat{a}_1 \hat{a}_2^+ \hat{a}_3^+$  and  $\hat{a}_1 \hat{a}_3^+ \hat{a}_2^+$  (for the direct processes) or  $\hat{a}_3 \hat{a}_2 \hat{a}_1^+$  and  $\hat{a}_2 \hat{a}_3 \hat{a}_1^+$  (for the reverse processes) contribute to these matrix elements. And as  $\Psi_{1,23} = \Psi_{1,32}$ , the kinetic equation takes the form

$$\begin{aligned} \frac{dn_1}{dt} = & -\frac{4\pi}{\hbar} \sum_2 \sum_3 |\Psi_{1,23}|^2 [n_1(n_2 + n_3 + 1) - n_2 n_3] \\ & \times \Delta(\mathbf{k}_1 - \mathbf{k}_2 - \mathbf{k}_3) \delta(\hbar\omega_1 - \hbar\omega_2 - \hbar\omega_3). \end{aligned} \quad (11.10)$$

Assuming now that the numbers  $n_2$  and  $n_3$  are equal to their *equilibrium* values and taking into account that  $dn_1/dt = 0$  if  $n_1 = \bar{n}_1$ , we make sure that (11.10) may be written in the form (11.7) and obtain

$$\omega_{r1} = \frac{2\pi}{\hbar} \sum_2 \sum_3 |\Psi_{1,23}|^2 (\bar{n}_2 + \bar{n}_3 + 1) \Delta(\mathbf{k}_1 - \mathbf{k}_2 - \mathbf{k}_3) \delta(\hbar\omega_1 - \hbar\omega_2 - \hbar\omega_3). \quad (11.11)$$

The existence of  $\Delta(\mathbf{k}_1 - \mathbf{k}_2 - \mathbf{k}_3)$  in (11.11) implies that the summation should be carried out over the values of one of the vectors  $\mathbf{k}_2$  and  $\mathbf{k}_3$ , and the relation  $\mathbf{k}_3 = \mathbf{k}_1 - \mathbf{k}_2$  must be taken into account in writing  $\Psi_{1,23}$  and the delta function.

Passing then, as in the calculation of  $M(T)$  in Section 7.3, to the integration

over the  $k_2$  space, we get

$$(\omega_{r1})_{3s} = \frac{V}{(2\pi)^2 \hbar^3} \int_{k_2} \int_{\theta_2=0}^{\pi} \int_{\varphi_2=0}^{2\pi} |\Psi_{1,23}|^2 (\bar{n}_2 + \bar{n}_3 + 1) \\ \times \delta(\hbar\omega_1 - \hbar\omega_2 - \hbar\omega_3) k_2^2 \sin \theta_2 dk_2 d\theta_2 d\varphi_2 \quad (11.12)$$

where  $\theta_2$  and  $\varphi_2$  are the angles of the vector  $k_2$ , and the limits of integration over  $k_2$  are determined by the energy and momentum conservation laws.

The existence of the delta function in (11.12) results in the integration over a surface in  $k_2$  space. Usually it is reasonable to pass from the delta function of the energy difference to the delta function of a coordinate in  $k_2$  space, e.g., to  $\theta_2$ . Then the integration over this coordinate can be eliminated using the properties of the delta function (Appendix C).

The calculations with formula (11.12) demand, in general, the use of computers. Analytical expressions can be derived in *high-temperature* approximation

$$\kappa T \gg \hbar\omega_1, \hbar\omega_2, \hbar\omega_3, \dots \quad (11.13)$$

Then,  $\bar{n}_{2,3} \simeq \kappa T / (\hbar\omega_{2,3})$ , and formula (11.12), with regard to (11.8), takes the form

$$(\Delta H_k)_{3s} \equiv \frac{2\omega_{r1}}{\gamma} \\ = \frac{1}{4} \gamma^2 \kappa T \omega_1 M_0 \int_{k_2} \int_{\theta_2=0}^{\pi} \int_{\varphi_2=0}^{2\pi} \frac{|\sin 2\theta_2 \exp(-i\varphi_2) + \sin 2\theta_3 \exp(-i\varphi_3)|^2}{\omega_2(\omega_1 - \omega_2)} \\ \times \delta(\omega_1 - \omega_2 - \omega_3) k_2^2 \sin \theta_2 dk_2 d\theta_2 d\varphi_2. \quad (11.14)$$

The given frequency  $\omega_1$  is the largest for the splitting process. Thus, the condition (11.13) reduces to  $\kappa T \gg \hbar\omega_1$ , which holds in the microwave range even at the liquid-helium temperature.

Sometimes the *high-frequency* approximation

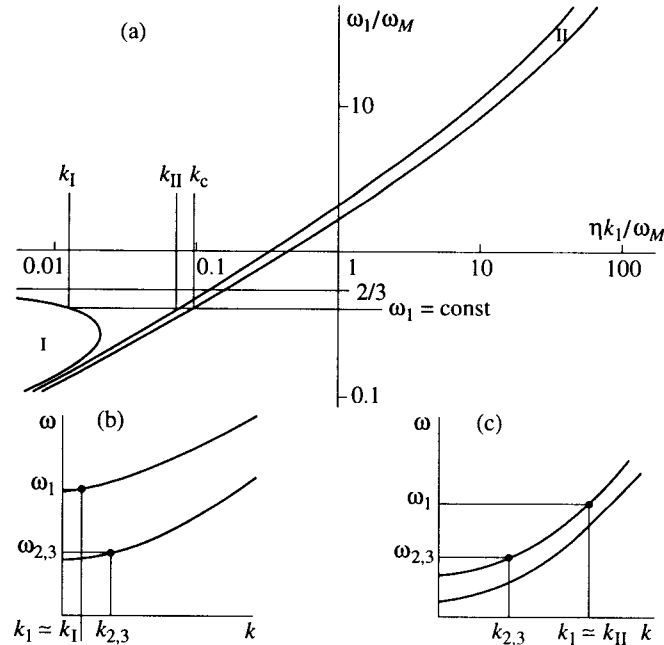
$$\omega_1, \omega_2, \omega_3, \dots \gg \gamma 4\pi M_0 \equiv \omega_M \quad (11.15)$$

can be used. Then, we can employ the approximate spin-wave dispersion expression (7.14) and, as in deriving (11.14), ignore the third Holstein-Primakoff transformation.

For the splitting of the uniform mode ( $k_1 = 0, \omega_1 = \omega_0$ ) it follows from the conservation laws that  $k_3 = -k_2$  and  $\omega_3 = \omega_2 = \omega_0/2$ . The latter relation holds only if  $\omega_0/2$  lies over the lower boundary of the spin-wave spectrum. The condition for this, in the case of a spheroid, is

$$\omega_0 < 2\gamma N_{\perp} M_0 \quad (11.16)$$

where  $N_{\perp}$  is the demagnetization factor in the direction normal to the axis of revolution. For a sphere, it follows from (11.16) that  $\omega_0 < 2\omega_M/3$ . This

**FIGURE 11.2**

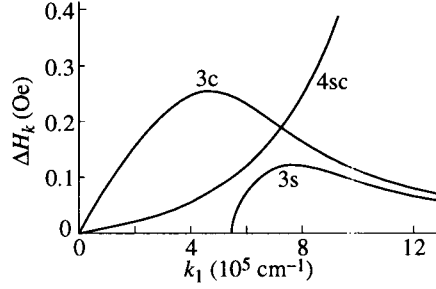
Three-magnon splitting of  $\pi/2$  magnons. (a) Regions in which the process is allowed. (b), (c) Frequencies and wave numbers of magnons in regions I and II, respectively (near their boundaries  $k_I$  and  $k_{II}$ ) [239, 157].

relation coincides with the condition (6.10) for the passage of  $\omega_0$  through the upper boundary of the non-exchange spin-wave spectrum.

A rather simple analytical expression for the contribution of three-magnon splitting to the dissipation parameter of the uniform mode can be found only in the high-frequency approximation (11.15), which contradicts condition (11.16). Therefore, this expression can be used only for a very rough estimate, which gives  $(\Delta H)_{3s} \sim 0.03$  Oe for YIG at 2.5 GHz.

The main method used in experimental investigation of spin-wave relaxation in ferrites is the measurement of the thresholds of parametric excitation of spin waves, especially under the longitudinal (parallel) pumping (Section 10.3). In this case, in certain limits of the constant magnetic field  $H_0$ , the magnons with  $\theta_k = \pi/2$  and  $k$  depending on  $H_0$  are excited. Let us consider the contribution of the three-magnon splitting to the relaxation of such magnons.

It was shown by Lamaire, Le Gall, and Dormann [239] that there are two regions of  $\omega_1$  and  $k_1$  in which the three-magnon splitting of magnons with  $\theta_k = \pi/2$  is allowed by the conservation laws (Figure 11.2). In the first region,  $\omega_1 < \omega_{10} \equiv 2\omega_M/3$  and  $k_1$  does not exceed  $k_1(\omega_1)$  [Figure 11.2(a)]. Magnons with small  $\theta_{2,3}$  are created in this region [Figure 11.2(b)]. The second region exists at all

**FIGURE 11.3**

Contributions of inherent spin-spin relaxation processes to the dissipation parameter of  $\pi/2$  magnons in YIG at room temperature [378].  $H_0 = 1.5$  kOe, frequency changes as  $k$  is varied, according to the magnon dispersion law.

frequencies but in very narrow ranges of  $k_1$ : from  $k_{II}$  to the limiting value  $k_c$ , which is determined (in an isotropic case) by the condition  $H_0 = 0$ , i.e., actually, by the rise of domains. Magnons with  $\theta_{2,3}$  equal to or near  $\pi/2$  are created in this region. Taking into account that  $\omega_2 = \omega_3$  always at the boundary of the region and assuming  $\theta_2 = \theta_3 = \pi/2$ , we get

$$\eta k_{II}^2 = \frac{2}{3} (\sqrt{4\omega_1^2 + \omega_M^2} - \sqrt{\omega_1^2 + \omega_M^2}). \quad (11.17)$$

For YIG at room temperature and  $f_1 \equiv \omega_1/2\pi = 4.5$  GHz (i.e., the pumping frequency  $f_p = 9$  GHz),  $k_{II} = 4.06 \times 10^5$  and  $k_c = 4.28 \times 10^5$ .

The contribution of three-magnon splitting to  $\Delta H_k$  of the  $\pi/2$  magnons calculated [378] in high-temperature and high-frequency approximations at fixed  $H_0$  and varying frequency is shown in Figure 11.3. However, in parallel-pumping experiments usually  $\omega_1 = \text{const}$  and  $H_0$  is varied. Then, as one can see from Figure 11.2, the splitting process also begins at some  $k_1$  value but, contrary to Figure 11.3, exists only in very narrow  $k_1$  and, hence,  $H_0$  ranges.

### 11.2.2 Three-magnon confluence

The kinetic equation (11.1) for the three-magnon confluence process takes the form

$$\begin{aligned} \frac{dn_1}{dt} = & \frac{2\pi}{\hbar} \sum_2 \sum_3 \left[ -|\langle n_1 - 1, n_2 - 1, n_3 + 1 | \mathcal{H}_{3d} | n_1, n_2, n_3 \rangle|^2 \right. \\ & \left. + |\langle n_1 + 1, n_2 + 1, n_3 - 1 | \mathcal{H}_{3d} | n_1, n_2, n_3 \rangle|^2 \right] \\ & \times \delta(\hbar\omega_1 + \hbar\omega_2 - \hbar\omega_3). \end{aligned} \quad (11.18)$$

The factor 1/2 before the sum is absent here because the states  $|n_1, n_2, n_3\rangle$  and  $|n_1, n_3, n_2\rangle$  are not equivalent. Writing the matrix elements in (11.18) analogously to (11.4) and (11.5), replacing  $n_2$  and  $n_3$  by their equilibrium values, and passing, as in the case of splitting, to the integration in the  $k_2$ -space, we obtain

$$(\omega_{r1})_{3c} = \frac{V}{2\pi^2\hbar^2} \int_{k_2} \int_{\theta_2=0}^{\pi} \int_{\varphi_2=0}^{2\pi} |\Psi_{3,12}|^2 (\bar{n}_2 - \bar{n}_3) \times \delta(\omega_1 + \omega_2 - \omega_3) k_2^2 \sin\theta_2 dk_2 d\theta_2 d\varphi_2. \quad (11.19)$$

Here, the limits of integration over  $k_2$  are determined by the conservation laws, and  $\Psi_{3,12}$  has the form analogous to (11.8).

The energy and momentum conservation laws can be satisfied for the confluence process only if  $k_1$  is larger than a certain quantity  $k_{1 \text{ min}}$ . For small  $k_1$  the values of  $k_2$  and  $k_3$  must be very large, but they are limited by the dimensions of the first Brillouin zone (Section 7.4). Such reasoning leads to the relation

$$k_{1 \text{ min}} = \xi \frac{\omega_1 a}{2\eta} \quad (11.20)$$

where  $a$  is a lattice constant,  $\eta$  is the nonuniform exchange constant (Section 7.1), and  $\xi$  is a coefficient of the order of unity, which depends on crystal structure and  $k_1$  direction. Regarding YIG as a ferromagnet with the lattice constant equal to the mean distance between  $\text{Fe}^{3+}$  ions, we get with (11.20) at  $f_1 = 4.5$  GHz that  $k_{1 \text{ min}} \sim 10^4$ . In other crystals and at higher frequencies the  $k_{1 \text{ min}}$  values can be much larger [157].

The high-temperature approximation is poorly applicable to the confluence process because  $\omega_2$  can be, and  $\omega_3$  is always, larger than  $\omega_1$ . Nevertheless, the contribution of this process to the dissipation parameter of  $\pi/2$  magnons was calculated in such an approximation [378]. With some assumption valid for YIG it was obtained at small (but, of course, larger than  $k_{1 \text{ min}}$ )  $k_1$  values:

$$(\Delta H_k)_{3c} = \frac{2(\omega_{r1})_{3c}}{\gamma} = \frac{\pi\gamma M_0 \kappa T k_1}{2D\omega_1} \quad (11.21)$$

where  $D = \eta/\gamma$ . An estimate using this formula gives  $(\Delta H_k)_{3c} = 0.2$  Oe for YIG at room temperature,  $f_1 = 4.5$  GHz, and  $k_1 = 10^5$ . The  $k_1$  dependence of  $(\Delta H_k)_{3c}$  at  $\omega_1 = \text{const}$  is shown in Figure 11.3.

The linear temperature dependence in (11.21) is characteristic of all three-magnon processes in high-temperature approximation. In another limiting case, at low temperatures the temperature dependence of  $(\omega_{r1})_{3c}$  is exponential, whereas  $(\omega_{r1})_{3c}$  does not depend on temperature in this case. The difference is easily understood: for the confluence process, as distinct from the splitting, thermal magnons ( $\omega_2, k_2$ ) are needed.

All three-magnon processes result in the change of the entire magnon number, and therefore, according to (7.72), can take part in the relaxation of  $M_z$ . According to (7.75), the length of the vector  $\mathbf{M}$  is also changed by three-magnon processes.

Hence, the use of the equations of motion (1.66) and (1.67) with dissipative terms that conserve  $|M|$  is, strictly speaking, not allowed when three-magnon processes are present. But in the case of small amplitudes and small dissipation all forms of the dissipative term are approximately equivalent (Section 1.4). Therefore, equations (1.66) and (1.67) are commonly used even in the presence of three-magnon processes.

### 11.2.3 Four-magnon scattering

The kinetic equation (11.6) for the four-magnon scattering takes the form

$$\begin{aligned} \frac{dn_1}{dt} = & \frac{2\pi}{\hbar} \frac{1}{2} \sum_2 \sum_3 \sum_4 |\Psi_{12,34} + \Psi_{12,43} + \Psi_{21,34} + \Psi_{21,43}|^2 \\ & \times [(n_1 + 1)(n_2 + 1)n_3n_4 - n_1n_2(n_3 + 1)(n_4 + 1)] \\ & \times \delta(\hbar\omega_1 + \hbar\omega_2 - \hbar\omega_3 - \hbar\omega_4). \end{aligned} \quad (11.22)$$

The factor  $1/2$  before the sum is inserted because the identical states  $|n_1, n_2, n_3, n_4\rangle$  and  $|n_1, n_2, n_4, n_3\rangle$  enter twice in summation. Replacing  $n_2, n_3,$  and  $n_4$  by their equilibrium values, we make sure that in this case the kinetic equation also acquires the form (11.7), and

$$\begin{aligned} (\omega_{r1})_{4sc} = & \frac{\pi}{2\hbar^2} \sum_2 \sum_3 \sum_4 |\Psi|^2 [\bar{n}_2(\bar{n}_3 + \bar{n}_4 + 1) - \bar{n}_3\bar{n}_4] \\ & \times \Delta(\mathbf{k}_1 + \mathbf{k}_2 - \mathbf{k}_3 - \mathbf{k}_4) \delta(\omega_1 + \omega_2 - \omega_3 - \omega_4) \end{aligned} \quad (11.23)$$

where  $\Psi = \Psi_{12,34} + \Psi_{12,43} + \Psi_{21,34} + \Psi_{21,43}$ .

The existence of the delta symbol in (11.23) allows one to exclude the summation over one of the wave vectors, e.g., over  $\mathbf{k}_4$ . Passing then to the integration over  $\mathbf{k}_2$  and  $\mathbf{k}_3$  spaces, we obtain

$$(\omega_{r1})_{4sc} = \frac{V^2 \hbar^2}{2^7 \pi^5} \int_{\mathbf{k}_2} \int_{\mathbf{k}_3} [n_2(n_3 + n_4 + 1) - n_3n_4] |\Psi|^2 \delta(\omega_1 + \omega_2 - \omega_3 - \omega_4) d\mathbf{k}_2 d\mathbf{k}_3. \quad (11.24)$$

In the high-temperature approximation (11.13) the 'statistical' factor in (11.24) takes the form

$$n_2(n_3 + n_4 + 1) - n_3n_4 = \frac{(\kappa T)^2 \omega_1}{\hbar^2 \omega_2 \omega_3 \omega_4} \quad (11.25)$$

and the dissipation parameter turns out to be proportional to  $T^2$ . But, as in the case of three-magnon confluence, the condition  $\hbar\omega_1 \ll \kappa T$  is not sufficient for this approximation to be valid.

For long-wavelength magnons, according to [199] (see also [214]),

$$|\Psi|^2 = \frac{2D(\gamma\hbar)^2}{M_0 V} k_1 k_2 \cos \varphi_{12} \quad (11.26)$$



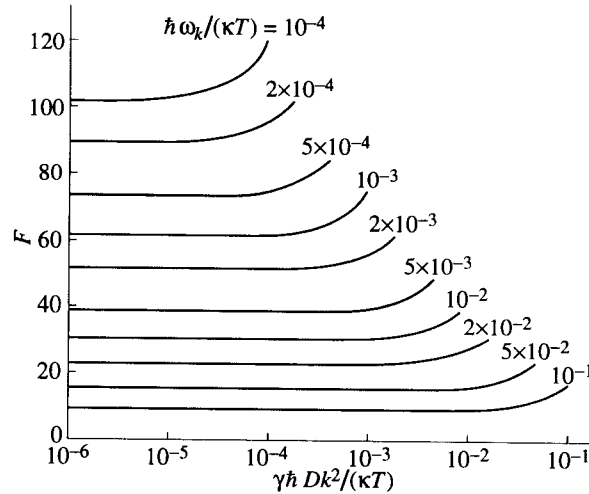


FIGURE 11.4

Factor  $F$  in (11.28), calculated in [20] according to [436].

where  $\varphi_{12}$  is the angle between  $k_2$  and  $k_1$ . After substituting (11.26) into (11.24) the factor  $k_1^2$  can be taken out of the integral. The  $k$  dependence of  $(\omega_{r1})_{4sc}$  is determined not only by the factor  $k^2$ . However, it leads to a fast increase of  $(\omega_{r1})_{4sc}$  with growing  $k_1$ .

The contribution of the four-magnon exchange scattering to the spin-wave relaxation was first calculated by Dyson [104]. Without regard for the dipole-dipole interaction and external magnetic field  $H_0$  Dyson obtained that at very low temperatures ( $\kappa T \ll \hbar \omega_1$ ) this contribution is proportional to  $k_1^3 T^{5/2}$ . For higher temperatures ( $\hbar \omega_1 < \kappa T < \kappa T_C$  where  $T_C$  is the Curie temperature) Kashtsheev and Krivoglaz [210] found, also without account for  $H_0$  and dipole-dipole interaction, that

$$(\omega_{r1})_{4sc} = A \omega_1 k_1^2 T^2 \ln^2 \frac{2\hbar \omega_1}{\xi \kappa T} \quad (11.27)$$

where  $A$  is a constant and  $\xi$  is a factor of the order of unity. Vaks, Larkin, and Pikin [415] and Wang [436], taking into account the external field  $H_0$ , obtained for the same temperature range an expression that can be written in the form

$$(\Delta H_k)_{4sc} = \frac{1}{48\pi} \frac{\omega_1}{\gamma^2} \left( \frac{k_1 \kappa T}{M_0 D} \right)^2 F \quad (11.28)$$

where  $F$  depends on  $\omega_1$ ,  $k_1$ , and  $T$ . This dependence is shown in Figure 11.4.

The considered four-magnon process plays an important role in the relaxation of secondary magnons (with  $k_2$  and  $k_3$  for three-magnon splitting,  $k_3$  for three-

magnon confluence,  $k_3$  and  $k_4$  for four-magnon scattering), as well as for magnons of next 'generations'. We shall see below that the contribution of four-magnon scattering can also be essential on the first stage of relaxation.

#### 11.2.4 Inherent processes for uniform precession

Of all the above-considered relaxation processes, only the three-magnon splitting at sufficiently low frequencies ( $\omega < 2\omega_M/3$  for  $\pi/2$  magnons) makes a contribution to the dissipation parameter not vanishing with  $k_1 \rightarrow 0$ . At the same time, it follows from numerous experimental data that the uniform-resonance linewidth  $\Delta H_0$  and the spin-wave dissipation parameter extrapolated to  $k_1 \rightarrow 0$  ( $\Delta H_k \rightarrow 0$ ) cannot be caused only by defects (Section 11.3). There should exist some inherent relaxation processes whose contributions to  $\Delta H_0$  and  $\Delta H_k \rightarrow 0$ , at all frequencies, are finite. The first attempt to solve this problem was made by Kasuya and Le Craw [212]. They pointed out that energy and momentum conservation laws can be satisfied by the three-magnon confluence process even for  $k_1 = 0$ , but under the condition that magnons with  $k_2$  and  $k_3$  belong to the higher (exchange) spin-wave branches of a ferrimagnet (Section 3.3). Kolokolov, L'vov, and Cherepanov [231] showed that such a process can yield a material part of observed  $\Delta H_0$  and  $\Delta H_k \rightarrow 0$  values in the ferrimagnet YIG.

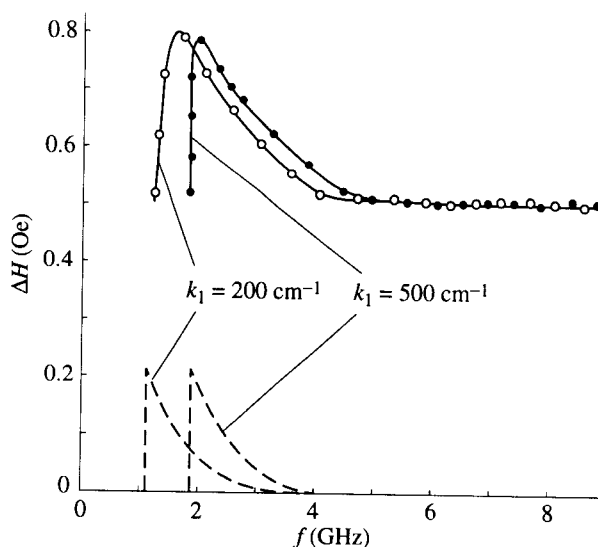
It should be noted that another three-particle confluence process exists, which gives the contribution to magnon relaxation not vanishing with  $k_1 \rightarrow 0$ . This is the confluence of a magnon with a phonon of the upper (optical) branch. It belongs to the spin-lattice relaxation processes and will be discussed in Section 12.5.

Four-magnon confluence and splitting processes caused by the dipole-dipole interaction can also take part in relaxation of magnons with  $k = 0$  [14]. However, their contributions are usually much less than the contributions of all above-mentioned processes.

#### 11.2.5 Experimental data

In most experimental investigations aimed at the study of inherent relaxation processes in magnetically ordered substances YIG single crystals were used. The comparison of the results of these experiments with theory is complicated by the fact that YIG is a ferrimagnet, whereas the majority of theories, in particular, all mentioned above except [212, 231], use the ferromagnetic model.

Let us discuss first the uniform-resonance linewidth  $\Delta H_0$ . Its minimal values for YIG are 0.2–0.3 Oe. The contribution of inherent processes to these values is hardly larger than  $\sim 0.1$  Oe. It should increase when, with decreasing frequency, the splitting process is 'turned on'. But in experiments on uniform resonance such an increase has not been observed because in spheres, used in such experiments, the 'turning on' of splitting is masked by the partial 'turning out' of the two-magnon relaxation processes (Section 11.3) at the same point  $\omega_0 = 2\omega_M/3$ . If such coincidence does not take place, the contribution of three-magnon splitting



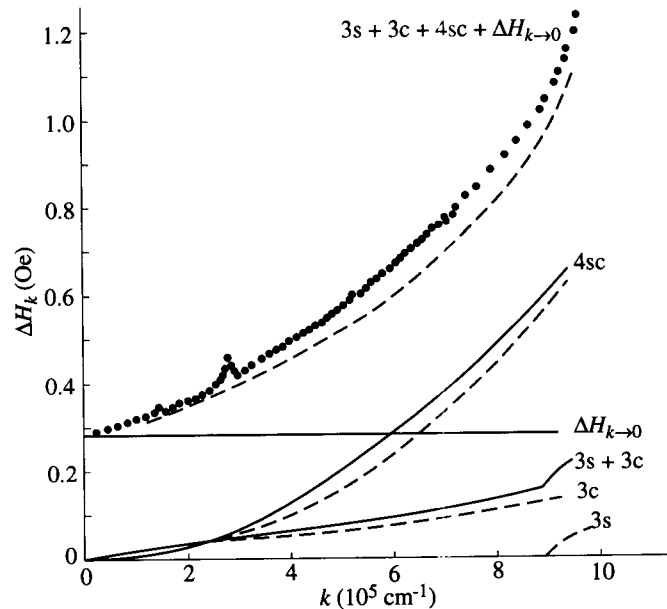
**FIGURE 11.5**

Frequency dependences of the dissipation parameter for surface magnetostatic wave (Section 6.2) in a tangentially magnetized YIG film [168]. Points represent experimental data; dashed lines denote calculated three-magnon-splitting contributions;  $k_1$  is the wave number of the magnetostatic wave.

can be observed. An example is given in Figure 11.5, where the frequency dependences of the surface-magnetostatic-wave dissipation parameter are plotted. The low-frequency maxima in these dependences results from the three-magnon splitting [168]. Contributions of this process were also observed in the frequency dependences of  $\Delta H_k \rightarrow 0$ , found from the measurements of threshold fields for spin-wave parametric excitation under parallel pumping (e.g., [376]).

For spin waves with  $k > 0$  excited parametrically, all the above-considered processes, 3s, 3c, and 4sc should give observable contributions. To compare them with the predictions of theory it is necessary, first of all, to separate the contributions of different processes to the entire linewidth  $\Delta H_k$  obtained experimentally. This has been performed in [20], for an YIG single crystal, with the assumption that the contribution of processes which work at  $k \rightarrow 0$ , does not depend on  $k$  and, therefore,  $\Delta H_k - \Delta H_{k \rightarrow 0}$  is the entire contribution of 3s-, 3c-, and 4sc-processes. The contributions of three- and four-magnon processes were separated using their different theoretical temperature dependences. The result of such separation is shown in Figure 11.6, together with the theoretical results. The contribution of 4sc-process was calculated with formula (11.28). The 3s- and 3c-contributions were found according to [378]. It should be emphasized that the temperature-dependent experimental values of  $M_0$  and  $D$  were used in all these calculations.

One can see from Figure 11.6 that for YIG the contribution of four-magnon

**FIGURE 11.6**

Contributions of different relaxation processes to the dissipation parameter of spin waves with  $\theta_k = \pi/2$  in a YIG sphere [20]. Pumping frequency 35.5 GHz, room temperature. Points represent experimental data obtained by parallel pumping method (Section 10.3). Solid lines denote the results of separation of different contributions, their calculated values are denoted by dashed lines.

exchange scattering dominates at sufficiently high temperatures and large  $k$  values. The contribution of three-magnon processes increases sharply at  $k$  value that is in a good agreement with the theoretical value (11.17) for the onset of the three-magnon dipole splitting in the second region of its existence (Figure 11.2), the first region being absent in this case. It follows from Figure 11.6 that there is a rather good agreement between the experimental contributions of three- and four-magnon processes and theoretical results obtained without any fitting of coefficients. It testifies that the assumptions made in deriving the formulae which were used in the calculations hold for YIG in the conditions of this experiment.

The situation becomes different for some other crystals with small  $\Delta H_k$ , in particular,  $\text{CdCr}_2\text{Se}_4$  and  $\text{EuO}$ . They are ferromagnets, and the above-considered theory of relaxation processes, based on the Heisenberg model of a ferromagnet, should be applicable better to these crystals than to the ferrimagnet YIG. However, their parameters (Table 11.2) differ greatly from the YIG parameters, and the assumptions good for YIG are poorly applicable to these ferromagnets. Therefore, the formulae, e.g., (11.28), which give good agreement with experiment in the

TABLE 11.2

Parameters of some ferro- and ferrimagnets with small  $\Delta H_k$ .

Substance	$4\pi M_0$ (at 4.2 K) (G)	$T_c$ (K)	$D$ (Oe cm <sup>2</sup> )	$\Delta H_{k \rightarrow 0}$ (Oe)
Y <sub>3</sub> Fe <sub>5</sub> O <sub>12</sub>	2470	560	$5.17 \times 10^{-9}$	0.2 (at 36 GHz)
CdCr <sub>2</sub> Se <sub>4</sub>	4450	130	$3.3 \times 10^{-10}$	0.6 (at 9 GHz)
EuO	24000	69.5	$1.0 \times 10^{-10}$	0.75 (at 36 GHz)

case of YIG, can be used now only for qualitative estimates. It follows from such estimates that the contributions of three-magnon dipole processes will be much larger for these crystals than for YIG ( $10^4$  times in the case of EuO) and can be observed even at liquid-helium temperature [21, 157]. The contribution of four-magnon process will increase to a smaller extent (25 times for EuO) and will be negligible, at low temperatures, in comparison with the contribution of three-magnon processes. The numerical calculations [157] carried out for EuO with the use of formulae (11.14) and (11.19) confirmed the above-stated considerations.

### 11.3 Two-magnon processes

It became clear in the late 1950s that large values and 'anomalous' (with low-temperature maxima) temperature dependences of the linewidth in many magnetic materials are caused by two noninherent relaxation processes (Figure 11.1): (i) spin-spin relaxation due to nonuniformities, (ii) indirect spin-lattice (and in some cases also spin-spin) relaxation via ions with strong spin-orbital coupling or via charge carriers.

The first of these relaxation channels is considered in this section.<sup>5</sup>

The following nonuniformities are the most important.

1. Heterogeneity of composition (chemical nonuniformities), in particular, disorder in distribution of ions over the lattice sites.
2. Variation of the directions of crystal axes in polycrystals or non-perfect single crystals.
3. Nonuniform stresses, in particular, caused by dislocations.
4. 'Geometrical' nonuniformities: pores, surface roughness.

The effect of nonuniformities on magnetic resonance can be described, in principle, in the independent-region approximation (used already in Section 2.4). In this approximation, the broadening and shift of resonance curves in a nonuniform

<sup>5</sup>The second will be studied in Chapter 13.

medium is not a result of some new relaxation mechanism but is simply due to the difference of resonance conditions in different regions of the sample (the oscillations in these regions are assumed to be independent). This approximation is usually appropriate for paramagnetic and antiferromagnetic (Section 3.2) resonances. But it is not applicable, as a rule, to ferromagnetic resonance. The dipole-dipole interaction (for large nonuniformities) or exchange interaction (if the nonuniformities are sufficiently small) leads to such strong coupling of the oscillations at different points that they cannot be regarded as independent even in the zero approximation. It should be spoken of different types of oscillations (eigenmodes) of the entire nonuniform sample. These modes form, practically, continuous groups near every mode of a uniform sample. The ac field excites the entire group, and so, the resonance curve is broadened and shifted. As in the independent-region approximation, this broadening is not a result of a new relaxation mechanism. However, as distinct from that approximation, now the broadening is due to the difference in resonance conditions of different *modes of the entire sample*.

The resonance in nonuniform samples was treated above in terms of normal modes. But the problem can also be attacked in terms of coupled modes. As such modes, the eigenmodes of a uniform sample are to be used. They are independent, uncoupled in the absence of nonuniformities, but become coupled if the nonuniformities are present. The coupling leads to the energy transfer from the initial mode (excited by the external field) to the modes coupled with it. In such treatment the nonuniformities give rise to a new relaxation mechanism. Thus, the distinction between dissipative and nondissipative resonance-line broadening is relative in the case of such strongly coupled systems as ferromagnets.

In the classical theory, the coupled-mode approach reduces to solving the coupled classical equations of motion (Section 11.1). In the quantum theory, the equations of motion must be quantum-mechanical (e.g., [336]), and the quantum-mechanical method of transition probabilities can be also used. It has already been mentioned that the probabilities are higher the smaller the number of quasiparticles that take part in the process. The two-magnon processes are forbidden in an ideal crystal by the momentum-conservation law. In a crystal with nonuniformities they are allowed and their probabilities can be large. Such processes can be referred to as the scattering of magnons by nonuniformities. When the initial mode is the uniform precession, these processes are usually called  $0-k$  processes.

### 11.3.1 Theory of two-magnon processes

Consider the relaxation of magnons with wave vector  $k_1$  caused by nonuniformities. Using the transition-probability method, assume that the perturbation energy can be regarded as the Zeeman energy of spins  $S_f$  in an effective field  $\mathbf{H}_{\text{ef}}(\mathbf{r}_f)$ . Suppose, for simplicity, that this field is directed along the  $z$ -axis, which coincides with the direction of constant magnetization  $M_0$ . Then the perturbation

Hamiltonian can be written, according to (7.86), as

$$\mathcal{H}_p = \gamma \hbar \sum_{f=1}^N \hat{S}_f^z H_{\text{ef}}(\mathbf{r}_f) \quad (11.29)$$

where  $N$  is the number of spins in the sample. Let us pass now, according to (7.91), to the operators  $\hat{a}_f^+$  and  $\hat{a}_f$  and then, using (7.105), to the operators  $\hat{a}_k^+$  and  $\hat{a}_k$ . Expand, at the same time, the field  $H_{\text{ef}}(\mathbf{r}_f)$  in the Fourier harmonics. Then, the bilinear part of the Hamiltonian (11.29) takes the form

$$\begin{aligned} \hat{\mathcal{H}}_{p2} &= \gamma \hbar \sum_{f=1}^N \frac{1}{\sqrt{N}} \sum_{\mathbf{k}_1} \exp(i\mathbf{k}_1 \mathbf{r}_f) \hat{a}_1 \frac{1}{\sqrt{N}} \sum_{\mathbf{k}_2} \exp(-i\mathbf{k}_2 \mathbf{r}_f) \hat{a}_2^+ \\ &\quad \times \frac{1}{\sqrt{N}} \sum_{\mathbf{k}_p} \exp(i\mathbf{k}_p \mathbf{r}_f) H_{\mathbf{k}} \end{aligned} \quad (11.30)$$

where

$$H_{\mathbf{k}} = \frac{1}{\sqrt{N}} \sum_{f=1}^N H_p(\mathbf{r}_f) \exp(-i\mathbf{k}_p \mathbf{r}_f) \quad (11.31)$$

is the amplitude of the  $k_p$ th harmonic of the field  $\mathbf{H}_{\text{ef}}$  and the sums in (11.30), except the first one, are over all allowed wave vectors in the first Brillouin zone.

As the perturbation is already taken into account by the effective field  $\mathbf{H}_{\text{ef}}$ , we can now regard the crystal as ideal, for which the expressions (7.103) hold. Then, the Hamiltonian (11.30) takes the form

$$\hat{\mathcal{H}}_{p2} = \frac{\gamma \hbar}{\sqrt{N}} \sum_{\mathbf{k}_1} \sum_{\mathbf{k}_2} \sum_{\mathbf{k}_p} H_{\mathbf{k}} \hat{a}_2^+ \hat{a}_1 \Delta(\mathbf{k}_2 - \mathbf{k}_1 + \mathbf{k}_p). \quad (11.32)$$

The matrix elements of  $\hat{\mathcal{H}}_{p2}$  that appear in the kinetic equation (11.6) for direct transitions should be written as [84]

$$\langle n_1 - 1, n_2 + 1 | \mathcal{H}_{p2} | n_1, n_2 \rangle = \sqrt{n_1(n_2 + 1)} \Psi_{1,2} \quad (11.33)$$

where

$$\Psi_{1,2} = \frac{\gamma \hbar}{\sqrt{N}} \sum_{\mathbf{k}_p} H_{\mathbf{k}} \Delta(\mathbf{k}_2 - \mathbf{k}_1 + \mathbf{k}_p) \equiv \frac{\gamma \hbar}{\sqrt{N}} H_{(\mathbf{k}_1 - \mathbf{k}_2)}. \quad (11.34)$$

For reverse transitions, the displacement  $1 \leftrightarrow 2$  must be made.

The kinetic equation now has the form

$$\frac{dn_1}{dt} = \frac{2\pi}{\hbar} \sum_{\mathbf{k}_2} |\Psi_{1,2}|^2 (n_2 - n_1) \delta(\hbar\omega_1 - \hbar\omega_2). \quad (11.35)$$

We assume, as usual,  $n_2 = \bar{n}_2$  and take into account that  $\bar{n}_1 = \bar{n}_2$  because magnons with  $\mathbf{k}_1$  and  $\mathbf{k}_2$  are degenerate. Then, according to (11.7), the relaxation

frequency is

$$\omega_{r1} = \frac{\pi}{\hbar^2} \sum_{k_2} |\Psi_{1,2}|^2 \delta(\omega_1 - \omega_2). \quad (11.36)$$

It is seen from (11.35) that the energy is conserved in each elementary two-magnon process. But the momentum conservation does not take place, the momentum  $\hbar(k_2 - k_1)$  is transferred to the crystal as a whole.

Passing, as in (11.2), from the summation over  $k_2$  values to integration over  $k_2$  space and taking into account (11.34), we obtain

$$\Delta H_k \equiv \frac{2\omega_{r1}}{\gamma} = \frac{\gamma}{(2\pi)^2} \frac{V}{N} \int_{k_2} H_{(k_1-k_2)} \delta(\omega_1 - \omega_2) k_2^2 \sin \theta_2 dk_2 d\theta_2 d\varphi_2. \quad (11.37)$$

Consider first the case in which the harmonics  $H_k$  of the effective field do not depend on  $k$ , i.e., the nonuniformities are chaotic. Then it can be shown, using (7.103), that

$$H_k^2 = \frac{1}{N} \sum_{f=1}^N H_{ef}(\mathbf{r}_f) \equiv H_p^2. \quad (11.38)$$

$H_p$  is the root-mean-square effective field of nonuniformities. Assuming the spin-wave spectrum to be independent of  $\varphi$  and getting rid of the integration over  $k_2$ , we obtain (omitting the subscript at  $\theta_2$ )

$$\Delta H_k = \frac{\gamma}{\pi} a^3 H_p^2 \int_0^{\theta_{\max}} \left( \frac{\partial \omega_k}{\partial k} \right)_{k=k_d(\theta)} k_d^2 \sin \theta d\theta. \quad (11.39)$$

Here,  $a = \sqrt[3]{V/N}$  is the mean distance between neighboring spins,  $k_d(\theta)$  is found from the condition of degeneration  $\omega_k(k_d, \theta) = \omega_1$ , and  $\theta_{\max}$  is either equal to  $\pi/2$  or is determined by the condition  $\omega_k(k = 0, \theta_{\max}) = \omega_1$  [Figure 11.7(a),(b)].

Consider, e.g., the relaxation of the uniform mode in an ellipsoid of revolution ( $k_1 = 0, \omega_1 = \omega_H + N_{\perp} \gamma M_0$ ) and take, for simplicity, the approximate spin-wave dispersion relation (7.14). Then the calculation with (11.39) leads to

$$\Delta H_0 = (2\pi)^{-1/2} I_1 a^3 M_0^{1/2} D^{-3/2} H_p^2 \equiv H_p \xi_{\text{ex}} \quad (11.40)$$

where  $I_1$  is a factor of the order 1, depending on  $N_{\perp}$ ; for a sphere  $I_1 = 0.217$ . The obtained linewidth can be regarded as a result of broadening the resonance line (on the order of  $H_p$ ) by the nonuniformities and 'further' narrowing it by the exchange interaction. The coefficient of exchange narrowing  $\xi_{\text{ex}}$  in (11.40) is, on the order of magnitude,

$$\xi_{\text{ex}} \sim \frac{H_p}{H_{\Lambda}} \sqrt{\frac{4\pi M_0}{H_{\Lambda}}} \quad (11.41)$$

where  $H_{\Lambda}$  is the 'molecular' field related to  $D$  and  $a$  by (7.119). For YIG,  $\xi_{\text{ex}}$  is of the order of  $10^{-4}$ . Thus, very high effective fields, of the order of  $10^5$  Oe, are needed to get an appreciable contribution ( $\sim 1$  Oe) to the linewidth.



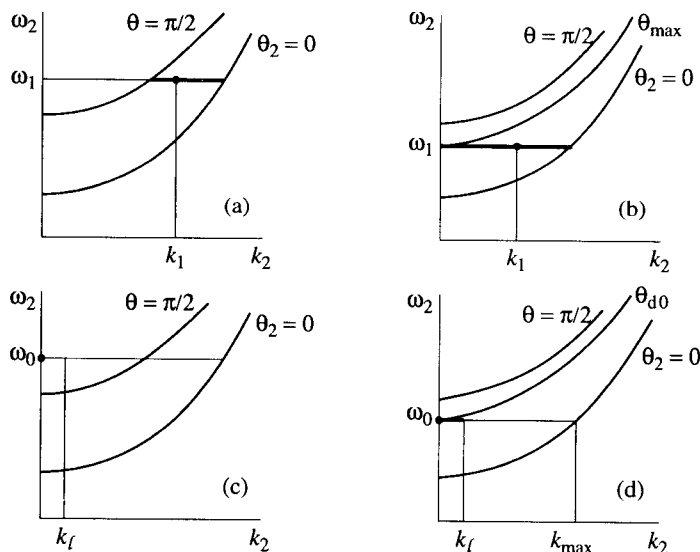


FIGURE 11.7

Routes of integration (shown by thick lines) in calculating the contributions of the two-magnon process to  $\Delta H_k$  for (a), (b) chaotic nonuniformities and (c), (d) large-scale nonuniformities; in the latter case,  $k_1 = 0$ .

Another limiting case is that of large-scale nonuniformities [Figure 11.7(c),(d)]. The amplitudes of harmonics  $H_k$  now have noticeable values only in a small  $k$ -range. Assume, e.g., that

$$H_k = \begin{cases} H_{k0} & \text{if } k < k_l \equiv 1/l \\ 0 & \text{if } k > k_l \end{cases} \quad (11.42)$$

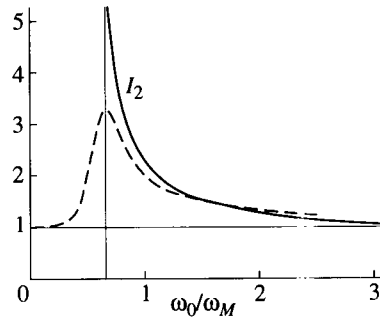
where  $l$  is a characteristic dimension of the nonuniformities. It can be shown that

$$H_{k0}^2 = 6\pi^2 \frac{l^3}{a^3} H_p^2. \quad (11.43)$$

Examining again the relaxation of the uniform mode in an ellipsoid of revolution, we substitute (11.42) into (11.37) and get rid of integration over  $\theta_2$ . Then, using the spin-wave spectrum (7.14), we obtain

$$\Delta H_0 = \frac{3}{2} \frac{l^3 H_p^2}{M_0} \int_0^{k_l} \frac{k^2}{\cos \theta_d(k)} dk \quad (11.44)$$

where the angle  $\theta_d(k)$  of degenerate spin waves is determined by the condition

**FIGURE 11.8**

Factors accounting for the density of degenerate states in the scattering of uniform-precession magnons by large-scale nonuniformities [338]. Solid line denotes  $I_2$  in (11.47); dashed line corresponds to the result obtained with the exchange term in the spin-wave dispersion law taken into account.

$\omega_k(k, \omega_d) = \omega_0$ , which yields

$$\cos \theta_d = \sqrt{\frac{N_z}{4\pi} + \frac{Dk^2}{2\pi M_0}}. \quad (11.45)$$

If  $k_l \ll k_{\max}$  [Figure 11.7(d)], the second term under the root in (11.45) can be neglected. Then,

$$\Delta H_0 \cong \frac{H_p^2}{2M_0 \sqrt{N_z/(4\pi)}} \equiv H_p \xi_d \quad (11.46)$$

where  $\xi_d$  is the coefficient of dipole narrowing, which was already introduced in Section 2.4. In this case (of large-scale nonuniformities), much smaller  $H_p$  values are needed to obtain an appreciable contribution to the linewidth than in the previous case of chaotic nonuniformities. For example,  $H_p$  should be  $\sim 10$  Oe to obtain  $\Delta H_0 = 1$  Oe in YIG.

Two assumptions have been made in deriving (11.46): the replacement of the spin-wave spectrum by the approximate expression (7.14) and the neglect of exchange contribution to this spectrum. Without the first assumption, Schlömann obtained for a sphere [338]

$$\Delta H_0 = \frac{\sqrt{3}}{2M_0} H_p^2 I_2(\omega_0/\omega_M). \quad (11.47)$$

The dependence  $I_2(\omega_0/\omega_M)$  is shown in Figure 11.8. The factor  $I_2$  tends to infinity at a point  $\omega_0 = 2\omega_M/3$  where the frequency of the considered mode approaches the upper boundary of the nonexchange spin-wave spectrum. At this point the density of states (in nonexchange approximation) tends to infinity, and it is the reason of  $\Delta H \rightarrow \infty$ . It should be emphasized that the singularity of

the density of states, and hence of  $\Delta H$ , is removed by taking into account the exchange contribution to the spin-wave spectrum [338] (Figure 11.8). It is also removed if the spin-wave dissipation or the influence of nonuniformities on the spin-wave spectrum is taken into consideration [349].

### 11.3.2 Disorder in distribution of ions over lattice sites

Passing now to the study of the influence of specific nonuniformities, we begin with the disorder in distribution of atoms (or ions) over the lattice sites. This problem was solved by Clogston, Suhl, Walker, and Anderson [76] using the method of coupled equations of motion. The same results can be obtained, as Callen [66] has shown, by the transition probability method. The results can be represented in the form of (11.40), but as the exact spin-wave dispersion relation was used, the factor  $I$  in (11.40) turned out to be dependent on the ratio  $H_{e0}/(4\pi M_0)$ .

The disorder in the distribution of ions takes place in ferrites with the inverse spinel structure (Section 3.3), e.g., in Ni and Mn ferrites. By the time when the work [76] was performed, the minimal  $\Delta H$  values in single crystals of these ferrites were  $\sim 40$  Oe. An assumption has been made in [76] that the nonuniformity is the variation of the pseudodipole interaction (Section 2.2). If the entire magnetocrystalline anisotropy of Ni ferrite would be caused by this interaction, its effective field (and the root-mean-square variation in the case of chaotic nonuniformities) should be of the order of  $10^5$  Oe. Such  $H_p$ , according to (11.40), would lead to the above-cited  $\Delta H$  value.

The results of later works have frustrated this optimistic picture. First, essentially smaller  $\Delta H$  values were obtained in ferrite single crystals with spinel structure, e.g., 1.2 Oe in nickel ferrite [454]. Second, it turned out (Section 2.2) that the origin of the anisotropy in ferrites is mainly the intraionic ('one-ion') interaction. Callen and Pittelly [67] and Haas and Callen [170] calculated the linewidth assuming the perturbation to be the variation of the intraionic spin-orbital interaction in the cases of, respectively, a nondegenerate and degenerate lowest energy level. The first case takes place for  $\text{Fe}^{2+}$  and  $\text{Ni}^{2+}$  ions at octahedral spinel sites, and the second takes place for  $\text{Co}^{2+}$  ions at such sites.

The results obtained in [67, 170] can be expressed in the form of (11.40). In the case of a nondegenerate level [67], the effective field  $H_p$  turned out to be proportional to  $c(1-c)(G_A - G_B)^2$ , where  $c$  and  $1-c$  are the relative concentrations of two sorts of ions distributed disorderly over the octahedral sites, and  $G_A$  and  $G_B$  are the constants of spin-orbital interaction for these ions. An estimate for  $\text{Fe}^{2+}$  as A ions,  $\text{Fe}^{3+}$  as B ions ( $G_B \simeq 0$ ), and  $c = 1/2$  results in  $\Delta H \simeq 10$  Oe. This value is much smaller than the experimental  $\Delta H$  values in ferrites containing  $\text{Fe}^{2+}$  ions even in smaller quantities. The spin-orbital interaction in  $\text{Ni}^{2+}$  ions is weaker than in  $\text{Fe}^{2+}$ , so, the experimental data [454] do not contradict the theory.

In the case of a degenerate level ( $\text{Co}^{2+}$  at octahedral sites), the contribution of ionic disorder is 20–30 Oe per 1 at. % of Co [170], which is much greater than the contribution of  $\text{Fe}^{2+}$ . But in both cases the theoretical values are smaller than the

experimental linewidths in ferrites containing  $\text{Co}^{2+}$  or  $\text{Fe}^{2+}$  ions, and, in addition, the experimental angular and temperature dependences differ essentially from the theoretical. The reason for this is that the scattering of magnons by the ionic disorder is masked by another, stronger mechanism of ionic relaxation, which will be discussed in detail in Chapter 13.

Thus, until now (1996), the contribution of the scattering of magnons by the disorder in distribution of ions over the lattice sites has not been discovered experimentally, although this mechanism was the first  $0-k$  process studied theoretically.

### 11.3.3 Anisotropy-field variations and pores in polycrystals

The independent-grain model (Section 2.4) is applicable to polycrystals if condition (2.64) holds. This condition is satisfied only for ferrites with very large anisotropy or near the compensation points. If (2.64) does not hold, the dipole narrowing takes place, and one can use the theory of magnon scattering by nonuniformities. The nonuniformities are now the variations of the directions of crystal axes, pores, and, in some cases, the inclusions of other phases.

We consider first the variations of the directions of crystal axes (and hence, of the anisotropy field), which are characteristic of polycrystals, though do not always make the largest contribution to the linewidth. The mean grain dimensions in polycrystals are usually of the order of a micrometer or more,<sup>6</sup> and therefore  $k_l \ll k_{\max}$  (Figure 11.7). So, the second of the above-considered limiting cases and, in particular, formula (11.46) are usually applicable to polycrystals.

In nontextured polycrystals, in which all directions of the crystal axes are equally probable, the root-mean-square value of the anisotropy field  $H_a$  must be substituted into (11.46) for  $H_p$ . In a cubic crystal, with allowance only for the first anisotropy constant,  $\bar{H}_a^2 = (16/24)H_{A1}^2$  [338] where  $H_{A1} = K_1/M_0$ . The estimate using (11.46) yields for YIG at room temperature  $\Delta H_a \sim 10$  Oe, which does not contradict the experiment (see below).

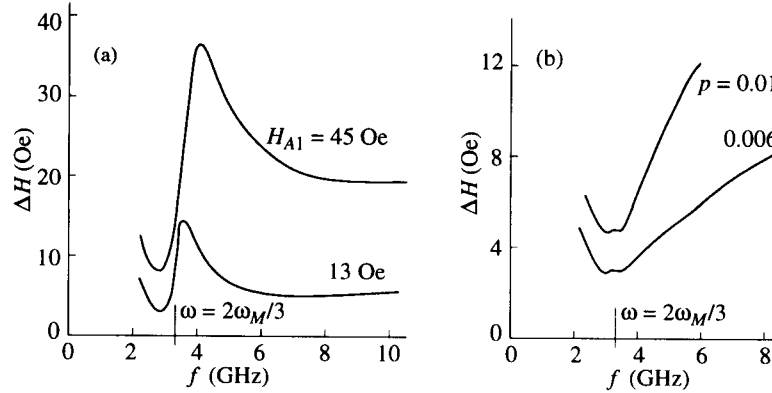
Formulae (11.46) and (11.47) can be used to calculate the contributions to  $\Delta H$  of other effective fields, e.g., the fields caused by nonuniform strains arising near dislocations. The theory for this case was developed by Barjyakhtar, Savchenko, and Tarasenko [40].

Consider now the contribution to ferromagnetic-resonance linewidth of the pores between grains in polycrystalline ferrites. The independent-region concept (Section 2.4) has given, in this case, the  $\Delta H$  values that agree with experiment on the order of magnitude. However, this agreement indicates only that the coefficient of dipole narrowing (Section 2.4) is of the order of unity.

The contribution of pores was calculated by Sparks, Loudon, and Kittel [378] using the transition-probability method. The same model of a spherical cavity as in the independent-region theory was used. The energy of the demagnetizing

---

<sup>6</sup>We do not touch on the nanocrystals, which have much smaller grains, though they are regarded now as a promising magnetic materials.

**FIGURE 11.9**

Frequency dependences of  $\Delta H$  in polycrystalline ferrites [209]. (a) The anisotropy contribution dominates ( $p \leq 0.003$ ). (b) The porosity contribution dominates ( $|H_{A1}| \approx 2$  Oe).

field of the cavity was expressed in operators  $\hat{a}_k^+$  and  $\hat{a}_k$ , and after calculations analogous to those performed in deriving (11.46) it was found that

$$(\Delta H)_p = \frac{4\pi V_p}{9 V_0} 4\pi M_0 \frac{G(\theta_{d0})}{\cos \theta_{d0}} \quad (11.48)$$

where  $V_p$  is the volume of the cavity,  $V_0$  is the volume of the sample,  $\theta_{d0} = \arccos(N_z/4\pi)^{1/2}$  is the polar angle of degenerate spin waves [Figure 11.7(d)], and

$$G(\theta_{d0}) = (3 \cos^2 \theta_{d0} - 1)^2. \quad (11.49)$$

Two assumptions [the same as in deriving (11.46)] were made in deriving (11.48): the approximate spin-wave dispersion relation (7.14) was used, and the second term in (11.45) was neglected. If the first assumption is not made, a singularity in the  $\Delta H(\omega)$  dependence arises when the uniform-resonance frequency  $\omega_0$  crosses the upper boundary of the non-exchange spin-wave spectrum. And if the second assumption is also given up, the singularity will be smoothed, as in the above-considered case of the anisotropy-field variations. If the sample contains many pores,  $V_p$  in (11.48) is the entire volume of all pores; the ratio  $V_p/V_0 \equiv p$  is called the porosity.

Expression (11.48), as distinct from (2.69), contains factors  $(\cos \theta_{d0})^{-1}$  and (11.49). The former takes into account the density of degenerate states and is present in all formulae for large-scale nonuniformities. The latter has appeared due to the specific, spherical shape of the cavities. Real pores in polycrystals, of course, are not spheres, and the behavior of  $\Delta H$  determined by the factor (11.49) should not be and has not been observed in experiment.

A lot of works were devoted to the experimental investigation of ferromagnetic

resonance in polycrystalline ferrites (e.g., [63, 160, 209]). In all of them, beginning with work by Buffer [63], the  $\Delta H$  maximum predicted by the two-magnon theory has been observed when the frequency of the relaxing mode crosses the upper boundary of the nonexchange spin-wave spectrum. But at first it was not clear by which contribution to  $\Delta H$  this maximum was determined, by the contribution of the anisotropy-field variations  $(\Delta H)_a$ , of pores  $(\Delta H)_p$ , or by both. To separate the contributions  $(\Delta H)_a$  and  $(\Delta H)_p$  we may use two methods: to employ their different temperature dependences, or (that is better) to vary separately anisotropy and porosity. In the latter case the contribution of each parameter should not change and must be as small as possible when the other is varied. In Figure 11.9 the data obtained by this method [209] are shown. When the anisotropy contribution dominates [Figure 11.9(a)], the observed  $\Delta H$  behavior agrees with the theory of magnon scattering by large-scale nonuniformities. But when the porosity contribution dominates [Figure 11.9(b)], the experimental dependences do not at all agree with the above-considered theory: no distinct maximum is observed at  $\omega_0 = 2\omega_M/3$ , the  $\Delta H$  values to the left of this point are not smaller than those to the right, and an essential increase of  $(\Delta H)_p$  is observed with growing frequency. As for the proportionality of  $(\Delta H)_p$  to  $M_0$  and  $p$  (obtained also in the independent-region theory), it is confirmed by all experiments.

### 11.3.4 Surface roughness

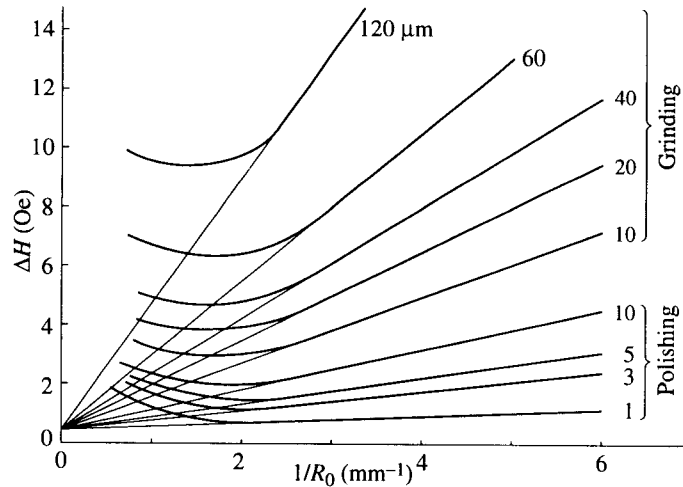
In high-quality single-crystal ferrite samples the surface roughness is the most significant factor causing the two-magnon scattering. Le Craw, Spencer, and Porter [251] were the first to ascertain the influence of this factor on the ferromagnetic-resonance linewidth. This influence is very important. The  $\Delta H$  values of carefully polished YIG spheres are as low as 0.3 Oe, but they grow to  $\sim 10$  Oe if the spheres are grinded using abrasive powder with 10  $\mu\text{m}$  grain.

The above-mentioned theory [378] was developed just to allow for surface roughness. The assumption has been made that the surface nonuniformities are semispherical pits covering the sample surface. The amplitude  $\Psi_{0k}$  should be halved twice, when passing from internal spheres to surface semispheres, to take into account the decrease of the scattering-center effectiveness and the decrease of its volume. The number of semispheres is found from the condition that they completely cover the surface. Then, instead of (11.48), we obtain

$$(\Delta H)_s = \frac{\pi R_s}{9 R_0} 4\pi M_0 \frac{G(\theta_{d0})}{\cos \theta_{d0}} \quad (11.50)$$

where  $R_0$  is the sample radius and  $R_s$  is the radius of semispheres. The dependences of  $(\Delta H)_s$  on  $M_0$  and  $R_0$  have clear physical meaning and agree with experiment (e.g., Figure 11.10).

Formula (11.50) does not give the frequency dependence of  $(\Delta H)_s$ , whereas the experimental values of  $(\Delta H)_s$ , as well as of  $(\Delta H)_p$ , increase with growing frequency. The allowance for exact spin-wave spectrum should lead, according to



**FIGURE 11.10**

Dependences of  $\Delta H$  on the radius  $R_0$  of ferrite spheres [452]. Bold lines represent experimental data at  $f = 9$  GHz and room temperature. Numbers at the curves denote the mean abrasive-grain dimensions in the final grinding or polishing. The increase of  $\Delta H$  at large  $R_0$  is related to excitation of nonuniform modes (Section 6.3).

the two-magnon theory, to maxima at the points where the frequency of the relaxing mode crosses the upper boundary of the non-exchange spin-wave spectrum. However, these maxima have never been observed in single-crystal samples with rough surface. The reason for this is, probably, the broad spectrum of the space harmonics of uniformities caused by their highly irregular shape; the degeneration with the non-exchange part of the spin-wave manifold does not then play a significant role. The same may be the reason of the above-mentioned 'anomalous' behavior of  $\Delta H_p$  in polycrystals.

The contribution of surface roughness is proportional to the ratio of the area of sample surface to the volume of the sample. Therefore, this contribution should be very large in thin films. Only the high quality of the surface of epitaxial YIG films grown on well polished substrates allows one to obtain rather small  $\Delta H$  values in such films (Section 6.2).

In conclusion, some general remarks should be made concerning the two-magnon relaxation processes.

These processes play a significant role not only at the first stage but also at subsequent stages of relaxation, leading to the spreading of energy over the entire region of the spin-wave manifold degenerate with the initial mode.

The existence of higher (exchange) branches of spin-wave spectrum in ferrimagnets does not materially influence the two-magnon processes because the modes the relaxation of which we are interested in are usually degenerate only with the

lowest (ferromagnetic) branch. In antiferromagnets the two-magnon processes play an important role (e.g., [255]). Very narrow antiferromagnetic-resonance lines were observed [233] just when the degeneration of the relaxing mode with spin waves did not take place.

Two-magnon processes do not make an *additive* contribution to the spin-wave dissipation parameter  $\Delta H_k$  found from the measurement of the spin-wave parametric excitation threshold. Nevertheless, these processes influence essentially the parametric excitation of spin waves (Section 10.3). They lead to the increase of the threshold of first-order parametric processes and to the smoothing of the second-order-process threshold.

Two-magnon processes, in which the entire number of magnons is conserved, do not take part, to a first approximation (without allowance for the dipole-dipole interaction), in the relaxation of  $M_z$ . However, the  $0 - k$  processes take part in the relaxation of the vector  $M$  length, which is determined, to the same approximation, by the number of all magnons except the magnons of uniform precession.

The dissipation parameter in magnetically ordered substances increases when the point of the second-order phase transition (Curie temperature for ferromagnets) is approached. This increase is sometimes associated with 'scattering of magnons by the magnetization fluctuations', and this process is assigned to the two-magnon processes. But such treatment cannot be regarded as correct. Fluctuations, including critical (which arise near the points of second-order phase transitions), are characteristic of an ideal crystal. Therefore, their effect on the relaxation should be treated in terms of inherent processes, which were considered (without taking fluctuations into account) in Section 11.2.



# 12

## *Magnetoelastic coupling*

### 12.1 Elastic properties and magnetoelastic interaction

So far the magnetic system of magnetically ordered substances was regarded as isolated. Now taking into account its coupling with other systems, we discuss, in the present chapter, the coupling with elastic system, i.e., with the vibrations of the crystal lattice. First of all, some general concepts of the theory of elasticity (e.g., [227, 113, 245]) will be briefly recalled.

#### 12.1.1 Elastic waves and oscillations

The elastic state of a solid regarded as a continuum is characterized by the *displacement* vector

$$\mathbf{u}(\mathbf{r}) = \mathbf{r} - \mathbf{r}_0 \quad (12.1)$$

where  $\mathbf{r}_0$  and  $\mathbf{r}$  are the position vectors of a point in the initial and the deformed states, respectively. Under certain conditions [245], which are approximately satisfied in the cases we are interested in, the deformation can be described by the symmetric *strain tensor*<sup>1</sup>

$$e_{pq} = \frac{1}{2} \left( \frac{\partial u_p}{\partial x_q} + \frac{\partial u_q}{\partial x_p} \right). \quad (12.2)$$

The tensor  $e_{pq}$  diagonal components, in the main axes of this tensor, represent the fractional extensions in the directions of these axes, and their sum is the fractional change of volume of a small element of the solid.

The force acting on a small volume element is the sum of the *elastic* force  $\delta f_{el}$  and the *body* force  $\delta f_b$ . The former is the net force caused by the action of all neighboring elements on the considered one. The latter is caused by external

---

<sup>1</sup>Here and hereafter in this chapter, we use, contrary to the previous chapters, the same notations (e.g.,  $e_{pq}$ ) for the entire tensor and its components.

fields, as gravitational and electromagnetic. In problems we will consider, this force may be neglected. The elastic force per unit volume can be presented in the form

$$f_{elp} = \sum_{q=1}^3 \frac{\partial \sigma_{pq}}{\partial x_q} \quad (12.3)$$

where  $\sigma_{pq}$  is the symmetric *stress tensor*. The stresses are usually caused by external forces applied to the surface of the body, and the boundary condition holds [245]

$$\sum_{q=1}^3 n_{0Sq} \sigma_{pq} = F_{ep} \quad \text{on } S \quad (12.4)$$

where  $F_e$  is the external force per unit area of the surface  $S$  and  $n_{0S}$  is the unit outward normal to  $S$ . In the case of uniform extension or compression in the direction of a unit vector  $n_{0F}$ ,

$$\sigma_{pq} = \pm \beta_p \beta_q \sigma \quad (12.5)$$

where  $\beta_{p,q}$  are the direction cosines of the vector  $n_{0F}$ . Such uniform deformation is approximately realized when, e.g., a rod is compressed in the direction of its axis;  $\sigma$  is then equal to the pressure applied to the flat surface of the rod.

The free energy density (or energy, in accordance with the footnote on the page 31) of an elastically strained solid is

$$U_{el} = \frac{1}{2} \sum_{p=1}^3 \sum_{q=1}^3 \sigma_{pq} e_{pq}. \quad (12.6)$$

Taking into account that  $\sigma_{pq}$  depends on  $e_{pq}$ , we can get

$$\sigma_{pq} = \frac{\partial U_{el}}{\partial e_{pq}}. \quad (12.7)$$

For small displacements the *Hooke law* holds:

$$\sigma_{pq} = \sum_{l=1}^3 \sum_{m=1}^3 c_{pqlm} e_{lm} \quad (12.8)$$

where  $c_{pqlm}$  are components of the fourth-rank tensor of elastic stiffness constants or *moduli of elasticity*<sup>2</sup> [227]. It follows from the symmetry of the tensors  $\sigma_{pq}$  and  $e_{pq}$  that the number of independent components  $c_{pqlm}$ , in general, is equal to 21. It decreases for all crystal systems except the triclinic. For the cubic system, there are three independent components:  $c_{pppp}$ ,  $c_{ppqq}$ , and  $c_{pqpp}$  (in coordinate system

<sup>2</sup>The inverse tensor  $(c_{pqlm})^{-1} = s_{pqlm}$  is called the tensor of elastic compliance constants [227]. However, there is no consensus on these terms, components  $c_{pqlm}$  are named sometimes 'elastic constants', and components  $s_{pqlm}$ , 'elastic moduli'.

with axes in  $\langle 100 \rangle$  directions). The following notations are used:  $c_{pppp} \equiv c_{11}$ ,  $c_{ppqq} \equiv c_{12}$ , and  $c_{pqpp} \equiv c_{44}$ . For an isotropic medium,

$$c_{11} - c_{12} = 2c_{44} \quad (12.9)$$

so that two independent components are left. It should be noted that (12.9) is *nearly* satisfied for some cubic crystals, too. For YIG at room temperature,  $c_{11} = 2.69 \times 10^{12}$ ,  $c_{12} = 1.077 \times 10^{12}$ , and  $c_{44} = 0.764 \times 10^{12}$  [387], so that  $2c_{44}/(c_{11} - c_{12}) = 0.947$ .

With allowance for Hooke's law the elastic energy of a cubic crystal takes the form

$$U_{el} = \frac{1}{2}c_{11}(e_{xx}^2 + e_{yy}^2 + e_{zz}^2) + c_{12}(e_{xx}e_{yy} + e_{yy}e_{zz} + e_{zz}e_{xx}) + 2c_{44}(e_{xy}^2 + e_{yz}^2 + e_{zx}^2). \quad (12.10)$$

The *equation of motion* for an elastically strained solid, without taking into account the body forces and dissipation, has the form

$$\rho \frac{\partial^2 \mathbf{u}}{\partial t^2} = \mathbf{f}_{el} \quad (12.11)$$

where  $\rho$  is the mass density, and  $\mathbf{f}_{el}$  is determined by (12.3). Using (12.8) and (12.2), this equation is transformed into

$$\rho \frac{\partial^2 u_p}{\partial t^2} = \sum_q \sum_l \sum_m c_{pqtm} \frac{\partial^2 u_m}{\partial x_q \partial x_l}. \quad (12.12)$$

In the case of a uniform plane wave [ $\mathbf{u} = \mathbf{u}_0 \exp(i\omega t - i\mathbf{q}\mathbf{r})$ ], the solution of (12.12) shows [227, 113] that there are *three normal* elastic waves with dispersion relations

$$\omega_j = v_j q \quad (j = 1, 2, 3). \quad (12.13)$$

For an isotropic solid and for a cubic crystal in the case when wave vector  $\mathbf{q}$  is parallel to the axis  $\langle 100 \rangle$ , one of the normal waves is *longitudinal* ( $\mathbf{u} \parallel \mathbf{q}$ ), with velocity

$$v_{\parallel} = \sqrt{\frac{c_{11}}{\rho}} \quad (12.14)$$

and the other two are *transverse* ( $\mathbf{u} \perp \mathbf{q}$ ), with

$$v_{\perp} = \sqrt{\frac{c_{44}}{\rho}}. \quad (12.15)$$

In YIG ( $\rho = 5.17$ ) at room temperature,  $v_{\parallel} = 7.209 \times 10^5$  and  $v_{\perp} = 3.843 \times 10^5$  [387]. The density of elastic-energy flow (the Umov vector) [113] is

$$\Pi_{el} = \rho \omega^2 u^2 \mathbf{v}_{\parallel, \perp}. \quad (12.16)$$

Normal waves in waveguides containing elastic media, as well as eigenoscillations of bounded bodies, are found by solving the elastic equations of motion, e.g., (12.12), subject to boundary conditions. If boundary surface is *free*, the boundary condition is

$$\sum_q n_{0q} \sigma_{pq} = 0 \quad \text{at } S. \quad (12.17)$$

If the surface is *fastened*,  $u = 0$  at  $S$ . It should be noted that waves in elastic *waveguides* are neither pure transverse nor pure longitudinal even in the above-mentioned cases (isotropic solid and cubic crystal with  $q \parallel \langle 100 \rangle$ ) when waves in unbounded medium are longitudinal or transverse. In systems bounded in the direction of propagation, e.g., in plates, elastic *standing waves* take place, similar to standing spin waves (Section 7.2). Their eigenfrequencies are determined by the plate thickness and by the character of boundary conditions. For conditions (2.17), the eigenfrequencies are  $\omega_{n\perp,\parallel} = nv_{\perp,\parallel}/d$  where  $n = 1, 2, 3 \dots$

The calculation of *elastic-oscillation* eigenfrequencies for bodies bounded in all directions presents essential difficulties. We will cite only the values of some of the lowest frequencies for an isotropic sphere with free surface and elastic parameters of YIG [249]:  $f_{T12} = 3.081 \times 10^5/d$  Hz,  $f_{S12} = 3.259 \times 10^5/d$  Hz,  $f_{S01} = 6.067 \times 10^5/d$  HZ where  $d$  is the sphere diameter in centimeters. The frequency  $f_{T12}$  corresponds to pure transverse oscillation (relative to the radius), and the other two correspond to mixed oscillations; figures in the subscripts indicate the numbers of variations along polar angle and radius.

Quantization of elastic waves and oscillations, similar to the magnetic case (Section 7.3), yields the quasiparticles (*phonons*) with energy  $\varepsilon = \hbar\omega$  and quasi-impulse  $p = \hbar q$ . A certain kind of phonons corresponds to each elastic normal wave.

So far we have considered, according to the classical theory of elasticity, an elastic continuum. In a *discrete* crystal lattice, analogous to discrete magnetic lattice (Section 7.4), the following new features appear: (i) the  $q$  range is limited to the first Brillouin zone, (ii) dispersion relations (12.13) are replaced by more complicated ones, and (iii) the  $3(n - 1)$  new, optical branches appear where  $n$  is the number of atoms in a primitive lattice cell (Figure 12.1).

### 12.1.2 Magnetoelastic energy and equations of motion

One of the reasons of coupling between magnetic and elastic systems in magnetically ordered substances is the dependence of exchange interaction on distances between magnetic atoms (or ions). Another reason is the dependence of magnetic (dipole-dipole) interaction on these distances. The third reason, usually the most essential, is the spin-orbital interaction. These reasons apart, we may write the phenomenological expressions for the magnetoelastic energy using [as for magnetocrystalline energy (Section 2.2)] only the symmetry considerations. We will restrict ourselves to the case of a cubic crystal, assume the exchange interaction to

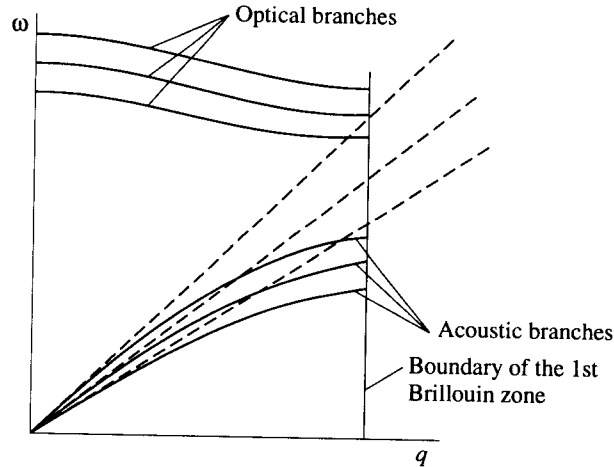


FIGURE 12.1

Elastic-wave spectrum in a continuum (dashed lines) and in a discrete crystal lattice (solid curves). Only three of  $3(n-1)$  optical branches are shown.

be isotropic, and direct the coordinate axes along the axes  $\langle 100 \rangle$ . Then, up to the terms of the first order in  $e_{pq}$  and of the second order in  $M_p$ , the *magnetoelastic energy* can be written in the form [340]

$$U_{\text{mel}} = \frac{B_1}{M_0^2} \sum_p M_p^2 e_{pp} + \frac{B_2}{M_0^2} \sum_p \sum_{q \neq p} M_p M_q e_{pq} + \frac{A_1}{M_0^2} \sum_p \sum_q \sum_{l \neq q} \frac{\partial M_p}{\partial x_q} \frac{\partial M_p}{\partial x_l} e_{ql} + \frac{A_2}{M_0^2} \sum_p \sum_q \left( \frac{\partial M_p}{\partial x_q} \right)^2 e_{qq} \quad (12.18)$$

where  $p, q, l = 1, 2, 3$ . (Terms of the first order in  $M_p$  cannot be present, as pointed out in Section 2.2.) The first two terms in (12.18) result from *relativistic* (magnetic and spin-orbital) interactions, and the last two terms, from the *exchange* interaction. The quantities  $B_1$ ,  $B_2$ ,  $A_1$ , and  $A_2$  are called magnetoelastic constants. For YIG at room temperature,  $B_1 = 3.48 \times 10^6$  and  $B_2 = 6.96 \times 10^6$  [387]. In an isotropic ferromagnet  $B_1 = B_2$ .

The magnetoelastic energy  $U_{\text{mel}}$  leads, first of all, to the change in the *equilibrium* elastic state of a magnetically ordered substance, namely, to the appearance of spontaneous strains  $e_{pq}^0$  caused by magnetization. This phenomenon is called *magnetostriction*, in a narrow sense (in a wider sense, the term 'magnetostriction' is used sometimes to denote all phenomena caused by magnetoelastic coupling). To find the strains  $e_{pq}^0$ , in the case of a ferromagnet magnetized to saturation, we have to minimize the sum of  $U_{\text{el}}$  and  $U_{\text{mel}}$ .

Consider a *cubic* crystal and neglect the exchange contribution to magnetoelastic

energy. Then, the magnetostrictive fractional elongations in the directions of the  $\langle 100 \rangle$  and  $\langle 111 \rangle$  axes, due to magnetization in the same directions, are [70]

$$\left(\frac{\delta l}{l}\right)_{100} \equiv \lambda_{100} = -\frac{2}{3} \frac{B_1}{c_{11} - c_{12}} \quad \left(\frac{\delta l}{l}\right)_{111} \equiv \lambda_{111} = -\frac{1}{3} \frac{B_2}{c_{44}}. \quad (12.19)$$

The quantities  $\lambda_{100}$  and  $\lambda_{111}$  are the *magnetostriction constants* of a cubic ferromagnet. Their values for YIG at room temperature are:  $\lambda_{100} = -1.4 \times 10^{-6}$  and  $\lambda_{111} = -2.4 \times 10^{-6}$ . The averaged magnetostrictive constant of a cubic polycrystal is [70]

$$\lambda_{\text{poly}} = \frac{2}{5} \lambda_{100} + \frac{3}{5} \lambda_{111}. \quad (12.20)$$

Substituting the magnetostrictive strains  $e_{pq}^0$  into expression (12.18) for the magnetoelastic energy (taking into account only its first two terms), we find that the part of this energy dependent on magnetization directions has the form [70]

$$U_{\text{mel}}^0 = K_{1\text{mel}}^0 (\alpha_1^2 \alpha_2^2 + \alpha_2^2 \alpha_3^2 + \alpha_3^2 \alpha_1^2) \quad (12.21)$$

where  $\alpha_{1,2,3}$  are the direction cosines of the magnetization, as in (2.32), and

$$K_{1\text{mel}}^0 = \frac{B_1^2}{c_{11} - c_{12}} - \frac{B_2^2}{2c_{44}}. \quad (12.22)$$

The energy (12.21) and the elastic energy caused by the magnetostrictive strains should be added to the energy of magnetocrystalline anisotropy. This results in renormalization of the anisotropy constant, as already pointed out in Section 2.2. If terms of higher order in  $\mathbf{M}$  components were taken into account in the magnetoelastic energy, the higher anisotropy constants would be renormalized in a similar manner. It should be noted that the considered renormalization, based on finding the equilibrium strains, is valid only in the *static* case or, approximately, for sufficiently slow changes of magnetization.

In the presence of *external* mechanical forces, the equilibrium strains can be found by minimizing the sum  $U_{\text{el}} + U_{\text{mel}} + U_{\text{el}}^e$  where  $U_{\text{el}}^e$  is the energy of elastic strains caused by external forces. Substituting the equilibrium strains into the mentioned sum, we can find an expression for the part  $U^e$  of the total energy depending on the external mechanical forces. For example, in the case of uniform compression of a uniformly magnetized sample of cubic crystal [70],

$$U^e = -\frac{3}{2} \sigma [\lambda_{100} (\alpha_1^2 \beta_1^2 + \alpha_2^2 \beta_2^2 + \alpha_3^2 \beta_3^2) + 2\lambda_{111} (\alpha_1 \alpha_2 \beta_1 \beta_2 + \alpha_2 \alpha_3 \beta_2 \beta_3 + \alpha_3 \alpha_1 \beta_3 \beta_1)] \quad (12.23)$$

where  $\sigma$  is the pressure and  $\beta_{1,2,3}$  are the direction cosines of compression axis (relative to the  $\langle 100 \rangle$  directions).

To study the *dynamic* processes under the action of magnetic and mechanical forces varying quickly in time we must use the equations of motion. If the magnetoelastic coupling is to be taken into account, these equations should be the

*coupled* equations for magnetization  $\mathbf{M}$  and elastic displacement  $\mathbf{u}$ . To obtain them we must insert the effective field of magnetoelastic interaction  $\mathbf{H}_{\text{mel}}$  into the Landau–Lifshitz equation and insert the force  $\mathbf{f}_{\text{mel}}$  caused by this interaction into the mechanical equation of motion (12.11). The effective field  $\mathbf{H}_{\text{mel}}$  can be found from the magnetoelastic energy, e.g., (12.18) using the general formula (2.7). To find the force  $\mathbf{f}_{\text{mel}}$  an expression similar to (12.3) is to be used where the magnetoelastic stresses  $\sigma_{\text{mel}pq}$  are obtained from magnetoelastic energy by the formula found from (12.7) with the replacement  $U_{\text{el}} \rightarrow U_{\text{mel}}$ .

Let us consider, as before, a *cubic* crystal magnetized along the  $\langle 100 \rangle$  axis and, restricting to not-too-fast variations of  $\mathbf{M}$  in space, retain in (12.18) only the first two, relativistic, terms. Suppose, for simplicity, that the condition of elastic isotropy (12.9) is satisfied, and assume the exchange interaction to be also isotropic. Then, without allowance for dissipation, we get the *coupled equations of motion* [249]:

$$\begin{aligned} \frac{\partial M_x}{\partial t} &= -\gamma \frac{B_2}{M_0} \left( \frac{\partial u_y}{\partial x} + \frac{\partial u_x}{\partial y} \right) M_x - \gamma \left[ H_{\text{ef}z} - D\nabla^2 \right. \\ &\quad \left. + 2 \frac{B_1}{M_0} \left( \frac{\partial u_y}{\partial y} - \frac{\partial u_z}{\partial z} \right) \right] M_y + \gamma H_{\text{ef}y} M_z - \gamma B_2 \left( \frac{\partial u_z}{\partial y} + \frac{\partial u_y}{\partial z} \right) \\ \frac{\partial M_y}{\partial t} &= \gamma \frac{B_2}{M_0} \left( \frac{\partial u_y}{\partial x} + \frac{\partial u_x}{\partial y} \right) M_y + \gamma \left[ H_{\text{ef}z} - D\nabla^2 \right. \\ &\quad \left. + 2 \frac{B_1}{M_0} \left( \frac{\partial u_x}{\partial x} - \frac{\partial u_z}{\partial z} \right) \right] M_x - \gamma H_{\text{ef}x} M_z + \gamma B_2 \left( \frac{\partial u_z}{\partial x} + \frac{\partial u_x}{\partial z} \right) \end{aligned} \quad (12.24)$$

$$\begin{aligned} \rho \frac{\partial^2 u_x}{\partial t^2} &= c_{44} \nabla^2 u_x + (c_{44} + c_{12}) \frac{\partial}{\partial x} \text{div} \mathbf{u} \\ &\quad + \frac{B_1}{M_0^2} \frac{\partial M_x^2}{\partial x} + \frac{B_2}{M_0^2} \left[ \frac{\partial}{\partial y} (M_x M_y) + \frac{\partial}{\partial z} (M_x M_z) \right] \\ \rho \frac{\partial^2 u_y}{\partial t^2} &= c_{44} \nabla^2 u_y + (c_{44} + c_{12}) \frac{\partial}{\partial y} \text{div} \mathbf{u} \\ &\quad + \frac{B_1}{M_0^2} \frac{\partial M_y^2}{\partial y} + \frac{B_2}{M_0^2} \left[ \frac{\partial}{\partial z} (M_y M_z) + \frac{\partial}{\partial x} (M_y M_x) \right] \\ \rho \frac{\partial^2 u_z}{\partial t^2} &= c_{44} \nabla^2 u_z + (c_{44} + c_{12}) \frac{\partial}{\partial z} \text{div} \mathbf{u} \\ &\quad + \frac{B_1}{M_0^2} \frac{\partial M_z^2}{\partial z} + \frac{B_2}{M_0^2} \left[ \frac{\partial}{\partial x} (M_z M_x) + \frac{\partial}{\partial y} (M_z M_y) \right]. \end{aligned} \quad (12.25)$$

The effective field  $\mathbf{H}_{\text{ef}}$ , the components of which appear in (12.24), involves external magnetic fields, both steady and ac, dipole–dipole (demagnetizing) field  $\mathbf{H}_M$ , and effective field of anisotropy  $\mathbf{H}_{\text{an}}$  (Section 2.3). The third projection of

the Landau–Lifshitz equation is not written because the component  $M_z$  can be determined from the condition of  $M$  conservation.

## 12.2 Effect of elastic stresses on ferromagnetic resonance

Consider the *uniform* oscillations of magnetization in a ferromagnet in the presence of elastic stresses. Note that uniform ac magnetization does not appear in the mechanical equations of motion (12.25), just as the uniform *displacement*  $u$  does not appear in the magnetic equations (12.24). Thus, the elastic vibrations occur independently of uniform magnetization oscillations. But elastic *strains*, as it is evident from (12.24), do affect the uniform magnetic oscillations.

Let us examine first the influence of the static *magnetostrictive* strains. Consider an ellipsoid of cubic single-crystal ferromagnet magnetized to saturation along one of its axes, which coincides with the  $\langle 100 \rangle$  cubic axis. Having found the equilibrium magnetostrictive strains and substituting them into (12.24), we make sure that these strains result in the appearance of an effective field

$$H_{\text{mel}} = \frac{2B_1}{M_0(c_{11} - c_{12})} \quad (12.26)$$

acting on ac magnetization. So, the ferromagnetic-resonance frequency, e.g., in the case of a sphere, is

$$\omega_0 = \gamma \left( H_{e0} + \frac{2K_1}{M_0} + H_{\text{mel}} \right). \quad (12.27)$$

One can see from this expression that at  $H_{e0} \rightarrow 0$  and  $K_1 \rightarrow 0$  (if no domains would arise) the resonance frequency  $\omega_0 \rightarrow \gamma H_{\text{mel}}$ . That is why the quantity  $\gamma H_{\text{mel}}$  is called *magnetoelastic gap*.

The effective field (12.26) differs from the effective field  $H_{\text{mel}}^0$ , which corresponds to the additional anisotropy constant (12.22) caused by magnetoelastic coupling:

$$H_{\text{mel}}^0 = 2 \frac{K_{1\text{mel}}^0}{M_0} = \frac{2}{M_0} \left( \frac{B_1^2}{c_{11} - c_{12}} - \frac{B_2^2}{2c_{44}} \right) = H_{\text{mel}} - \frac{B_2^2}{M_0 c_{44}}. \quad (12.28)$$

For an isotropic sphere ( $B_1 = B_2$ , and  $c_{11} - c_{12} = 2c_{44}$ ),  $H_{\text{mel}}^0 = 0$ , whereas  $H_{\text{mel}} \neq 0$ . The physical reason of this difference, as Turov and Shavrov pointed out (e.g., [41]), is the following: in the dynamic case, we consider now, the magnetization vector is precessing in the ‘frozen’ crystal lattice (deformed by static stresses), while in the static (or quasistatic) case, discussed in the previous section, elastic strains *had time to follow* the magnetization changes.

For YIG at room temperature,  $H_{\text{mel}}^0 = 0.4$  Oe and  $H_{\text{mel}} = 0.5$  Oe, so that magnetoelastic ‘corrections’ are close to each other and both are small as compared with the magnetocrystalline-anisotropy field ( $H_{A1} = 2K_1/M_0 \cong 80$  Oe



at room temperature). Therefore, the 'illegal' use of static anisotropy constants in ferromagnetic-resonance calculations or, on the contrary, the use of anisotropy constants found from resonance measurements (Section 2.3) in calculations of static processes, do not lead (in this case!) to essential errors.

Examining the influence of *external* elastic stresses on ferromagnetic resonance, we restrict our treatment to uniform oscillations in a spheroid of cubic ferromagnet compressed uniformly in the direction of its axis. It follows from (12.23) that the effective demagnetization factors of magnetoelastic interaction have the form

$$N_{pq}^{\sigma} = -\frac{3\sigma}{M_0^2} [(\lambda_{100} - \lambda_{111}) \Delta_{pq} + \lambda_{111}] \beta_p \beta_q \quad (12.29)$$

where  $\sigma$  and  $\beta_{pq}$  have the same meaning as in (12.22),  $\lambda_{100}$  and  $\lambda_{111}$  are determined by (12.19), and  $\Delta_{pq}$  is the Kronecker delta symbol. The effective demagnetization factors  $N_{pq}^{\sigma}$ , being added to demagnetization factors of magnetocrystalline anisotropy and shape, determine the ferromagnetic-resonance frequency  $\omega_0$ .

If  $M_0$  and the pressure (i.e., the vector  $n_{0F}$ ) are both directed along the same  $\langle 100 \rangle$  axis, coinciding with the axis of the spheroid, then, using the method of effective demagnetization factors (Section 12.1), we get, with regard to (12.29),

$$\frac{\omega_0}{\gamma} = H_{e0} + (N_{\perp} - N_z) M_0 + \frac{2K_1}{M_0} + \frac{3\sigma\lambda_{100}}{M_0}. \quad (12.30)$$

If  $M_0$  and  $n_{0F}$  are parallel to the  $\langle 111 \rangle$  axis coinciding with the spheroid axis, then

$$\frac{\omega_0}{\gamma} = H_{e0} + (N_{\perp} - N_z) M_0 - \frac{4}{3} \frac{K_1}{M_0} + \frac{3\sigma\lambda_{111}}{M_0}. \quad (12.31)$$

Formulae (12.30) and (12.31) can be used in the measurement of magnetostriction constants  $\lambda_{100}$  and  $\lambda_{111}$  [372]. If  $M_0$  lies in the  $\{110\}$  plane and the pressure is applied along the axis  $\langle 111 \rangle$  perpendicular to this plane, the expression for the frequency  $\omega_0$  will depend on the angle between  $M_0$  and the  $\langle 100 \rangle$  axis and contain  $\lambda_{100}$  and  $\lambda_{111}$ . The both constants can then be measured in one experiment. The effective magnetostriction constant (12.20) can be found from similar measurement on a polycrystalline sample.

### 12.3 Magnetoelastic waves

We proceed now to study the *nonuniform* magnetic and elastic modes, which are coupled with each other according to equations (12.24) and (12.25). This coupling manifests itself in that the plane waves cease to be pure magnetic (spin) and pure elastic waves and become *coupled* (or *mixed*) magnetoelastic waves. Turov and Irkhin [411] were the first to pay attention to this fundamental fact. Later, magnetoelastic waves were studied by Kittel [222], Akhiezer, Bar'yakhtar,

and Peletminskii [12] (see also [14]), Vlasov and Ishmukhametov [424], and Schlömann [340].

### 12.3.1 Normal waves

We will restrict ourselves to a *cubic* ferromagnet (regarded as elastically isotropic) magnetized to saturation along the  $\langle 100 \rangle$  axis; equations (12.24) and (12.25) hold in this case. To get the *dispersion law* for normal magnetoelastic waves we must linearize these equations and substitute  $M_{x,y} = m_{0x,y} \exp(i\omega t - i\mathbf{k}\mathbf{r})$  and  $u_{x,y,z} = u_{0x,y,z} \exp(i\omega t - i\mathbf{k}\mathbf{r})$  into them. Then we obtain a system of five coupled homogeneous linear algebraic equations for complex amplitudes  $m_{0x,y}$  and  $u_{0x,y,z}$ .<sup>3</sup> The condition of compatibility of these equations will yield the dispersion law.

In the case of  $\mathbf{k} \parallel \mathbf{M}_0$ , the dipole-dipole field  $\mathbf{H}_M$  vanishes, as one can see from (7.12). Neglecting the magnetocrystalline anisotropy, we obtain from the linearized equations (12.24) and (12.25)

$$\begin{aligned} i\omega m_x + \gamma (H_0 + Dk^2) m_y - i\gamma k B_2 u_y &= 0 \\ i\omega m_y - \gamma (H_0 + Dk^2) m_x + i\gamma k B_2 u_x &= 0 \\ \omega^2 \rho u_x - k^2 c_{44} u_x - ik \frac{B_2}{M_0} m_x &= 0 \\ \omega^2 \rho u_y - k^2 c_{44} u_y - ik \frac{B_2}{M_0} m_y &= 0 \end{aligned} \quad (12.32)$$

$$\omega^2 \rho u_z - k^2 c_{11} u_z = 0. \quad (12.33)$$

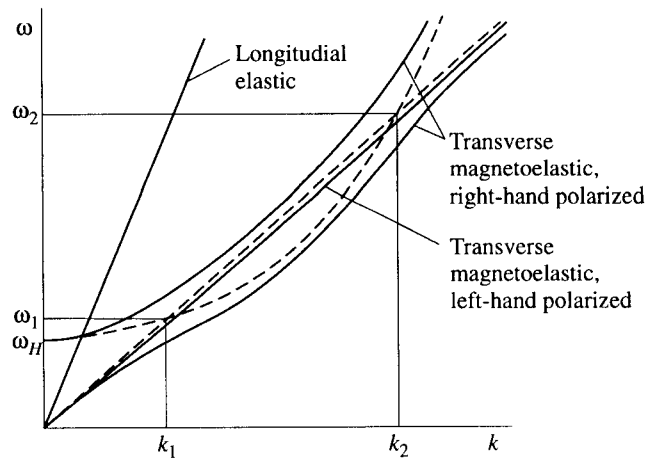
Equation (12.33) is decoupled from the others and describes a *pure elastic* longitudinal wave with linear dispersion relation and velocity (12.14). The system of four coupled equations (12.32) describes transverse *magnetoelastic* waves. After turning to circular variables  $m_{\pm} = m_x \pm im_y$  and  $u_{\pm} = u_x \pm iu_y$ , system (12.32) reduces to two independent systems for components with different senses of rotation. The condition of compatibility of equations in each system results in the equation

$$(\omega \mp \omega_m) (\omega^2 - \omega_{el\perp}^2) \mp \frac{\gamma B_2^2}{\rho M_0} k^2 = 0. \quad (12.34)$$

Here,  $\omega_m = \gamma (H_0 + Dk^2)$  is the frequency of an unperturbed spin wave,  $\omega_{el\perp} = v_{\perp} k \equiv \sqrt{c_{44}/\rho} k$  is the frequency of an unperturbed transverse elastic wave, the upper and the lower signs relate to the waves with right-hand and left-hand circular polarization, respectively.

Equation (12.34) has the form characteristic of all *coupled* waves. In the absence of coupling ( $B_2 = 0$ ), it gives the dispersion curves of the unperturbed waves.

<sup>3</sup>The subscripts 0 will be omitted hereafter.

**FIGURE 12.2**

Dispersion characteristics for normal magnetoelastic waves propagating in a cubic crystal in the direction of  $\mathbf{M}_0$ , which coincides with the  $\langle 100 \rangle$  axis. Dashed curves correspond to uncoupled magnetic and transverse elastic waves.

They *cross* at two values  $k_1$  and  $k_2$  of the wave number (Figure 12.2), which are the roots of the equation  $\omega_m = \omega_{e\perp}$ . The corresponding frequencies  $\omega_1$  and  $\omega_2$  are called sometimes the frequencies of magnetoelastic (or magnetoacoustic) resonance. At not-too-large  $H_0$  values and, hence, at sufficiently low frequencies (for YIG, at frequencies lower than  $\sim 100$  GHz),

$$k_1 \simeq \frac{\omega H}{v_{\perp}} \quad k_2 \simeq \frac{v_{\perp}}{\gamma D}. \quad (12.35)$$

The last term in (12.34) can be written as  $\xi \gamma M_0 \omega_{e\perp}^2$  where

$$\xi = \frac{B_2^2}{c_{44} M_0^2} \quad (12.36)$$

is a dimensionless coupling parameter. Usually  $\xi \ll 1$ , e.g.,  $\xi = 3.3 \times 10^{-3}$  for YIG at room temperature.

The spectrum of magnetoelastic waves with *right-hand* polarization, which is obtained by solving equation (12.34) with the upper signs, contains *two branches* (Figure 12.2). They can be regarded (in terms of coupled modes) as a result of the repelling of spin-wave and elastic-wave dispersion curves. The separation  $\delta\omega$  of the frequencies of two branches is minimal at the crossing points  $k_1$  and  $k_2$ . At the lower point

$$\delta\omega_1 = \gamma \sqrt{2\xi M_0 (H_0 + Dk_1^2)}. \quad (12.37)$$

So, the minimal fractional separation is of the order of  $\xi^{1/2}$ .

The spectrum of the *left-hand* polarized magnetoelastic wave, which is the solution of (12.34) with lower signs, has one branch (Figure 12.2). It differs only slightly from the dispersion curve of the transverse elastic wave. Thus, in the considered case, there are *three normal waves*: a right-hand circularly polarized magnetoelastic wave (with spectrum consisting of two branches), a left-hand circularly polarized magnetoelastic wave, and a longitudinal pure elastic wave.

The  $m$  and  $u$  components for normal magnetoelastic waves can be found from the linearized equations (12.32) and (12.33). The longitudinal elastic wave has only the component  $u_z$ . For the left-hand polarized wave the magnetic component  $m_-$  is, of course, very small. For the right-hand polarized magnetoelastic wave

$$\left| \frac{m_+}{u_+} \right| = \left| \frac{\gamma B_2 k}{\omega - \omega_m} \right| = \left| \frac{(\omega^2 - \omega_{el\perp}^2) \rho M_0}{B_2 k} \right|. \quad (12.38)$$

One can see from (12.38) that, far from the crossing points,  $m_+$  is small and  $u_+$  is large at the segments ('half-branches') at which  $\omega$  is close to  $\omega_{el\perp}$ . On the contrary,  $m_+$  is large and  $u_+$  is small at the half-branches at which  $\omega$  is close to  $\omega_m$ . These half-branches (and the waves at them) can be named, respectively, *quasielastic* and *quasimagnetic*. The magnetic-energy flow density can be expressed as [348]

$$\Pi_m = \frac{1}{2} \frac{H_0}{M_0} m_+^2 v_{m\text{gr}} \quad (12.39)$$

where  $v_{m\text{gr}}$  is the magnetic (spin) wave group velocity. It can be shown, with the help of (12.39) and (12.16), that  $\Pi_{el}$  dominates at quasielastic half-branches,  $\Pi_m$  dominates at quasimagnetic branches, and these flows are equal at the crossing points.

The difference in  $k$  values of magnetoelastic waves with different senses of polarization rotation leads, as in the case of electromagnetic waves (Section 4.2), to the turn of polarization of an elliptically, in particular, of a linearly polarized wave, i.e., to the Faraday effect [424, 271].

Consider now the waves propagating in the direction *perpendicular* to the steady magnetization. In this case, it follows from the linearized equations (12.24) and (12.25) that there are also three normal waves: a longitudinal pure elastic wave, a transverse pure elastic wave with  $\mathbf{u} \perp \mathbf{M}_0$ , and a transverse magnetoelastic wave with  $\mathbf{u} \parallel \mathbf{M}_0$ . The dispersion equation for the magnetoelastic wave is

$$(\omega^2 - \omega_m^2) (\omega^2 - \omega_{el\perp}^2) - \frac{\gamma B_2^2}{\rho M_0} \omega_M k^2 = 0 \quad (12.40)$$

where now  $\omega_m = [(\omega_H + Dk^2) (\omega_H + Dk^2 + \omega_M)]^{1/2}$  is the frequency of a spin wave with  $\theta_k = \pi/2$ . The spectrum determined by (12.40) consists of two branches nearing each other at the points of crossing of the unperturbed magnetic and elastic dispersion curves. The minimal separation  $\delta\omega$  of the branches at the lower crossing point is of the same order as  $\delta\omega_1$  given by (12.37).

Far from the crossing points, the half-branches of the spectrum are quasimagnetic or quasielastic. On the quasimagnetic half-branches, the magnetic components  $m_x$  and  $m_y$  prevail, and on the quasielastic half-branches, the elastic component  $u_z$  prevails. Suppose that, 'at the input' of a certain section of a ferromagnet, there is a transverse magnetoelastic wave with polarization different from polarizations of the above-considered normal waves, i.e., with  $\mathbf{u}$  directed at an arbitrary angle with respect to  $\mathbf{M}_0$ . Then, the polarization of the propagating wave will transform, similar to such a transformation of an electromagnetic wave that propagates perpendicularly to  $\mathbf{M}_0$  (Section 4.2).

For arbitrary directions of  $\mathbf{M}_0$  (with respect to the cubic axes) and of  $\mathbf{k}$  (with respect to  $\mathbf{M}_0$ ), the situation is found to be much more complicated. Magnetoelastic-wave spectra now depend on  $B_2$  and  $B_1$ ; independence of  $B_1$  takes place only if both vectors  $\mathbf{M}_0$  and  $\mathbf{k}$  are directed along the  $\langle 100 \rangle$  axes. For  $\theta_k$  not equal to zero or  $\pi/2$ , as well as for  $\theta_k$  equal to zero or  $\pi/2$  but  $\mathbf{M}_0$  not parallel to  $\langle 100 \rangle$  or  $\langle 110 \rangle$ , the *longitudinal* elastic wave is also coupled with magnetic waves.

### 12.3.2 Damping and excitation

To allow for damping of magnetoelastic waves we have to insert, into equations of motion or directly into dispersion relations, the parameters that describe dissipation in magnetic and elastic systems. For example, the replacements  $\omega_m \rightarrow \omega_m + i\omega_m''$  and  $\omega_{el} \rightarrow \omega_{el} + i\omega_{el}''$  can be made. Then, if the losses are *small*, we get, e.g., in the case of  $\mathbf{k} \parallel \mathbf{M}_0$ ,

$$\omega'' = \frac{2\omega_{el}(\omega - \omega_m)\omega_{el}'' + (\omega^2 - \omega_{el}^2)\omega_m''}{2\omega(\omega - \omega_m) + (\omega^2 - \omega_{el}^2)}. \quad (12.41)$$

One can see that magnetic and elastic losses are additive in this approximation, and, near the crossing points,  $\omega'' = (\omega_m'' + \omega_{el}'')/2$ . Far from the crossing points,  $\omega'' \simeq \omega_m''$  at the quasimagnetic half-branches, and  $\omega'' \simeq \omega_{el}''$  at the quasielastic half-branches. The wave decrement  $k''$  can be found using formula (6.7).

It should be emphasized that this is true only in the case of small losses. For *arbitrary losses*, as in the case of pure spin waves (Section 7.1), the complex dispersion equation must be solved. For stationary waves,  $\omega$  in this equation is real, and  $k = k' - ik''$ . It turns out that branches of the dependence  $\omega(k', k'')$  repel only if the losses do not exceed certain values. In the opposite case, the branches intersect. This general property of any coupled waves will also be discussed in Section 14.2 for coupled spin-electromagnetic waves in metals.

Magnetoelastic waves can be *excited* either 'magnetically', when ac magnetization is directly excited by ac magnetic field, or 'elastically', when ac elastic displacement is directly excited by some mechanic forces. *Elastic* excitation (as well as receiving) can be realized, e.g., with the use of a piezoelectric transducer pasted to the ferrite sample, as in Figure 9.3(b). *Magnetic* excitation of magnetoelastic waves always takes place, strictly speaking, when spin waves are to be

excited, e.g., in films (Sections 6.2 and 7.2). But in most cases, the waves are excited at quasimagnetic half-branches, far from crossing points, and the elastic displacements can be neglected, as well as the influence of magnetoelastic coupling on the spectrum.

Another method of magnetic excitation of magnetoelastic waves is the excitation by a uniform ac magnetization, which becomes possible owing to *boundary conditions*. Consider, following Le Craw and Comstock [249], a thin ferromagnetic plate magnetized normally to its surface (in  $z$  direction) and put in a uniform ac magnetic field. The right-hand circular ac magnetization excited by this field is regarded as given. For oscillations depending only on  $z$ , we can find from (12.24) and (12.25), neglecting the exchange interaction, the equation

$$\omega^2 \rho u_+ + \left( c_{44} + \frac{\gamma B_2^2}{M_0(\omega - \omega_H)} \right) \frac{\partial^2 u_+}{\partial z^2} = 0. \quad (12.42)$$

It *does not contain*  $m_+$ , but this component comes into play through the boundary conditions. Assuming the surfaces of the plate to be free, we use the boundary conditions (12.17). To find the stresses that appear in these conditions we use the expressions obtained from (12.7) by the substitution  $U_{el} \rightarrow U_{el} + U_{mel}$ . Then, using (2.10) and (2.18), we get the boundary condition

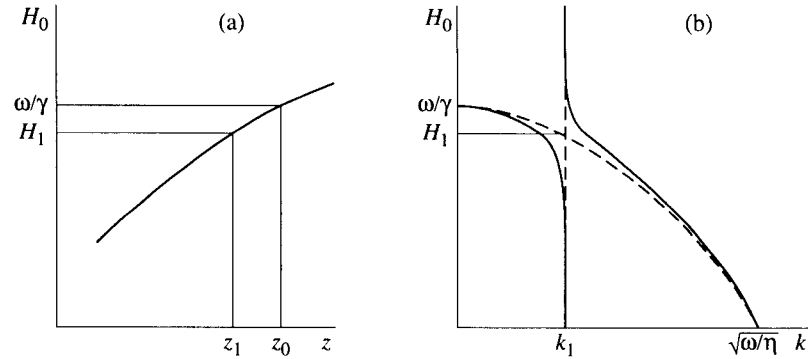
$$\left( c_{44} + \frac{\gamma B_2^2}{M_0(\omega - \omega_H)} \right) \frac{\partial u_+}{\partial z} + \frac{B_2}{M_0} m_+ = 0. \quad (12.43)$$

Thus, the problem is reduced to solving a *homogeneous* (i.e., without a driving term) equation (12.42) subject to a *nonhomogeneous* boundary condition (12.43). Note that in the problem of standing spin waves (Section 7.2) the boundary conditions were homogeneous, but the equation was nonhomogeneous, it contained the given ac field.

Solution of (12.42) subject to (12.43) shows [249] that  $u_+$  in the plate is a sum of a uniform displacement and an infinite number of resonance terms, which correspond to standing magnetoelastic waves. Such a plate can be used as a transducer for excitation of transverse circularly polarized elastic waves.

### 12.3.3 Magnetoelastic waves in nonuniform steady magnetic field

So far, studying magnetoelastic waves, we assumed the internal steady magnetic field to be uniform within the sample. Nonuniformity of this field results in some new phenomena, one of which is the transformation of quasimagnetic waves into quasielastic and vice versa. Consider, e.g., a right-hand circularly polarized wave propagating along  $M_0$ . The spectrum of this wave is plotted in Figure 12.3(a) in coordinates  $H_0(k)$  at  $\omega = \text{const}$ . If the field  $H_0$  depends on coordinate  $z$  in the direction of propagation, as shown in Figure 12.3(b), the character of the wave will change with its propagation. Assume that the dependence  $H_0(z)$  is *smooth* enough, so that the condition (7.60) is satisfied. Then the wave will all the time

**FIGURE 12.3**

Magnetoelastic waves in nonuniform steady magnetic field  $H_0$ : (a) dependence of  $H_0$  on a coordinate in the direction of propagation, coinciding with the  $\mathbf{H}_0$  direction; (b) dispersion characteristics  $H_0(k)$  at  $\omega_k = \text{const}$ .

belong to the same branch of the spectrum and, therefore, will *transform* from quasimagnetic into quasielastic or vice versa in passing the crossing point.

If, on the contrary, the field *gradient is large*, so that inequality (7.60) is not satisfied, then partial excitation of a wave at the other branch will take place near the crossing. Hence, the complete transformation of the character of the wave, as it passes the crossing point, *will not occur*. These qualitative considerations are confirmed by the theory developed by Schlömann and Joseph [346–348]. It should be noted that, in these considerations, we have used the ‘language’ of normal modes. In terms of coupled modes, they would sound in the following manner: in passing the crossing point, the spin wave transforms partly into the elastic wave (or vice versa) due to coupling between them; the transformation is more complete the smaller the  $H_0$  gradient and, hence, the larger the length and the time of interaction.

Nonuniform internal steady magnetic field  $H_0$  can be realized, e.g., in a cylindrical ferrite rod placed into uniform external field  $H_{e0}$ . It was pointed out in Section 7.2 that ‘turning surfaces’ (where  $H_0 = \omega/\gamma$ ) are present in such rod at appropriate  $H_{e0}$  values. Near such a surface ( $z = z_0$  in Figure 12.3), a spin wave (or, strictly speaking, a quasimagnetic magnetoelastic wave) arises, in a uniform ac magnetic field, and propagates towards the crossing surface  $z = z_1$ . Passing this surface, it transforms into a quasielastic (practically, very near pure elastic) wave. Similar transformation takes place in the case of  $\mathbf{k} \perp \mathbf{M}_0$ , which can be realized in a normally magnetized ferrite disk (Section 7.2.). Both ‘geometries’ can be used in designing magnetoelastic microwave delay lines. Great attention was paid in the 1960s to the investigation of such delay lines (e.g., [387]). But this problem later lost its urgency because of the development of delay lines using magnetostatic waves in films (Section 6.2).

## 12.4 Parametric excitation of magnetoelastic waves

In the present section the effect of magnetoelastic coupling on the parametric-excitation processes (studied in detail, but without allowance for this coupling, in Chapter 10) will be considered. Two kinds of problems arise here: (i) the allowance for the fact that the parametrically excited modes are *not pure magnetic* but magnetoelastic, (ii) the investigation of the parametric excitation *caused* by magnetoelastic interaction. Let us consider first the former problem.

### 12.4.1 Longitudinal pumping of magnetoelastic waves

The magnetoelastic coupling should result in the *increase* of the longitudinal-pumping threshold. This becomes especially clear if we use the coupled-mode 'language': the parametrically excited spin waves excite linearly the elastic waves, and, therefore, the damping of spin waves and, hence, the threshold increase. It is evident that the increase becomes essential as the *crossing point* is approached.

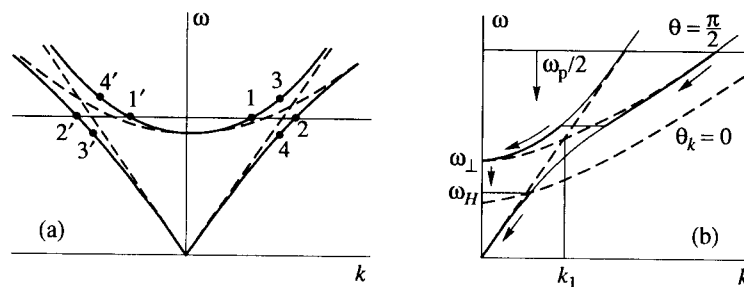
The presence of two magnetoelastic branches allows the conservation laws for longitudinal pumping to be satisfied in a degenerate, as well as in a nondegenerate, case [Figure 12.4(a)]. But the threshold in the degenerate case usually is lower.

Suppose now that, at a constant value of the steady field, the pumping frequency is varied [Figure 12.4(b)]. If  $\omega_p/2$  essentially exceeds the crossing frequency  $\omega_1$ , the waves at quasimagnetic branch are excited, and the threshold is, practically, the same as without allowance for magnetoelastic coupling. As  $\omega_p/2$  approaches  $\omega_1$ , the threshold increases, and at  $\omega_p/2 \simeq \omega_1$  the threshold point jumps onto another branch [Figure 12.4(b)] where the threshold is now lower. With further decrease of  $\omega_p$ , the threshold lowers approaching its pure magnetic value. At  $\omega_p/2 < \omega_H$  the parametric excitation of spin waves, without magnetoelastic interaction, is impossible. This interaction being taken into account, the waves on the quasielastic branch can be excited but with very high threshold. The sharp peak of  $h_{z \text{ thr}}$ , at the point of crossing of pure magnetic and elastic dispersion curves, was first observed by Turner [408] and then investigated theoretically by Morgenthaler [290].

We will restrict our treatment to the case for which equations (12.24) and (12.25) are valid. From these equations, for a wave with components  $M_x$ ,  $M_y$ , and  $u_z$  propagating in the  $x$  direction, it follows that

$$\begin{aligned}
 \frac{\partial M_x}{\partial t} &= - \left( \omega_H - \gamma D \frac{\partial^2}{\partial x^2} + \gamma h_z \cos \omega_p t \right) M_y \\
 \frac{\partial M_y}{\partial t} &= \left( \omega_H + \omega_M - \gamma D \frac{\partial^2}{\partial x^2} + \gamma h_z \cos \omega_p t \right) M_x + \gamma B_2 \frac{\partial u_z}{\partial x} \\
 \rho \frac{\partial^2 u_z}{\partial t^2} &= c_{44} \frac{\partial^2 u_z}{\partial x^2} + \frac{B_2}{M_0} \frac{\partial M_x}{\partial x}.
 \end{aligned} \tag{12.44}$$



**FIGURE 12.4**

Parametric excitation of magnetoelastic waves under longitudinal pumping. (a) The spectrum of magnetoelastic waves propagating perpendicularly to  $\mathbf{M}_0$ , points indicate the frequencies of unstable-wave pairs: degenerate (1, 1' and 2, 2') and nondegenerate (3, 3' and 4, 4'). (b) Movement of the frequencies of a degenerate pair with decreasing pumping frequency.

To find the threshold value of  $h_z$  we will *not* (as distinct from Chapter 10) turn from  $M_x$ ,  $M_y$ , and  $u_z$  to normal variables. We will directly examine the solutions of (12.44) which correspond to the parametrically excited waves with frequency  $\omega_p/2$  and wave vectors  $x_0 k$  and  $-x_0 k$ . The condition for threshold is that these waves *do not damp in spite of losses*.

The solutions, as yet without losses, are

$$M_{x,y} = \text{Re} \left[ m_{k\ x,y} \exp \left( i \frac{\omega_p}{2} t - ikx \right) + m_{-k\ x,y} \exp \left( i \frac{\omega_p}{2} t + ikx \right) \right]$$

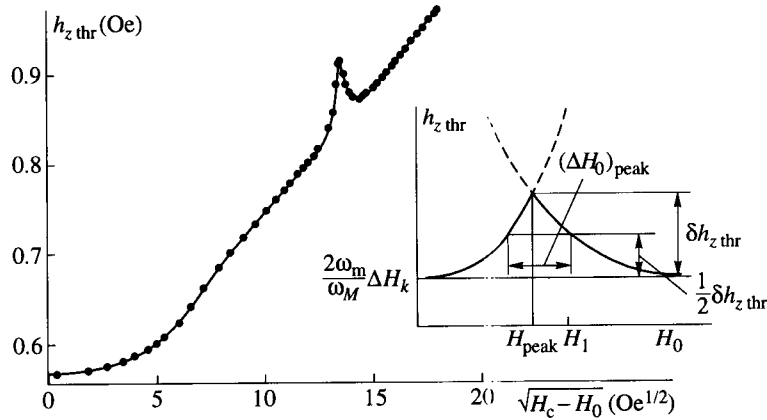
$$u_z = \text{Re} \left[ u_{k\ z} \exp \left( i \frac{\omega_p}{2} t - ikx \right) + u_{-k\ z} \exp \left( i \frac{\omega_p}{2} t + ikx \right) \right]. \quad (12.45)$$

Substituting (12.45) into (12.44), allowing for losses by replacements  $\omega_m \equiv [(\omega_H + Dk^2)(\omega_H + \omega_M + Dk^2)]^{1/2} \rightarrow \omega_m + i\omega_m''$  and  $\omega_{el} \equiv \sqrt{c_{44}/\rho} \rightarrow \omega_{el} + i\omega_{el}''$ , and equating to zero the determinant of the obtained system of six algebraic equations, we can obtain an expression for  $h_{z\ \text{thr}}$  values at both branches of the magnetoelastic spectrum. The analysis of this expression supports the qualitative conclusions made above.

Near the crossing point, the mentioned general expression for  $h_{z\ \text{thr}}$  reduces to [290]

$$h_{z\ \text{thr}} \cong \min \left\{ \frac{2\omega_m}{\omega_M} \Delta H_k + 2 \frac{\omega_m^2 - \omega_p^2/4}{\omega_{el}^2 - \omega_p^2/4} \frac{\omega_{el}^2}{Q_{el}\gamma\omega_M} \right\} \quad (12.46)$$

where  $Q_{el} = \omega_{el}/(2\omega_{el}'')$  is the elastic quality factor,  $\Delta H_k = 2\omega_m''/\gamma$ , and 'min' means that the lowest value must be chosen from two  $h_{z\ \text{thr}}$  values at different branches. When these values become equal, the jump of the threshold point occurs from one branch onto the other. It is easy to make sure that the second term in the braces in (12.46) is always positive, so that the magnetoelastic coupling always results in increasing the threshold.



**FIGURE 12.5**

Dependence of the threshold field, for longitudinal pumping of magnetoelastic waves, on the internal steady magnetic field  $H_0$ . Points represent experimental data for a YIG sphere with  $\mathbf{M}_0 \parallel \langle 100 \rangle$  at 194 K and  $f_p = 23.2$  GHz [304]. The inset shows the threshold field values near the crossing point calculated with formula (12.46).

An experimental dependence of  $h_{z \text{ thr}}$  on the steady magnetic field at  $\omega_p = \text{const}$  is plotted in Figure 12.5. The inset shows this dependence in a small  $H_0$  range calculated with formula (12.46). One can see that the intersection of  $h_{z \text{ thr}}$  vs  $H_0$  curves for two branches, and so, the threshold maximal value occurs at the field  $H_{\text{peak}}$  somewhat smaller than the field  $H_1$  at which the unperturbed magnetic and elastic dispersion curves cross at frequency  $\omega_p/2$ . The expression for  $H_1$  follows from the conditions  $\omega_m = \omega_{\text{el}} = \omega_p/2$ :

$$H_1 = H_c - \frac{D\omega_p^2}{4v_{\perp}^2}. \quad (12.47)$$

The parameters of the curve  $h_{z \text{ thr}}$  vs  $H_0$  (Figure 12.5, inset) can be obtained from (12.46):

$$\delta H_{z \text{ thr}} = \frac{D\omega_p^2}{v_{\perp}^2 Q_{\text{el}}} \left( \frac{1}{2} + \frac{\gamma H_1}{\omega_M} \right) \quad (12.48)$$

$$(\Delta H_0)_{\text{peak}} = \frac{\gamma B_2 \omega_p}{v_{\perp}^2 \omega_M} \sqrt{\frac{\pi D H_1}{\rho (1/2 + \gamma H_1 / \omega_M)}} \quad (12.49)$$

$$H_1 - H_{\text{peak}} = \frac{\gamma \Delta H_k Q_{\text{el}} (\Delta H_0)_{\text{peak}}}{2\omega_M (H_c - H_1)} \sqrt{1 + \frac{\omega_M}{\gamma H_1}}. \quad (12.50)$$

Using these expressions, the values of  $B_2$ ,  $Q_{\text{el}}$ , and  $D$  can be found (however, with low precision) from experimental curves  $h_{z \text{ thr}}$  vs  $H_0$ .

We have considered in some detail the case of  $M_0 \parallel \langle 100 \rangle$ . In other cases, in particular when  $M_0 \parallel \langle 111 \rangle$ , the longitudinal elastic wave is also coupled, as pointed out in the previous section, to the magnetic system. Then, *two* magnetoelastic peaks, transverse and longitudinal, are observed on the curves  $h_{z \text{ thr}} \text{ vs } H_0$ .

Magnetoelastic waves are the modes that are actually excited under transverse pumping, as well. The influence of this circumstance on the threshold values is essential, of course, only near the crossings of magnetic and elastic spectra. In both cases, of longitudinal and transverse pumping, the excitation of waves at the lower *quasielastic* half-branch [Figure 12.4(b)] is possible at low frequencies ( $\omega_p/2 < \omega_H$ ). Such parametric excitation was observed [405] under transverse pumping at frequency  $f_p = 1.32$  GHz in a hexaferrite single-crystal sphere.

#### 12.4.2 Parametric excitation caused by magnetoelastic coupling

Now the magnetoelastic nonlinearity is the *reason* of parametric excitation. The excited waves may also be magnetoelastic. But, if the magnetoelastic coupling is *absent* in linear approximation, the excited waves are pure magnetic or pure elastic. This case is of the most interest, especially when the parametric excitation caused by pure magnetic nonlinearity is impossible.

As an example, consider parametric excitation, under uniform transverse pumping, of spin and longitudinal elastic waves propagating in the direction of  $M_0$ , which coincides with the  $\langle 100 \rangle$  axis in a cubic crystal. From equations (12.24) and (12.25), assuming magnetic and elastic isotropy, we get in the present case the following system:

$$\begin{aligned} \frac{\partial M_x}{\partial t} &= - \left( \omega_H + \gamma D \frac{\partial^2}{\partial z^2} - 2 \frac{B_1}{M_0} \frac{\partial u_z}{\partial z} \right) M_y \\ \frac{\partial M_y}{\partial t} &= \left( \omega_H + \gamma D \frac{\partial^2}{\partial z^2} - 2 \frac{B_1}{M_0} \frac{\partial u_z}{\partial z} \right) M_x \\ \rho \frac{\partial^2 u_z}{\partial t^2} &= c_{11} \frac{\partial^2 u_z}{\partial z^2} - \frac{B_1}{M_0^2} \frac{\partial}{\partial z} (M_x^2 + M_y^2). \end{aligned} \quad (12.51)$$

Here,  $M_x$  and  $M_y$  contain the components of uniform pumping magnetization and the components of the excited spin wave with the wave vector  $\mathbf{k} = z_0 \mathbf{k}$ . The excited elastic wave has (as the pumping is uniform) the wave vector  $\mathbf{q} = -z_0 \mathbf{k}$ . Assuming the pumping magnetization to be circularly polarized with right-hand rotation, we may write

$$\begin{aligned} M_x &= M_0 a_0^0 \cos \omega_p t + \text{Re} [m_{k_x} \exp(i\omega_1 t - ikz)] \\ M_y &= M_0 a_0^0 \sin \omega_p t + \text{Re} [m_{k_y} \exp(i\omega_1 t - ikz)] \\ u_z &= \text{Re} [u_{-k} \exp(i\omega_2 t + ikz)]. \end{aligned} \quad (12.52)$$

Substituting (12.52) into (12.51), we obtain a system of equations in  $m_{kx}$ ,  $m_{ky}$ , and  $u_{-k}^*$  containing the pumping amplitude  $a_0^0$ . Allowing for losses, as usual, by replacements  $\omega_1 \rightarrow \omega_1 + i\gamma\Delta H_k/2$  and  $\omega_2 \rightarrow \omega_2 + i\omega_2/(2Q_{el})$ , we find from the condition of compatibility of the equations that

$$a_{0\text{thrmel}}^0 = \frac{1}{B_1} \sqrt{\frac{c_{11}M_0\Delta H_k}{Q_{el}}}. \quad (12.53)$$

The dissipation parameters  $\Delta H_k$  and, especially,  $1/Q_{el}$  decrease with decreasing  $k$ . Therefore, low threshold should be observed at such values of  $\omega_p$  and  $H_0$  at which  $k \rightarrow 0$ . However, the plane-wave theory is not applicable for small  $k$  values, and *eigenmodes* of the sample, magnetic and elastic, are excited. For a sphere, these are the Walker modes (Section 6.3) and some of the lowest elastic modes (Section 12.1). The threshold amplitude, in this case, is of the order of (12.53).

If the pumping frequency is high enough, so that the magnetic parametric-excitation process of the first order at ferromagnetic resonance is forbidden (Section 10.2), it is worthwhile to compare the threshold (12.53) with the threshold (10.26) for the *second-order* magnetic process. An estimate shows that, for YIG, the ratio  $a_{0\text{thrmel}}^0/a_{0\text{thr2}}^0$  can be as small as 0.1, provided that  $Q_{el}$  is not reduced by an external mechanical load. Just under this condition, the considered magnetoelastic parametric excitation of an elastic mode (named the magnetoacoustic resonance, MAR) was observed in a YIG sphere by Spencer and Le Graw [380].

Spin waves excited parametrically under longitudinal or transverse magnetic pumping can act as pumping for magnetoelastic parametric excitation [188]. This effect was named the secondary MAR.

### 12.4.3 Elastic pumping

The role of pumping in parametrical excitation of magnetoelastic waves can also be played by an elastic mode. Consider again the case of  $M_0 \parallel \langle 100 \rangle$ . Assume that the pumping wave is a *longitudinal elastic* wave that propagates along  $M_0$  (in  $z$  direction), and the excited waves are magnetoelastic waves with wave vectors  $k_1$  and  $k_2$  propagating in  $xz$  plane. Suppose that  $k_{1,2} \gg q_p$  and, hence,  $k_{1x} \simeq k_{2x} \equiv k$ . Then, equations (12.24) will take the form

$$\begin{aligned} \frac{\partial M_x}{\partial t} &= - \left( \omega_H + \gamma D k^2 - \frac{2\gamma B_1}{M_0} \frac{\partial u_z}{\partial z} \right) M_y \\ \frac{\partial M_y}{\partial t} &= \left( \omega_H + \gamma D k^2 - \frac{2\gamma B_1}{M_0} \frac{\partial u_z}{\partial z} \right) M_x \end{aligned} \quad (12.54)$$

where  $u_z = u_p \cos(\omega_p t - q_p z)$  is a given quantity.

Comparing (12.54) with the equations of motion for longitudinal magnetic pumping (Section 10.3), we see that the elastic pumping wave is equivalent to

magnetic longitudinal field

$$h_{z\text{ef}} = -\frac{2B_1}{M_0} \frac{\partial u_z}{\partial z} \equiv -\frac{2B_1}{M_0} q_p u_p \sin(\omega_p t - q_p z). \quad (12.55)$$

As  $q_p$  is small, we may ignore the wave nature of this field and, regarding the excited waves as pure magnetic, use formula (10.42). Then, we get

$$u_{p\text{thr}} = \frac{v_{\parallel} \Delta H_k}{4\pi\gamma B_1} \quad (12.56)$$

where  $v_{\parallel}$  is the longitudinal elastic-wave velocity (12.14). Estimating, with the use of (12.16), the threshold value of the elastic energy flow, we find for YIG the value of  $\sim 0.1 \text{ W cm}^{-2}$ , which does not contradict the experiment [272]. For pumping of spin (strictly speaking, quasimagnetic) waves by transverse elastic wave, the threshold turns out to be almost the same as in the above-considered case. The threshold for excitation of elastic and magnetic, or of two elastic, waves are much higher [258].

## 12.5 Spin-lattice relaxation

The energy of magnetic oscillations and waves is ultimately transferred, mostly, to the crystal lattice. This transfer is performed, as pointed out in Section 11.1, by direct and indirect spin-lattice relaxation processes. Indirect processes will be studied in Chapters 13 and 14. In the present section we consider the direct processes, the cause of which is the magnetoelastic interaction.

Because of the noncoherent, statistical nature of spin-lattice relaxation processes the quantum-mechanical approach is to be used in the theory of these processes. The theory based on the Heisenberg model of ferromagnet (Section 1.1) was developed by Akhiezer in his famous work [10] repeatedly cited above.

In this theory, the operator  $\hat{r}_f$  of a spin radius-vector ( $f$  denotes the lattice site) is presented, analogously to (12.1), in the form of  $\hat{r}_f = \hat{r}_{f0} + \hat{u}_f$ , and the Heisenberg Hamiltonian is expanded in series in terms of the displacement operator  $\hat{u}_f$ . Limiting the treatment to the zero- and first-order terms in this series, we turn from spin operators  $\hat{S}_f$ , as in Section 7.4, to the operators  $\hat{a}_k^+$  and  $\hat{a}_k$ , and from operators  $\hat{u}_f$ , to the operators  $b_q^+$  and  $b_q$  of creation and annihilation of phonons. The Hamiltonian, then, takes the form

$$\hat{\mathcal{H}} = \hat{\mathcal{H}}_0 + \hat{\mathcal{H}}_{\text{mel}2} + \hat{\mathcal{H}}_{\text{mel}3} + \dots \quad (12.57)$$

where  $\hat{\mathcal{H}}_0$  is the unperturbed Hamiltonian used in Section 7.4 and 11.2 and the other terms describe the magnetoelastic interaction. They contain operators  $b_q^+$  and  $b_q$  in the first power, and the operators  $\hat{a}_k^+$  and  $\hat{a}_k$  in the increasing powers: the term  $\hat{\mathcal{H}}_{\text{mel}2}$ , in the first power,  $\hat{\mathcal{H}}_{\text{mel}3}$ , in the second power, and so on.

However, the *main* source of the magnetoelastic coupling, the *spin-orbital* interaction, cannot be treated on the basis of the Heisenberg model, which does not involve orbital moments. Abrahams and Kittel [2] proposed to evolve a quantum-mechanical theory of magnetoelastic relaxation using *phenomenological* expressions, e.g., (12.18), for the magnetoelastic energy. This proposal was realized by Kaganov and Tsukernik [200].

In this theory the projections of  $\mathbf{M}$  and  $\mathbf{u}$  in (12.18) (regarded as operators) are expressed in terms of the operators  $\hat{a}_k^+$ ,  $\hat{a}_k$  and  $\hat{b}_j^+$ ,  $\hat{b}_j$ , respectively. According to [200] (see also [14]),

$$\hat{\mathbf{u}} = \sqrt{\frac{\hbar}{2\rho V}} \sum_j \sum_q \frac{\mathbf{p}_{0qj}}{\omega_{qj}} \left[ \hat{b}_{qj} \exp(-i\mathbf{q}\mathbf{r}) + \hat{b}_{qj}^+ \exp(i\mathbf{q}\mathbf{r}) \right]. \quad (12.58)$$

Here,  $\rho$  is the mass density,  $V$  is the sample volume,  $\mathbf{p}_{0qj}$  ( $j = 1, 2, 3$ ) are the unit vectors of phonon polarization, showing the directions of  $\mathbf{u}$  for each of three normal elastic waves with a given wave vector  $\mathbf{q}$ , and  $\omega_{qj}$  are the frequencies of these waves.

Consider an isotropic medium, i.e., assume in (12.18)  $B_1 = B_2 \equiv B$ . Then, using (12.58) and the formulae that express  $\mathbf{M}$  projections in terms of  $\hat{a}_k$  and  $\hat{a}_k^+$  (Section 7.4), we obtain from (12.18) the Hamiltonian in the form (12.57) where

$$\hat{\mathcal{H}}_{\text{mel}2} = \sum_j \sum_{\mathbf{k}} \sum_{\mathbf{q}} \left( \Psi_{\mathbf{k},\mathbf{q}j} \hat{a}_{\mathbf{k}} \hat{b}_{\mathbf{q}j}^+ + \text{H. c.} \right) \Delta(\mathbf{k} - \mathbf{q}) \quad (12.59)$$

$$\begin{aligned} \hat{\mathcal{H}}_{\text{mel}3} = & \sum_j \sum_{\mathbf{k}_1} \sum_{\mathbf{k}_2} \sum_{\mathbf{q}} \left[ \left( \Psi_{\mathbf{k}_1\mathbf{k}_2,\mathbf{q}j} \hat{a}_{\mathbf{k}_1} \hat{a}_{\mathbf{k}_2} \hat{b}_{\mathbf{q}j}^+ + \text{H. c.} \right) \Delta(\mathbf{k}_1 + \mathbf{k}_2 - \mathbf{q}) \right. \\ & \left. + \left( \Psi_{\mathbf{k}_1,\mathbf{k}_2,\mathbf{q}j} \hat{a}_{\mathbf{k}_1} \hat{a}_{\mathbf{k}_2}^+ \hat{b}_{\mathbf{q}j}^+ + \text{H. c.} \right) \Delta(\mathbf{k}_1 - \mathbf{k}_2 - \mathbf{q}) \right]. \quad (12.60) \end{aligned}$$

Here, H.c. denotes the Hermitian conjugate of the quantity written before it, and  $\Delta$  is the Kronecker symbol (Appendix C); the expressions for the amplitudes  $\Psi_{\mathbf{k},\mathbf{q}j}$ ,  $\Psi_{\mathbf{k}_1\mathbf{k}_2,\mathbf{q}j}$ , and  $\Psi_{\mathbf{k}_1,\mathbf{k}_2,\mathbf{q}j}$  are given in [200].

The terms in (12.59) and (12.60), as in the case of the isolated magnetic system (Section 11.2), correspond to *elementary processes* of annihilation and creation of quasiparticles, in the present case, of magnons and phonons. In these processes, as one can see from (12.59) and (12.60), the impulse conservation takes place. (Energy is also conserved in each elementary process, in the first approximation of the perturbation theory, similar to magnon processes treated in Section 11.1.) The bilinear Hamiltonian (12.59) describes two-particle elementary processes of magnon-phonon conversion. After the diagonalization of it, together with the quadratic Hamiltonians of magnetic and elastic systems, a Hamiltonian that describes the mixed quasiparticles corresponding to magnetoelastic waves would be obtained.

The Hamiltonian (12.60) describes the three-particle elementary processes, which are basic to the spin-lattice relaxation. The terms with amplitudes  $\Psi_{\mathbf{k}_1\mathbf{k}_2,\mathbf{q}j}$

correspond to the elementary processes of *two-magnon confluence* with creation of a phonon, and the Hermitian conjugate terms correspond to the splitting of a phonon into two magnons. The terms with amplitudes  $\Psi_{k_1, k_2 q j}$  correspond to the elementary processes of splitting a magnon into magnon and phonon. These processes (as well as the reverse ones, the magnon–phonon confluence) were named the *Cherenkov processes*, by analogy with the Cherenkov–Vavilov effect of light radiation by an electron retarded in a medium (e.g., [246]). The condition of this effect (the electron velocity must exceed the velocity of light in the medium) transforms, in our case, into

$$v_{\text{m gr}} > v_{\text{el}}. \quad (12.61)$$

This condition can be satisfied at sufficiently large  $k$  values, as one can see, e.g., from Figure 12.2.

The process of two-magnon confluence into a phonon can be caused only by the relativistic interactions, just as the processes in the isolated magnetic system occurring with the change of the entire number of magnons (Section 11.2). But the Cherenkov processes, in which the number of magnons *remains constant*, can be caused by relativistic, as well as by *exchange* interactions. The ratio of their contributions to  $\Psi_{k_1, k_2 q j}$ , at  $k_1 \simeq k_2 \equiv k$ , is [200]

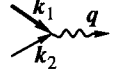
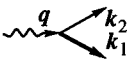

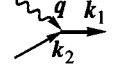
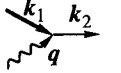

$$\frac{(\Psi_{k_1, k_2 q j})_{\text{ex}}}{(\Psi_{k_1, k_2 q j})_{\text{rel}}} \sim \frac{M_0 D k^2}{B}. \quad (12.62)$$

This ratio, for YIG, is of the order of unity at  $k \sim 10^6$ . At smaller  $k$  values the relativistic contribution is dominant, and at larger  $k$  values the exchange contribution dominates. It is worth noting that the direct Cherenkov process (splitting of a magnon into magnon and phonon) underlies the parametric excitation of magnetic and elastic waves under magnetic pumping, and the splitting of a phonon into two magnons is the basis of parametric excitation of magnetic modes under elastic pumping.

The above-discussed three-particle elementary processes form the basis of the processes of direct spin–lattice relaxation in magnetically ordered substances shown in Table 12.1. Note that, as distinct from Section 11.2, now there is no need in considering four-particle processes. In the case of spin–lattice relaxation, three-particle processes can be caused by exchange interaction, and, hence, their probabilities are always larger than the probabilities of four-particle processes.

To obtain the *relaxation frequencies* of the processes shown in Table 12.1 we can use the theory based on calculating the transition probabilities in the first approximation of the nonstationary perturbation theory (Section 11.1). Without dwelling on these calculations, we cite only some results [100] (see also [14, 171]). It turns out that the contribution of all these processes to the dissipation of *uniform* magnetization oscillations, as well as their contribution to the dissipation of spin waves with  $k \lesssim 10^5$ , is negligible. This contribution increases with growing  $k$ . In substances in which the indirect spin–lattice processes do not play any important

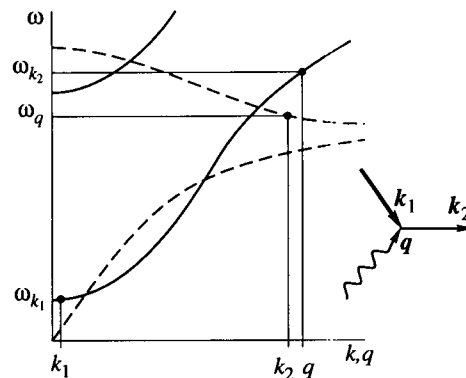
**TABLE 12.1**  
Processes of direct spin–lattice relaxation.<sup>a</sup>

Process	Amplitude	Elementary processes	
		direct	reverse
Magnon confluence	$\Psi_{k_1, k_2, q_j}$		
Cherenkov processes	Splitting $\Psi_{k_1, k_2, q_j}$		
	Confluence $\Psi_{k_2, k_1, q_j}$		

<sup>a</sup> Relaxation of magnons with wave vector  $k_1$  is considered.

role, the direct processes shown in Table 12.1 transfer the energy into the lattice. This energy was ‘smeared’ out over the magnetic system by spin–spin processes (Chapter 11) at ‘early stages’ of relaxation.

For uniform ferromagnetic resonance and spin waves with small  $k$ , in ‘good’ samples of single-crystal ferrites, as YIG, an essential difficulty arises in explaining the very first of the mentioned relaxation stages, which mainly determines the observed  $\Delta H_0$  and  $\Delta H_{k \rightarrow 0}$  values. It was already pointed out in Section 11.2 that *Kasuya–Le Graw processes* [212] (see also [376]), both magnon–magnon and



**FIGURE 12.6**

Spectra of magnons (solid curves) and phonons (dashed curves). Points indicate the frequencies for a magnon–phonon Kasuya–Le Graw process. Note that the condition  $k_1 = k_2 - q$  need not be satisfied because the vectors  $k_1$ ,  $k_2$ , and  $q$ , for which the impulse conservation holds, are, in general, not parallel to each other.



magnon–phonon, can be important at this stage. A distinctive feature of Kasuya–Le Graw processes is the participation of magnons or phonons at *upper* branches of their spectra. The magnon–phonon Kasuya–Le Graw process is the confluence of a small- $k$  magnon with phonon at the upper (optical) branch of the elastic-wave spectrum resulting in creation of a magnon with large  $k$  (Figure 12.6). It should be noted that such a process leads to the energy transfer, not from the spin system into the lattice but in the opposite direction. However, it results in annihilation of the considered small- $k$  magnons and, hence, makes a contribution to their dissipation parameter. Of course, the energy transferred into the spin system by this process is returned into the lattice by other processes, the probabilities of which are large enough because of high  $k$  values of magnons created in the Kasuya–Le Graw process.

Estimates show that the contribution of the magnon–phonon Kasuya–Le Graw processes, as well as of the magnon–magnon ones (Section 11.2), to the linewidth of high-quality single-crystal ferrites is essential. For YIG, it is of the order of 0.1 Oe, which is a noticeable part, if not a dominant one, of the entire value of  $\Delta H_{k \rightarrow 0}$  in YIG.



# 13

## *Ionic anisotropy and relaxation*

### 13.1 Anisotropy caused by impurity ions

As mentioned in Section 11.1, the impurity ions with strong spin–orbital coupling give rise to an effective relaxation process which we, for brevity, refer to as *ionic* process. These ions are also a source of anisotropy in ferromagnetic resonance.

Among the considered ions there are all ions with partly filled 3d or 4f shells, except such that either have no orbital angular momentum (are in the S state) or have a quenched orbital angular momentum. The latter means that the lowest energy level of such an ion in the particular crystal is an orbital singlet. The ions  $\text{Mn}^{2+}$ ,  $\text{Fe}^{3+}$ ,  $\text{Eu}^{2+}$ ,  $\text{Gd}^{3+}$  are in the S state, and  $\text{Cr}^{3+}$  in the octahedral environment is an example of ions with quenched orbital angular momentum. It should be noted that ions with zero or quenched orbital momentum, first of all,  $\text{Fe}^{3+}$  ions, are the main magnetic ions in all soft magnetic materials, including microwave ferrites. Ions with strong spin–orbital coupling emerge either as a result of the impurities in the starting materials or due to the change of the main-ion valencies. In some cases the ions with strong spin–orbital coupling are added purposely, e.g., to increase the threshold of parametric spin-wave excitation (Chapter 10).

#### 13.1.1 Energy levels of ions

The angular momenta  $\mathbf{J}$  of ions with partially filled 3d or 4f shells are vector sums of orbital and spin angular momenta of all electrons of these shells. The interaction of electrons is such in this case (the Russel–Saunders coupling [336]) that it is reasonable to first sum the spin angular momenta of all electrons ( $\sum_n \mathbf{s}_n = \mathbf{S}$ ) and their orbital angular momenta ( $\sum_n \mathbf{l}_n = \mathbf{L}$ ), and only then to sum  $\mathbf{S}$  and  $\mathbf{L}$  ( $\mathbf{S} + \mathbf{L} = \mathbf{J}$ ).

It was pointed out in Section 1.1 that the eigenvalues of the operator  $\hat{S}$  and  $\hat{L}$  projections onto the axis of quantization are:  $S, (S - 1), \dots, (-S)$  and  $L, (L - 1), \dots, (-L)$ , where  $S$  and  $L$  are, respectively, the spin and the orbital quantum numbers. The eigenvalues of the operator  $\hat{J}$  projections are:  $J, (J - 1), \dots, (-J)$ ,

and the quantum number  $J$  can take the values  $(S + L), (S + L - 1), \dots, |S - L|$ . The values of  $S$  and  $L$  in the ground state are determined by the empirical Hund rules (e.g. [243, 336]).

The energy levels of a *free* ion, without allowance for spin-orbital and intraionic spin-spin interactions, depend only on  $S$  and  $L$  and are  $(2S + 1)(2L + 1)$ -fold degenerate. The mentioned interactions split the levels into  $(2J + 1)$ -fold degenerate multiplets with different  $J$  values. The lowest multiplet is that with  $J = |S - L|$  if the shell is less than half filled, and with  $J = S + L$  if it is more than half filled. The  $S$ ,  $L$ , and  $J$  values of free 3d and 4f ions in the ground states are given in Tables 13.1 and 13.2.

An external *magnetic* field splits each multiplet into  $(2J + 1)$  equidistant levels with intervals (1.18). An external *electric* field removes the degeneration, completely or partly, depending on the symmetry of the field and the value of  $J$ . A field with orthorhombic or lower symmetry splits the multiplet completely if  $J$  is an integer (i.e., the number of 3d or 4f electrons is even), or splits it into  $J + 1/2$  Kramers doublets if  $J$  is a half-integer. Fields with higher symmetries split the multiplets partly. The cubic field does not split them at all if  $J < 2$ . The five-fold degenerate multiplet with  $J = 2$  is split by the cubic field into a doublet and a triplet, the seven-fold degenerate multiplet with  $J = 3$  is split into a singlet and two triplets [1].

Ions in a *crystal* interact electrostatically with the neighboring ions. The part of the energy of this interaction that depends on mutual orientations of the ionic spins is referred to as the *exchange energy*. It can be described by the use of the effective exchange (or 'molecular') field (Section 1.1), which results in the splitting of ionic levels similar to the splitting in a magnetic field. The rest of the interaction with the neighboring ions is described by means of the so-called *crystal field*, which has the same symmetry as the local environment of the ion.

Considering the influence of different interactions on the ionic energy levels, we must begin with the strongest interaction and then pass to weaker and weaker ones. The sequence of them is different for 3d and 4f ions. For 3d ions, the influence of the crystal field is the strongest and should be taken into account first. Then the exchange interaction follows, and only after it the spin-orbital coupling is to be taken into account. The case of the so-called intermediate crystal field [1] is usually realized. In this case the energy of interaction between 3d electrons is higher than their energy in the crystal field, and the energy spectrum is determined first of all by the values of  $S$  and  $L$ . The action of the crystal field is stronger for the 3d ions than the spin-orbital interaction (which leads to the formation of the total angular momentum  $J$ ). Therefore, the energy levels of 3d ions are determined mainly by the action of the crystal field onto the *orbital* multiplets.

The *cubic* component of the crystal field is always the greatest. Therefore, it is reasonable to first find the structure of energy levels in the cubic crystal field, and then to take into account, as perturbations, the trigonal, tetragonal, and orthorhombic crystal-field components. The splitting of orbital multiplets with  $L = 2$  and  $L = 3$  by the cubic field is shown in Table 13.3. It should be noted that the crystal

**TABLE 13.1**  
Quantum numbers of free 3d ions in the ground state [1].

Ions	V <sup>2+</sup>		Cr <sup>2+</sup>		Mn <sup>2+</sup>		Fe <sup>2+</sup>		Co <sup>2+</sup>		Ni <sup>2+</sup>		Cu <sup>2+</sup>	
	V <sup>3+</sup>	Cr <sup>3+</sup>	Mn <sup>3+</sup>	Fe <sup>3+</sup>	Co <sup>3+</sup>	Ni <sup>3+</sup>								
	V <sup>4+</sup>	Cr <sup>4+</sup>	Mn <sup>4+</sup>	Fe <sup>4+</sup>										
Number of 3d electrons	1	2	3	4	5	6	7	8	9					
Spin angular momentum	1/2	1	3/2	2	5/2	2	3/2	1	1/2					
Orbital angular momentum	2	3	3	2	0	2	3	3	2					
Total angular momentum	3/2	2	3/2	0	5/2	4	9/2	4	5/2					
Notation of the term	<sup>2</sup> D <sub>3/2</sub>	<sup>3</sup> F <sub>2</sub>	<sup>4</sup> F <sub>3/2</sub>	<sup>5</sup> D <sub>0</sub>	<sup>6</sup> S <sub>5/2</sub>	<sup>5</sup> D <sub>4</sub>	<sup>4</sup> F <sub>9/2</sub>	<sup>3</sup> F <sub>4</sub>	<sup>2</sup> D <sub>5/2</sub>					

**TABLE 13.2**  
Quantum numbers of free 4f ions in the ground state [1].

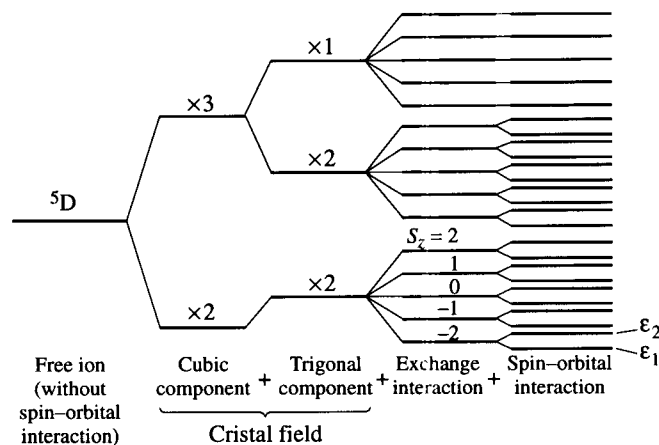
Ions	Sm <sup>2+</sup> Eu <sup>2+</sup>													
	Ce <sup>3+</sup>	Pr <sup>3+</sup>	Nd <sup>3+</sup>	Pm <sup>3+</sup>	Sm <sup>3+</sup>	Eu <sup>3+</sup>	Gd <sup>3+</sup>	Tb <sup>3+</sup>	Dy <sup>3+</sup>	Ho <sup>3+</sup>	Er <sup>3+</sup>	Tm <sup>3+</sup>	Yb <sup>3+</sup>	Yb <sup>3+</sup>
Number of 4f electrons	1	2	3	4	5	6	7	8	9	10	11	12	13	13
Spin angular momentum	1/2	1	3/2	2	5/2	3	7/2	3	5/2	2	3/2	1	1/2	1/2
Orbital angular momentum	3	5	6	6	5	3	0	3	5	6	6	5	3	3
Total angular momentum	5/2	4	9/2	4	5/2	0	7/2	6	15/2	8	15/2	6	7/2	7/2
Notation of the term	<sup>2</sup> F <sub>5/2</sub>	<sup>3</sup> H <sub>4</sub>	<sup>4</sup> I <sub>9/2</sub>	<sup>5</sup> I <sub>4</sub>	<sup>6</sup> H <sub>5/2</sub>	<sup>7</sup> F <sub>0</sub>	<sup>8</sup> S <sub>7/2</sub>	<sup>7</sup> F <sub>6</sub>	<sup>6</sup> H <sub>15/2</sub>	<sup>5</sup> I <sub>8</sub>	<sup>4</sup> I <sub>15/2</sub>	<sup>3</sup> H <sub>6</sub>	<sup>2</sup> F <sub>7/2</sub>	<sup>2</sup> F <sub>7/2</sub>

**TABLE 13.3**  
Splitting of orbital multiplets by the cubic crystal field.

Orbital angular momentum	Degeneracy before splitting	Number of 3d electrons	Examples of ions	Degeneracy after splitting (in order of increasing energy)	
				Environment	Environment
				octahedral	tetrahedral
2	5	1 or 6 4 or 9	Fe <sup>2+</sup> Co <sup>3+</sup> Cr <sup>2+</sup> Mn <sup>3+</sup> Fe <sup>4+</sup>	3; 2	2; 3
				2; 3	3; 2
3	7	3 or 8 2 or 7	Cr <sup>3+</sup> Ni <sup>2+</sup> Cr <sup>4+</sup> Co <sup>2+</sup>	1; 3; 3	3; 3; 1
				3; 3; 1	1; 3; 3

field on octahedral sites of spinels and garnets (Section 3.3) contains a trigonal component, which results in splitting of the triplet into a singlet and a doublet.

In Figure 13.1, a 'sequential' splitting of the orbital multiplet <sup>5</sup>D of ions Cr<sup>2+</sup>, Mn<sup>3+</sup>, or Fe<sup>4+</sup> on an octahedral site is shown. The cubic crystal-field component, according to Table 13.3, splits the <sup>5</sup>D multiplet into orbital doublet and triplet. The trigonal component splits the triplet. The exchange interaction removes the spin degeneration, i.e., splits each level into five doublets or singlets, according to their



**FIGURE 13.1**  
Splitting of energy levels of d<sup>4</sup> ions in the octahedral environment. ×3, ×2, and ×1 denote the orbital degeneracy.

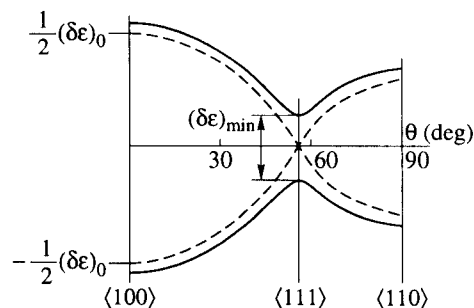


FIGURE 13.2

Splitting of the lowest doublet of  $d^4$  or  $d^6$  ions on octahedral lattice sites by spin-orbital interaction without (dashed lines) and with (solid lines) allowance for perturbations.

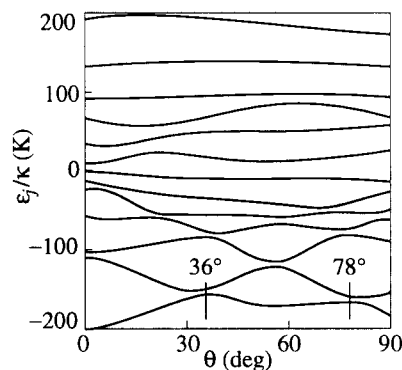


FIGURE 13.3

Angular dependence of  $Tb^{3+}$  energy levels on one of the nonequivalent dodecahedral YIG lattice sites, calculated from experimental data on ferromagnetic resonance in Tb-doped YIG [100].  $\theta$  is the angle between  $M_0$  and the  $\langle 100 \rangle$  axis in the  $\{110\}$  plane.

orbital degeneracy. And finally, the weakest, spin-orbital interaction splits the doublets. This splitting depends essentially on the direction of  $M_0$  with respect to the crystal axes. It has been shown [182] that the angular dependence of the lowest levels has the form (Figure 13.2)

$$\varepsilon_{1,2} = \pm \frac{(\delta\varepsilon)_0}{2} \left( 1 - \frac{3}{4} (\sin^2 2\theta + \sin^4 \theta \sin^2 2\varphi) \right)^{1/2} \quad (13.1)$$

where  $\theta$  and  $\varphi$  are the  $M_0$  angles in the spherical coordinate system with the axis coinciding with the  $\langle 100 \rangle$  direction. One can see that there is a crossing of levels in the  $\langle 111 \rangle$  direction. It is replaced by a *near-crossing* if some perturbations are taken into account (Figure 13.2).

For 4f ions, the spin-orbital interaction is the strongest. It combines  $S$  and  $L$  into the total angular momentum  $J$ . The multiplets with different  $J$  are split

by the crystal and exchange fields, as the orbital multiplets of 3d ions. For 4f ions with small spin angular momenta, e.g.,  $\text{Yb}^{3+}$ , the splitting in crystal field is much stronger than the exchange splitting. But for 4f ions with large spin angular momenta, such as  $\text{Tb}^{3+}$  or  $\text{Ho}^{3+}$  (Table 13.2), these splittings are of the same order, which leads to 'accidental' crossings of levels at some  $M_0$  angles. Different interactions, which have not been taken into account, result in replacement of the crossings by near-crossings (Figure 13.3).

### 13.1.2 One-ion theory of ferromagnetic-resonance anisotropy

Let us examine the influence of the ions with strong spin-orbital coupling on the condition for ferromagnetic resonance (not yet touching on the dynamic contribution of the ions, which will be considered in the next section).

The *free energy* of the ions can be found from the general formula [244]

$$U_i = -\kappa T \ln \left[ \sum_l \sum_\nu N_{l\nu} \sum_j \exp \left( -\frac{\varepsilon_{l\nu j}}{\kappa T} \right) \right] \quad (13.2)$$

where  $l$  denotes the sort of ions,  $\nu$  denotes the nonequivalent crystal site, and  $j$  is the number of the level. In the case of small concentration of the ions, which we are interested in, the contributions of different ions on different sites can be regarded as independent and additive, and we may study them one by one using formula (2.29). To obtain the condition for resonance we must substitute the sum of the following terms into (2.24): the ionic free energy (2.29), the Zeeman energy (2.26), and, in general, the energy of demagnetizing fields. But the last term may be omitted in the case of a sphere, which we consider for simplicity. For small concentration of ions, neglecting the intrinsic anisotropy of the main magnetic system, we may regard  $\theta$  and  $\varphi$  as coinciding with the given angles  $\theta_H$  and  $\varphi_H$  of the external magnetic field.

Let us take into account only *two lowest energy levels*. Then, it is easy to obtain from (2.32) (omitting a constant term)

$$U_i = N\varepsilon_0 - N\kappa T \ln \left( \cosh \frac{\delta\varepsilon}{2\kappa T} \right) \quad (13.3)$$

where  $\varepsilon_0 = (\varepsilon_1 + \varepsilon_2)/2$  and  $\delta\varepsilon = \varepsilon_2 - \varepsilon_1$  depend, in general, on the angles  $\theta$  and  $\varphi$ . Substituting the sum of (13.3) and (2.26) into (2.24) and neglecting the terms of the second order in  $N$ , we find [163]

$$\begin{aligned} H_{\text{res}} \equiv \frac{\omega}{\gamma} + \delta H = \frac{\omega}{\gamma} + \frac{N}{2M_0} \left\{ -(\varepsilon_0)_{\theta\theta} + \frac{(\delta\varepsilon)_{\theta\theta}}{2} \tanh \frac{\delta\varepsilon}{2\kappa T} \right. \\ \left. + \frac{(\delta\varepsilon)_{\theta}^2}{4\kappa T} \left( \cosh \frac{\delta\varepsilon}{2\kappa T} \right)^{-2} + \frac{1}{\sin^2 \theta} \left[ -(\varepsilon_0)_{\theta\theta} \right. \right. \\ \left. \left. + \frac{(\delta\varepsilon)_{\varphi\varphi}}{2} \tanh \frac{\delta\varepsilon}{2\kappa T} + \frac{(\delta\varepsilon)_{\varphi}^2}{4\kappa T} \left( \cosh \frac{\delta\varepsilon}{2\kappa T} \right)^{-2} \right] \right\}. \quad (13.4) \end{aligned}$$



Here the indices  $\theta$  and  $\varphi$  denote, as in (2.26), the partial derivatives with respect to the corresponding angles.

### 13.1.3 Near-crossing energy levels

The two-level approximation is good at low temperatures and, without severe restriction on the temperature, in two important particular cases: (i) low-lying doublet split by spin-orbital (for 3d ions) or exchange (for 4f ions) interaction, leading to the near-crossing of levels, as in Figure 13.2, (ii) 'accidental' near-crossing of two lowest levels, as in Figure 13.3.

Consider, first, the case of the lowest *orbital doublet* split by spin-orbital interaction. Assume  $M_0$  to lie in the  $\{110\}$  plane. Then, according to (13.1), there is a level crossing in the  $\langle 111 \rangle$  direction replaced, as it has been mentioned, by near-crossing. To take this into account we may change (13.1):

$$\varepsilon_{1,2} = \pm \frac{(\delta\varepsilon)_0}{2} \left( 1 - \frac{3}{4} (\sin^2 2\theta + \sin^4 \theta \sin^2 2\varphi) + \xi^2 \right)^{1/2} \quad (13.5)$$

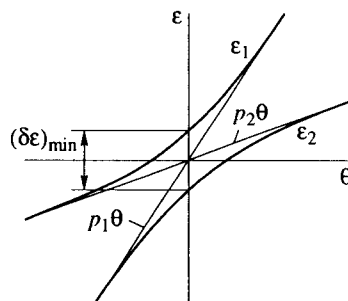
where  $\xi = (\delta\varepsilon)_{\min}/(\delta\varepsilon)_0$  (Figure 13.2). Then, using the formula (13.4), we obtain, e.g.,

$$(\delta H)_{111} = \frac{N(\delta\varepsilon)_0}{M_0\xi} \tanh \frac{(\delta\varepsilon)_{\min}}{2\kappa T}. \quad (13.6)$$

It should be noted that  $(\delta H)_{111}$  remains finite in the limiting case of pure crossing:

$$[(\delta H)_{111}]_{\xi \rightarrow 0} = \frac{1}{2} \frac{N(\delta\varepsilon)_0^2}{M_0\kappa T}. \quad (13.7)$$

Consider now an *asymmetrical*, 'accidental' near-crossing of two levels (Figure 13.4). Near the point  $\theta = 0$  the angular dependence of the levels can be



**FIGURE 13.4**  
Near-crossing of energy levels.

approximated by the roots of the equation

$$(\varepsilon - p_1\theta)(\varepsilon - p_2\theta) - \frac{1}{4}(\delta\varepsilon)_{\min}^2 = 0. \quad (13.8)$$

Suppose (as the calculation is only an estimate) that the terms containing derivatives with respect to  $\varphi$  make the same contribution to  $\delta H$  as the terms with derivatives with respect to  $\theta$ . Then, using (13.4) and (13.8), we obtain that at the point of near-crossing

$$\delta H = \frac{N(p_1 - p_2)}{2M_0(\delta\varepsilon)_{\min}} \tanh \frac{(\delta\varepsilon)_{\min}}{2\kappa T}. \quad (13.9)$$

Giant  $H_{\text{res}}$  peaks at the points of near-crossings of the impurity-ion energy levels were explained by Kittel [224]. The expressions for  $\delta H$  given in [225] follow from (13.9) in the limiting cases  $(\delta\varepsilon)_{\min} \ll \kappa T$  and  $(\delta\varepsilon)_{\min} \gg \kappa T$ .

#### 13.1.4 Experimental data

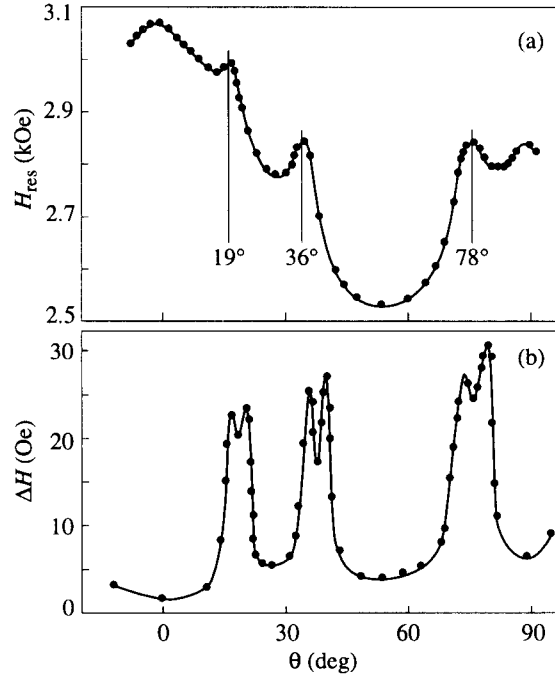
The influence of the ions with strong spin-orbital coupling on ferromagnetic resonance was first observed by Dillon and Nielsen [98] in the case of impurity 4f ions in YIG single crystals.

The experimental angular dependences of  $H_{\text{res}}$  in YIG with small addition of Tb are shown in Figure 13.5. Two  $H_{\text{res}}$  angular maxima, at  $\theta = 36^\circ$  and  $\theta = 78^\circ$ , of the three observed, are caused by the near-crossings shown in Figure 13.3. The third maximum, at  $\theta = 19^\circ$ , is caused by the ions on another nonequivalent lattice site.

Let us compare the height of the maxima in Figure 13.5 with the theoretical value (13.9). The concentration  $N$  can be easily found by taking into account that the edge of an elementary YIG cubic crystal cell (which contains eight 'molecules'  $\text{Y}_3\text{Fe}_5\text{O}_{12}$ ) is 12.5 Å [138] and only 1/3 of the ions occupy the lattice sites that correspond to Figure 13.3. The magnetization  $M_0$  may be assumed to be the same as for pure YIG (195 G at 4.2 K). The values for  $p_1 - p_2 \simeq 120\kappa$  and  $(\delta\varepsilon)_{\min} \simeq 5\kappa$  are found from Figure 13.3. Then, using (13.9), we obtain  $\delta H = 250$  Oe, whereas the experimental value (Figure 13.5) is approximately 200 Oe.

The 'strange' values of the angles,  $\theta = 19^\circ$ ,  $38^\circ$ , and  $78^\circ$ , were explained by Huber [185]. He showed that all these angles correspond to the same angle  $71^\circ$  between  $M_0$  and one of the local axes.

Big  $H_{\text{res}}$  peaks in the  $M_0$  directions in which energy-level near-crossings take place were also observed [98] in YIG doped with other non-Kramers 4f ions: with  $\text{Pr}^{3+}$ , in the directions  $\langle 100 \rangle$ , and with  $\text{Ho}^{3+}$ , in all directions lying in the  $\{100\}$  planes. The contributions of Kramers ions,  $\text{Nd}^{3+}$ ,  $\text{Sm}^{3+}$ ,  $\text{Dy}^{3+}$ ,  $\text{Er}^{3+}$ , and  $\text{Yb}^{3+}$ , were also great, but sharp maxima were not observed, except for  $\text{Yb}^{3+}$ . In the last case, very sharp 'anomalous'  $H_{\text{res}}$  peaks were observed owing to the near-crossings of levels of  $\text{Yb}^{3+}$  ions that penetrate onto octahedral lattice sites [99].



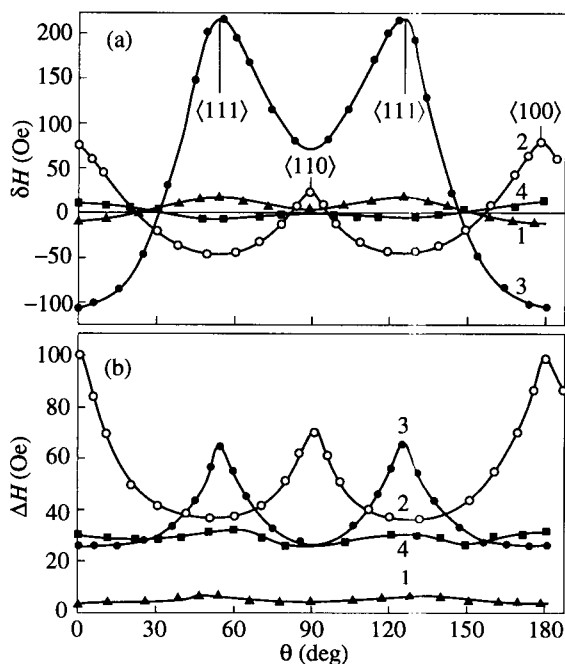
**FIGURE 13.5**

Angular dependences of  $H_{res}$  and  $\Delta H$  for  $Y_{3-x}Tb_xFe_5O_{12}$  garnet ( $x = 4 \times 10^{-4}$ ) at frequency 8.9 GHz and temperature 4.2 K [156].

The influence of 3d ions with strong spin-orbital coupling on the ferromagnetic-resonance anisotropy in ferrites was also investigated. For YIG, the ions  $Fe^{2+}$  and  $Fe^{4+}$  are of the most interest [401, 402].  $Fe^{2+}$  ions arise in small amounts in the process of crystal growth due to oxygen vacancies and  $Si^{4+}$  and  $Pt^{4+}$  ions penetrating into the lattice.  $Fe^{4+}$  ions arise as a result of penetration of Pb used as a solvent in the growth of YIG crystals.

Analogous reasons lead to the appearance of  $Fe^{2+}$ ,  $Fe^{4+}$ , and  $Mn^{3+}$  ions in ferrites with spinel structure [236, 297].  $Co^{2+}$  ions arise in these materials when small amounts of cobalt are added to control the anisotropy or to raise the threshold of spin-wave parametric excitation (Chapter 10). All the mentioned 3d ions usually have no sharp near-crossings of the energy levels, and their main effect is the appearance of low-temperature  $\Delta H$  maxima to be studied in the next section.

An interesting example of the influence of ions with strong spin-orbital coupling on ferromagnetic-resonance anisotropy is that of  $Cr^{2+}$  and  $Cr^{4+}$  ions in the ferromagnet  $CdCr_2Se_4$  [417]. The anisotropy of this crystal is small because the main magnetic ions  $Cr^{3+}$  have quenched orbital momenta. However, distinct



**FIGURE 13.6**

Angular dependences of  $\delta H = H_{\text{res}} - \omega/\gamma$  and  $\Delta H$  for  $\text{CdCr}_2\text{Se}_4$  (curves 1) and  $\text{Cd}_{1-x}\text{Ag}_x\text{Cr}_2\text{Se}_4$  ( $x = 0.015$ ): as grown (curves 2), after annealing in vacuum (curves 3), and after subsequent annealing in Se vapor (curves 4) [34]. Measurements were performed at frequency 9.1 GHz and temperature 4.2 K.

$H_{\text{res}}$  maxima are observed in  $\langle 111 \rangle$  directions [Figure 13.6(a), curve 1]. They are caused by  $\text{Cr}^{2+}$  ions arising in the course of crystal growth due to Se vacancies. The lowest energy levels of these ions have been shown in Figure 13.2.

But if  $\text{CdCr}_2\text{Se}_4$  crystals are grown with small addition of Ag [Figure 13.6(a), curve 2], the maxima in  $\langle 111 \rangle$  directions disappear and maxima in  $\langle 100 \rangle$  and  $\langle 110 \rangle$  directions arise. They are caused by  $\text{Cr}^{4+}$  ions, which emerge owing to the substitution of  $\text{Ag}^+$  ions for  $\text{Cd}^{2+}$  ions. The  $\text{Cr}^{4+}$  ions in octahedral cubic environment have a low-lying orbital triplet (Table 13.3). It is split into a doublet and a singlet by the trigonal crystal-field component present on octahedral spinel sites. The singlet and the lowest level of the doublet (split by the spin-orbital interaction, as in Figure 13.2) are believed to approach each other in  $\langle 100 \rangle$  and  $\langle 110 \rangle$  directions.

The Ag-doped sample was then annealed in vacuum. This resulted in the rise of Se vacancies and, hence, of the  $\text{Cr}^{2+}$  ions. Strong  $H_{\text{res}}$  maxima caused by these ions appeared in  $\langle 111 \rangle$  directions [Figure 13.6(a), curve 3]. The subsequent annealing of the sample in Se vapor resulted in the disappearance of these maxima (curve 4) due to the 'healing' of Se vacancies. It should be noted that in other

crystals, e.g., in  $\text{HgCr}_2\text{Se}_4$ , the  $\text{Cr}^{2+}$  and  $\text{Cr}^{4+}$  ions can coexist, being localized near the defects that have caused them. The  $H_{\text{res}}$  maxima in  $\langle 111 \rangle$  and  $\langle 100 \rangle$  directions are then observed at the same time [107].

An important assumption has been made in this section (it will be removed in Section 13.2): the relaxation time of the ionic energy-level populations is much shorter than the period of oscillations. The anisotropy obtained above with this assumption does not depend on frequency and coincides with the anisotropy measured in a constant field, e.g., by the method of torque moments (Section 2.2). It gives grounds to name such anisotropy the *static* anisotropy, although it manifests itself in such a dynamic process as ferromagnetic resonance.

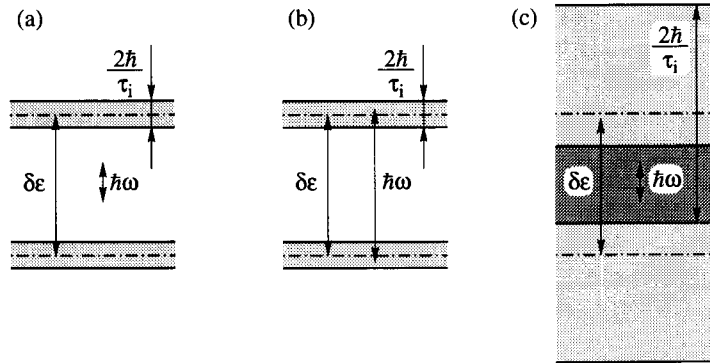
## 13.2 Ionic relaxation processes

The contribution of the ionic relaxation process to the ferromagnetic-resonance linewidth of ferrites was observed, as it became clear afterwards, in the early 1950s. But this process was understood only after Dillon and Neilsen [97] and Spencer, Le Craw, and Clogston [379] discovered the low-temperature  $\Delta H$  maxima in YIG single crystals with rare-earth impurity ions. To explain these maxima a theory known as the theory of *fast relaxation* was developed by Kittel, De Gennes, and Portis [224, 87]. According to this theory, the  $\Delta H$  maxima appear at such temperatures at which the relaxation frequency of ion-level populations  $1/\tau_i$  becomes equal to  $\delta\varepsilon/\hbar$  where  $\delta\varepsilon$  is the energy interval between the lowest levels.

It soon became apparent however, that the predictions of the fast-relaxation theory do not agree, in most cases, with experiment. Besides, the  $1/\tau_i$  values can hardly be so large at the temperatures of  $\Delta H$  maxima, as it is necessary according to this theory. Dillon [94] and Teale and Tweedale [403] proposed another mechanism to determine the behavior of  $\Delta H$  in YIG with rare-earth impurities. It was given the name of *slow relaxation*. According to this mechanism, the  $\Delta H$  maxima are observed at such temperatures at which  $1/\tau_i$  is equal to the frequency  $\omega$  of the ac field. It has turned out that the theory developed earlier by Clogston [75] for the case of *interionic* electron transitions (Section 14.1) is also the proper theory for the *intraionic* slow relaxation.

### 13.2.1 Transverse relaxation

The fast relaxation falls into the transverse relaxation mechanisms, for which the excitation of ions is accomplished by means of direct transitions between ionic energy levels. This excitation is analogous, in some sense, to the paramagnetic resonance [1, 15], with the difference that it is performed by the magnons of the main magnetic system, rather than by quanta of an external field. Different cases of such excitation are shown in Figure 13.7. Case (c) corresponds to the

**FIGURE 13.7**

Transverse ionic relaxation: (a) transition probability is very small, (b) resonance relaxation, (c) fast relaxation.

fast-relaxation mechanism.

A macroscopic model was first used by Kittel [224] in the theory of fast relaxation. Both systems, the main magnetic system and the ions, were regarded as sublattices (Section 3.1) with magnetizations, respectively,  $M_1$  and  $M_2 = N_2 \mathfrak{M}_2$  where  $N_2$  is the concentration and  $\mathfrak{M}_2$  is the magnetic moment of the ions. The Landau–Lifshitz equations of motion were written for both sublattices neglecting the intrinsic anisotropy and dissipation of the first sublattice and assuming the exchange interaction between the sublattices to be antiferromagnetic. The solution of these coupled equations, in the case of small  $N_2$ , results in

$$\Delta H = \frac{2\gamma_1 M_{20}}{\gamma_2 M_{10}} \frac{\omega_E \tau_i}{1 + \omega_E^2 \tau_i^2}. \quad (13.10)$$

Here,  $\omega_E \simeq \Lambda \gamma_2 M_{10}$  where  $\Lambda$  is the constant of the exchange interaction between the sublattices. The relaxation time  $\tau_i$  is defined by

$$\frac{1}{\tau_i} = \Lambda \frac{M_{10}}{M_{20}} \gamma_2 \lambda_2 \quad (13.11)$$

where  $\lambda_2$  is the dissipation parameter (Section 1.4) of the second sublattice; its value can be arbitrarily large.

It was mentioned in Section 3.3 that the system of rare-earth ions on dodecahedral lattice sites in garnets, even in the case of high concentrations, can be regarded as a sublattice only at low temperatures. The concentration of ions in the above-considered theory being small, this theory needs justification all the more. The microscopic theory [87] developed for the case of high temperatures can serve as such justification. Its result coincides with the high-temperature limit ( $\omega_E \tau_i \ll 1$ ) of (13.10) if  $\tau_i$  defined by (13.11) is equal to the relaxation time of the level populations in microscopic theory.

It should be emphasized that in both theories, the macroscopic and the microscopic, two essential assumptions were made: (i) the exchange interaction was regarded as isotropic, and (ii) the interaction of orbital moments with the lattice (which could be taken into account by means of the crystal field) was neglected. With these assumptions, the dc components of  $\mathcal{M}_1$  and  $\mathcal{M}_2$  are parallel, and the ac effective field  $\Lambda m_1$  acting on the ions, which is transversal with respect to  $\mathcal{M}_{10}$ , is transversal also with respect to  $\mathcal{M}_{20}$ . That is why the fast relaxation is regarded as a case of transverse relaxation.

A general theory of transverse relaxation was developed by Van Vleck [419]. Two systems coupled with each other by isotropic exchange interaction are considered in this theory. The first is described by the magnetization  $\mathcal{M}_1$ , which satisfies the Landau–Lifshitz equation. The second consists of ions, which are characterized by their energy levels. Taking into account two lowest of them, the following formula was obtained for the case of a sphere:

$$\delta H + i \frac{\Delta H}{2} = \frac{N_2 \mathcal{M}_{20} \gamma_1}{M_{10} \gamma_2} H_0 \frac{\delta \varepsilon}{2\hbar} \left[ \left( \omega - \frac{\delta \varepsilon}{\hbar} - \frac{i}{\tau_1} \right)^{-1} + \left( \omega + \frac{\delta \varepsilon}{\hbar} - \frac{i}{\tau_1} \right)^{-1} \right] \tanh \frac{\delta \varepsilon}{2\kappa T} \quad (13.12)$$

where  $M_{10}$  and  $\mathcal{M}_{20}$  are the values at  $T \rightarrow 0$ . In the limiting case of *fast* relaxation ( $\omega \ll \delta \varepsilon / \hbar$ ,  $1/\tau_1 \sim \delta \varepsilon / \hbar$ ), the expression for  $\Delta H$  following from (13.12) reduces to (13.10), and  $\delta H$  becomes much smaller than  $\Delta H$ .

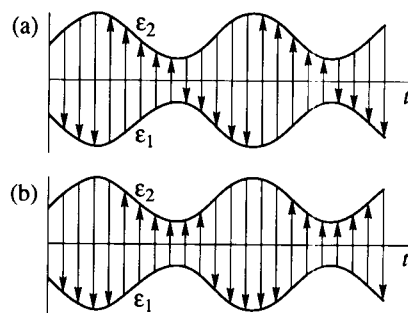
Let us cite now the distinctive features of the fast-relaxation mechanism.

1. The resonance linewidth remains finite at  $T \rightarrow 0$  and passes through a maximum when  $1/\tau_1 = \delta \varepsilon / \hbar$ ; the position of the maximum depends on  $\omega$  only because of the frequency dependence of  $\tau_1$ .
2. The height of the maximum grows with increasing  $\omega$ .
3. The dynamic shift of the resonance field  $\delta H$  is small as compared with  $\Delta H$ .

In the case of resonance relaxation [ $\omega \sim \delta \varepsilon / \hbar$ ,  $1/\tau_1 \ll \delta \varepsilon / \hbar$ , Figure 13.7(b)] the maximal  $\Delta H$  value can be much larger than for the fast relaxation, but it diminishes sharply when  $\omega$  departs from the resonance frequency  $\delta \varepsilon / \hbar$ .

### 13.2.2 Longitudinal (slow) relaxation

The mechanism of slow relaxation (referred also to as *longitudinal* relaxation) is based on the modulation of ionic energy levels by the oscillations of the magnetic system. Consider, first, this mechanism qualitatively (Figure 13.8). The interval  $\delta \varepsilon$  between two lowest energy levels is modulated with frequency  $\omega$ . The *equilibrium* populations of the levels change with the same frequency, and transitions between the levels occur all the time ‘trying’ to restore the continuously disturbed equilibrium.

**FIGURE 13.8**

Transitions between ion energy levels in the course of modulation of the levels: (a) in the absence and (b) in the presence of retardation.

Suppose, first, that the transitions occur without retardation with respect to the change of  $\delta\varepsilon$  [Figure 13.8(a)], i.e., from the lower level onto the upper one when  $\delta\varepsilon$  is decreasing, and vice versa. Then, the average energy  $U_1$ , transferred by the ions to the lattice, is equal to zero, as evident from Figure 13.8(a). But if there is a retardation [Figure 13.8(b)], i.e., the ionic system has a finite relaxation time  $\tau_1$ , then  $U_1$  is finite and positive. In a stationary regime this energy is compensated by the energy expended by the magnetic system on the modulation of energy levels. However, if the retardation is very large ( $\tau_1 \rightarrow \infty$ ), the transitions 'have no time' to occur, and again  $U_1 = 0$ . One can believe that the energy transferred from the magnetic system to the ions and from them to the lattice is maximal when  $1/\tau_1 = \omega$ .

The considered mechanism is like the Debay mechanism of dielectric relaxation (e.g., [227]) or the Gorter mechanism of paramagnetic relaxation [68, 144]. From the latter it differs in that the modulation of energy levels is accomplished by magnons instead of photons. It is the same difference as the above-mentioned difference between transverse relaxation and paramagnetic resonance. A mechanism analogous to the slow intraionic relaxation was proposed earlier, for electron transitions between  $\text{Fe}^{2+}$  and  $\text{Fe}^{3+}$  ions in ferrites, by Wijn and van der Heide [444] and, in a particular case of ferromagnetic resonance, by Jager, Galt, and Merritt [450]. The theory of this mechanism was developed by Clogston [75]. It is fully applicable to our case of slow ionic relaxation based on *intraionic* transitions.

Proceeding to the study of the Clogston theory, consider again two coupled systems: magnetic and ionic. The first is characterized by the vector  $\mathbf{M}$  that satisfies the Landau–Lifshitz equation. The second consists of  $N$  ions characterized by the energy levels  $\varepsilon_j$  and their populations  $N_j$ , so that  $\sum_j N_j = N$ . The coupling of the systems is not specified in the theory, it is assumed only that the coupling leads to the variation of the levels with certain frequency  $\omega$ . The *equilibrium* populations of the levels  $N_{j\infty}$  are determined by the instantaneous  $\varepsilon_j$  values and are changing with the same frequency. The *instantaneous* populations  $N_j$  are also changing with the frequency  $\omega$  but, of course, do not coincide with  $N_{j\infty}$  due to



the retardation mentioned above. The main assumption of the theory is

$$\frac{dN_j}{dt} = \frac{N_{j\infty} - N_j}{\tau_i}. \quad (13.13)$$

It means that all populations relax to their equilibrium values with *the same* relaxation frequency  $1/\tau_i$ .

Substituting  $N_{j\infty} = (N_{j\infty})_0 + n_{j\infty} \exp(i\omega t)$  and  $N_j = (N_j)_0 + n_j \exp(i\omega t)$  into (13.13) and regarding the amplitudes  $n_{j\infty}$  and  $n_j$  as small with respect to  $(N_{j\infty})_0$  and  $(N_j)_0$ , we obtain

$$N_j = (N_j)_0 + \frac{n_{j\infty}}{1 + i\omega\tau_i} \exp(i\omega t). \quad (13.14)$$

We will restrict ourselves to the case of uniform oscillations and neglect all anisotropies except one caused by the considered ionic system. Then, the free energy may be written as

$$U = -\mathbf{M}\mathbf{H} + \sum_j N_j \varepsilon_j - S_j T \quad (13.15)$$

where the entropy  $S_j = -\kappa \sum_j N_j \ln(N_j/N)$  [244]. The first term in the right-hand side of (13.15) is the free energy of the magnetic system (which includes the entropy term, as  $\mathbf{M}$  is the magnetization at a given temperature, see Section 2.1). It should be noted that now we may not use formula (13.2) for the free energy of the ionic system because it is valid only in the equilibrium.

The linearized equation of motion for the eigenoscillations of the magnetic system is

$$i\omega \mathbf{m} = -\gamma \mathbf{m} \times \mathbf{H}_{\text{ef}0} - \gamma \mathbf{M}_0 \times \mathbf{h}_{\text{ef}} \quad (13.16)$$

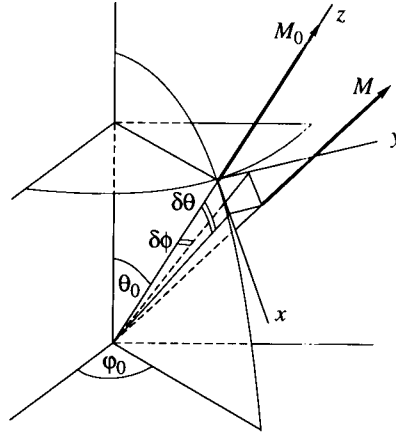
where  $\mathbf{H}_{\text{ef}0}$  and  $\mathbf{h}_{\text{ef}}$  are, respectively, the dc and the ac components of the effective field

$$\mathbf{H}_{\text{ef}} = -\left(\frac{\partial U}{\partial \mathbf{M}}\right)_{N_j=\text{const}}. \quad (13.17)$$

It is very important that the differentiation in (13.17) is carried out at constant populations  $N_j$ . Indeed, the right-hand side of (13.16) is the force moment acting on the system; in calculating it, the partial derivatives of energy must be taken with respect to the angles, i.e., to the  $\mathbf{M}$  components, and populations  $N_j$  are to be regarded as constant factors. So, in calculating  $\mathbf{H}_{\text{ef}}$  by (13.17) the last term of  $U$  in (13.15) must not be taken into account.

In the considered theory the Cartesian coordinate system with the  $z$ -axis directed along  $\mathbf{M}_0$  is used (Figure 13.9). In this system,  $m_x = M_0 \delta\theta$  and  $m_y = M_0 \delta\phi$  where  $\delta\theta = \theta - \theta_0$  and  $\delta\phi = (\varphi - \varphi_0) \sin \theta_0$ . The components of  $\mathbf{H}_{\text{ef}}$  in this system, according to (13.16) and (13.15), are

$$H_{\text{ef}x} = -\frac{1}{M_0} \sum_j N_j \frac{\partial \varepsilon_j}{\partial \theta} \quad H_{\text{ef}y} = -\frac{1}{M_0} \sum_j N_j \frac{\partial \varepsilon_j}{\partial \phi} \quad H_{\text{ef}z} = 0 \quad (13.18)$$



**FIGURE 13.9**  
Coordinate system in the Clogston theory.

where the populations  $N_j$  are determined by (13.14). These components and the derivatives  $\partial \varepsilon_j / \partial \theta$  and  $\partial \varepsilon_j / \partial \phi$  are expanded in series near the point  $\theta_0, \varphi_0$ . They are substituted into the projections of (13.16), and only the terms of the first order are retained. The condition of compatibility of the obtained equations gives the complex frequency  $\omega = \omega' + i\omega''$ . In the case of small ion concentration, neglecting the terms with products of  $N_{j\infty}$  or their derivatives, we obtain

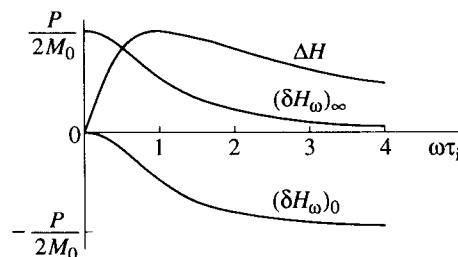
$$\begin{aligned} \delta H &\equiv H_0 - \frac{\omega'}{\gamma} = (\delta H)_\infty + (\delta H_\omega)_\infty \\ (\delta H)_\infty &= -\frac{1}{2M_0} \sum_j N_{j\infty} \left( \frac{\partial^2 \varepsilon_j}{\partial \theta^2} + \frac{\partial^2 \varepsilon_j}{\partial \phi^2} \right) \\ (\delta H_\omega)_\infty &= \frac{1}{2M_0} P \frac{1}{1 + \omega^2 \tau_i^2} \end{aligned} \quad (13.19)$$

$$\Delta H \equiv \frac{2\omega''}{\gamma} = \frac{1}{M_0} P \Omega \quad (13.20)$$

$$P = - \sum_j \left( \frac{\partial N_{j\infty}}{\partial \theta} \frac{\partial \varepsilon_j}{\partial \theta} + \frac{\partial N_{j\infty}}{\partial \phi} \frac{\partial \varepsilon_j}{\partial \phi} \right) \quad (13.21)$$

$$\Omega = \frac{\omega \tau_i}{1 + \omega^2 \tau_i^2}. \quad (13.22)$$

All the derivatives in (13.19) and (13.21) are taken at equilibrium angles  $\theta_0$  and  $\varphi_0$ .

**FIGURE 13.10**

Frequency dependences of  $\Delta H$  and of the resonance-field dynamic shifts in the theory of slow relaxation.

The expressions (13.19) can be rewritten in the form

$$\begin{aligned} \delta H &= (\delta H)_0 + (\delta H_\omega)_0 \\ (\delta H)_0 &= -\frac{1}{2M_0} \sum_j \left[ \frac{\partial}{\partial \theta} \left( N_{j\infty} \frac{\partial \varepsilon_j}{\partial \theta} \right) + \frac{\partial}{\partial \phi} \left( N_{j\infty} \frac{\partial \varepsilon_j}{\partial \phi} \right) \right] \\ (\delta H_\omega)_0 &= \frac{1}{2M_0} P \frac{\omega^2 \tau_i^2}{1 + \omega^2 \tau_i^2}. \end{aligned} \quad (13.23)$$

As  $(\delta H_\omega)_0 \rightarrow 0$  when  $\omega \tau_i \rightarrow 0$  (Figure 13.10), the term  $(\delta H)_0$  is the *static* shift of the resonance field. It coincides, as it can be shown, with the  $\delta H$  value obtained in Section 13.1. The term  $(\delta H_\omega)_\infty$  in (13.19) approaches zero when  $\omega \tau_i \rightarrow \infty$ , so  $(\delta H)_\infty$  is the resonance-field shift when the populations of the levels 'have no time' to relax to their quickly changing equilibrium values. According to [68], this shift can be named *adiabatic*. It is interesting that both quantities  $(\delta H)_0$  and  $(\delta H)_\infty$  are obtained by double differentiation of the equilibrium energy  $\sum_j N_{j\infty} \varepsilon_j$  with respect to the angles  $\theta$  and  $\phi$ . The first differentiation (which is related to the calculation of the effective field) is performed in both cases at  $N_{j\infty} = \text{const}$ . The second differentiation is performed at  $N_{j\infty} = \text{const}$  in calculating  $(\delta H)_\infty$ , and taking into account the angular dependences of  $N_{j\infty}$ , in calculating  $(\delta H)_0$ .

Important relations

$$(\delta H_\omega)_0 = \omega^2 \tau_i^2 (\delta H_\omega)_\infty = -\frac{1}{2} \omega \tau_i \Delta H \quad (13.24)$$

follow directly from (13.19), (13.23), (13.20), and (13.22).

Further development of the slow-relaxation theory was performed by Hartmann-Boutron [174] in two directions. First, it was shown that the anisotropy of exchange interaction results in the modulation of ionic energy levels by the oscillations of magnetization. Indeed, the anisotropy of the exchange interaction between magnetic and ionic systems leads to the fact that the transverse (with respect to  $\mathbf{M}_0$ )

ac magnetization gives rise to the longitudinal (with respect to  $\mathfrak{M}_0$ ) ac effective field acting on the ions. This field modulates, even in the first (linear) approximation, the energy levels of the ions. It should be noted that another cause of the appearance of the longitudinal ac field modulating the ionic energy levels is the crystal field, which also leads to nonparallelism of  $\mathfrak{M}_0$  and  $M_0$  if the spin-orbital interaction is present.

The second direction in which the slow-relaxation theory was improved by Hartmann-Boutron [174] is the replacement of (13.13) by the more general equation

$$\frac{dN_j}{dt} = -(N_j - N_{j\infty}) \sum_{j'=j} \frac{1}{\tau_{jj'}} + \sum_{j' \neq j} (N_{j'} - N_{j'\infty}) \frac{1}{\tau_{j'j}}. \quad (13.25)$$

The first term in the right-hand side of this equation represents the number of ions leaving per unit time the considered level. The second term is the number of ions coming onto this level from all others. The 'reverse' terms, analogous to the second term in (13.25), were omitted in Sections 11.2, 11.3, and 12.5; studying the relaxation of magnons, we assumed the numbers of all quasiparticles, except the considered ones to be equal to their equilibrium values. It should be noted that in some cases this assumption is not valid even for the relaxation of quasiparticles, and particularly, in two cases. The first case is when the number of primary quasiparticles is large, as for the nonlinear damping of parametrically excited magnons (Section 10.5). The second case is when a certain region of the secondary-quasiparticle spectrum is overfilled due to some other process. This situation is analogous to one considered in this chapter. Magnetic oscillations modulate *all* the ionic levels, and the difference between the instantaneous and equilibrium populations of *all* levels is not to be neglected.

Consider now the important particular case of *two energy levels*. In this case,  $N_1 + N_2 = N_{1\infty} + N_{2\infty} = N$ , and equations (13.13) for  $N_1$  and  $N_2$  with the *same* relaxation frequency

$$\frac{1}{\tau_1} = \frac{1}{\tau_{12}} + \frac{1}{\tau_{21}} \quad (13.26)$$

follow from (13.25).

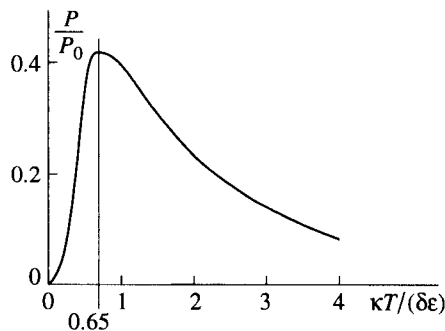
The distribution of ions over the levels in equilibrium state is the Boltzmann distribution [244]

$$N_{1,2\infty} = \exp\left(\frac{-\varepsilon_{1,2} + \mu}{\kappa T}\right) \quad (13.27)$$

where  $\mu$  is the chemical potential. Finding it from the condition  $N_{1\infty} + N_{2\infty} = N$ , we get

$$N_{1,2} = N \left[ 1 + \exp\left(\mp \frac{\delta\varepsilon}{\kappa T}\right) \right]^{-1}. \quad (13.28)$$

Substituting  $\varepsilon_{1,2} = \varepsilon_0 \mp \delta\varepsilon/2$  and  $N_{1,2\infty}$  from (13.28) into (13.21), we obtain

**FIGURE 13.11**

Temperature dependence of the factor  $P/P_0$  given by (13.29), in the case of two levels.

(for  $\epsilon_0$  not depending on  $\theta$  and  $\varphi$ )

$$P = P_0 \frac{\delta\epsilon}{\kappa T} \left( \cosh \frac{\delta\epsilon}{2\kappa T} \right)^{-2} \quad P_0 = \frac{N}{4\delta\epsilon} \left[ \left( \frac{\partial}{\partial\theta} \delta\epsilon \right)^2 + \left( \frac{\partial}{\partial\phi} \delta\epsilon \right)^2 \right]. \quad (13.29)$$

The static resonance-field shift  $(\delta H)_0$  calculated with (13.23) coincides, as it should, with (13.4).

The *frequency dependence* of the linewidth  $\Delta H$  is determined by the factor  $\Omega$  in (13.20). The linewidth approaches zero when  $\omega\tau_1 \rightarrow 0$  and when  $\omega\tau_1 \rightarrow \infty$  and passes through a maximum when  $\omega\tau_1 = 1$  (Figure 13.10), in accordance with the above-stated qualitative consideration. The  $\Delta H$  *temperature dependence* is determined by both factors  $P$  and  $\Omega$  because  $\tau_1$  depends on  $T$ . The relaxation time  $\tau_1$  usually decreases with growing temperature (see below), and the factor  $\Omega$  has a maximum at such temperature  $T_\Omega$  at which  $\omega\tau_1(T) = 1$ . The factor  $P$ , according to (13.29), passes through a maximum at  $\kappa T_P = 0.65\delta\epsilon$  (Figure 13.11). The function  $\delta H(T)$  can have one maximum or two, depending on the difference between  $T_\Omega$  and  $T_P$ . The dynamical shift  $(\delta H_\omega)_0$ , according to (13.23), has a temperature minimum near  $T_P$ .

Thus, the distinctive features of the slow (or longitudinal) relaxation mechanism are the following.

1.  $\Delta H$  approaches zero at  $T \rightarrow 0$  and has two temperature maxima; one of them, caused by the relaxation factor  $\Omega$ , is shifted to the higher temperatures with increasing frequency; very often the two maxima merge into one.
2. The height of the  $\Delta H$  temperature maximum depends slightly on frequency; the only reason of this dependence is the difference in positions of the  $\Omega$  and  $P$  maxima.
3. The angular dependences of  $\Delta H$  pass through minima when  $\partial(\delta\epsilon)/\partial\theta$  and  $\partial(\delta\epsilon)/\partial\phi$  go to zero, e.g., at the points of near-crossing of the ionic levels.

4. The dynamic shift of the resonance field is always negative; the ratio of its absolute value to  $\Delta H$  is proportional to frequency.

### 13.2.3 Relaxation of ionic-level populations

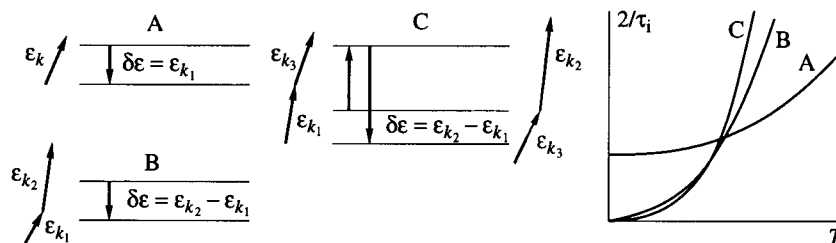
The processes of relaxation of the ionic-level populations, which determine the  $\tau_i$  values, are similar to, in some respects, the relaxation processes in paramagnetic substances [15]. However, the spin–spin (i.e., in our case, the ion–ion) relaxation does not now play an important role, as distinct from paramagnets, because the interaction between the ions is much weaker than their interaction with the magnetic system. Besides, the exchange splitting of the levels (Section 13.1) is much greater in ferromagnetic materials than the splitting in an external field, in the case of paramagnets. And, finally, along with the relaxation processes involving phonons, analogous processes with the participation of magnons (ion–magnon processes) can take place. Such processes were investigated theoretically by Buishvili [64] and Huber [186].

Processes in which more than two quasiparticles, phonons or magnons, take part are of negligible probability. For one-particle or so-called direct processes, the relaxation time, as Orbach [305] has shown, is

$$\tau_i = \tau_0 \tanh \frac{\delta\varepsilon}{2\kappa T}. \quad (13.30)$$

Here,  $\tau_0$  is also a function of  $\delta\varepsilon$ , and the character of this function depends on which interaction leads to the process. The orbital–lattice interaction dominates in the case of ion–phonon processes, and  $\tau_0$  decreases with growing  $\delta\varepsilon$ . For ion–magnon processes, the exchange interaction plays the main role, and the dependence of  $\tau_0$  on  $\delta\varepsilon$  is different for different ions [186]. For example, close to the near-crossings of energy levels,  $\tau_0$  decreases with growing  $\delta\varepsilon$  for  $\text{Yb}^{3+}$  ions on dodecahedral sites in YIG and increases for  $\text{Tb}^{3+}$  ions on the same sites.

The two-quasiparticle Raman and Orbach processes [305] (Figure 13.12) do



**FIGURE 13.12**

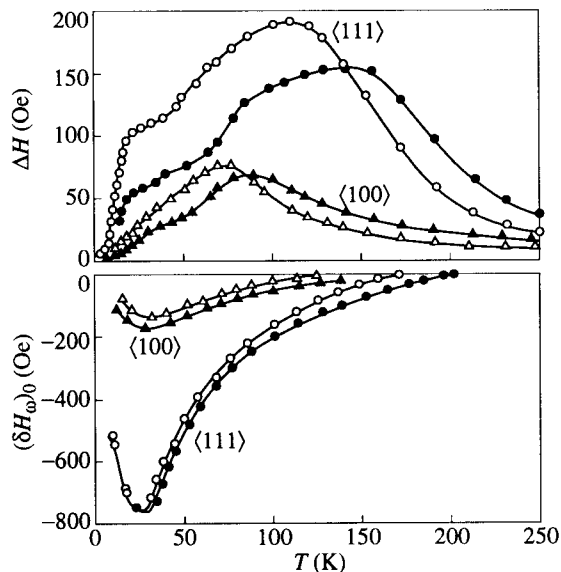
Elementary processes of the relaxation of ionic-level populations and temperature dependences of their contributions to the relaxation frequency (schematically): direct processes (A), Raman processes (B), and Orbach processes (C).

not differ in their final result. But, for the Orbach process, a third, higher level is needed. This leads to different temperature dependences. For Raman processes,  $\tau_1$  is proportional to  $T^{-7}$  in the case of non-Kramers ions and to  $T^{-9}$  in the case of Kramers ions. The  $\tau_1$  temperature dependence for Orbach processes is exponential. One can see from Figure 13.12 that direct processes dominate at low temperatures, whereas Raman and Orbach processes dominate at high temperatures.

#### 13.2.4 Experimental data

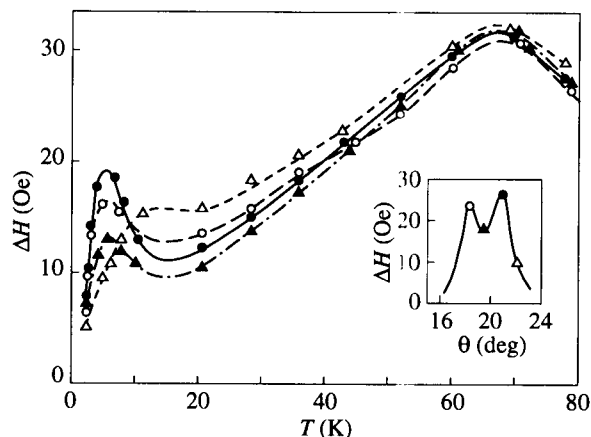
Discussing the results of experimental investigations of ionic relaxation processes, we must take into consideration that the ions are often situated on several nonequivalent lattice sites. The energy levels are different for ions on different sites due to different orientations of  $M_0$  with respect to the local crystal axes. Thus, all expressions for  $\Delta H$  and  $\delta H$  are to be replaced by their sums over all nonequivalent sites.

Let us consider first the rear-earth ions in garnets. It has been mentioned above that the two-level model is well applicable to a low-lying doublet and to an 'accidental' near-crossing of levels.  $\text{Yb}^{3+}$  ions on dodecahedral garnet sites are a good example of the first case.



**FIGURE 13.13**

Temperature dependences of  $\Delta H$  and the dynamic resonance-field shift for a  $\text{Y}_{3-x}\text{Yb}_x\text{Fe}_5\text{O}_{12}$  garnet ( $x = 0.153$ ) for different orientations of  $M_0$  [74]. Open circles correspond to frequency  $f = 9$  GHz and full circles, to  $f = 16.8$  GHz.



**FIGURE 13.14**

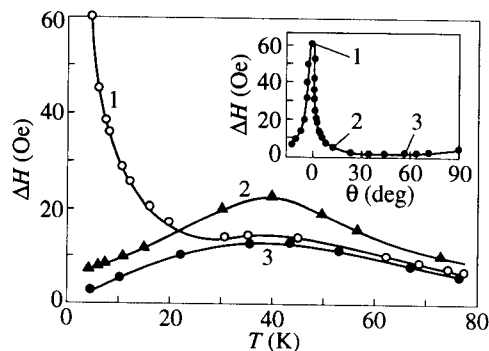
Temperature and angular dependences of  $\Delta H$  for a  $\text{Y}_{3-x}\text{Tb}_x\text{Fe}_5\text{O}_{12}$  garnet ( $x = 3 \times 10^{-4}$ ) in the vicinity of one of the near-crossings of  $\text{Tb}^{3+}$  energy levels [373]. Frequency  $f = 8.66$  GHz. The temperature dependences are shown for the angles denoted by corresponding symbols on the  $\Delta H$  vs  $\theta$  curve.

The ferromagnetic resonance in a YIG single crystal with a small addition of Yb was thoroughly investigated by Clarke, Tweedale, and Teale [74] (Figure 13.13). The  $\delta H$  values presented in this figure were obtained by subtracting the static resonance-field shift (measured by the torque-moment method) and the electrodynamic shift (Section 5.3) from the measured  $H_{\text{res}} - \omega/\gamma$  values. The  $\Delta H$  values are the directly measured quantities and represent, practically, the contributions only of the ionic relaxation mechanism. The data shown in Figure 13.13 agree with the above-mentioned features of the slow-relaxation mechanism. The  $\tau_1$  values found from these data decrease from  $\sim 10^{-9}$  to  $\sim 10^{-12}$  with growing temperature.

The experimental data for other Kramers rare-earth ions ( $\text{Nd}^{3+}$ ,  $\text{Sm}^{3+}$ ,  $\text{Dy}^{3+}$ , and  $\text{Er}^{3+}$ ) [94] seem to be consistent with the supposition that the slow relaxation mechanism plays the main role for these ions, too. But the absence of a sufficiently-low-lying doublet makes difficult the qualitative interpretation of the data.

In YIG doped with *non-Kramers* ions  $\text{Tb}^{3+}$ ,  $\text{Ho}^{3+}$ , and  $\text{Pr}^{3+}$ , the 'anomalous'  $\Delta H$  angular dependences caused by near-crossings of energy levels were observed [94, 373, 156, 9]. In the case of  $\text{Tb}^{3+}$ , strong absorption bands take place at low temperatures for three  $M_0$  directions in which the near-crossings occur (Figure 13.5). To explain these absorption bands in the framework of the slow-relaxation theory one has to assume the relaxation frequency  $1/\tau_1$  (that is less than  $\omega$  at such temperatures) to increase sharply with decreasing  $\delta\varepsilon$ . This assumption, made in [373], was confirmed theoretically by Huber [186]. He showed that the contribution of the above-mentioned direct ion-magnon processes dominates in



**FIGURE 13.15**

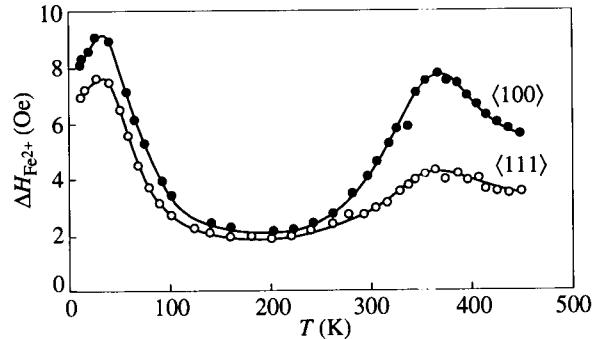
Temperature and angular dependences of  $\Delta H$  for  $Y_{3-x}Pr_xFe_5O_{12}$  garnet ( $x = 9 \times 10^{-4}$ ) measured at frequency  $f = 9$  GHz [156]. The temperature dependences are shown for angles denoted by corresponding numbers on the  $\Delta H$  vs  $\theta$  curve (measured at  $T = 4.2$  K).

this case at low temperatures and leads to the assumed dependence of  $1/\tau_1$  on  $\delta\varepsilon$ . The minimal  $\delta\varepsilon$  value can be estimated as  $\sim 2.5 \text{ cm}^{-1}$  and the relaxation time  $\tau_1$ , as  $\sim 10^{-10}$  s. One can see from Figure 13.5 that there are minima at the centers of all absorption bands, in agreement with the slow-relaxation theory.

The  $\Delta H$  temperature dependences in YIG doped with Tb are plotted, for one of the absorption bands, in Figure 13.14. Two maxima in these dependences can be associated with the contributions of different levels: the near-crossing pair (low-temperature maximum) and all other levels (high-temperature one). It is seen from Figure 13.14 that at high temperatures, when the relaxation frequency  $1/\tau_1$  of the near-crossing levels exceeds  $\omega$ , the angular absorption bands transform into angular minima. This has been observed for other 4f ions, too, [164] and is in agreement with the slow-relaxation theory if we suppose that  $1/\tau_1$  increases with the decrease of  $\delta\varepsilon$ .

In YIG with  $Ho^{3+}$  ions, sharp  $\delta H$  maxima and strong absorption bands were observed [9] when  $M_0$  directions lay in one of the  $\{100\}$  planes. In these directions, as has already been mentioned, the near-crossings of  $Ho^{3+}$  energy levels take place. The absorption bands, as in the case of  $Tb^{3+}$ , were split into two maxima, in agreement with the slow-relaxation theory.

The temperature and angular dependences of  $\Delta H$ , for YIG with small addition of Pr, are plotted in Figure 13.15. In this case,  $\Delta H$  grows monotonically with decreasing temperature (at least, down to 4.2 K) and  $\Delta H$  angular maxima are not split. The same features were observed [99] in YIG with addition of Yb for  $M_0$  directions ( $\theta = 30^\circ$  and  $\theta = 90^\circ$ ) in which the  $Yb^{3+}$  ions penetrating onto *octahedral* lattice sites have near-crossing of energy levels (Section 13.1). The  $\delta\varepsilon$  value can be so small in both cases, of Pr and Yb on octahedral sites, that the contribution of the transverse relaxation is possible.



**FIGURE 13.16**

Temperature dependences of the contribution of  $\text{Fe}^{2+}$  ions to  $\Delta H$  for Ge-doped YIG at different  $M_0$  orientations [172].  $f = 9.25$  GHz,  $\text{Fe}^{2+}$  concentration  $z = 0.2$  mol % (with respect to  $\text{Fe}^{3+}$  ions),  $\Delta H_{\text{Fe}^{2+}} = \Delta H|_{z=0.2} - \Delta H|_{z=0}$ . © 1972 Elsevier Science Ltd.

The influence of  $\text{Fe}^{2+}$  ions on ferromagnetic resonance in YIG was detected as early as in 1961 [165, 381] and was investigated in detail later on (e.g., [401, 175]). In addition to the *intraionic* transitions considered above, the electron transitions between  $\text{Fe}^{2+}$  and neighboring  $\text{Fe}^{3+}$  ions are possible in this case. Their influence on ferromagnetic resonance will be studied in Section 14.1. We mention here only that the characteristic frequencies for such transitions are usually much lower than the frequencies  $1/\tau_i$  for the *intraionic* transitions. The temperature dependences of  $\Delta H$  in YIG containing  $\text{Fe}^{2+}$  ions are plotted in Figure 13.16. The low-temperature maxima in these dependences are caused by *intraionic* transitions and can be described in terms of the slow-relaxation theory. The high-temperature maxima are due to *interionic* electron transitions.  $\text{Fe}^{4+}$  ions, which arise in YIG as a result of the substitution of two-valent ions for the three-valent ions (e.g.,  $\text{Ca}^{2+}$  for  $\text{Y}^{3+}$ ), lead to  $\Delta H$  temperature maxima [402] similar to such caused by  $\text{Fe}^{2+}$  ions. The reason for this is the same level splitting (Table 13.3) for  $\text{Fe}^{2+}$  ions in an octahedral environment (which is preferred by these ions) and for  $\text{Fe}^{4+}$  ions in a tetrahedral environment.

$\text{Fe}^{2+}$  and  $\text{Fe}^{4+}$  ions can arise in YIG single crystals and epitaxial films grown from highly pure starting materials, without any additions, as a result of ions  $\text{Pt}^{4+}$  penetrating into the lattice from the crucible and of  $\text{Pb}^{2+}$  ions penetrating from the melt. The diminishing of the amount of these ions, or compensation of their effect, e.g., by small addition of Ca if  $\text{Pt}^{4+}$  ions dominate, is a necessary condition for obtaining YIG crystals or films with small  $\Delta H$  values.

Ferromagnetic resonance in YIG with small additions of Mn and Co was also investigated [169, 388]. However, the interpretation of these experiments presents problems because these elements can have different valencies, can occupy different lattice sites, and can stimulate the change of valency of Fe ions.

The 3d ions with strong spin-orbital coupling in ferrites with *spinel* structure can exert, as White suggested [440], the same influence on ferromagnetic-resonance anisotropy and linewidth as the above-discussed ions in YIG. It soon became clear that the slow-relaxation mechanism also operates in spinels. But the above-mentioned difficulties in interpretation arise here, as well. The most attention was paid to the ferrite  $\text{Mn}_{1-x}\text{Fe}_{2-y}\text{O}_4$ , in which the fast relaxing ions  $\text{Mn}^{3+}$  and  $\text{Fe}^{2+}$  can exist [236]. Two  $\Delta H$  temperature maxima were observed in some samples of this ferrite [73], the low-temperature caused by  $\text{Mn}^{3+}$  ions and the high-temperature caused by  $\text{Fe}^{2+}$  ions.

The ferromagnetic crystals with spinel structure  $\text{MCr}_2\text{X}_4$  ( $\text{M} = \text{Cd}, \text{Hg}$  and  $\text{X} = \text{S}, \text{Se}$ ) are also good objects for studying the ionic relaxation processes. In Figure 13.6 the  $\Delta H$  angular dependences for one of these crystals have been shown. The  $\Delta H$  maxima in  $\langle 100 \rangle$  and  $\langle 110 \rangle$  directions are caused by the near-crossings of levels of the  $\text{Cr}^{4+}$  ions, which arise due to Ag addition in the course of the crystal growth. The maxima in  $\langle 111 \rangle$  directions are caused by  $\text{Cr}^{2+}$  ions, which arise due to Se vacancies emerging in the process of annealing the sample. The slow-relaxation mechanism appears to dominate in this case, too, even though some of its characteristic features ( $\Delta H$  low-temperature maxima and splitting of the  $\Delta H$  angular maxima) have not been observed. Both were observed in another crystal of this group,  $\text{HgCr}_2\text{Se}_4$  [107].

It follows from the considered examples that the ionic relaxation process is widely present in non-metallic ferro- and ferrimagnetic substances. In many cases, especially at low temperatures, this process forms the main channel of relaxation in ferromagnetic resonance. The ionic relaxation process makes essential contributions to energy dissipation in antiferromagnetic crystals (e.g., [354]) and in magnetically ordered metals (Section 14.2), as well.

The ionic relaxation process is based on the transitions between energy levels of individual ions. Therefore, the contributions of this mechanism to the spin-wave dissipation parameter  $\Delta H_k$  should not depend essentially on the wave number  $k$ .



# 14

---

## *Interaction of magnetic oscillations and waves with charge carriers*

---

### **14.1 Effect of charge carriers in semiconductors**

Until now, studying oscillations and waves in magnetically ordered substances, we did not take into account the conductivity, i.e., regarded these substances as dielectrics. But actually they are, usually, semiconductors or metals. True, the ferrites used in microwave engineering (as well as in most experiments on ferromagnetic resonance and spin waves) are semiconductors with such small conductivity that the effect of charge carriers can be neglected. However, for some ferrites with larger conductivity (e.g., [236]), this effect is essential. Moreover, there are magnetic semiconductors [284], which combine magnetic ordering with conductivity as large as for 'good' semiconductors. And, finally, there are ferromagnetic, ferrimagnetic, and antiferromagnetic metals, in which charge carriers have the determinative impact on all dynamic magnetic processes.

The theoretical treatment of magnetic oscillations and waves in conducting media is based on simultaneous solution of the Maxwell equations, equation of motion of the magnetization, and equations of motion of the charge carriers. The peculiarities of the solutions and the nature of the observed phenomena depend, first of all, on the relationship between the dimensions of the sample and the skin depth  $\delta$  (Section 4.2). In the present section the limiting case of  $\delta \gg d$  will be considered, where  $d$  is the characteristic dimension of the sample, i.e., the radius of a sphere or the thickness of a plate. This case is realized, in the microwave region, for spheres of common ferrites, as well as for thin films of materials with much larger conductivity.

#### **14.1.1 Damping of magnetic oscillations caused by conductivity**

Let us consider the contribution of conductivity to the dissipation parameter of magnetization oscillations (in the case of  $\delta \gg d$ ) using, as an example, the uniform

oscillations in a small ferromagnetic sphere [155]. The method of successive approximations may be applied. The magnetization in a nonconducting sphere will be the zero approximation. In the first approximation, the electric field induced by this magnetization will be found. The Joule losses of the current excited by this field will contribute to the damping of magnetic oscillations.

We will limit ourselves to the oscillations near ferromagnetic resonance and assume the resonance line to be sufficiently narrow. Then,  $|m| \gg |h_e|$  (where  $m$  is the ac magnetization and  $h_e$  is the external ac field), the polarization of  $m$  is near circular, i.e.,  $m \simeq m(x_0 - iy_0)$ , and the ac magnetic induction is

$$b = h + 4\pi m = h_e - \frac{4\pi}{3}m + 4\pi m \simeq \frac{8\pi}{3}m. \quad (14.1)$$

To find the ac electric field we have to substitute the zero-order induction (14.1) into the first of equations (6.4). The result of such calculation, performed by Pistol'kors and Sui Yangshen [316], can be represented in the form

$$e_1 = \frac{4\pi}{3}k_0 [(-x_0 + iy_0)z + z_0(x - iy)]m. \quad (14.2)$$

It is worth nothing that, for sufficiently narrow resonance line and not too small a sample, the field  $e_1$  turns out to be much larger than the field  $h_e$  and, hence, much larger than the electric field in the resonator or waveguide in which the sample is placed. Assume, e.g., that the radius of the sphere  $R = 0.5$  mm,  $M_0 = 139$  G, and  $\Delta H = 0.5$  Oe. Then, taking into account that  $m \simeq M_0 h_e / \Delta H$  (Section 1.5), we get, at  $\lambda_0 = 2\pi/k_0 = 3$  cm, the electric field at the surface of the sphere  $e_{1 \max} \simeq 100 h_e$ . According to (5.46) and (1.120), a resonator containing such a sphere will have a quality factor  $Q \sim 5$ . It is easy to make sure that  $e_{1 \max}$  will be, then, as large as  $10 \text{ kV cm}^{-1}$  when the power absorbed in the resonator is only  $\sim 1$  W.

According to (4.75), the power of electric losses caused by the field  $e_1$  is

$$P_\sigma = \frac{\omega \varepsilon''}{8\pi} \int_V |e_1|^2 dV \quad (14.3)$$

where the integration is over the sphere volume. This power is drawn from the energy of magnetic oscillations and makes a contribution to the dissipation parameter

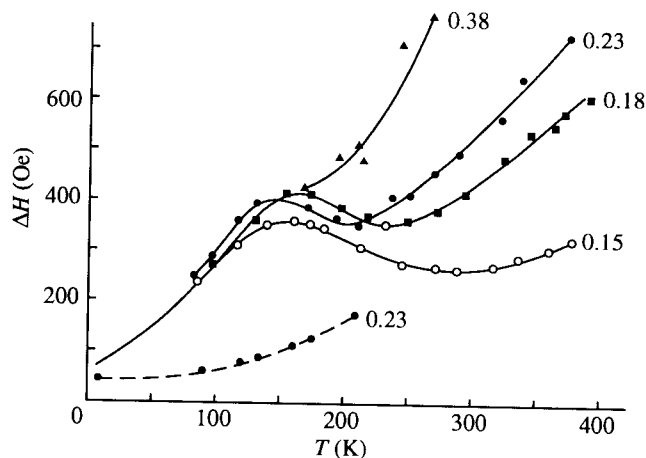
$$\Delta H_\sigma = \frac{P_\sigma}{\gamma W_0} \quad (14.4)$$

where  $W_0$  is the energy of the uniform oscillation mode. According to (7.68),

$$W_0 = \frac{\omega m^2}{2\gamma M_0}. \quad (14.5)$$

After integrating in (14.3) with regard for (14.2), we get from (14.4)

$$\Delta H_\sigma = \frac{4}{45} \varepsilon'' 4\pi M_0 (k_0 R)^2. \quad (14.6)$$

**FIGURE 14.1**

Temperature  $\Delta H$  dependences for single-crystal spheres of ferrite  $\text{Ni}_{0.75}\text{Fe}_{0.25}^{2+}\text{Fe}_2^{3+}\text{O}_4$  at frequency 24 GHz [450]. Numbers by the curves denote the sphere diameters in millimeters. Solid lines correspond to  $M_0 \parallel (111)$ , and dashed line corresponds to  $M_0 \parallel (100)$ .

Thus, the contribution of conductivity to the linewidth is a *dimensional effect*.

The value of  $\varepsilon''$  is less than 0.01 for stoichiometric single-crystal ferrites, as well as for most of polycrystalline microwave ferrites. For spheres of such materials with  $R < 1$  mm, the values of  $\Delta H_\sigma$  are negligibly small (less than  $\sim 0.02$  Oe). But they become essential for materials with higher conductivity, e.g., for ferrites containing  $\text{Fe}^{2+}$ . The conductivity of such materials and, hence,  $\Delta H_\sigma$  increase with growing temperature (Figure 14.1).

Formulae similar to (14.6) were obtained by Maryško [270] for other sample shapes. The order of the values and the dependence on frequency and the characteristic sample dimensions remain the same as in (14.6). Analogous calculations can be carried out for nonuniform oscillations and for spin waves. But it is obvious that the  $\Delta H_\sigma$  values will be much smaller because the role of  $2R$  will be played by the wavelength  $2\pi/k$  or—for nonuniform modes—by the distance at which the ac magnetization phase changes by  $2\pi$ .

### 14.1.2 Influence of interionic electron transitions

In some ferrites, the 'jumping' mechanism (referred also to as the valency-exchange or Verwey's mechanism) is the dominant mechanism of conductivity (e.g. [236]). In such substances, along with the main magnetic ions, e.g.,  $\text{Fe}^{3+}$ , there exist ions of the same element but with other valences ( $\text{Fe}^{2+}$  or  $\text{Fe}^{4+}$ ). Such ions are usually fast-relaxing ions. Their contributions to ferromagnetic-resonance anisotropy and relaxation caused by the intraionic transitions were studied in detail in the preceding chapter. But the *interionic* transitions, i.e., the transitions of

electrons between these ions and the neighboring ions with the main valency, can occur, as well. These transitions are associated with getting over certain (usually rather low, of the order of 0.1 eV) energy barriers and are caused by the thermal motion. If an electric field is applied, a prevailing direction of the transitions appears, and an electric current arises. In a high-frequency electric field, the inertia of the transitions manifests itself, and electrical losses appear. They pass through a maximum when the frequency of the field  $\omega$  becomes equal to the relaxation frequency  $1/\tau_e$  associated with the transitions.

Prevailing directions of such thermally activated transitions can be determined as well by the magnetization and can change (with delay  $\tau_e$ ) with the variation of the magnetization direction, e.g., at ferromagnetic resonance. The theory considered in Section 13.2 is fully applicable to the interionic transitions; moreover, it was developed by Clogston just for this case. The energy levels  $\varepsilon_j$  are now the levels of the complexes that differ in the appearance of an extra electron (as in the case of  $\text{Fe}^{2+}$ ) or in the lack of an electron (as for  $\text{Fe}^{4+}$ ) at different neighboring ions. Then, the difference in  $\varepsilon_j$  values is due to the difference in angles between the direction of  $\mathbf{M}$  and the local axes of ions. Thus, the number of levels is equal to the number of nonequivalent lattice sites that can be occupied by the considered ions.

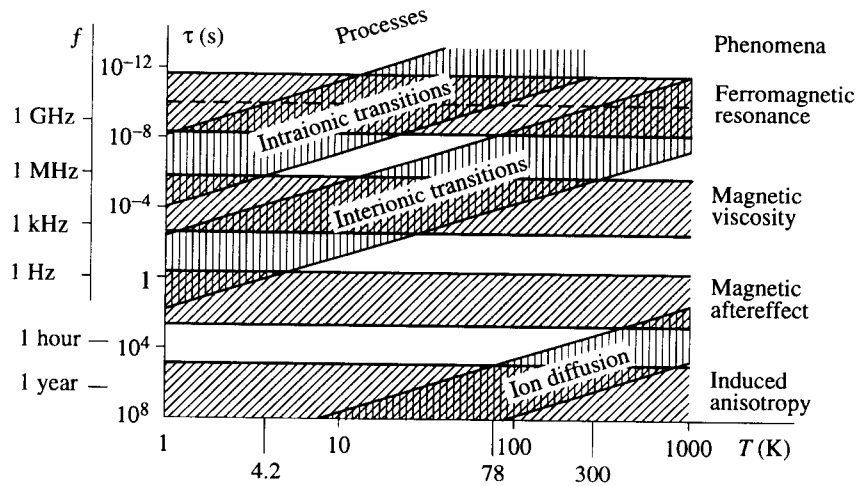
$\text{Fe}^{2+}$  ions prefer the octahedral sites [236], and there are *four* such nonequivalent sites in spinel and garnet structures (Section 3.3). That is why Clogston examined the model with four levels  $\varepsilon_j$  and found, using formula (13.20), that  $\Delta H$  is maximal when  $\mathbf{M}_0 \parallel \langle 100 \rangle$  and is minimal when  $\mathbf{M}_0 \parallel \langle 111 \rangle$ . Such anisotropy (resulting from the interionic  $\text{Fe}^{3+}$ - $\text{Fe}^{2+}$  transition) was observed for the high-temperature maximum of  $\Delta H$  in YIG with a Ge addition [172]. As to the experimental data for the Ni-Fe ferrite (which Clogston tried to compare his theory with), in that case the  $\Delta H$  anisotropy has the reversed sign (Figure 14.1). It later became clear that no contradiction exists here because the temperature  $\Delta H$  maxima in Ni-Fe ferrite are caused by intraionic transitions (Section 13.2).

It should be noted that at very low temperatures the interionic electron transitions, practically, do not occur at all during the time 'at the disposal' of experimentalists; this is one of the reasons of the induced anisotropy in ferrites (e.g., [236]). At higher temperatures, when  $\tau_e$  becomes comparable with the time of experiment, the retarded interionic transitions lead to nonstationary phenomena known as magnetic aftereffects. At still higher temperature, when  $1/\tau_e$  becomes comparable with the frequency  $\omega$  of the ac magnetic field, the same transitions result in magnetic viscosity, i.e., in the losses described by the imaginary part of the permeability. And when  $1/\tau_e$  becomes as high as the ferromagnetic-resonance frequency (usually at temperatures higher than the room temperature), the above-mentioned contributions of interionic transitions to  $H_{\text{res}}$  and  $\Delta H$  take place.

The interionic transitions can occur under the influence of light, which leads to the interesting photomagnetic effects, in particular, to the light-induced magnetocrystalline anisotropy. This phenomenon was investigated, in the case of YIG with addition of Si, by Dillon, Gyorgy, and Remeika [96].

One note more: the diffusion of atoms or ions in the crystal lattice can also





**FIGURE 14.2**

Characteristic time vs temperature for different processes and regions in which these processes manifest themselves in different phenomena (schematically). The dashed line corresponds to the experimental data shown in Figure 14.1.

lead to the induced magnetocrystalline anisotropy or, at higher temperatures, to the magnetic aftereffect. As the characteristic time of the diffusion is much longer than the relaxation time of electron transitions, the phenomena caused by the diffusion are shifted to much higher temperatures. The positions of all mentioned phenomena on frequency and time scales are shown—quite schematically—in Figure 14.2.

### 14.1.3 Interaction of spin waves with charge carriers

Let us discuss now the influence of charge carriers on the propagation of magnetic waves. The permittivity  $\epsilon$  cannot be regarded now as a real scalar quantity, as in Chapters 6 and 7, but it is a tensor with complex components depending on frequency and, in general, on the wave vector. To find this tensor we must use the equations of motion of the charge carriers. Because of the distribution of carriers over the velocities  $\mathbf{V}$ , the function of the equation of motion is fulfilled now by the *Boltzmann kinetic equation* for the distribution function  $f(\mathbf{V}, \mathbf{r}, t)$  (e.g., [253]). Having found this function for each type of carriers, at given values of the electric field  $\mathbf{E}$  and magnetic field  $\mathbf{H}$ , we can then calculate all quantities depending on the carriers, in particular, the concentrations  $N_s(\mathbf{r}, t) = \int f(\mathbf{V}, \mathbf{r}, t) d\mathbf{V}$  and the mean velocity

$$\bar{\mathbf{V}}_s(\mathbf{r}, t) = \frac{1}{N_s} \int \mathbf{V} f_s(\mathbf{V}, \mathbf{r}, t) d\mathbf{V} \quad (14.7)$$

where  $s$  denotes the type of carriers. The current density

$$\mathbf{J} = \sum_s e_s N_s \bar{\mathbf{V}}_s \quad (14.8)$$

where  $e_s$  is the charge of the  $s$ -type carrier. If the Ohm law holds, the conductivity  $\vec{\sigma}$  and (for harmonic processes) the complex permittivity (4.18) can be obtained. (The 'dielectric constant'  $\epsilon_d$ , in the microwave frequency range, can be regarded, really, as a constant.)

In the problem of interaction of magnetic waves with charge carriers, the so-called *hydrodynamic* approximation (e.g., [317]) can be used. The carriers of each type are entirely characterized, then, by the following parameters: concentration  $N_s$ , mean velocity  $\bar{\mathbf{V}}_s$ ,<sup>1</sup> and mean frequency of collisions  $1/\tau_s$ . The equation of motion in this approximation can be written as

$$\frac{\partial \mathbf{V}_s}{\partial t} + (\mathbf{V}_s \nabla) \mathbf{V}_s = \frac{e_s}{m_s} \left( \mathbf{E} + \frac{1}{c} \mathbf{V}_s \times \mathbf{B} \right) + \frac{\nabla P}{m_s N_s} - \frac{\mathbf{V}_s}{\tau_s} \quad (14.9)$$

where  $m_s$  is the carrier mass and  $P$  is the pressure. This equation can be derived, with appropriate assumptions, from the Boltzmann kinetic equation. It can be regarded, as well, as the Newton equation of motion for carriers in a volume element moving with the velocity  $\mathbf{V}_s$ . The left-hand side of (14.9) is the total derivative  $d\mathbf{V}_s/dt$ . The terms in the right-hand side are: the Lorentz force, the force caused by pressure gradient, and the frictional force caused by the collisions. We limit ourselves to one type of carriers (electrons) with the charge  $e_0$  and neglect the 'pressure' term in (14.9).

All quantities in (14.9) are the sums of steady and alternating components. Regarding the latter as small and assuming that their dependence on time is harmonic, we obtain the *linearized* equation for the complex amplitudes

$$i\omega \mathbf{v} + (\mathbf{V}_0 \nabla) \mathbf{v} = -\frac{|e_0|}{m_e} \left( \mathbf{e} + \frac{1}{c} \mathbf{V}_0 \times \mathbf{b} + \frac{1}{c} \mathbf{v} \times \mathbf{B}_0 \right) - \frac{\mathbf{v}}{\tau}. \quad (14.10)$$

(An assumption has been made that the steady velocity  $\mathbf{V}_0$  does not depend on coordinates.)

We will consider the solutions of (4.10) for a *uniform plane wave* propagating along or perpendicularly to the direction of the steady magnetization (Figure 14.3). In both cases the drift velocity  $\mathbf{V}_0$  will be parallel to the direction of propagation.

In the first case ( $\mathbf{k} \parallel \mathbf{V}_0 \parallel \mathbf{B}_0$ ), projecting (14.10) onto axes  $x$  and  $y$  (the  $z$ -axis is directed, as usual, along  $\mathbf{B}_0$ ) and passing to the circular variables  $v_{\pm} = v_x \pm iv_y$ , etc., we get

$$v_{\pm} \left( i\omega \mp i\omega_B - ikV_0 + \frac{1}{\tau} \right) = -\frac{|e_0|}{m_e} \left( e_{\pm} \pm \frac{i}{c} V_0 b_{\pm} \right) \quad (14.11)$$

<sup>1</sup>In what follows, the mean velocity will be denoted, simply, by  $\mathbf{V}_s$ .

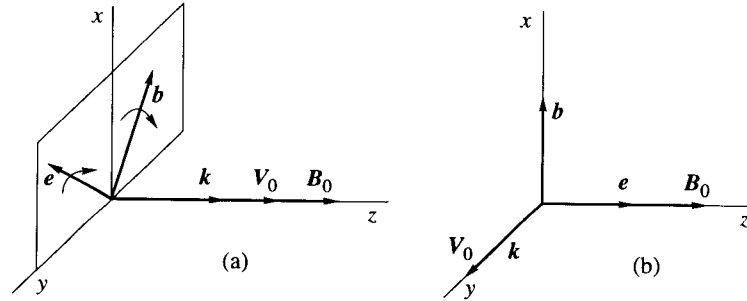


FIGURE 14.3

Particular cases of wave propagation in a medium with drifting charge carriers.

where  $\omega_B = |e_0|B_0 / (m_e c)$  is the cyclotron frequency. To exclude  $b_{\pm}$  we use the Maxwell equation (4.7), from which it follows  $b_{\pm} = \pm i (ck/\omega) e_{\pm}$ .

Linearizing (14.8), in our case of one type of carriers, we get

$$\mathbf{j} = -|e_0| (N_0 \mathbf{v} + n \mathbf{V}_0). \quad (14.12)$$

But the second term in the parentheses is small, and we neglect it. Passing in (14.12) to the circular components of  $\mathbf{j}$  and  $\mathbf{v}$ , we find, using (14.11), the conductivity  $\sigma_{\pm}$ , and, finally, taking into account (1.18), we obtain

$$\epsilon_{\pm} = \epsilon_d - \frac{\omega_p^2}{\omega} \frac{1 - kV_0/\omega}{\omega - kV_0 \mp \omega_B - i/\tau} \quad (14.13)$$

where

$$\omega_p = \sqrt{\frac{4\pi N_0 e_0^2}{m_e}} \quad (14.14)$$

is the Langmuir plasma frequency [317].

We are interested in the influence of carriers on the *slow* (spin) waves in a ferromagnet (Section 4.2). In the case of  $\mathbf{k} \parallel \mathbf{B}_0$ , the wave with right-hand circular polarization is such a wave. Therefore, we must take the upper signs in (14.13). In the second particular case ( $\mathbf{k} \perp \mathbf{B}_0$ ), the wave with electric field  $\mathbf{e}$  directed along  $\mathbf{B}_0$  is the slow wave. For this direction of  $\mathbf{e}$ , proceeding analogously to the previous case, we find

$$\epsilon_{\parallel} = \epsilon_d - \frac{\omega_p^2}{\omega} \frac{1 - kV_0/\omega}{\omega - kV_0 - i/\tau}. \quad (14.15)$$

Thus, in both cases the tensor  $\vec{\epsilon}$  components are complex and depend on  $\omega$ ,  $k$ , and, in the first case, also on the steady magnetic field. Electromagnetic waves in such media, the so-called *electrokinetic* waves, have been thoroughly investigated (e.g., [557]). The waves with circular polarization propagating along  $\mathbf{B}_0$  are called

helicons, and the linearly polarized waves propagating perpendicularly to  $\mathbf{B}_0$  are called the cyclotron waves.

Separating the real and the imaginary parts of the obtained expressions for  $\vec{\epsilon}$  components, we get, in the first case,

$$\epsilon''_{\pm} = \frac{\omega_p^2}{\omega\tau} \frac{1 - kV_0/\omega}{(\omega - kV_0 \pm \omega_B)^2 + (1/\tau)^2}. \quad (14.16)$$

In the second case, in the expression for  $\epsilon''_{\parallel}$  the term  $\pm\omega_B$  is absent. In both cases  $\epsilon''$  decreases with the growth of  $V_0$  and becomes equal to zero at  $V_0 = \omega/k \equiv v_{ph}$ . This means that the electric losses are compensated by the drift of the carriers. The mechanism of the compensation is that the Lorentz force  $|e_0|/(m_e c)\mathbf{V}_0 \times \mathbf{b}$  excites the ac current in the direction antiparallel to the ac electric field  $\mathbf{e}$ . When  $V_0 > v_{ph}$ , the quantity  $\epsilon''$  becomes negative. And if there are no other losses, except those caused by the conductivity, then a wave propagating in such medium will be *amplified*. The energy will be drawn from the source that accelerates the carriers.

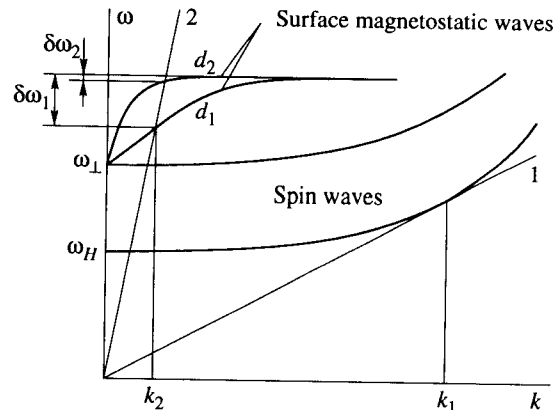
It is easy to make sure that, when  $V_0$  and  $\mathbf{k}$  make an arbitrary acute angle, the condition of loss compensation is

$$kV_0 > \omega. \quad (14.17)$$

It is worth noting that this condition coincides with the condition of the Cherenkov radiation [246] of electromagnetic energy by electrons moving in dielectric with velocity  $V_0$ .

Suppose now that the medium is a magnetically ordered one, e.g., a ferromagnet. Then, to obtain the dispersion relations of electromagnetic waves in such a medium we have to find the solutions of Maxwell's equations, the equations of motion of charge carriers, and the Landau-Lifshitz equation of motion of magnetization; the boundary conditions should be, of course, taken into account. For waves in semiconductors (but not in metals, see Section 14.2) all the characteristic dimensions, including the carrier mean free path, are smaller than the wavelength in the microwave range. Under this condition, we may seek the solutions of Maxwell's equations with the parameters  $\vec{\epsilon}$  and  $\vec{\mu}$  found *beforehand* from the corresponding equations of motion.

For an *unbounded* medium, the formulae given in Section 4.2 can be used, e.g., formula (4.42), for waves propagating along  $\mathbf{M}_0$ , and formula (4.53), for waves that propagate perpendicularly to  $\mathbf{M}_0$ . The waves for which the dispersion relations are found in such a way are *mixed magneto-electrokinetic* waves. They have been investigated in detail in many important cases (e.g., [386]). These mixed waves, analogously to the magnetoelastic waves (Section 12.3), can be regarded (in terms of coupled waves) as a result of the interaction of magnetic (spin) waves in a nonconducting medium and electrokinetic waves in a medium with  $\mu = 1$ . Similar to the magnetoelastic waves (Section 12.3), the interaction is the strongest near the crossing points of the dispersion curves for the unperturbed waves. Far



**FIGURE 14.4**

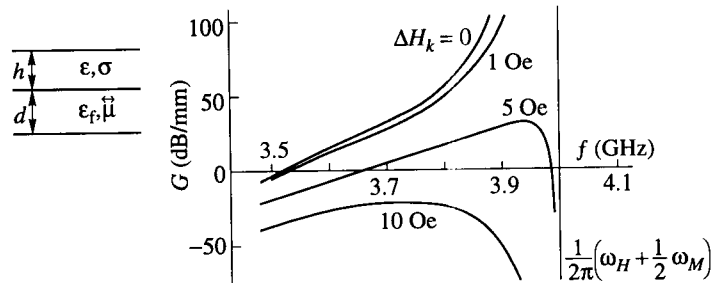
Dispersion curves for spin waves in an infinite medium and for surface nonexchange magnetostatic waves in tangentially magnetized films. The straight line 1 corresponds to  $v_{\text{ph min}}$  of spin waves, and the straight line 2 corresponds to a certain drift velocity.  $\delta\omega_1$  and  $\delta\omega_2$  are the frequency bands in which (without allowance for magnetic losses) the amplification by drifting charge carriers is possible in films with thicknesses, respectively,  $d_1$  and  $d_2$ .

enough from these points, the spectrum of mixed waves consists of the magnetic and the electrokinetic branches more or less perturbed by the interaction.

With allowance for losses (caused both by the conductivity and the imaginary parts of  $\vec{\mu}$  components) the dispersion equations for the mixed waves become complex. In the case of stationary waves,  $\omega$  is real and the solutions of these equations have the form  $k = k' - ik''$ . And if the drift velocity and the concentration of the carriers are large enough, the losses are compensated,  $k''$  becomes negative, and the *amplification* of the wave takes place. Not too near the crossing point, we may speak of the amplification of spin waves by drifting carriers. The possibility of such an amplification was predicted by Trivelpiece *et al.* [406] and investigated theoretically by Akhiezer, Bar'yakhtar, and Peletminskii [13] (see also [14]) on the model of an *electron beam* piercing the ferromagnet. The beam velocity should be, in any case, larger than the minimal spin-wave phase velocity, which according to (7.9) is  $v_{\text{ph min}} = \sqrt{\eta\omega}$ . For YIG at microwave frequencies,  $v_{\text{ph min}} \sim 10^5$ . Such beam velocities are easily achievable in vacuum, but the model of an electron beam piercing a ferromagnetic sample is hardly realizable.

The amplification of spin waves by drifting carriers in a *semiconductor* was investigated by Makhmudov and Bar'yakhtar [268]. It was later shown [80] that for full compensation of losses, i.e., for amplification, such parameters are needed ( $\Delta H < 0.3$  Oe,  $V_0 \sim 10^6$ ) which can hardly be obtained in one substance.

Therefore, great attention has been paid to the problem of amplification of waves in *composite structures* that contain adjoining layers of 'good' weakly conducting ferrite and of 'good' nonmagnetic semiconductor. This problem was first studied by Schlömann [350] on a model of a semi-infinite ferrite and a thin semiconductor

**FIGURE 14.5**

Calculated frequency dependence of the amplification coefficient of the surface magnetostatic wave in a ferrite-semiconductor structure [49].  $d = 3.6 \mu\text{m}$ ,  $h = \infty$ ,  $V_0 = 3 \times 10^7 \text{ cm s}^{-1}$ ,  $H_0 = 553 \text{ Oe}$ ,  $M_0 = 139 \text{ G}$ ,  $\epsilon_f = 17$  (YIG),  $\epsilon = 17.7$ ,  $\sigma = 191 \Omega^{-1} \text{ cm}^{-1}$ . © 1978 IEEE.

layer. Lukomskii and Tsvirko [260] and Bini, Millanta, and Rubino [49] investigated the problem for a surface magnetostatic wave (Section 6.2) in a thin ferrite film. It was shown that, if magnetic losses are not taken into account, amplification begins at  $V_0/v_{\text{ph}} = 1$  ( $k = k_2$  in Figure 14.4) and intensifies with the growth of this ratio. It is seen from Figure 14.4 that the frequency band of the amplification is larger the thinner the ferrite film.

The allowance for *magnetic losses* in the ferrite film leads to the narrowing of the frequency band in which the amplification takes place (Figure 14.5): from the low-frequency side of the band, because the amplification begins now at  $V_0/v_{\text{ph}} > 1$ , and from the high-frequency side, because the contribution of magnetic losses to  $k''$  increases with growing  $k'$  due to the decrease of the group velocity.

The amplification of magnetic waves by drifting charge carriers—despite repeated attempts—has not been as yet reliably observed in experiment. The main reasons for this are: the difficulty of combining the necessary parameters in one substance (for uniform magnetic semiconductor) and narrow frequency band and criticality of the conductivity value (for composite structures).

It should be noted that the above-considered amplification of a stationary wave (described by negative  $k''$  at real  $\omega$ ) is often referred to as the *convective* instability; the increase of the field amplitudes in time (described by negative  $\omega''$ ) is called the *absolute* instability.

## 14.2 Ferromagnetic resonance and spin waves in metals

In this section, magnetic oscillations and waves in ferromagnetic metals will be studied. Transition metals of the 3d or iron group (Fe, Co, and Ni), some rare-earth metals (Gd, Dy, Ho, Er), and many alloys belong to this class. Magnetic oscillations and waves in ferromagnetic metals are of fundamental interest for

the study of interaction between the magnetic system and charge carriers. At the same time, they are of interest, from a practical point of view, as the means for measurement of parameters of ferromagnetic metals. The application of ferromagnetic metals in microwave engineering is also not ruled out.

In metals (e.g., [24, 253]), the electrons of the outer, *s* shells are collectivized and form the electron 'liquid' with the density (number of electrons per 1 cm<sup>3</sup>)  $n \sim 10^{22}$ . The lattice of positive ions is immersed into this liquid. The presence of the lattice results in the fact that the energy spectrum of electrons in metal consists of energy bands separated by forbidden gaps. The upper band (or several upper bands) in metals is not entirely filled. The boundary (at  $T = 0$ ) between the filled and the unfilled electron states in the *k*-space (where *k* is the quasi-wave vector) is called Fermi surface. The maximal energy of the filled states is the Fermi energy  $\varepsilon_F$  [24]. In the isotropic case the Fermi surface is a sphere with radius  $k_F = (3\pi^2 n)^{1/3}$ .

In magnetically ordered, in particular, in ferromagnetic metals, the positive ions immersed in the electron liquid are the ions of elements with unfilled 3d or 4f shells. It should be noted that the direct exchange interaction of the spin moments of these ions cannot assure the magnetic ordering (as well as in nonmetallic crystals, Section 3.1), and the indirect exchange interaction plays an important role. In metals the exchange interaction via the collectivized *s* electrons, the Ruderman–Kittel–Kasuya–Iosida (RKKI) interaction is the most essential. In the case of 4f metals the ionic magnetic moments, to a good approximation, can be regarded as localized. For 3d metals the delocalization of 3d electrons and their hybridization with *s* electrons takes place.

In the microwave range, the penetration length of electromagnetic field into metal (the skin depth)  $\delta$  is of the order of  $10^{-4}$  cm. This leads to the most important distinction of magnetic oscillations and waves in metals from such processes in weakly conducting media, e.g., ferrites. The conductivity can be neglected in the study of magnetic waves in metals only if the dimension of the sample (in the direction of the wave propagation) is much less than  $\delta$ , as, e.g., in the case of standing spin waves in thin films (Section 7.2).

The second peculiarity of magnetic oscillations in metals is also caused by high density of conduction electrons. This peculiarity is the great contribution of relaxation processes in which these electrons take part to the damping of oscillations.

### 14.2.1 Thin-film model

The ferromagnetic resonance in metals (and, in general, the ferromagnetic resonance) was first observed by Griffiths [149] in thin films of Fe, Ni, and Co magnetized tangentially to the film surfaces. The obtained resonance conditions were originally incomprehensible: the apparent *g*-factor (found from the ratio of  $\omega$  to  $H_0$ ) turned out to be several times larger than two. This 'anomaly' was explained by Kittel [219], who took into consideration the ac demagnetizing field

and showed that formula (1.93) holds in this case.<sup>2</sup> Soon it became clear that for *bulk* metallic samples magnetized tangentially to the surface the ferromagnetic-resonance frequency is approximately equal to

$$\omega = \omega_{\perp} \equiv \gamma [H_0 (H_0 + 4\pi M_0)]^{1/2} \quad (14.18)$$

where, as distinct from (1.93),  $H_0$  is the *internal* steady field. Expression (14.18) follows from (1.92) if the demagnetization factors for the ac field are assumed to be the same as for a thin surface layer, and the demagnetization factor for the steady field, to be as for the entire sample. This assumption defines the so-called *thin-film model* for ferromagnetic resonance in bulk metallic samples.

Formula (14.18) can be generalized to the case when the steady magnetization  $M_0$  makes an arbitrary angle  $\theta$  with the normal to the sample surface. In the coordinate system with  $z'$ -axis coinciding with the normal, all components of the demagnetization tensor  $\vec{N}$  are equal to zero, except  $N_{3'3'} = 4\pi$ . Passing to the coordinate system with  $z$ -axis coinciding with  $M_0$  direction and using formula (1.92), we get

$$\omega = \gamma [H_0 (H_0 + 4\pi M_0 \sin^2 \theta)]^{1/2}. \quad (14.19)$$

If  $\theta = \pi/2$ , expression (14.18) follows from (14.19), and if  $\theta = 0$  (normal magnetization),  $\omega = \omega_H = \gamma H_0$ .

If the angle between  $M_0$  and the normal varies over the sample surface, the thin-film model can be used for calculation of the resonance-curve shape in the 'independent-grain' approximation (Section 2.4). Similarly to expression (2.61), without allowance for internal dissipation, we get

$$\chi''(\omega, H_0) = \frac{\pi}{4} M_0 \int_S \delta [H_0 - H_{\text{res}}(\omega)] dS \quad (14.20)$$

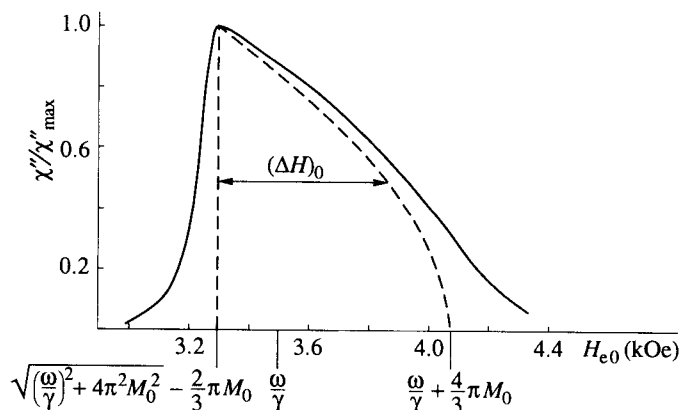
where  $S$  is the sample surface. For a sphere,  $H_{\text{res}}$  is determined by (14.19). Then, the calculation by (14.20) results in the resonance curve  $\chi''(H_{e0})$  shown in Figure 14.6. The width of this curve on the  $(1/2) \chi''_{\text{max}}$  level is

$$(\Delta H)_0 = \frac{3}{2} \pi M_0 + \sqrt{\left(\frac{\omega}{\gamma}\right)^2 + \frac{1}{4} (\pi M_0)^2} - \sqrt{\left(\frac{\omega}{\gamma}\right)^2 + 4 (\pi M_0)^2}. \quad (14.21)$$

If  $\omega/\gamma \gg 2\pi M_0$ , then  $(\Delta H)_0 \simeq (3/2)\pi M_0$ . It should be noted that such nonuniform broadening of the resonance curve is the main reason why spherical samples are not used in experiments on ferromagnetic resonance in metals.

<sup>2</sup>Having extended this idea to the case of an arbitrary ellipsoid, Kittel obtained [220] the famous formula (1.93).





**FIGURE 14.6**

Ferromagnetic-resonance absorption curves in a metal sphere according to the thin-film model. The dashed curve is calculated by formula (14.20) with  $\omega/\gamma = 8\pi M_0$ ; the solid curve is drawn schematically making allowance for the intrinsic losses.

### 14.2.2 Theory without allowance for exchange interaction

The above-considered thin-film model, which is based on the assumption of a uniform ac magnetization in the thin surface layer, is very crude. In reality, electromagnetic waves are excited at the surface of a metallic sample and propagate with large damping into metal. A theory of ferromagnetic resonance in metal must be based on examining these waves. If the conductivity of the metal is so large that  $\delta \ll \lambda_0$  (where  $\lambda_0$  is the wavelength outside the metal), the waves in the metal are propagating along the normal to the surface. And if the radius of curvature of the surface is much larger than  $\delta$ , the waves may be regarded as plane waves.

Without taking into account the electrokinetic effects mentioned in the previous section (their influence is usually negligible in the frequency range we are interested in) and neglecting the electrical crystalline anisotropy, we will regard the permittivity (4.18) as a scalar quantity. Its real part can be neglected for usual ferromagnetic metals at microwave frequencies. Thus, we assume that  $\epsilon = -i\epsilon'' = -i4\pi\sigma/\omega$ . If magnetic losses are not taken into account, then, neglecting the magnetocrystalline anisotropy, we will take expressions (1.54) for the tensor  $\mu$  components. Allowing for magnetic losses, we will use the expressions that are obtained from (1.54) by the substitution (1.68).

It was shown in Section 4.2 that, in the case of scalar  $\epsilon$ , effective permeabilities can be introduced for normal waves in a ferromagnet. When  $M_0$  is perpendicular to the metal surface (normal magnetization) so that the waves in metal propagate along  $M_0$ , the two waves with circular polarization are the normal waves, and  $\mu_{\text{ef}1,2} = \mu \pm \mu_a$ . In the case of tangential magnetization (with respect to the surface) the two waves with different linear polarization of vectors  $e$  and  $b$  are

the normal waves. In this case,  $\mu_{\text{ef}1} = \mu_{\perp}$  and  $\mu_{\text{ef}2} = 1$ . It is obvious that the normal waves with parameters depending on frequency and magnetic field in a *resonance* manner exert the most important influence on ferromagnetic resonance. In the case of normal magnetization, the *right-hand* circularly polarized wave with  $\mu_{\text{ef}} = \mu + \mu_a$  is such a wave, and for tangential magnetization, the *extraordinary* wave with  $\mu_{\text{ef}} = \mu_{\perp}$ . The resonance conditions for these effective permeabilities are just the conditions that are given by the thin-film model:  $\omega = \omega_H$  in the former case and  $\omega = \omega_{\perp}$  in the latter case. However, both normal waves for each direction of magnetization are to be taken into account in the strict theory.

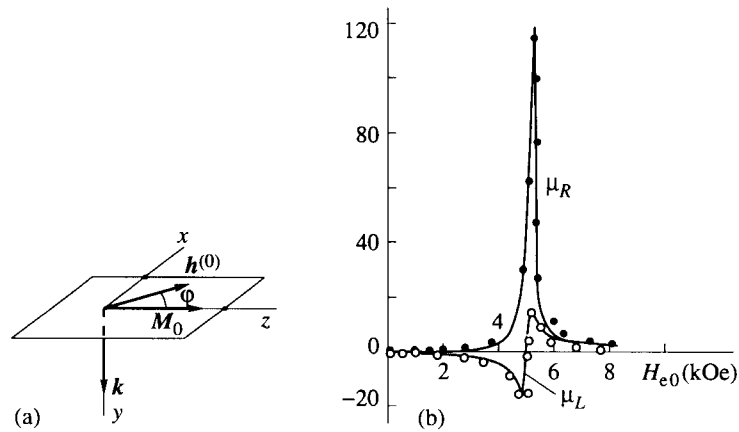
The final result of the theory of ferromagnetic resonance in a metallic sample (as well as in a nonmetallic one), which permits an experimental test, must consist in determining how the parameters of an electromagnetic system with such a sample vary in the region of resonance. For an electromagnetic resonator, the resonance frequency and the quality factor are such parameters, and for a waveguide, the coefficients of transmission and reflection. This problem having been solved, it becomes possible to obtain the parameters of the metal from the measured dependences of the resonator or waveguide parameters on frequency or magnetic field. The solution of the mentioned problem consists in obtaining the electromagnetic fields in the resonator (or in the waveguide) and in the sample (which can be a part of the waveguide or resonator wall). As we, for the present, do not take into account the exchange interaction, the solution must satisfy only the ordinary electrodynamic boundary conditions. The incident power at the input of the system should be regarded as the known quantity.

A strict solution of this problem would be very difficult, and the method of successive approximations is to be used. As a zero approximation, we can take the magnetic field  $h^{(0)}$  in the considered system near the surface of the metallic sample, assuming its conductivity to be infinite. Then, using the boundary conditions at the surface, we find magnetic and electric fields of both normal waves in metal. The sum of their electric fields at the surface is equal to the tangential component of the electric field  $e^{(1)}$  of the resonator or the waveguide in the first approximation. Using the fields  $h^{(0)}$  and  $e^{(1)}$ , all parameters of the considered system can be calculated. It is worth noting that the influence of these parameters on the field  $h^{(0)}$  can be taken into account, which makes the problem self-consistent and allows one to increase the accuracy of the solution.

Let us consider a hollow resonator; a part  $S_1$  of its surface is the ferromagnetic metal, and the remainder ( $S_0 - S_1$ ) is perfectly conducting. To find the changes of the resonator frequency and quality factor caused by the ferromagnetic metal we can use the Slater perturbation formula (4.96). This formula can be transformed by introducing the *surface impedance*  $\zeta_s$ , defined in the following way:

$$(\mathbf{n}_0 \times \mathbf{e}) \mathbf{h}^* = \zeta_s \mathbf{h} \mathbf{h}^*. \quad (14.22)$$

Here,  $\mathbf{e}$  and  $\mathbf{h}$  are the fields in the resonator at the surface and  $\mathbf{n}_0$  is a unit normal to the surface. If  $h^{(0)}$  is linearly polarized, the impedance  $\zeta_s$  is the ratio  $e_{\tau}/h$  where  $e_{\tau}$  is the projection of  $\mathbf{e}$  onto the direction perpendicular to  $\mathbf{h}$  and  $\mathbf{n}_0$ . With



**FIGURE 14.7**

Ferromagnetic resonance in metal magnetized tangentially to its surface: (a) coordinate axes; (b) field dependence of  $\mu_R$  and  $\mu_L$  for permalloy [54]; the curves were calculated with parameters chosen to fit the experimental points.

allowance for (14.22), formula (4.96) takes the form

$$\frac{\omega - \omega_0}{\omega_0} + i \frac{1}{2Q} = \frac{ic\zeta_s}{2\omega_0 W_0} \int_{S_1} |h^{(0)}|^2 dS \quad (14.23)$$

where  $\omega_0$  is the eigenfrequency of the resonator with walls of infinitely conducting metal,  $W_0$  is determined by (4.84), and the prime at  $\omega'$  is omitted.

Consider first, following Young and Uehling [455], the case of *tangential magnetization* ( $M_0 \perp n_0$ ). Assume that the field  $h^{(0)}$  makes an angle  $\varphi$  with  $M_0$  (Figure 14.7). The normal waves in metal are: (i) the wave with components  $h_{1x}$ ,  $h_{1y}$ , and  $e_{1z}$ , for which  $k_1 = k_0 \sqrt{\epsilon \mu_{\perp}}$  and the wave impedance  $\zeta_1 = e_{1z}/h_{1x} = \sqrt{\mu_{\perp}/\epsilon}$ ; (ii) the wave with components  $h_{2z}$  and  $e_{2x}$ , for which  $k_2 = k_0 \sqrt{\epsilon}$  and  $\zeta_2 = \sqrt{1/\epsilon}$ . From the boundary conditions (the continuity of  $h_x$  and  $h_z$  at  $S_1$ ) it follows that  $h_{1x}(y=0) = h^{(0)} \sin \varphi$  and  $h_{2z}(y=0) = h^{(0)} \cos \varphi$ . Substituting  $h^{(0)}$  and the electric field  $e^{(1)} = x_0 \zeta_2 h^{(0)} \cos \varphi + z_0 \zeta_1 h^{(0)} \sin \varphi$  into (4.96), we get

$$\frac{\omega - \omega_0}{\omega_0} + i \frac{1}{2Q} = \frac{ic(\sqrt{\mu_{\perp}} \sin^2 \varphi + \cos^2 \varphi)}{2\omega_0 W_0 \sqrt{\epsilon}} \int_{S_1} (h^{(0)})^2 dS. \quad (14.24)$$

From the experimental point of view, the entire contribution of the ferromagnetic wall (14.24) is not of the most interest. Of the prime interest is the *change* of this contribution, either when we replace an 'ordinary' wall by the ferromagnetic one or when we pass from the  $H_0$  value at ferromagnetic resonance to its value far from resonance (where  $\mu_{ef} \cong 1$ ). To find this change we have to subtract from (14.24)

an analogous expression but with  $\mu_{\perp} = 1$  and, in general, with other permittivity  $\varepsilon_0$ . Then, taking into account that  $\varepsilon = -i4\pi\sigma/\omega$  and  $\varepsilon_0 = -i4\pi\sigma_0/\omega$ , we obtain

$$\frac{\omega - \omega_0}{\omega_0} + \frac{i}{2} \left( \frac{1}{Q} - \frac{1}{Q_0} \right) = \frac{1}{4W_0} \left\{ \delta_1 \left[ (i\sqrt{\mu_{\perp R}} - \sqrt{\mu_{\perp L}}) \sin^2\varphi + (i-1) \cos^2\varphi \right] + (1-i)(\delta_1)_0 \right\} \int_{S_1} (h^{(0)})^2 dS. \quad (14.25)$$

Here,  $\mu_{\perp R}$  and  $\mu_{\perp L}$  are determined by expressions (4.38) and (4.39),  $\delta_1$  is given by formula (4.40), and  $(\delta_1)_0$  is given by the same formula but with the replacement of the conductivity of the ferromagnet near resonance  $\sigma$  by the conductivity  $\sigma_0$  of the 'ordinary' wall or of the ferromagnet far from resonance.

The case of *normal magnetization* can be treated in a similar manner [455]. Waves with right-hand and left-hand circular polarization are now the normal waves. If the field  $h^{(0)}$  is linearly polarized, the amplitudes of the normal waves at the surface are equal to  $h^{(0)}/2$ . Finding then  $e^{(1)} = e_+ + e_-$  and using the perturbation formula (4.96), we get expressions resembling (14.24) or (14.25). Near ferromagnetic resonance the normal wave with left-hand polarization may be neglected, and we get

$$\frac{\omega - \omega_0}{\omega_0} + i\frac{1}{2Q} = \frac{\delta_1}{8W_0} (i\sqrt{\mu_{+R}} - \sqrt{\mu_{+L}}) \int_{S_1} (h^{(0)})^2 dS \quad (14.26)$$

where  $\mu_{+R} = |\mu + \mu_a| + (\mu'' + \mu_a'')$  and  $\mu_{+L} = |\mu + \mu_a| - (\mu'' + \mu_a'')$  (Section 4.2).

Thus, having measured the shift of the frequency and the change of the quality factor of a resonator with a ferromagnetic-metal wall, it is possible to find the quantities  $\mu_{\perp R}$  and  $\mu_{\perp L}$  or  $\mu_{+R}$  and  $\mu_{+L}$ , according to the direction of magnetization. The result of such measurement and calculation performed by Bloembergen in one of the first works on ferromagnetic resonance [54] is shown in Figure 14.7.

### 14.2.3 Influence of exchange interaction

Because of the skin effect, the ac magnetization near the surface of ferromagnetic metal is strongly *nonuniform*, and, hence, the exchange interaction should be taken into account. Kittel and Herring pointed out as early as in 1950 [228] that the exchange interaction must lead to the broadening of the ferromagnetic-resonance curve in metals by the quantity

$$\Delta H_{\text{ex}} \sim \frac{D}{\delta^2} \quad (14.27)$$

and to the decrease of the resonance field of the same order. This can be justified in the following manner: the magnetization wave damping out on the distance  $\sim \delta$  can be expanded into the Fourier integral in the undamped spin waves with the

mean  $k$  value  $\bar{k} \sim 1/\delta$ ; their resonance fields form a distribution with the width and the shift of the maximum of the order of  $D\bar{k}^2 \sim D/\delta^2$ .

However, the  $\delta$  value in (14.27) depends on the permeability and, hence, on the linewidth, to which the exchange interaction makes the above-mentioned contribution. Akhiezer, Bar'yakhtar, and Kaganov [11] showed that this *self-consistent* chain of relations can be used in the following way to estimate the value of  $\Delta H_{\text{ex}}$ . According to (4.39),

$$\delta = \frac{\delta_1}{\sqrt{\mu_{\text{ef}} R}} \quad (14.28)$$

where  $\delta_1$  is the skin depth in a nonmagnetic medium. Near resonance, we may assume

$$\mu_{\text{ef}} R \simeq (\mu_{\text{ef}}'')_{\text{res}} = \frac{\beta 4\pi M_0}{\Delta H_0 + \Delta H_{\text{ex}}} \quad (14.29)$$

where  $\Delta H_0$  is the contribution of all other sources of resonance-line broadening except exchange interaction and  $\beta$  is a factor of the order of unity. It is easy to make sure that  $\beta = 2$  in the case of normal magnetization and  $\beta = (\omega_H + \omega_M)/(\omega_H + \omega_M/2)$  in the case of tangential magnetization. It follows from (14.27)–(14.29) that

$$\Delta H_{\text{ex}} (\Delta H_0 + \Delta H_{\text{ex}}) = \frac{\beta D 4\pi M_0}{\delta_1^2}. \quad (14.30)$$

In particular, if  $\Delta H_{\text{ex}} \gg \Delta H_0$ , then

$$\Delta H_{\text{ex}} \simeq \frac{1}{\delta_1} \sqrt{\beta D 4\pi M_0} \equiv \frac{2\pi}{c} \sqrt{2\beta D M_0 \sigma \omega}. \quad (14.31)$$

As  $\sigma$  and  $M_0$  decrease with increasing temperature, the exchange contribution to the linewidth manifests itself at low temperatures.

In this estimate, as in all the preceding reasoning, it was assumed that the *normal* skin effect took place (e.g., [246]), which is the case when the electron mean free path  $l_e \ll \delta$ . Then,  $\sigma$  does not depend on the skin depth and, for metals at microwave frequencies, slightly differs from the static conductivity. In the case of *anomalous* skin effect [253] when  $l_e > \delta$ , some electrons—in greater quantity the larger the ratio  $l_e/\delta$ —leave the skin layer before they undergo a collision. This can approximately be taken into account if  $\sigma$  in the expression for  $\delta$  is replaced by

$$\sigma_{\text{ef}} = \nu \sigma \frac{\delta}{l_e} \quad (14.32)$$

where  $\nu$  is a factor given by the theory of anomalous skin effect [253] ( $\nu = 5.16$  in the absence of magnetic field). Taking (14.32) into account, we obtain, instead of (14.30),

$$\Delta H_{\text{ex}}^{3/2} (\Delta H_0 + \Delta H_{\text{ex}}) = \frac{\beta \nu 4\pi M_0 D^{3/2}}{\delta_1^2 l_e}. \quad (14.33)$$

Now, in the case of  $\Delta H_{\text{ex}} \gg \Delta H_0$ ,

$$\Delta H_{\text{ex}} \simeq \left( \frac{\beta \nu 4\pi M_0}{l_e} \right)^{2/5} \frac{D^{3/5}}{\delta_1^{4/5}}. \quad (14.34)$$

The finite value of  $\Delta H_{\text{ex}}$ , in the absence of magnetic dissipation (that determines  $\Delta H_0$ ), and the increase of  $\Delta H_{\text{ex}}$  with decreasing  $\delta_1$ , witnesses the fact that the dissipation of energy of magnetic oscillations is accomplished (for both the normal and the anomalous skin effect) by the conducting electrons.

A *strict* theory of ferromagnetic resonance in metals with allowance for exchange interaction can be developed in the same way as the nonexchange theory considered above. But now we must use the expressions for tensor  $\vec{\mu}$  components found with regard for this interaction, e.g., the expressions obtained from (7.8) by the replacement (1.68). Substituting these expressions into (4.42), we get (in the case of normal magnetization, i.e., for  $\theta_k = 0$ ) a quadratic equation in  $k^2$  for each direction of the polarization rotation. In the case of tangential magnetization ( $\theta_k = \pi/2$ ), we get from (4.53) a cubic equation in  $k^2$  for the extraordinary wave; for the ordinary wave,  $k^2 = k_0^2 \epsilon$ . So, in both considered cases (and in an arbitrary case, as well) there are now *four* normal waves.

The dispersion relations for these waves were studied by Patton [310]. It turns out that two of the four waves are the waves with right-hand rotation of the vector  $m$  polarization (Larmor branches, in terms of [310], denoted by the subscripts +), and the other two are the waves with left-hand rotation (anti-Larmor branches denoted by the subscript -). One of the two waves with the same rotation of polarization is an 'electromagnetic' (E) wave with large  $v_{\text{ph}}$  and comparatively weak effect of exchange interaction; the other is a 'spin' (S) wave. The Larmor 'spin' wave ( $S_+$ ), at large  $k'$  values, turns into an ordinary spin wave, and the anti-Larmor 'spin' wave has a very large damping.

If the dissipation parameter exceeds a certain value (e.g.,  $\alpha > \alpha_{\text{cr}} = 0.013$  for permalloy), the branches  $E_+$  and  $S_+$  do not intersect in the  $\omega(k', k'')$  space (Figure 14.8) and conserve their character in the entire space. But their projections onto  $\omega(k')$  plane do intersect. At  $\alpha < \alpha_{\text{cr}}$  these branches, as well as their projections, repel. This is a general feature of all mixed (or coupled) waves; we have already encountered it for magnetoelastic waves (Section 12.3).

The magnetic-field amplitudes of all four normal waves in metal can be expressed in terms of the field  $h^{(0)}$  at the surface by the use of four boundary conditions: two electromagnetic and two supplementary (exchange) conditions (Section 7.2). These conditions, with the use of the expressions for tensor  $\vec{\mu}$  components, result in the equations for magnetic-field amplitudes. Then, using the wave impedances of the normal waves, we find (as in the above-considered nonexchange case) the electric fields of these waves. Their sum gives the field  $e^{(1)}$  at the surface. Then we can either find the surface impedance  $\zeta_s$  or, for a ferromagnetic-metal wall of a resonator, apply the perturbation formula (4.96).

Consider now in more detail the case of *tangential* magnetization assuming

**TABLE 14.1**  
Parameters of ferromagnetic metals<sup>a</sup> [47, 126].

Metal	$T_C$ (K)	$4\pi M_0$ (G)	$\sigma$ ( $\Omega^{-1} \text{ cm}^{-1}$ )	$g$	$\alpha^b$	D (Oe $\text{cm}^2$ )
Fe	1043	21 580	$1.03 \times 10^5$	2.088	0.0023	$2.2 \times 10^{-9}$
Fe <sub>97</sub> Si <sub>3</sub>		21 148				
Ni <sub>77</sub> Fe <sub>23</sub>		11 000				$2.5 \times 10^{-9}$
Ni	631	6 084	$1.46 \times 10^5$		0.027	$3.1 \times 10^{-9}$
Co	1904	17 900	$1.60 \times 10^5$		0.027	

<sup>a</sup>The values of all parameters (except  $T_C$ ) are given at room temperature.

<sup>b</sup>The Landau–Lifshitz dissipation parameter  $\lambda_1$  and the exchange constant  $A$ , encountered in many works on ferromagnetic resonance in metals, are related to the parameters cited in the table as follows:  $\lambda_1 = \gamma\alpha M_0$ ,  $A = DM_0/2$ .

$\mathbf{h}^{(0)} \perp \mathbf{M}_0$ , i.e.,  $\varphi = \pi/2$  in Figure 14.7(a). The ordinary wave (with  $\mu_{\text{ef}} = 1$ ) is not excited then, and the field in metal consists of three normal waves: an ‘electromagnetic’ wave and two ‘spin’ waves. Their complex wave numbers  $k_j$  ( $j = 1, 2, 3$ ) are determined by a cubic equation in  $k^2$ , which is obtained by substituting the expression for  $\mu_{\perp}$  (with regard to exchange interaction and dissipation) into (4.53). The wave impedances of the normal waves  $\zeta_j = e_{jz}/h_{jx}$  for the considered strongly conducting metal, according to (4.56) and (4.53), have the form

$$\zeta_j = \frac{ick_j}{4\pi\sigma}. \quad (14.35)$$

This problem was first solved by Ament and Rado [16], with the assumption of the exchange boundary conditions (7.42) ( $\xi = 0$ ). In the *low-frequency* limit,

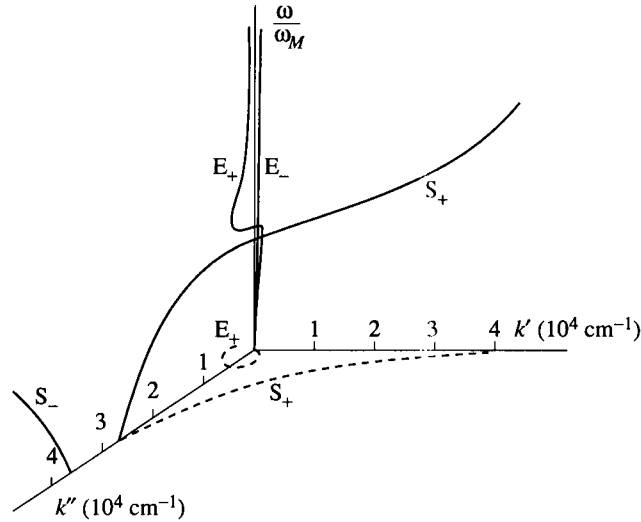
$$\omega \ll \omega_M \quad \omega_H \ll \omega_M \quad p \equiv \gamma\sqrt{D4\pi M_0}/\delta_1 \ll \omega_M \quad (14.36)$$

the obtained expression for the surface impedance has the form

$$\zeta_s = \frac{c}{4\pi} (1+i) \frac{\sqrt{\omega_M}}{\sigma\delta_1} \frac{[\omega_H - \omega^2/\omega_M + i\alpha\omega + 2(1+i)p]^{1/2}}{\omega_H - \omega^2/\omega_M + i\alpha\omega + (1+i)p}. \quad (14.37)$$

Conditions (14.36) are satisfied and, hence, formula (14.37) is approximately valid in the entire centimeter-wavelength range for metals in which the ferromagnetic resonance is usually measured (Table 14.1).

One can see from (14.37) that for  $\alpha = 0$  and  $p = 0$ , i.e., without allowance for dissipation and exchange interaction, the resonance frequency (at which  $\zeta \rightarrow \infty$ )  $\omega_{\text{res}} \simeq \sqrt{\omega_H\omega_M}$ , which is the low-frequency limit of (14.18). The allowance for dissipation ( $\alpha \neq 0$ ,  $p = 0$ ) results in a finite real part of the impedance at resonance and in finite linewidth. If the linewidth is defined at the level  $(\zeta_s^2)' = (\zeta_s^2)'_{\text{res}}/2$ ,

**FIGURE 14.8**

Dispersion curves of normal waves in metal for tangential magnetization and  $\theta_k = \pi/2$  [310].  $H_0 = 1135$  Oe,  $\alpha = 0.03$ , other parameters correspond to permalloy (Table 14.1). Dashed curves are projections of the solid curves  $S_+$  and  $E_+$  onto the plane  $(k', k'')$ .

it is equal to  $2\alpha\omega$ , i.e., it coincides with the 'usual' linewidth  $\Delta H$  defined at the level  $\chi'' = \chi''_{\text{res}}/2$ . This coincidence is caused by the fact that, for a strongly conducting metal (if only one of the normal waves is taken into account),

$$\zeta_s^2 = i \frac{\omega}{4\pi\sigma} \mu_{\text{ef}} \quad (14.38)$$

and hence,  $(\zeta_s^2)' = (\omega/\sigma) \chi''_{\text{ef}}$ . The shift of the resonance line with respect to its position at  $\alpha = 0$  turns out to be of the second order in  $\alpha$ , as in the case of 'usual' ferromagnetic resonance in weakly conducting samples (Section 1.5).

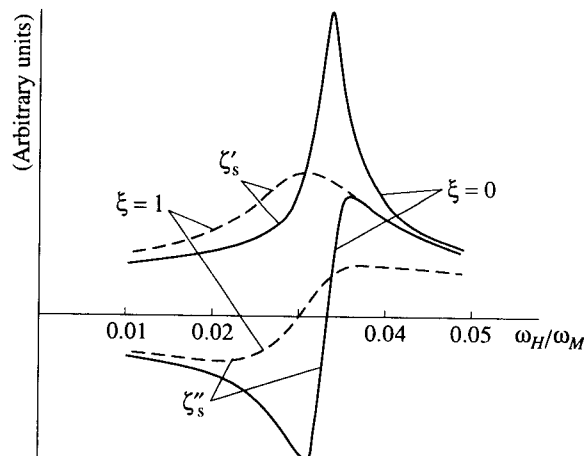
But if  $p \neq 0$  and is large as compared with  $\alpha\omega$ , then, as one can see from (14.37), the resonance-line shift and the linewidth are of the same order. Defining them as in the case of  $p = 0$  and assuming for simplicity that  $\alpha = 0$ , we get

$$\Delta H_{\text{ex}} = \frac{1.26}{\delta_1} \sqrt{D 4\pi M_0} \quad (14.39)$$

$$(\delta H_{\text{res}})_{\text{ex}} = -\frac{0.78}{\delta_1} \sqrt{D 4\pi M_0}. \quad (14.40)$$

It should be noted that the estimate (14.31) is in a good agreement with (14.39) (in the low-frequency limit  $\beta = 2$ ).



**FIGURE 14.9**

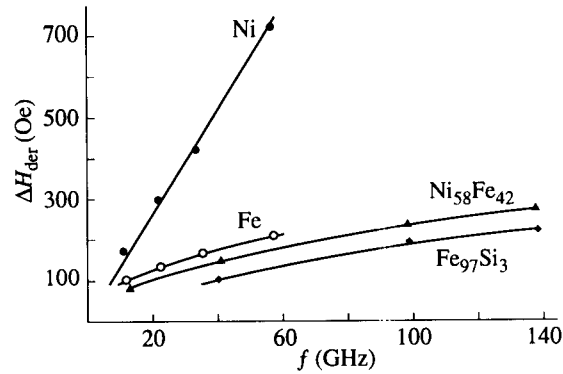
Calculated field dependences of the surface impedance in the case of tangential magnetization for two values of the pinning parameter  $\xi$  [129]. Frequency is 11.5 GHz, all parameters correspond to iron at room temperature (Table 14.1).

Later, Kaganov and Yui Lu [195, 202] showed that the value of the *pinning parameter*  $\xi$  (Section 7.2) makes a strong influence on the ferromagnetic resonance in metals: the quantities  $\Delta H_{\text{ex}}$  and  $(\delta H_{\text{res}})_{\text{ex}}$  increase with increasing  $\xi$ . The numerical calculations by Frait and Mac Faden [126] and the theory by Fraitova [127–129] (Figure 14.9) confirmed this dependence.

The case of *normal* magnetization can be analyzed in a similar manner. Two waves with the right-hand and two waves with the left-hand circular polarization are now the normal waves. This problem was solved for  $\xi = 0$  by V. L. Gurevich [167]. The obtained expression for  $\zeta_s$  in the low-frequency limit differs from (14.37) by the replacement of  $\omega^2/\omega_M$  with  $\omega$ . Formulae (14.39) and (14.40) are valid in this case, too.

The ferromagnetic resonance in metal with anomalous skin effect was also investigated in [167] for the case of normal magnetization. The expression for  $\Delta H_{\text{ex}}$ , when the exchange contribution dominates, differs from the estimate (14.34) only by a factor of the order of unity. The case of tangential magnetization with the anomalous skin effect was studied by Blank and Kaganov [50].

Thus, the contribution of the exchange interaction (together with conductivity) to the ferromagnetic-resonance linewidth and the resonance-field shift are of the *same order* and are proportional (if they dominate) to the *square root* of frequency. Meanwhile, the contribution of magnetic losses to  $\Delta H$  in metals is usually proportional to  $\omega$ , as the dissipation parameter  $\alpha$  is approximately independent of frequency. Therefore, the advantageous conditions for observing the exchange contribution are low frequencies and, of course, low temperatures

**FIGURE 14.10**

Frequency dependences of ferromagnetic-resonance linewidths at room temperature [126, 47].  $\Delta H_{\text{der}} = \Delta H/3^{1/2}$  (Section 1.4).

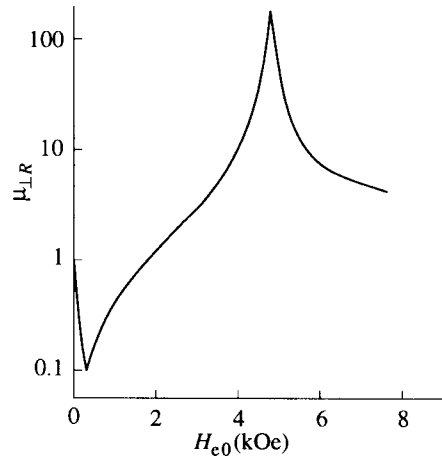
because the conductivity of metals increases with decreasing frequency. At rather low frequency (however, at room temperature) the exchange contribution was first observed by Rado and Weertman [325].

Estimates, with the use of (14.39) and the data of Table 14.1, show that the frequency at which the magnetic and the exchange contributions to  $\Delta H$  at room temperature become comparable is equal to  $\sim 300$  GHz for Fe and to  $\sim 1$  GHz, for Ni. For these metals, at microwave frequencies and room temperature, the limiting cases are realized when either one or the other contribution dominates. The exchange contribution also dominates for permalloy and silicon iron. Figure 14.10 gives a good illustration of this: the linewidth is proportional to  $\omega$  for Ni and is proportional to the square-root of  $\omega$  for Fe and other metals.

#### 14.2.4 Antiresonance

The processing of experimental data on the basis of the strict theory of ferromagnetic resonance in metals allows the separation of the magnetic contribution to  $\Delta H$  and makes it possible to find the dissipation parameter  $\alpha$  even in the case (as for Fe) when the exchange contribution dominates. But it is obvious that the accuracy of such a procedure cannot be high. For a more accurate determination of the magnetic dissipation parameter the measurement of the antiresonance linewidth can be used.

Antiresonance point (Section 4.2) is the frequency or steady magnetic field value at which the real part of the effective permeability  $\mu_{\text{ef}}$  becomes equal to zero and the imaginary part does not pass through a maximum, as distinct from resonance, but passes through a minimum. The condition of antiresonance (4.59) does not depend on the angle between the direction of magnetization and the

**FIGURE 14.11**

Effective permeability of supermalloy vs steady magnetic field for tangential magnetization [449].

direction of the wave propagation. One can see from (4.59) that antiresonance can be observed only at  $\omega > \omega_M$ , e.g., for Fe, at  $\omega/(2\pi) \gtrsim 60$  GHz. It can be shown that, to a first approximation (for small losses), the imaginary part of the effective permeability at antiresonance is

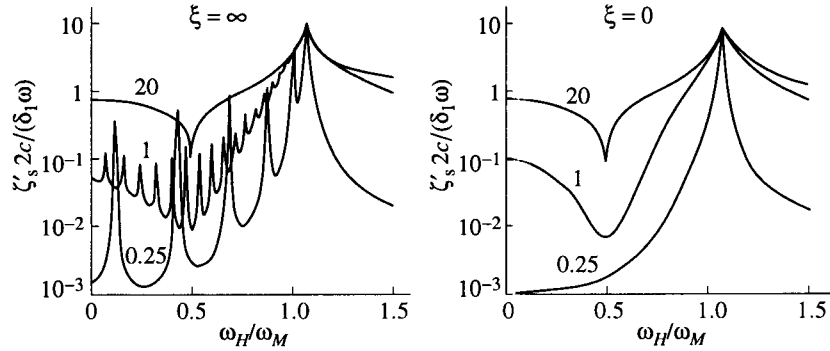
$$(\mu''_{\text{ef}})_{\text{antires}} = \frac{\alpha\omega}{\omega_M} \quad (14.41)$$

for any direction of magnetization. The antiresonance linewidth  $\Delta H_{\text{antires}}$  can be defined as the interval between  $\omega$  or  $H_0$  points at which  $\mu''_{\text{ef}} = 2(\mu''_{\text{ef}})_{\text{antires}}$ . It is easy to make sure that, independently of the magnetization direction,  $\Delta H_{\text{antires}}$  coincides, to a first approximation, with the resonance linewidth  $\Delta H = \alpha\omega/\gamma$ .

Expressions (4.59) and (14.41) have been obtained without allowance for exchange interaction. However, the skin depth, according to (4.39), becomes large near antiresonance, and there is *no need* to take into account the exchange interaction. Thus, measuring the parameters of an electromagnetic system with a metallic sample near antiresonance, we can determine independently the magnetic dissipation parameter  $\alpha$ .

The absorption minimum at antiresonance was first observed by Yager [449] (Figure 14.11). Simultaneous measurements of the linewidth at resonance and at antiresonance were used [124] to determine the values of  $\alpha$  and the pinning parameter  $\xi$ . The simultaneous measurements of the resonance and antiresonance magnetic fields allowed one to obtain precise values of magnetization [324] and  $g$ -factor [123].

The increase of the skin depth at antiresonance results in a great increase of the



**FIGURE 14.12**

Calculated field dependences of the real part of the surface impedance for tangentially magnetized metal films of different thickness  $d$  [92].  $\omega = 1.5\omega_M$ ,  $\alpha = 10^{-4}$ ,  $D/(4\pi M_0\delta_1^2) = 5 \times 10^{-5}$ , numbers by the curves are the values of  $d/\delta_1$ . © 1974 Jpn. J. Appl. Phys.

power *percolating through a film* of ferromagnetic metal. This effect was predicted by Kaganov [196]. It was observed first by Heinrich and Meshcherjakov [177] and later on, by others (e.g., [77]).

It should be noted that, if the thickness of the film is comparable with the skin depth, then the calculation of the percolation through the film, as well as of the reflection from it (determined by the surface impedance), demands the regard for the boundary conditions at *both sides* of the film. In general, the electrodynamic and the exchange boundary conditions must be taken into account; but near antiresonance there is no need for the latter. The results of such calculations carried out by De Wames and Wolfram [92] are shown in Figure 14.12. The symmetric excitation, i.e., the excitation by the same ac field at both sides of the film, was assumed. One can see from this figure that the influence of the pinning parameter becomes stronger with diminishing film thickness. In the case of  $\xi = \infty$ , sharp peaks caused by 'space quantization' are superimposed onto the dependence  $\zeta'_s(H_0)$  that is characteristic of an infinite metal.

#### 14.2.5 Processes of magnetic relaxation

The measurements of magnetic dissipation parameter  $\alpha$  in metals show that this parameter is practically independent of frequency. Its dependence on temperature is usually weak in perfect samples. Let us discuss now what relaxation processes determine this parameter.

All processes investigated in Chapters 11–13 can exist in metals. In addition, the process in which the conduction electrons are involved can be present. The contributions of *inherent* magnon processes (Section 11.2) to  $\Delta H$  in metals should

be of the same order as in dielectrics or semiconductors (ferrites), i.e., of the order of 0.1 Oe. At the same time, the linewidths even in perfect metallic samples turn out to be several tens of oersteds. So, the intrinsic magnon processes do not play any noticeable role in metals. *Two-magnon* processes caused by defects (Section 11.3) are effective in metals because of large steady magnetization. They lead to high  $\Delta H$  values in 'bad' samples, e.g., in samples with not sufficiently well polished surfaces. The two-magnon processes caused by nonuniform anisotropy fields are effective in polycrystals. The contributions of two-magnon processes caused by nonuniform elastic stresses are large in poorly annealed samples. But if proper attention is paid to the quality of samples, as in all good works on ferromagnetic resonance in metals, the contributions of all two-magnon processes are small.

The *ionic* relaxation processes (Section 13.2) can also play an important role in metals, especially at low temperatures. It is conceivable that the sharp rise of  $\Delta H$  in Ni at low temperature and high  $\Delta H$  values in Co [48] result from this process. However, it is obvious that rather high  $\Delta H$  values in all ferromagnetic metals, which weakly depend on frequency and temperature, should be caused mainly by the *electron-magnon* processes.

To realize these processes we consider, following Turov [409], the interaction between the charge carriers (electrons) and the magnetic system of a ferromagnet. Electrons are characterized by the operators of orbital impulse  $\hat{p}$  and spin  $\hat{s}$ . The magnetic system is characterized by the magnetization  $M$ . Then, the Hamiltonian of the interaction of an electron with the magnetic system will have the form [409]

$$\hat{\mathcal{H}}_1 = -2\mu_B \mathbf{A} \hat{p} - 2\mu_B \mathbf{H} \hat{s} - 2 \frac{I}{M_0} M \hat{s} \quad (14.42)$$

where  $\mu_B = |e_0| \hbar / (2m_e c)$  is the Bohr magneton,  $\mathbf{A}$  is the vector potential of the electromagnetic field, and  $I$  is the exchange integral that characterizes the interaction of carriers ( $s$  electrons) with the magnetic system.

All the above-studied effects caused by the interaction of magnetic oscillations and waves with charge carriers resulted from the first term in (14.42). Now we will briefly consider the phenomena determined by the other two terms, i.e., by the interaction of the magnetic system with *spins* of the conduction electrons. The energy of this interaction can be written in the form

$$U = \sum_{s=\pm 1/2} \int_V \psi^*(\mathbf{r}, s) \hat{\mathcal{H}} \psi(\mathbf{r}, s) dV \quad (14.43)$$

where  $\psi(\mathbf{r}, s)$  is the wave function of the conduction electrons,  $\hat{\mathcal{H}}$  is the sum of the last two terms in (14.42), and integration is over the volume of the sample. We substitute the last two terms of  $\hat{\mathcal{H}}_1$  into (14.43), pass from  $\psi(\mathbf{r}, s)$  and  $\psi^*(\mathbf{r}, s)$  to the operators  $\hat{b}_{q,s}^+$  and  $\hat{b}_{q,s}$  of creation and annihilation of electrons with impulse  $\hat{p} = \hbar \hat{q}$  and spin  $s$ , and express  $M$  in terms of the operators  $\hat{c}_k^+$  and  $\hat{c}_k$  of the magnon creation and annihilation (Section 7.4). Then, the energy  $U$  will contain

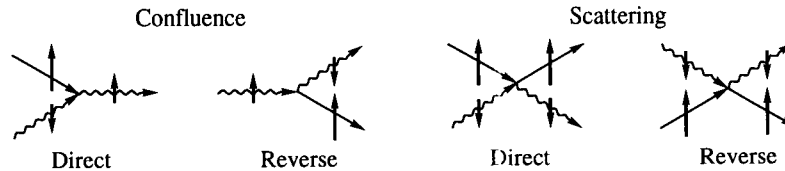


FIGURE 14.13

Elementary processes with conservation of the total spin, which underlie the three-particle and four-particle magnon relaxation processes. Straight lines denote magnons, and wavy lines denote conduction electrons.

terms of different order with products of operators  $\hat{b}_{q's}^+$ ,  $\hat{b}_{q's}$ ,  $\hat{c}_k^+$ , and  $\hat{c}_k$ .

The quadratic terms containing the products  $\hat{b}_{q's}^+ \hat{b}_{q's}$  give the correction to the energy of the carriers caused by their interaction with the magnetic system. The terms of third, fourth, and higher order in  $\hat{b}_{q's}^+$ ,  $\hat{b}_{q's}$ ,  $\hat{c}_k^+$ , and  $\hat{c}_k$  correspond to the elementary processes of creation and annihilation of electrons and magnons. These elementary processes underlie the magnon relaxation processes resulting from the interaction of magnons with the spins of charge carriers. In such low-energy processes, electrons cannot arise or annihilate, only their  $q$  and  $s$  values change. Hence, the operators  $\hat{b}_{q's}^+$  and  $\hat{b}_{q's}$  appear only in pairs. It is very important that the  $sd$  (or  $sf$ ) exchange interaction, like the exchange interaction within the magnetic system (Section 11.2), leads only to processes in which the total spin of the interacting particles is *conserved*. The elementary processes that satisfy this condition are shown in Figure 14.13. The three-particle processes are, in general, more probable. But they are forbidden if the turn-over of the conduction-electron spin is connected with the increase of the electron energy by a value exceeding the energy of the relaxing magnon. Then, the main contribution to the magnon relaxation will be made by the *four-particle* process. This is the case for ferromagnetic metals where the mentioned increase of the  $s$  electron energy, i.e., the  $sd$  exchange splitting of the conduction band, is of the order of 1 eV.

The magnon relaxation frequency determined by such four-particle elementary processes, without turn-over of the electron spin, was calculated by Lutovinov and Reizer [262]:

$$\omega_r = \frac{3\pi}{64} \left( \frac{\hbar k}{S p_F} \right)^2 \frac{\hbar \omega \kappa T}{\gamma D p_F^2} \ln \frac{\kappa T}{\hbar \omega} \quad (14.44)$$

where  $S$  is the spin of magnetic ions,  $p_F = \hbar k_F$  is the Fermi impulse of electrons,  $\omega$  is the magnon frequency, and  $k$  is the magnon wave number. In ferromagnetic resonance the  $k$  value is of the order of  $\delta^{-1}$ , where  $\delta$  is the skin depth depending, in its turn, on  $\Delta H$ . Assuming the considered process to be the dominant one, it is easy to obtain, by the same method as used in deriving expression (14.31),

$$\Delta H = \frac{\sqrt{3}\pi}{2} \frac{\hbar^2 \omega}{c \gamma S p_F^2} \sqrt{\frac{\beta \kappa T 4\pi M_0 \sigma}{\hbar D} \ln \frac{\kappa T}{\hbar \omega}}. \quad (14.45)$$

One can see from (14.45) that the linewidth is approximately proportional to  $\omega$  and (if the temperature dependences of  $M_0$  and  $\sigma$  are taken into account) weakly depends on temperature. Both the above-mentioned features agree with experiment. Estimates using (14.45) are also in agreement with the experimental  $\Delta H$  values in metals.

It should be noted that spin waves propagating in metal along its surface cannot be excited linearly by the ac field of a resonator or a waveguide because the wavelength of this field is much larger than  $1/k$  of the spin waves. But pairs of such spin waves can be excited parametrically (Chapter 10), as it was observed in thin films [79, 46] and thin wires [234].





---

## *Appendix A*

---

### **Units and constants**

The CGS (Gaussian) units are used in this book. The relations between them and the SI units are given in Table A.1. The table includes only the quantities, with few exceptions, that appear in the text.

The energy of particles and quasiparticles is often measured in special units, which are defined in the following manner.

The electronvolt is the energy  $|e_0|V$  obtained by an electron in passing the potential difference  $V = 1$  V.

The inverse centimeter is the energy quantum  $2\pi\hbar c/\lambda$  of electromagnetic radiation with the wavelength in vacuum  $\lambda = 1$  cm.

The kelvin is the mean energy  $\kappa T$  per two degrees of freedom of an ideal gas at temperature  $T = 1$  K.

The oersted is the energy equal to the Zeeman splitting  $\gamma\hbar H \equiv g\mu_B H$  of electron energy levels, with  $g$ -factor  $g_s = 2.0023$ , in magnetic field  $H = 1$  Oe.

Values of these units and the relations between them are given in Table A.2. Energy, especially thermal, is also measured in calories:  $1 \text{ cal} = 4.1868 \times 10^7 \text{ erg}$ .

Values of the fundamental physical constants, which could be used in calculations on the subjects of this book, are given in Table A.3.

**TABLE A.1**  
 Relations between CGS and SI units [357]. If  $a_{\text{CGS}}$  and  $a_{\text{SI}}$  are the units,  $A_{\text{CGS}}$  and  $A_{\text{SI}}$  are the values of a quantity measured in these units, and  $K$  are the factors given in the table, then  $a_{\text{SI}} = a_{\text{CGS}}K$ , and  $A_{\text{SI}} = A_{\text{CGS}}/K$ .

Name	Quantity	CGS			SI		
		Notation in text	Dimension	Name of unit	Notation	Name of unit	Dimension
Length		$l, d, \text{etc.}$	L	centimeter	cm	meter	L
Time		$t, \tau$	T	second	s	second	T
Velocity		$v$	$L T^{-1}$	$\text{cm s}^{-1}$	$\text{cm s}^{-1}$	$\text{m s}^{-1}$	$L T^{-1}$
Angle		$\theta, \varphi, \text{etc.}$	1	radian	rad	radian	1
Angular velocity		$\omega$	$T^{-1}$	$\text{rad s}^{-1}$	$\text{rad s}^{-1}$	$\text{rad s}^{-1}$	$T^{-1}$
Cyclic frequency		$\omega$	$T^{-1}$	$\text{s}^{-1}$	$\text{s}^{-1}$	$\text{s}^{-1}$	$T^{-1}$
Frequency		$f$	$T^{-1}$	hertz	Hz	hertz	$T^{-1}$
Mass		$m$	M	gram	g	kilogram	M
Momentum, impulse		$p$	$L M T^{-1}$	$\text{g cm s}^{-1}$	$\text{g cm s}^{-1}$	$\text{kg m s}^{-1}$	$L M T^{-1}$
Moment of momentum		$L, S$	$L^2 M T^{-1}$	$\text{g cm}^2 \text{s}^{-1}$	$\text{g cm}^2 \text{s}^{-1}$	$\text{kg m}^2 \text{s}^{-1}$	$L^2 M T^{-1}$
Force		$F$	$L M T^{-2}$	dyne	dyn	newton	$L M T^{-2}$
Pressure		$P$	$L^{-1} M T^{-2}$	dyne $\text{cm}^{-2}$	$\text{dyn cm}^{-2}$	pascal	$L^{-1} M T^{-2}$
Work, energy, thermodynamic potentials		$W, \varepsilon$	$L^2 M T^{-2}$	erg	erg	joule	$L^2 M T^{-2}$
Energy volume density [energy] <sup>a</sup>		$U$	$L^{-1} M T^{-2}$	$\text{erg cm}^{-3}$	$\text{erg cm}^{-3}$	$\text{J m}^{-3}$	$L^{-1} M T^{-2}$
Power		$P$	$L^2 M T^{-3}$	$\text{erg s}^{-1}$	$\text{erg s}^{-1}$	watt	$L^2 M T^{-3}$
Energy-flow surface density (Poynting vector)		$\Pi$	$M T^{-3}$	$\text{erg cm}^{-2} \text{s}^{-1}$	$\text{erg cm}^{-2} \text{s}^{-1}$	$\text{W m}^{-2}$	$M T^{-3}$
Elastic strain		$\bar{\epsilon}$	1				1

Quantity			CGS			SI		
Name	Notation in text	Dimension	Name of unit	Notation	<i>K</i>	Notation	Name of unit	Dimension
Elastic stress Module of	$\vec{\sigma}$	$L^{-1} M T^{-2}$		dyn cm <sup>-2</sup>	10	Pa		$L^{-1} M T^{-2}$
elasticity	$c_{pqlm}$	$L^{-1} M T^{-2}$		dyn cm <sup>-2</sup>	10	Pa		$L^{-1} M T^{-2}$
Electric charge	$e$	$L^{3/2} M^{1/2} T^{-1}$	electrostatic unit	esu	$2.9979 \times 10^9$	C	coulomb	TI
Electric charge volume density	$\rho$	$L^{-3/2} M^{1/2} T^{-1}$		esu cm <sup>-3</sup>	$2.9979 \times 10^3$	C m <sup>-3</sup>		$L^{-3} T I$
Electric field	$E$	$L^{-1/2} M^{1/2} T^{-1}$	<sup>b</sup>	statvolt cm <sup>-1</sup> = dyn esu <sup>-1</sup>	$3.3356 \times 10^{-5}$	V m <sup>-1</sup>		$L M T^{-3} I^{-1}$
Electric potential	$\varphi$	$L^{1/2} M^{1/2} T^{-1}$	statvolt	statvolt = erg cm <sup>-1</sup>	$3.3356 \times 10^{-3}$	V	volt	$L^2 M T^{-3} I^{-1}$
Capacitance	$p$	L		cm	$8.9876 \times 10^{11}$	F	farad	$L^{-2} M^{-1} T^4 I^2$
Electric dipole moment	$P$	$L^{5/2} M^{1/2} T^{-1}$		esu cm	$2.9979 \times 10^{11}$	C m		LT I
Polarization	$P$	$L^{-1/2} M^{1/2} T^{-1}$	<sup>b</sup>	esu cm <sup>-2</sup>	$2.9979 \times 10^5$	C m <sup>-2</sup>		$L^{-2} T I$
Electric susceptibility	$\vec{\epsilon}$	1			$8.9876 \times 10^9$	F m <sup>-1</sup>		$L^{-3} M^{-1} T^4 I^2$
Permittivity	$D$	1		statvolt cm <sup>-1</sup> = dyn esu <sup>-1</sup>	$8.9876 \times 10^9$	F m <sup>-1</sup>		$L^{-3} M^{-1} T^4 I^2$
Electric induction (displacement)	$I$	$L^{-1/2} M^{1/2} T^{-1}$	<sup>b</sup>	esu s <sup>-1</sup>	$2.9979 \times 10^5$	C m <sup>-2</sup>		$L^{-2} T I$
Current	$j$	$L^{3/2} M^{1/2} T^{-2}$		esu cm <sup>-2</sup> s <sup>-1</sup>	$2.9979 \times 10^5$	A m <sup>-2</sup>	ampere	I
Current density	$R$	$L^{-1/2} M^{1/2} T^{-2}$		cm <sup>-1</sup> s	$1.1126 \times 10^{-12}$	$\Omega$	ohm	$L^2 M T^{-3} I$
Resistance	$\rho$	$L^{-1} T$		s	$1.1126 \times 10^{-10}$	$\Omega$ m		$L^3 M T^{-3} I$
Resistivity		T		cm s <sup>-1</sup>	$8.9876 \times 10^{11}$	S	siemens	$L^{-2} M^{-1} T^3 I^2$
Conductance		$L T^{-1}$						

TABLE A.1 Continued.

Name	Quantity				CGS				SI			
	Notation in text	Dimension	Name of unit	Notation	$K$	Notation	Name of unit	Notation	Dimension			
Conductivity	$\vec{\sigma}$	$T^{-1}$		$s^{-1}$		$s^{-1}$		$S m^{-1}$	$L^{-3} M^{-1} T^3 I^2$			
Magnetic field	$\mathbf{H}$	$L^{-1/2} M^{1/2} T^{-1}$	oersted	Oe	$8.9876 \times 10^9$	Oe		$A m^{-1}$	$L^{-1} I$			
Magnetic potential	$\psi$	$L^{1/2} M^{1/2} T^{-1}$	gilbert	Gi	1.2566	Gi		A	I			
Magnetic moment	$\mathfrak{M}$	$L^{5/2} M^{1/2} T^{-1}$		esu cm	$10^3$	esu cm		$A m^2$	$L^2 I$			
Magnetization	$\mathbf{M}$	$L^{-1/2} M^{1/2} T^{-1}$	gauss <sup>b</sup>	G	$10^{-3}$	G		$A m^{-1}$	$L^{-1} I$			
Magnetic induction	$\mathbf{B}$	$L^{-1/2} M^{1/2} T^{-1}$	gauss <sup>b</sup>	G	$10^4$	G		T	$M T^{-2} I^{-1}$			
Magnetic flux	$\Phi$	$L^{3/2} M^{1/2} T^{-1}$	maxwell	Mx	$10^8$	Mx		Wb	$L^2 M T^{-2} I^{-1}$			
Inductance		L		cm	$10^9$	cm		H	$L^2 M T^{-2} I^{-2}$			
Magnetic susceptibility	$\vec{\chi}$	1			$7.9577 \times 10^{-2}$				1			
Permeability	$\vec{\mu}$	1			$10^7$			$H m^{-1}$	$L M T^{-2} I^{-2}$			
Magnetoelastic constants	$B_{1,2}$	$L^{-1} M T^{-2}$		erg $cm^{-3}$	10	erg $cm^{-3}$		$J m^{-3}$	$L^{-1} M T^{-2}$			
Temperature	$T$	$L M T^{-2}$		erg cm	$10^5$	erg cm		$J m^{-1}$	$L M T^{-2}$			
Heat capacity		$\Theta$	kelvin	K	1	K		K	$\Theta$			
Fractional heat capacity [heat capacity] <sup>a</sup>	$c_{p,v}$	$L^2 M T^{-2} \Theta^{-1}$		erg $K^{-1}$	$10^7$	erg $K^{-1}$		$J K^{-1}$	$L^2 M T^{-2} \Theta^{-1}$			
Entropy		$L^{-1} M T^{-2} \Theta^{-1}$		erg $cm^{-3} K^{-1}$	10	erg $cm^{-3} K^{-1}$		$J m^{-3} K^{-1}$	$L^{-1} M T^{-2} \Theta^{-1}$			
Entropy density [entropy] <sup>a</sup>	$S$	$L^2 M T^{-2} \Theta^{-1}$		erg $K^{-1}$	$10^7$	erg $K^{-1}$		$J K^{-1}$	$L^2 M T^{-2} \Theta^{-1}$			
		$L^{-1} M T^{-2} \Theta^{-1}$		erg $cm^{-3} K^{-1}$	10	erg $cm^{-3} K^{-1}$		$J m^{-3} K^{-1}$	$L^{-1} M T^{-2} \Theta^{-1}$			

<sup>a</sup> Contracted names of quantities used in the text are given in brackets.

<sup>b</sup> Oersted is commonly used as the magnetic field  $\mathbf{H}$  unit, and gauss, as the magnetization  $\mathbf{M}$  or magnetic induction  $\mathbf{B}$  unit in the CGS system. However, all quantities  $\mathbf{H}$ ,  $\mathbf{M}$ ,  $\mathbf{B}$ ,  $\mathbf{E}$ ,  $\mathbf{P}$ , and  $\mathbf{D}$  have the same dimension in this system and, hence, may be measured in the same units, e.g., in oersteds.

**TABLE A.2**

Special energy units. The numbers in the table (analogous to the factor  $K$  in Table A.1) are the ratios of units in appropriate rows to units in appropriate columns.

Unit	Erg	Electron-volt (eV)	Inverse centimeter (cm <sup>-1</sup> )	Kelvin (K)	Oersted (Oe)
Erg	1	$6.2415 \times 10^{11}$	$5.0341 \times 10^{15}$	$7.2429 \times 10^{15}$	$5.3852 \times 10^{19}$
Electronvolt	$1.6022 \times 10^{-12}$	1	$8.0655 \times 10^3$	$1.1604 \times 10^4$	$8.6280 \times 10^7$
Inverse centimeter	$1.9864 \times 10^{-16}$	$1.2398 \times 10^{-4}$	1	1.4388	$1.0697 \times 10^4$
Kelvin	$1.3807 \times 10^{-16}$	$8.6174 \times 10^{-5}$	0.69504	1	$7.4351 \times 10^3$
Oersted	$1.8570 \times 10^{-20}$	$1.1590 \times 10^{-8}$	$9.3481 \times 10^{-5}$	$1.3450 \times 10^{-4}$	1

**TABLE A.3**

Values of some fundamental physical constants [78].

Constant	Notation and relation to other constants	Value in CGS system
Velocity of light in vacuum	$c$	$2.997925 \times 10^{10}$
Electron charge	$e_0$	$-4.80321 \times 10^{-10}$
Electron mass at rest	$m_e$	$9.10939 \times 10^{-28}$
Electron specific charge	$e_0/m_e$	$-5.27281 \times 10^{17}$
Proton mass at rest	$m_p \cong 1836 m_e$	$1.67262 \times 10^{-24}$
Neutron mass at rest	$m_n = 1839 m_e$	$1.67493 \times 10^{-24}$
Atomic mass unit	$m_0 = m(^{12}\text{C})/12$	$1.66054 \times 10^{-24}$
Avogadro number	$N_A = 1/m_0$	$6.02214 \times 10^{23}$
Planck constant	$\hbar = h/(2\pi)$	$1.05457 \times 10^{-27}$
Fine-structure constant	$\alpha = e_0^2/(\hbar c)$	$7.29735 \times 10^{-3} \cong 1/137$
Bohr radius	$a_0 = \hbar^2/(m_e e_0^2)$	$5.29177 \times 10^{-9}$
Electron-spin $g$ -factor	$g_S = 2[1 + \alpha/(2\pi) - 0.328\alpha^2/\pi^2]$	2.002319
Bohr magneton	$\mu_B =  e_0 \hbar/(2m_e c)$	$9.27402 \times 10^{-21}$
Electron-spin gyromagnetic ratio	$\gamma_S = g_S  e_0 /(2m_e c) \equiv g_S \mu_B/\hbar$	$1.76086 \times 10^7$
Nuclear magneton	$\mu_n =  e_0 \hbar/(2m_p c)$	$5.05079 \times 10^{-24}$
Proton magnetic moment	$\mathfrak{M}_p = 2.79285 \mu_n$	$1.41061 \times 10^{-23}$
Neutron magnetic moment	$\mathfrak{M}_n = 1.91304 \mu_n$	$9.66237 \times 10^{-24}$
Magnetic flux quantum	$\Phi_0 = \pi \hbar c/ e_0 $	$2.06783 \times 10^{-7}$
Boltzmann constant	$\kappa$	$1.38066 \times 10^{-16}$
Constant of gravitation	$G$	$6.67259 \times 10^{-8}$
Standard acceleration of gravity	$g_{\text{norm}}$	$9.80665 \times 10^2$



---

## Appendix B

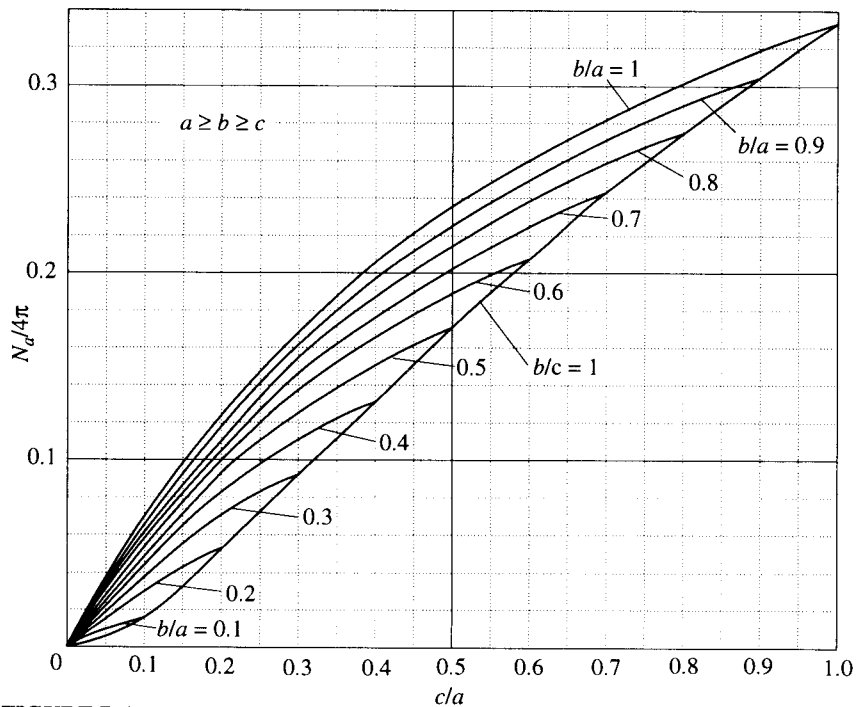
---

### Demagnetization factors

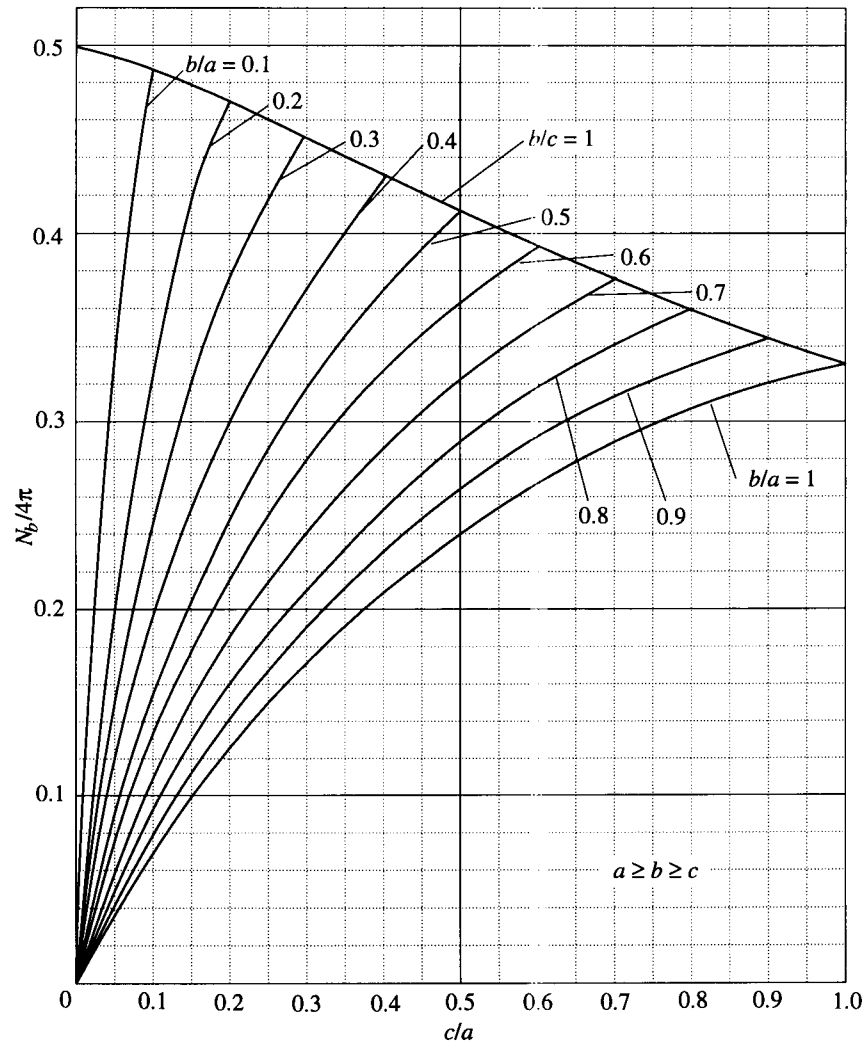
The demagnetization factors  $N_{a,b,c}$  (Section 1.5) of an ellipsoid with axes  $a$ ,  $b$ , and  $c$  ( $a \geq b \geq c$ ) placed in a medium with  $\mu = 1$  are determined (e.g., [131]) by the expression

$$N_a = 2\pi abc \int_0^\infty \frac{dt}{(a^2 + t) \sqrt{(a^2 + t)(b^2 + t)(c^2 + t)}} \quad (B.1)$$

and analogous expressions for  $N_b$  and  $N_c$ . The curves of  $N_{a,b,c}$  vs the ratios of the ellipsoid axes, calculated by Osborn [306], are plotted in Figures B.1, B.2, and B.3.

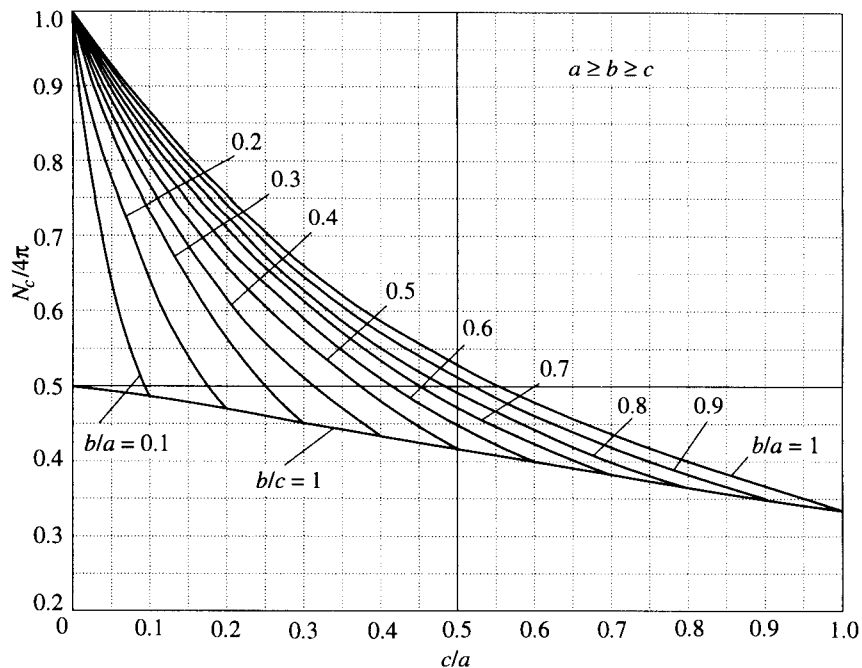


**FIGURE B.1**  
Demagnetization factors of an ellipsoid in the direction of the larger axis [306].



**FIGURE B.2**  
Demagnetization factors of an ellipsoid in the direction of the middle axis [306].





**FIGURE B.3**

Demagnetization factors of an ellipsoid in the direction of the smaller axis [306].

For an ellipsoid of revolution (spheroid), rather simple formulae [321] follow from (B.1); in the case of  $a > b = c$  (prolate spheroid),

$$N_a = 4\pi \frac{1 - \xi^2}{\xi^2} \left( \frac{1}{2\xi} \ln \frac{1 + \xi}{1 - \xi} - 1 \right) \quad (B.2)$$

and in the case of  $a = b > c$  (oblate spheroid),

$$N_c = 4\pi \frac{1 - \xi^2}{\xi^2} \left( 1 - \frac{1}{\xi} \arctan \xi \right) \quad (B.3)$$

where  $\xi = \sqrt{a^2 - c^2}/a$  in both cases.



---

## Appendix C

---

### Dirac delta function and Kronecker delta symbol

The Dirac delta function  $\delta(x)$  is defined as (e.g., [243, 84, 336])

$$\delta(x) = \begin{cases} 0 & \text{at } x \neq 0 \\ \infty & \text{at } x = 0 \end{cases}$$
$$\int_a^b \delta(x) dx = 1 \quad \text{if } a < 0 < b. \quad (C.1)$$

It should be noted that  $\delta(x)$  is not a function in the usual sense but a symbolic or generalized function. The main property of it, which can be regarded as its definition, is

$$\int_a^b f(x) \delta(x - x_0) dx = f(x_0) \quad \text{if } a < x_0 < b \quad (C.2)$$

where  $f(x)$  is an arbitrary function continuous at  $x = x_0$ .

Some other useful properties of  $\delta(x)$  are

$$\delta(-x) = \delta(x) \quad (C.3)$$

so that  $\delta(x)$  is an even function;

$$\delta(Cx) = \frac{1}{|C|} \delta(x) \quad (C.4)$$

where  $C$  is a constant;

$$x\delta(x) = 0 \quad (C.5)$$

$$f(x)\delta(x - x_0) = f(x_0)\delta(x - x_0) \quad (C.6)$$

$$\int \delta(a - x)\delta(x - b) dx = \delta(a - b). \quad (C.7)$$

The function  $\delta(x)$  can be represented as a limit of sequences of some analytical functions, e.g.,

$$\delta(x) = \lim_{k \rightarrow \infty} \frac{\sin(kx)}{\pi x} \quad (C.8)$$

or as an integral, e.g.,

$$\delta(x) = \frac{1}{2\pi} \int_{-\infty}^{+\infty} \exp(ikr) dk. \quad (C.9)$$

The delta function can be related by a symbolic expression

$$\delta(x) = \frac{d}{dx} U(x) \quad (C.10)$$

to the unit (or step) function

$$U(x) = \begin{cases} 0 & \text{at } x < 0 \\ 1 & \text{at } x > 0 \end{cases} \quad (C.11)$$

(the value of  $U(x)$  at  $x = 0$  can be defined, e.g., as 1/2). The derivative of  $\delta(x)$  can be introduced by

$$\int_a^b f(x) \delta'(x - x_0) dx = -f'(x_0) \quad \text{if } a < x_0 < b. \quad (C.12)$$

A three-dimensional delta function is defined as

$$\delta(\mathbf{r}) = \delta(x) \delta(y) \delta(z). \quad (C.13)$$

Its main property is

$$\int_{\mathbf{r}} f(\mathbf{r}) \delta(\mathbf{r} - \mathbf{r}_0) d\mathbf{r} = f(\mathbf{r}_0) \quad (C.14)$$

where integration is performed over the entire  $\mathbf{r}$  space. Extending (C.9), we get

$$\delta(\mathbf{r}) = \frac{1}{(2\pi)^3} \int_{\mathbf{k}} \exp(i\mathbf{k}\mathbf{r}) d\mathbf{k} \quad (C.15)$$

where integration is carried out over the  $\mathbf{k}$  space.

The Kronecker delta symbol is defined as

$$\Delta_{mn} = \begin{cases} 0 & \text{if } n \neq m \\ 1 & \text{if } n = m \end{cases} \quad (C.16)$$

where  $m$  and  $n$  are any discrete quantities, e.g., integers, or as

$$\Delta(\mathbf{k}) = \begin{cases} 0 & \text{if } \mathbf{k} \neq 0 \\ 1 & \text{if } \mathbf{k} = 0 \end{cases} \quad (C.17)$$

where  $\mathbf{k}$  is a scalar or a vector, continuous or discrete.

---

## *Bibliography*

---

- [1] Abragam, A. and Bleaney, B. I., *Electron Paramagnetic Resonance of Transition Ions*, Clarendon Press, Oxford, (1970).
- [2] Abrahams, E. and Kittel, C., Spin-lattice relaxation in ferromagnets, *Phys. Rev.*, **88**, No. 5, 1200, (1952).
- [3] Adam, J. D., Analog signal-processing with microwave magnetics, *Proc. IEEE*, **76**, No. 2, 159, (1988).
- [4] Adam, J. D. and Collins, J. H., Microwave magnetostatic delay devices based on epitaxial yttrium iron-garnet, *Proc. IEEE*, **64**, No. 5, 794, (1976).
- [5] Adam, J. D., Daniel, M. R., Emtage, P. R., and Talisa, S. H., *Magnetostatic Waves*, Academic Press, New York, (1991).
- [6] Adam, J. D. and Stitzer, S. N., A magnetostatic wave signal-to-noise enhancer, *Appl. Phys. Lett.*, **36**, No. 6, 485, (1980).
- [7] Adams, M. J., *An Introduction to Optical Waveguides*, Wiley, New York, (1981).
- [8] Adkins, L. R. and Glass, H. L., Magnetostatic volume wave propagation in multiple ferrite layers, *J. Appl. Phys.*, **53**, No. 12, 8928, (1982).
- [9] Ageev, A. N. and Gurevich, A. G., Ferromagnetic resonance in yttrium garnet with holmium impurity, *Sov. Phys. Solid State*, **11**, No. 8, 1712, (1970).
- [10] Akhiezer, A. I., Theory of the relaxation processes in ferromagnetics at low temperatures, *J. Phys. (USSR)*, **10**, No. 3, 217, (1946).
- [11] Akhiezer, A. I., Bar'yakhtar, V. G., and Kaganov, M. I., On the problem of the width of ferromagnetic resonance lines, *Fiz. Met. Metalloved*, **6**, No. 5, 932, (1958), (in Russian).
- [12] Akhiezer, A. I., Bar'yakhtar, V. G., and Peletminskii, S. V., Coupled magnetoelastic waves in ferromagnets and ferroacoustic resonance, *Sov. Phys. JETP*, **8**, No. 1, 157, (1959).
- [13] Akhiezer, A. I., Bar'yakhtar, V. G., and Peletminskii, S. V., Coherent amplification of spin waves, *Sov. Phys. JETP*, **18**, No. 1, 235, (1964).
- [14] Akhiezer, A. I., Bar'yakhtar, V. G., and Peletminskii, S. V., *Spin Waves*, North Holland, Amsterdam, (1968).

- [15] Altshuler, S. A. and Kozyrev, B. M., *Electron Paramagnetic Resonance in Compounds of Transition Elements*, Halsted Press, New York, (1975).
- [16] Ament, W. S. and Rado, G. T., Electromagnetic effects of spin wave resonance in ferromagnetic metals, *Phys. Rev.*, **97**, No. 6, 1558, (1955).
- [17] Anderson, P. W., The concept of spin-lattice relaxation in ferromagnetic materials, *Phys. Rev.*, **88**, No. 5, 1214, (1952).
- [18] Anderson, P. W., Exchange in insulators: superexchange, direct exchange, and double exchange, in [267], Vol. I, p. 25.
- [19] Anderson, P. W. and Suhl, H., Instability in the motion of ferromagnets at high microwave power levels, *Phys. Rev.*, **100**, No. 6, 1788, (1955).
- [20] Anisimov, A. N. and Gurevich, A. G., Attenuation of spin waves due to four-magnon scattering, *Sov. Phys. Solid State*, **18**, No. 1, 20, (1976).
- [21] Anisimov, A. N., Shukyurov, A. S., Gurevich, A. G., and Emiryan, L. M., Longitudinal pumping of spin waves in ferromagnetic chromium chalcogenide spinels, *Sov. Phys. JETP*, **57**, No. 4, 818, (1983).
- [22] Arkad'ev, V. K., Absorption of electric waves in parallel wires, *Zh. Russk. Fiz.-Khim. Obshchestva, Otdel Fiz.*, **44**, No. 4, 165, (1912), (in Russian).
- [23] Artman, J. O., Microwave resonance relations in anisotropic single-crystal ferrites, *Phys. Rev.*, **105**, No. 1, 62, (1957).
- [24] Ashcroft, N. W. and Mermin, N. D., *Solid State Physics*, Holt, Rinehart, and Winston, New York, (1976).
- [25] Auld, B. A., Coupling of electromagnetic and magnetostatic modes in ferrite-loaded cavity resonators, *J. Appl. Phys.*, **34**, No. 6, 1629, (1963).
- [26] Auld, B. A., Transversely pumped magnetoelastic instabilities, *J. Appl. Phys.*, **36**, No. 3, Pt. 1, 689, (1965).
- [27] Auld, B. A. and Mechta, K. B., Magnetostatic waves in a transversely magnetized rectangular rod, *J. Appl. Phys.*, **38**, No. 10, 4081, (1967).
- [28] Ayres, W. P., Millimeter-wave generation experiment utilizing ferrites, *IRE Trans. Microwave Theory Tech.*, **MTT-7**, No. 1, 62, (1959).
- [29] Bacon, G. E., *Neutron Diffraction*, Clarendon Press, Oxford, (1962).
- [30] Bady, I., Frequency doubling using ferrite slabs, particularly planar ferrites, *IRE Trans. Microwave Theory Tech.*, **10**, No. 1, 55, (1962).
- [31] Bady, I. and Schlömann, E., Spin wave excitation in planar ferrites, *J. Appl. Phys.*, **33**, No. 3, 1377, (1962).
- [32] Bailey, G. C. and Vittoria, C. V., Spin-wave resonance fields, linewidths, and intensities of a permalloy film: theory and experiment, *Phys. Rev. Lett.*, **28**, No. 2, 100, (1972).
- [33] Bairamov, A. I., Gurevich, A. G., Karpovich, V. I., Kalinnikov, V. T., Aminov, T. G., and Emiryan, L. M., Ferromagnetic resonance in silver-doped  $\text{CdCr}_3\text{Se}_4$  crystal, *Sov. Phys. Solid State*, **18**, No. 3, 396, (1976).

- [34] Bairamov, A. I., Gurevich, A. G., Emiryan, L. M., and Parfenova, N. N., Influence of selenium vacancies on ferromagnetic resonance in silver-doped  $\text{CdCr}_2\text{Se}_4$  crystals, *Sov. Phys. Solid State*, **19**, No. 9, 1563, (1977).
- [35] Bajorek, C. H. and Wilts, C. H., Evidence for partial surface spin pinning in ferromagnetic resonance, *J. Appl. Phys.*, **42**, No. 11, 4324, (1971).
- [36] Bar'yakhtar, V. G., Phenomenological description of relaxation processes in magnetic materials, *Sov. Phys. JETP*, **60**, No. 4, 863, (1984).
- [37] Bar'yakhtar, V. G., Bogdanov, A. N., and Yablonskii, D. A., The physics of magnetic domains, *Sov. Phys. Usp.*, **31**, No. 9, 810, (1988).
- [38] Bar'yakhtar, V. G., Ivanov, B. A., and Sukstanskii, A. L., On spin waves in ferromagnet with domain structure, *Sov. Phys. Solid State*, **21**, No. 10, 1729, (1979).
- [39] Bar'yakhtar, V. G., and Kaganov, M. I., Non-uniform resonance and spin waves, in [115], p. 231.
- [40] Bar'yakhtar, V. G., Savchenko, M. A., and Tarasenko, V. V., Effect of dislocations on the line width of uniform ferro- and antiferromagnetic resonance, *Sov. Phys. JETP*, **27**, No. 5, 858, (1968).
- [41] Bar'yakhtar, V. G., and Turov, E. A., Magnetoelastic excitations, in [382], Pt. 2, p. 333.
- [42] Baryshev, D. A., Vashkovskii, A. V., Grechushkin, K. V., and Stal'makhov, A. V., Propagation of a ratio pulse of a magnetostatic wave in a ferrite waveguide, *Sov. Tech. Phys. Lett.*, **16**, No. 2, 84, (1990).
- [43] Becker, R., Dynamics of Bloch walls and the high-frequency permeability, *J. Phys. Radium*, **12**, No. 3, 332, (1951), (in French).
- [44] Becker, R., *Electromagnetic Fields and Interactions*, Blaisdell, (1964).
- [45] Beeman, D. E., Magnetostatic modes in antiferromagnets and canted antiferromagnets, *J. Appl. Phys.*, **37**, No. 3, 1136, (1966).
- [46] Berteaud, A. J. and Pascard, H., Nonlinear behavior of ferromagnetic thin films, *J. Appl. Phys.*, **37**, No. 5, 2035, (1966).
- [47] Bhagat, S. M., Hirst, L. L., and Anderson, J. R., Ferromagnetic resonance in nickel and iron, *J. Appl. Phys.*, **37**, No. 1, 194, (1966).
- [48] Bhagat, S. M. and Lubitz, P., Temperature variation of ferromagnetic relaxation in the 3d transition metals, *Phys. Rev.*, **B10**, No. 1, 179, (1974).
- [49] Bini, M., Millanta, L., and Rubino, N., Interaction of magnetic waves with drifting charges, *IEEE Trans. Magn.*, **MAG-14**, No. 5, 811, (1978).
- [50] Blank, A. Y. and Kaganov, M. I., Contribution to the theory of spatial dispersion in a ferromagnetic metal in a strong magnetic field, *Sov. Phys. JETP*, **22**, No. 3, 561, (1966).
- [51] Blankenship, A. C. and Hunt, R. L., Microwave characteristics of fine-grain high-power garnets and spinels, *J. Appl. Phys.*, **37**, No. 3, 1066, (1966).
- [52] Bloch, F., On the theory of ferromagnetism, *Z. Phys.*, **61**, No. 3/4, 206, (1930), (in German).

- [53] Bloch, F., Nuclear induction, *Phys. Rev.*, **70**, No. 7/8, 460, (1946).
- [54] Bloembergen, N., On the ferromagnetic resonance in nickel and supermalloy, *Phys. Rev.*, **78**, No. 5, 572, (1950).
- [55] Bloembergen, N., *Nonlinear Optics*, Benjamin, New York, (1965).
- [56] Bloembergen, N. and Damon, R. W., Relaxation effects in ferromagnetic resonance, *Phys. Rev.*, **85**, No. 4, 699, (1952).
- [57] Bloembergen, N. and Wang, S., Relaxation effects in para- and ferromagnetic resonance, *Phys. Rev.*, **93**, No. 1, 72, (1954).
- [58] Bongianini, W. L., Magnetostatic propagation in a dielectric layered structure, *J. Appl. Phys.*, **43**, No. 6, 2541, (1972).
- [59] Borovik-Romanov, A. S. and Kreines, N. M., Light scattering from spin waves, in [382], Pt. 1, p. 81.
- [60] Borovik-Romanov, A. S. and Orlova, M. P., Magnetic properties of cobalt and manganese carbonates, *Sov. Phys. JETP*, **4**, No. 4, 531, (1957).
- [61] Bozorth, R., *Ferromagnetism*, Van Nostrand, Princeton, (1961).
- [62] Brown, W. F., Jr., *Micromagnetics*, Interscience, New York, (1963).
- [63] Buffler, C. R., Ferromagnetic resonance near the upper limit of the spin wave manifold, *J. Appl. Phys.*, **30**, No. 4, Suppl., 172S, (1959).
- [64] Buishvili, L. L., Spin-lattice relaxation in ferrites with paramagnetic impurities, *Sov. Phys. Solid State*, **3**, No. 12, 2689, (1962).
- [65] Burkov, V. D., Vashkovskii, A. V., and Kil'dishev, V. N., Excitation of magnetoacoustic resonance in ferrite disks, *Radio Eng., Electron.* **15**, No. 4, 648, (1970).
- [66] Callen, H. B., A ferromagnetic dynamical equation, *J. Phys. Chem. Solids*, **4**, No. 4, 256, (1958).
- [67] Callen, H. B. and Pittelli, E., Anisotropic ferromagnetic resonance linewidth in ferrites, *Phys. Rev.*, **119**, No. 5, 1523, (1960).
- [68] Casimir, H. B. and du Pre, F. K., On the thermodynamic interpretation of paramagnetic relaxation phenomena, *Physica*, **5**, No. 6, 507, (1938).
- [69] Charap, S. H. and Artman, J. O., Magnetostatic modes of stripe domain, *J. Appl. Phys.*, **49**, No. 3, 1585, (1978).
- [70] Chikazumi, S., *Physics of Magnetism*, R. E. Krieger, Malabar, Fl., (1986).
- [71] Chivileva, O. A., Gurevich, A. G., Anisimov, A. N., Gusev, B. N., Vugal'ter, G. A., and Sher, E. S., Threshold fields in parametric excitation of spin waves by a surface magnetostatic wave, *Sov. Phys. Solid State*, **29**, No. 6, 1020, (1987).
- [72] Chivileva, O. A., Gurevich, A. G., Anisimov, A. N., and Emiryan, L. M., Effect of a cubic anisotropy on the spectrum of surface spin waves in a film with a {111} surface, *Sov. Phys. Solid State*, **29**, No. 1, 61, (1987).
- [73] Clarke, B. H., Resonance relaxation in  $Mn_xFe_yO_4$  by slow relaxing manganese and ferrous ions, *J. Phys. Chem. Solids*, **27**, No. 2, 353, (1966).



- [74] Clarke, B. H., Tweedale, K., and Teale, R. W., Rare-earth ion relaxation time and  $G$  tensor in rare-earth-doped yttrium iron garnet, 1. Ytterbium, *Phys. Rev.*, **139**, No. 6A, A1933, (1965).
- [75] Clogston, A. M., Relaxation phenomena in ferrites, *Bell Syst. Tech. J.*, **34**, No. 4, 739, (1955).
- [76] Clogston, A. M., Suhl, H., Walker, L. R., and Anderson, P. W., Ferromagnetic resonance line width in insulating materials, *J. Phys. Chem. Solids*, **1**, No. 3, 129, (1956).
- [77] Cochran, J. F., Heinrich, B., and Dewar, G., Ferromagnetic antiresonance transmission through supermalloy at 24 GHz, *Can. J. Phys.*, **55**, No. 9, 787, (1977).
- [78] Cohen, E. R. and Taylor, B. N., The fundamental physical constants, *Phys. Today*, **41**, No. 8, Pt. 2, BG9 (1988).
- [79] Comly, J. B. and Jones, R. V., Parallel-pumped instabilities in magnetic metal films, *J. Appl. Phys.*, **36**, No. 3, Pt. 2, 1201 (1965).
- [80] Coutinho, M. D., Filho, Miranda, L. C. M., and Rezende, S. M., Spin wave amplification in ferromagnetic semiconductors, *Phys. Status Solidi B*, **57**, No. 1, 85, (1973).
- [81] Damon, R. W., Thermally-induced nonlinear effects in ferromagnetic resonance, *Phys. Status Solidi*, **8**, No. 2, K89, (1965).
- [82] Damon, R. W. and Eshbach, J. R., Magnetostatic modes of ferromagnetic slab, *J. Phys. Chem. Solids*, **19**, No. 3/4, 308, (1961).
- [83] Davies, J. T., Effect of nonuniform magnetization on the spin-wave spectrum in thin ferromagnetic films, *J. Appl. Phys.*, **35**, No. 3, Pt. 2, 804 (1964).
- [84] Davydov, A. S., *Quantum Mechanics*, Nauka, Moscow, (1973), (in Russian).
- [85] Dedukh, L. M., Kabanov, Yu. P., and Nikitenko, V. I., An experimental study of the spectrum of spin waves localized on a Bloch line, *Sov. Phys. JETP*, **70**, No. 2, 317, (1990).
- [86] de Gennes, P. G., Theory of neutron scattering by magnetic crystals, in [267], Vol III, p. 115.
- [87] de Gennes, P. G., Kittel, C., and Portis, A. M., Theory of ferromagnetic resonance in rare-earth garnets, 2. Line widths, *Phys. Rev.*, **116**, No. 2, 323, (1959).
- [88] Denton, R. T., Theoretical and experimental characteristics of ferromagnetic amplifier using longitudinal pumping, *J. Appl. Phys.*, **32**, No. 3, Suppl., 300S, (1961).
- [89] Deryugin, I. A., Zaporozhets, V. V., and Melkov, G. A., Nonlinear ferromagnetic resonance, *JETP Lett.*, **5**, No. 10, 292, (1967).
- [90] De Wames, R. E. and Wolfram, T., Dipole-exchange spin waves in ferromagnetic films, *J. Appl. Phys.*, **41**, No. 3, 987, (1970).

- [91] De Wames, R. E. and Wolfram, T., Experimental test for pinned spins in ferromagnetic resonance, *Phys. Rev. Lett.*, **26**, No. 23, 1445, (1971).
- [92] De Wames, R. E. and Wolfram, T., Spin-wave resonance in conducting films: parallel resonance, *Jpn. J. Appl. Phys.*, **13**, No. 1, 68, (1974).
- [93] Dillon, J. F., Jr., Ferromagnetic resonance in thin discs of manganese ferrite, *Bull. Am. Phys. Soc.*, **1**, No. 3, 125, (1956).
- [94] Dillon, J. F., Jr., Ferrimagnetic resonance in rare-earth-doped yttrium iron garnet. 3. Linewidth, *Phys. Rev.*, **127**, No. 5, 1495, (1962).
- [95] Dillon, J. F., Jr., Domains and domain walls, in [267], Vol. III, p. 415.
- [96] Dillon, J. F., Jr., Gyorgy, E. M., and Remeika, J. P., Photoinduced uniaxial magnetic anisotropy and optical dichroism in silicon-doped yttrium iron garnet [YIG(Si)], *J. Appl. Phys.*, **41**, No. 3, 1211, (1970).
- [97] Dillon, J. F., Jr. and Nielsen, J. W., Effects of rare-earth impurities on ferrimagnetic resonance in yttrium iron garnet, *Phys. Rev. Lett.*, **3**, No. 1, 30, (1959).
- [98] Dillon, J. F., Jr. and Nielsen, J. W., Ferrimagnetic resonance in rare-earth doped yttrium iron garnet. 1. Field for resonance, *Phys. Rev.*, **120**, No. 1, 105, (1960).
- [99] Dillon, J. F., Jr., Remeika, J. P., and Walker, L. R., Low-temperature anomaly in ferrimagnetic resonance of ytterbium-doped yttrium iron garnet, *J. Appl. Phys.*, **38**, No. 5, 2235, (1967).
- [100] Dillon, J. F., Jr. and Walker, L. R., Ferrimagnetic resonance in rare-earth doped yttrium iron garnet. 2. Terbium substitution, *Phys. Rev.*, **124**, No. 5, 1401, (1961).
- [101] Dirac, P. A. M., Quantum mechanics of many-electron systems, *Proc. R. Soc. London*, **A123**, No. 792, 714, (1929).
- [102] Dorfmann, J., Some comments to understanding the mechanism of magnetic phenomena, *Z. Phys.*, **17**, No. 2, 98, (1923), (in German).
- [103] Döring, W., On the inertia of the walls between domains, *Z. Naturforsch.*, **3a**, No. 7, 373, (1948), (in German).
- [104] Dyson, F. J., General theory of spin-wave interactions, *Phys. Rev.*, **102**, No. 5, 1217, (1956).
- [105] Dyson, F. J., Thermodynamic behavior of an ideal ferromagnet, *Phys. Rev.*, **102**, No. 5, 1230, (1956).
- [106] Dzyaloshinskii, I. E., A thermodynamical theory of 'weak' ferromagnetism in antiferromagnetics, *Sov. Phys. JETP*, **5**, No. 6, 1259, (1957).
- [107] Emiryan, L. M., Gurevich, A. G., Shukyurov, A. S., and Berzhanskii, V. N., Characteristics of a ferromagnetic resonance in magnetic semiconductor  $\text{HgCr}_2\text{Se}_4$ , *Sov. Phys. Solid State*, **23**, No. 10, 1700, (1981).
- [108] Emtage, P. R., Interaction of magnetostatic waves with a current, *J. Appl. Phys.*, **49**, No. 8, 4475, (1978).

- [109] Epstein, P. S., Theory of wave propagation in a gyromagnetic medium, *Rev. Mod. Phys.*, **28**, No. 1, 3, (1956).
- [110] Eremenko, V. V., Krivoruchko, V. N., Lavrinenko, N. M., and Yablonskii, D. A., Excitation of exchange magnetic oscillations in  $\text{CsMnF}_3$  by an alternating electric field, *Sov. Phys. Solid State*, **30**, No. 12, 2070, (1988).
- [111] Eshbach, J. R., Spin-wave propagation and the magnetoelastic interaction in yttrium iron garnet, *J. Appl. Phys.*, **34**, No. 4, Pt. 2, 1298, (1963).
- [112] Eshbach, J. R. and Damon, R. W., Surface magnetostatic modes and surface spin waves, *Phys. Rev.*, **118**, No. 5, 1208, (1960).
- [113] Fedorov, F. I., *Theory of Elastic Waves in Crystals*, Plenum, New York, (1968).
- [114] *Ferromagnetic Materials*, Wohlfarth, E.P., Ed., North-Holland, New York, Vol. 1 and Vol. 2, (1980); Vol. 3, (1982).
- [115] *Ferromagnetic Resonance*, Vonsovskii, S. V., Ed., Pergamon Press, Oxford, (1965).
- [116] Filippov, B. N., Spin-system spectrum and high-frequency properties of ferromagnetic monocrystals containing plane defects, *Sov. Phys. JETP*, **28**, No. 1, 109, (1969).
- [117] Filippov, B. N., Oscillations of magnetization in ferromagnetic plates. I, *Fiz. Met. Metalloved*, **32**, No. 5, 911, (1971), (in Russian).
- [118] Filippov, B. N. and Tityakov, I. G., Oscillations of magnetization in ferromagnetic plates. II, *Fiz. Met. Metalloved*, **35**, No. 1, 28, (1973), (in Russian).
- [119] Fletcher, P. C. and Bell, R. O., Ferrimagnetic resonance modes in spheres, *J. Appl. Phys.*, **30**, No. 5, 687, (1959).
- [120] Fletcher, P. C. and Kittel, C., Considerations on the propagation and generation of magnetostatic waves and spin waves, *Phys. Rev.* **120**, No. 6, 2004, (1960).
- [121] Fletcher, P. C. and Solt, I. H., Jr., Coupling of the magnetostatic modes, *J. Appl. Phys.*, **30**, No. 4, Suppl., 181S, (1959).
- [122] Foner, S., Antiferromagnetic and ferrimagnetic resonance, in [267], Vol. 1, p. 383.
- [123] Frait, Z., G-factor in pure polycrystalline iron, *Czech. J. Phys.*, **B27**, No. 2, 185, (1977).
- [124] Frait, Z. and Fraitova, D., Ferromagnetic resonance and surface anisotropy in iron single-crystals, *J. Magnet. and Magn. Mater.*, **15/18**, Pt. 2, 1081, (1980).
- [125] Frait, Z. and Fraitova, D., Spin-wave resonance in metals, in [382], Pt. 2, p. 1.
- [126] Frait, Z. and Mac Faden, H., Ferromagnetic resonance in metals. Frequency dependence, *Phys. Rev.*, **139**, No. 4A, A1173, (1965).

- [127] Fraitova, D., An analytical theory of FMR in bulk metals (parallel configuration). 1. Dispersion-relations, *Phys. Status Solidi B*, **120**, No. 1, 341, (1983).
- [128] Fraitova, D., An analytical theory of FMR in bulk metals (parallel configuration). 2. Penetration depth, *Phys. Status Solidi B*, **120**, No. 2, 659, (1983).
- [129] Fraitova, D., An analytical theory of FMR in bulk metals (parallel configuration). 3. Surface impedance, *Phys. Status Solidi B*, **124**, No. 2, 587, (1984).
- [130] Frenkel, Ya. I., Elementary theory of the magnetic and electric properties of metals at zero temperature, *Z. Phys.*, **49**, No. 1-2, 31, (1928), (in German).
- [131] Frenkel, Ya. I., *Electrodynamics*, Vol. 2, ONTI, Leningrad, (1936), (in Russian).
- [132] Galt, J. K., Motion of individual domain walls in a nickel-iron ferrite, *Bell Syst. Tech. J.*, **33**, No. 5, 1023, (1954).
- [133] Gann, V. V., Nonuniform resonance in a ferromagnetic plate, *Sov. Phys. Solid State*, **8**, No. 11, 2537, (1967).
- [134] Ganguly, A. K. and Webb, D. C., Microstrip excitation of magnetostatic surface-waves-theory and experiment, *IEEE Trans. Magn.*, **23**, No. 12, 998, (1975).
- [135] Geschwind, S. and Clogston, A. M., Narrowing effect of dipole forces on inhomogeneously broadened lines, *Phys. Rev.*, **108**, No. 1, 49, (1957).
- [136] Geschwind, S. and Walker, L. R., Exchange resonances in gadolinium iron garnet near the magnetic compensation temperature, *J. Appl. Phys.*, **30**, No. 4, Suppl., 163S, (1959).
- [137] Gilinskii, I. A. and Shcheglov, I. M., Theory of the excitation of surface magnetostatic waves, *Sov. Phys. Tech. Phys.*, **30**, No. 12, 1380, (1985).
- [138] Gilleo, M. A., Ferromagnetic insulators: garnets, in [114], Vol. 2, p. 1.
- [139] Gintsburg, M. A., Gyrotropic waveguide, *Dok. Akad. Nauk SSSR*, **95**, No. 3, 489, (1954), (in Russian).
- [140] Gintsburg, M. A., On the waves in a gyrotropic medium, *Izv. Akad. Nauk SSSR, Ser. Fiz.*, **18**, No. 4, 444, (1954), (in Russian).
- [141] Gintsburg, M. A., Surface waves on the boundary of a gyrotropic medium, *Sov. Phys. JETP*, **7**, No. 6, 1123, (1958).
- [142] Gintsburg, M. A., Exchange effects in ferromagnetic resonance, *Sov. Phys. JETP*, **8**, No. 4, 730, (1958).
- [143] Golovenchits, E. I., Gurevich, A. G., and Sanina, V. A., Magnetic resonance in the uniaxial ferromagnet  $\text{RbNiF}_3$ , *Sov. Phys. Solid State*, **10**, No. 10, 2334, (1969).
- [144] Gorter, C. J., *Paramagnetic Relaxation*, Elsevier, Amsterdam, (1948).
- [145] Gubanov, A. I., Quasi-classical theory of amorphous ferromagnetics, *Sov. Phys. Solid State*, **2**, No. 3, 468, (1960).

- [146] Gubler, I. E., Making of small ferrite spheres, *Prib. Tekh. Eksp.*, No. 5, 145, (1960), (in Russian).
- [147] Gottlieb, P., Nonlinear effects of crystalline anisotropy on ferrimagnetic resonance, *J. Appl. Phys.*, **31**, No. 11, 2059, (1960).
- [148] Gottlieb, P. and Suhl, H., Saturation of ferrimagnetic resonance with parallel pumping, *J. Appl. Phys.*, **33**, No. 4, 1508, (1962).
- [149] Griffiths, J. H. E., Anomalous high-frequency resistance of ferromagnetic metals, *Nature*, **158**, No. 4019, 670, (1946).
- [150] Gulyaev, Yu. V., Bugaev, A. S., Zil'berman, P. E., Ignat'ev, I. A., Konovalov, A. G., Lugovskoi, A. V., Mednikov, A. M., Nam, B. P., and Nikolaev, E. I., Giant oscillations in the transmission of quasi-surface spin waves through a thin yttrium-iron garnet (YIG) film, *JETP Lett.*, **30**, No. 9, 565, (1979).
- [151] Gurevich, A. G., *Cavity Resonators and Waveguides*, Sov. Radio, Moscow, (1952), (in Russian).
- [152] Gurevich, A. G., Quadratic relations for media with tensor parameters, *Radiotekh. Elektron*, **2**, No. 8, 960, (1957), (in Russian).
- [153] Gurevich, A. G., *Ferrites at Microwave Frequencies*, Consultants Bureau, New York, (1963).
- [154] Gurevich, A. G., Ferrite ellipsoid in a waveguide, *Radiotekh. Elektron*, **8**, No. 5, 780, (1963), (in Russian).
- [155] Gurevich, A. G., Electric-loss induced width of ferromagnetic resonance curve, *Sov. Phys. Solid State*, **16**, No. 6, 1159, (1974).
- [156] Gurevich, A. G., Ageev, A. N., and Klinger, M. I., Resonance in ferrimagnets containing paramagnetic ions with near-crossing energy levels, *J. Appl. Phys.*, **41**, No. 3, 1295, (1970).
- [157] Gurevich, A. G., Anisimov, A. N., Samokhvalov, A. A., and Solin, N. I., Spin-wave damping in ferromagnet EuO, *Acta Phys. Pol.*, **A68**, No. 3, 467, (1985).
- [158] Gurevich, A. G. and Bogomaz, M. A., Nonreciprocal phase shifts and decrement of waves in a waveguide with a ferrite plate, *Radiotekh. Elektron*, **3**, No. 9, 1133, (1958), (in Russian).
- [159] Gurevich, A. G. and Gubler, I. E., Ferromagnetic resonance in yttrium ferrite single crystals, *Sov. Phys. Solid State*, **1**, No. 12, 1693, (1960).
- [160] Gurevich, A. G., Gubler, I. E., and Safant'evskii, A. P., Ultrahigh frequency properties of yttrium and lutecium iron garnets, *Sov. Phys. Solid State*, **1**, No. 12, 1706, (1960).
- [161] Gurevich, A. G., Gubler, I. E., and Titova, A. G., Temperature relationships of the width of the resonance curve and processes of relaxation in ferrite monocrystals, *Sov. Phys. Solid State*, **3**, No. 1, 13, (1961).
- [162] Gurevich, A. G., Drabkin, G. M., Lazebnik, I. M., Mal'tsev, E. I.,

- Marchik, I. I., and Starobinets, S. S., Scattering of neutrons by parametrically excited spin waves, *Sov. Phys. Solid State*, **10**, No. 2, 511, (1968).
- [163] Gurevich, A. G., Karpovich, V. I., Rubal'skaya, E. V., Bairamov, A. I., Lapovok, B. L., and Emiryman, L. M., Ferromagnetic-resonance in  $\text{CdCr}_2\text{Se}_4$  with Fe addition, *Phys. Status Solidi B*, **69**, No. 2, 731, (1975).
- [164] Gurevich, A. G., Mêng Hsien-chên, and Starobinets, S. S., Anisotropy of resonance line width in yttrium garnet with rare-earth impurities, *Sov. Phys. Solid State*, **5**, No. 2, 540, (1963).
- [165] Gurevich, A. G., Safant'evskii, A. P., Solov'ev, V. I., and Sher, E. S., Effect of induced anisotropy on ferromagnetic resonance, *Bull. Acad. Sci. USSR, Phys. Ser.*, **25**, No. 11, 1374, (1961).
- [166] Gurevich, A. G., Sanina, V. A., Golovenchits, E. I., and Starobinets, S. S., Resonance in magnetically ordered crystals with anisotropic g factors, *J. Appl. Phys.*, **40**, No. 3, 1512, (1969).
- [167] Gurevich, V. L., Skin effect and ferromagnetic resonance, *Sov. Phys. JETP*, **6**, No. 6, 1155, (1957).
- [168] Gusev, B. N., Gurevich, A. G., Anisimov, A. N., Chivileva, O. A., Vinnik, M. A., and Berezin, I. L., Frequency dependences of the attenuation and nonlinearity threshold of surface spin waves in films, *Sov. Phys. Solid State*, **28**, No. 10, 1669, (1986).
- [169] Gyorgy, E. M., Le Craw, R. C., and Sturge, M. D., Influence of Jahn-Teller ions on acoustic and magnetic properties of YIG, *J. Appl. Phys.*, **37**, No. 3, 1303, (1966).
- [170] Haas, C. W. and Callen, H. B., Ferromagnetic resonance linewidth in cobalt-substituted ferrites, *Phys. Rev.*, **122**, No. 1, 59, (1961).
- [171] Haas, C. W. and Callen, H. B., Ferromagnetic relaxation and resonance line widths, in [267], Vol. I, p. 449.
- [172] Hansen, P., Tolksdorf, W., and Schuldt, G., Magnetostriction of germanium-substituted yttrium iron-garnet, *J. Appl. Phys.*, **43**, No. 11, 4740, (1972).
- [173] Hartfield, W. B. and Auld, B. A., Electromagnetic shock waves in gyromagnetic media, *J. Appl. Phys.*, **34**, No. 10, 2941, (1963).
- [174] Hartmann-Boutron, F., Effect of rare-earth impurities on the ferrimagnetic resonance and nuclear relaxation in yttrium iron garnet, *J. Appl. Phys.*, **35**, No. 3, Pt. 2, 889, (1964).
- [175] Hartwick, T. S. and Smit, J., Ferromagnetic resonance in Si-doped YIG, *J. Appl. Phys.*, **40**, No. 10, 3995, (1969).
- [176] Healy, D. W., Ferromagnetic resonance in nickel ferrite as a function of temperature, *Phys. Rev.*, **86**, No. 6, 1009, (1952).
- [177] Heinrich, B. and Meshcheryakov, V. F., Passage of electromagnetic wave through a ferromagnetic metal in the antiresonance region, *JETP Lett.*, **9**, No. 11, 378, (1969).

- [178] Heisenberg, W., On the theory of ferromagnetism, *Z. Phys.*, **49**, No. 9-10, 619, (1928), (in German).
- [179] Helzain, J., *Nonreciprocal Microwave Junctions and Circulators*, Wiley, New York, (1975).
- [180] Herring, C. and Kittel, C., On the theory of spin waves in ferromagnetic media, *Phys. Rev.*, **81**, No. 5, 869, (1951).
- [181] *High Frequency Processes in Magnetic Materials*, Srinivasan, G. and Slavin, A. N., Eds., World Scientific, Singapore, (1994).
- [182] Hoekstra, B., van Staple, R. P., and Voermans, A. B., Magnetic anisotropy of tetrahedral ferrous ions in  $\text{CdCr}_2\text{S}_4$ , *Phys. Rev.*, **B6**, No. 7, 2762, (1972).
- [183] Hogan, C. L., The ferromagnetic Faraday effect at microwave frequencies and its applications, *Bell. Syst. Tech. J.*, **31**, No. 1, 1, (1952).
- [184] Holstein, T. and Primakoff, H., Field dependence of the intrinsic domain magnetization of a ferromagnet, *Phys. Rev.*, **58**, No. 12, 1098, (1940).
- [185] Huber, D. L., Energy levels of the terbium ion in the iron garnet, *J. Appl. Phys.*, **36**, No. 3, Pt. 2, 1005, (1965).
- [186] Huber, D. L., Spin-magnon relaxation in terbium-doped YIG, *Solid State Commun.*, **4**, No. 9, 435, (1966).
- [187] Hurd, R. A., The magnetic fields of a ferrite ellipsoid, *Can. J. Phys.*, **36**, No. 8, 1072, (1958).
- [188] Ikola, R. J., New excitation mechanism for magnetoacoustic resonance in YIG, *J. Appl. Phys.*, **36**, No. 10, 3260, (1965).
- [189] Ishak, W. S., Magnetostatic-wave technology: A review, *Proc. IEEE*, **76**, No. 2, 171, (1988).
- [190] Jaffe, D., Cacheris, J. C., and Karayianis, N., Ferrite microwave detector, *Proc. IRE*, **46**, No. 3, 594, (1958).
- [191] Jordan, E. C. and Balmain, K. G., *Electromagnetic Waves and Radiating Systems*, Prentice-Hall, Englewood, NJ, (1968).
- [192] Joseph, R. I. and Schlömann, E., Theory of magnetostatic modes in long, axially-magnetized cylinders, *J. Appl. Phys.*, **32**, No. 6, 1001, (1961).
- [193] Joseph, R. I. and Schlömann, E., Dependence of the phonon-instability threshold for parallel pumping on crystal orientation and magnetic-field strength, *J. Appl. Phys.*, **41**, No. 6, 2513, (1970).
- [194] Kaczer, J. and Murtinova, L., Demagnetizing energy of periodic magnetic distributions, *Phys. Status Solidi A*, **23**, No. 1, 79, (1974).
- [195] Kaganov, M. I., Excitation of standing spin waves in a film, *Sov. Phys. JETP*, **12**, No. 1, 114, (1961).
- [196] Kaganov, M. I., Selective transparency of ferromagnetic films, *JETP Lett.*, **10**, No. 7, 214, (1969).
- [197] Kaganov, M. I. and Chubukov, A. V., Spin waves in magnetic dielectrics. Current status of the theory, in [382], Pt. 1, p. 1.

- [198] Kaganov, M. I. and Paash G., Impedance of ferromagnetic metal near antiresonance, *Sov. Phys. JETP*, **43**, No. 3, 580, (1976).
- [199] Kaganov, M. I. and Tsukernik, V. M., Phenomenological theory of kinetic processes in ferromagnetic dielectrics, Pt. 1, Relaxation in a gas of spin waves, *Sov. Phys. JETP*, **7**, No. 6, 1107, (1958).
- [200] Kaganov, M. I. and Tsukernik, V. M., Phenomenological theory of kinetic processes in ferromagnetic dielectrics. Pt. 2. Interaction of spin waves with phonons, *Sov. Phys. JETP*, **9**, No. 1, 151, (1959).
- [201] Kaganov, M. I. and Tsukernik, V. M., Nonresonance absorption of the energy of an alternating magnetic field by a ferromagnetic dielectric, *Sov. Phys. JETP*, **10**, No. 3, 587, (1960).
- [202] Kaganov, M. I. and Yui Lu, Effect of the boundary condition for the magnetic moment on spin-wave resonance in metals, *Bull. Acad. Sci. USSR, Phys. Ser.*, **25**, No. 11, 1388, (1962).
- [203] Kales, M. L., Modes in wave guides containing ferrites, *J. Appl. Phys.*, **24**, No. 5, 604, (1953).
- [204] Kales, M. L., Chait, H. M., and Sakiotis, N. G., A nonreciprocal microwave component, *J. Appl. Phys.*, **24**, No. 6, 816, (1953); Erratum, *ibid*, No. 12, 1528.
- [205] Kalinikos, B. A., Dipole-exchange spin-wave spectrum of magnetic films, in [254], p. 89.
- [206] Kalinikos, B. A. and Kovshikov, N.G., Private communication.
- [207] Kalinikos, B. A., Kovshikov, N. G., and Kozhus', N. V., Parametric excitation of a series of quasisurface spin waves in thin ferromagnetic films, *Sov. Phys. Solid State*, **27**, No. 9, 1681, (1985).
- [208] Kanamori, J., Anisotropy and magnetostriction of ferromagnetic and antiferromagnetic materials, in [267], Vol. 1, p. 127.
- [209] Kasatkina, T. S., Yakovlev, Yu. M., Matskevich, S. L., and Berestovaya, I. K., Relaxation processes in polycrystalline garnets near the upper limit of the spin wave spectrum, *Sov. Phys. Solid State*, **25**, No. 6, 999, (1983).
- [210] Kashcheev, V. N. and Krivoglaz, M. A., The effect of spin-spin and spin-phonon reaction in a ferromagnetic on the energy distribution of scattered neutrons, *Sov. Phys. Solid State*, **3**, No. 5, 1117, (1961).
- [211] Kasuya, T., The relaxation process in ferromagnetic resonance absorption, *Prog. Theor. Phys.*, **12**, No. 6, 802, (1954).
- [212] Kasuya, T. and Le Craw, R. C., Relaxation mechanisms in ferromagnetic resonance, *Phys. Rev. Lett.*, **6**, No. 5, 223, (1961).
- [213] Kazakov, G. T. and Filimonov, Yu. A., Interaction of magnetostatic waves with carriers of charge in laminated structures, *Sov. Phys. J.*, **32**, No. 1, 1, (1989).



- [214] Keffer, F., Spin waves, in *Encyclopedia of Physics*, Vol. XVIII/2, *Ferromagnetism*, Wijn, H. P. J., Ed., Springer-Verlag, Berlin, (1966).
- [215] Khlebopros, R. G. and Mikhailovskaya, L. V., Left-handed polarization of spin oscillations in the spectrum of a ferromagnet, *Sov. Phys. Solid State*, **12**, No. 8, 1986, (1971).
- [216] Kirov, S. A. and Pil'shchikov, A. I., Intensity and shape of ferromagnetic resonance absorption line in a sample with a domain structure, *Sov. Phys. Solid State*, **19**, No. 1, 80, (1977).
- [217] Kirov, S. A., Pil'shchikov, A. I., and Syr'ev, N. E., Magnetostatic-type oscillations in specimen with a domain structure, *Sov. Phys. Solid State*, **16**, No. 10, 1970, (1975).
- [218] Kirzhnits, D. A., Superconductivity and elementary particles, *Sov. Phys. Usp.*, **21**, No. 5, 470, (1978).
- [219] Kittel, C., Interpretation of anomalous Larmor frequencies in ferromagnetic resonance experiment, *Phys. Rev.*, **71**, No. 4, 270, (1947).
- [220] Kittel, C., On the theory of ferromagnetic resonance absorption, *Phys. Rev.*, **73**, No. 2, 155, (1948).
- [221] Kittel, C., Theory of antiferromagnetic resonance, *Phys. Rev.*, **82**, No. 4, 565, (1951).
- [222] Kittel, C., Interaction of spin waves and ultrasonic waves in ferromagnetic crystals, *Phys. Rev.*, **110**, No. 4, 836, (1958).
- [223] Kittel, C., Excitation of spin waves in a ferromagnet by a uniform RF field, *Phys. Rev.*, **110**, No. 6, 1295, (1958).
- [224] Kittel, C., Theory of ferromagnetic resonance in rare earth garnets, 1.  $g$  values, *Phys. Rev.*, **115**, No. 6, 1587, (1959).
- [225] Kittel, C., Theory of ferromagnetic resonance in rare earth garnets, 3. Giant anisotropy anomalies, *Phys. Rev.*, **117**, No. 3, 681, (1960).
- [226] Kittel, C., *Quantum Theory of Solids*, Wiley, New York, (1967).
- [227] Kittel, C., *Introduction to Solid State Physics*, Wiley, New York, (1976).
- [228] Kittel, C. and Herring, C., Effect of exchange interaction on ferromagnetic microwave resonance absorption, *Phys. Rev.*, **77**, No. 5, 725, (1950).
- [229] Kojima, H., Fundamental properties of hexagonal ferrites with magnetoplumbite structure, in [114], Vol. 3, p. 305.
- [230] Kolokolov, I. V., L'vov, V. S., and Cherepanov, V. B., Spin-wave spectra and thermodynamics of yttrium iron garnet, a twenty-sublattice ferrimagnet, *Sov. Phys. JETP*, **57**, No. 3, 605, (1983).
- [231] Kolokolov, I. V., L'vov, V. S., and Cherepanov, V. B., Magnon interaction and relaxation in yttrium iron garnet, a twenty-sublattice ferrimagnet, *Sov. Phys. JETP*, **59**, No. 5, 1131, (1984).
- [232] Korchagin, Yu. A., Khlebopros, R. G., and Chistyakov, N. S., Spin-wave resonance spectrum in a thin ferromagnetic layer with mixed boundary conditions, *Sov. Phys. Solid State*, **14**, No. 7, 1826, (1973).

- [233] Kotthaus, J. P. and Jaccarino, V., Antiferromagnetic-resonance linewidths in  $\text{MnF}_2$ , *Phys. Rev. Lett.*, **28**, No. 25, 1649, (1972).
- [234] Kraus, L., Anisimov, A. N., Gurevich, A. G., and Atlasman, A. V., Parametric spin-wave excitation in amorphous ferromagnetic wires, *JETP Lett.*, **37**, No. 2, 123, (1983).
- [235] Krivchenkov, V. D. and Pil'shchikov, A. I., Magnetostatic types of precession in an anisotropic sphere, *Sov. Phys. JETP*, **16**, No. 2, 410, (1963).
- [236] Krupička, S. and Novák, P., Oxide spinels, in [114], Vol. 2, p. 189.
- [237] Krutsenko, I. V., L'vov, V. S., and Melkov, G. A., Spectral density of parametrically excited waves, *Sov. Phys. JETP*, **48**, No. 3, 561, (1978).
- [238] Krutsenko, I. V. and Melkov, G. A., Parametric excitation of second group of spin waves in ferrites, *Sov. Phys. Solid State*, **21**, No. 1, 163, (1979).
- [239] Lamaire, B., Le Gall, H., and Dormann, J. L., Splitting of parametric magnons in ferromagnetic crystals, *Solid State Commun.*, **5**, No. 6, 499, (1967).
- [240] Landau, L. D., Possible explanation of the field dependence of the susceptibility at low temperatures, in Landau L. D., *Collected Papers*, ter Haar, D., Ed., Pergamon, Oxford, (1967).
- [241] Landau, L. D. and Lifshitz, E. M., To the theory of the dispersion of the ferromagnetic-body permeability, in Landau L. D., *Collected Papers*, ter Haar, D., Ed., Pergamon, Oxford, (1965).
- [242] Landau, L. D. and Lifshitz, E. M., *Course of Theoretical Physics*, Vol. 1, *Mechanics*, Pergamon, Oxford, (1976).
- [243] Landau, L. D. and Lifshitz, E. M., *Course of Theoretical Physics*, Vol. 3, *Quantum Mechanics, Nonrelativistic Theory*, Pergamon Press, Oxford, (1981).
- [244] Landau, L. D. and Lifshitz, E. M., *Course of Theoretical Physics*, Vol. 5, *Statistical Physics*, Pergamon Press, Oxford, (1980).
- [245] Landau, L. D. and Lifshitz, E. M., *Course of Theoretical Physics*, Vol. 7, *Theory of elasticity*, Pergamon Press, Oxford, (1986).
- [246] Landau, L. D. and Lifshitz, E. M., *Course of Theoretical Physics*, Vol. 8, *Electrodynamics of Continuous Media*, Pergamon Press, Oxford, (1984).
- [247] Lax, B. and Button, K. J., *Microwave Ferrites and Ferrimagnetics*, McGraw-Hill, New York, (1962).
- [248] Lebedeva, E. V., Pil'shchikov, A. I., and Sedletskaia, N. S., Conditions for parametric excitation of spin waves in samples with a regular domain structure, *Sov. Phys. JETP*, **45**, No. 2, 350, (1977).
- [249] Le Craw, R. C. and Comstock, R. L., Magnetoelastic interaction in ferromagnetic dielectrics, in *Physical Acoustics, Principles and Methods*, Mason, W. P., Ed., Vol. 3, Pt. B, *Lattice Dynamics*, Academic Press, New York, (1965).

- [250] Le Craw, R. C., Remeika, J. P., and Matthews, H., Angular momentum compensation in narrow line width ferrimagnets, *J. Appl. Phys.*, **36**, No. 3, Pt. 2, 901, (1965).
- [251] Le Craw, R. C., Spencer, E. C., and Porter, C. S., Ferromagnetic resonance line width in yttrium iron garnet single crystals, *Phys. Rev.*, **110**, No. 6, 1311, (1958).
- [252] Le Craw, R. C. and Walker, L. R., Temperature dependence of the spin-wave spectrum of yttrium iron garnet, *J. Appl. Phys.*, **32**, No. 3, Suppl., 167S, (1961).
- [253] Lifshitz, I. M., Azbel' M. Ya., and Kaganov, M. I., *Electron Theory of Metals*, Plenum, New York, (1973).
- [254] *Linear and Nonlinear Spin Waves in Magnetic Films and Superlattices*, Cottam, M. G., Ed., World Scientific, Singapore, (1994).
- [255] Loudon, R. and Pincus, P., Effect of dipolar fields on the antiferromagnetic spin-wave spectrum, *Phys. Rev.*, **132**, No. 2, 673, (1963).
- [256] Louisell, W. H., *Coupled Mode and Parametric Electronics*, Wiley, New York, (1960).
- [257] Luborski, F. E., Amorphous ferromagnets, in [114], Vol. 1, p. 451
- [258] Lukomskii, V. P., Parametric amplification of magnetoelastic waves, *Sov. Phys. Solid State*, **9**, No. 2, 467, (1967).
- [259] Lukomskii, V. P. and Kuz'ko, A. V., Magnetoelastic instability of spin waves in ferromagnets, *Sov. Phys. Solid State*, **11**, No. 5, 1052, (1969).
- [260] Lukomskii, V. P. and Tsvirko, Yu. A., Amplification of magnetoelastic waves in ferromagnetic films due to the drift current of carriers, *Sov. Phys. Solid State*, **15**, No. 3, 492, (1973).
- [261] Lutovinov, V. S., Melkov, G. A., Taranenko, A. Yu., and Cherepanov, V. B., First-order kinetic instability of spin waves in ferrite, *Sov. Phys. JETP*, **68**, No. 2, 432, (1989).
- [262] Lutovinov, V. S. and Reizer, M. Yu., Relaxation processes in ferromagnetic metals, *Sov. Phys. JETP*, **50**, No. 2, 355, (1979).
- [263] Lutsenko, A. L. and Melkov, G. A., Ferrite frequency doubler with the efficiency of 60%, *Radiotekh. Elektron.*, **18**, No. 11, 2284, (1973), (in Russian).
- [264] L'vov, V. S. and Fal'kovich, G. E., On the interaction of parametrically excited spin waves with thermal spin waves, *Sov. Phys. JETP*, **55**, No. 5, 904, (1982).
- [265] L'vov, V. S. and Prozorova, L. A., Spin waves above the threshold of parametric excitation, in [382], Pt. 1, p. 233.
- [266] Macdonald, J. R., Ferromagnetic resonance and the internal field in ferromagnetic materials, *Proc. Phys. Soc. London*, **64**, No. 383A, 968, (1951).

- [267] *Magnetism. A Treatise on Modern Theory and Materials*, Rado, G.T. and Suhl, H., Eds., Academic Press, New York. Vol. 1, Vol. 3, (1963); Vol. 2A, (1965); Vol. 2B, Vol. 4, (1966).
- [268] Machmudov, Z. Z. and Bar'yakhtar, V. G., Instability of electric current in semiconductors due to spin-wave excitation, *Sov. Phys. Solid State*, **7**, No. 7, 1677, (1966).
- [269] Manuilova, A. A. and Bogdanova, L. P., Ferromagnetic resonance in unsaturated yttrium garnet single crystals, *Sov. Phys. Solid State*, **6**, No. 9, 2152, (1965).
- [270] Marysko, M., Eddy-current line width contribution and propagation effects in low resistivity ferrites, *Phys. Status Solidi A*, **28**, No. 2, K159, (1975).
- [271] Matthews, H. and Le Craw, R. C., Acoustic wave rotation by magnon-phonon interaction, *Phys. Rev. Lett.*, **8**, No. 10, 397, (1962).
- [272] Matthews, H. and Morgenthaler, F. R., Phonon-pumped spin-wave instabilities, *Phys. Rev. Lett.*, **13**, No. 21, 614, (1964).
- [273] Mathews, J. and Walker, R. L., *Mathematical Methods of Physics*, Benjamin, New York, (1965).
- [274] Melchor, L. J., Ayres, W. P., and Vartanian, P. H., Microwave frequency doubling from 9-KMC to 18-KMC in ferrites, *Proc. IRE*, **45**, No. 5, 643, (1957).
- [275] Melkov, G. A., Nonlinear relaxation of spin waves in ferrites, *Sov. Phys. JETP*, **34**, No. 1, 198, (1972).
- [276] Melkov, G. A., Ferromagnetic resonance in large ferrite spheres, *Izv. Vyssh. Uchebn. Zaved. Radioelectron.*, **18**, No. 9, 107, (1975) (in Russian).
- [277] Melkov, G. A., Size effects in parametric excitation of spin waves in ferrites, *Sov. Phys. JETP*, **43**, No. 4, 690, (1976).
- [278] Melkov, G. A. and Artyukh, N. N., Ferrite amplifier with dielectric resonator, *Izv. Vyssh. Uchebn. Zaved. Radioelectron.*, **16**, No. 1, 127, (1973) (in Russian).
- [279] Melkov, G. A. and Lutzenko, A. L., Doubling of frequency using ferrites, *Radiotekh. Elektron.*, **18**, No. 2, 350, (1973) (in Russian).
- [280] Melkov, G. A., Safonov, V. L., Taranenko, A. Yu., and Sholom, S. V., Kinetic instability and Bose condensation of nonequilibrium magnons, *J. Mag. Mag. Materials*, **132**, No. 1-3, 180, (1994).
- [281] Melkov, G. A. and Sholom, S. V., Parametric excitation of spin waves by local pumping, *Sov. Phys. Solid State*, **29**, No. 11, 1870, (1987).
- [282] Melkov, G. A. and Sholom, S. V., Parametric excitation of spin waves by a surface magnetostatic wave, *Sov. Phys. JETP*, **69**, No. 2, 403, (1989).
- [283] Melkov, G. A. and Sholom, S. V., Amplification of surface magnetostatic waves by a parametric pump, *Sov. Phys. Tech. Phys.*, **35**, No. 8, 943, (1990).
- [284] Methfessel, S. and Mattis, D. C., *Magnetic Semiconductors*, Springer-Verlag, Berlin, (1968).

- [285] Mikaelyan, A. L., *Theory and Application of Ferrites at Microwave Frequencies*, Gosenergoizdat, Moscow, (1963) (in Russian).
  - [286] Mikaelyan, A. L. and Anton'yants, V. Ya., Mixing of microwave frequencies by use of ferrites, *Radiotekh. Elektron.*, **5**, No. 1, 90, (1960) (in Russian).
  - [287] Mikhailovskaya, L. V. and Bogomaz, I. V., Magnetostatic oscillations in a ferromagnetic film with domain structure, *Sov. Phys. Solid State*, **19**, No. 8, 1315, (1977).
  - [288] Miles, P. A. Westphal, W. B., and von Hippel, A., Dielectric spectroscopy of ferromagnetic semiconductors, *Rev. Mod. Phys.*, **29**, No. 3, 279, (1957).
  - [289] Monosov, Ya. A., On the theory of nonlinear phenomena in ferrites at microwave frequencies, Pt. I, Parametrically coupled magnetostatic oscillations in ferrite under the action of pumping, *Radiotekh. Elektron.*, **5**, No. 1, 59, (1960), (in Russian).
  - [290] Morgenthaler, F. R., Longitudinal pumping of magnetoelastic waves in ferrimagnetic ellipsoids, *J. Appl. Phys.*, **34**, No. 4, Pt. 2, 1289, (1963).
  - [291] Morgenthaler, F. R., An overview of electromagnetic and spin angular-momentum mechanical waves in ferrite media, *Proc. IEEE*, **76**, No. 2, 138, (1988).
  - [292] Moriya, T., Week ferromagnetism, in [267], Vol. 1, p. 85.
  - [293] Morse, P. M. and Feshbach, H., *Methods of Theoretical Physics*, Pts. 1, 2, McGraw-Hill, New York, (1953).
  - [294] Nagamiya, T., Theory of antiferromagnetism and antiferromagnetic resonance absorption, *Prog. Theor. Phys.*, **6**, No. 3, 342; 350, (1951).
  - [295] Nagamiya, T., A tentative interpretation of Bickford observation of the resonance absorption in magnetite below its transition point, *Prog. Theor. Phys.*, **10**, No. 1, 72, (1953).
  - [296] Neel, L., Magnetic properties of ferrites; ferromagnetism and antiferromagnetism, *Ann. Phys. (Paris)*, **3**, No. 2, 137, (1948), (in French).
  - [297] Nicolas, J., Microwave ferrites, in [114], Vol. 2, p. 243.
  - [298] Nikol'skii, V. V., Measurement of parameters of ferrites at microwave frequencies, *Radiotekh. Elektron.*, **1**, No. 4, 447; No. 5, 638, (1956), (in Russian).
  - [299] Nikol'skii, V. V., The gyrotropic perturbation of a waveguide, *Radiotekh. Elektron.*, **2**, No. 2, 157, (1957), (in Russian).
  - [300] *Nonlinear Phenomena and Chaos in Magnetic Materials*, Wigen, P. E., Ed., World Scientific, Singapore, (1994).
  - [301] O'Dell, T. H., *Magnetic Bubbles*, Macmillan, London, (1974).
  - [302] Okaya, A. and Barash, L. F., The dielectric microwave resonator, *Proc. IRE*, **50**, No. 10, 2081, (1962).
  - [303] O'Keeffe, T. W. and Patterson, R. W., Magnetostatic surface-wave propagation in finite samples, *J. Appl. Phys.*, **49**, No. 9, 4886, (1978).
-

- [304] Olson, F. A., Study of magnetoelastic interactions by parallel pumping, *J. Appl. Phys.*, **34**, No. 4, Pt. 2, 1281, (1963).
- [305] Orbach, R., Spin-lattice relaxation in rare-earth salts, *Proc. R. Soc. London, Ser. A*, **264**, No. 131, 458, (1961).
- [306] Osborn, J. A., Demagnetizing factors of the general ellipsoid, *Phys. Rev.*, **67**, No. 11/12, 351, (1945).
- [307] Ozhogin, V. I., Indirect parallel pumping and biresonance frequency doubling in antiferromagnetic substances, *Sov. Phys. JETP*, **31**, No. 6, 1121, (1970).
- [308] Parekh, J. P. and Tuan, H. S., Theory of magnetostatic forward volume wave convolvers, *IEEE Trans. Magn.*, **MAG-20**, No. 5, 1249, (1984).
- [309] Passell, L., Dietrich, O. W., and Als-Nilsen, J., Neutron scattering from the Heisenberg ferromagnets EuO and EuS, 1. The exchange interactions, *Phys. Rev. B*, **14**, No. 11, 4897, (1976).
- [310] Patton, C. E., Classical theory of spin-wave dispersion for ferromagnetic metals, *Czech. J. Phys.*, **B26**, No. 8, 925, (1976).
- [311] Patton, C. E. and Van Hook, H. J., Microwave loss in ultralow-linewidth substituted garnets, *J. Appl. Phys.*, **43**, No. 6, 2872, (1972).
- [312] Perekalina, T. M., Askochinskii, A. A., and Sannikov, D. G., Resonance of domain walls in cobalt ferrite, *Sov. Phys. JETP*, **13**, No. 2, 303, (1961).
- [313] Petrakovskii, G. A., Influence of the magnetocrystalline anisotropy on the parametric excitation of spin waves in ferrite single crystals, *Izv. Vyssh. Uchebn. Zaved. Fiz.*, No. 6, 29, (1962), (in Russian).
- [314] Pil'shchikov, A. I., Instability of spin waves in a sample with domain structure, *Sov. Phys. JETP*, **39**, No. 2, 328, (1974).
- [315] Pippin, J. E., Frequency doubling and mixing in ferrites, *Proc. IRE*, **44**, No. 8, 1054, (1956).
- [316] Pistol'kors, A. A. and Sui Yangshen, Oscillations of a small gyrotropic sphere in the field of a plane wave, *Radiotekh. Elektron.*, **5**, No. 1, 3, (1960), (in Russian).
- [317] Platzman, P. M. and Wolf, P. A., *Waves and Interactions in Solid State Plasmas*, Academic Press, New York, (1973).
- [318] Plumier, R., Magnetostatic modes in a sphere and polarization current corrections, *Physica (Utrecht)*, **28**, No. 4, 423, (1962).
- [319] Polder, D., On the theory of ferromagnetic resonance, *Philos. Mag.*, **40**, No. 300, 99, (1949).
- [320] Polder, D. and Smit, J., Resonance phenomena in ferrites, *Rev. Mod. Phys.*, **25**, No. 1, 89, (1953).
- [321] Polivanov, K. M., *Ferromagnets*, Gosenergoizdat, Moscow, (1957), (in Russian).

- [322] Pomeranchuk, I. Ya., The heat conductivity of paramagnetic dielectrics at low temperatures, *Zh. Exp. Theor. Fiz.*, **11**, No. 2-3, 226, (1941), (in Russian).
- [323] Prozorova, L. A. and Borovik-Romanov, A. S., Parametric excitation of spin waves in antiferromagnetic  $\text{CsMnF}_3$ , *JETP Lett.*, **10**, No. 7, 201, (1969).
- [324] Püst, L. and Frait, Z., FMR and FMAR measurement of saturation magnetization of the Fe-3WT-percent Si single-crystals between 3.5-K and 300-K, *Solid State Commun.*, **45**, No. 2, 103, (1983).
- [325] Rado, G. T. and Weertman, J. R., Spin-wave resonance in a ferromagnetic metal, *J. Phys. Chem. Solids*, **11**, No. 3/4, 315, (1959).
- [326] Reggia, R. and Spencer, E. G., A new technique in ferrite phase shifting for beam scanning of microwave antennas, *Proc IRE*, **45**, No. 11, 1510, (1957).
- [327] Rezende, S. M., Azevedo, A., and de Aguiar, F. M., Spin-wave instabilities, auto-oscillations, chaos, and control of chaos in YIG spheres, in [254], p. 335.
- [328] Roberts, R. W., Auld, B. A., and Schell, R. R., Magnetodynamic mode ferrite amplifier, *J. Appl. Phys.*, **33**, No. 3, Suppl., 1267, (1962).
- [329] Rodrigue, G. P., Meyer, H., and Jones, R. V., Ferrimagnetic resonance effects and miscellaneous: resonance measurements in magnetic garnets, *J. Appl. Phys.*, **31**, No. 5, Suppl., 3765, (1960).
- [330] Rosenbaum, F. J., Integrated Ferromagnetic Devices, in *Advances in Microwaves*, Young, L. and Sobol, H., Eds., Vol. 8, Academic Press, New York, (1974), p. 203.
- [331] Rubinstein, B. E., Titova, A. G., and Lapovok, B. L., Compensation of sublattice magnetic moments in yttrium iron-gallium garnet, *Sov. Phys. Solid State*, **7**, No. 6, 1328, (1965).
- [332] Sakiotis, N. G., Chait, H. N., and Kales, M. L., Nonlinearity of microwave ferrite media, *IEEE Trans. Antennas Propag.*, **AP-4**, No. 2, 111, (1956).
- [333] Salanskii, N. M. and Erukhimov, M. Sh., *Physical Properties and Applications of Magnetic Films*, Nauka, Sibirskoe Otdelenie, (1975), (in Russian).
- [334] Samokhvalov, A. A., Morozov, Yu. N., Volkenshtein, N. V., Zotov, T. D., and Karpenko, B. V., Spin-wave theory and the temperature dependence of the magnetization of  $\text{EuO}$  and  $\text{Eu}_{0.97}\text{Gd}_{0.03}\text{O}$  single crystals, *Sov. Phys. Solid State*, **12**, No. 10, 2312, (1977).
- [335] Shcheglov, I. M., Gilinskii, I. A., and Sorokin, V. G., Theory of excitation of surface magnetostatic waves. II. Numerical results and comparison with experiments, *Sov. Phys. Tech. Phys.*, **32**, No. 5, 573, (1987).
- [336] Schiff, L. I., *Quantum Mechanics*, McGraw-Hill, New York, (1968).
- [337] Schlömann, E. and Zeender, J. R., Ferromagnetic resonance in polycrystalline nickel ferrite aluminate, *J. Appl. Phys.*, **29**, No. 3, 341, (1958).
- [338] Schlömann, E., Spin-wave analysis of ferromagnetic resonance in polycrystalline ferrites, *J. Phys. Chem. Solids*, **6**, No. 2/3, 242, (1958).

- [339] Schlömann, E., Ferromagnetic resonance in polycrystalline ferrites with large anisotropy, 1. General theory and application to cubic materials with a negative anisotropy constant, *J. Phys. Chem. Solids*, **6**, No. 2/3, 257, (1958).
- [340] Schlömann, E., Generation of phonons in high power ferromagnetic resonance experiments, *J. Appl. Phys.*, **31**, No. 9, 1647, (1960).
- [341] Schlömann, E. and Jones, R. V., Ferromagnetic resonance in polycrystalline ferrites with hexagonal crystal structure, *J. Appl. Phys.*, **30**, No. 4, Suppl., 177S, (1959).
- [342] Schlömann, E., Ferrimagnetic resonance in the compensation region, in *Solid State Physics in Electronics and Telecommunication*, Academic Press, New York, London, Vol. 3, p. 322, (1960).
- [343] Schlömann, E., Green, J. J., and Milano, U., Recent developments in ferromagnetic resonance at high power levels, *J. Appl. Phys.*, **31**, No. 5, Suppl., 386S, (1960).
- [344] Schlömann, E., Ferromagnetic relaxation caused by interaction with thermally excited magnons, *Phys. Rev.*, **121**, No. 5, 1312, (1961).
- [345] Schlömann, E. and Joseph, R. I., Instability of spin waves and magnetostatic modes in a microwave magnetic field applied parallel to dc field, *J. Appl. Phys.*, **32**, No. 6, 1006, (1961).
- [346] Schlömann, E., Generation of spin waves in nonuniform magnetic fields, 1. Conversion of electromagnetic power into spin-wave power and vice versa, *J. Appl. Phys.*, **35**, No. 1, 159, (1964).
- [347] Schlömann, E. and Joseph, R. I., Generation of spin waves in nonuniform dc magnetic fields, 2. Calculation of the coupling length, *J. Appl. Phys.*, **35**, No. 1, 167, (1964).
- [348] Schlömann, E. and Joseph, R. I., Generation of spin waves in nonuniform magnetic fields, 3. Magnetoelastic interaction, *J. Appl. Phys.*, **35**, No. 8, 2382, (1964); Erratum, *ibid* **36**, No. 3, Pt. 1, 875, (1965);
- [349] Schlömann, E., Inhomogeneous broadening of ferromagnetic resonance lines, *Phys. Rev.*, **182**, No. 2, 632, (1969).
- [350] Schlömann, E., Amplification of magnetostatic surface wave by interaction with drifting charge carriers in crossed electric and magnetic fields, *J. Appl. Phys.*, **40**, No. 3, 1422, (1969).
- [351] Schlömann, E., Microwave behavior of partially magnetized ferrites, *J. Appl. Phys.*, **41**, No. 1, 204, (1970).
- [352] Schlömann, E., Circulators for microwave and millimeter-wave integrated-circuits, *Proc. IEEE*, **76**, No. 2, 188, (1988).
- [353] Schwob, P. K., Tachiki, M., and Everett, G. E., Determination of exchange integrals  $J_1$  and  $J_2$  and magnetic surface-anisotropy energy in EuS from standing-spin-wave resonance, *Phys. Rev. B*, **10**, No. 1, 165, (1974).



- [354] Searle, C. W. and Wang, C. T., Magnetic-resonance properties of pure and titanium-doped hematite, *J. Appl. Phys.*, **39**, No. 2, Pt. 2, 1025, (1968).
- [355] Seavey, M. H., Jr. and Tannenwald, P. E., Direct observation of spin-wave resonance, *Phys. Rev. Lett.*, **1**, No. 5, 168, (1958).
- [356] Seidel, H., The character of waveguide modes in gyromagnetic media, *Bell Syst. Tech. J.*, **36**, No. 2, 409, (1957).
- [357] Sena, L. A., *Units of Measure of Physical Quantities and Their Dimensions*, Nauka, Moscow, (1988), (in Russian).
- [358] Seshadri, S. R., Surface magnetostatic modes of a ferrite slab, *Proc. IEEE*, **58**, No. 3, 506, (1970).
- [359] Sethares, J. C., Magnetostatic surface-wave transducers, *IEEE Trans. Microwave Theory Tech.*, **MTT-27**, No. 11, 902, (1979).
- [360] Sievers, A. J. and Tinkham, M., Far infrared spectra of rare-earth iron garnets, *Phys. Rev.*, **129**, No. 5, 1995, (1963).
- [361] Sigal, M. A., Magnetostatic oscillations in a uniaxial crystal with plane-parallel domain structure, *Sov. Phys. Tech. Phys.*, **34**, No. 10, 1173, (1989).
- [362] Sigal, M. A. and Kostenko, V. I., Ferromagnetic resonance in a uniaxial crystal plate with a bubble domain lattice magnetized along the easy axis, *Sov. Phys. Solid State*, **22**, No. 1, 67, (1980).
- [363] Skomal, E. N. and Medina, M. A., Study of a microwave ferrimagnetic multiple signal conversion process, *J. Appl. Phys.*, **30**, No. 4, Suppl., 161S, (1959).
- [364] Skrotskii, G. V. and Alimov, Yu. I., Ferromagnetic resonance in a circularly polarized electromagnetic field of arbitrary amplitude, *Sov. Phys. JETP*, **8**, No. 6, 1035, (1959).
- [365] Skrotskii, G. V. and Alimov, Yu. I., Effect of specimen shape on ferromagnetic resonance in a strong radio-frequency field, *Sov. Phys. JETP*, **9**, No. 4, 899, (1959).
- [366] Skrotskii, G. V. and Kurbatov, L. V., Phenomenological theory of ferromagnetic resonance, in [115], p. 12.
- [367] Slater, J. C., Microwave electronics, *Rev. Mod. Phys.*, **18**, No. 4, 441, (1946).
- [368] Slavin, A. N., Kalinikos, B. A., and Kovshikov, N. G., Spin-wave envelope solitons in magnetic films, in [300], p. 209.
- [369] Slavin, A. N., Srinivasan, G., Cordone, S. S., and Cherepanov, V. B., Instability mechanism of collective spin-wave oscillations in finite-size ferrite samples, *J. Appl. Phys.*, **75**, No. 10, Pt. 2A, 5610, (1994).
- [370] Smart, J. S., *Effective Field Theories of Magnetism*, Saunders, Philadelphia, (1966).
- [371] Smit, J. and Beljers, H. G., Ferromagnetic resonance absorption in  $\text{BaFe}_{12}\text{O}_{19}$ , a highly anisotropic crystal, *Philips Res. Rep.*, **10**, No. 2, 113, (1955).

- [372] Smith, A. B. and Jones, R. V., Magnetostriction constants from ferromagnetic resonance, *J. Appl. Phys.*, **34**, No. 4, Pt. 2, 1283, (1963).
- [373] Solov'ev, V. I. and Gurevich, A. G., Ferromagnetic resonance in yttrium garnet doped with terbium, *Sov. Phys. Solid State*, **7**, No. 6, 1420, (1965).
- [374] Soohoo, R. F., *Magnetic Thin Films*, Harper & Row, New York, (1965).
- [375] Soohoo, R. F., *Microwave Magnetics*, Harper & Row, New York, (1985).
- [376] Sparks, M., *Ferromagnetic Relaxation Theory*, McGraw-Hill, New York, (1964).
- [377] Sparks, M., Theory of three-magnon ferromagnetic relaxation frequency for low temperature and small wave vectors, *Phys. Rev.*, **160**, No. 2, 364, (1967).
- [378] Sparks, M., Loudon, R., and Kittel, C., Ferromagnetic relaxation, 1. Theory of the relaxation of the uniform precession and the degenerate spectrum in insulators at low temperatures, *Phys. Rev.*, **122**, No. 3, 791, (1961).
- [379] Spencer, E. G., Le Craw, R. C., and Clogston, A. M., Low-temperature linewidth maximum in yttrium iron garnet, *Phys. Rev. Lett.*, **3**, No. 1, 32, (1959).
- [380] Spencer, E. G. and Le Craw, R. C., Magnetoacoustic resonance in yttrium iron garnet, *J. Appl. Phys.*, **30**, No. 4, Suppl., 149S, (1959).
- [381] Spencer, E. G., Le Craw, R. C., and Linares, R. C., Low-temperature ferromagnetic relaxation in yttrium iron garnet, *Phys. Rev.*, **123**, No. 6, 1937, (1961).
- [382] *Spin Waves and Magnetic Excitations*, Borovik-Romanov, A. S. and Sinha, S. K., Eds., Pts. 1, 2. North-Holland, Amsterdam, (1988).
- [383] Srinivasan, G., Patton, C. S., and Emtage, P. E., Brillouin light scattering on yttrium iron garnet films in magnetostatic wave device structure, *J. Appl. Phys.*, **61**, No. 6, 2318, (1987).
- [384] Stancil, D. D. and Morgenthaler, F. R., Guiding magnetostatic surface waves with nonuniform in-plane fields, *J. Appl. Phys.*, **54**, No. 3, 1613, (1983).
- [385] Stauss, G. H., Rubinstein, M., Feinleib, J., Dwight, K., Menyuk, K., and Wold, A., Nuclear magnetic resonance and magnetization studies of  $\text{CdCr}_2\text{Se}_4$ , *J. Appl. Phys.*, **39**, No. 2, 667, (1968).
- [386] Steele, M. C. and Vural, B., *Wave Interaction in Solid State Plasmas*, McGraw-Hill, New York, (1969).
- [387] Strauss, V., Magnetoelastic properties of yttrium iron garnet, in *Physical Acoustics, Principles and Methods*, Mason, W. P., Ed., Vol. 4, Pt. B, *Applications to Quantum and Solid State Physics*, Academic Press, New York, (1967).
- [388] Sturge, M. D., Gyorgy, E. M., Le Craw, R. C., and Remeika, J. P., Magnetic behavior of cobalt in garnets, 3. Magnetocrystalline anisotropy and ferromagnetic resonance of cobalt-doped yttrium iron garnet, *Phys. Rev.*, **180**, No. 2, 413, (1969).

- [389] Sugimoto, M., Properties of ferroxplana-type hexagonal ferrites, in [114], Vol. 3, p. 393.
- [390] Suhl, H., Ferromagnetic resonance in nickel ferrite between one and two kilomegacycles, *Phys. Rev.*, **97**, No. 2, 555, (1955).
- [391] Suhl, H., The nonlinear behavior of ferrites at high microwave signal levels, *Proc. IRE*, **44**, No. 10, 1270, (1956).
- [392] Suhl, H., The theory of ferromagnetic resonance at high signal powers, *J. Phys. Chem. Solids*, **1**, No. 4, 209, (1957).
- [393] Suhl, H., Theory of the ferromagnetic microwave amplifier, *J. Appl. Phys.*, **28**, No. 11, 1225, (1957).
- [394] Suhl, H., Origin and use of instabilities in ferromagnetic resonance, *J. Appl. Phys.*, **29**, No. 3, 416, (1958).
- [395] Suhl, H., Note on the saturation of the main resonance in ferromagnetics, *J. Appl. Phys.*, **30**, No. 12, 1961, (1959).
- [396] Suhl, H., Some nonlinear effects in magnetically ordered materials, in [300], p. 13.
- [397] Suhl, H. and Walker, L. R., Topics in guided wave propagation through gyromagnetic media, Pt. I, The completely filled cylindrical guide, *Bell Syst. Tech. J.*, **33**, No. 3, 579, (1954); Pt. II, Transverse magnetization and non-reciprocal helix, *ibid.*, No. 4, 939; Pt. III, Perturbation theory and miscellaneous results, *ibid.*, No. 5, 1133.
- [398] Sui Yang Shen,, Methods of solving the problem of oscillations of a small gyrotropic sphere, Pt. 1, The method of successive approximations, *Radiotekh. Elektron*, **5**, No. 12, 1951, (1960), (in Russian).
- [399] Tamm, I. E., *Fundamentals of the Theory of Electricity*, Gostekhizdat, Moscow, (1949) (in Russian).
- [400] Tannenwald, P. E. and Weber, R., Exchange integral in cobalt from spin-wave resonance, *Phys. Rev.*, **121**, No. 3, 715, (1961).
- [401] Tchernev, D. I., Effect of low-temperature magnetic anneal on the linewidth of garnets containing  $\text{Fe}^{2+}$  ions, *J. Appl. Phys.*, **38**, No. 3, 1046, (1967).
- [402] Tchernev, D. I., Temperature dependence of the linewidth of garnets containing  $\text{Fe}^{4+}$  ions, *J. Appl. Phys.*, **39**, No. 2, Pt. 1, 826, (1968).
- [403] Teale, R. W. and Tweedale, K., Ytterbium-ion relaxation in ferrimagnetic resonance, *Phys. Lett.*, **1**, No. 7, 298, (1962).
- [404] Tien, P. K. and Suhl, H., A traveling-wave ferromagnetic amplifier, *Proc. IRE*, **46**, No. 4, 700, (1958).
- [405] Tokheim, R. E., Winslow, D. K., and Auld, B. A., Parametric excitation of acoustic wave instabilities in ferromagnets, *J. Appl. Phys.*, **35**, No. 3, Pt. 2, 1010, (1964).
- [406] Trivelpiece, A. W., Ignatus, A., and Holscher, P. C., Backward waves in longitudinally magnetized ferrite rods, *J. Appl. Phys.*, **32**, No. 2, 259, (1961).
-

- [407] Tsukernik, V. M., Quantum mechanics of a spin wave in a ferromagnet, *Sov. Phys. Solid State*, **10**, No. 4, 795, (1968).
- [408] Turner, E. H., Interaction of phonons and spin waves in yttrium iron garnet, *Phys. Rev. Lett.*, **5**, No. 3, 100, (1960).
- [409] Turov, E. A., Features of ferromagnetic resonance in metals, in [115], p. 144.
- [410] Turov, E. A., *Physical Properties of Magnetically Ordered Crystals*, Academic Press, New York, (1965).
- [411] Turov, E. A. and Irkhin, Yu. P., On the spectrum of oscillations for ferromagnetic elastic medium, *Fiz. Met. Metalloved.*, **3**, No. 1, 15, (1956), (in Russian).
- [412] Tyablikov, S. V., *Methods of Quantum Theory of Magnetism*, Nauka, Moscow, (1975), (in Russian).
- [413] Ubbink, J., Poulis, J. A., Gerritsen, H. J., and Gorter, C. J., Antiferromagnetic resonance in copper chloride, *Physica (Utrecht)*, **18**, No. 6/7, 361, (1952).
- [414] Vaks, V. G., Larkin, A. I., and Pikin, S. A., Thermodynamics of an ideal ferromagnetic substance, *Sov. Phys. JETP*, **26**, No. 1, 188, (1968).
- [415] Vaks, V. G., Larkin, A. I., and Pikin, S. A., Spin waves and correlation functions in a ferromagnet, *Sov. Phys. JETP*, **26**, No. 3, 647, (1968).
- [416] Vashkovskii, A. V., Stal'makhov, A. V., and Shakhnazaryan, D. G., Formation, reflection, and refraction of magnetostatic wave beams, *Sov. Phys. J.*, **31**, No. 11, 908, (1988).
- [417] van Staple, R. P., Sulfospinels, in [114], Vol. 3, p. 603.
- [418] Van Vleck, J. H., Ferromagnetic resonance. *Physica (Utrecht)*, **17**, No. 3/4, 234, (1951).
- [419] Van Vleck, J. H., Ferrimagnetic resonance of rare-earth-doped iron garnets, *J. Appl. Phys.*, **35**, No. 3, Pt. 2, 882, (1964).
- [420] Vendik, O. G. and Chartorizhskii, D. N., Dispersion equation for nonuniform oscillations of the magnetization in a ferromagnetic plate, *Sov. Phys. Solid State*, **12**, No. 5, 1209, (1970).
- [421] Vendik, O. G., Kalinikos, B. A., and Chartorizhskii, D. N., Instability of spin-waves in thin ferromagnetic films, *Sov. Phys. Solid State*, **16**, No. 9, 1785, (1975).
- [422] Vendik, O. G., Kalinikos, B. A., and Chartorizhskii, D. N., Instability of spin waves in tangentially magnetized ferromagnetic films, *Sov. Phys. Solid State*, **19**, No. 2, 222, (1977).
- [423] Vittoria, C., *Microwave Properties of Magnetic Films*, World Scientific, Singapore, (1994).
- [424] Vlasov, K. B. and Ishmukhametov, B. Kh., Rotation of the plane of polarization of elastic waves in magnetically polarized magneto-elastic media, *Sov. Phys JETP*, **10**, No. 3, 531, (1960).

- [425] Vlasov, K. B. and Onoprienko, L. G., Resonance effects in magnetically uniaxial ferrite single crystals having domain structure, *Phys. Met. Metallogr. (USSR)*, **15**, No. 1, (1963).
- [426] *Handbook of Microwave Ferrite Materials*, von Aulock, W. H., Ed., Academic Press, New York, (1965).
- [427] Vonsovskii, S. V., Conductivity of ferromagnets at low temperatures, *Zh. Eksp. Teor. Fiz.*, **18**, No. 2, 219, (1948), (in Russian).
- [428] Vugal'ter, G. A. and Gilinskii, I. A., Excitation and reception of magnetostatic waves by a microstrip transducer, *Sov. Phys. Tech. Phys.*, **30**, No. 11, 1332, (1985).
- [429] Vugal'ter, G. A. and Gilinskii, I. A., Magnetostatic waves (a review), *Izv. Vyssh. Uchebn. Zaved. Radiofiz.*, **32**, No. 10, 1187, (1989), (in Russian).
- [430] Vugal'ter, G. A., Gusev, B. N., Gurevich, A. G., and Chivileva, O. A., Excitation of magnetostatic surface wave by a coplanar transducer, *Sov. Phys. Tech. Phys.*, **31**, No. 1, 87, (1986).
- [431] Vugal'ter, G. A. and Makhalin, K. N., Reflection and excitation of magnetostatic surface waves on the metal strip, *Sov. Phys. Tech. Phys.*, **30**, No. 3, 296, (1985).
- [432] Walker, L. R., Magnetostatic modes in ferromagnetic resonance, *Phys. Rev.*, **105**, No. 2, 390, (1957).
- [433] Walker, L. R., Resonant modes of ferromagnetic spheroid, *J. Appl. Phys.*, **29**, No. 3, 318, (1958).
- [434] Wangsness, R. K., Sublattice effects in magnetic resonance, *Phys. Rev.*, **91**, No. 5, 1085, (1953).
- [435] Wangsness, R. K., Susceptibility tensor and the Faraday effect in ferrimagnetics, *Phys. Rev.*, **95**, No. 2, 339, (1954).
- [436] Wang, J. Shy-Yih, Energy width of ferromagnetic-exchange magnons in a magnetic field, *Phys. Rev. B*, **6**, No. 5, 1908, (1972).
- [437] Weiss, M. T., Solid-state microwave amplifier and oscillator using ferrites, *Phys. Rev.*, **107**, No. 1, 317, (1957).
- [438] Weiss, M. T., Microwave and low-frequency oscillation due to resonance instabilities in ferrites, *Phys. Rev. Lett.*, **1**, No. 7, 239, (1958).
- [439] White, R. L. and Solt, I. H., Multiple ferromagnetic resonance in ferrite spheres, *Phys. Rev.*, **104**, No. 1, 56, (1956).
- [440] White, R. L., Ferromagnetic resonance line widths and g-factors in ferrites, *Phys. Rev. Lett.*, **2**, No. 11, 465, (1959).
- [441] Wiese, G., Buxman, L., Kabos, P., and Patton, C. E., Parallel-pumping fine structure at 9.4 GHz for in-plane magnetized yttrium iron garnet thin films, *J. Appl. Phys.*, **75**, No. 2, 1041, (1994).
- [442] Wigen, P. E., Kooi, C. F., Shanabarger, M. R., and Rossing, T. D., Dynamic pinning in thin-film spin-wave resonance, *Phys. Rev. Lett.*, **9**, No. 5, 206, (1962).

- [443] Wickersheim, K. A., Spectroscopic study of the ytterbium-iron exchange interaction in ytterbium iron garnet, *Phys. Rev.*, **122**, No. 5, 1376, (1961).
- [444] Wijn, H. P. J. and van der Heide, H. A., A Richter type after-effect in ferrites containing ferrous and ferric ions, *Rev. Mod. Phys.*, **25**, No. 1, 98, (1953).
- [445] Wohlfarth, E. P., Band magnetism and applications, in *Magnetism. Selected Topics*, Foner, S., Ed., Gordon and Breach, New York, (1976), p. 59.
- [446] Wolf, W. P., Effect of crystalline electric fields on ferromagnetic anisotropy, *Phys. Rev.*, **108**, No. 5, 1152, (1957).
- [447] Wolf, W. P., Ferrimagnetism, *Rep. Prog. Phys.*, **24**, 212, (1961).
- [448] Wolfram, T. and De Wames, R. E., Experimental test for pinned spins in ferromagnetic resonance: parallel resonance, *Solid State Commun.*, **9**, No. 2, 171, (1971).
- [449] Yager, W. A., Additional ferromagnetic resonance absorption measurements on supermalloy, *Phys. Rev.*, **75**, No. 2, 316, (1949).
- [450] Yager, W. A., Galt, J. K., and Merritt, F. R., Ferromagnetic resonance in 2 nickel-iron ferrites, *Phys. Rev.*, **99**, No. 4, 1203, (1955).
- [451] Yakovlev, Yu. M., Spin-wave instabilities in isotropic ferromagnets for alternating and constant magnetic fields of arbitrary orientation, *Sov. Phys. Solid State*, **10**, No. 8, 1911, (1969).
- [452] Yakovlev, Yu. M., Private communication.
- [453] Yakovlev, Yu. M. and Burdin, Yu. N., Angular variation of the ferromagnetic resonance frequency in an arbitrary oriented plane of a cubic crystal, *Sov. Phys. Solid State*, **8**, No. 11, 2147, (1967).
- [454] Yakovlev, Yu. M., Rubal'skaya, E. V., Godes, L. G., Lapovok, B. L., and Bushueva, T. N., Single crystals of ferrite spinels with narrow ferromagnetic resonance lines, *Sov. Phys. Solid State*, **13**, No. 4, 952, (1971).
- [455] Young, J. A. and Uehling, E. A., The tensor formulation of ferromagnetic resonance, *Phys. Rev.*, **94**, No. 3, 544, (1954).
- [456] Yu, J. T., Turk, R. A., and Wigen, P. E., Exchange-dominated surface spin waves in thin yttrium-iron-garnet films, *Phys. Rev. B*, **11**, No. 1, 420, (1975).
- [457] Yukawa, T., Yamada, J., Abe, K., and Ikenoue, J., Effects of metal on dispersion-relation of magnetostatic surface-waves, *Jpn. J. Appl. Phys.*, **16**, No. 12, 2187, (1977).
- [458] Zakharov, V. E. and L'vov, V. S., Parametric excitation of spin waves in ferromagnets with magnetic inhomogeneities, *Sov. Phys. Solid State*, **14**, No. 10, 2513, (1973).
- [459] Zakharov, V. E., L'vov, V. S., and Starobinets, S. S., Turbulence of spin waves beyond their parametric excitation threshold, *Sov. Phys. Usp.*, **17**, No. 6, 896, (1974).
- [460] Zautkin, V. V., Zakharov, V. E., L'vov, V. S., Musher, S. L., and Starobinets, S. S., Parallel spin-wave pumping in yttrium garnet single crystals, *Sov. Phys. JETP*, **35**, No. 5, 926, (1972).

- [461] Zavoiskii, E. K., Magnetic spin resonance in ferromagnets in centimeter wave-length range, *Zh. Eksp. Teor. Fiz.*, **17**, No. 10, 883, (1947).
- [462] Zhang, Z., Zhou, L., Wigen, P. E., and Ounadjela, K., Using ferromagnetic resonance as a sensitive method to study temperature dependence of interlayer exchange coupling, *Phys. Rev. Lett.*, **73**, No. 2, 336, (1994).
- [463] Zil'bermann, P. E., Golubeva, N. S., and Temiryazev, A. G., Parametric excitation of spin waves by spatially localized pumping in tangentially magnetized iron-yttrium garnet films, *Sov. Phys. JETP*, **70**, No. 2, 353, (1990).
- [464] Zil'bermann, P. E., Temiryazev, A. G., and Tikhomirova, M. P., Excitation and propagation of exchange spin waves in yttrium iron garnet films, *Sov. Phys. JETP*, **81**, No. 1, (1995).
- [465] Zotov, T. D. and Sukrov'tseva, M. M., Temperature dependence of spontaneous magnetization of an yttrium iron garnet single crystal, *Sov. Phys. Solid State*, **11**, No. 3, 521, (1969).





---

## ***Subject Index to the Bibliography***

---

This index contains numbers of references in the Bibliography classified according to their subjects. In Subsections A.1, A.2, and A.3, the references are listed in alphabetical order. In each item of subsections B.1 through B.9 the order is chronological. Some specialized issues of journals which are devoted to problems treated in the book are given in Section C.

---

### **A. Manuals and monographs**

#### **A.1. Mathematics and general physics**

7, 24, 29, 44, 55, 84, 113, 131, 151, 191, 226, 227, 242, 243, 244, 245, 246, 253, 256, 273, 317, 336, 357, 386, 399

#### **A.2. Magnetism and magnetic resonance**

1, 14, 15, 61, 62, 70, 114, 115, 267, 284, 301, 321, 333, 370, 374, 382, 410, 412

#### **A.3. Microwave magnetic processes, materials, and devices**

5, 115, 159, 179, 181, 247, 254, 285, 297, 300, 375, 376, 423, 426

---

### **B. Articles in journals and chapters in collective monographs**

#### **B.1. Magnetism: ground states, thermodynamics, etc.**

Ferromagnetism 130, 178, 101, 241, 306, 427, 446, 145, 18, 95, 208, 385, 194, 445, 334, 257, 417, 37

Antiferromagnetism and ferrimagnetism 240, 296, 60, 106, 342, 447, 292, 465, 138, 236, 229, 389

**B.2. Uniform oscillations of magnetization (Chapters 1, 2, and 3)**

Ferromagnetic resonance<sup>1</sup> 22, 102, 241, 149, 461, 219, 220, 319, 418, 266, 176, 371, 390, 23, 339, 341, 146, 159, 366, 453, 166, 143, 462  
 Antiferromagnetic resonance 221, 294, 413, 122, 166, 233, 110  
 Peculiarities of resonance in ferrimagnets 434, 435, 337, 136, 329, 342, 122, 360, 250, 331, 230

**B.3. Electrodynamics of gyrotropic media and microwave ferrite devices (Chapters 4 and 5)**

Fundamentals of electrodynamics of gyrotropic media 367, 319, 183, 140, 141, 109, 152  
 Ferrite-loaded waveguides and microwave devices based on them 203, 204, 139, 140, 397, 299, 326, 356, 158  
 Resonators and waveguide junctions with ferrite 298, 187, 316, 398, 328, 25, 154, 330, 276, 352

**B.4. Nonuniform oscillations of magnetization and spin waves (Chapters 6 and 7)**

Nonexchange magnetostatic waves 112, 192, 406, 82, 39, 27, 358, 134, 4, 457, 108, 303, 359, 6, 8, 308, 137, 428, 431, 430, 72, 335, 189, 3, 416, 429, 42  
 Nonuniform oscillations (Walker's modes) 93, 439, 432, 433, 119, 121, 318, 235, 45  
 Spin waves in unbounded media 52, 184, 180, 104, 105, 142, 252, 255, 214, 407, 414, 415, 230, 291  
 Spin waves in bounded bodies and nonuniform fields 223, 355, 325, 120, 195, 400, 442, 111, 83, 346, 347, 348, 133, 116, 90, 91, 117, 35, 448, 215, 118, 232, 92, 353, 456, 150, 384, 206, 205, 464

**B.5. Oscillations and waves in unsaturated ferromagnet (Chapter 8)**

Oscillations of domain walls 103, 43, 132, 288, 312  
 Ferromagnetic resonance and spin waves in the presence of domains 295, 320, 288, 425, 269, 351, 217, 216, 248, 287, 69, 38, 362, 361, 85

**B.6. Nonlinear processes (Chapters 9 and 10)**

One-mode nonlinear processes 315, 274, 190, 438, 364, 365, 28, 363, 147, 286, 30, 173, 81, 89, 263, 279

*Parametric excitation of spin waves:*

Thresholds under transverse pumping 56, 57, 19, 391, 392, 394, 31, 46, 51, 421, 206, 422, 234, 168, 71, 463, 464

---

<sup>1</sup>Only general theory and basic experiments are referred to in this item; for special topics in ferromagnetic resonance see Subsections B.5, B.7, B.8, and B.9 of this index.

Thresholds under longitudinal pumping 343, 201, 345, 313, 79, 323, 307, 458, 314, 20, 277, 237, 238, 21, 207, 281, 282, 441, 451

Above-threshold state 392, 395, 148, 275, 460, 459, 264, 265, 261, 283, 280, 369, 396, 327, 368

Instability of magnetostatic oscillations and waves; ferromagnetic amplifier 393, 437, 404, 289, 88, 345, 328, 278

### **B.7. Spin–spin relaxation (Chapter 11)**

General phenomenology and inherent processes 68, 10, 53, 144, 17, 104, 66, 199, 210, 212, 378, 344, 171, 376, 366, 214, 239, 377, 415, 436, 20, 36, 157, 168

Two-magnon processes 211, 76, 135, 338, 251, 63, 67, 160, 161, 170, 378, 381, 452, 40, 349, 454, 233, 311, 209, 231

### **B.8. Magnetoelastic interactions (Chapter 12)**

Magnetoelastic waves 411, 222, 12, 424, 440, 271, 111, 372, 249, 348, 387, 65, 41

Magnetoelastic nonlinearities 380, 340, 408, 290, 304, 272, 405, 188, 249, 26, 258, 259, 193

Spin-lattice relaxation 2, 10, 200, 212

### **B.9. Interactions of magnetic system with other systems, except lattice (Chapters 13 and 14)**

Anisotropy and relaxation caused by ions with strong spin-orbital coupling 75, 251, 87, 97, 224, 379, 440, 98, 225, 100, 165, 305, 64, 94, 403, 164, 174, 419, 74, 185, 373, 73, 169, 186, 99, 354, 402, 175, 388, 9, 156, 172, 182, 163, 33, 34, 107, 401

Interaction with charge carriers in semiconductors 444, 75, 450, 13, 268, 350, 80, 260, 155, 270, 49, 213

Ferromagnetic resonance and spin waves in metals 149, 449, 54, 228, 16, 455, 167, 11, 202, 126, 409, 47, 50, 177, 196, 32, 48, 198, 310, 77, 123, 262, 124, 127, 128, 324, 129, 125

Interactions with slow neutrons and light<sup>2</sup> 443, 210, 29, 86, 162, 96, 309, 383, 59

---

## **C. Special issues of journals devoted to topics discussed in the book**

1. Proceedings of the IRE, **44**, No. 2, (1956).
2. Circuits, Systems, and Signal Processing, **4**, No. 1–2, (1985).
3. Proceedings of the IEEE, **76**, No. 2, (1988).

---

<sup>2</sup>Only a few works (referred to in the text) are given on these topics not discussed in the book.



---

## *Index*

---

- Aftereffect, magnetic, 366
- Amplification of spin waves by drifting charge carriers, 371, 372
- in magnetic semiconductor, 371
  - in a structure ferromagnet-semiconductor, 372
- Angular momentum, *see* Moment of momentum
- Anisotropy constants, 39
- measurement, 43
  - renormalization, 40, 316, 318
- Anisotropy field, 43, 44
- Antiferromagnetic resonance, 68, 80
- damping, 72
  - easy axis of anisotropy, steady magnetic field
    - arbitrary oriented, 75
    - parallel to the axis, 70, 71, 73
    - perpendicular to the axis, 70, 74
  - easy plane of anisotropy, steady magnetic field
    - lying in the plane, 77, 78
    - perpendicular to the plane, 76
  - in weak ferromagnets, 78
  - influence of shape and dimensions of the sample, 80
  - line width, 73
  - susceptibility, 72
  - temperature dependence, 80
- Antiferromagnets, 59
- antiferromagnetic ordering
    - layered (Landau-type), 60, 61
    - staggered (Neel-type), 60
  - ground states, 65, 66
    - easy axis of anisotropy, 68, 70, 73
    - easy plane of anisotropy, 76, 77
  - vector of antiferromagnetism, 74
  - weak ferromagnet, 59, 60, 65
- Antiresonance, 15, 22, 103, 384
- line width (in metals), 385
- Bigyrotropic medium, 94
- electrodynamical equations, 95
  - for harmonic  $z$ -dependence, 95
- Bohr magneton, 4, 395
- Boltzmann constant, 5, 395
- Boundary conditions
- elastic, 314
  - electrodynamical, 92
  - periodical (Born-von Karman), 200
  - supplementary (exchange), 186
- Brillouin function, 5, 66
- Butterfly curve, 258
- Chaos above spin-wave-instability threshold, 279
- Charge-carrier influence on magnetic waves, 367
- Charge-conservation equation, 92

- Cherenkov condition of amplification, 370
- Circular waveguide with longitudinally magnetized ferrite
  - completely filled, 118
  - with ferrite rod, 119
- Circulator, 122
  - Faraday-type, 121
  - symmetric-junction, 145
- Coincidence of subsidiary absorption with main resonance, 254
- Collision integral, 287
- Compensation points, 67, 83, 89
- Conductivity contribution to ferromagnetic-resonance relaxation
  - in a sphere, 364
  - of interionic electron transitions, 366
- Conservation of magnetization-vector length, 10, 234
- Convective instability, *see* Amplification of spin waves by drifting charge carriers
- Corpuscule-wave duality, 199
- Coupled-wave approach, 120
- Coupling of magnetic modes at high power level, 245
- Creation and annihilation operators
  - of magnons, 208
  - of spin deviations, 207
- Critical wavelength, 117
- Crystal field, 338
- Curie constant, 6
- Curie law, 6
- Curie temperature (point), 1, 7
- Curie-Weiss law, 7
  
- Damon-Eshbach wave, 160
- Degeneration of uniform oscillations
  - with spin waves, 149, 183
- Demagnetization factors, 23, 397
- Demagnetization tensor, 23
  
- Detection of magnetization oscillations, 235
- Dimensional effects in ferromagnetic resonance, 136, 365
- Dipole-dipole (magnetic, relativistic) interaction, 2, 38
  - Hamiltonian, 212
- Dirac delta function, 21, 401
- Displacement vector, 311
- Dissipation parameters, 17, 18
- Dissipative terms
  - Gilbert, 17
  - Landau-Lifshitz, 17
  - modified Bloch, 18
- Domain structures
  - bubble, 218
  - stripe, 217
- Domain walls, 215
  - Bloch, 216
  - mass, 220
  - Neel, 217
- Domain-wall oscillations
  - dynamic susceptibility, 220
  - eigenfrequency, 220
  - equation of motion, 219
  - line width, 221
  - quality factor, 220
  
- Effective demagnetization factors, 35, 43
  - of cubic anisotropy, 47
  - of uniaxial anisotropy, 44
- Effective field, 33
  - of exchange interaction, 179
  - of magnetocrystalline anisotropy, 43, 44, 64
- Effective permeability, 16, 97
- Effective pumping, 275
- Elastic force, 311
- Elastic waves
  - in continuum, 313
  - in discrete crystal lattice, 314
- Elastic-stress effect on ferromagnetic resonance

- magnetostrictive stresses, 318
  - external stresses, 319
- Electrokinetic waves, 370
  - cyclotron waves, 370
  - helicons, 370
- Electron paramagnetic resonance, 4
- Ellipticity, 26
  - of spin wave, 256
  - of uniform oscillations, 26, 238
- Energy losses, 108
- Energy-balance equation, 107
- Energy-flow density
  - elastic (Umov vector), 313
  - electromagnetic (Poynting vector), 107, 166
- Equations of motion
  - elastic, 313
  - magnetoelastic, 317
  - of domain wall, 219
  - of magnetization,
    - in anisotropic ferromagnet (Landau–Lifshitz equation), 33
    - in isotropic ferromagnet, 9
    - linearized, 11, 18, 24, 34
    - with dissipative terms, 17
  - of sublattice magnetizations, 64
- Equilibrium magnetization directions
  - in anisotropic ferromagnet, 32
    - cubic, 43
    - uniaxial, 41
  - in antiferromagnet, 65, 66, *see also* Antiferromagnets
  - in ferrimagnet, 81, 82
  - in isotropic ferromagnet
    - ellipsoid, 23
    - unbounded, 11
- Exchange boundary conditions, 186
  - for ac magnetization, 188
    - free spins, 188
    - perfect pinning, 189
- Exchange field, 179
- Exchange energy, 7, 33, 338
  - Hamiltonian, 7, 206
    - nonuniform term, 179
    - of antiferromagnet, 64
- Exchange integral, 7
- Exchange interaction, 7
  - anisotropy of, 38
  - indirect, 7, 63, 373
- External susceptibility tensor, 27
- Faraday effect
  - for plane wave, 100, 101
  - in circular waveguide, 119, 120
- Fast relaxation, *see* Ionic relaxation
- Fast-relaxing ions, *see* Ions with strong spin–orbital coupling
- Fermi surface, 373
- Ferrimagnetic resonance, 81, 89
  - exchange modes, 85, 88, 89
  - in antiparallel ground state
    - allowance for shape and anisotropy, 88, 89
    - damping, 87
    - effective parameters, 84, 88
    - eigenfrequencies, 83
    - line width, 88
    - susceptibility, 87
  - in noncollinear ground state, 86
- Ferrimagnets, 59
  - equilibrium orientations of sublattice magnetizations, 81
- Ferrite microwave devices
  - circulator, 122
  - Faraday-type, 121
  - field-displacement-type, 129
  - filter, 142
  - isolator, 122
  - modulator, 122
  - nonlinear devices, 279
  - phase shifter, 122
  - resonance-type, 128
- Ferrite parametric amplifier, 267
- Ferrite resonator, *see* Magnetodynamic oscillations

- Ferrites with
  - garnet structure, 62
  - hexagonal structure, 62
  - spinel structure, 61
- Ferromagnetic resonance, 13
  - in a film, 50
    - of cubic ferromagnet, 51
  - in a small ellipsoid
    - eigenfrequency, 24
    - external susceptibility, 27
    - line width, 28
    - losses, 26
    - polarization, 26
  - in a sphere of anisotropic ferromagnet
    - cubic, 47
    - uniaxial, 45
  - in polycrystals, 53
  - in the presence of domains, 222
    - ellipsoid of uniaxial ferromagnet, 224
    - sphere of cubic ferromagnet, 226
  - influence of sample dimensions, 136, 365
  - measurement, 138
- Ferromagnetic resonance in bulk metal
  - nonexchange theory, 375
    - normal magnetization, 377
    - tangential magnetization, 377
  - self-consistent estimate of exchange influence, 378
  - theory allowing for exchange, 380
    - anomalous skin-effect, 383
    - effect of pinning-parameter, 383
    - normal magnetization, 383
    - tangential magnetization, 381
- Field-displacement effect, 127
- Filter (microwave, ferrite), 140, 142
  - filter-circulator, 142
- Fine-structure constant, 3, 395
- Four-magnon scattering, 288, 294, 298
- Free-energy density
  - elastic, 312, 313
  - magnetoelastic, 315, 316
  - of ferromagnet, 32
  - of ions, 342
- Frequency doubling, 236, 238
  - using magnetocrystalline anisotropy, 239
  - using magnetodynamic oscillations, 239
- Frequency mixing, 242
- g*-factor, *see* Spectroscopic splitting factor
- Group velocity
  - nonexchange magnetostatic waves in films, 154, 156, 161
  - spin waves, 182
- Growth anisotropy, 51
- Gyromagnetic ratio, 3, 10, 33
- Gyrotropy, 12
- 'Hard' parametric excitation of spin waves, 278
- Harmonic generation
  - second harmonic, 236, 238, *see also* Frequency doubling
  - third harmonic, 241
- Heisenberg model, 8, 205
  - diagonalization of the Hamiltonian, 206
- High-frequency approximation, 290, 291
- High-temperature approximation, 290, 294
- Holstein-Primakoff transformations, 206, 213
- Hooke law, 312
- Hydrodynamic approximation, 368



- Impedance
  - surface (of metal), 377, 381
  - wave, 99, 102
- Independent-grain (region) approximation, 54, 56, 300
- Induced anisotropy, 366, 367
  - by light, 366
- Induction electric field at ferromagnetic resonance, 364
- Instability of ferromagnetic resonance in strong ac field
  - caused by
    - magnetocrystalline anisotropy, 234
    - shape anisotropy, 233
- Interaction of magnons, 214
- Internal magnetic (dipole) field of magnetization wave, 181, 189
- Internal magnetic energy, 34, 65
- Ionic anisotropy
  - experimental data
    - 3d ions in YIG and spinel ferrites, 345
    - 4f ions in YIG, 344
    - chromium ions in ferromagnets, 345
  - one-ion theory, 342
    - low-lying doublet, 342
    - near-crossing levels, 343
- Ionic relaxation, 347
  - experimental data
    - 3d ions in garnets and spinels, 360
    - 4f ions in garnets, 358
    - in metals, 386
  - longitudinal (slow), 347, 349, 355
    - case of two energy levels, 354
  - Clogston theory, 350
  - dynamic anisotropy, 352
  - frequency and temperature dependences of line
    - width, 355
    - Hartmann–Boutron theory, 354
    - relaxation of ionic-level populations, 356
    - transverse, 347, 349, 360
      - Kittel fast-relaxation theory, 348
      - Van Vleck theory, 349
- Ions with strong spin–orbital coupling, 337
  - contribution to anisotropy, 337, *see also* Ionic anisotropy
  - contribution to line width, 347, *see also* Ionic relaxation
  - free energy, 342
  - splitting of energy levels, 337
    - 3d ions, 338, 339
    - 4f ions, 339, 342
- Isolator, 122
  - Faraday-type, 122
  - field-displacement, 129
  - resonance, 128
- Kasuya–Le Craw processes
  - magnon–magnon, 295
  - magnon–phonon, 296, 335
- Kerr effect, 102
- Kinetic equation (for numbers of quasiparticles), 287, 292
- Kronecker delta symbol, 132, 402
- Landé factor, *see* Spectroscopic splitting factor
- Landau–Lifshitz equation, 33
- Limitation of parametric-spin-wave growth above threshold, 271
  - nonlinear damping, 276
  - phase mechanism, 274
  - phase mechanism and nonlinear damping, 277
  - reaction of spin waves on pumping, 271

- Line width
  - antiresonance (in metals), 385
  - dipole narrowings, 55
  - exchange narrowings, 302
  - in ferrimagnets, 88
  - of antiferromagnetic resonance, 73
  - of domain-wall oscillations, 221
  - of ferromagnetic resonance
    - due to conductivity, 363
    - due to exchange interaction and conductivity in metals, 383
    - due to porosity, 56, 306, 308
    - due to surface roughness, 309
    - in polycrystals, 35, 306, 308
    - in single crystals, 28
  - spin-wave due to
    - four-magnon scattering, 295, 298
    - inherent processes in YIG (experimental data), 297
    - three-magnon confluence, 293
    - three-magnon splitting, 291
- Lorentz lemma, 104
- Lorentz resonance curve, 20
- Magnetic dipoles, 2
- Magnetic domains, 1, 215
- Magnetic gyration vector, 12, 94, 105
- Magnetic moment, 3
  - eigenvalues, 4, 337
  - elementary, 1, 2
- Magnetic spectra, 221
- Magnetic susceptibility tensor, 12
  - circular components, 14, 22
  - of polycrystal, 53
  - with losses, 19, 22
- Magnetic-flux quantum, 395
- Magnetization, 9, 92
- Magnetization processes
  - displacement, 218
  - rotation, 218
- Magneto-electrokinetic waves, 370
- Magnetoacoustic resonance (MAR), 330
  - secondary, 330
- Magnetocrystalline anisotropy, 31
  - origins, 37
  - phenomenological description, 39
    - antiferromagnets and ferrimagnets, 64, 81
    - cubic ferromagnet, 40
    - uniaxial ferromagnet, 34
- Magnetodynamic oscillations, 135
  - of a ferrite sphere, 136
- Magnetoelastic
  - constants, 315
  - energy, 315, 316
  - equations of motion, 317
    - linearized, 320
  - gap, 318
  - peaks on 'butterfly' curve, 326, 329
- Magnetoelastic waves, 319
  - damping, 323
  - excitation, 323
    - in a thin plate by ac magnetic field, 324
  - parametric excitation, 326, 330
  - propagating parallel to steady magnetization, 320
  - propagating perpendicularly to steady magnetization, 322
  - transformation in nonuniform steady magnetic field, 324
- Magnetostatic approximations
  - first (for electric field), 147, 166
  - limits of validity, 152
  - zero, 147, 148
- Magnetostatic equations, 93
- Magnetostatic nonexchange waves, 148

- applications, 170
- energy flow, 166
- excitation, 168
- in anisotropic ferromagnet, 150
- in plates (films), 153, 170
  - backward volume, 155
  - forward volume, 153
  - surface, 159, 161, *see also* Surface magnetostatic waves
- in the presence of domains, 230
- in waveguides with finite cross section
  - film of small width, 165
  - metallized rectangular rod, 163
  - round rod, 164
- losses, 167
- Magnetostatic potential, 132, 149
- Magnetostriction, 315
  - constants, 316
- Magnon dispersion law
  - classical (small- $k$ ) limit, 183, *see also* Spin waves
  - quantum-mechanical, 209
  - cubic spin lattices, 209
- Magnons, 199
  - numbers of, 200
  - spin and magnetic moment, 203
  - statistics, 203
  - thermal, 202
    - contribution to heat capacity, 205
    - contribution to temperature dependence of magnetization, 203, 212
    - time of life, 185, 202, 214
- Material equations, 92
- Maxwell equations, 91
  - for complex amplitudes of ac quantities, 93
- Measurement of
  - $\vec{\mu}$  components and  $\epsilon$  of ferrites, 137
  - anisotropy constants, 43
  - ferromagnetic-resonance parameters, 138
  - threshold field (longitudinal pumping), 257
- Moduli of elasticity, 312
  - cubic crystal, 312
  - isotropic medium, 313
- Molecular field, 6, 211
- Moment of momentum, 2
  - eigenvalues, 2
- Monodomain particles, 218
- Morin temperature (point), 60
- Narrowing of resonance line
  - dipole, 55, 307
  - exchange, 302
- Natural ferromagnetic resonance, 226, 229
  - Polder–Smit formula, 229
- Near-crossing of energy levels, 341, 343
  - $H_{\text{res}}$  peaks at, 344
- Nearest-neighbor approximation, 209
- Neel temperature of
  - antiferromagnet, 60, 66
  - ferrimagnet, 66
- Nonlinear ferrite microwave devices
  - power limiter, 279
  - filter-limiter, 280
  - small-signal suppressor (signal-to-noise-ratio enhancer), 280
- Nonlinear ferromagnetic resonance
  - in an ellipsoid of revolution, 232
  - in a sphere, 231
- Nonlinear magnetization oscillations, methods of approximate analysis using condition of magnetization-vector-length conservation, 234

- recurrent equations for magnetization terms, 236
- Nonlinear shift of spin-wave frequency, 250, 275
- Nonreciprocal waveguide junctions
  - matrix approach, 143
  - three-port, 145
  - two-port, 144
- Nonreciprocity, 104
  - in circular waveguide with longitudinally magnetized ferrite, 119
  - in rectangular waveguide with transversely magnetized ferrite, 126
- Nonuniform exchange constant, 180, 204, 210
- Nonuniform magnetostatic oscillations, 170
  - coupling of modes, 177, 300
  - excitation, 176
  - in antiferromagnet, 178
  - in ellipsoid of revolution, 175
  - in metallized cylinder, 171
  - in a sphere, 171
  - in samples with domains, 229
  - orthogonality relations, 176
- Number-of-magnons operator, 208
- One-ion anisotropy, 38, 342
- Onsager principle, 106
- Overlapping integral, 263
- Parallel (longitudinal) pumping, *see* Parametric excitation of spin waves
- Paramagnetic magnetization, 4
- Paramagnetic susceptibility of
  - antiferromagnet, 66
  - ferrimagnet, 66
  - ferromagnet, 5
- Parametric excitation of
  - magnetic and elastic modes, caused by magnetoelastic nonlinearity, 329
  - magnetoelastic waves under
    - elastic pumping, 330
    - magnetic pumping, 326
  - nonexchange magnetostatic waves, 264
  - Walker modes, 263
- Parametric excitation of spin waves, 245
  - under longitudinal (parallel) pumping, 246, 255
    - critical magnetic field, 256
    - effect of magnetocrystalline anisotropy, 258
    - effect of nonuniformities, 259
    - in thin films, 266
    - measurements, 257
    - spin-wave parameters, 256, 257
    - threshold ac field, 256
  - under nonuniform pumping
    - by a running wave, 269
    - by surface magnetostatic wave in a film, 269
    - local, 268
  - under oblique pumping, 261
    - in unsaturated samples, 262
  - under transverse pumping, 246
    - Suhl theory, 246
    - first-order threshold, 250
    - second-order threshold, 251
- Permeability tensor, 14
  - anisotropic ferromagnet, 43
  - designation of components, 94
  - isotropic ferromagnet, 15
    - with losses, 22
  - with exchange interaction, 180
- Permittivity, 94
  - in the presence of drifting carriers, 368
- Perturbation
  - lemmas, 109
  - of a resonator, 111

- cylindrical with ferrite sphere, 137
  - with ferromagnetic-metal wall, 114
- of a waveguide, 110
  - circular with ferrite rod, 120
- quasistatic approximation of internal field, 111, 113
- Phase shifter, 122
  - latching, 130
  - Reggia–Spencer, 123
- ‘Physical’ region (of spin-deviation space), 207
- Pinning parameter, 188
- Plank constant, 3, 395
- Polder tensor, *see* Magnetic susceptibility tensor
- Poynting vector, 108, 166
- Propagating spin waves in films, 194
  - dispersion characteristics, 196
  - ways of theoretical treatment, 194
- Pseudodipole interaction, 38
- Quality factor, 27
  - of domain-wall oscillations, 220
  - of small ferromagnetic ellipsoid, 27
- Rectangular waveguide with transversely magnetized ferrite
  - completely filled, 123
  - with ferrite plate, 125
- Relaxation frequency, 287
- Relaxation processes in metals, 386
  - electron–magnon, 387
  - four-particle, 388
  - exchange-conductivity, 383
  - ionic, 386
  - magnon–magnon, 386
  - two-magnon, 386
- Relaxation processes, methods of study
  - coupled equations of motion, 285
  - transition probability, 285
- Relaxation processes near Curie temperature, 310
- Relaxation time, 287
- Resonators with ferrite
  - cylindrical with ferrite sphere, 137
  - eigenoscillations, 131
  - forced oscillations, 131
  - use in measurements
    - of  $\vec{\mu}$  components and  $\epsilon$  of ferrites, 137
    - of ferromagnetic-resonance parameters, 138
  - waveguide resonators, 133
- Ruderman–Kittel–Kasuya–Iosida (RKKI) interaction, 373
- Saturation of main resonance, 254
- Scattering matrix of waveguide junction, 143
- Secondary quantization, 207
- Self-consistent field acting on a ferrite sample in waveguide, 139
- Self-oscillations above spin-wave-instability threshold, 279
- Shape anisotropy, 31
- Skin depth, 98, 363, 373
- Skin effect
  - anomalous, 379, 383
  - normal, 98
- Slow branches, 100, 103, 147, 162
- Slow relaxation, *see* Ionic relaxation
- Smearing out of spin-wave-instability threshold, 274
- Smit–Suhl formula, 36
- Soft mode, 74, 86, 90
- Space dispersion, 181
- Spectroscopic splitting factor, 3, 4, 10, 33
  - electron-spin, 3, 395

- Spherical-coordinate method, 35
- Spin waves
- damping, 184
  - dispersion law in anisotropic ferromagnet, 183
  - dispersion law in isotropic ferromagnet, 180
    - classical (continuum), 180, 182
    - degeneration with uniform oscillations, 149, 183
    - phase velocity, 181
    - quantum-mechanical, 209, *see also* Magnon dispersion law
  - excitation in nonuniform steady magnetic field, 198
  - in films, 189, *see also* Standing spin waves in films *and* Propagating spin waves in films
    - in films of small width, 197
  - in metals, 380
  - in samples of finite dimensions, 197
  - in the presence of domains, 229
  - parametric excitation, 245, *see also* Parametric excitation of spin waves
  - polarization, 184
- Spin-lattice relaxation processes, 284, 331
- direct, 331
    - Cherenkov, 333
    - phonon Kasuya-Le Craw, 296, 335
    - two-magnon confluence, 333
  - indirect
    - caused by charge carriers, 363, *see also* Charge-carrier effects in ferromagnetic resonance
    - ionic, 347, *see also* Ionic relaxation
- Spin-spin relaxation processes, 283
- experimental data for parametric magnons, 297, 299
    - in yttrium iron garnet, 297
  - inherent, in ferrites, 288, *see also* Three-magnon relaxation processes *and* Four-magnon scattering
  - inherent, in metals, 386
  - two-magnon, 299, *see also* Two-magnon relaxation processes
- Spin-flop transition, 69
- Spin-stiffness constant, *see* Nonuniform exchange constant
- Spin-wave instabilities, *see* Parametric excitation of spin waves
- Spin-wave resonance (SWR), *see* Standing spin waves in films
- Splitting of low-lying doublet, 341
- Spontaneous magnetization, 1, 7
- Stability of above-threshold state
  - external and internal, 278, 279
- Standing spin waves in films, 189
  - excitation by uniform ac field, 192
  - hyperbolic modes, 191
  - in normally magnetized film, 189
  - in tangentially magnetized film, 193
- Strain tensor, 311
- Stress tensor, 312
- Sublattice model, 63
  - equations of motion, 64, 67
  - equilibrium conditions, 65
- Subsidiary absorption, 252, 254
- Surface impedance, 377, 381
- Surface magnetostatic waves, 157
  - in film of small width, 165
  - in plates (films) and planar structures, 159, 161, 162

- Damon–Eshbach, 160
  - on boundary of ferromagnet with dielectric, 159
  - with metal, 157
- Thin-film model (of FMR in metals), 374
  - line width of a metal sphere, 374
- Three-halves-power law, 204
- Three-magnon relaxation processes, 288
  - confluence, 288
    - Kasuya–Le Craw process, 295
    - of parametric  $\pi/2$  magnons, 293
  - participation in  $M_z$  and  $|M|$  relaxation, 294
  - splitting, 288, 289
    - of magnetostatic-wave magnons, 297
    - of parametric  $\pi/2$  magnons, 291
    - of uniform mode, 290
- Threshold ac magnetic fields (under transverse pumping)
  - first-order instability, 252
    - at resonance, 252
    - off resonance, 252
  - influence of pumping-field polarization, 254
  - second-order instability, 254
- Transducers for magnetostatic waves, 168, 169
  - radiation resistance, 170
- Transmission and reflection in waveguides with small ferrite samples
  - infinite waveguide, 139
  - short-circuited waveguide, 141
  - two coupled waveguides, 141
- Transparency of metal films, 385
- Turning surface, 198
- Two-magnon processes, 259, 273, 299
  - disordered distribution of ions over lattice sites, 305
  - general theory, 300
    - chaotic nonuniformities, 302
    - large-scale nonuniformities, 303, 308
  - in metals, 386
  - 0- $k$  processes, 300, 302
  - pores, 307, 308
  - roughness of sample surface, 309
  - variation of crystal-axis directions, 306, 308
- Two-quantum absorption, 241
- Uniform plane waves in
  - gyrotropic dielectric, 97
  - gyrotropic metal, 98
  - longitudinally magnetized ferrite, 98, 100
  - transversely magnetized ferrite, 102, 103
- Viscosity, magnetic, 366
- Walker equation, 150
  - generalized, 149
  - in anisotropic ferromagnet, 150
- Walker modes, *see* Nonuniform magnetostatic oscillations
- Waveguides with magnetized ferrite
  - circular, 118, 119
  - coaxial, 129
  - plane (optical), 120
  - rectangular, 123, 125
- Weak ferromagnets, 59, 60, 65
  - antiferromagnetic resonance, 78
- Weiss theory of ferromagnetism, 6
- Y-circulator, 145
- Yttrium iron garnet, 62, 296, 299
- Zeeman energy, 4, 34, 37, 65

